2023

Advancement of an Inhouse Aerospace Vehicle Design Synthesis System through the Introduction of a Novel Database-Knowledgebase System and by Improving the Geometry and Aerothermodynamic Disciplinary Processes

Samuel Atchison

ADVANCEMENT OF AN INHOUSE AEROSPACE VEHICLE DESIGN SYNTHESIS SYSTEM THROUGH THE INTRODUCTION OF A NOVEL DATABASE-KNOWLEDGEBASE SYSTEM AND BY IMPROVING THE GEOMETRY AND AEROTHERMODYNAMIC DISCIPLINARY PROCESSES

by

SAMUEL ATCHISON

Presented to the Faculty of the Graduate School of

The University of Texas at Arlington in Partial Fulfillment

of the Requirements

for the Degree of

MASTER OF SCIENCE IN AEROSPACE ENGINEERING

The University of Texas at Arlington

MAY 2023

ACKNOWLEDGEMENTS

I would like to first thank God for helping me through this journey. It has been a difficult one, but He has helped give me the strength to push through and has truly blessed me with this opportunity. I pray He continues to watch over me in the journey after.

Secondly, I must thank my wife. If it was not for her strength and believing in me that I could finish this, I'm not sure that I could have. She has been with me every step of the way of my graduate career, and there are no words to express how truly thankful I am for her sticking by my side. I pray that God continues to be with us in our marriage and our journey in life together.

Next, I want to thank my family. They have been supportive of me through this and have always helped me when I needed it. I pray that God blessed them as they have blessed me with my life.

Next, I want to thank my supervising professor and committee chairman, Dr. Chudoba. I thank him for giving me a chance to prove myself, when at the time I was not showing my full potential. I thank him for always being accommodating of me with the craziness of my life, and for the many opportunities I have been blessed with while being a researcher in the AVD Laboratory. I have learned so much, and I will never forget this experience. I pray that God blesses him, his family, and the prosperity of the AVD Laboratory.

I also want to thank the AVD Laboratory members that I have had the honor of working with and spending my graduate career with through these years. I want to thank Ian, who I have spent the most time with, for guiding me when I joined the AVD Laboratory, and for helping me with some of the work presented here. I want to thank Cody, Thomas, and Tony for being my new friends within the lab. While Covid prevented our initial time together, I thank them for the time and laughs we shared during this relatively short time. I also want to thank the previous lab members Stenila and Harin. I want to thank Stenila for her help with some of the work presented here and for her help with the publishing process on our conference papers. I thank Harin for guiding me as well, especially with my writing process on this thesis. I pray that God watches over all of them and blesses them in their life.

Lastly, I want to thank my committee members, Dr. Robert Taylor, and Dr. Animesh Chakravarthy, for being interested in my work, for being willing to be my committee members, and for taking the time out of their day to attend my defense. I pray that God watches over them as well.

This research effort would not have happened without all your help, and I truly thank everyone from the bottom of my heart. I pray that God blesses you, in the name of the Father, Son, and the Holy Spirt, Amen.

ABSTRACT

ADVANCEMENT OF AN INHOUSE AEROSPACE VEHICLE DESIGN SYNTHESIS SYSTEM THROUGH THE INTRODUCTION OF A NOVEL DATABASE-KNOWLEDGEBASE SYSTEM AND BY IMPROVING THE GEOMETRY AND AEROTHERMODYNAMIC DISCIPLINARY PROCESSES

SAMUEL ATCHISON, M.S.

The University of Texas at Arlington, 2023

Supervising Professor: Bernd Chudoba

Throughout the years of aerospace vehicle design, the process in which a vehicle is designed has drastically improved from being primarily developed through trial and error, to using sophisticated synthesis systems. While the trial-and-error process had its uses with providing the fundamental knowledge of how aircraft behave and can be designed, the increase in knowledge and technology allowed the possibility of more vehicle configurations to be explored without the need to build each one. This increase should have led to a revolution of vehicle designs, and while there have been some novel ones, it seems that the general design of aerospace vehicles has begun to stagnate. In short, as our knowledge of aerospace vehicle design has increased, the design freedom for new vehicles has decreased.

One possible reason for this contradictory situation is that as the knowledge of a specific vehicle configuration grew, it reduced the need or the want to explore beyond it. Keeping the same configuration, or at least close to it, reduces the risk involved with its design, but other vehicle configurations that may potentially prove to be more beneficial are left unexplored. Another possible reason is that the full knowledge from each vehicle design is not completely passed down from generation to generation. While the knowledge of design has generally increased over the years, this issue with knowledge retention keeps designers from reaching their full potential by having to redesign past vehicles and configurations. These issues are especially prevalent for high-speed aerospace vehicles.

The Aerospace Vehicle Design (AVD) Laboratory has been tackling these issues for many years, and their solution was the Aerospace Vehicle Design Synthesis (AVDS) system. This synthesis system provides a generic design methodology to open up the solution space topographies and allow more unconventional vehicle configurations to be explored. Each

generation of AVD researchers has improved upon this system to increase its capabilities, and the research presented herein introduces the author's contribution.

First, to further help the knowledge retention issue, the Vehicle Configuration Compendium (VCC) is introduced. This compendium is a self-contained parametric library that combines a comprehensive database and knowledgebase of past-to-present aerospace vehicles to aid design engineers by making the past always available. The power of this system was shown within a NASA-funded study regarding hypersonic commercial transportation, with two of the vehicle verification studies out of seven provided herein.

Lastly, to improve the capabilities of AVDS to increase the solution space topographies, improvements of the geometry and aerothermodynamic disciplinary processes were accomplished. For the geometry disciplinary process, a parametric 3D modeling software was used in conjunction with AVDS to generate models that could be used for method and synthesis verification, synthetic data, and to use more complex scaling methods to explore more possibilities within a solution space. For the aerothermodynamics disciplinary process, a method was developed to calculate the structural index parameter, a parameter that can be used during conceptual design to represent the structural and aerothermal effects that the vehicle may experience. This method was verified against historic data from when it was originally developed, and new maps were generated to visualize how the parameter is affected by temperature, cruise time, and TPS material. These improvements to AVDS with the VCC and the disciplinary methods, will assist future researchers in their quest of aerospace vehicle design.

TABLE OF CONTENTS

ACKNOWLEDGEMENTS iii
ABSTRACT iv
TABLE OF CONTENTS vi
LIST OF FIGURES ix
LIST OF TABLES xiii
NOMENCLATURE xv
CHAPTER 1 : INTRODUCTION 1
1.1 Research Motivation and Objectives 1
1.2 Aerospace Vehicle Design Phases 8
1.3 Aerospace Vehicle Design Synthesis (AVDS) 14
1.4 The Vehicle Configuration Compendium (VCC) 18
1.5 NASA Hypersonic, Commercial Transportation Feasibility Study 25
CHAPTER 2 : AEROSPACE VEHICLE DESIGN SYNTHESIS (AVDS) OVERVIEW 29
2.1 AVDS Introduction 29
2.2 History of AVDS 29
2.3 Aerospace Vehicle Design Synthesis-Python (AVDS-PYTHON) 32
CHAPTER 3 : VEHICLE CONFIGURATION COMPENDIUM (VCC) OVERVIEW 41
3.1 VCC Introduction 41
3.2 VCC Background Development 48
3.3 VCC Alpha Software Development 66
CHAPTER 4 : VSP MODEL CREATION AND USE 75
4.1 VSP Overview 75
4.2 VSP Model Creation Process 76
4.3 VSP use for the VCC 80
4.4 VSP use for AVDS 84
CHAPTER 5 : VCC METHOD AND SYNTHESIS VERIFICATION 108
5.1 X-43A Methods and Synthesis Verification 109
5.2 XB-70 Methods and Synthesis Verification 125
CHAPTER 6 : PARAMETER TREND INVESTIGATION 153
6.1 Purpose of Parameter Trend Investigation 153
6.2 Case Study: Istr Investigation 154
6.3 Summary of Other Parameter Trends Investigated 175

CHAPTER 7 : AEROTHERMODYNAMICS DISCIPLINE DEVELOPMENT FOR AVDS 179
7.1 Aerothermodynamics Discipline Overview 179
7.2 Development of Aerothermodynamic Methods for AVDS 182
CHAPTER 8 : FUTURE WORK 229
8.1 Improvement to the Vehicle Configuration Compendium (VCC) 229
8.2 VCC Synthetic Development 230
8.3 Geometry Module of AVDS 231
8.4 Improvements to Aerothermodynamics Method 232
CHAPTER 9 : SUMMARY OF CONTRIBUTIONS 235
REFERENCES 237
APPENDIX A VERIFICATION VEHICLE INPUTS AND ASSUMPTIONS FOR AVDS^{CE} 249
APPENDIX B VEHICLE BIBLIOGRAPHIES 254
B.1. X-51 Bibliography 255
B.2. X-43A Bibliography 256
B.3. XB-70 Bibliography 262
B.4. SR-71 Bibliography 266
B.5. Concorde Bibliography 269
B.6. Sänger-II Bibliography 275
B.7. NASP/X-30/Orient Express Bibliography 281
APPENDIX C DATABASE VEHICLE 'SNAPSHOTS' 294
APPENDIX D VEHICLE GEOMETRIC METHODS USED WITHIN AVDS 299
D.1 AVDS Configuration Evaluation (AVDS^{CE}) Geometric Method 300
D.2 AVDS Parametric Sizing (AVDS^{PS}) Geometric Method 302
APPENDIX E AEROTHERMODYNAMIC DISCIPLINARY METHODS FOR AVDS 305
APPENDIX F MATERIAL PROPERTIES 312
E.1 Insulation Material Properties 313
E.2 Structural Material Properties 317
APPENDIX G STRUCTURAL INDEX (I_{STR}) SENSITIVITY MAPS 319
G.1 Variation of Structural Index with an Aluminum 2024 Structure 320
G.2 Variation of Insulation Thickness with an Aluminum 2024 Structure 321
G.3 Variation of Structural Index with a Beryllium Aluminum Structure 322
G.4 Variation of Insulation Thickness with a Beryllium Aluminum Structure 323
G.5 Variation of Structural Index with a Graphite Epoxy Structure 324
G.6 Variation of Insulation Thickness with a Graphite Epoxy Structure 325

G.7 Variation of Structural Index with a Titanium 6Al-4V Structure 326
G.8 Variation of Insulation Thickness with a Titanium 6Al-4V Structure 327

LIST OF FIGURES

Fig. 1.1 HOTOL Schematic [4]. 3
Fig. 1.2 Hypersonic investment over time [5]. 4
Fig. 1.3 Personnel in hypersonics [6]. 5
Fig, 1.4 Generic aerospace vehicle design phases, modified from [10]. 9
Fig. 1.5 Design cycle design knowledge, design freedom, and discipline integration [11]. 10
Fig. 1.6 Fundamental steps to aerospace vehicle conceptual design [13]. 12
Fig. 1.7 Master timeline summarizing the professional engagement at (a) conceptual design (CD) level and (b) strategic decision-maker (CxO) support level. Industry exposure from 1989-2002, academic research exposure from 2002-today [14]. 15
Fig. 1.8 Knowledge retention issue demonstrated [26]. 19
Fig. 1.9 Data-Information-Knowledge cycle [28]. 20
Fig. 1.10 Example of future workstation for aerospace conceptual design [31]. 23
Fig. 1.11 Historical timeline leading to development of the VCC [30]. 25
Fig. 1.12 Study approach to develop hypersonic civil flight vehicle [14]. 26
Fig. 1.13 Verification and trade vehicles selected for tool verification studies and design trade studies for three different baseline geometries: (a) wing-body (WB), (b) blended-body (BB), and all-body (AB) [14]. 28
Fig. 2.1 Aerospace Vehicle Design Synthesis (AVDS) methodology and software development timeframe since 2002 [14]. 30
Fig. 2.2 Evolution of AVDS system through various programming languages [11,13,34]. 31
Fig. 2.3 AVDS Configuration Evaluation ($AVDS^{CE}$) synthesis process [14]. 34
Fig. 3.1 Example of a GUI for the database side of the VCC. 42
Fig. 3.2 Example of vehicle ‘snapshot’. 43
Fig. 3.3 Overview of main configurations with vehicle examples for each one [15]. 45
Fig. 3.4 Example of cross-section categories. 46
Fig. 3.5 Examples of knowledgebase continuum lines [39]. 46
Fig. 3.6 Example of a GUI for the knowledgebase side of the VCC. 47
Fig. 3.7 Vehicle configuration compendium (VCC) buildup process. 50
Fig. 3.8 Example of *Zotero* GUI with X-51 references. 51
Fig. 3.9 Example of *EndNote* GUI with X-51 references. 52
Fig. 3.10 First page of two of X-51 bibliography. 53
Fig. 3.11 Bibliography separated into primary disciplines for X-51. 55
Fig. 3.12 Excel sheet of identifying primary information in reviewed references for X-51. 55
Fig. 3.13 Examples of extracted data for X-51. 56
Fig. 3.14 Example of digitization of data. 57
Fig. 3.15 SQLite Studio Interface – Data storage with discipline codes. 58
Fig. 3.16 VCC statistics covering number of references and data richness of verification vehicles, and the relevant data-element extraction by discipline [14]. 60
Fig. 3.17 VCC statistics covering number of references and data richness of trade vehicles, and the relevant data-element extraction by discipline [14]. 61
Fig. 3.18 Absolute data richness of X-51. 64
Fig. 3.19 Relative data richness for X-51. 65
Fig. 3.20 Types of sources found for X-51. 66
Fig. 3.21 VCC Graphical User Interface (GUI) flowchart. 68
Fig. 3.22 Screen #1 of Software – Viewer chooses between database or knowledgebase path. 69
Fig. 3.23 User selects from list of vehicles. 70
Fig. 3.24 Vehicle ‘snapshot’ displayed. 71
Fig. 3.25 Bibliography displayed. 71
Fig. 3.26 Data displayed for chosen discipline. 72
Fig. 3.27 VCC interface – initiating knowledgebase. 73
Fig. 3.28 VCC interface – comparing configurations. 73
Fig. 3.29 VCC interface – viewing knowledge graphic for a specific discipline. 74
Fig. 4.1 Top-view portion of a 3-view of a representative vehicle for shaping within VSP [42]. 77
Fig. 4.2 Match input fuselage length of model to top-view of representative vehicle. 78
Fig. 4.3 Shape fuselage model to top-view of representative vehicle. 78
Fig. 4.4 Complete top-view of VSP model compared to top-view of representative vehicle. 79
Fig. 4.5 Four-view of the VSP model representing the Sänger II first stage. 80

Fig. 4.6 Examples of vehicles within the geometry characteristics compendium. 82
Fig. 4.7 Geometry method creation process for AVDS using X-43A. 84
Fig. 4.8 Example of advanced parameter linking for X-43A model. 85
Fig. 4.9 MATLAB GUI for data map creation from VSP models. 86
Fig. 4.10 Schematic of parameters to determine the vertical tail planform area [48]. 89
Fig. 4.11 Schematic of parameters to determine the horizontal tail planform area [48]. 89
Fig. 4.12 Change in tau with the addition of a constant width section (spatula) into the vehicle [33]. 93
Fig. 4.13 Change in tau with increasing the max height of the vehicle [33]. 93
Fig. 4.14 Tau scaling of the X-51. 95
Fig. 4.15 Height variation for tau scaling for the X-43A. 96
Fig. 4.16 Spatula width variation for tau scaling of the X-43A. 96
Fig. 4.17 Wingtip droop variation of the XB-70. 98
Fig. 4.18 Mach number variation for the scaling of Concorde. 102
Fig. 4.19 Length variation for tau scaling of Concorde. 102
Fig. 4.20 Mach number variation for scaling of Sänger HST-230. 104
Fig. 4.21 Height variation for tau scaling of Sänger HST-230. 104
Fig. 4.22 Mach number variation for tau scaling of Orient Express. 105
Fig. 4.23 Height variation for tau scaling of Orient Express. 106
Fig. 5.1 Three-view of X-43A [60]. 110
Fig. 5.2 Four-view of the VSP model representing the X-43A. 111
Fig. 5.3 Example of unusable data due to lack of axis values [71]. 112
Fig. 5.4 Lift coefficient versus angle of attack at Mach 7 for X-43A [72]. 112
Fig. 5.5 Lift-curve slope for the X-43A at varying Mach. 113
Fig. 5.6 Static pressure distribution along nozzle throat [75]. 114
Fig. 5.7 Static pressure distribution along diffuser duct [75]. 114
Fig. 5.8 Specific impulse vs mach number for X-43A, but with no y-axis values [73]. 115
Fig. 5.9 Specifc impulse vs mach number with full axes [74]. 115
Fig. 5.10 X-43A flight mission profile [73]. 116
Fig. 5.11 X-43A flight 2 Mach number, angle of attack, and dynamic pressure [76]. 116
Fig. 5.12 X-43A flight 2 engine test phases [77]. 116
Fig. 5.13 X-43A flight 2 engine test, parameter identification, and recovery maneuver phases [77]. 116
Fig. 5.14 Comparison of the AVDS^{CE} X-43A trajectory data and the X-43A flight #2 trajectory data from VCC for dynamic pressure and time. 119
Fig. 5.15 Comparison of the AVDS^{CE} X-43A trajectory data and the X-43A flight #2 trajectory data from VCC for Mach number and time. 119
Fig. 5.16 Proportions of calculated weights for the X-43A. 121
Fig. 5.17 Comparison of calculated weights to reference weight. 121
Fig. 5.18 Three-view of XB-70 [94]. 127
Fig. 5.19 Four-view of the VSP model representing the XB-70. 127
Fig. 5.20 Verification results of lift coefficient versus Mach for the XB-70. 130
Fig. 5.21 Verification results of drag coefficient versus Mach for the XB-70. 130
Fig. 5.22 Altitude vs net thrust [117]. 132
Fig. 5.23 Change in throat area [118, 119]. 132
Fig. 5.24 Capture mass flow ratio for XB-70 [104, 106]. 132
Fig. 5.25 Thrust data for various test flights [104, 120]. 132
Fig. 5.26 Derivation of thrust, TET, and T_{ab} for the XB-70 engine (YJ-93) with no afterburner. 133
Fig. 5.27 Verification of thrust as function of altitude for the XB-70 engine J-93. 135
Fig. 5.28 XB-70 wing-tip folding schedule as a function of Mach number [95]. 136
Fig. 5.29 XB-70 mission profile with annotated wing-tip folding schedule [121]. 136
Fig. 5.30 Altitude and Mach number trajectory data used for the surrogate trajectory [104]. 137
Fig. 5.31 Comparison of XB-70 flight speed limits to RS-70 flight speed limits [122]. 137
Fig. 5.32 XB-70A subsonic climb with max thrust (with afterburner) [123]. 137
Fig. 5.33 XB-70A supersonic climb with max thrust (with afterburner) [123]. 137
Fig. 5.34 XB-70B mission profile [130]. 138
Fig. 5.35 XB-70A and XB-70B flight envelopes [122]. 139
Fig. 5.36 XB-70A Mach 3.0 cruise altitude, range, and thrust settings [123]. 139
Fig. 5.37 XB-70A descent altitude, mach number, and speed for various weights [123]. 140
Fig. 5.38 XB-70A descent time, distance traveled, and fuel used (with change in gross weight) [123]. 140

Fig. 5.39 Digitized XB-70 altitude and mach number mission profile [104,122]. 141
Fig. 5.40 Comparison of the AVDS^{CE} XB-70 trajectory data and the XB-70 trajectory data from VCC for altitude and Mach number. 144
Fig. 5.41 AVDS^{CE} XB-70 altitude and range mission profile for a 50,000 lb payload. 145
Fig. 6.1 Structural concept for hypersonic vehicles [33]. 157
Fig. 6.2 Representative structural specific weights for a near-term demonstrator [33]. 158
Fig. 6.3 Propulsion integrated configurations, 78° leading edge angle [33]. 159
Fig. 6.4 Summary of the available design space for four different configuration concepts [33]. 159
Fig. 6.5 Selected structural indices for the Sänger EHTV and LAPCAT II missions [13]. 161
Fig. 6.6 Sänger II design space for two structural indices [13]. 161
Fig. 6.7 Vehicle configuration sensitivity to I_{str}. (*W/S* denotes the wing loading, or weight over surface) [142]. 162
Fig. 6.8 Superposition of structural indices provides the final constraint to determine the technical solution space [18]. 164
Fig. 6.9 Definition of structural capability indices used for this study [18]. 164
Fig. 6.10 I_{str} vs I_{perf} with varying spatula width and tau [143]. 166
Fig. 6.11 I_{str} vs I_{perf} with varying vehicle cross-section and tau [143]. 166
Fig. 6.12 Structural index vs. number of passengers. 168
Fig. 6.13 Structural index vs. payload weight. 168
Fig. 6.14 Structural index vs. total planform area. 169
Fig. 6.15 Structural index vs. industrial capability index. 170
Fig. 6.16 Structural index vs. wetted area. 171
Fig. 6.17 Temperature versus Mach number [33,145,146,147]. 173
Fig. 6.18 Temperature versus Mach number reduction to usable correlation. 173
Fig. 6.19 Structural index vs temperature with verification vehicles and used correlation line [33]. 174
Fig. 6.20 Propulsion index vs. cruise mach number. 176
Fig. 6.21 Propulsion index vs. mission range. 177
Fig. 6.22 Industry capability index vs. total planform area. 178
Fig. 7.1 Air flow chemistry boundaries [33]. 180
Fig. 7.2 Temperature behind a normal shock wave as a function of freestream velocity at a standard altitude of 52 km [150]. 181
Fig. 7.3 Altitude vs. mach with constant equilibrium temperature solution space [33]. 186
Fig. 7.4 Coefficient of lift vs. angle of attack at various mach numbers [151]. 187
Fig. 7.5 Constant equilibrium temperature lines for temperature of 1700 °F [151]. 188
Fig. 7.6 Constant equilibrium temperature solution space for 1700 °F [151]. 189
Fig. 7.7 Calculated lift loading lines at a value of 19 psf at various angles of attack. 190
Fig. 7.8 Digitized constant equilibrium temperature lines. 191
Fig. 7.9 Overlay of constant equilibrium temperature lines and 19 psf lift loading lines. 192
Fig. 7.10 Overlay of constant equilibrium temperature lines and 19 psf and 210 psf loading lines. 192
Fig. 7.11 Outlining the boundary of the solution space with the overlayed temperature and lift loading lines. 193
Fig. 7.12 Final created constant equilibrium temperature solution space. 193
Fig. 7.13 Comparison of digitized to calculated constant equilibrium temperature lines. 196
Fig. 7.14 Comparison of the generated constant equilibrium temperature solution spaces. 196
Fig. 7.15 Schematic of a thermal protection system with temperature distribution [152]. 198
Fig. 7.16 Representative finite element model of a thermal protection system [162]. 199
Fig. 7.17 Temperature of each node of the thermal protection system over time [162]. 200
Fig. 7.18 Temperature through the thickness of the thermal protection system at various times [162]. 200
Fig. 7.19 Calculated temperature of each node of the thermal protection system over time. 201
Fig. 7.20 Updated calculated temperature of each node of the thermal protection system over time. 202
Fig. 7.21 Calculated temperature through the thickness of the thermal protection system at various times. 203
Fig. 7.22 Illustration of simplified problem [163]. 204
Fig. 7.23 Simplified heating and pressure histories for BP9740 [163]. 205
Fig. 7.24 Maximum structural temperature rise vs insulation thickness [163]. 206
Fig. 7.25 Comparison of Blosser series results with AVD results (linear interpolation). 207
Fig. 7.26 Comparison of Blosser series results with AVD results (spline interpolation). 207
Fig. 7.27 Results for temperature method comparison. 208
Fig. 7.28 Total structural weight vs wetted area. 211
Fig. 7.29 Verification between selected method and results by Czysz. 215
Fig. 7.30 Verification between selected method and results by Czysz (reduced). 215
Fig. 7.31 Structural index sensitivity map for varying insulation material. 217
Fig. 7.32 Insulation thickness sensitivity map for varying insulation material. 219

Fig. 7.33 Structural index sensitivity map for varying structural material. 221
Fig. 7.34 Insulation thickness sensitivity map for varying structural material. 222
Fig. 7.35 Structural index sensitivity map for varying radiation shield material. 224
Fig. 7.36 Structural index sensitivity map for varying cruise time. 226
Fig. 7.37 Structural index sensitivity map for varying average atmospheric pressure (P_{avg}) 228
Fig. C.1 X-51 database 'snapshot'. 295
Fig. C.2 X-43A database 'snapshot'. 295
Fig. C.3 SR-71 database 'snapshot'. 296
Fig. C.4 XB-70 database 'snapshot'. 296
Fig. C.5 Concorde database 'snapshot'. 297
Fig. C.6 Sänger II database 'snapshot'. 297
Fig. C.7 NASP X-30 database 'snapshot'. 298
Fig. G.1 Structural index vs surface design temperature at a cruise time of 2 hrs. 320
Fig. G.2 Structural index vs surface design temperature at a cruise time of 3 hrs. 320
Fig. G.3 Structural index vs surface design temperature at a cruise time of 4 hrs. 320
Fig. G.4 Structural index vs surface design temperature at a cruise time of 5 hrs. 320
Fig. G.5 Insulation thickness vs surface design temperature at a cruise time of 2 hrs. 321
Fig. G.6 Insulation thickness vs surface design temperature at a cruise time of 3 hrs. 321
Fig. G.7 Insulation thickness vs surface design temperature at a cruise time of 4 hrs. 321
Fig. G.8 Insulation thickness vs surface design temperature at a cruise time of 5 hrs. 321
Fig. G.9 Structural index vs surface design temperature at a cruise time of 2 hrs. 322
Fig. G.10 Structural index vs surface design temperature at a cruise time of 3 hrs. 322
Fig. G.11 Structural index vs surface design temperature at a cruise time of 4 hrs. 322
Fig. G.12 Structural index vs surface design temperature at a cruise time of 5 hrs. 322
Fig. G.13 Insulation thickness vs surface design temperature at a cruise time of 2 hrs. 323
Fig. G.14 Insulation thickness vs surface design temperature at a cruise time of 3 hrs. 323
Fig. G.15 Insulation thickness vs surface design temperature at a cruise time of 4 hrs. 323
Fig. G.16 Insulation thickness vs surface design temperature at a cruise time of 5 hrs. 323
Fig. G.17 Structural index vs surface design temperature at a cruise time of 2 hrs. 324
Fig. G.18 Structural index vs surface design temperature at a cruise time of 3 hrs. 324
Fig. G.19 Structural index vs surface design temperature at a cruise time of 4 hrs. 324
Fig. G.20 Structural index vs surface design temperature at a cruise time of 5 hrs. 324
Fig. G.21 Insulation thickness vs surface design temperature at a cruise time of 2 hrs. 325
Fig. G.22 Insulation thickness vs surface design temperature at a cruise time of 3 hrs. 325
Fig. G.23 Insulation thickness vs surface design temperature at a cruise time of 4 hrs. 325
Fig. G.24 Insulation thickness vs surface design temperature at a cruise time of 5 hrs. 325
Fig. G.25 Structural index vs surface design temperature at a cruise time of 2 hrs. 326
Fig. G.26 Structural index vs surface design temperature at a cruise time of 3 hrs. 326
Fig. G.27 Structural index vs surface design temperature at a cruise time of 4 hrs. 326
Fig. G.28 Structural index vs surface design temperature at a cruise time of 5 hrs. 326
Fig. G.29 Insulation thickness vs surface design temperature at a cruise time of 2 hrs. 327
Fig. G.30 Insulation thickness vs surface design temperature at a cruise time of 3 hrs. 327
Fig. G.31 Insulation thickness vs surface design temperature at a cruise time of 4 hrs. 327
Fig. G.32 Insulation thickness vs surface design temperature at a cruise time of 5 hrs. 327

LIST OF TABLES

Table 1.1 Aircraft and aerospace vehicle class IV synthesis systems [15]. 16
Table 1.2 List of important AVDS studies. 17
Table 1.3 Aerospace database survey [30]. 21
Table 1.4 Vehicles considered for verification and trades [14]. 27
Table 2.1 AVDS^{CE} X-51 inputs and assumptions [14]. 35
Table 2.2 Summary of AVDS^{CE} code information for the four verification vehicles [14]. 36
Table 2.3 Comparison of the AVDS^{PS} process and the AVDS^{CE} process [14]. 37
Table 2.4 Inputs and assumptions for solution space generation [14]. 38
Table 2.5 Summary of AVDS^{PS} code information as applied to the three trade vehicles [14]. 40
Table 3.1 Summary of data sought for each discipline (not an exhaustive list). 62
Table 4.1 Verification of Sänger II first stage VSP model [43]. 80
Table 4.2 Vertical and aft-horizontal tail coefficients [48]. 89
Table 5.1 Disciplinary methods utilized in the AVDS^{CE} system for sizing the X-43A. 109
Table 5.2 Verification of X-43A VSP model [59]. 111
Table 5.3 Verification results comparison for the X-43A lift-curve slope at Mach 7. 113
Table 5.4 Verification results comparison for the X-43A Specific Impulse at Mach 6.83. 115
Table 5.5 Summary of determined X-43A flight 2 trajectory attributes for the AVDS X-43A surrogate trajectory. 117
Table 5.6 X-43A flight 2 surrogate trajectory flight segments and their parameters. 118
Table 5.7 X-43A Synthesis weight verification data. 120
Table 5.8 X-43A weight verification results. 122
Table 5.9 AVDS^{CE} X-43A inputs and assumptions. 122
Table 5.10 Comparison of the AVDS^{CE} X-43A sizing results with (VCC) actual X-43A data. The results shown are the verification results where no silane ignition phase is considered (Case 1). 124
Table 5.11 Comparison of the AVDS^{CE} X-43A sizing results with (VCC) actual X-43A data. The results shown are the verification results where a 1.5 second silane ignition phase has been considered (Case 2). 125
Table 5.12 Disciplinary methods utilized in the AVDS^{CE} system for sizing the XB-70. 126
Table 5.13 Verification of XB-70 VSP model [93]. 128
Table 5.14 Verification data for XB-70 compiled from VCC. 129
Table 5.15 Subsonic verification error results for the XB-70. 131
Table 5.16 Supersonic verification error results for the XB-70. 131
Table 5.17 Component efficiency used for the YJ-93. 132
Table 5.18 YJ-93 sizing results with afterburner (sea level). 134
Table 5.19 Summary of J-93/YJ-93 engine specification. 135
Table 5.20 B-70, RS-70, XB-70, and YB-70 mission ranges and cruise attributes. 138
Table 5.21 XB-70 surrogate trajectory input parameters. 141
Table 5.22 Part one of the inputs and results from using the XB-70A flight manual to predict XB-70A performance for a mission that is similar to the surrogate XB-70 trajectory. 142
Table 5.23 Part two of the inputs and results from using the XB-70A flight manual to predict XB-70A performance for a mission that is similar to the surrogate XB-70 trajectory. 143
Table 5.24 XB-70, XB-70A-1, and XB-70A-2 mission ranges and cruise attributes. 145
Table 5.25 XB-70A-1 and XB-70A-2 takeoff gross weights, empty weights, and fuel weights. 146
Table 5.26 Comparison of the AVDS^{CE} XB-70 and the VCC XB-70 flight manual calculated ranges and fuel weights. 147
Table 5.27 XB-70 weight data for verification part 1, units are lb [140]. 148
Table 5.28 XB-70 weight data for verification part 2, units are lb [140]. 148
Table 5.29 XB-70 weights estimation verification results. 149
Table 5.30 AVDS^{CE} XB-70 inputs and assumptions [14]. 150
Table 5.31 Comparison of the AVDS^{CE} XB-70 sizing results to the (VCC) actual XB-70 data. The results shown are the verification results with a 50,000 lb payload. 152
Table 6.1 Summary of how $I_{str,}$ I_p, and *ICI* behave when decreasing and increasing the level of technical capability required to develop a design. 154
Table 6.2 Range of Structural Indices Encompassed by Investigation [33]. 156
Table 7.1 List of material properties used for I_{str} sensitivity study. 213
Table 7.2 Variables for I_{str} verification study. 215
Table 7.3 Variables for I_{str} sensitivity study 1. 216

Table 7.4 Variables for I_{str} sensitivity study 2. 220
Table 7.5 Variables for I_{str} sensitivity study 3. 224
Table 7.6 Variables for I_{str} sensitivity study 4. 225
Table 7.7 Variables for I_{str} sensitivity study 5. 227
Table A.1 AVDS^{CE} X-51 inputs and assumptions [14]. 250
Table A.2 AVDS^{CE} X-43A inputs and assumptions [14]. 251
Table A.3 AVDS^{CE} XB-70 inputs and assumptions [14]. 252
Table A.4 AVDS^{CE} SR-71 inputs and assumptions [14]. 253
Table F.1 Material properties of saffil [171]. 313
Table F.2 Material properties for saffil cont. [171]. 313
Table F.3 Material properties for q-felt [172]. 314
Table F.4 Material properties for q-felt cont. [172]. 314
Table F.5 Material properties for cerrachrome [173]. 315
Table F.6 Material properties of AETB-8 [174]. 315
Table F.7 Material properties of AFRSI [174]. 316
Table F.8 Material properties of LI-900 [164]. 316
Table F.9 Material properties of aluminum 2024-T4 [175]. 317
Table F.10 Material properties of titanium 6Al-4V [175]. 317
Table F.11 Material properties of aluminum-beryllium alloy AM162 [176]. 318
Table F.12 Material properties of graphite/epoxy [177]. 318

NOMENCLATURE

Abbreviations

AB	All Body
AETB	Alumina Enhanced Thermal Barrier
AFRL	Air Force Research Laboratory
AFRSI	Advanced Reusable Surface Insulation
AI	Artificial Intelligence
AIAA	American Institute of Aeronautics and Astronautics
ARC	Aerospace Research Central
ATSp	Access To Space
AVD	Aerospace Vehicle Design
AVDS	Aerospace Vehicle Design Synthesis
BB	Blended Body
BP	Body Point
CATIA	Computer Aided Three-Dimensional Interactive Application
C/C	Carbon-Carbon Composite
CD	Conceptual Design
CE	Configuration Evaluation
CEA	Chemical Equilibrium Applications
CFD	Computational Fluid Dynamics
c.g.	Center of Gravity
CL	Configuration Layout
CVI	Chemical Vapor Infiltrated
DARPA	Defense Advanced Research Projects Agency
DBS	Data-Base System
DD	Detailed Design
DTIC	Defense Technical information Center
EADS	European Aeronautics Defense and Space Company
EIS	Entry Into Service
EHTV	European Hypersonic Transport Vehicle
ESP	Engineering Sketch Pad
FE	Finite Element
FEM	Finite Element Method
FWC	Flying-Wing Configuration
GHV	Generic Hypersonic Vehicle
GUI	Graphical User Interface
HAP	Hypersonic Air-breathing Propulsion
HASA	Hypersonic Aerospace Sizing Analysis
HOTOL	Horizontal Takeoff and Landing
HST	Hypersonic Transport
HTP	Hypersonic Technology Project
HyFAC	Hypersonic Research Facilities Study
KBS	Knowledge-Based System
KEAS	Knots Equivalent Airspeed

LAPCAT	Long-Term Advanced Propulsion Concepts and Technologies
m.a.c	Mean Aerodynamic Chord
MATLAB	MATrix LABoratory
MCAIR	McDonnell Aircraft Company
MDAO	Multi-Disciplinary Analysis and Optimization
MMC	Metal Matrix Composite
NASA	National Aeronautics and Space Administration
NASP	National Aero-Space Plane
NPSS	Numerical Propulsion System Simulation
NTRS	NASA Technical Report Server
OEW	Operating Empty Weight (empty weight)
OFWC	Oblique-Flying-Wing Configuration
OWC	Oblique-Wing Configurations
OWE	Operating Weight Empty (dry weight)
OWE_w	Operating Weight Empty (weight budget)
OWE_v	Operating Weight Empty (volume budget)
PAX	Passengers
PD	Preliminary Design
PDF	Portable Document Format
PrADO	Preliminary Aircraft Design and Optimization
PS	Parametric Sizing
RCG	Reaction Cured Glass
RSR	Rapid Solidification Rate
SEP	Société Européenne de Propulsion
SFC	Specific Fuel Consumption
SiC	Silicon Carbide
SQLite	Structured Query Language
SSTO	Single Stage to Orbit
TAC	Tail-Aft Configuration
TET	Turbine Entry Temperature
TFC	Tail-First Configuration
TOGW	Takeoff Gross Weight
TPS	Thermal Protection System
TSC	Triple-Surface Configuration
UTA	University of Texas at Arlington
VAB	Vehicle Analysis Branch
VCC	Vehicle Configuration Compendium
VDK	Vandenkerckhove
VSP	Vehicle Sketch Pad
WB	Wing Body
WR	Weight Ratio

Symbols

AR	Aspect ratio
AR_{droop}	New Aspect ratio with wing droop effect
b_{droop}	New wingspan with wing droop effect
b_n	Coefficients of series solution for $\tau > \tau_h$
b_{tip}	Span of portion of wing that droops
b_w	Wingspan
C_D	Coefficient of drag
C_{D_0}	Zero-lift drag coefficient
$C_{D,base}$	Base drag coefficient
c_f	Local skin-friction coefficient
C_H	Heat-transfer coefficient
C_{HT}	Horizontal tail coefficient
C_{in}	Root chord of portion of wing that droops
C_L	Coefficient of lift
C_{L_α}	Lift curve slope
c_m	Coefficients of series solution for $0 < \tau \leq \tau_h$
c_p	Specific heat capacity of the material
C_p	Specific heat coefficient of air for constant pressure
C_{tip}	Tip chord
C_{VT}	Vertical tail coefficient
$\bar{c}_w$	Mean aerodynamic chord of the wing
d	Thickness of the material
f_{ke}	Fraction of the insulator temperature range
f_{thr}	Fraction of the surface temperature range
$Fuel\ Volume_{wing}$	Fuel volume in the wing
g	Gravitational acceleration
H_{cabin}	Cabin height
H_{engine}	Height of the engine
I_p	Propulsion index
I_{perf}	Performance efficiency index
I_{sp}	Specific impulse
I_{str}	Structural index
I_T	Integrated surface temperature rise from the initial temperature
ICI	Industrial Capability Index
K	Scaling coefficient
k	thermal conductivity of the material
K_{str}	Structural parameter
K_v	Scaled propellant volume fraction
K_w	Ratio of wetted surface area to planform area
L/D	Lift to drag ratio
L_{cabin}	Cabin length
l_{HT}	Length from the ¼ m.a.c of the horizontal tail to the ¼ m.a.c of the wing
l_{VT}	Length from the ¼ m.a.c of the vertical tail to the ¼ m.a.c of the wing
$\dot{m}_0$	Mass flow rate of the air

$\dot{m}_f$	Mass flow rate of the fuel
m	Leading-edge flow parameter
M_∞	Freestream mach number
$M_{original}$	Original mach number
n_z	Load factor
P_2	Pressure behind shockwave
P_∞	Freestream pressure
P_{avg}	Average atmospheric pressure
Pr	Prandtl number
$P_{S.L}$	Sea-level pressure
$\dot{q}_{aero}$	Aerodynamic heating heat transfer rate
$\dot{q}_{conv}$	Convective heat transfer rate
$\dot{q}_{rad}$	Radiation heat transfer rate (radiation cooling)
q	Dynamic pressure
R	Gas constant
r	Recovery factor
Re_x^*	Reference reynolds number at x-location along flat plate
S	Characteristic area
S_{HT}	Planform area of the horizontal tail
S_{pln}	Total planform area
$S_{pln,droop}$	New total planform area with wing droop effect
S_{side}	Side area
$S_{side,droop}$	New side area with wing droop effect
S_{tail}	Tail reference area
S_{VT}	Planform area of the vertical tail
S_w	Wing area
S_{wet}	Wetted surface area
$S_{wing,droop}$	New wing area with wing droop effect
$S_{wet_{nacelle}}$	Wetted surface area of the nacelle
$S_{X\text{-}section\ max}$	Max x-section reference area
T	Temperature
t	Time
T^*	Reference temperature
t/c	Thickness to chord ratio
T/W	Thrust to weight ratio
T_0	Total temperature
T_2	Temperature behind shockwave
T_{ab}	Temperature after the afterburner
T_{aw}	Adiabatic wall temperature
T_{ce}	Temperature to use for calculating insulation specific heat capacity
T_{cs}	Temperature to use for calculating structural specific heat capacity
T_h	Applied surface temperature rise of insulator
t_h	Duration of heat pulse
T_i	Initial temperature
T_{ke}	Temperature to use for calculating insulation conductivity
T_m	Maximum structural temperature rise

T_{mx}	Maximum surface temperature for a surface temperature history
T_{thr}	Threshold temperature for truncating insulator temperature rise integral
T_w	Wall temperature
V_2	Velocity behind shockwave
Vol_{cabin}	Cabin volume
V_{tot}	Total vehicle volume
W/S	Wing loading
W_{cabin}	Cabin width
W_{crew}	Crew weight
W_{fuel}	Fuel weight
$W_{payload}$	Payload weight
W_{str}	Structural weight
x	Nondimensionalized spatial variable
x_t	Location along the flat plate

Greek Letters

α	Angle of attack
β	Ratio of insulator conductance/area to insulator heat capacity/area
γ	Ratio of insulator to structural heat capacity/area
δ_{droop}	Angle of wing droop
Δ	Sweep angle
Δt	Time step
Δy	Node length
ε	Surface emissivity
θ	Nondimensionalized temperature
θ_{tip}	Interior angle of the wing, measure from centerline to leading-edge
λ	Eigenvalue
Λ_{new}	New leading-edge sweep
$\Lambda_{original}$	Original leading-edge sweep
μ^*	Reference coefficient of viscosity
ν_{sb}	Stefan-Boltzmann constant
ρ	Aircraft density, density of the material
ρ^*	Reference air density
ρ_{fuel}	Fuel density
ρ_{ppl}	Bulk propellant density
τ	Küchemann parameter, nondimensionalized time
τ_{droop}	New Küchemann parameter with wing droop effect
τ_h	Nondimensionalized duration of heat pulse

CHAPTER 1: INTRODUCTION

1.1 Research Motivation and Objectives

With the first successful powered flight in history by the Wright Brothers at Kitty Hawk, North Carolina in December of 1903, the aeronautical engineering field, and soon after aerospace, has only been around for almost 120 years [1]. In that relatively short period, the aircraft advanced to the point of achieving Mach 10 in-atmosphere with the X-43A, and even taking humans to the moon with the Apollo program. While there have been numerous aerospace vehicles developed during this time, the time it takes from a vehicle to be designed to operational has greatly increased today. According to Ben Rich, vice president of Lockheed and former director of Skunk Works (1975-1991), during his 40-year career, he worked on 27 different airplanes, with the engineers of today being lucky to work on even one [2]. He states that *"...we are entering an era in which there may be twenty- to thirty- year lapse between generations of military aircraft."* Even though he specifically states for a military aircraft, if this becomes the case, in another 120 years only 4-6 military aircraft will have been designed, produced, and operated. This shows the significant increase in time to completely design a vehicle today than it has been in the past, despite the increase in available technology to help the design engineer. From a design point of view, there are two issues of note that contribute to this increase in time: (1) the design space investigated during the conceptual design phase, and (2) the lack of data and knowledge retention between aerospace vehicle contracts.

For the design space investigated during the conceptual design phase, this contributes to the time to design a vehicle through the number of points investigated and the selection of a design point, or a handful of design points, that meet the wanted requirements to move through the design

phases. Out of the three design phases (conceptual, preliminary, and detail), conceptual design contributes the least amount of time to the overall design but has the greatest impact on the design and production. This means that an unviable design selected during the conceptual design phase will cause a large loss in time with trying to move forward with the design and make it viable. An example of this is British Aerospace's SSTO (Single Stage to Orbit) spaceplane design, HOTOL (Horizontal Takeoff and Landing) shown in Fig. 1.1. As observed, the engines, wing, and payload are located at the rear of the vehicle, with the forebody of the vehicle mainly containing liquid hydrogen fuel. This configuration has severe stability issues due to the extreme changes in the center of gravity during ascent. When fully loaded, the stability of the vehicle is manageable, but as the fuel is used during flight, the center of gravity moves to the rear, which destabilizes the vehicle and reduces control power making it both unstable and uncontrollable. To mitigate this issue, many design alterations were considered, but with all of them resulting in a decrease in payload capability, the project was canceled due to the operational disadvantage [3].

From this example, it is noted that this issue of stability should have been identified in the early conceptual design phase before moving forward to the other design phases. This resulted in major time and money loss from a critical design flaw that potentially could have been avoided. This leads back to the design space investigated, if HOTOL was a design point selected within a design space, then either a portion of where HOTOL was located within it was incorrect, or the total design space was incorrect to begin with. To correct this issue, the design space investigated may have had to get larger to allow more possible design points, or new methods and assumptions have to be used to make the design space more accurate to produce viable designs. Both options increase the time it takes to select a design point and move forward, and while this extra time during the conceptual design phase may have saved the project with finding a viable design, this

extra time may have not been possible. With this, an accurate, robust, and relatively fast synthesis system that can also expand the design space in which it produces by allowing conventional and unconventional designs may be required to mitigate this issue.

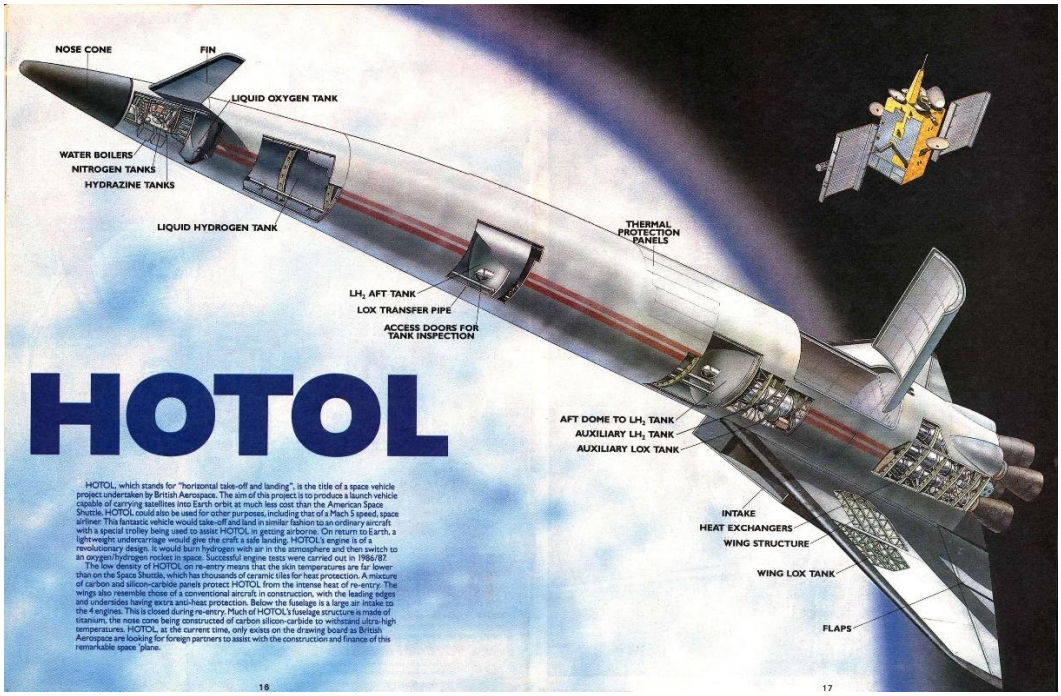

Fig. 1.1 HOTOL schematic [4].

For the lack of aerospace vehicle data and knowledge retention, this contributes to the time to design a vehicle through having to recreate past designs, or relearning past lessons. There are several possible factors that contribute to this issue of not passing on data and knowledge to others, or it being unavailable to the current generation of engineers, with a few of them being: (1) the data/knowledge is not readily available, and requires time and resources to obtain it, (2) it is of a secretive or proprietary nature, (3) a number of past engineers who worked on the aerospace projects are retiring faster than it can be passed on, and (4) the data/knowledge is intentionally destroyed, thereby setting the aerospace industry back that many years they took to obtain it in the first place.

The first three factors presented are the most common, especially in the field of hypersonics, with the fourth being rare, but arguably the most devastating as there is no way to recover the destroyed data and knowledge. For the first lack of retention factor, with the amount of documentation that occurs during a project, if these documents are not stored in an easily accessible location, then when it is needed for another project, time is required to find and then extract the wanted information for the new project. Even if the documents are stored in an easily accessible location, time would still be required to sort through the documents to find the wanted information, but not as long as trying to find it first. This factor is heightened for hypersonic projects as it continually goes through a cyclic cycle where interest rises, then almost instantly falls off with possible decades before the next rise as shown in Fig. 1.2. This allows documents to sit for decades, unused, with the fear of eventually being lost and forgotten.

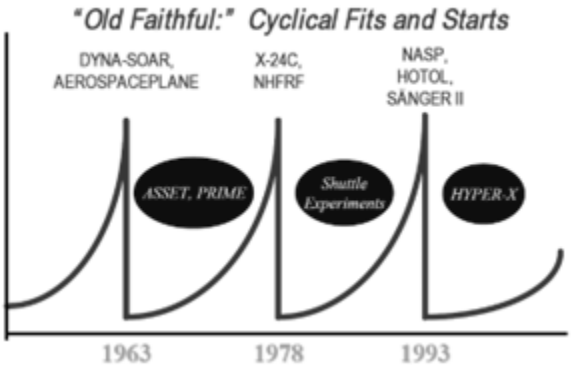

Fig. 1.2 Hypersonic investment over time [5].

For the second factor, while hypersonic projects are often of a secretive or proprietary nature, therefore publishing very little publicly, the hope is that at least internally, the information of these projects are kept alive with each generation of engineers with that company learning from them. The issue with this though, is that each company must conduct its own study of the same configuration, making multiple redundant studies while possibly obtaining the same conclusions.

In terms of data and knowledge retention, it is highly inefficient, but in terms of national security, it may be a necessary 'evil'. For the third factor, Fig. 1.3 below aptly portrays this issue. As shown, the number of personnel in hypersonics has continually decreased throughout the years, and the age of the remaining personnel is primarily around the retirement age. This causes an imminent problem where large amounts of personnel will retire and the knowledge that they have accumulated through the years and from the number of hypersonic projects they worked on, will retire with them, leaving the younger generation to relearn what has already been learned. Assuming that the age of retirement is around 65 years old from Fig. 1.3, this means that the majority of the personnel in hypersonics currently, have been alive for over half as long as the aeronautical engineering discipline has been around, and even more so for aerospace. If nothing is done to obtain as much knowledge from them as possible before they leave, then the loss will be as devastating as the fourth provided factor, the intentional destruction of this knowledge.

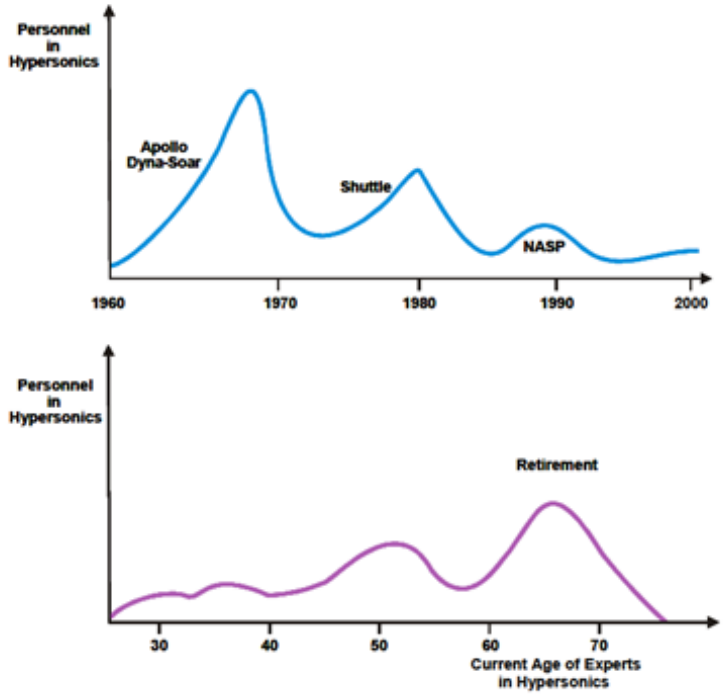

Fig. 1.3 Personnel in hypersonics [6].

For the extreme case of the lack of data and knowledge retention, an example that portrays the effects of destroying data and knowledge is the relationship between the YB-49 and the B-2 stealth bomber. The YB-49 is a flying wing that was developed by Northrop who, after the cancellation of the program, deliberately destroyed the hardware and design documentation of this vehicle [7]. The problem of this destruction did not occur until 35 years later during the conceptual design of the B-2. For the design of the B-2, no one on the team had any knowledge from the YB-49, with Northrop having a hard time finding any company employee who had experience with the previous flying wings. Besides the issue of employees, they could not even find any data or basic flying wing information through the company archives [8]. This greatly set back the design of the B-2 with the Northrop team having to recreate and relearn what the previous generation of Northrop engineers destroyed.

All these examples of issues that contribute, or have contributed, to the lack of data and knowledge retention within the aerospace industry, is perfectly summed up by Santayana, "*Progress, far from consisting in change, depends on retentiveness … Those who cannot remember the past are condemned to fulfil it* [9]." With this, a central system that contains past-to-present data, information, and knowledge of hypersonic vehicles, allowing it to be available to the design engineer 'at the fingertips', without the need for each engineer to extensively investigate the wanted vehicle themselves from past documentation, may be required to mitigate these issues.

With the two issues discussed and how each effects the time it takes to design a vehicle, solutions have been conceived to attempt to solve these issues. For the first issue of the creation of the design space and the importance of making it as reliable as possible, the Aerospace Vehicle Design (AVD) Laboratory has been tackling this issue through the creation of an inhouse synthesis system called AVDS (Aerospace Vehicle design Synthesis). This system aims to create more

accurate solutions spaces and to investigate both conventional and unconventional designs to open the solution space further to observe as many potential design points as possible. Since its creation, this system has been continually developed through each generation of AVD researchers. Part of the study that will be presented here is the author's contributions to this system through the improvement of the geometry and aerothermodynamics methods used within it.

For the second issue of a lack of data and knowledge retention within the aerospace industry, an idea for a compendium that will assist future engineers with storing, maintaining, and passing on accumulated aerospace vehicle data and knowledge, will be introduced. This compendium, called the Vehicle Configuration Compendium (VCC), will not only assist future design engineers, but will also improve AVDS by allowing it to draw the data, information, and knowledge, stored within to use within the synthesis process, thus potentially making a new version of AVDS that uses a functioning AI design approach. Part of the study that will be presented here is the author's contributions to the development of this system, and its use with AVDS.

1.1.1 Research Objectives

The objectives in which the research conducted here wishes to accomplish are:

1. Develop the foundation of a standalone system with a database and knowledgebase to assist the design engineer.
2. Incorporate a few prime hypersonic vehicles into this system to showcase its usefulness in synthesis verification and disciplinary method development.
3. Improve the geometric function of AVDS and the VCC using the 3D modeling software *OpenVSP*.

4. Improve the aerothermodynamics discipline within AVDS by updating the maps and calculation of the Structural Index (I_{str}) parameter.

Through the accomplishments of these objectives, the author hopes to provide some advancement to the aerospace vehicle design field through the improvement of an already accomplished synthesis system, and through the development of a design tool consisting of a database and knowledgebase that can assist the design engineer by providing and using past-to-present aerospace vehicle design information.

1.2 Aerospace Vehicle Design Phases

Before moving forward, an overview of the aerospace vehicle design phases is presented as AVDS and the VCC act within a specific design phase, the conceptual design (CD) phase. The phases of aerospace vehicle design are classically separated into (1) conceptual design (CD), (2) preliminary design (PD), and (3) detail design (DD), which occurs sequentially as provided (CD, PD, then DD). This process through the design phases is provided visually in Fig, 1.4. Beginning with the provided mission in which the vehicle must be designed for, the conceptual design phase (CD) identifies and evaluates sets of possible concepts and configurations that satisfy the mission requirements. This phase has the highest level of design freedom, allowing drastic changes between considered configurations. A problem with this level of design freedom though, is that unlimited possibilities can be explored, but the time constraints during this phase usually allow only a limited range of configurations and concepts. The time constraints can also contribute to the stagnation of vehicle design, as legacy and conventional vehicle configurations allow quicker turnaround time, leaving the possible design space vastly unexplored. Once the selected sets of concepts and configurations are evaluated, the configuration that is deemed to fit the mission

requirements the most, or have the best performance from this initial analysis, is then moved on to the preliminary design (PD) phase.

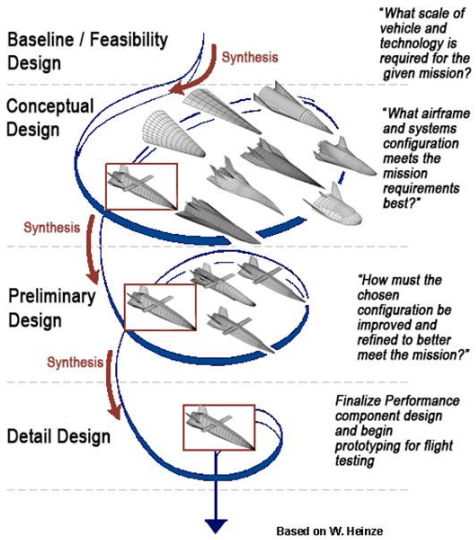

Fig, 1.4 Generic aerospace vehicle design phases, modified from [10].

With the selected configuration from CD, the PD phase then refines this configuration by making small changes to improve the design further. This means that the overall configuration remains the same (cross-sectional shape, tail configuration, etc.), while small changes (nose shape, spatula, etc.) are made where necessary. These refinements can be accomplished with increased fidelity level tools compared to the ones used for CD, optimization, and wind tunnel testing. Once the changes are investigated to obtain the best design possible that meets the mission requirements, this refined vehicle design is then moved on to the final phase of aerospace vehicle design, the detail design (DD) phase.

With the refined vehicle design from PD, the DD phase then locks this design in place and the manufacturing process is begun. This is where detailed part schematics are generated, parts are

manufactured, and the vehicle is being geared towards flight-testing. Again, each of these phases can be visualized within Fig, 1.4.

From the above discussion, it is noted that as the vehicle design moves through each phase, the freedom of design decreases as the knowledge about the vehicle increases. With each phase, the configuration is further fixed, and with the addition of increased fidelity level tools, more knowledge about the design is obtained. This relationship is shown within Fig. 1.5. The relationship of the discipline integration level throughout each phase is also shown. Using the conceptual design (CD) phase as an example, the integration of each discipline should be the same, or contribute the same amount, to the design of the vehicle. This figure shows though that aerodynamics is usually favored, followed closely by propulsion, but the other disciplines such as structures and stability & control are greatly lacking during the initial phase of design. This may explain why the stability issue of HOTOL was missed until later in the design process.

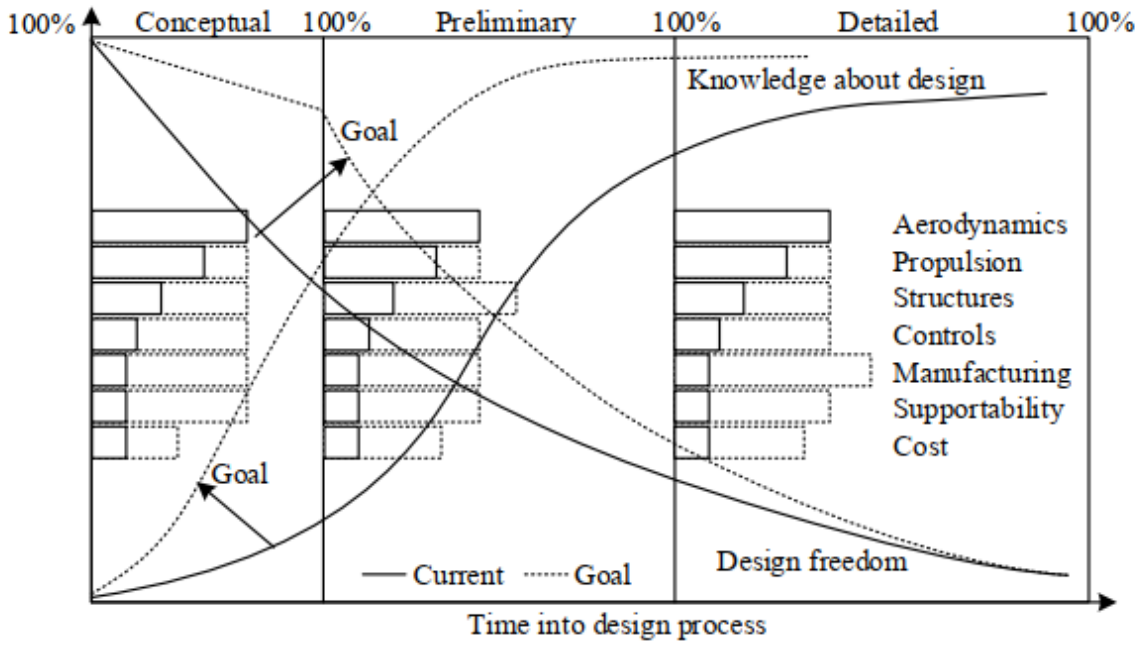

Fig. 1.5 Design cycle design knowledge, design freedom, and discipline integration [11].

1.2.1 Significance and Breakdown of Conceptual Design

Out of the three design phases, the conceptual design (CD) phase is considered the most crucial due to any decisions here affecting the whole design from beginning to end. Also, if designs are not carefully evaluated and selected during this phase, it can lead to major losses in time and money with the design being a 'dead horse', or unviable design. At the end of the CD phase, it can be assumed that approximately 80% of the vehicle configuration is determined [12]. With the CD phase being where knowledge about the design is the least (refer to Fig. 1.5), the ability to accurately investigate and select a design that meets the mission requirements, and that stays viable through the rest of the design phases is key for a design engineer. For the CD phase, while every aerospace company has their own method of completing this phase, which is typically proprietary, a review of publicly available 'by-hand' methods (e.g., design texts, course materials) and 'computer-integrated' methods (e.g. synthesis systems) has been previously completed (refer to [13]) and was determined that CD may be broken down into three distinct subphases: (1) Parametric Sizing (PS), (2) Configuration Layout (CL), and (3) Configuration Evaluation (CE). These subphases are visualized in Fig. 1.6.

The first step of the conceptual design (CD) phase, the parametric sizing (PS) subphase, as explained by Gary Coleman, a former AVD researcher, "*... serves to establish the 1st order solution space for the mission and gives the designer an idea related to the gross geometry, weight, and cost of performing the mission* [13]." As per Fig. 1.6, this subphase takes the mission specifications that are provided, the technology level (whether current or expected future capability), and the combination of vehicle concepts and configurations, to generate a solution space topography. This is where both conventional and unconventional vehicle configurations should be explored to create as large a solution space as possible, so that a greater variety of

vehicles are considered for the mission. While time constraints and synthesis system capabilities may limit the number of configurations that can be explored, this issue can be resolved as written by Gary Coleman, "*with a well calibrated and flexible parametric sizing tool-box, designers can quickly screen configurations and technologies which warrant further conceptual design work* [13]."

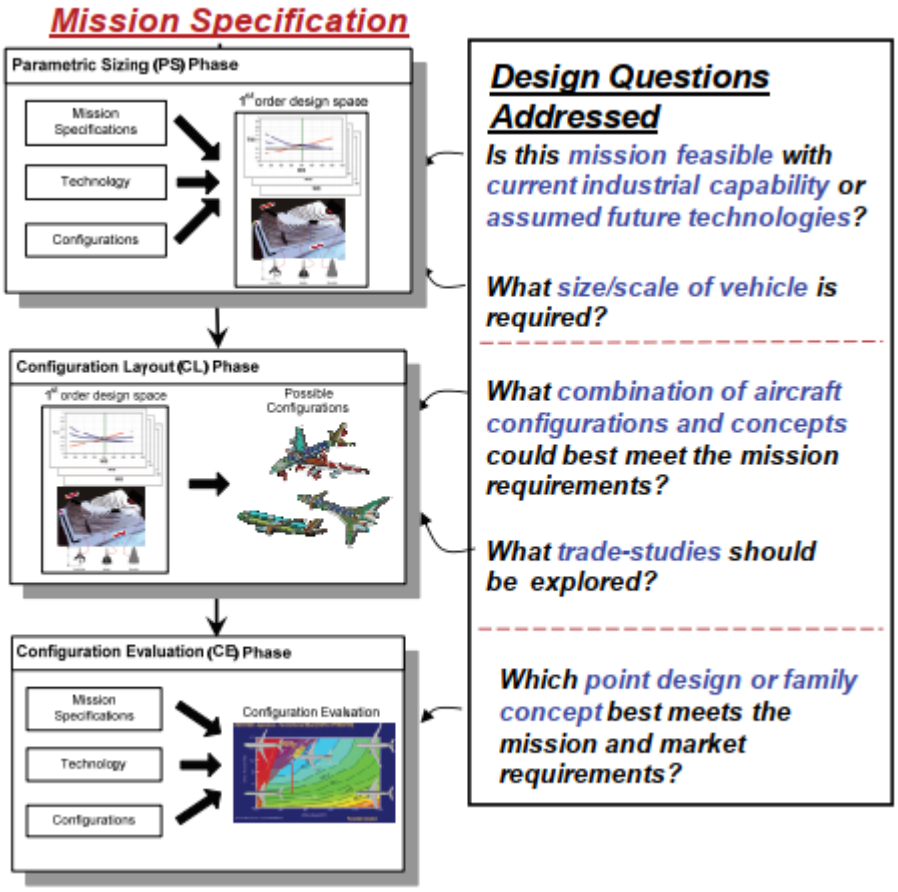

Fig. 1.6 Fundamental steps to aerospace vehicle conceptual design [13].

Once the design space is generated, the baseline vehicles that meet the mission requirements are then identified, which allows the parametric sizing (PS) subphase to move to the configuration layout (CL) subphase. During the CL subphase, this is where the sized values from PS are used to map out locations of the internal features (e.g., landing gear, fuel, payload, etc.) and

to further define the external features, such as in the case for a wing, while the wing area is known, the wing sweep, taper ratio, etc. are not yet known. Also, during this phase, some of the assumptions used during PS may be determined to not be valid, such as assumed volumes, which would then require the return to the PS subphase to correct them. Once the layout of each configuration considered within CL has been established, then they are moved to the configuration evaluation (CE) subphase where the proposed vehicles are thoroughly evaluated.

The configuration evaluation (CE) subphase is where the proposed vehicle configurations from CL are subjected to a more detailed analysis and a series of disciplinary checks to determine whether the vehicles satisfy the mission requirements. This subphase is similar to PS with containing weight estimation, trajectory analysis, constraint analysis, and convergence, but is operated at a higher fidelity level. This higher fidelity level, which can include CFD and FEM, is to thoroughly check each configuration through each discipline, and to check critical assumptions that were used during PS. It also checks and refines the design decisions made during CL, where even if they appear to work within CL, once the design goes through the multidisciplinary analysis of CE, the weight and balance may be off, the aerodynamics may be inadequate, etc. which would need to be corrected. During CE, sensitivity and technological trade studies are conducted around the selected baseline to further refine the design, but the design spaces generated are not as large as PS, as the trades are on a smaller scale. As an example, the Mach number could be traded for PS which would greatly change the design and shape of each configuration, but for CE the trades are more focused, such as trading nose width or wing thickness, which refines the selected area of the solution space topography. These still provide perturbations, but only change the design slightly. Once CE is completed for each configuration, the design spaces are compared and the design point that best matches the mission requirements is selected. It is possible that none of the

points meet the mission requirements or disciplinary checks, and if this occurs, then the designer must return to PS and modify the inputs and assumptions.

With the subphases of conceptual design (CD) as described, both AVDS and the VCC are developed to assist the design engineers during this phase to increase the accuracy in which design spaces are generated and explored, and in which design points are selected and evaluated.

1.3 Aerospace Vehicle Design Synthesis (AVDS)

The Aerospace Vehicle Design Synthesis (AVDS) system is a next-generation generic synthesis methodology and software developed by the AVD Laboratory to function in three primary modes: (1) aerospace vehicle design, (2) technology forecasting, and (3) strategic decision-maker support. The concept of this system was initiated in 1992 during the author's supervisor's (Dr. Chudoba's) involvement with the future project departments of EADS Airbus GmbH, Airbus UK (British Aerospace), Airbus France (Aérospatiale Aéronautique), Airbus Industrie, and Fairchild Dornier, where he was responsible for conceptual design process development and application addressing conventional and unconventional flight vehicles [14]. From this initiation, inspiration was found from *AeroMach*, *PrADO*, Paul Czysz's Hypersonic Convergence, and Küchemann's Breguet Range, that eventually led to the creation of AVDS, which is continually developed today. A timeline of this involvement is showcased in Fig. 1.7.

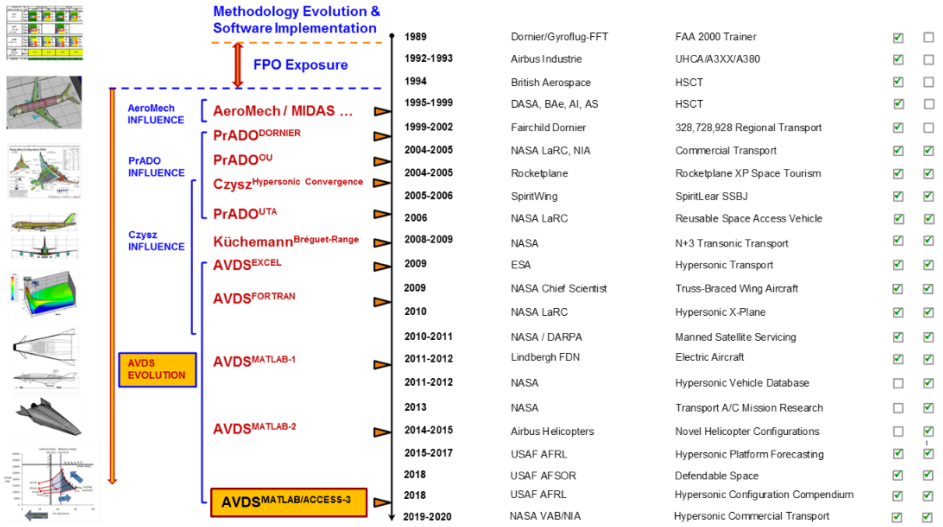

Fig. 1.7 Master timeline summarizing the professional engagement at (a) conceptual design (CD) level and (b) strategic decision-maker (CxO) support level. Industry exposure from 1989-2002, academic research exposure from 2002-today [14].

During this time, synthesis approaches were gathered and categorized from Class I to Class IV by their 'modeling complexity' (e.g., empirical, analytical, numeric, parametric, etc.) and categorized from Class I to Class IV [15]. Class IV synthesis systems are the ones used currently by industry that typically focus on singular configurations and concepts, or for a 'classical'/conventional flight vehicle and system. This synthesis system class "*...operate[s] by sizing the main components independently, and 'assembling' them into very simple geometric relationships* [16]", meaning that the vehicles designed are typically non-integrated, or have a low level of integration, allowing the wing, fuselage, engines, etc., to be sized separately. Table 1.1 shows an overview of the gathered Class IV synthesis systems with their acronyms and originator. While this limitation has become the norm due to the difficulty in synthesizing the range of individual design-disciplines for both conventional and unconventional vehicle designs [14], AVDS was developed to overcome this limitation, and thereby becoming one of the few, if not only, next-generation Class V synthesis systems. Class V synthesis systems are categorized to be configuration-independent (generic) with more rigorous disciplinary engineering analysis methods

and are linked to a sophisticated design synthesis framework to allow a wider range of design alternatives to be considered [15]. While it is unknown whether there are other specific Class V synthesis systems being developed, there are Class IV systems, a very small number at least, that are considered state-of-the-art in their design environment and have the potential to become Class V. Two examples are *SENSxx* [17] and *PrADO* [10].

Table 1.1 Aircraft and aerospace vehicle class IV synthesis systems [15].

AAA	Advanced Airplane Analysis	DARcorporation
ACDC	Aircraft Configuration Design Code	Boeing Defense and Space Group
ACDS	Parametric Preliminary Design System for Aircraft and Spacecraft Configuration	Northwestern Polytechnical University
ACES	Aircraft Configuration Expert System	Aeritalia
ACSYNT	AirCraft SYNThesis	NASA
ADAM	-	McDonnell Douglas
ADAS	Aircraft Design and Analysis System	Delft University of Technology
ADROIT	Aircraft Design by Regulation Of Independent Tasks	Cranfield University
ADST	Adaptable Design Synthesis Tool	General Dynamics/Fort Worth Division
AIDA	Artificial Intelligence Supported Design of Aircraft	Delft University of Technology
AircraftDesign	-	University of Osaka Prefecture
APFEL	-	IABG
AProg	Auslegungs Programm	Dornier Luftfahrt
ASAP	Aircraft Synthesis and Analysis Program	Vought Aeronautics Company
ASCENT	-	Lockheed Martin Skunk Works
ASSET	Advanced Systems Synthesis and Evaluation Technique	Lockheed California Company
AVID	Aerospace Vehicle Interactive Design	N.C. State University, NASA LaRC
AVSYN	-	Ryan Teledyne
BEAM	-	Boeing
CAAD	Computer-Aided Aircraft Design	SkyTech
CAAD	Computer-Aided Aircraft Design	Lockheed-Georgia Company
CACTUS	-	Israel Aircraft Industries
CADE	Computer Aided Design and Evaluation	McDonnell Douglas Corporation
CAP	Configuration Analysis Program	North American Rockwell (B-1 Division)
CAPDA	Computer Aided Preliminary Design of Aircraft	Technical University Berlin
CAPS	Computer Aided Project Studies	BAC Military Aircraft Devision
CASP	Combat Aircraft Synthesis Program	Northrop Corporation
CASTOR	Computer Aircraft Synthesis and Trajectory Optimization Routine	Loughborough University
CDS	Configuration Development System	Rockwell International
CISE	-	Grumman Aerospace Corporation
COMBAT	-	Cranfield University
CONSIZ	CONfiguration SIZing	NASA Langley Research Center
CPDS	Computerized Preliminary Design System	The Boeing Company
DesignSheet	-	Rockwell International
DRAPO	Definition et Realisation d' Avions Par Ordinateur	Avions Marcel Dassault/Breguet Aviation
DSP	Decision Support Problem	University of Houston
EASIE	Environment for Application Software Integration and Execution	NASA Langley Research Center
ESCAPE	-	BAC (Commercial Aircraft Devision)
ESP	Engineer's Scratch Pad	Lockheed Advanced Development Co.
FASTPASS	Flexibly Analysis for Synthesis, Trajectory, and Performance for Advanced Space Systems	Lockheed Martin Astronautics
FLOPS	FLight OPtimization System	NASA Langley Research Center
FPDB & AS	Future Projects Data Banks & Application Systems	Airbus Industrie
FPDS	Future Projects Design System	Hawker Siddeley Aviation Ltd
FVE	Flugzeug VorEntwurf	Stemme GmbH & Co. KG
GASP	General Aviation Synthesis Program	NASA Ames Research Center
GPAD	Graphics Program for Aircraft Design	Lockheed-Georgia Company
HASA	Hypersonic Aerospace Sizing Analysis	NASA Lewis Research Center
HESCOMP	HElicopter Sizing and Performance COMputer Program	Boeing Vertol Company
HiSAIR/Pathfinder	High Speed Airframe Integration Research	Lockheed Engineering and Sciences Co.
Holist	-	-
ICAD	Interactive Computerized Aircraft Design	USAF-ASD
ICADS	Interactive Computerized Aircraft Design System	Delft University of Technology
IDAS	Integrated Design and Analysis System	Rockwell International Corporation
IDEAS	Integrated DEsign Analysis System	Grumman Aerospace Corporation
IKADE	Intelligent Knowledge Assisted Design Environment	Cranfield University
IMAGE	Intelligent Multi-Disciplinary Aircraft Generation Environment	Georgia Tech
IPAD	Integrated Programs for Aerospace-Vehicle Design	NASA Langley Research Center
MacAirplane	-	Notre Dame University
MIDAS	Multi-Disciplinary Integrated Design Analysis & Sizing	DaimlerChrysler Military
MIDAS	Multi-Disciplinary Integration of Deutsche Airbus Specialists	DaimlerChrysler Aerospace Airbus
MVA	Multi-Variate Analysis	RAE (BAC)
MVO	MultiVariate Optimisation	RAE Farnborough

ODIN	Optimal Design INtegration System	NASA Langley Research Center
OPDOT	Optimal Preliminary Design of Transports	NASA Langley Research Center
Paper Airplane	-	MIT
PASS	Program for Aircraft Synthesis Studies	Stanford University
PIANO	Project Interactive ANalysis and Optimisation	Lissys Limited
POP	Parametrisches Optimierungs-Programm	Daimler-Benz Aerospace Airbus
PrADO	Preliminary Aircraft Design and Optimisation	Technical University Braunschweig
PreSST	Preliminary SuperSonic Transport Synthesis and Optimisation	DRA UK
PROFET	-	IABG
RCD	Rapid Conceptual Design	Lockheed Martin Skunk Works
RDS	-	Conceptual Research Corporation
Rubber Airplane	-	MIT
SENSxx	-	DaimlerChrysler Aerospace Airbus
SSP1	System Synthesis Program	University of Maryland
SSSP	Space Shuttle Synthesis Program	General Dynamics Corporation
SYNAC	SYNthesis of AirCraft	General Dynamics
TASOP	Transport Aircraft Synthesis and Optimisation Program	BAe (Commercial Aircraft) LTD
TRANSYN	TRANsport SYNthesis	NASA Ames Research Center
TRANSYS	TRANsportation SYStem	DLR (Aerospace Research)
VDEP	Vehicle Design Evaluation Program	NASA Langley Research Center
Vehicles	-	Aerospace Corporation
VizCraft	-	Virginia Tech
WIPAR	Waverider Interactive Parameter Adjustment Routine	DLR Braunschweig
X-Pert	-	Delft University of Technology
-	Dialog System for Preliminary Design	TsAGI
-	Hypersonic Aircraft Conceptual Design Methodology	Turin Polytechnic
-	Design Methodology for Low-Speed High Altitude UAV's	Cranfield University (Altman)
-	Preliminary Design of Civil Transport Aircraft	ONERA
-	Numerical Synthesis Methodology for Combat Aircraft	Cranfield University (Siegers)
-	Synthesis Model for Supersonic Aircraft	Stanford University (Van der Velden)
-	Spreadsheet Analysis Program	Loughborough University

With the previous discussion, the uniqueness of AVDS and its capabilities have been introduced. Since its initial development and with the collaboration with NASA and AFRL, AVDS has been verified as a best-practice design-to-mission vehicle synthesis framework that is able to address conventional and especially unconventional vehicle designs, including hypersonic vehicles [14]. A list of the major studies that AVDS has contributed to is provided in Table 1.2. Due to its uniqueness and its niche in the aerospace vehicle design environment, it is important to continually update and develop this system to keep it at the forefront of vehicle design.

Table 1.2 List of important AVDS studies.

Date	Contractor	Study	Reference
June 2010	NASA	VAB Hypersonic Endurance Demonstrator Contract	[18]
January 2011	NASA/DARPA	Manned Geostationary Satellite Servicing Contract	[19]
June 2015	AFRL	AFRL Hypersonic Demonstrator Contract 1	[20]
March 2016	AFRL	AFRL Hypersonic Demonstrator Contract 2	[21]
September 2018	-	Generic Hypersonic Vehicle Design Configuration Verification	[22]
September 2018	-	A Paradigm-Shift in Aerospace Vehicle Design Synthesis and Technology Forecasting	[23]
June 2019	-	A Sizing-Based Approach to Evaluate Near Term Hypersonic Demonstrators: Demonstrator-Carrier Constraints and Sensitivities	[24]
March 2020	-	A Sizing Study Comparison of Hypersonic Demonstrator Vehicles with a Pre-Cooled Turbojet Cycle	[25]
April 2021	NASA	NASA Hypersonic Commercial Study	[14]

1.4 The Vehicle Configuration Compendium (VCC)

The Vehicle Configuration Compendium (VCC) is a system that is being built to assist design engineers in a multitude of roles throughout the conceptual design phase. It assists by providing a central location of past-to-present aerospace vehicle data, information, and knowledge that is easily accessible by the design engineer, and can be used to: (1) create statistics and disciplinary trends, (2) verify multi-fidelity methods (from analytical to CFD), (3) provide a 'snapshot' of important vehicle characteristics and design data to allow design engineers to familiarize themselves with the stored vehicles, and (4) enable designers to develop new understanding through the creation and comparison of aerospace vehicle data trends.

With this functionality, the hope of the VCC is not only to assist through the conceptual design phase, but also to mitigate the knowledge retention issue as previously discussed. Fig. 1.8 perfectly showcases the current situation within the aerospace field with the 'non-ideal situation' of knowledge retention, and the 'ideal situation' being where the VCC hopes to bring it to. While 100% knowledge retention may not be possible due to the nature of secret and sensitive projects, as close to 100% as possible can be achieved through the projects that are publicly available. This would increase progress and innovation, as it would reduce the amount of time that the next generation of engineers must spend relearning the same information and coming to, hopefully, the same conclusions as from legacy projects.

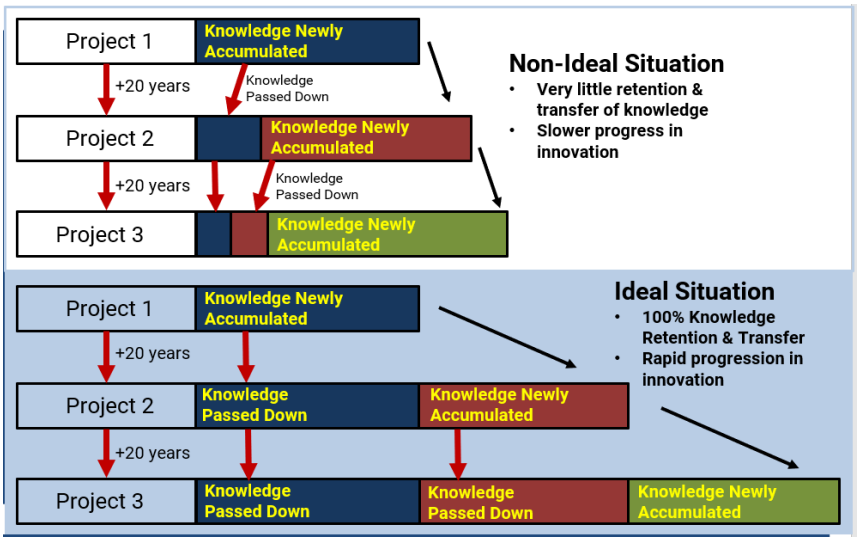

Fig. 1.8 Knowledge retention issue demonstrated [26].

To provide a clear understanding of what is meant by data, information, and knowledge that is stored within the VCC, the following definitions are adopted from Dr. Bernd Chudoba [15].

- Data is characterized by being a set of discrete, objective facts about events. It has little relevance or purpose when considered by itself but is important for the creation of information. When gathering data for the VCC, this would consist of tabulated values for the vehicle such as weight and length but would also include plots such as for aerodynamic characteristics of the vehicle.
- Information is simply data when meaning and value is added to it. "*Information must inform, thus it has a meaning and it is organized to some purpose*." When gathering information for the VCC, this would consist of contextual information about the data that is collected to allow a better understanding of the vehicle.
- Knowledge "… *represents a mixture of experience, values, contextual information, and expert insight that provides a setting for evaluating and incorporating new experiences and information.*" When gathering knowledge for the VCC, this would consist of plots or

figures that contain continuum guidelines with multiple configurations of vehicles presented. It would also consist of design experiences and insights for a specific vehicle and/or configuration.

From these definitions, it is clear that the terms, data, information, and knowledge are not interchangeable, and that they are related to each other. Davenport and Prusak sum up this relationship as "*Knowledge derives from information as information derives from data* [27]." A visual of this relationship between data, information, and knowledge, is provided in Fig. 1.9.

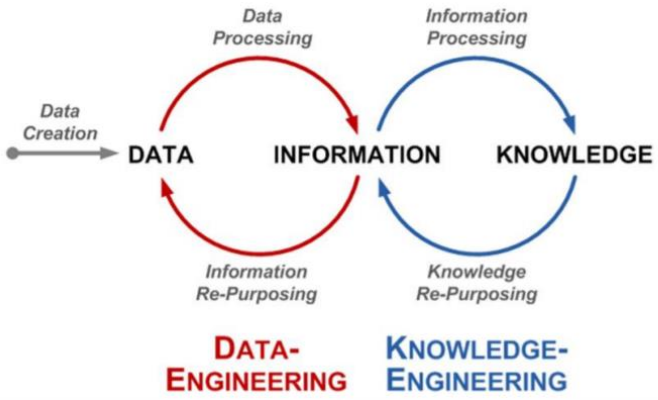

Fig. 1.9 Data-Information-Knowledge cycle [28].

1.4.1 Survey of Current Aerospace Databases

Before developing the VCC though, an investigation into the options that are currently available must be conducted to avoid redundancy in systems, and to determine the differences between these options and the VCC, if any. Table 1.3 presents a total of 47 aerospace specific databases that have been surveyed to provide a reference of aerospace related database concepts. As the VCC is specifically for aerospace vehicles, with the current effort being in high-speed vehicles, other generalized engineering databases were excluded as they would not provide an accurate representation of what is available for the aerospace field. Table 1.3 also provides a breakdown of the types of data available within each database.

From this survey, it was determined that none of the aerospace databases considered accumulates parametric information pertaining to high-speed vehicle design, in which is envisioned for the VCC. It was discovered that most of these databases simply compile publications and journals. While these publication databases do contribute to the retention of knowledge and can assist design engineers by containing the information they may seek, the brunt of the work is put on the designers to search for and extract the needed data, which can also be incredibly time-consuming. This process can contribute partially to the lack of knowledge retention, not due to the data not being there, but due to the time sink involved of sorting through the material. This time sink would either not allow enough time for all the available information to be found, or extremely limit the number of vehicles that can be investigated. This issue is aptly stated by previous AVD researcher Eric Haney in his dissertation, "…*Though practicing engineers spend the majority of their time identifying, organizing, and transforming data* [29], *there remains an opportunity to advance research into systematically developing, utilizing and thus formalizing the data & knowledge domains…*" [28]. This development that Haney mentions for the data & knowledge domains is exactly what the VCC advances by becoming a parametric compendium that stores, displays, and allows the manipulation of, the gathered data, information, and knowledge of high-speed vehicles, and provides them to the design engineers to significantly reduce this time sink.

Table 1.3 Aerospace database survey [30].

Name	**Data Formats Available**						
	Journals	Abstracts	Text books	Technical Reports	Graphs	Interactive Tools	Spreadsheets
Advanced Technologies & Aerospace Collection	X	X	X	X	-	-	-
AERADE Reports Archive	-	-	-	X	-	-	-
Aerodesign.de	-	-	-	-	X	-	X
Aerospace and High Performance Alloys Database	-	-	-	-	X	-	X
Aerospace Structural Metals Database	-	-	-	-	X	-	X
AeroWeb Database System	-	-	-	-	-	-	X
AIAA ARC	X	X	X	X	-	-	-
Airfleets	-	-	-	-	-	-	X
Agile Novel Overall Aircraft Design Database	-	-	-	-	-	X	-
AHS International – The Vertical Flight Society Publications	X	-	-	X	-	-	-

Aircraft Bluebook	-	-	-	-	-	X	-
Airfoiltools.com	-	-	-	-	-	X	X
Airframes.org	-	-	-	-	-	-	X
Airline Monitor	-	-	-	-	-	-	X
Air University Library Index to Military Periodicals	-	X	X	-	-	-	-
Airliners.net	-	-	-	-	-	-	X
AUVSI Unmanned Systems and Robotics Database	-	-	-	-	-	X	X
AviationDB	-	-	-	-	-	X	-
Aviation Safety Network	-	-	-	-	-	-	X
Aviation Week Intelligence Network	-	-	-	X	-	-	X
Aviatorsdatabase.com							
CAPA Centre for Aviation	-	-	-	X	X	X	X
Cirium	-	-	-	-	X	-	X
Civil Aerospace Medical Institute Publications	-	X	-	X	-	-	-
DTIC Online	-	-	-	X	-	-	-
Encyclopedia of Aerospace Engineering	-	-	-	-	X	-	X
Eurocontrol Aircraft Performance Database	-	-	-	-	X	-	X
Evolution of Flight, 1784-1991	X	X	X	X	-	-	-
FAA	-	-	-	-	-	X	-
ForeFlight	-	-	-	-	-	-	X
ICAO Data+	-	-	-	-	X	X	X
IOP Electronic Journals	X	-	-	-	-	-	-
Jane's All the World's Aircraft	-	-	-	-	X	-	X
Janes.com	-	-	-	-	X	X	X
NASA Technical Reports Server	X	X	-	X	-	-	-
National Technical Reports Library [48]	-	-	-	X	-	-	-
NewSpace Global	-	-	-	X	-	-	X
NTSB Aviation Accident Database & Synposes	-	-	-	X	-	-	X
Opensky	-	-	-	-	-	X	-
Princeton University Aerospace Database	X	X	X	X	-	-	-
RisingUp Aviation	-	-	-	-	-	-	X
Scramble Military Database	-	-	-	-	-	-	X
SKYbrary	-	-	-	-	-	-	X
Space Report Online	-	-	-	X	X	X	X
Stargazer	-	-	-	-	-	-	X
TischLibrary – Aerospace database	X	X	X	X	-	-	-
U.S. Military Aircraft Database	-	-	-	-	-	-	X

With the stored data, information, and knowledge within the VCC, it can improve synthesis systems through the verification of the used disciplinary and synthesis methods, along with improving the inputs and assumptions used within it. While this is true for any synthesis system, for this study, the VCC was used to improve AVDS along these lines. The VCC is currently being developed as a standalone system, so any use of the data or disciplinary trends used within AVDS is a manual process of entering it from the VCC. In the future, it is planned that the VCC will be integrated with AVDS to automate this process, and to fully create a conceptual design tool suite. This suite is portrayed within Fig. 1.10, which visualizes a future aerospace conceptual designer's workstation consisting of three screens with each one having a purpose. The VCC would occupy two of them, where the database and knowledgebase functions can be used in tandem, along with the third screen being occupied by AVDS where the synthesis process is completed. This 'Cockpit' Design System would ideally provide everything that a design engineer would need 'at the fingertips'.

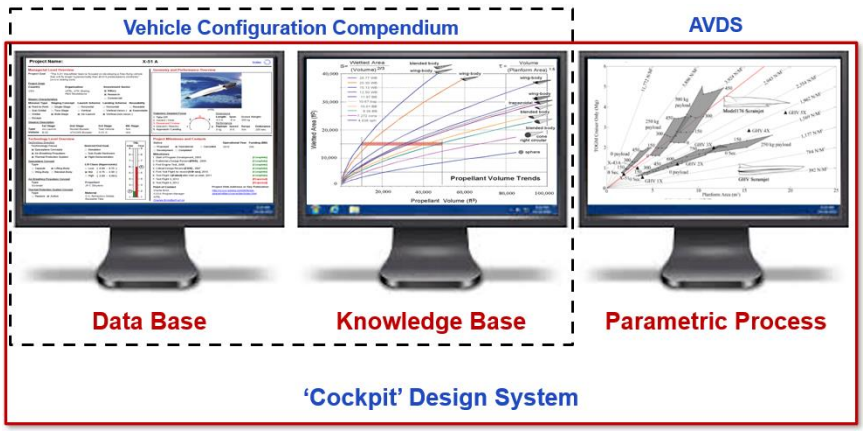

Fig. 1.10 Example of future workstation for aerospace conceptual design [31].

1.4.2 Historic Progression of the VCC

This notion of a combined database and knowledgebase system which grew into the VCC began during the doctoral research of Dr. Bernd Chudoba [15]. In his dissertation, as he discusses about the lack of computer systems used within the conceptual design level of aerospace vehicle design when compared to the preliminary and detailed design levels, he mentions that "…*a combination of a Data-Base System (DBS) containing information on existing designs, and a Knowledge-Based System (KBS) with knowledge about the design process, coupled to analysis packages organized in a multidisciplinary synthesis system, should provide the designer with a great deal of assistance in all stages…* [15]." Dr. Chudoba goes on further to state that what are commonly missing from conceptual design methodologies though are "*…an up-to-date DBS and KBS for making data, information, and knowledge readily available for design-decision making…* [15]." With these observations, along with a report called "Stability and Control Characteristics of Subsonic, Supersonic, and Hypersonic Aircraft Configurations" which is a vast collection of stability and control derivatives and parameters for a variety of aircraft configurations and flight scenarios that was developed alongside Dr. Chudoba's dissertation, the foundation for the VCC was created.

Once the Aerospace Vehicle Design (AVD) laboratory was founded in 2002, this database-knowledgebase concept has been steadily worked towards through the intentional collecting and archiving of conceptual design data, information, and knowledge through every research activity that the AVD Laboratory has participated in. The idea of this concept has also steadily improved through research and publications conducted on this topic by AVD researchers, with two notable Ph.D. dissertations with 1) by Eric Haney being on data engineering for aerospace forecasting [28], and 2) by Xiao Peng being on the formalization of Knowledge Engineering as an engineering science discipline [32].

Research on the VCC officially began at the end of 2018 with the author of this work and another researcher, Ramlingham Pillai. They were joined the following year by Stenila Simon. With the initiation of the NASA-funded study on the feasibility of hypersonic commercial transportation, this research effort was fast tracked to be able to provide digitized verification data for 7 high-speed vehicles, namely the X-51, X-43A, XB-70, SR-71, Concorde, Sänger-II, and Orient Express/NASP X-30. This effort took under a year to accomplish, which would not have been possible without the previous years of data collection. Towards the end of the NASA-study in 2020, the software for the VCC was initiated by Stenila with the author helping with determining the layout. The alpha version was completed in 2021, with future iterations and integration with AVDS being conducted by future AVD researchers. This timeline of the development of the VCC is also provided visually in Fig. 1.11.

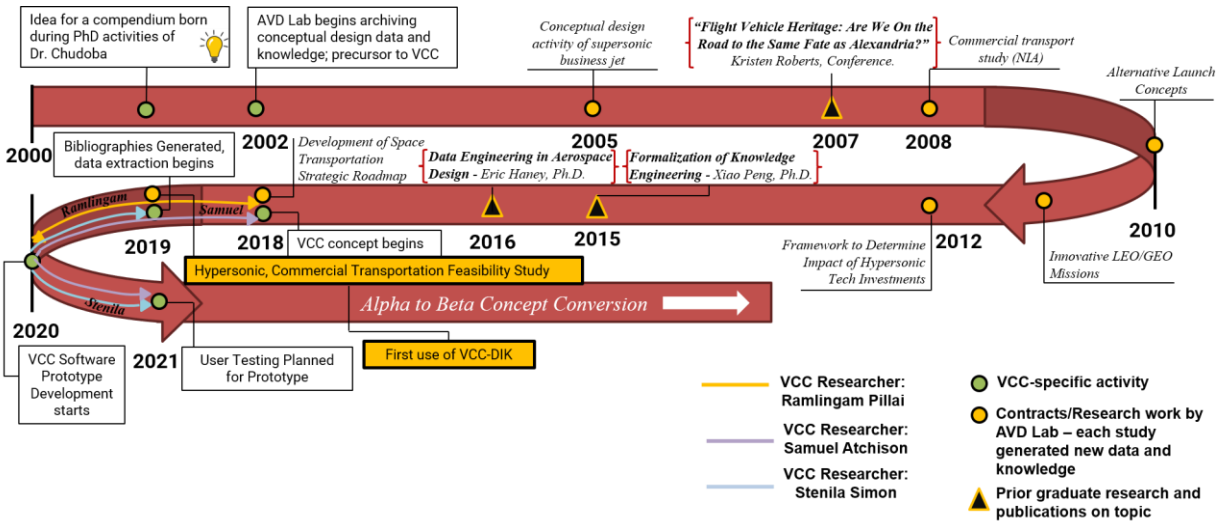

Fig. 1.11 Historical timeline leading to development of the VCC [30].

1.5 NASA Hypersonic, Commercial Transportation Feasibility Study

As the majority of the research conducted and presented here was completed during the NASA Hypersonic, Commercial Transportation Feasibility study, a small description of this study is provided. This study was sponsored by the Hypersonic Technology Project (HTP) at NASA Langley Research Center and was performed over 16 months from January of 2020 to April of 2021 [14]. The objectives of this study were to (1) explore the feasibility and practicality of corporate to medium-size commercial hypersonic transports, (2) provide possible baseline vehicles for two Entry Into Service (EIS) dates, and (3) to produce a library of hypersonic cruise vehicle continuum solution-space topographies. The approach taken to complete these objectives is provided in Fig. 1.12. For further information, the final report can be requested through NASA.

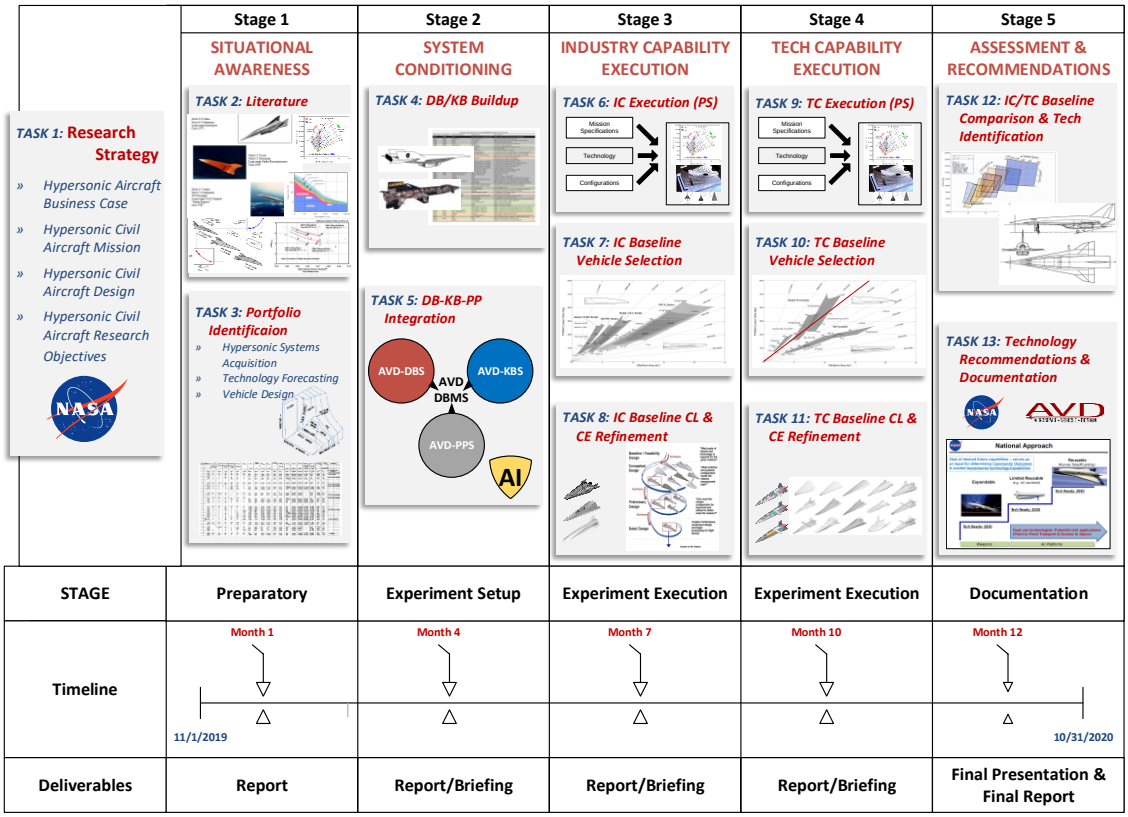

Fig. 1.12 Study approach to develop hypersonic civil flight vehicle [14].

1.5.1 Vehicle Selection

During this study, a literature review of past-to-present high-speed vehicles was conducted for the purpose of identifying relevant data and knowledge to the planning and development of civil hypersonic aircraft, and to select vehicles to (1) verify and calibrate AVDS, and (2) to serve as initiating geometries for the solution space screening trade studies [14]. For the selection of the vehicles, these were separated and termed verification and trade vehicles respectively. Table 1.4 summarizes the vehicles that were considered along with the decision-criteria considered. The final vehicles selected are shown in Fig. 1.13.

Table 1.4 Vehicles considered for verification and trades [14].

	Configuration	Flown	Speed Regime	Commercial/ Research/ Military	Engine Type	Reference Availability
X-51	AB	Yes	Hypersonic	Military	Scramjet	Low
X-43A	AB	Yes	Hypersonic	Research	Scramjet	High
XB-70	WB	Yes	Supersonic	Military/ Research	Turbojet	High
SR-71	BB	Yes	Supersonic	Military	Turbojet engine with compressor bleed	Medium
Concorde	WB	Yes	Supersonic	Commercial	Turbojet	High
Sänger II	BB	No	Hypersonic	Commercial	Turboramjet	Medium
Orient Express	AB	No	Hypersonic	Commercial	Combined turbine and dual-mode ramjet engine	Low
Stratofly	AB	No	Hypersonic	Commercial	Air Turbo-Rocket and Dual-Mode Ramjet	Low
X-15	WB	Yes	Hypersonic	Research	Liquid rocket	Medium
SR-72	BB	No	Hypersonic	Military/Research	Combined turbine and dual-mode ramjet engine	N/A
GHV	BB	No	Hypersonic	Research	Scramjet	Low
HSCT Vehicles	WB/AB	No	Supersonic	Commercial	Various proposed turbine-based variable cycle engines	N/A
ZHEST	WB	No	Supersonic	Commercial	Turbofans, rockets, and ramjets	N/A
TU-144	WB	Yes	Supersonic	Commercial	Turbofan	Medium
Boom	WB	No	Supersonic	Commercial	N/A	N/A
Aerion AS2	WB	No	Supersonic	Commercial	Turbofan	N/A
Hermeus	WB	No	Hypersonic	Commercial	N/A	N/A
LAPCAT Vehicles	WB/AB	No	Hypersonic	Commercial	Pre-cooled turbofan/ramjet engine	Medium
ATLLAS Vehicles	WB	No	Supersonic/ Hypersonic	Commercial	Combined turbine and dual-mode ramjet engine	Low
HYCAT Vehicles	WB/BB	No	Hypersonic	Commercial	Turbojet-Ramjet and Turbojet-Scramjet	Low

As shown, four vehicles were selected to be verification vehicles, while three were selected to be trade vehicles. As mentioned, the verification vehicles were used to verify/calibrate disciplinary tools and to verify the correctness of AVDS, and the trade vehicles were used as the initiating geometries (wing-body [WB], blended-body [BB], and all-body [AB]) for the solution space screening trade studies. With the introduction of the trade vehicles though, AVDS was split

into a configuration evaluation version (AVDS^{CE}) and a parametric sizing version (AVDS^{PS}), with different fidelity level disciplinary methods used. Due to this split, the trade vehicles were also used to verify/calibrate the disciplinary tools and synthesis system for AVDS (specifically AVDS^{PS}). This split is further detailed within the next chapter. These 7 selected vehicles created the foundation of the VCC presented here.

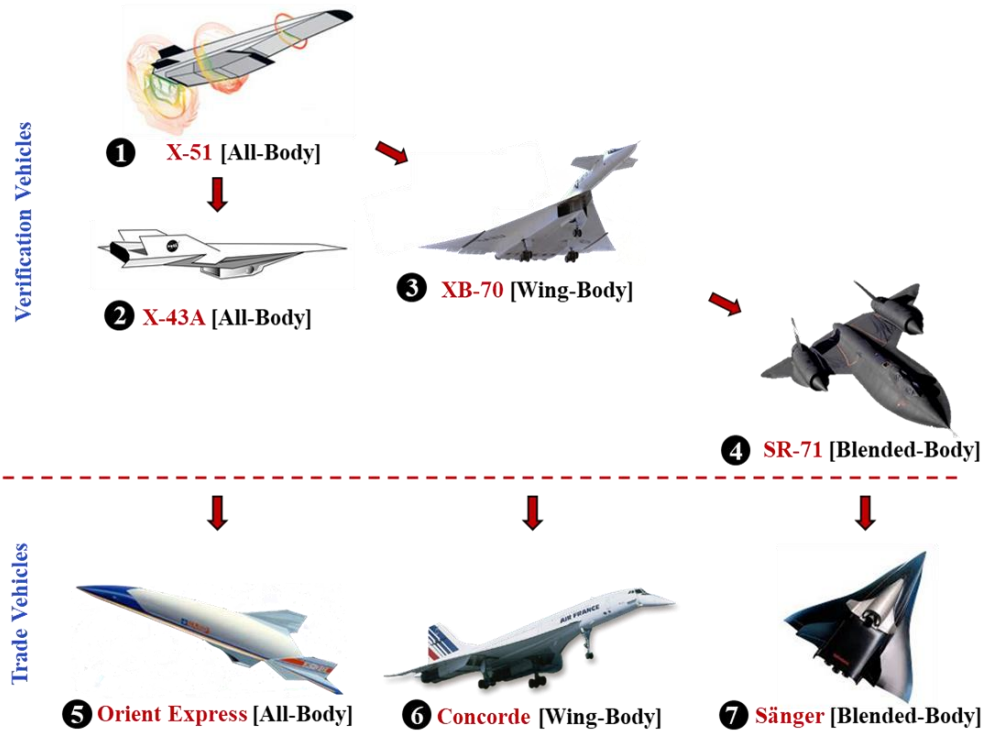

Fig. 1.13 Verification and trade vehicles selected for tool verification studies and design trade studies for three different baseline geometries: (a) wing-body (WB), (b) blended-body (BB), and all-body (AB) [14].

CHAPTER 2: AEROSPACE VEHICLE DESIGN SYNTHESIS (AVDS) OVERVIEW

2.1 AVDS Introduction

The Aerospace Vehicle Design Synthesis (AVDS) system is a next-generation synthesis methodology and software that was initiated in 2002 and has been growing and evolving over the last 20 years. It provides three primary modes: (1) aerospace vehicle design, (2) technology forecasting, and (3) strategic decision-maker support. AVDS has produced several landmark studies, earning it to be an industry-rated, -validated and -endorsed aerospace system design and technology forecasting system [14]. This system is the heart and soul of the AVD Laboratory with each generation of researchers leaving their mark by continually expanding the capabilities of AVDS and increasing its reliability within the aerospace community. As the research presented here is for the improvement of AVDS with the creation of the Vehicle Configuration Compendium (VCC) and improvements to the disciplinary methods for geometry and aerothermodynamics, a review of the history of AVDS and its current methodology is required.

2.2 History of AVDS

Through the years that AVDS has been developed, there have been several iterations expanding across three programming languages. These principal eras of AVDS development can be identified as (a) AVDS-Fortran, (b) AVDS-MATLAB, and (c) AVDS-Python, with the most current version being in the Python language. Figure 2.1 provides a timeline of each era along with indications of major tool utilization contracts, with examples of the software from each programming generation of AVDS shown in Fig. 2.2 below. AVDS-Fortran was developed primarily by Gary Coleman and has been verified by sizing the vehicles B777-300ER, the Learjet

24, Sänger II, and LAPCAT [13]. As this was the first version of AVDS, the foundation of the sizing methodology was developed, and was heavily influenced by Paul Czysz's Hypersonic Convergence [33]. While there have been changes overall such as the disciplinary methods used, the geometric modeling method used, how constraint analysis is used, etc., the fundamentals and purpose of AVDS have not changed since this Fortran version. For the other two programming languages, the MATLAB version was developed primarily by Lex Gonzales with support from Amen Omoragbon and Amit Oza [34-36], and verified primarily with the vehicles GHV, X-20, and X-51A [34,37]. The Python version was developed primarily by Thomas McCall [11] with verification with the vehicles X-51A, X-43A, XB-70, SR-71, Concorde, Sänger II, and Orient Express [14]. The primary developers for each programming version accomplished this task as part of their doctoral research, with each version also spawning several master theses to continually improve the functionality of AVDS.

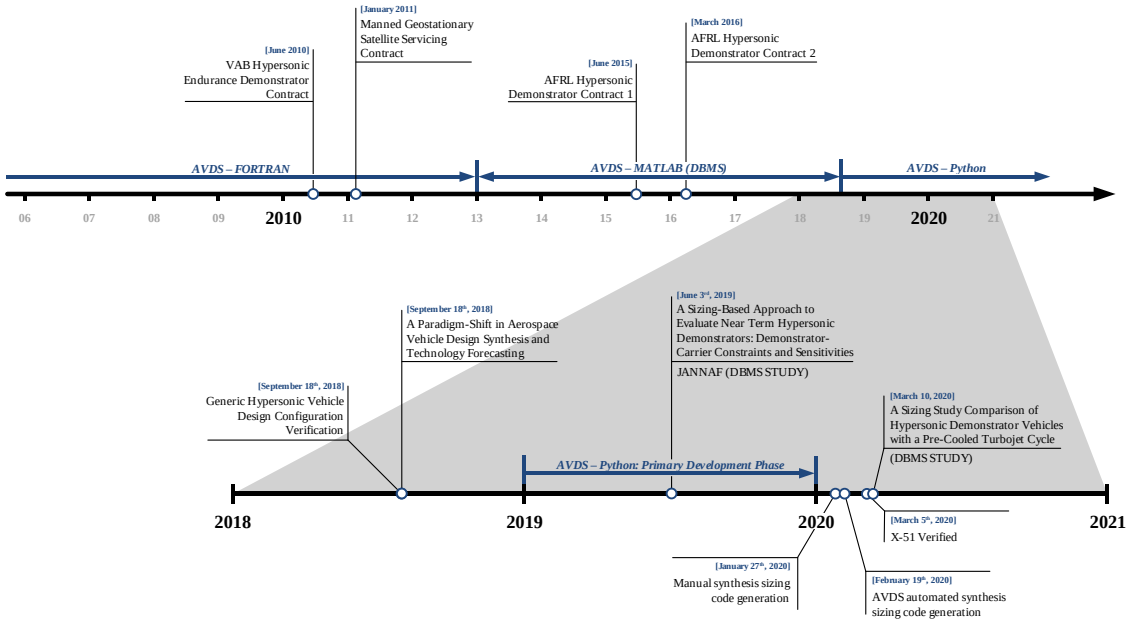

Fig. 2.1 Aerospace Vehicle Design Synthesis (AVDS) methodology and software development timeframe since 2002 [14].

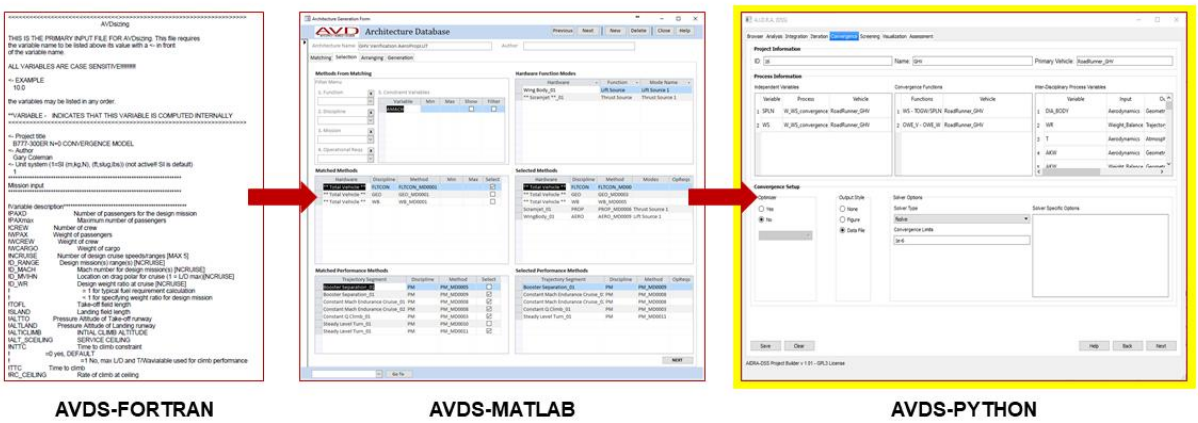

Fig. 2.2 Evolution of AVDS system through various programming languages [11,13,34].

While AVDS has gone through three programming languages, this was not due to doctoral work needing to be done, but these were changed due to practical factors such as ease of use, knowledge of language, connectivity to other applications, etc. For example, Fortran is not a programming language that is taught during the engineering program at UTA, so the knowledge of this language is lacking therefore the use of it in AVDS would require the learning of this language, at least fundamentally, to be able to run the system. This does not include the additional study to make any modifications that would be required when testing different high-speed vehicles. So, instead of requiring each future member that enters the AVD Laboratory to learn Fortran, the language was changed to allow members to only need to familiarize themselves with the methodology of AVDS before running studies and/or improving upon the system.

The ease of use and lack of knowledge reasons for the previous change are not the same reasons for the change from MATLAB to Python though. This change was primarily due to wanting to improve AVDS to the point of eventually becoming an artificial intelligence (AI) design and research assistant [11]. Python was selected as it is one of the most popular languages for AI development due to it being easy-to-use with flexible tools, extensible, providing several

prebuilt libraries, and a large community with experience already that could potentially help in this development [38]. Even though new members to the AVDS Lab would have to learn this language, which was one of the reasons that Fortran was changed to MATLAB, Python is easy to learn due to the syntax being similar to the English language, so with the knowledge gained of the MATLAB language, the transition to Python is a simple matter [38].

2.3 Aerospace Vehicle Design Synthesis-Python (AVDS-PYTHON)

For AVDS-Python, the first time it was verified and used was during the NASA study mentioned in Chapter 1. During this study, two versions of AVDS were created, a configuration evaluation version ($AVDS^{CE}$) and a parametric sizing version ($AVDS^{PS}$). These two different versions were created due to the requirements of the study.

The configuration version ($AVDS^{CE}$) was the original version which was verified with the verification vehicles (X-51, X-43A, XB-70, and SR-71). When it came to verify the trade vehicles (Concorde, Sänger II, and Orient Express) though, and in turn run the trade studies with those vehicles as the base, the amount of trades that wanted to be conducted became an issue with $AVDS^{CE}$ as the fidelity of the methods, while applicable to conceptual design, was not practical, from a synthesis condition time and effort point of view, for the number of trade points and the different geometric configurations. The issue was not realized until that point as verifying $AVDS^{CE}$ with the verification vehicles only required a single point verification or a small solution space. A large or broad solution space screening was determined to not be practical for $AVDS^{CE}$.

The parametric sizing version ($AVDS^{PS}$) was created to counteract this issue by reducing the fidelity of the methods further and modifying the sizing methodology to allow a larger number of trades to be conducted. This version was then verified with the trade vehicles to verify the

applicability of this system before running the trade study. A further explanation of the different versions, along with their differences are explained below.

2.3.1 Configuration Evaluation Version ($AVDS^{CE}$)

For $AVDS^{CE}$, a Nassi-Shneiderman diagram is provided in Fig. 2.3 depicting the synthesis process in which a vehicle is sized. This process begins with the inputs that are required for the mission, along with any independent design variables for each of the disciplines considered (in this case: geometry, aerodynamics, propulsion, trajectory, weight, and volume). The inputs for the X-51 verification vehicle are provided in Table 2.1 as an example of some of the inputs required for $AVDS^{CE}$. The inputs for all the verification vehicles are provided in Appendix A. As will be shown in the next section, the inputs and assumptions for $AVDS^{PS}$ is greatly reduced and more uniform compared to $AVDS^{CE}$ to make the synthesis system more generic to handle the wanted trade space. For the vehicles in which a small trade space is developed (the X-51 and X-43), additional inputs such as the tau value and spatula width are provided to create these solution spaces. The tau value is a dimensionless geometric parameter that relates the total vehicle volume to the total vehicle planform area, $\tau = V_{tot}/S_{pln}^{1.5}$. This relationship also makes it known as a slenderness parameter as if the planform area is kept constant and tau increases, the volume of the vehicle must increase, making it stouter, while if tau decreases, the volume decreases making the vehicle slimmer. This relation is reversed if volume is kept constant, but it effects the 'slenderness' of the vehicle. After the inputs, two initial guess-values are provided to the system to start the sizing process. These inputs are the planform area and wing loading. Using the input guess-values and tau values (if scaled with it), the geometry method then scales the baseline vehicle to match the guessed planform area and input tau value.

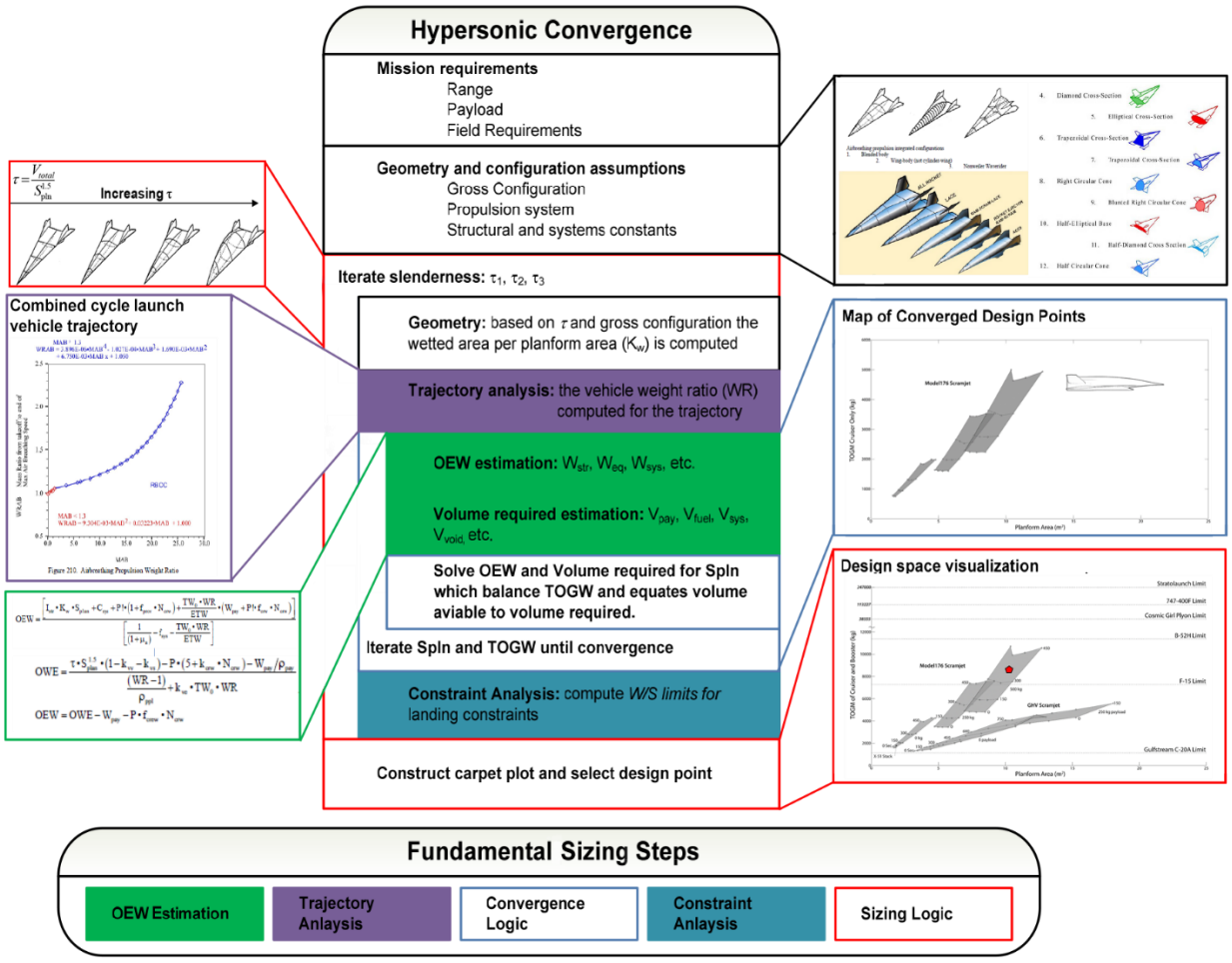

Fig. 2.3 AVDS Configuration Evaluation (AVDS^{CE}) synthesis process [14].

Once the vehicle is scaled, the trajectory analysis is performed using this new geometry. The trajectory analysis is split into multiple segments with different equations of motion depending on the type of trajectory. Within each trajectory segment, the aerodynamic and propulsion discipline is conducted to provide the required information for the trajectory. Once the trajectory analysis is completed, the total fuel fraction (or weight ratio in the case of trans-atmospheric launchers) for the scaled vehicle is determined. The fuel fraction is then provided to the weight and volume discipline where the takeoff gross weight (TOGW) is determined.

The TOGW for the scaled vehicle requires the payload weight, crew weight, operating empty weight (OEW), and the fuel weight, which the payload and crew weight are determined

from the inputs of the vehicle regardless of how it is scaled. The fuel weight is determined from the fuel fraction from the trajectory analysis and the guess TOGW. The guess TOGW can be determined from the guess wing loading and planform area. Finally, the OEW can be determined, but it is calculated in two different ways. It is first converted into the operating weight empty (OWE), where OWE = OEW + $W_{payload}$ + W_{crew}. It is then calculated twice, once using weight methods and the second time using volume methods with densities. These two calculations must converge to the same value to determine OEW. Once converged and the TOGW for the scaled vehicle is determined with the converged OEW value, the guessed wing loading value is compared to the scaled TOGW divided by the guessed planform area to determine if they match. If the values match, then the design is considered converged. If not, then the system iterates the guessed values until the design is converged. A solution space of converged design points is then generated if multiple trade inputs were used, such as tau, where a constraint analysis can be applied to separate the feasible designs from the non-feasible ones.

Table 2.1 AVDS^{CE} X-51 inputs and assumptions [14].

Variable Discipline	Variable	Value
Geometry	Küchemann's tau	0.214
Propulsion	Area ratio of viscous captured flow to inviscid captured flow	0.95
	Reference fuel equivalence ratio	1
	Design Mach	6
Trajectory	Constant *q* climb segment: Start altitude, m	18,517
	Constant *q* climb segment: Start velocity, m/s	1,416
	Constant *q* climb segment: End altitude, m	19,290
	Constant *q* climb segment: Maximum longitudinal acceleration, m/s^2	0.1
	Constant *q* climb segment: Minimum longitudinal acceleration, m/s^2	0.01
	Constant Mach endurance cruise segment: Cruise endurance time, sec	109
Weights and Volume	Number of crew	0
	Number of passengers	0
	Weight of unmanned fixed systems, N	2,053
	Weight of each crew member, N/person	-
	Weight fixed manned systems per crew member, N/person	-
	Weight of each passenger, N/person	-
	Weight of passenger provisions per passenger, N/person	-
	Weight of variable systems per vehicle dry weight	0.0161
	Weight of cargo, N	0
	Minimum dry weight (OEW) margin	0.1
	Volume of provision for each crew member, m^3/person	-
	Volume per crew member, m^3/person	-
	Volume of manned fixed systems per crew member, m^3/person	-
	Volume of each passenger space, m^3/person	-
	Volume of variable systems per total vehicle volume, m^3	0.1
	Volume of vehicle void space per total vehicle volume, m^3	0.1

Volume of unmanned fixed system, m^3	0.3724
Error band around the structural fraction, $m^{-0.138}$	-0.02
Cargo density, kg/m^3	-
Fuel density, kg/m^3	800

With each of the four verification vehicles verified within AVDS^{CE}, a comparison of the sizing code for each can be compared as shown in Table 2.2. First looking at the number of sizing code versions for each vehicle, it shows that the number of versions created decreases from the X-51 to the SR-71. As the order of these vehicles portray the order in which each was verified, this decrease demonstrates a growth in robustness and effectiveness of the AVDS^{CE} methodology and software. This decrease in sizing code versions is despite an increase in number of source code lines, subfunctions, and number of independent parameters, which also shows an increase in proficiency of using AVDS^{CE} with each vehicle.

Table 2.2 Summary of AVDS^{CE} code information for the four verification vehicles [14].

	X-51	X-43A	XB-70	SR-71
Total Sizing Code Versions	15	13	8	4
Sizing Code Magnitude (Number of Source Code Lines)	3,869	3,636	7,039	6,453
Number of Subfunctions	36	30	78	64
Number of Trajectory Segments	4	2	10	10
Number of Independent Sizing and Mission Parameters	21	23	50	52

2.3.2 Parametric Sizing Version (AVDS^{PS})

With the configuration evaluation version of AVDS (AVDS^{CE}) discussed, the parametric sizing version (AVDS^{PS}) is now discussed along with how the AVDS methodology was modified for CE to PS. As AVDS^{PS} is a modified version of AVDS^{CE} the underlying synthesis process remains the same, but the primary difference is in the convergence logic and the fidelity level of the disciplinary methods as previously mentioned. Table 2.3 provides a summary of the primary differences between these two versions of AVDS.

Table 2.3 Comparison of the AVDS^{PS} process and the AVDS^{CE} process [14].

AVDS Parametric Sizing (AVDS^{PS})	AVDS Configuration Evaluation (AVDS^{CE})
Convergence Criteria: 1. OEW $f(S_{pln}, K_v, \tau_{vol}, I_p,)$ – OEW $f(I_{str}, S_{wet}, K_w, K_{str})$ < error tolerance	Convergence Criteria: 1. $OWE_w - OWE_v$ < error tolerance 2. W/S – $TOGW/S_{pln}$ < error tolerance
Solver Guess Inputs: 1. S_{pln}	Solver Guess Inputs: 1. W/S 2. S_{pln}
Solver method: Differential-evolution: stochastic method, minimizes objective function, finds global minimum	Solver method: fsolve: root finding function
Primary Convergence Outputs: 1. OWE 3. TOGW 2. OEW 4. S_{pln} OWE = *f*(correlation parameters)	Primary Convergence Outputs: 1. OWE_w 4. W/S 2. OWE_v 5. TOGW 3. OEW 6. S_{pln} OWE = *f*(weight and volume buildup)
Method Attributes: - Geometry: Uses geometry code (VSP Modeled). - Aerodynamics: HyFAC method aerodynamics, Küchemann method aerodynamics, rapid configuration aerodynamics, etc. - Propulsion: Considers rapid configuration propulsion method. - Trajectory: Simplified climb, cruise, descent equations for estimating fuel fraction. - Weight and Volume: Less input weight assumptions required; volume is taken into account through correlation parameters, but not part of convergence. - Stability and Control: Geometry correlated inherent static stability determination (future capability).	Method Attributes: - Geometry: Uses geometry code (VSP Modeled). - Aerodynamics: HyFAC aero (current), replace with low order CFD (future capability). - Propulsion: NPSS Modeling (current), Heiser and Pratt scramjet model, etc. - Trajectory: Analysis of each trajectory segment as function of aerodynamic and propulsion system characteristics at each flight condition, 3DOF. - Weight and Volume: Weight and volume calculations based on detailed weight and volume buildup; many weight and volume assumptions are required for increasing the design detail considered. - Stability and Control: Implement *AeroMech* (future capability).
Other Attributes: - Uses a reference vehicle limited to geometric scaling (current). - I_{str} assumed to be a function of payload weight and temperature (through Mach number). - Mostly dependent on correlation parameters. - Capable of doing wide-range screening of vehicles leading to a selection of baseline vehicle.	Other Attributes: - Uses a reference vehicle limited to geometric scaling. - Evaluation of baseline design selected from AVDS^{PS} and AVDS^{CL} - Uses consistent method buildup instead of correlation parameters. - Capable of doing small trade space (reduced screening capability due to focus on point-design refinement)

AVDS^{PS} begins with the basic inputs for the mission along with any independent design variables in each of the disciplines considered. Compared to AVDS^{CE}, the inputs and assumptions for AVDS^{PS} are significantly less as shown in Table 2.4. They are also more uniform as the number of inputs across the three vehicles used within AVDS^{PS} is the same, while the number of inputs for the four vehicles used within AVDS^{CE} varies greatly between them. After setting up the inputs,

the process starts with an initial guess-value of planform area only, no wing loading guess-value. As with AVDS^{CE}, other inputs for sizing can be entered as well such as a tau value for tau scaling. Using the planform guess-value and the tau value (if used), the geometry method scales the baseline geometric model of the vehicle to match the input planform area guess and tau value. The geometric properties required for each discipline are provided from this scaled model.

After the vehicle is scaled from the inputs, the trajectory analysis is performed. Instead of having multiple segments within the trajectory analysis and equations of motion for each, the trajectory is simplified into three segments (climb, cruise, and descent), and simple estimation equations are used to determine the fuel consumed and rage covered in each segment. For each segment of the trajectory, the mission inputs and geometric values from the scaled model are used within the aerodynamics discipline to provide an *L/D* ratio, and the propulsion discipline to provide the installed specific fuel consumption (SFC) values, with the additional inputs of selected fuel properties and efficiency. At the completion of the trajectory analysis, the total fuel fraction is determined, and then used within the weight method.

Table 2.4 Inputs and assumptions for solution space generation [14].

Discipline	Variable	Concorde	Sänger HST-230	Orient Express
Mission	Cruise Mach number	2	4.4	6
	Number of passengers	100	230	80
	Number of crew	8	9	2
	Range	3,500 nmi	5,670 nmi	7,000 nmi
Geometry	Tau	0.0550	0.0826	0.0884
Propulsion	Fuel	Jet-A	Hydrogen	Methane
	Processing efficiency	0.90	0.85	0.94
	Fuel mass addition	No	No	No
	Internal losses	No	No	No
	Thermal recovery	No	No	Yes
Aerodynamics	Propulsive lift	No	No	No
Trajectory	Climb acceleration	0.10 g	0.10 g	0.10 g
	SFC average climb	Table 7.42	Table 7.42	Table 7.42
	SFC cruise	Table 7.42	Table 7.42	Table 7.42
	Fuel reserve fraction	0.06	0.04	0.00
	Taxi in/out time	24 min	24 min	24 min
	Cruise altitudes	55,000 ft	80,000 ft	100,000 ft
	Centrifugal lift	Yes	Yes	Yes
Weights	Weight per PAX	284.5 lbs	284.5 lbs	284.5 lbs
	Weight per crew	176.5 lbs	176.5 lbs	176.5 lbs
	Cargo weight per PAX	10 lbs	10 lbs	10 lbs

	I_{str}	5.27	5.68	3.5
	K_v	0.1052	0.156	0.18
	K_{str} error band	0.035	-0.035	0.035
Other Constraints		Underbody propulsion system	Underbody propulsion system	Underbody propulsion system

As mentioned, the convergence criterion for AVDS^{PS} is different compared to the convergence criterion used within AVDS^{CE}. As with AVDS^{CE}, OEW is calculated twice, but instead of having one based on weight and the other based on volume, weight estimations correlated with geometric parameters, structural parameters, a propulsion index, and a structural index are used. These two OEW values must converge to the same value in order for the design to be considered converged. While the PS version is more weight focused instead of having a dedicated volume relation as the CE version does, the fuel volume of the scaled vehicle is accounted for within a volume correlation parameter, K_v. This correlation parameter is described further within Paul Czysz's Hypersonic Convergence [33]. The operating weight empty (OWE), where OWE = OEW + $W_{payload}$ + W_{crew}, can be determined from the converged OEW, and the TOGW can be determined from OWE and the weight ratio (WR), which was determined from the fuel fraction, where WR = TOGW/OWE. A solution space of the converged design points is then generated where constraint analysis can be applied to separate the feasible designs from the infeasible designs.

While both AVDS^{PS} and AVDS^{CE} have been verified and can create solution spaces from the converged points, as discussed, the PS version can create a wide-ranging solution space due to the reduced inputs required and the decrease in fidelity levels of the methods compared to the smaller solution space generated for the CE version. It may seem that with the PS version, there may not be a need for the CE version of AVDS, but with the higher-level fidelity methods of CE

compared to the PS version, AVDS^{CE} can be used to fine tune the promising design candidates selected from the AVDS^{PS} broader solution space.

With each of the three trade vehicles verified within AVDS^{PS}, a comparison of the sizing code for each can be compared as shown in Table 2.5. First looking at the number of sizing code versions for each vehicle, it shows that the number of versions created decreases from the Concorde to the Orient Express. As the order of these vehicles portray the order in which each was verified, this decrease demonstrates a growth in robustness and effectiveness of the AVDS^{PS} methodology and software. It should also be noted that in comparison to the number of sizing code versions produced in AVDS^{CE}, this number is greatly reduced for AVDS^{PS}. This is primarily due to the disciplinary methods being less complex. For the number of subfunctions, trajectory segments, and independent sizing and mission parameters, all three vehicles had the same number. This is due to the change of making the PS version more generic to create the broader solution spaces, so the disciplinary methods between these three vehicles are primarily the same, except for slight differences in the geometry and aerodynamic methods. This is also shown in the sizing code magnitude, or the number of source code lines, as all three vehicles are close to the same number.

Table 2.5 Summary of AVDS^{PS} code information as applied to the three trade vehicles [14].

	Concorde	Sänger HST-230	Orient Express HST-80
Total Sizing Code Versions	8	2	1
Sizing Code Magnitude (Number of Source Code Lines)	2,106	2,224	2,182
Plot Code Magnitude (Number of Source Code Lines)	5,347	5,347	5,347
Number of Subfunctions	16	16	16
Number of Trajectory Segments	3	3	3
Number of Independent Sizing and Mission Parameters	14	14	14

CHAPTER 3: VEHICLE CONFIGURATION COMPENDIUM (VCC) OVERVIEW

3.1 VCC Introduction

The Vehicle Configuration Compendium, or VCC, is a tool introduced as a solution to the retention and usage of data-information-knowledge of historical legacy high-speed vehicles as mentioned within the problem statement of Chapter 1. It is a system designed to assist the conceptual designer by providing a central location of data, information, and design knowledge for various high-speed aerospace vehicles. This is accomplished by organizing the VCC into two functions, the 'database' and the 'knowledgebase'.

3.1.1 Database

The database side of the VCC is used to store vehicle data and information pertaining primarily to disciplinary information such as geometry, aerodynamics, etc. This stored data comes in the form of (a) tables for parameters that are normally not presented via plots (e.g., geometry and weight data) and (b) digitized plots of parameters that are primarily presented via a plot (e.g., C_L vs α, and C_L vs C_D). These plots are digitized from their respective sources to obtain a uniform figure format within VCC, and to obtain the raw data that makes up the plot to allow access to a specific point if interested. An example of the database in an early GUI concept layout is shown in Fig. 3.1. This illustrates the main points wanted for each vehicle within the database where (1) the vehicle disciplinary data is organized and separated into the primary disciplines of synthesis, aerodynamics, aerothermodynamics, geometry, performance, propulsion, weight & balance, and stability & control, (2) each collected data and information is clearly and easily visualized, and (3) a model developed within NASA's Vehicle Sketch Pad (*OpenVSP*) which allows a 3D view of the

wanted vehicle, the ability to obtain representative geometric values for unknown parameters, and to use within a synthesis system such as AVDS.

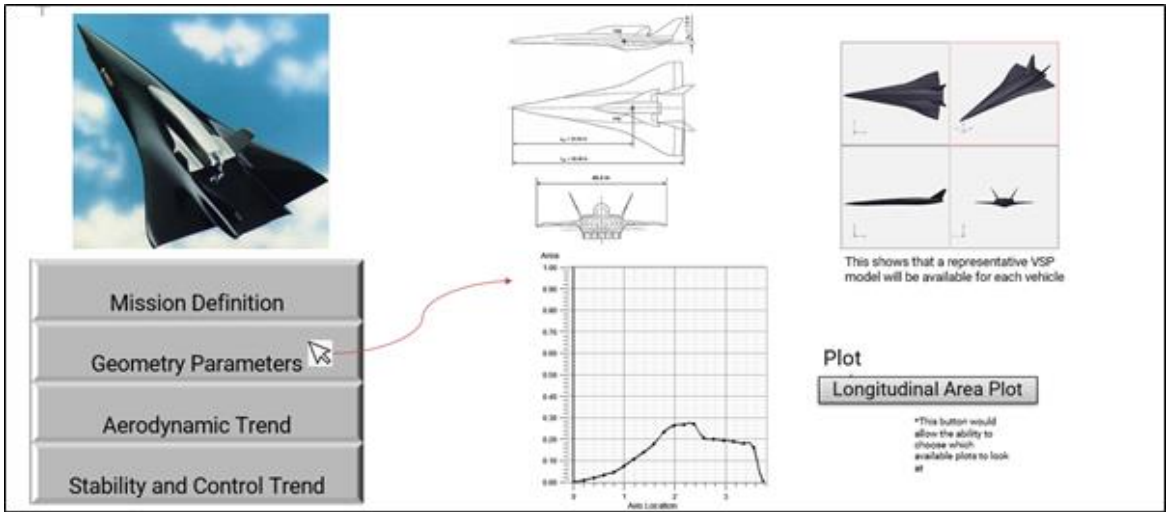

Fig. 3.1 Example of a GUI for the database side of the VCC.

With this, the database then provides three functions to assist the design engineer and synthesis systems, such as AVDS, by (1) providing aerospace vehicle statistics, (2) allowing aerospace vehicle method verification (disciplinary and multidisciplinary), and (3) providing an aerospace vehicle decomposition (mission, hardware, etc.). The aerospace vehicle statistics function allows a reasonable range of values to be determined for specified parameters for vehicles with the same mission, speed, range, etc. This is useful when certain independent variables are required to be assumed within a synthesis system, as a 'best-guess' or 'in-the-ball-park' value can be selected from similar historic vehicles.

Next, the aerospace vehicle method verification function would allow disciplinary methods selected for a synthesis system to be verified against real data (wind tunnel, ground tests, flight data, simulation, etc.) to determine if these methods are applicable for the wanted vehicle

configuration/mission. It would also allow verification and calibration of multidisciplinary methods, or how the synthesis system functions, by comparing sizing results to the actual vehicle.

Lastly, the aerospace vehicle decomposition function breaks down the mission, hardware, etc. of each vehicle within the database for the purpose of providing an overview, or a 'snapshot', of the components of the vehicle. This function primarily assists design engineers by acquainting them with mission/configuration highlights of each high-speed vehicle stored within the database. An example of a 'snapshot' for the X-51 is shown in Fig. 3.2.

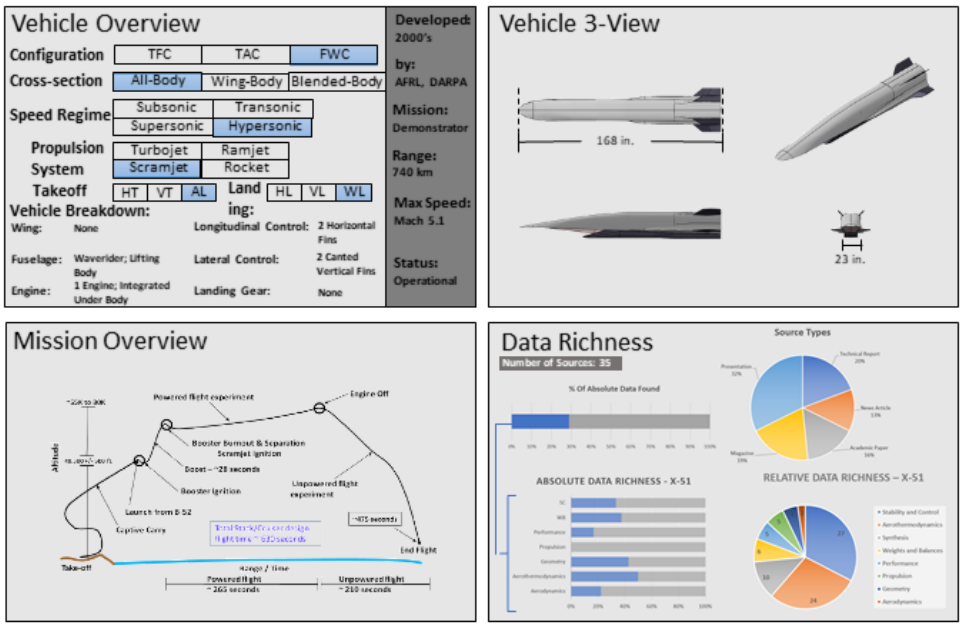

Fig. 3.2 Example of vehicle 'snapshot'.

3.1.2 Knowledgebase

The knowledgebase function of the VCC utilizes the data pool gathered within the database side to generate meaningful comparisons, continuum design trends, and best-practice guidelines for the range of relevant vehicle configurations and concepts obtained. This means that the effectiveness of the knowledgebase is dependent on the number of high-speed vehicles stored within the database and how rich the amount of publicly available data is for each one. The

knowledgebase side of the VCC provides two functions to assist the design engineer and synthesis systems by (1) allowing aerospace vehicle configuration comparisons and (2) the ability to develop configuration and trend-based disciplinary analysis methods. The aerospace vehicle configuration function would be used to compare the stored vehicle data within the database function to determine how configuration choices affect disciplinary performance, such as aerodynamics, weights, etc. The trend-based disciplinary analysis method generation function takes the comparison function a step further by adding trendlines to the available data to either supplement current disciplinary methods used within the synthesis system, or to develop a new method for calculating a particular parameter if there are no, or lack of, methods for it.

For the comparisons within these two functions, the stored vehicles are mainly categorized first by their longitudinal/pitch control layout, and then by their cross-section. The pitch control layout is the overall category each vehicle is first assigned as this configuration greatly effects the primary disciplines, such as aerodynamics, while the second category of cross-section does affect these as well, it primarily effects volume efficiency and the size the vehicle to contain the wanted contents. Figure 3.3 below shows a representative configuration layout for each configuration with corresponding examples of subsonic and supersonic/hypersonic vehicles. Currently only three of these configurations are represented within the VCC with Concorde representing the Tail-Aft Configuration (TAC) where the pitch control is aft of the wing, the XB-70 representing the Tail-First Configuration (TFC) where the pitch control is in front of the wing, and then the other five vehicles, X-51, X-43A, SR-71, Sänger II, and NASP/Orient Express, represent the Flying-Wing Configuration (FWC) where the pitch control is integrated into the wing. The last three configurations shown are the Triple-Surface Configuration (TSC) where the pitch controls are in front and aft of the wing, the Oblique-Wing Configuration (OWC) which is similar to the TAC,

except the wing is not perpendicular to the incoming airflow, and lastly the Oblique-Flying-Wing Configuration (OFWC) which is similar to the FWC, except, as with the OWC, the wing is not perpendicular to the incoming airflow.

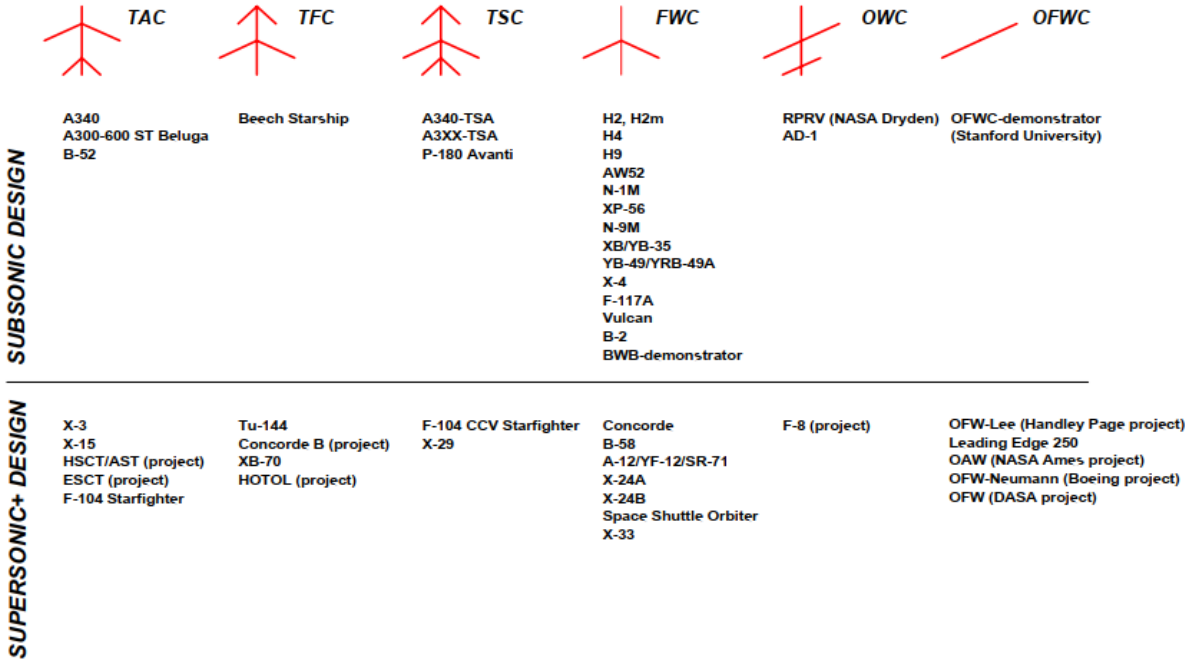

Fig. 3.3 Overview of main configurations with vehicle examples for each one [15].

After the overall configuration, each vehicle is then defined by their cross-section. The cross-section is broken down into three categories, the wing-body (WB), the blended-body (BB), and the all-body (AB). A wing-body cross-section is where there is a clear distinction between the fuselage and the wing, a blended-body cross-section is where there is a fuselage and wing, but there is no clear distinction between the two, and an all-body cross-section is where the vehicle only has a fuselage, but is shaped to generate usable lift, this is also known as a lifting-body. A representative example of each category of vehicle cross-section is shown in Fig. 3.4.

Fig. 3.4 Example of cross-section categories.

While many other categories could be used for these vehicles and their comparisons, these two are the primary ones as they allow overall disciplinary comparisons due to the configuration of the vehicle to determine how each configuration performs in terms of aerodynamics, weight, volume efficiency, aerothermodynamics, etc. Examples of continuum lines, or guidelines, to assist the design engineer through the comparison of the configurations are shown in Fig. 3.5.

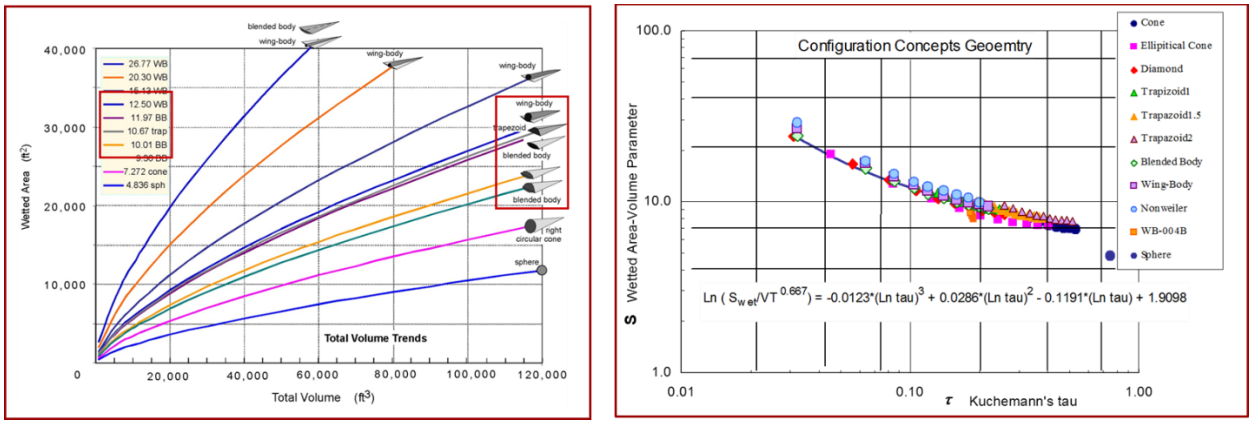

Fig. 3.5 Examples of knowledgebase continuum lines [39].

With this, an early example GUI layout for the Knowledgebase was generated as shown in Fig. 3.6. This layout highlights the primary elements wanted within the GUI. The single figure is the primary focus of the Knowledgebase as it provides a visual of the data stored within the Database superimposed together. This allows the design engineer to observe past knowledge stored within the Knowledgebase and to create new knowledge from the legacy vehicles through their configurations. The other two elements shown are the ability to select the axes in which are displayed to determine the interactions of the gathered parameters and the ability to select the

configurations which are displayed, whether it be all the configurations available (TAC, TFC, etc.), a single configuration such as observing only the stored Flying-Wing Configuration (FWC) vehicles, or a combination of comparing certain configurations and/or cross-sections. If there is something missing from this initial layout, it would be the ability to select pre-defined knowledgebase plots which have already been determined to provide valuable knowledge and/or provide design guidelines. This would provide design engineers with a starting point within the Knowledgebase and then allowing the ability to investigate other possible design guidelines through changing the axes and configuration comparisons.

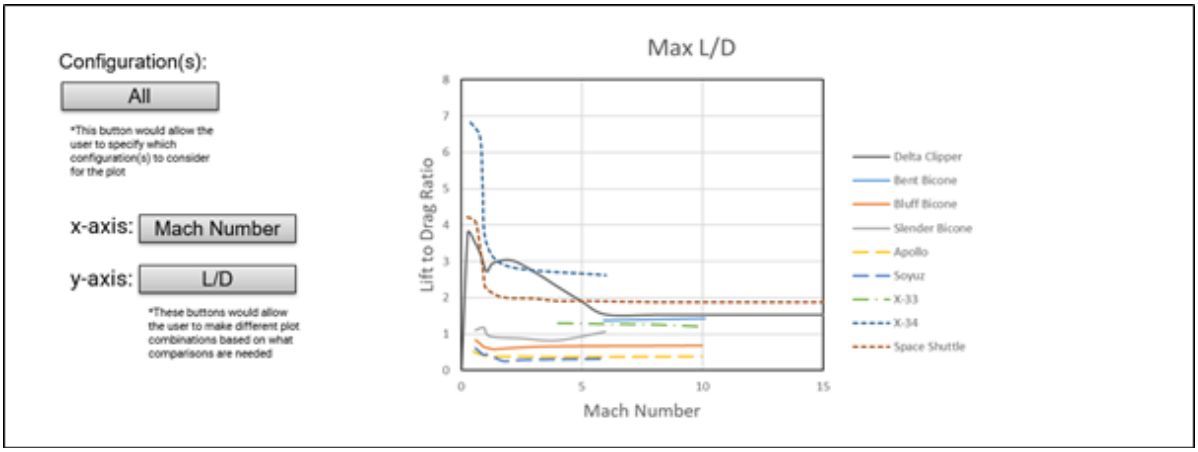

Fig. 3.6 Example of a GUI for the knowledgebase side of the VCC.

As the purpose and functions of the Database and Knowledgebase within the VCC have been defined, the next section describes the process each vehicle currently within the VCC went through when developing the Database. This section is strictly over the Database as it is the foundation of the VCC with it providing everything from verification data to what is used within the Knowledgebase. For specific uses of the VCC, the reader is directed to Chapter 5 where the power of the Database is shown with the verification of disciplinary methods and AVDS for

selected vehicles and Chapter 6 where the power of the Knowledgebase is shown with developing/discovering a method to determine the structural index, I_{str}.

3.2 VCC Background Development

As the Database side presents the foundation for everything within the VCC, the most important aspect is the authenticity of the underlying vehicle data accumulated. This strive for authenticity is summarized within a statement much in the same manner as that of Jane's all the World's Aircraft and the do-it-yourself Haynes car maintenance manuals. These two world-renown resources are known for their authenticity within their respective fields. In analogy, the VCC has adopted a similar quality standard related to source data selection and internal organization. The statement of authenticity for the VCC currently reads:

> Following the quality standard championed by Jane's and Haynes, the Vehicle Configuration Compendium (VCC) strives to provide the design engineer with impartial, accurate information, that draws on the 30 years of legacy material and experience available to the Aerospace Vehicle Design (AVD) Laboratory. The VCC is committed to the credibility and authenticity of the information stored, not to be influenced by outside entities, but to assist the designer through the ability to verify the accuracy of design tools, to rapidly extract lessons learned from past-to-present efforts, and through the ability to compare similar and dissimilar configuration and concept permutations at a parametric level. Through the selection, extraction, digitization, and organization of data gathered from reliable and complete source bibliographies for each vehicle, the

critical design parameters originally stemming from simulation, experimental and/or flight test data resources, are preserved and custom-presented to the practitioner.

With this, there are five principal steps required to develop the Database side of the VCC for each vehicle: (1) A comprehensive bibliography is generated for each vehicle, (2) Each reference entry within the bibliography is reviewed, (3) relevant conceptual to preliminary design material is identified and then (4) extracted and sorted into the primary discipline categories in VCC. After all the data that has been identified to be pertinent to conceptual and preliminary design is extracted, it is then (5) digitized to recreate the extracted plots which are now available for interpolation and extrapolation routines, if desired within the Knowledgebase side. Once the digitization process is complete, the newly digitized data for each vehicle is stored in a single location for the use of the VCC within the software to be developed. The process of building up the VCC is shown in Fig. 3.7.

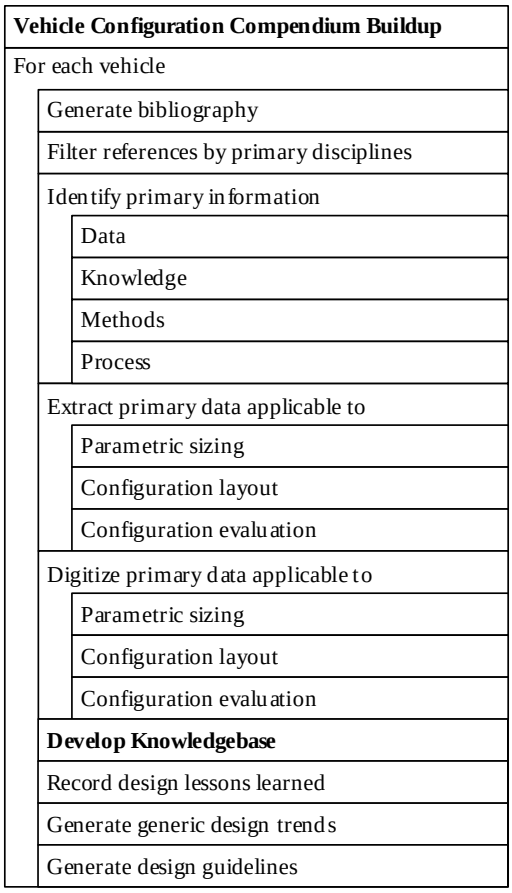

Fig. 3.7 Vehicle configuration compendium (VCC) buildup process.

3.2.1 Bibliography Generation

As introduced earlier, the process starts with the generation of the bibliography. First, the references of each individual vehicle readily available in the AVD Laboratory are collected, digitally and physically, with all available documents being stored in *Zotero*, see Fig. 3.8. *Zotero* is a free reference management software and is primarily used for the storage and organization of documents. *Zotero* is useful with the addition of its downloadable *Google Chrome* add-on (allows from an activation button near the web address bar, the document along with any metadata, or data such as title, author(s), publication location, etc., to be saved in *Zotero* without the need to be entered manually). While this makes the collection of digital source documents easier, any print documents are scanned with a high-quality scanner and converted into digital copies to be saved

and organized along with the others. Note that these copies though do not have metadata, so all information is manually entered for the bibliography later. Having completed the resources provided by the AVD Laboratory, a complementing online search is executed utilizing scholarly databases such as NASA NTRS, DTIC, and AIAA's ARC. This step further supplements and completes the vehicle bibliography and source material search.

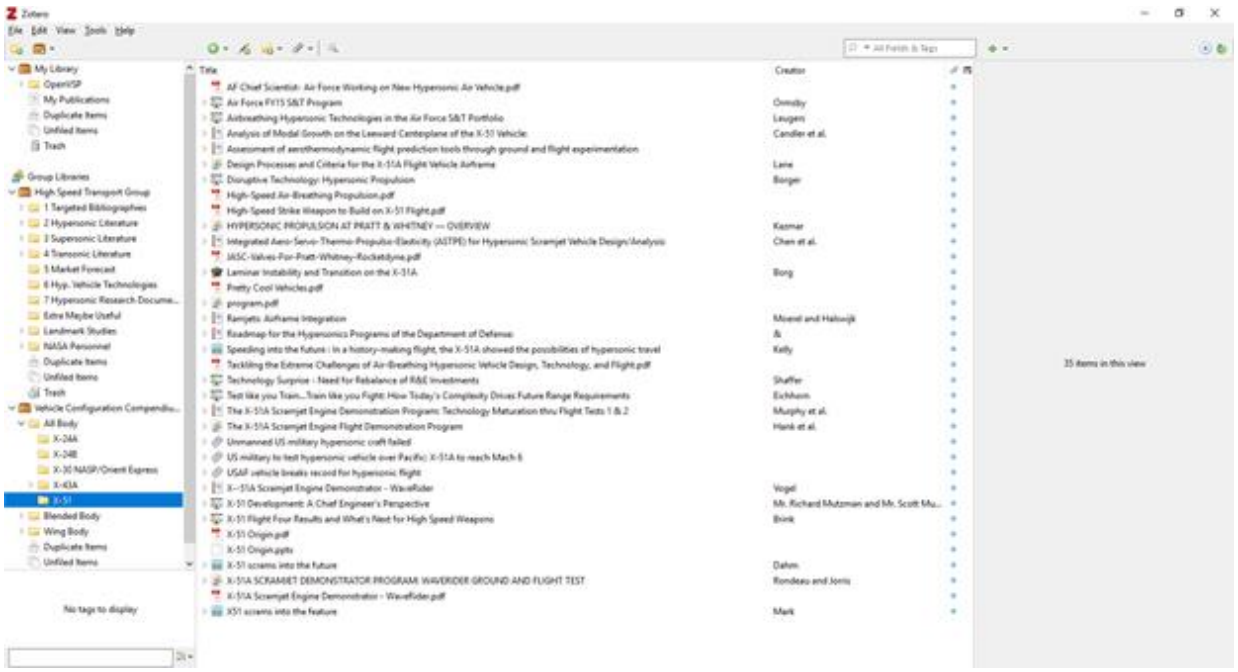

Fig. 3.8 Example of *Zotero* GUI with X-51 references.

Once all relevant documents have been added to *Zotero*, these are then exported into *EndNote* for completing the bibliography. The reason *EndNote* is used for the bibliography creation instead of *Zotero* for all of it, is that *EndNote* is more user-friendly than *Zotero* for formatting of the references, developing and modifying the style of the bibliography since it is connected to Word, making the final creation of the bibliography easier, along with allowing easier citations in report writing. The reason *EndNote* is not used for the storage and organization of the documents is because *EndNote* does not allow multiple sublevels for in-depth separation of the documents, does not have an easy way to add the attached PDFs, and requires a paid license for

each user to have access. By using both together, the documents can be easily stored, neatly organized, and shared by everyone in the AVD Laboratory through free accounts in *Zotero*, easily export files from *Zotero* to *EndNote*, and then have a user-friendly environment for the in-depth details of each reference and the final creation of the bibliography. The *EndNote* GUI showing the documents gathered for the X-51 is shown in Fig. 3.9.

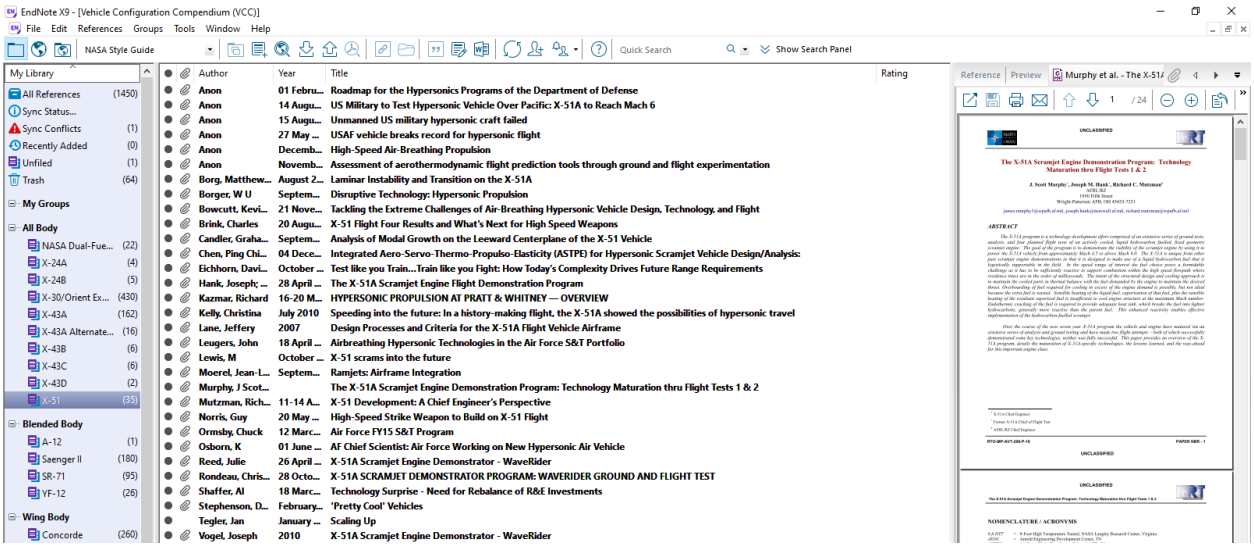

Fig. 3.9 Example of *EndNote* GUI with X-51 references.

After all the gathered documents have been exported into *EndNote*, each reference is checked to make sure that all relevant information required to fill out the bibliography is added, for example title, author(s), conference location, publisher, etc. This varies depending on the document type, but these are completed as thoroughly as possible. Once each reference is completed, the final bibliography can be created. This is accomplished by copying and pasting the references and their format from *EndNote* into a Word document. With the list of references in the Word document, these are converted into a numbered list to allow the numbers to automatically update with the addition or subtraction of references. After the creation of the numbered list, the bibliography is formatted through a set process defined in the AVD Laboratory. An example of a

created bibliography is shown in Fig. 3.10. The bibliography for each of the 7 selected vehicles currently within the VCC is provided in Appendix B.

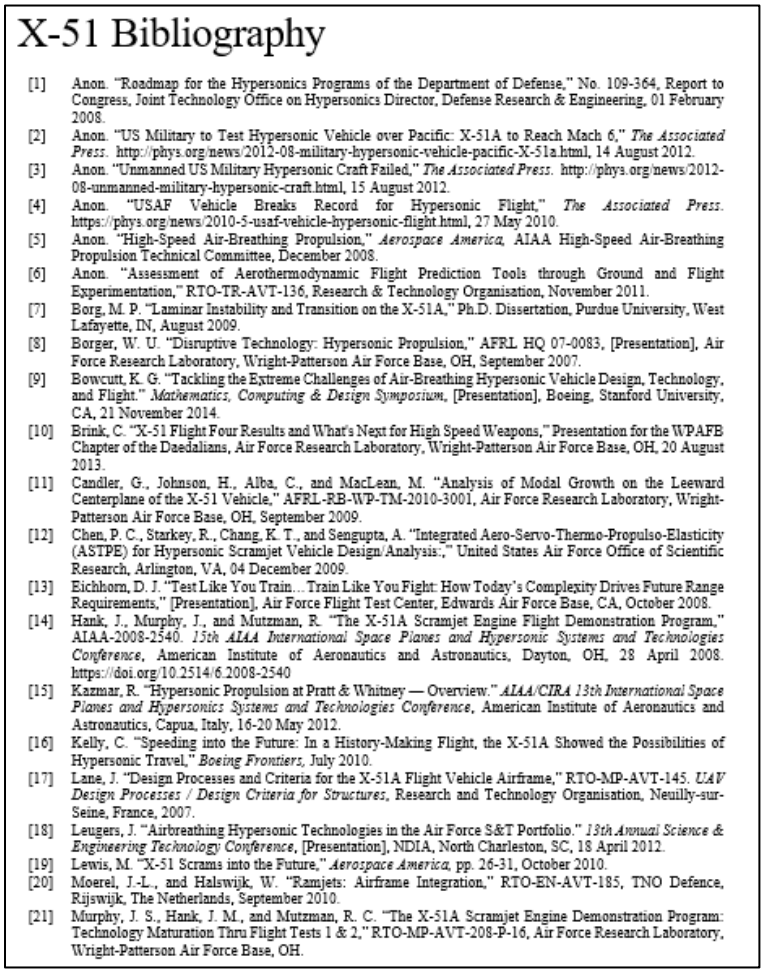

X-51 Bibliography

[1] Anon. "Roadmap for the Hypersonics Programs of the Department of Defense," No. 109-364, Report to Congress, Joint Technology Office on Hypersonics Director, Defense Research & Engineering, 01 February 2008.

[2] Anon. "US Military to Test Hypersonic Vehicle over Pacific: X-51A to Reach Mach 6," *The Associated Press*. http://phys.org/news/2012-08-military-hypersonic-vehicle-pacific-X-51a.html, 14 August 2012.

[3] Anon. "Unmanned US Military Hypersonic Craft Failed," *The Associated Press*. http://phys.org/news/2012-08-unmanned-military-hypersonic-craft.html, 15 August 2012.

[4] Anon. "USAF Vehicle Breaks Record for Hypersonic Flight," *The Associated Press*. https://phys.org/news/2010-5-usaf-vehicle-hypersonic-flight.html, 27 May 2010.

[5] Anon. "High-Speed Air-Breathing Propulsion," *Aerospace America*, AIAA High-Speed Air-Breathing Propulsion Technical Committee, December 2008.

[6] Anon. "Assessment of Aerothermodynamic Flight Prediction Tools through Ground and Flight Experimentation," RTO-TR-AVT-136, Research & Technology Organisation, November 2011.

[7] Borg, M. P. "Laminar Instability and Transition on the X-51A," Ph.D. Dissertation, Purdue University, West Lafayette, IN, August 2009.

[8] Borger, W. U. "Disruptive Technology: Hypersonic Propulsion," AFRL HQ 07-0083, [Presentation], Air Force Research Laboratory, Wright-Patterson Air Force Base, OH, September 2007.

[9] Bowcutt, K. G. "Tackling the Extreme Challenges of Air-Breathing Hypersonic Vehicle Design, Technology, and Flight." *Mathematics, Computing & Design Symposium*, [Presentation], Boeing, Stanford University, CA, 21 November 2014.

[10] Brink, C. "X-51 Flight Four Results and What's Next for High Speed Weapons," Presentation for the WPAFB Chapter of the Daedalians, Air Force Research Laboratory, Wright-Patterson Air Force Base, OH, 20 August 2013.

[11] Candler, G., Johnson, H., Alba, C., and MacLean, M. "Analysis of Modal Growth on the Leeward Centerplane of the X-51 Vehicle," AFRL-RB-WP-TM-2010-3001, Air Force Research Laboratory, Wright-Patterson Air Force Base, OH, September 2009.

[12] Chen, P. C., Starkey, R., Chang, K. T., and Sengupta, A. "Integrated Aero-Servo-Thermo-Propulso-Elasticity (ASTPE) for Hypersonic Scramjet Vehicle Design/Analysis:," United States Air Force Office of Scientific Research, Arlington, VA, 04 December 2009.

[13] Eichhorn, D. J. "Test Like You Train…Train Like You Fight: How Today's Complexity Drives Future Range Requirements," [Presentation], Air Force Flight Test Center, Edwards Air Force Base, CA, October 2008.

[14] Hank, J., Murphy, J., and Mutzman, R. "The X-51A Scramjet Engine Flight Demonstration Program," AIAA-2008-2540. *15th AIAA International Space Planes and Hypersonic Systems and Technologies Conference*, American Institute of Aeronautics and Astronautics, Dayton, OH, 28 April 2008. https://doi.org/10.2514/6.2008-2540

[15] Kazmar, R. "Hypersonic Propulsion at Pratt & Whitney — Overview." *AIAA/CIRA 13th International Space Planes and Hypersonics Systems and Technologies Conference*, American Institute of Aeronautics and Astronautics, Capua, Italy, 16-20 May 2012.

[16] Kelly, C. "Speeding into the Future: In a History-Making Flight, the X-51A Showed the Possibilities of Hypersonic Travel," *Boeing Frontiers*, July 2010.

[17] Lane, J. "Design Processes and Criteria for the X-51A Flight Vehicle Airframe," RTO-MP-AVT-145. *UAV Design Processes / Design Criteria for Structures*, Research and Technology Organisation, Neuilly-sur-Seine, France, 2007.

[18] Leugers, J. "Airbreathing Hypersonic Technologies in the Air Force S&T Portfolio." *13th Annual Science & Engineering Technology Conference*, [Presentation], NDIA, North Charleston, SC, 18 April 2012.

[19] Lewis, M. "X-51 Scrams into the Future," *Aerospace America*, pp. 26-31, October 2010.

[20] Moerel, J.-L., and Halswijk, W. "Ramjets: Airframe Integration," RTO-EN-AVT-185, TNO Defence, Rijswijk, The Netherlands, September 2010.

[21] Murphy, J. S., Hank, J. M., and Mutzman, R. C. "The X-51A Scramjet Engine Demonstration Program: Technology Maturation Thru Flight Tests 1 & 2," RTO-MP-AVT-208-P-16, Air Force Research Laboratory, Wright-Patterson Air Force Base, OH.

Fig. 3.10 First page of two of X-51 bibliography.

3.2.2 Identification, Extraction, and Organization of Vehicle Data

With the bibliography complete, the references are then searched for the purpose of sorting them into the eight (8) primary discipline categories (synthesis, aerodynamics, aerothermodynamics, geometry, weight & balance, performance, propulsion, and stability & control), and to identify and extract primary information along the same disciplines of relevant to conceptual/preliminary design. Example references from the X-51 bibliography sorted into the

primary disciplines are shown in Fig. 3.11. Even though most documents have information that pertains to multiple disciplines, during the sorting process, the references are deposited only under the discipline for which it carries most information. As the references are searched and sorted, the identification of relevant information and the extraction of this information is completed at the same time. For the identification of relevant information, only figures, tables, data, etc. that is useful for conceptual design is considered. For information to be considered useful for conceptual design, it can be of use in any of the 3 phases of conceptual design, parametric sizing (PS), configuration layout (CL), and/or configuration evaluation (CE). This means that higher-order CFD simulations, flight test data, and wind tunnel data are all valid sources of information if the data meets the requirement previously stated. Figure 3.12 shows how the identified information is documented. The information for each vehicle is kept within a single spreadsheet, showing which references have relevant data and which discipline it falls under.

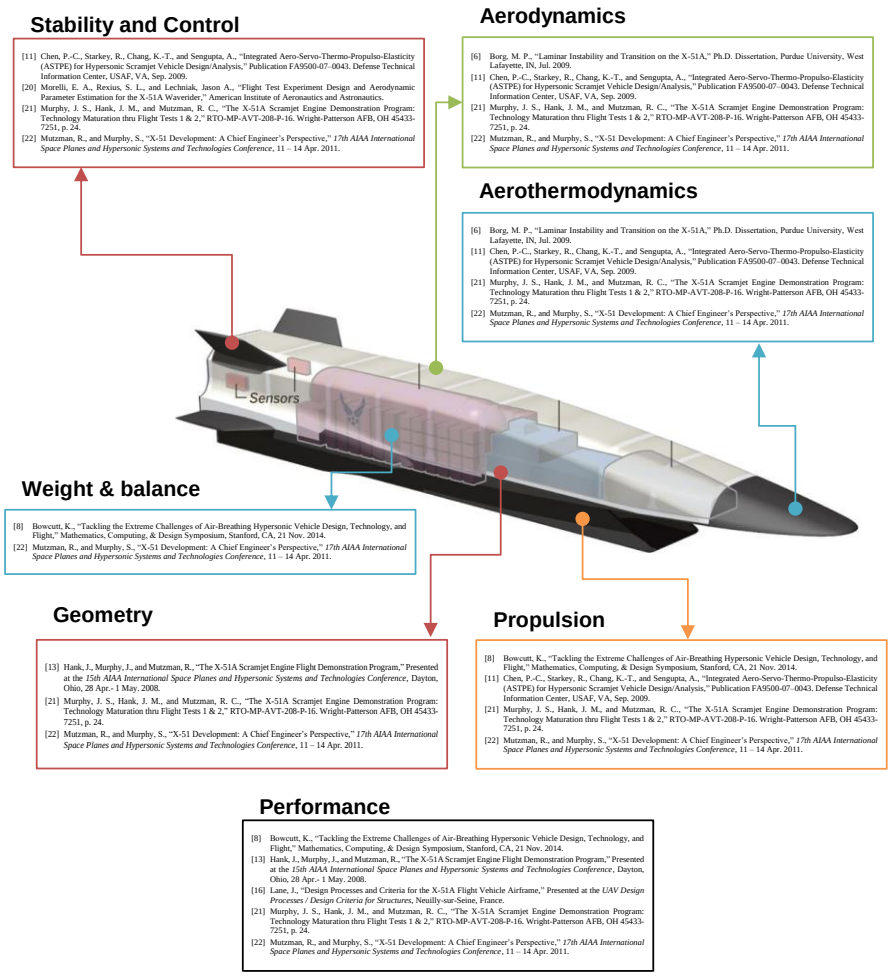

Fig. 3.11 Bibliography separated into primary disciplines for X-51.

Document #	Discipline:	Synthesis	Geometry	Aerodynamics	Aerotherm/TPS	Propulsion	S&C	W&B	Performance
[1]	Data								
	Info					SCRAMBLE subscale reusable scramjet			Typical attributes of cruise weapons
	Knowledge								
	Methods								
	Process								
[2]	Data								
	Info						Failure due to faulty control fin		
	Knowledge								
	Methods								
	Process								
[3]	Data		Length	Mach no					
	Info								
	Knowledge								
	Methods								
	Process								
[6]	Data			Boundary layer thickness, transition Reynolds number, stagnation	Temperature along vehicle span Centerline temperature				
	Info								
	Knowledge								
	Methods			Empirical transition prediction methods, hot-wire anemometry					
	Process								
[7]	Data								General Flight path trajectory
	Info								
	Knowledge	Payload mass fraction vs staging velocity				Isp vs. Mach			
	Methods								
	Process								
[8]	Data		General dimensions, component locations			Scramjet components layout		Operating weight, cruiser launch weight, booster vs interstage weight, fuel weight	Flight test profile
	Info					Propellant fraction required			
	Knowledge					Isp vs. Mach			
	Methods		"GEODUCK"						
	Process	Phoenix Integration's "ModelCenter"							

Fig. 3.12 Excel sheet of identifying primary information in reviewed references for X-51.

As the spreadsheet for the relevant identified information is being filled out, the information is also extracted at the same time. The extraction process consists of cutting out an image using a snipping tool, such as *Screenpresso*, and storing these images in a single location to be accessed after the identifying and extracting process is completed. Examples of some of the extracted data for the X-51 are shown in Fig. 3.13.

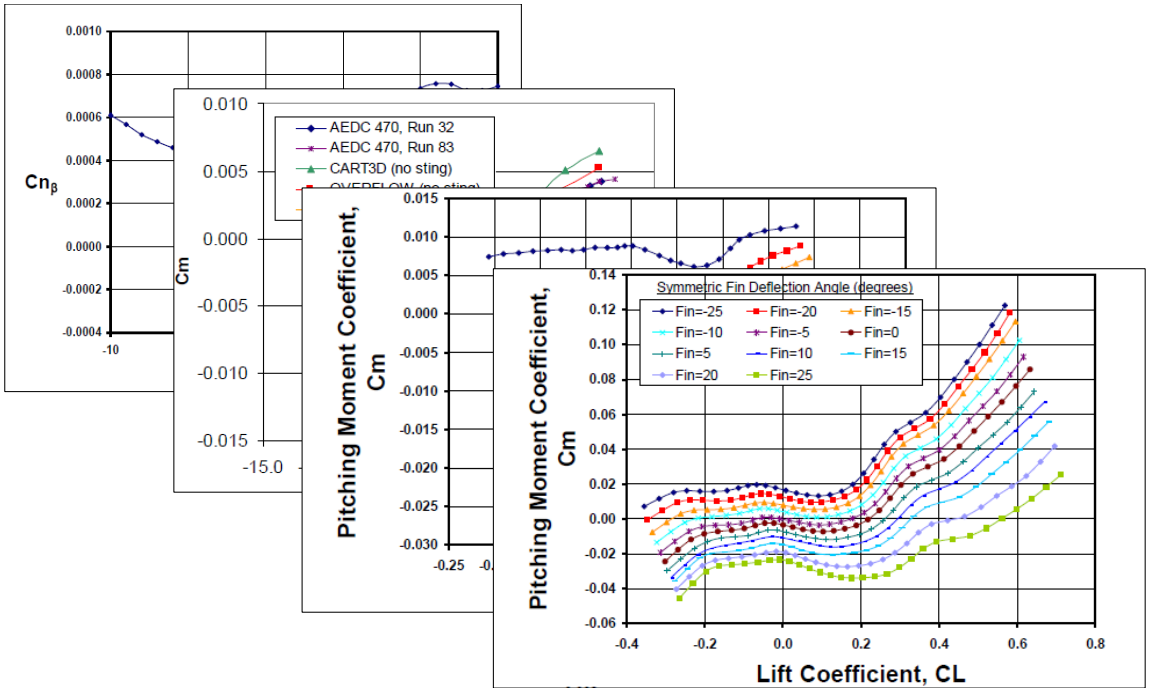

Fig. 3.13 Examples of extracted data for X-51.

3.2.3 Digitization Process

Once all references in the bibliography are reviewed and the relevant data is identified and extracted, the extracted data is digitized. For tables and single point values, these are recreated by simply creating a table in excel and entering the information from the extracted tables into it. Any figures gathered that help show what these single point values are, are added alongside the table, such as a 3-view figure with how dimensions are defined alongside a table of dimensions. For plots, a plot digitizer is required to change a picture of a plot into individual data points along the

trend line, so that it can be re-plotted to show the new digitized plot. The re-plotting of the digitized plot is to compare the original to the new one to make sure that the digitization process was completed correctly and to have a standard way of visualizing these plots. Examples of some of the data that has been digitized for the X-51 are shown in Fig. 3.14.

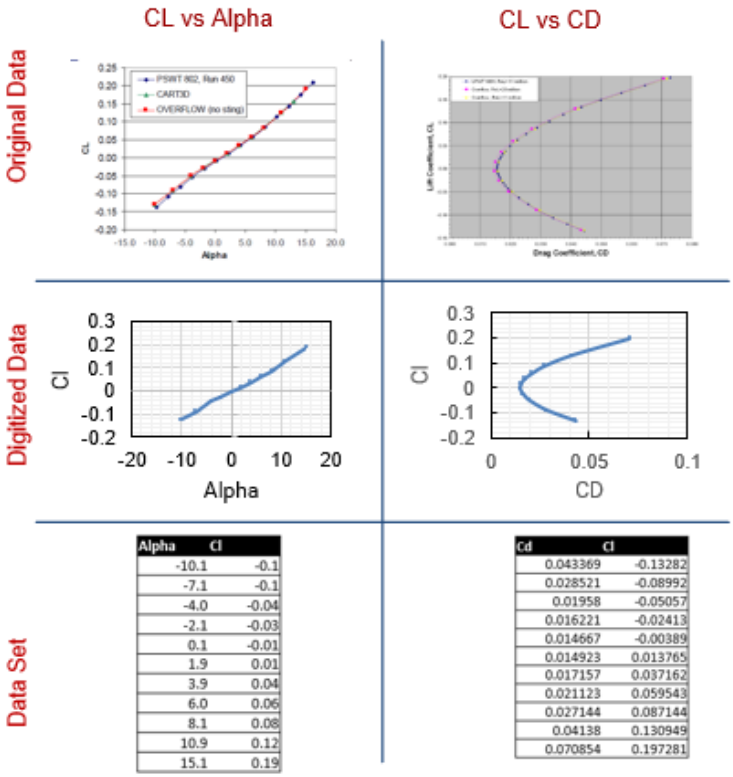

Fig. 3.14 Example of digitization of data.

3.2.4 Storage of Vehicle Data for Database use

With the digitization process completed, the data is then stored in a single location. From this location, the VCC can access the stored information to display and use within the in-development software for the Database and Knowledgebase. It also allows other systems developed within the AVD Laboratory to access this information as well as to use the stored data for verification in case studies, with the latter being one of the main purposes for the Database side of the VCC. The

location selected for this stored data is an SQLite database to allow easier use within the VCC software, and potentially any other software that is developed.

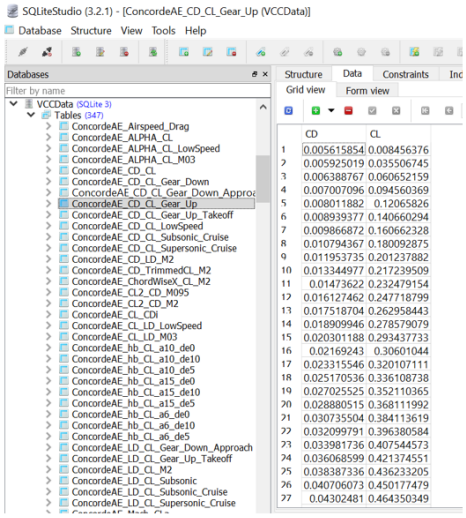

Discipline Codes

SY	Synthesis
GE	Geometry
AE	Aerodynamics
AT	Aerothermodynamics
PR	Propulsion
PE	Performance
SC	Stability and Control
WB	Weights and Balances

Fig. 3.15 SQLite Studio Interface – Data storage with discipline codes.

The digitized data has been stored and organized within the SQLite database as shown in Fig. 3.15. For easy indexing of the data tables, a naming format was selected to make the entered digitized data uniform and to make it easier to call the specific wanted data within the code of the VCC software. The selected naming format is 'VehicleName|Discipline_X-axis_Y-axis_Auxiliary_Information'. The 'Auxiliary_Information' portion of the naming format is only required if clarification is needed. An example for a standard digitized data entry would be 'ConcordeAE_CD_CL', where Concorde is the vehicle name, AE is the Aerodynamics discipline, CD is the drag coefficient being on the x-axis of the original figure, and CL is the lift coefficient being on the y-axis of the original figure. The table within Fig. 3.15 shows the naming/code used for each discipline. When multiple figures have the same x- and y-axis parameters, the auxiliary information comes in to distinguish between them. As also shown in Fig. 3.15, Concorde has several data entries with the 'CD_CL' naming, so they are distinguished with the additional

naming of ‘Gear_Up’, ‘Gear_Down’, etc. This turns the standard data entry of ‘ConcordeAE_CD_CL’ to ‘ConcordeAE_CD_CL_Gear_Up’ and ‘ConcordeAE_CD_CL_Gear_Down’ respectively.

3.2.5 Current Database Statistics

As mentioned during the vehicle selection section in Chapter 1, during the NASA contract in which the majority of this research was accomplished, the 7 selected vehicles were separated between verification and trade vehicles. With the digitized data stored within the SQLite database, statistics can be shown on the data that was extracted and the references that were collected. Statistics for the verification vehicles and the trade vehicles are shown in Fig. 3.16 and Fig. 3.17 respectively.

3.2.5.1 Verification Vehicles

For the verification vehicles, the total number of references assembled is 413 (34 for X-51, 162 for X-43A, 123 for XB-70, and 94 for SR-71) and the total amount of extracted data entries (table, figure, etc.) for all the disciplines for these vehicles is 479 (16 for X-51, 61 for X-43A, 225 for XB-70, and 177 for SR-71). When observing the overall number of references available for each vehicle, the X-43A has generated the most references with XB-70 closely behind. Comparing this to the data richness chart measuring relevant conceptual design data-elements, the references for the XB-70 provided the highest data-richness followed by the SR-71. It is noted that even if a vehicle is documented by many references, this does not automatically translate into high data-richness or usefulness as shown with the X-43A. This can be attributed to publication repetition, overall technical depth covered, and of course the design life-cycle focus of the publication.

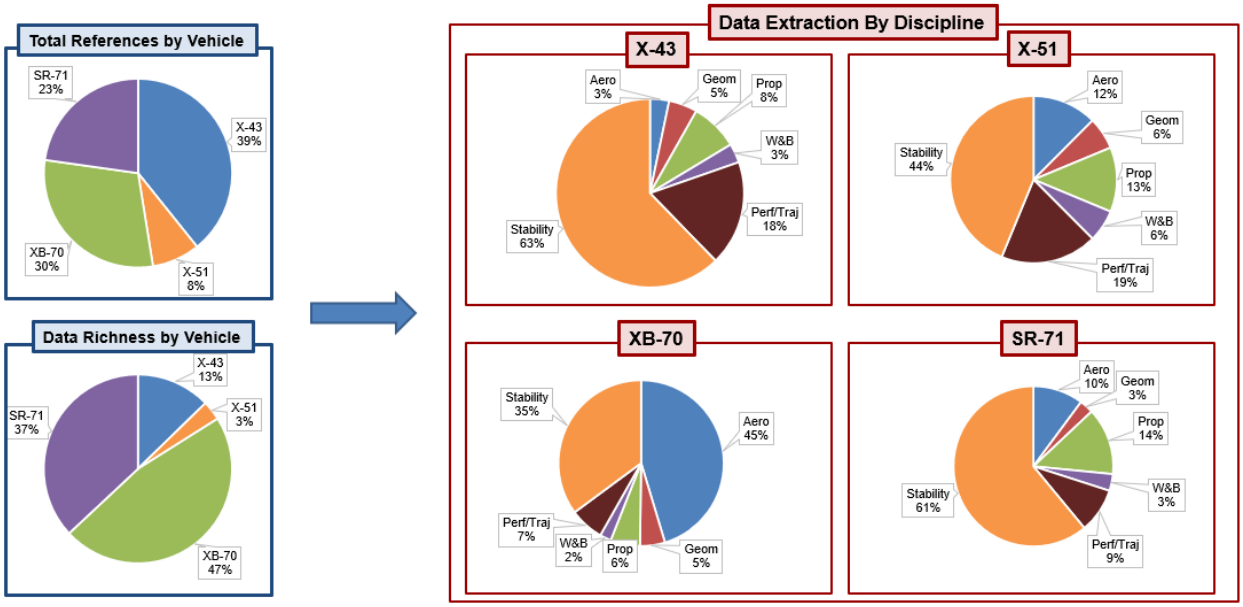

Fig. 3.16 VCC statistics covering number of references and data richness of verification vehicles, and the relevant data-element extraction by discipline [14].

Now looking at the right side of Fig. 3.16, the data extracted by vehicle is broken down to show the percentage of each disciplinary data extracted compared to the total amount of the extracted data for that vehicle. Comparing these breakdowns, it shows that for most of these vehicles, stability & control has the most available data while geometry and weight & balance has the least available overall. The exception is the XB-70 where the most available data is for the aerodynamics discipline. It is noted that while the geometry and weight & balance disciplines have the least available data overall compared to the other disciplines, it may have more useful data overall for conceptual design than the other disciplines. This particular form of data richness, which is separate from the database statistics, is discussed in section 3.2.6.

3.2.5.2 Trade Vehicles

For the trade vehicles, shown in Fig. 3.17, the total number of references assembled is 863 (258 for Concorde, 180 for Sänger HST-230, and 425 for NASP/Orient Express HST-80) and the total amount of extracted data entries for all the disciplines for these vehicles is 529 (121 for

Concorde, 185 for Sänger HST-230, and 223 for NASP/Orient Express HST-80). Comparing these results to the verification vehicles values of 413 and 479 respectively, it shows that over half of all the gathered references and extracted data come from the trade vehicles.

When observing the number of references assembled for each vehicle, it shows that the NASP/Orient Express HST-80 provides both the most references and extracted data. This is in contrast to the verification vehicles where the vehicle with the most refences did not offer the most extracted data. A reason that this may be the case for NASP is because the references are not separated into the several configuration derivatives that the NASP program considered, but all derivatives are pooled into one compendium. Note that most of the references are for the orbital-access NASP vehicle, whilst the specific configuration wanted for the NASA study, the in-atmosphere Orient Express HST-80, only had a couple of references available.

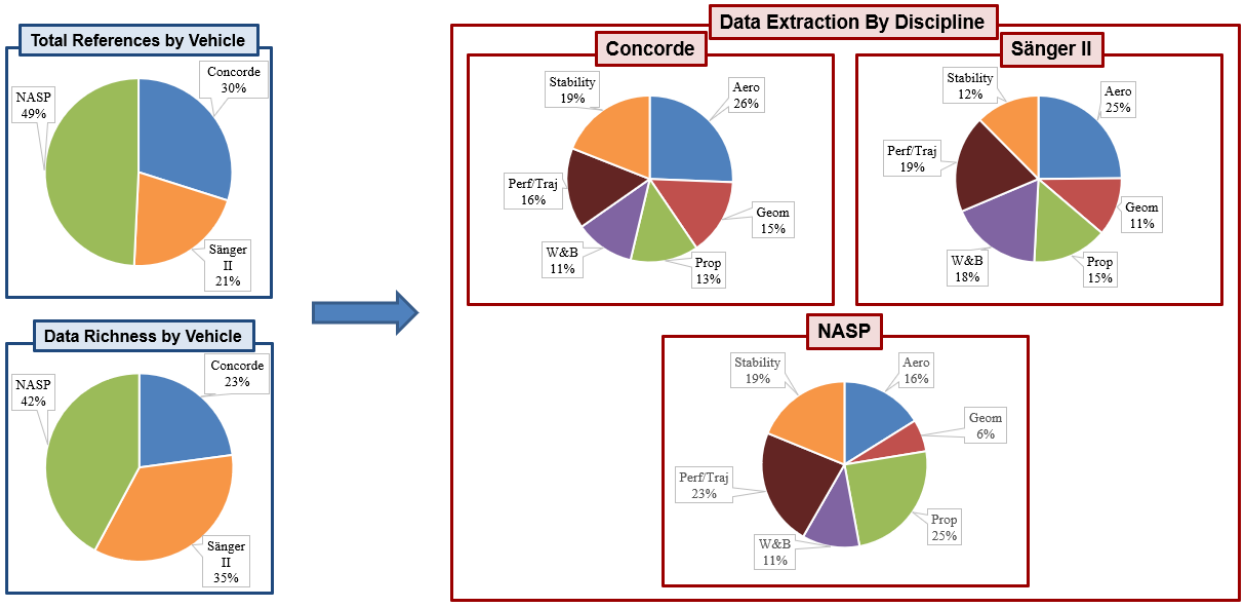

Fig. 3.17 VCC statistics covering number of references and data richness of trade vehicles, and the relevant data-element extraction by discipline [14].

Looking at the right side of Fig. 3.17, the breakdown of the data-elements extracted for each discipline is more evenly distributed when compared to the breakdown of the verification vehicles. While most of the verification vehicles focused on stability & control as the dominant discipline, most trade vehicles focused on aerodynamics in contrast. As with the verification vehicles, these statistics show the amount of extracted disciplinary data with respect to the total amount extracted and do not show how much of these are useful for conceptual design.

3.2.6 Data Richness

While the statistics of the database for each vehicle provides valuable insight into the amount of information available for each vehicle and discipline, to obtain the full picture of the usefulness of the extracted data, the amount for each discipline that is useful for conceptual design must be known. For this research, the parameters that are determined to be useful for conceptual design are the ones that are used within the method and synthesis verification for AVDS, the input deck that runs AVDS, or within systems that assist AVDS, such as *OpenVSP*. A summary of some data for each discipline that was determined to be useful for conceptual design is shown in Table 3.1. This summary is not an exhaustive list and is regularly updated when new data is required.

Table 3.1 Summary of data sought for each discipline (not an exhaustive list).

Synthesis	**Geometry**	**Aerodynamics**	**Aerothermodynamics**
Optimization data	3-view drawings	Lift Coefficient	TPS Materials
Varying engine design studies	Length	Drag Coefficient	Maximum Temperature
Slenderness ratio	Wingspan	Pitching moment	Dynamic pressure
Küchemann's Tau	Height	Lift force	Nose temperature
Vehicle solution spaces	Wing sweep angle	Drag force	Heating rates
Vehicle trade studies	Aspect ratio	*L/D* ratio	Density
	Component layout	Moments	

Taper ratio	Area ruling
Planform area	Angle of attack
Wing area	
Frontal area	
Side area	

Propulsion	**Stability & Control**	**Weights & Balances**	**Performance**
Fuel type	Pitch moment	Empty weight	Mission profile
Fuel consumption	Pitch rate	Takeoff Gross Weight	Maximum velocity
Thrust required	Rolling moment	Dry weight	Range
Thrust available	Roll rate	Fuel weight	Maximum altitude
Pressure ratio	Yawing moment	Payload weight	Separation characteristics for two-stage systems
Inlet area	Yaw rate	Center of gravity shift	Flight path
Mass flow ratio	Sideslip angle	Empty weight fraction	
	Control surface areas	Span loading distribution	

With this list of conceptual design parameters wanted for each discipline, a data richness scale can be determined by comparing these with what was able to be obtained through the gathered resources for each vehicle. This form of data richness has come to be called ‘absolute’ data richness as it is compared to a set list of design parameters. The ‘absolute’ data richness determined for the X-51 is shown in Fig. 3.18.

For the ‘absolute’ data richness, a total value is provided to show how much of all the parameters were able to be gathered, along with a breakdown of each discipline to show how many of the wanted parameters for each discipline were able to be gathered. As shown, the total ‘absolute’ data richness for the X-51 is about 29%, with only aerothermodynamics reaching about 50% of the wanted parameters and 0% being found for propulsion for the individual disciplines. This low data richness value is to be expected for the X-51 as it was a very difficult vehicle to

gather sources for and much of its data is not publicly available. For other vehicles with many resources available, this value will potentially be greater. It is noted that while the parameters being compared to are for AVDS or assisting systems, for the ones that are not found, other methods are selected to determine a reasonable value as a substitute.

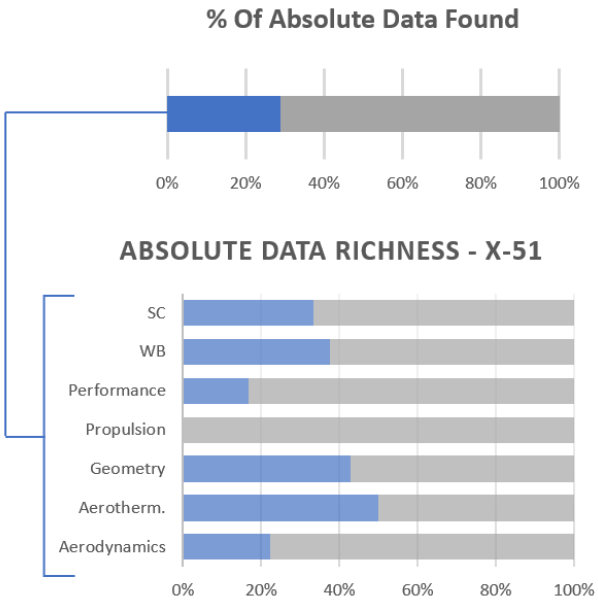

Fig. 3.18 Absolute data richness of X-51.

With the 'absolute' data richness described, and the data statistics previously shown, a full insight into the data richness of a vehicle can be obtained. The data statistics was renamed to 'relative' data richness as it is a measure of how many parameters per discipline against the total amount gathered. This provides a view of the relative weight of the amount of information found for each discipline, but as it does not compare to a set list, only against itself, many of these parameters may not be useful for conceptual design. The 'relative' data richness for the X-51 is shown in Fig. 3.19.

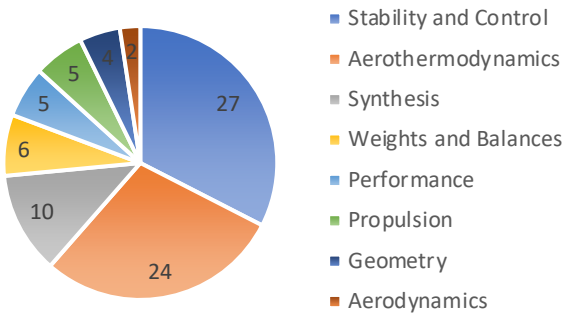

Fig. 3.19 Relative data richness for X-51.

The 'relative' data richness for the X-51 shows that the majority of the gathered parameters are for the stability control discipline closely followed by aerothermodynamics. This now allows the comparison between the 'absolute' and 'relative' data richness. Comparing these two, it is observed that while the stability and control discipline has the most data relatively, it is fourth overall when compared to the wanted list. Also, geometry is second to the least data gathered relatively, but second to the most obtained when compared to the wanted list. This shows the reasoning behind having both data richness scales to provide insight into the data gathered for each vehicle.

These data richness scales are provided for each vehicle within the 'snapshot' mentioned previously for the database as was shown in Fig. 3.2. The 'snapshot' for all 7 vehicles is provided in Appendix C. While it does not necessarily provide insight into the data richness of a vehicle, another figure that is provided within the 'snapshot' for each vehicle is the source breakdown of the gathered references. This does provide a view of the percent number of technical reports and academic papers compared to the news articles and magazines, which may potentially explain why a certain vehicle has a plethora of references, but a low data richness overall. The breakdown of

the sources for the X-51 is shown in Fig. 3.20. The accumulation of these three figures is provided within the 'Data Richness' section of the 'snapshot' for each vehicle in the VCC.

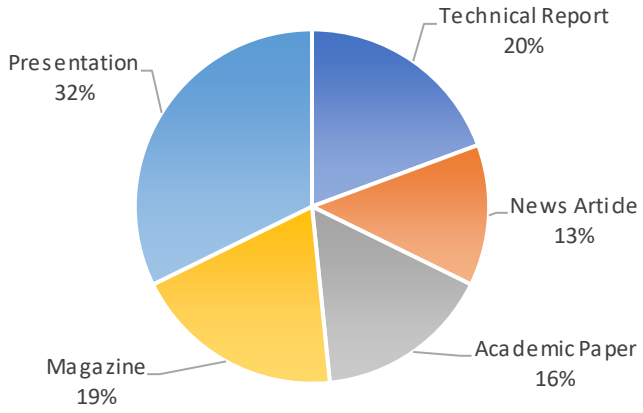

Fig. 3.20 Types of sources found for X-51.

3.3 VCC Alpha Software Development

With the process developed for the background of the VCC, which allows more vehicles to be added in the future, the alpha version of the software can then be developed. This alpha version provides an initial look into how the VCC could look and operate, while testing the usability of the database and the knowledgebase. While not accomplished during this research effort, the alpha version could also be tested in fully integrating with AVDS. The full integration would allow AVDS to pull directly from the VCC's database when running verification studies, or superimpose synthesis results into the knowledgebase for comparison with past vehicles. Currently, the VCC is a standalone system, so these are accomplished manually.

As the VCC software is in the alpha version phase, the graphical user interface, GUI, that is developed may change to make it more visually appealing and/or more user-friendly as more vehicles are eventually added, such as adding a search function, as it goes through the other

development phases of beta, and eventual release, but the overall flow in which it runs should not change. Figure 3.21 below shows the proposed flow structure for the VCC GUI.

As shown, once the software has begun, the user is first offered the choice of 'View Data' or 'Compare Data' which leads them to the database or knowledgebase respectively. If 'View Data' (the database side) is selected, the user is then given the option to select from a list of vehicles, which in this case are the 7 vehicles data is currently extracted for. When a vehicle is selected, the configuration and mission breakdown, along with the data richness discussed previously, and a 4-view of the vehicle is provided in a 'snapshot' as shown in Fig. 3.2. This is a quick overview of the vehicle before accessing the stored data for it. Along with this 'snapshot', a menu is provided that allows the further selection of the discipline that is wanted. Once the discipline is selected, a final choice of either 'View all data' or selecting a specific figure is presented. The 'View all data' option presents every digitized data in an organized manner, while the selecting a specific figure option pulls up the wanted figure and encompasses the full area in which all the data would have shared. This allows users to see what is available, but also to view enlarged views of each figure.

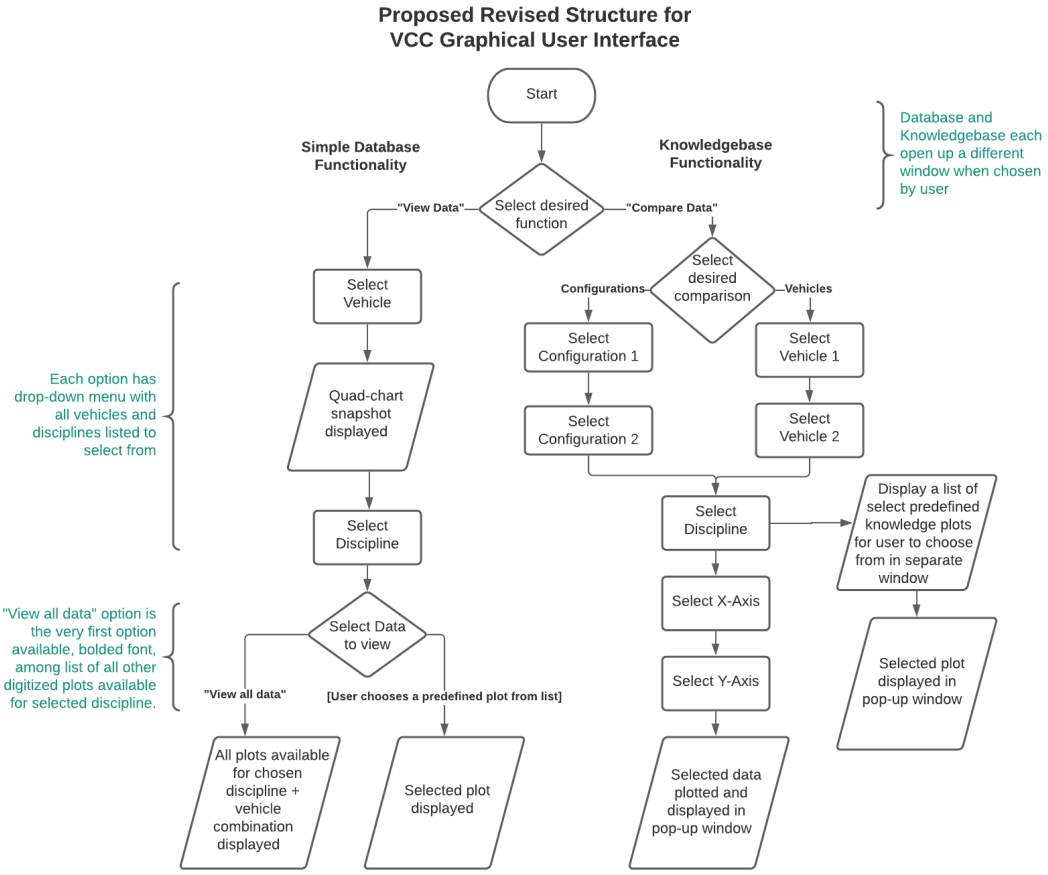

Fig. 3.21 VCC Graphical User Interface (GUI) flowchart.

At the start of the software, if the user selects the ‘Compare Data’ (knowledgebase side) option, then they are first presented with another option in which they can select whether to compare certain configurations or vehicles. Once the selection is made, the user is then directed to select one of the primary disciplines, which give the option to either select from a list of predefined knowledge plots, or to select the wanted x-axis and y-axis parameters related to that discipline if it is not within the predefined list. Either option will display the wanted data in which the user can then learn from the past knowledge or gleam new knowledge through the exploration of parameter combinations and configuration selections.

Using the flowchart above, the software GUI was then developed following its format. It is noted that while the layout for this GUI was discussed and agreed upon by the current VCC researchers, Stenila Simon and the author, the actual coding of the alpha version was completed by Stenila.

At the start of the VCC software, as mentioned in the flowchart, two options are presented which leads to the database side and the knowledgebase side of the VCC. Along with these options, the authenticity statement, or disclaimer, discussed earlier is displayed. This assures the user from the start of the authenticity of the data contained within the VCC and is displayed as such to be clearly visible. These are shown in Fig. 3.22.

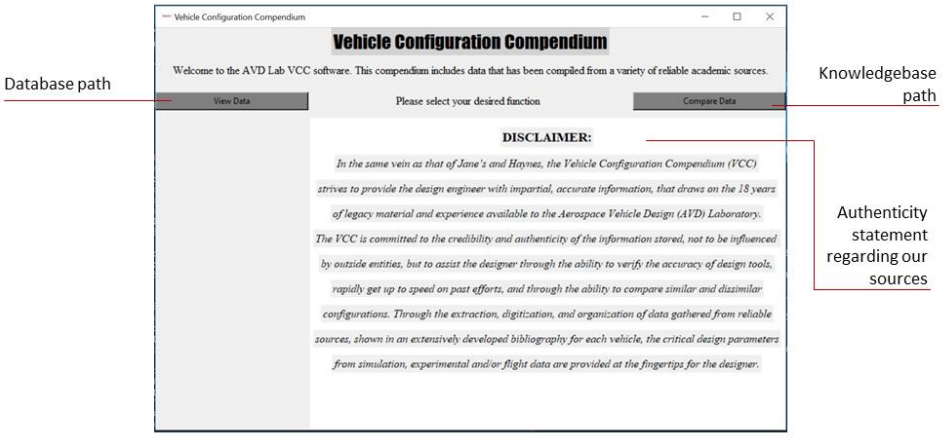

Fig. 3.22 Screen #1 of Software – Viewer chooses between database or knowledgebase path.

Following the database side first, when 'View Data' is selected, a list of the vehicles currently within the VCC is shown on the left-hand side of the GUI. As the alpha version only has 7 vehicles, they are all shown when given the option to select a vehicle, but when more vehicles are added, a drop down menu and/or a search bar can be added for easier viewing of the vehicles stored. This is shown in Fig. 3.23.

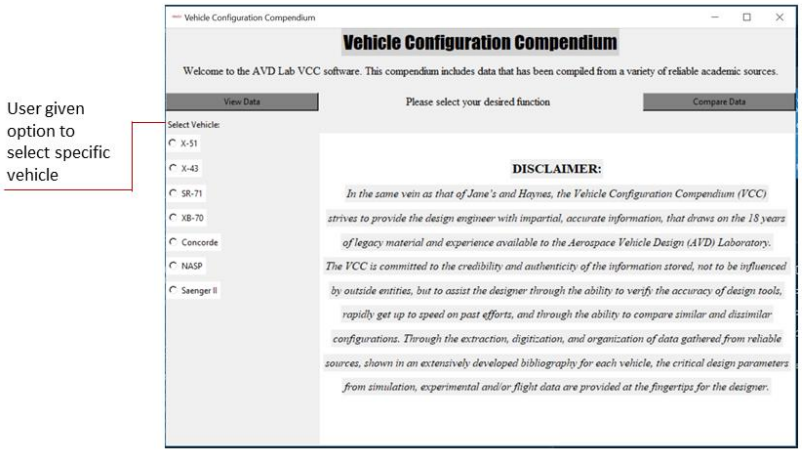

Fig. 3.23 User selects from list of vehicles.

Once a vehicle is selected, a 'snapshot' of that vehicle is displayed, along with a list of the eight primary disciplines on the left-hand side of the GUI. As previously discussed, the 'snapshot' provides a general overview of the vehicle by showing a breakdown of the configuration and mission, a 4-view of the vehicle (3-view plus isometric view), and the data richness that was determined during the entry into the VCC. Within the section that provides the configuration breakdown, named 'Vehicle Overview', additional information such as year it was developed, company that developed the vehicle, etc. Within the 'Data Richness' section, there is a button that can be selected that will display the generated bibliography for that vehicle. These are shown in Fig. 3.24 and Fig. 3.25 respectively.

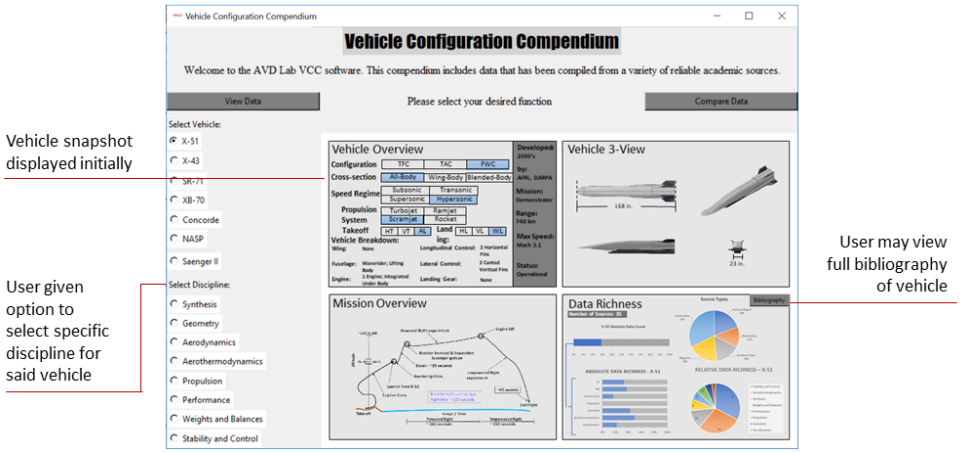

Fig. 3.24 Vehicle 'snapshot' displayed.

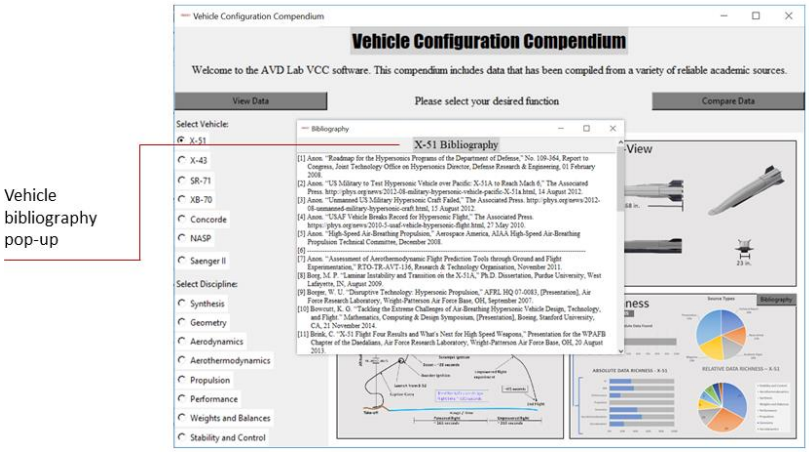

Fig. 3.25 Bibliography displayed.

Finally, after getting acquainted with the chosen vehicle through the 'snapshot', a discipline, such as stability and control, can be selected. When a discipline is selected, and depending on whether the user wants to view all data or a particular figure, the corresponding selection will display the wanted data. Figure 3.26 shows an example of the stability and control discipline for the X-51. As shown, each figure follows a uniform style for visual purposes and organized into a 3x3 grid. Even though it is not shown, if more figures are available for that discipline, the user will currently have to flip through 'pages' with each set presenting a 3x3 grid

of new data until all is shown. Along with each figure, a reference number is provided that is used with the bibliography of the vehicle to show the original source of the data.

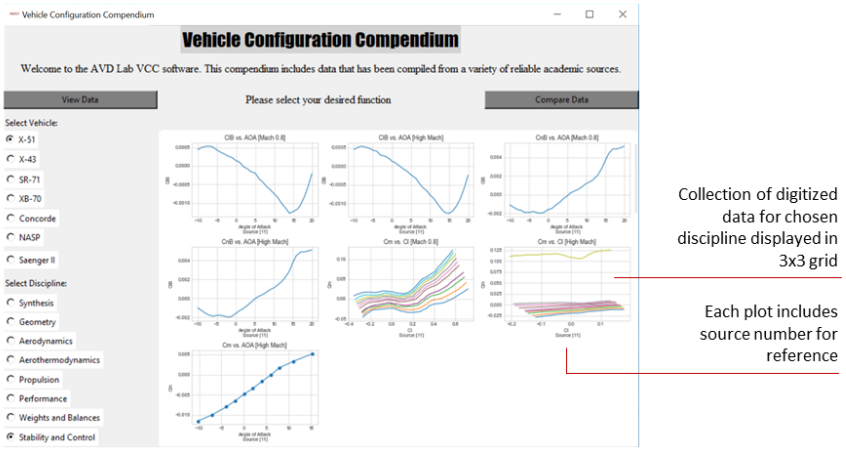

Fig. 3.26 Data displayed for chosen discipline.

Now following the knowledgebase side, when 'Compare Data' is selected, the user is presented the option to either compare vehicle configuration or cross-section. These two are the primary categories in which the vehicles are categorized as previously discussed. If, for example, that the user selects to compare configurations, then a list of the current configurations within the VCC is provided on the left-hand side of the GUI. Each configuration that is selected for comparison then displays a representative diagram with some of the vehicles within that category so the user is made aware of which configurations are being compared and the corresponding vehicles. These are shown in Fig. 3.27 and Fig. 3.28 below.

Fig. 3.27 VCC interface – initiating knowledgebase.

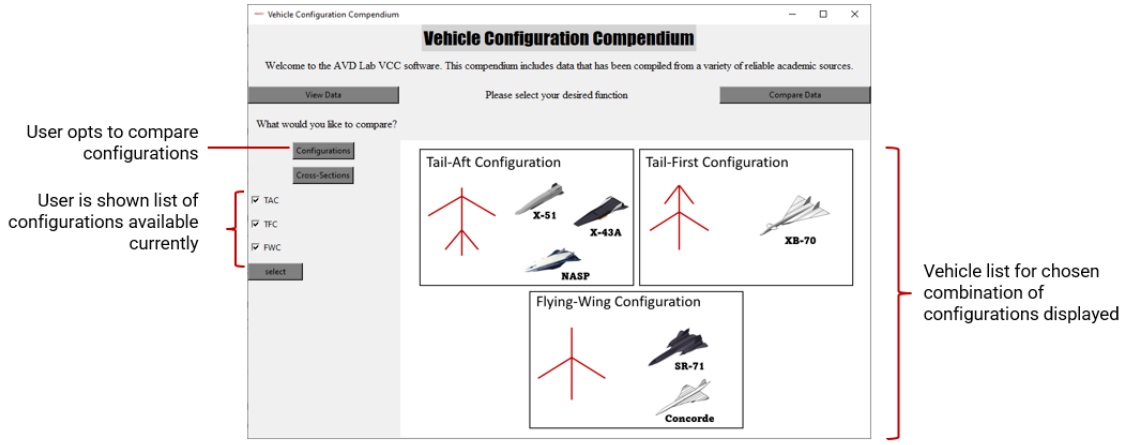

Fig. 3.28 VCC interface – comparing configurations.

After selecting the desired configurations or cross-sections for comparison, a list of the primary disciplines is shown on the left-hand side of the GUI in which the user can select from. When the user selects a discipline, they are able to view predefined knowledge plots, or select parameters for the x- and y-axis that correspond with that discipline. From their selection, the knowledge plot is then displayed as shown in Fig. 3.29. In the case of the predefined knowledge plots, these are annotated with legends that contain configuration/cross-section information so that they can be easily identified, identifiers for which data points are for which vehicle, and any trend that have been observed from the comparison previous. While the selecting of the axes by the user

will provide a legend to indicate which data is for the corresponding configuration/cross-section, any additional annotations as displayed for the predefined plots will not be available as this realm is for exploring possible trends that have not been defined yet.

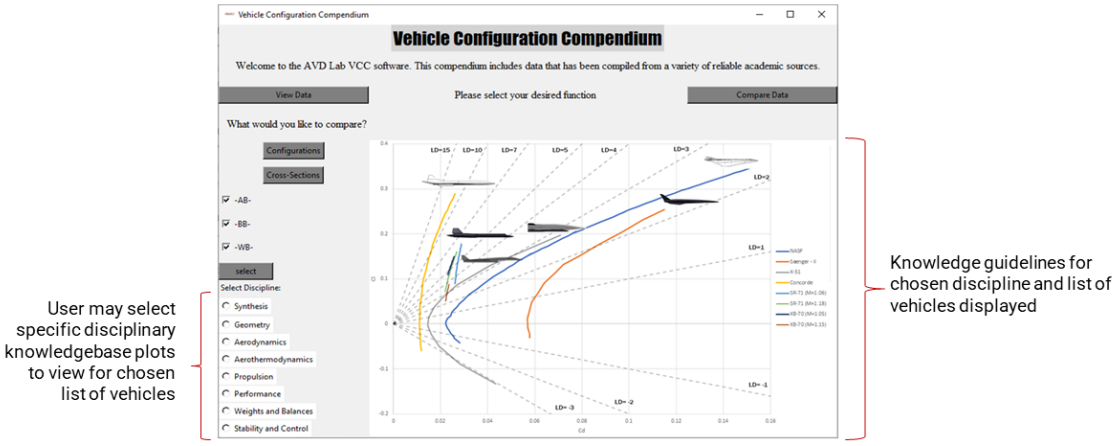

Fig. 3.29 VCC interface – viewing knowledge graphic for a specific discipline.

CHAPTER 4: VSP MODEL CREATION AND USE

4.1 VSP Overview

OpenVSP, or Vehicle Sketch Pad, is a parametric aircraft geometry tool that allows the creation of 3D models which are defined by common engineering parameters. This tool, which was developed by NASA and released as an open-source project in 2012 under NASA's Open Source Agreement [40], is the primary geometry modeling tool used in the AVD Laboratory. This is because with it being a parametric geometry tool, it is useful during the conceptual design phase as it uses common engineering parameters to define the geometry without detailed modeling, such as would be required for *SolidWorks* and *CATIA*.

Other parametric aircraft geometry tools were investigated as well, such as the *Engineering Sketch Pad* (ESP). This tool is a solid-modeling, feature-based, web-enabled system for constructing and modifying parametric geometry [41]. It is like *OpenVSP* but was created for the MDAO community to integrate 3D modeling for multi-fidelity analysis through the conceptual design phase. Another difference is that ESP is a web-enabled system, or also known as a browser-based tool, which uses a web browser such as *Chrome*, *FireFox*, *Safari*, etc., to run the system. This allows easier use as only access to the internet is required without the need to download software, and more portable, as it could even be used on a tablet [41].

While ESP could provide uses that VSP cannot, especially with its web-based system and MDAO potential, VSP is still currently used within the AVD Laboratory. This is because the in-house developed tools were created with VSP in mind, so to switch to ESP would require conversion time. Also, VSP has been used for years within the AVD Laboratory, so time would also be required to build up knowledge and proficiency in another modeling system. This would

be worthwhile if ESP proved to provide better benefits than VSP for the purposes of AVD, but this is not the focus of this research and is set on the next conceptual design geometry researcher.

With this, VSP is used within the VCC and AVDS system. For the VCC, it provides a geometry characteristics compendium, or a library of VSP models, where each vehicle entered allows a complete record of outer mold line geometric data, which contains a combination of verified and synthetic data. For AVDS, the VSP model provides a base for the sizing process of the system, allows methods to be verified using originally unknown values, scaling laws can be generated for each model depending on the trades used within AVDS, and the AVDS synthesis system itself can be verified using these models. These are further discussed below.

4.2 VSP Model Creation Process

Before further discussing the use of VSP within the VCC and AVDS, the process in which these models are created needs to be mentioned. This is because the method in which these models are generated determines how reliable the values that are not inputs into VSP are. For example, the length and span of each vehicle are generally known, but the side area is not. So, while the length and span of the vehicle can be trusted, if the overall shaping of the vehicle does not follow the original or verified against a known value that is not an input, then the side area or other unknown original parameter may not present an accurate representation of its value.

For the shaping of the VSP model, a 3-view of the respective vehicle is used as shown in Fig. 4.1 with the top-view used as an example. The following process will be shown for the top-view, but the front and side view are used as well to shape the front, sides, placement of the wings, tails, angles, etc. Everything that is not available within the extracted data housed within the VCC is provided with the 3-view. An important assumption made is that the selected 3-view provides

accurate proportions, which is verified through the input length and span, that they match the drawing, and through verifying with an output value such as planform area.

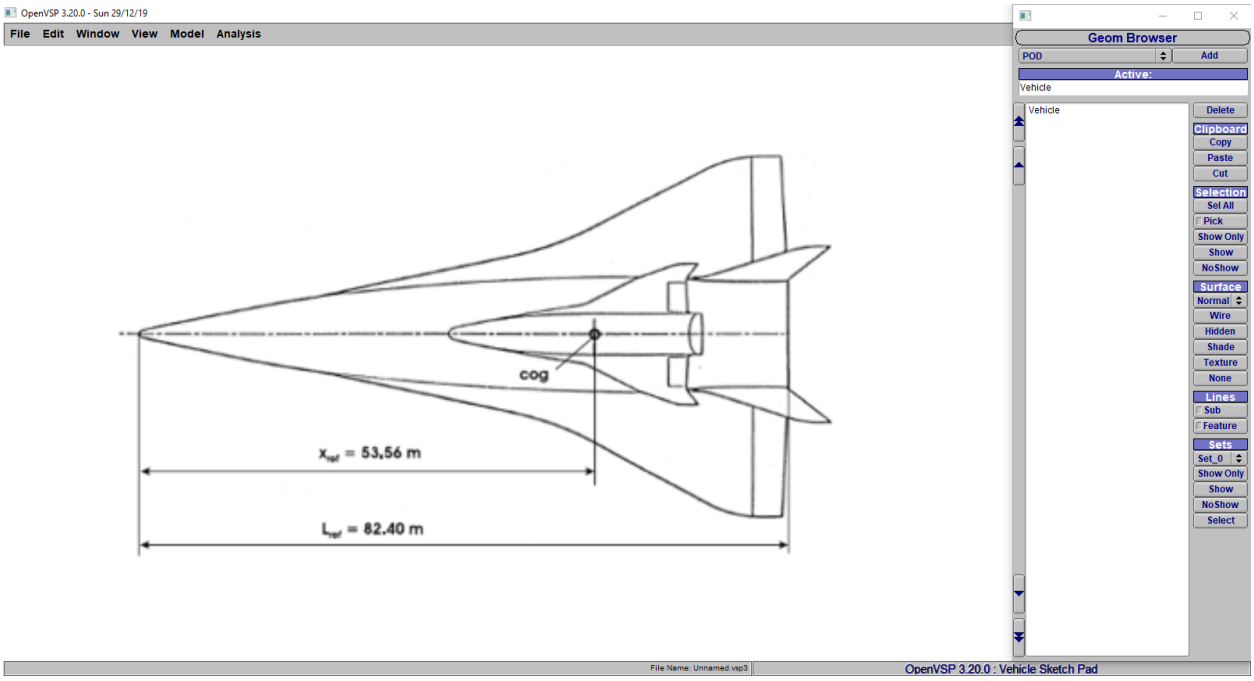

Fig. 4.1 Top-view portion of a 3-view of a representative vehicle for shaping within VSP [42].

For each vehicle, it needs to be broken down into separate parts to be able to model, such as fuselage, wing, vertical tail, horizontal tail, engine, etc. This varies depending on the vehicle, but generally the fuselage is started with and then built off of. Starting with the fuselage, the length of the vehicle is entered into the model and then positioned to match the length of the vehicle as shown in Fig. 4.2. This positioning is to allow the shaping of the fuselage as shown in Fig. 4.3. Once the top-view of the fuselage is complete, then the other views, side-view, and front-view, are used to model the rest of the fuselage.

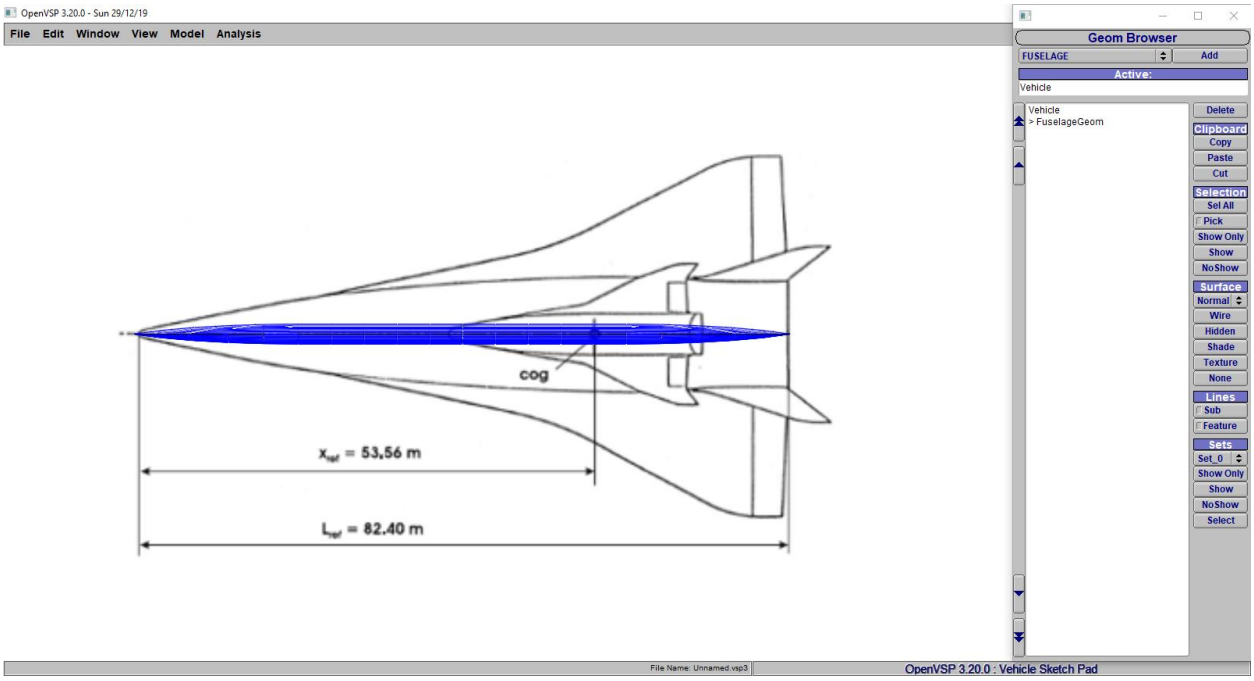

Fig. 4.2 Match input fuselage length of model to top-view of representative vehicle.

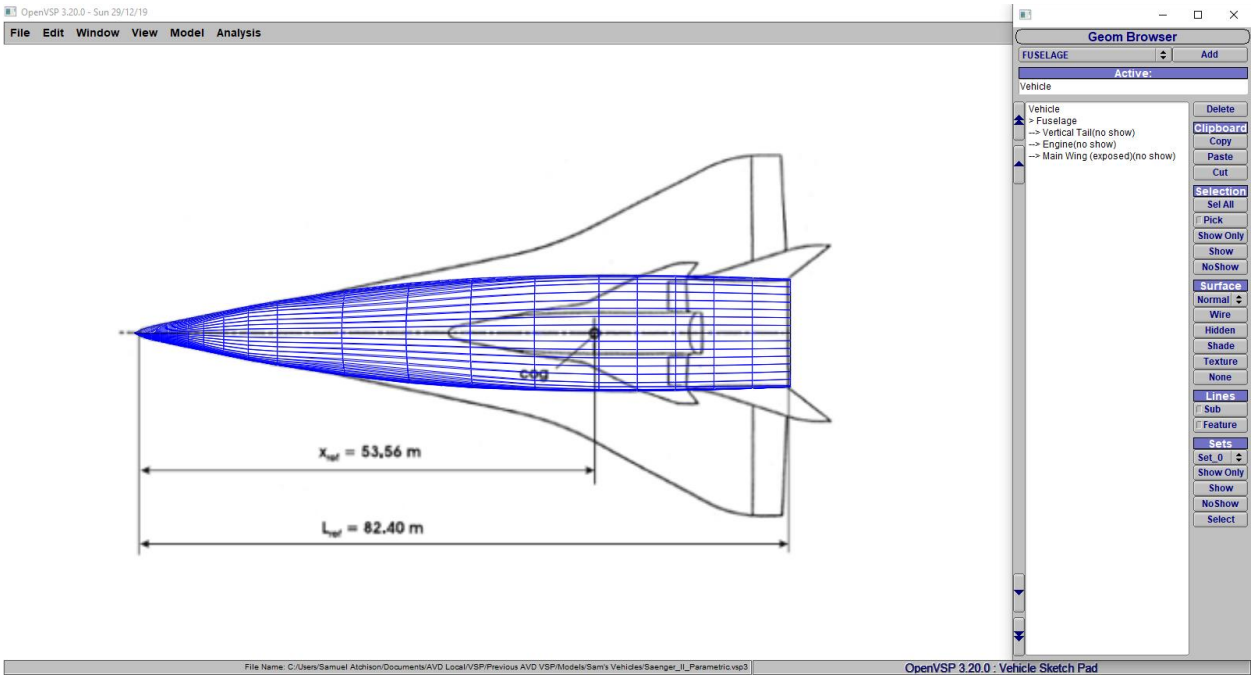

Fig. 4.3 Shape fuselage model to top-view of representative vehicle.

After the fuselage is modeled, then the other components of the vehicle are modeled, which in the case of the example vehicle are the wing, vertical tail, and engine. Figure 4.4 shows the completed top-view of the VSP model of the 3-view. For this model, the length of the vehicle was

known as shown in the 3-view, and the span was known which was provided within the VCC. As shown, the 3-view that was used to shape the vehicle appears to be correctly proportioned as the input length and span match with the drawing.

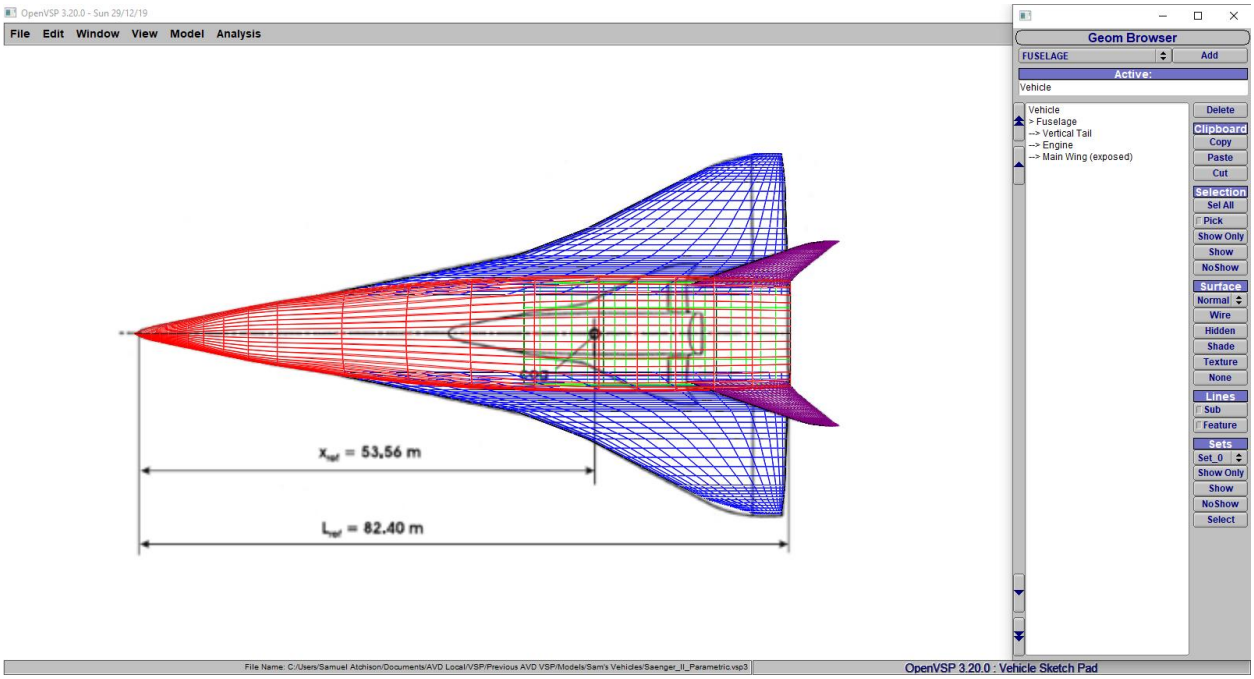

Fig. 4.4 Complete top-view of VSP model compared to top-view of representative vehicle.

Once the model is shaped on all 3-views, it is considered complete, and the model is then verified to the extracted data that was not input into the model such as the planform area. This verification of the model is important as while the model does follow the 3-view, and the inputs appear to be proportioned correctly, some things could still be incorrect with the drawing, or the model was not shaped to perfection, that could produce a large error compared to what the verification value, in this case the planform area, should be. The completed model for this vehicle is shown in Fig. 4.5, along with Table 4.1 showing the verification of the model. As shown, this model is within 1% of the original value, and is therefore considered verified. This means that other unknown geometric values such as the side area, frontal area, vertical tail, and horizontal tail

areas, etc. are deemed to be acceptable substitute values as they should provide an accurate representation of the actual value of this vehicle. This is especially important for method verification within AVDS, as will be further discussed in section 4.4.3.

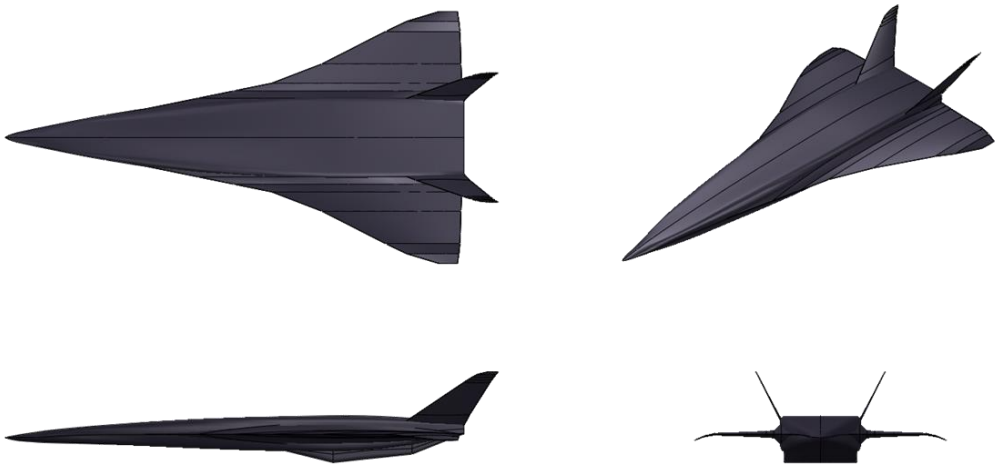

Fig. 4.5 Four-view of the VSP model representing the Sänger II first stage.

Table 4.1 Verification of Sänger II first stage VSP model [43].

	Actual (VCC)	VSP Model	% Error
S_{pln} (m^2)	1,658.0	1,649.8	0.49

4.3 VSP use for the VCC

4.3.1 Geometry Characteristics Compendium

One of the main uses for VSP within the VCC is to generate the geometry characteristics compendium, a geometry model subset within VCC. As most of the legacy geometry information is available through 3-views and/or isometric visuals, this geometry compendium of the VCC will consist of models of each legacy vehicle considered created through VSP with the 3-views as discussed previously. One of the purposes of this compendium is to obtain previously unknown

geometry values for the respective vehicle, such as areas, lengths, and widths of vehicle components. Each legacy model will be verified using the method discussed in section 4.2 above, allowing them to be used to extract previously unknown geometric information with a certain level of reliability. This reliability level is connected to the amount of verification data available for the respective vehicle. The more verification data available, the more reliable the model is and vice versa.

Another use for the models within the geometry characteristics compendium is to represent the foundation from which new design efforts are initiated. This is linked to its use with AVDS and is further explained in section 4.4 below, but briefly, this means that these geometries provide the base geometry of new designs and can be modified for new missions, configurations, update with modern technology, etc. The reasoning behind this is that these geometries provide a base understanding of how they behave, whether through flight tests or research through the development of the concept. This base understanding can then be expanded upon with alternate configurations, such as adding a canard to Concorde, or exploring new missions with the available geometry. While this does produce a new geometry, the base provides a starting point of a familiar vehicle instead of being completely from scratch. An example of some of the vehicles within this geometry characteristics compendium is shown in Fig. 4.6.

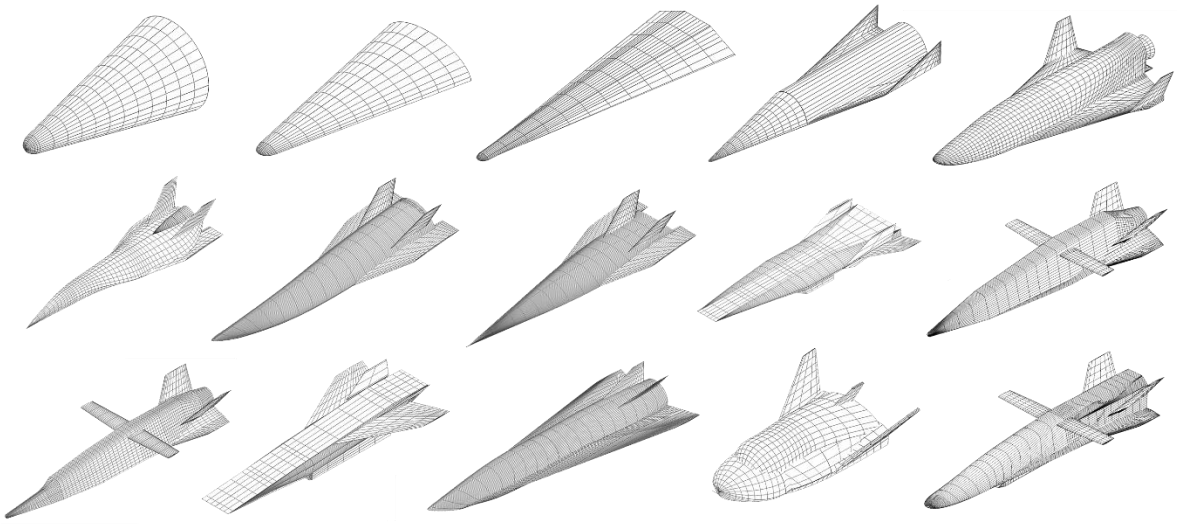

Fig. 4.6 Examples of vehicles within the geometry characteristics compendium.

4.3.2 VCC Synthetic

A future consideration for the VCC but is tied in with the geometry characteristics compendium due to the VSP models, is a concept called VCC Synthetic. One of the main purposes of the VCC is to assist the design engineer by allowing easy access actual data of legacy vehicles in one location for learning about the past, verifying methods, synthesis systems, etc., but most of this information is not available for hypersonic vehicles in the public domain, such as for the X-51. In this case, while some information can be verified, most of the data obtained through the synthesis system is synthetic, or artificial, due to having no way to verify it directly with what is available.

This synthetic data may at first seem unreliable, but depending on the verification process, and how much verification data is available, it may provide an accurate representation of what the value should be. An example is with the VSP model of the vehicle, or the geometry characteristics compendium. The VSP models contained within the geometry compendium are created through known data, such as lengths, spans, and 3-views, and then further verified through outputs such as

planform area, to determine how close the created model is to the actual values. With these verified models, any unknown external geometric information can then be obtained with reasonable accuracy. Using this verified model within AVDS, as will be further discussed in the next section, the synthesis system can be verified for this point allowing other disciplines to generate synthetic data as well.

This leads to VCC Synthetic, where instead of only having the actual data, the synthetic data can be added as well to have a complete vehicle compendium with no missing holes in the information. The actual data will always prevail over the synthetic, and any previously unknown data found later will be used to verify again that the system was correct and then either directly replace the synthetic data or replace and create new synthetic data with the updated information. An example of this is for the X-51. For the X-51, relatively no propulsion data was available, so reasonable assumptions had to be made to allow sizing and verification of the vehicle. As the vehicle was verified to what was known, synthetic propulsive data could then be generated and assumed to be relatively accurate to how the X-51 was flown. If propulsive data is released in the future, then the synthetic propulsive data within the VCC can be compared, verified, and either directly replace the information, or must verify the synthesis system again with the new information. This whole process though begins with the synthetic data within the geometry characteristic compendium, and while VCC Synthetic is not created at this point in time with the main focus being to build an alpha version of the VCC itself, this is a possible future use of the verified VSP models.

4.4 VSP use for AVDS

4.4.1 Base for AVDS Sizing

For AVDS, the VSP model, or the geometry discipline in general, provides the base for the sizing methodology. This is due to all the other disciplines (e.g., Aerodynamics, Propulsion, Stability and Control) requiring some geometric input to function, and that scaling laws are developed using the VSP model for the sizing process. Due to its importance for the sizing process, this increases the need of having verified models to decrease the possible error produced from the synthetic values from the model. It is noted that while this geometry method serves as the base for AVDS in terms of sizing, it is not the same for convergence which has its own requirements to deem a vehicle successfully converged. The convergence requirement is briefly discussed in Chapter 2. A summary of the creation of the geometry method using the X-43A is shown in Fig. 4.7.

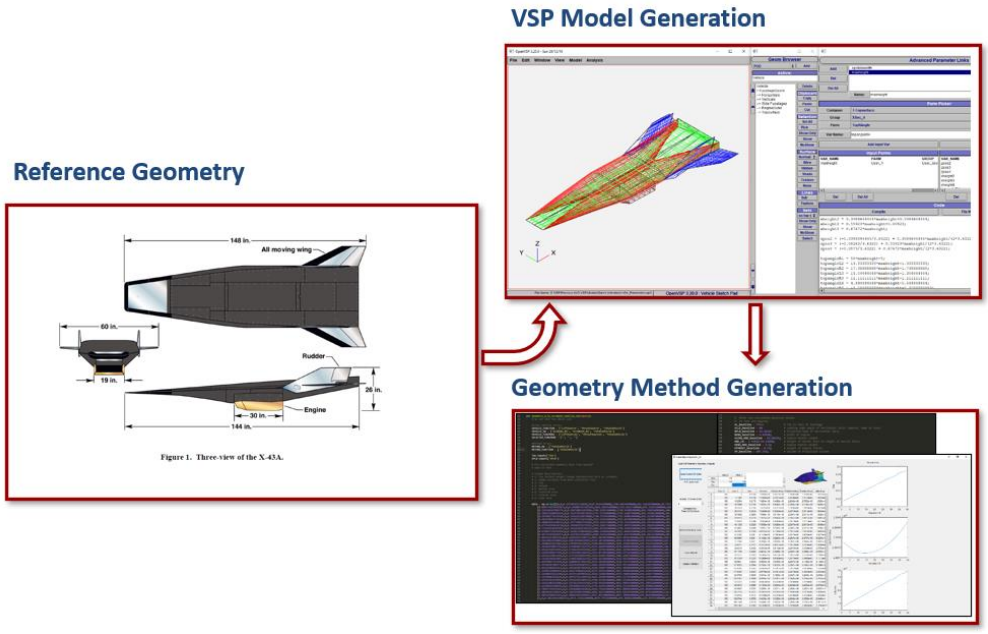

Fig. 4.7 Geometry method creation process for AVDS using X-43A.

The reference geometry and part of the VSP model generation were discussed in section 4.2 where the 3-view of the selected vehicle is used to create the model, and any other available geometric data is used to verify the model. Another part of the VSP model generation is to develop scaling laws depending on the trades explored within AVDS, and to code the model within *OpenVSP* to change depending on the selected scaling. Figure 4.8 shows a larger version of the 'VSP model generation' section of Fig. 4.7 that shows the 'Advanced Parameter Links' module within VSP that allows this.

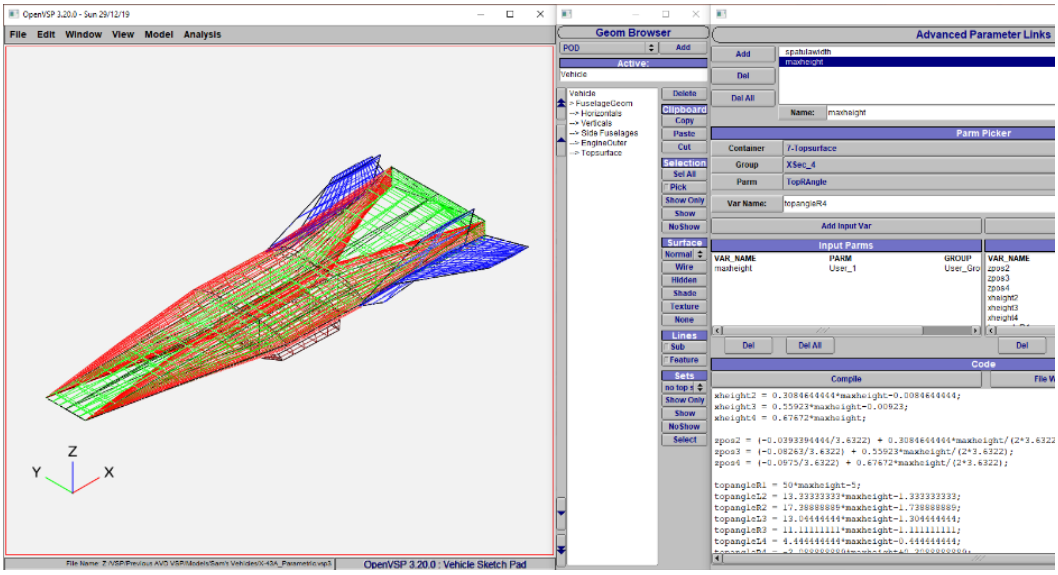

Fig. 4.8 Example of advanced parameter linking for X-43A model.

For the 'Geometry Method Generation' section shown in Fig. 4.7, there are two processes within this final step, 1) generate data maps using an in-house developed MATLAB code by previous AVD researcher James Haley that uses an entered VSP model, varies the geometry through the scaling laws, and extracts wanted information from each model such as planform area, side area, etc., and 2) enter these data maps and other required inputs/outputs within a python code to use within AVDS. Figure 4.9 shows the GUI of the developed MATLAB code. This is the primary process for the geometry method generation as the VSP model and MATLAB GUI allow

for more complex changes with the geometry or configuration without having to determine analytical equations to calculate its effect. Using the VSP models also allows the geometric information used to be from the complex verified geometry model instead of a simplified geometry model.

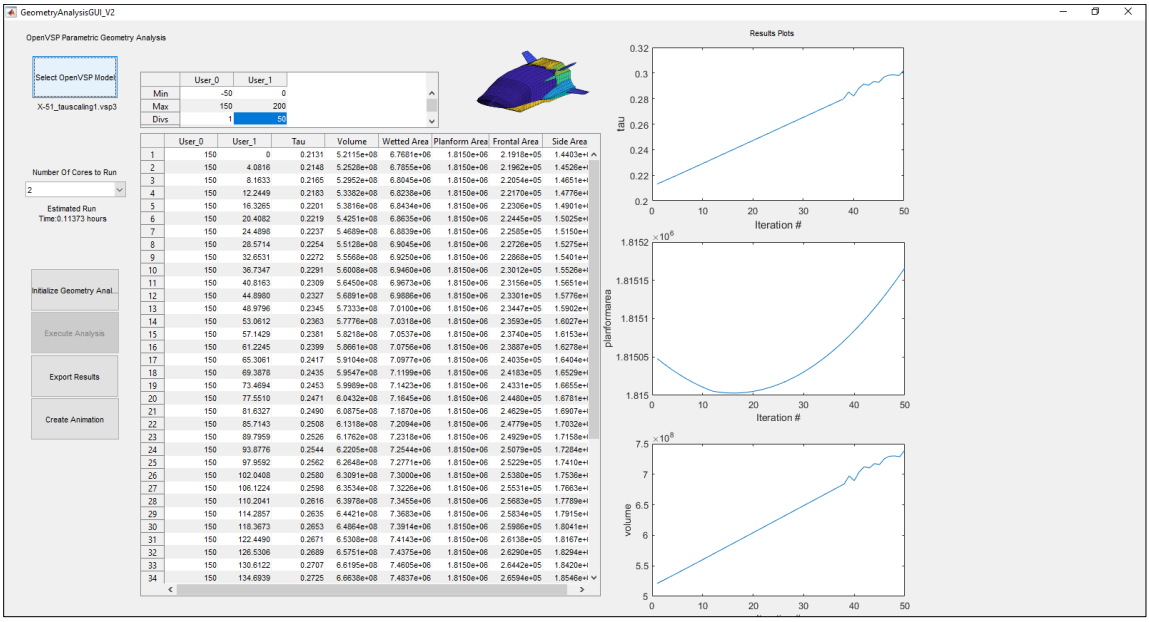

Fig. 4.9 MATLAB GUI for data map creation from VSP models.

4.4.2 Scaling Laws

4.4.2.1 Overview

As mentioned previously, the VSP models provide the base for AVDS sizing due to being able to develop scaling laws for each vehicle depending on the trades wanted to explore in the synthesis system. A scaling law can be defined as:

A law stating that two quantities are proportional, which is known to be valid at certain magnitudes and is used to calculate the value of one of the quantities at another magnitude [44,45].

Before scaling laws could be developed, different types of scaling needed to be investigated to determine how geometric scaling is accomplished to guide the ones created for the

wanted sizing trades. The scaling methods that will be explored can be split into three types, 1) Classical, 2) Modern, and 3) Tau. Classical scaling methods are those that have been traditionally used or established such as square-cube law and photographic scaling, while modern scaling methods are more recent methods developed that may be unique for a certain case or considered a non-traditional method. Tau scaling is a method introduced to the author of Hypersonic Convergence, P.A. Czysz, at McDonnell Aircraft Company that used the cross-sectional geometry of highly swept bodies to increase the volume without significantly increasing the wetted area [39]. These three scaling types are discussed below.

4.4.2.2 Classical Scaling Methods

For the classical scaling methods, the primary ones investigated were the square-cube law and photographic scaling. While the square-cube law is considered a separate scaling law to photographic scaling, these two are usually used in conjunction. This is because photographic scaling affects the square-cube law, and the square-cube law can also be seen as a limit to photographic scaling. Photographic scaling is considered a classical method as traditionally, aircraft companies used this type of scaling as the primary approach for conducting design trades, along with constant gross weight analysis [39]. Using a general aerospace vehicle as an example, photographic scaling would allow an increase or decrease in volume by multiplying a constant factor to all dimensions of the considered vehicle without changing the configuration characteristics. While it would be able to become larger or smaller through this, and thus increasing/decreasing the volume by the cube of the multiplier due to the square-cube law, the wetted area would also increase/decrease but by the square of the multiplier, which in terms of aerodynamics, can greatly affect the drag that is experienced. So, if a vehicle is being scaled as it

requires more volume, only applying photographic scaling to obtain this volume could prove to be detrimental to the size and weight of the design as the vehicle could be unnecessarily large.

Another potential issue with photographic scaling is with the scaling of engines. This is because if an engine is made uniformly larger or smaller, it may or may not perform the way it was designed. While it could be considered that engines can be photographically scaled [46], another solution to consider is that the volume, or space, for the propulsion system could consist of modules of the wanted engine [47]. With these issues of photographic scaling observed, it was determined that it could still be used if it was not the only scaling law used on the considered vehicle/design trade, and that these issues are kept in mind during design, such as making sure the design is not being overly large due to this scaling.

A last example of a classical scaling method is the sizing of the vertical and horizontal tail. The equations to determine the required tail area for the vertical or horizontal tail are shown in Eqns. 1 and 2 respectively. A schematic of how the parameters within these equations are defined are shown in Fig. 4.10 and Fig. 4.11. While these are used for the sizing of these tails, what makes these scaling methods as well are the scaling parameters, or coefficients, of C_{VT} and C_{HT}. The vertical and horizontal tail are scaled by the type of aircraft that they are, such as sail plane, homebuilt, general aviation, etc., as shown in Table 4.2. These coefficients scale the required tail areas as all the other parameters within the equations could be constant between aircraft type, but the coefficient would scale the area to what the type of aircraft, or mission, would generally have. This is a classic scaling method as this process is traditionally how the tail areas are sized/scaled, with the scaling coefficients extending to canard and other different tail types (e.g., T-Tail, V-Tail) as well.

$$S_{VT} = C_{VT}\frac{b_w S_w}{l_{VT}} \quad (1)$$

$$S_{HT} = C_{HT}\frac{\bar{c}_w S_w}{l_{HT}} \quad (2)$$

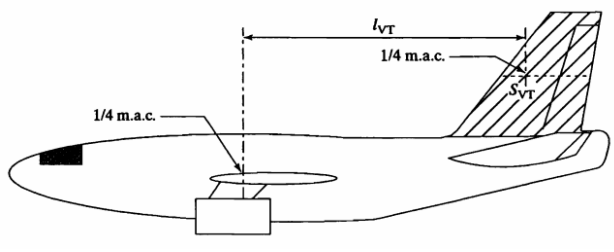

Fig. 4.10 Schematic of parameters to determine the vertical tail planform area [48].

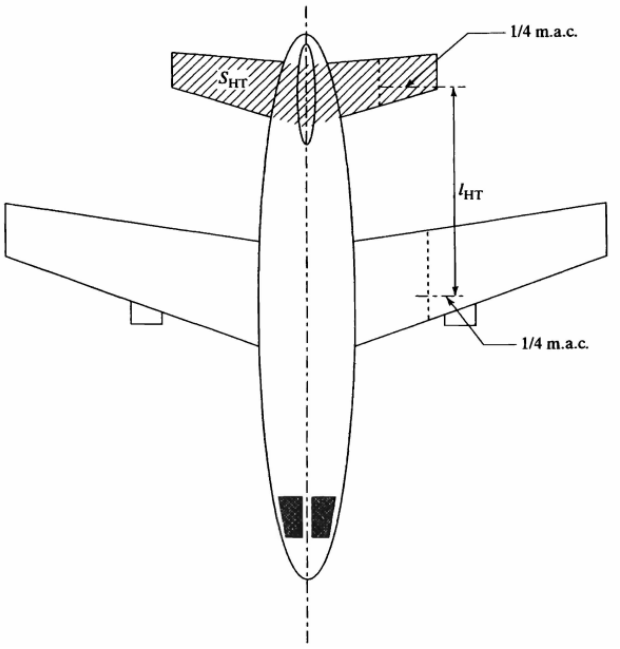

Fig. 4.11 Schematic of parameters to determine the horizontal tail planform area [48].

Table 4.2 Vertical and aft-horizontal tail coefficients [48].

	C_{VT}	C_{HT}
Sail Plane	0.02	0.50
Homebuilt	0.04	0.50
General Aviation (Single Engine)	0.04	0.70
General Aviation (Twin Engine)	0.07	0.80
Twin Turboprop	0.08	0.90
Combat Jet Trainer	0.06	0.70
Combat Jet Fighter	0.07	0.40
Military Transport/Bomber	0.08	1.00
Commercial Jet Transport	0.09	1.00

4.4.2.3 Modern Scaling Methods

For the modern scaling methods, as mentioned, these are being defined as methods that are more modern and/or methods that are not traditionally used to scale the geometric properties of a vehicle, such as the ones described above. While a couple of examples will be shown, it is noted that a plethora of scaling laws could be developed for each of these parameters as, especially in the early phases of design, the vehicles have a high degree of design freedom [49]. This means that the scaling laws that are shown are examples of possibilities of ones that could be used, and they show some of the primary, or dominant, parameters that are considered for scaling.

The first scaling law shown below in Eq. 3 is by Werner and Wislicenus who used physics-based laws and historical data to derive this scale for the vehicle characteristic area (S), such as planform area [50]. The main vehicle drivers for this scaling law are takeoff gross weight (TOGW), aircraft density (ρ), and gravitational acceleration (g). As with the tail area sizing discussed previously, the constant K in this case is the scaling factor, or coefficient, in which the characteristic area is determined from the vehicle class in which it is categorized. Each vehicle considered using this scaling law could have the same TOGW and mass density, but still have a different characteristic area due to its vehicle class.

$$S = K\left\{\frac{TOGW}{\rho g}\right\}^{\frac{2}{3}} \tag{3}$$

The second scaling law shown is a set of scaling laws derived by Raymer for use in vehicle multi-disciplinary optimization [51,52]. These are shown in Eqns. 4 to 7. The main drivers shown for these scaling laws is the wing area (S_w), thickness to chord ratio (t/c), sweep (Λ), and thrust to weight ratio (T/W). Out of these four drivers though, the one that occurred the most is the wing area, meaning that the wing area is a very important scaling parameter. Comparing Eqn. 4 below

to Eqns. 1 and 2 above, these equations determine the same parameter of tail area, but the way they are scaled are different. This shows how different scaling laws can be developed for a wanted parameter. While wing area is used in both scaling laws, the one produced by Raymer requires less parameters as it is only a function of wing area. Even though Raymer's scaling law for tail area has less parameters, it may still produce reasonable results compared to the traditional method depending on the set of vehicles used for the derivation in which the constant value *K* is from.

$$S_{tail} = K_1 (S_w)^{\frac{3}{2}} \tag{4}$$

$$S_{X-section\,max} = K_2 S_w \frac{t}{c} \cos(\Delta) \tag{5}$$

$$Fuel\,Volume_{wing} = K_3 S_w^{\frac{3}{2}} \tag{6}$$

$$S_{wet_{nacelle}} = K_4 \frac{T}{W} \tag{7}$$

An interesting note of these scaling laws is that over half of them are a form of power law. This shows the determination that many observed physical phenomena follow power laws [53], many empirical regressions best fit are power laws [54], and that dimensional consistency is easier when using power laws [49]. This means that when a scaling law equation is being derived, the best starting point is to use a power law. As will be shown when discussing the scaling laws developed for use within AVDS, analytical equations were not derived to determine the vehicles geometric properties after scaling. This is because, while the vehicle is scaled by the created laws, or a process, the laws are not explicit as shown above, as a VSP model is used for scaling and extracting the wanted values. Scaling the vehicle in this way allows more complex scaling and removes the need to analytically determine the wanted values. This only works when using a known geometry as the base for scaling. Even though analytical equations are not derived, the

investigation into these scaling methods provides a foundation of how scaling is traditionally accomplished and what parameters are considered to be the main drivers.

4.4.2.4 Tau Scaling

Tau scaling, as the name suggests, is where a vehicle is scaled by the nondimensional volume parameter tau, τ. This parameter, shown in Eqn. 8 below, was introduced by Küchemann [55] but is credited by him to J. Collingbourne who used it in an unpublished source. Tau was selected to use for scaling as it is an essential parameter relating configuration concept geometric properties across a diverse spectrum of configurations and to the sizing process as Hypersonic Convergence and AVDS converge on volume and weight for sizing [33]. Also, as previously mentioned, it allows the increase of volume of the vehicle without significantly increasing the wetted area, unlike photographic scaling. While it was originally used for highly swept bodies, it is not limited to those configurations. Observing Eqn. 8 in terms of scaling, it is noted that any type of scaling that is not photographic could be considered a type of tau scaling. This is because any disproportionate change in total volume (V_{tot}) and planform area (S_{pln}), would change the vehicle's tau value, while a photographic scaling of the vehicle would not. In the case for AVDS, tau scaling is referred to the deliberate change in a vehicles geometry to match the wanted tau value.

$$\tau = \frac{V_{tot}}{S_{pln}^{1.5}} \tag{8}$$

An example would be if a constant width to a hypersonic cruiser was added to either add, or increase, a spatula width, then the tau value of the vehicle would decrease as the planform area would increase faster than the volume increases. This example is shown in Fig. 4.12 below where a spatula width was added to reduce the wave drag. While this addition changed the tau value, it

was not the purpose of the addition, so it is not considered tau scaling. If the spatula width was added to match a specific tau value though, then it would be considered tau scaling. An example of tau scaling would be if the spatula vehicle wanted the same tau value that it previously had, then an additional geometry parameter would need to be varied to either increase the volume of the vehicle faster than the planform area or increase the volume and keep the planform area constant. An increase in tau using the latter process of increasing volume and keeping the planform area constant by increasing the max height of the vehicle is shown in Fig. 4.13. Using these geometric changes in conjunction, the same tau value of the vehicle before the addition of the spatula width could be achieved by increasing the max height of the spatula vehicle.

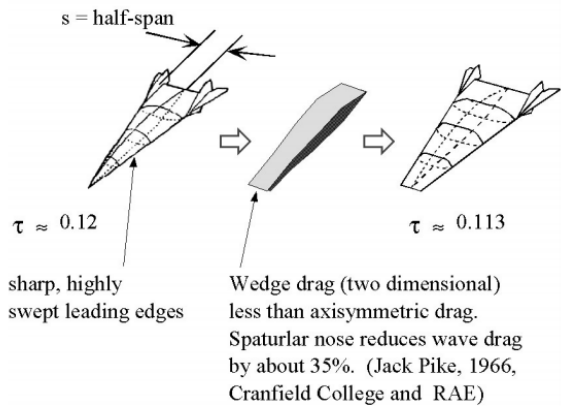

Fig. 4.12 Change in tau with the addition of a constant width section (spatula) into the vehicle [33].

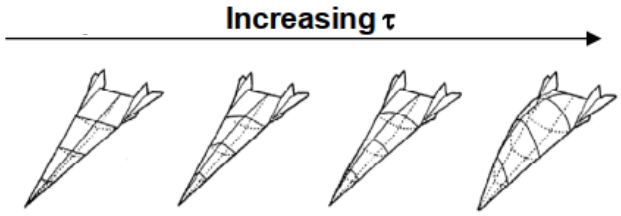

Fig. 4.13 Change in tau with increasing the max height of the vehicle [33].

4.4.2.5 Scaling Laws used with AVDS^{CE}

With the different types of scaling explored, scaling laws were created for each vehicle used within the NASA study. As mentioned, AVDS primarily scales the vehicle by the tau value, so the scaling laws developed keep this in mind. Photographic scaling is still used within the sizing process, but this type of scaling is to provide a starting point in which the vehicle is then tau scaled. The conjunction of these two scaling processes allows the overall volume of the vehicle to increase

or decrease by changing the size depending on the input planform area, and then adjust the volume to match the input tau without changing the size. These two processes are iterated together until a converged volume and weight are achieved. As photographic scaling does not affect the overall geometry configuration, only scaling laws that affect the tau value were constructed. For the seven vehicles below, they can be separated into two categories as mentioned in Chapter 1, verification vehicles (X-51, X-43A, XB-70, and SR-71) and trade vehicles (Concorde, Sänger II, and Orient Express). While all the vehicles went through a verification process within AVDS, the verification vehicles were only used for verification and testing purposes, while the trade vehicles were the main configurations used for the study to create results for NASA. The scaling laws developed for each vehicle reflect the category that it is in.

4.4.2.5.1 X-51

The first vehicle considered for scaling was the X-51. As mentioned, this vehicle belongs with the verification vehicles which used the AVDS^{CE} version, so as the primary function of the verification vehicles was to verify and test the AVDS system, and with it being the first vehicle, only one geometry-parameter was chosen to vary. The geometric parameter considered was the max height, as this is also the parameter used to vary tau, or tau scale, within Hypersonic Convergence as shown previously in section 4.4.2.4. The height ranges from a minimum height to a maximum height and is shown in Fig. 4.14. It also shows that the planform remains constant for the entire geometry-parameter range as only the max height is being changed. This is why, as shown, tau increases with increase in max height as volume is increasing without a change in planform area.

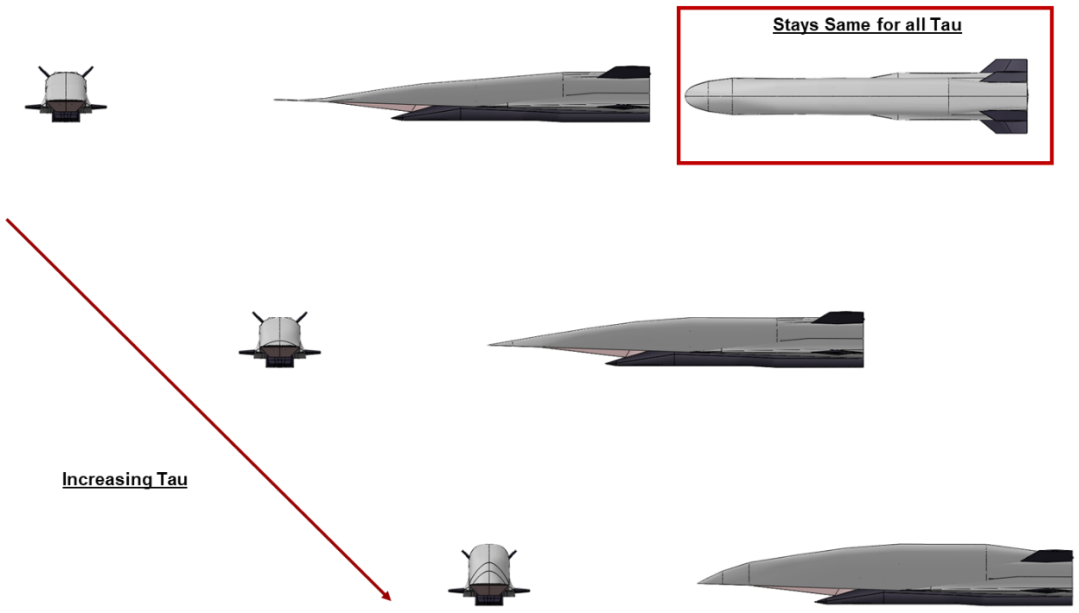

Fig. 4.14 Tau scaling of the X-51.

4.4.2.5.2 X-43A

The next vehicle considered for scaling was the X-43A. This vehicle also belongs with the verification vehicles, but instead of only one geometric parameter varying as with the X-51, two geometric parameters were varied to determine how AVDS would function with multiple varying geometric parameters. The parameters considered were the fuselage height and the spatula width as shown in Fig. 4.15 and Fig. 4.16 respectively. For the height variation, the change in tau is the same as for the X-51 where an increase in height increases tau due to the volume increasing but the planform area remaining constant. For the spatula width variation, both volume and planform are changing, but as shown, tau increases with decrease in spatula width, which means that the planform area decreases faster than the volume does for this geometry. The combination of these two varying geometric parameters creates unique tau scaled geometries to use during sizing.

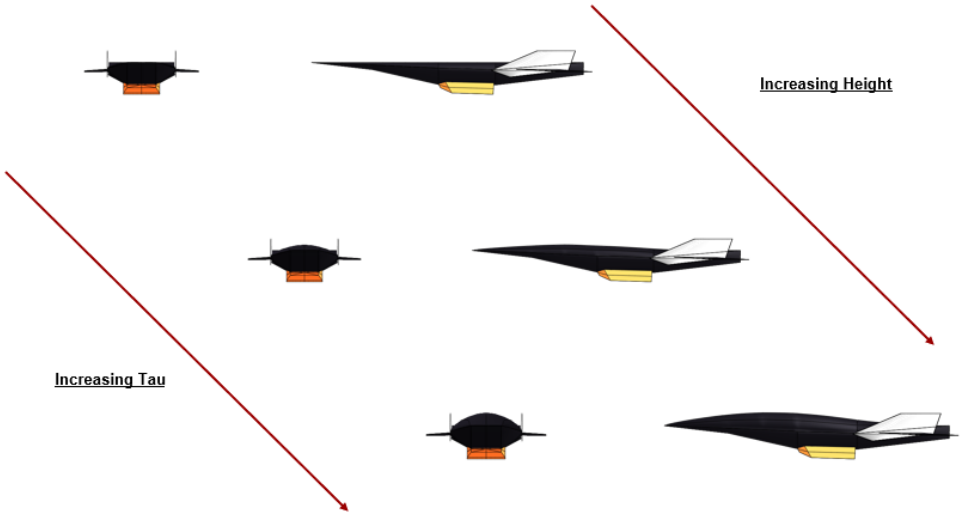

Fig. 4.15 Height variation for tau scaling for the X-43A.

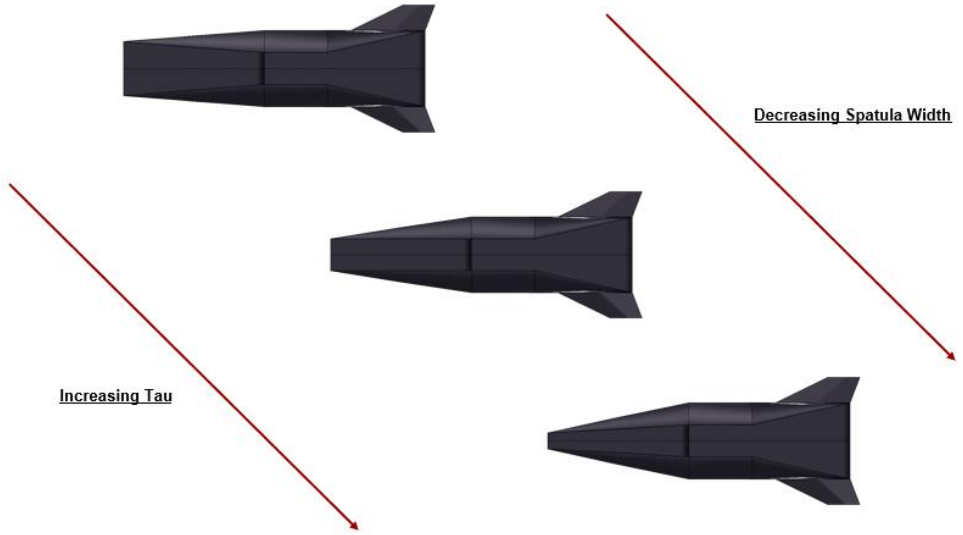

Fig. 4.16 Spatula width variation for tau scaling of the X-43A.

4.4.2.5.3 XB-70 Valkyrie

The next verification vehicle considered was the XB-70. This vehicle was selected due to it having waverider effects (compression lift) and variable drooping wing tips. Initially, the scaling developed for the XB-70 involved increasing the diameter of the fuselage and varying the aspect ratio of the wing. The primary reason that scaling for varying the aspect ratio of the wing was removed was due to the compression lift effects still being investigated, and how it would affect with changes in wing geometry.

Another reason, which is also why the increase in the diameter of the fuselage was removed from the scaling, is that these single or multiple geometric changes were already investigated with the X-51 and X-43A. With this, the geometric parameter that was investigated for the scaling was the variable drooping wing tip. This parameter was considered a form of tau scaling as while the wing tip droop does not affect the total volume (it remains constant), the planform of the vehicle changes. This is shown in Fig. 4.17 below where an increase in wing tip droop angle increases the tau value.

Unlike the previous vehicles, this wing tip droop changes during the flight profile, which means that the tau value is changing as well. This created an issue for sizing as primarily, a tau value is an input, the vehicle is scaled to that tau value, and it remains constant at that tau value during sizing. This is not the case for the XB-70, so a tau value would have to be selected in which the vehicle is sized, and the effects of the wing tip droop must be considered during the trajectory as some disciplinary methods use the tau value as an input as well. The tau value that was selected to size for the input tau is the undrooped wing tips geometry, or 0° wing tip droop, and analytical equations were developed to calculate the changing geometric properties through the trajectory. These equations are shown in Appendix D.

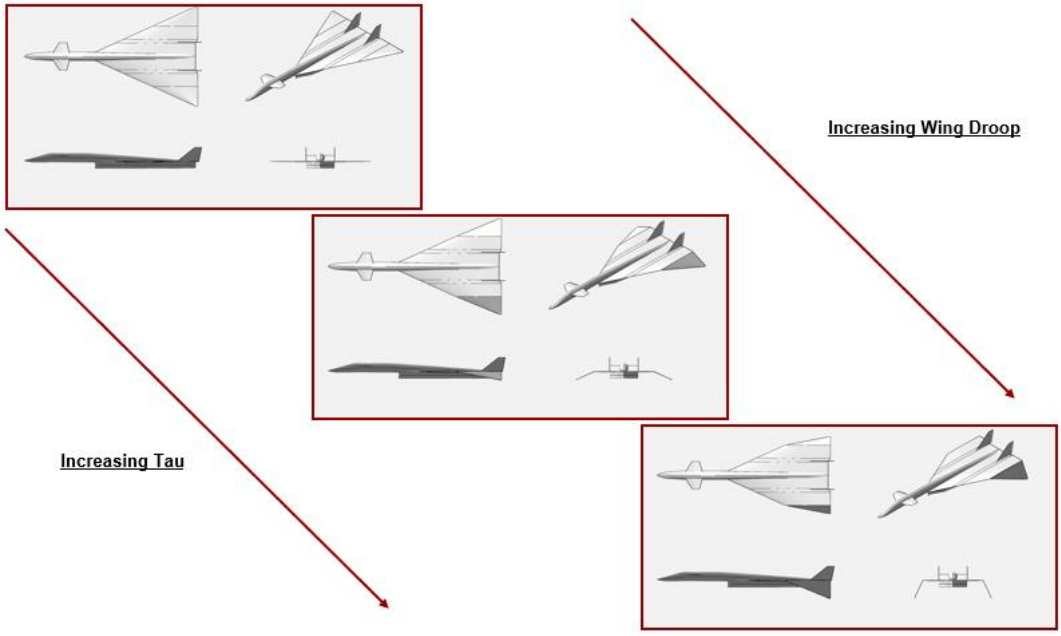

Fig. 4.17 Wingtip droop variation of the XB-70.

4.4.2.5.4 SR-71 Blackbird

The last verification vehicle that was considered was the SR-71. As most of the scaling tests to use within AVDS were accomplished with the previous verification vehicles, tau scaling was not used for this one. This vehicle was still verified within AVDS, but one of its purposes was not to test scaling features as it was for the others. The reason this vehicle was still used for verification is because of its geometry cross-section. As mentioned in Chapter 3, there are three cross-section configurations that vehicles can be separated into, all-body, wing-body, and blended-body. The verification vehicles were also selected using these, as disciplinary methods will vary based on this. The X-51 and X-43A cover the all-body cross-section, and the XB-70 covers the wing-body cross-section, but a blended-body cross-section was required, so the SR-71 was used. This is why the vehicle was still used for verification, to test out the required disciplinary methods to size it, and no specific tau scaling was used.

4.4.2.6 Scaling Laws used with AVDS^{PS}

For the trade vehicles' tau scaling method, it was changed from having independent geometry variations, or having geometry as a separate trade from what is already being conducted such as was done with the verification vehicles, to geometry changes being dependent on the trades conducted for the study, specifically for number of passengers (PAX), and Mach number. This means that when PAX, or Mach number changes, the geometry of the vehicle will change correspondingly, instead of having the geometry change separately from those trades, such as with the spatula width for the X-43A vehicle. The tau value is used as an input as well, but its purpose is the same as that of the verification vehicles where the input tau value is what the vehicle is tau scaled to in conjunction with the other trades.

As these trades, the PAX and Mach number, are not strictly related to the geometry, scaling laws were needed to be created to link these mission parameters to the geometry. First considering PAX, the passenger cabin layout was examined, specifically for high-speed transports, and correlations were created to determine the cabin dimensions as a function of passengers. These correlations are shown in Appendix D. With these correlations, one PAX scaling law was developed for wing-body cross-section configurations, and another for blended-body and all-body cross-section configurations. For the wing-body configuration, the dimensions of the fuselage are limited by the outer dimensions of the passenger cabin, so for the scaling, the relationship between the Concorde fuselage width and passenger cabin width is kept constant, and the height and width of the fuselage is scaled by the passenger cabin width and height for the corresponding PAX. For the blended-body and all-body cross-section configurations, the passenger cabin layout has more freedom on how it can be arranged compared to wing-body vehicles, so only the passenger cabin

volume is used to limit or scale the vehicle size. The required passenger cabin volume is determined by using the passenger cabin geometry correlations.

Next, considering the mission trade of flight Mach number, a leading-edge flow parameter is used to determine how the leading-edge sweep, and therefore the wing, changes with a variation in Mach number [56]. This is completed by keeping this parameter constant, which theoretically means that the flow perpendicular to the leading edge is kept the same. This parameter and corresponding Mach number scaling method is shown in Appendix D.

While both the PAX and Mach number trades contribute to a tau change, these are not considered a tau trade. The tau trade requires an input tau in which the vehicle is scaled to. With this and the PAX and Mach number mission trade inputs, the geometry is first modified by the scaling laws for PAX and Mach number, and then varies a single geometry parameter, such as height or length of the vehicle, to obtain the input tau value, overall generating a differently scaled vehicle for each parameter. Using these scaling laws for the trade vehicles, the scaling of each one is shown below.

4.4.2.6.1 Concorde

Starting with Concorde, which is the wing-body trade vehicle, the process explained above has been implemented. For the PAX trade, the Concorde fuselage diameter to passenger cabin diameter has been kept constant, so that when the passenger cabin dimensions are calculated from a PAX input, the fuselage diameter will increase or decrease to keep the baseline ratio constant. Then, as mentioned, the wing is scaled by keeping the leading-edge flow parameter constant, which means that for a given Mach number, a new leading-edge sweep can be calculated to theoretically keep the flow perpendicular to the wing leading-edge. This assumption of keeping the leading-edge flow parameter constant was determined through the observation that the leading-

edge sweep of the baseline vehicle, in this case Concorde, was selected through its relationship with the cruise Mach number and other constraints, so to maintain these, the relationship between the Mach number and leading-edge sweep was kept constant. Then, after determining the new leading-edge sweep angle with the input Mach number, the rest of the wing geometry is changed by keeping the root chord constant, which allows the span to change with the change in leading-edge sweep. A visualization of the effects of increasing Mach number on geometry and how the overall tau is affected, is shown in Fig. 4.18.

With the PAX and Mach number geometry changes defined, the last input, tau, can be defined. As discussed in section 4.4.2.4, tau is a function of total volume and total planform area. With a furnished tau from the trades and a total planform area provided by the initial guess and iteration of the AVDS system, the total volume of the vehicle can be calculated. Using this approach, the remaining unconstrained geometry parameters are adjusted to match the total volume. This is accomplished through a combination of photographically scaling the wing and increasing or decreasing the length of the fuselage. A visualization of the fuselage length variation along with the effects on overall tau is shown in Fig. 4.19. The minimum length of the fuselage is limited by the determined passenger cabin length and the root chord of the wing. Since the wing-body vehicle has several independently changing geometry elements (each element being able to be considered separate from each other), the MATLAB GUI which has been used to create data maps for the verification vehicles would not work for this case, as too many geometric parameters are being changed. With this, analytical equations were created to calculate the geometric properties of the vehicle with the inputs described above. These equations allow a solver to be used to determine what combination of photographic scaling of the wing and length of the vehicle

is required to obtain the calculated total volume and input total planform area to match the input tau value.

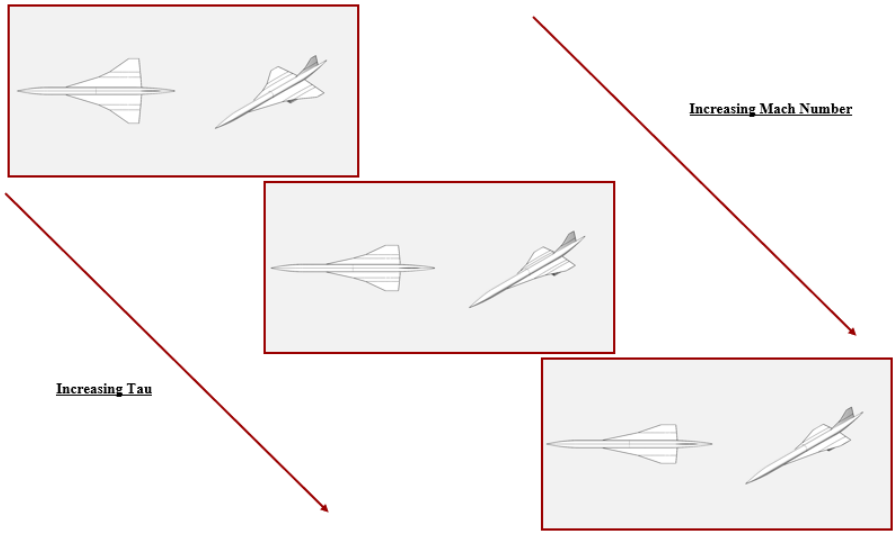

Fig. 4.18 Mach number variation for the scaling of Concorde.

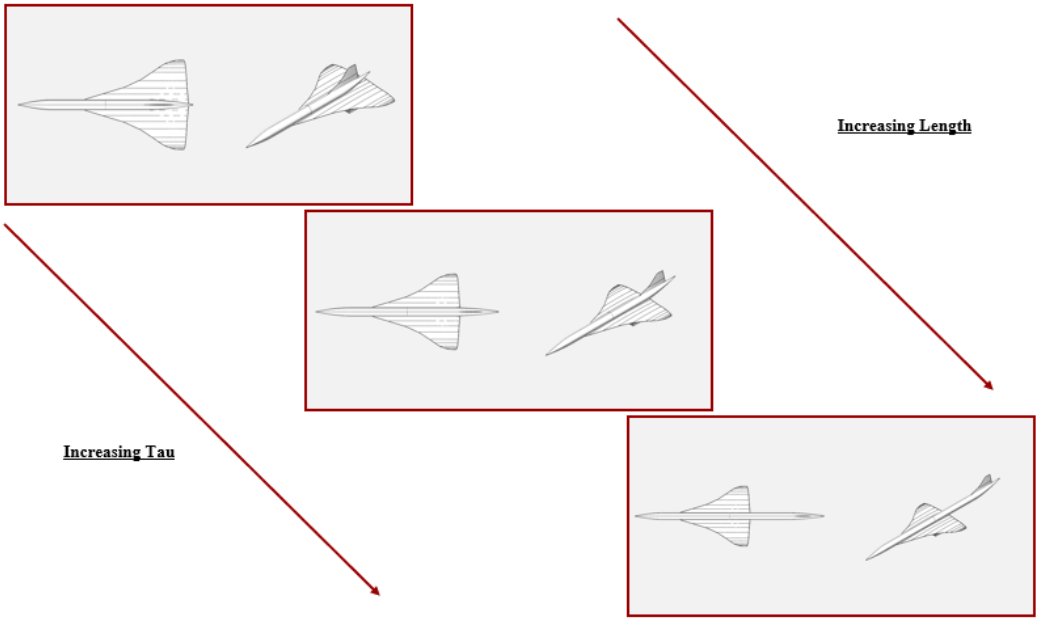

Fig. 4.19 Length variation for tau scaling of Concorde.

4.4.2.6.2 Sänger HST-230

For the Sänger HST-230, the geometry was scaled with the same trades as was used for Concorde, which were the mission trades of PAX and Mach number, and the geometric trade of tau. Since Sänger HST-230 is a blended-body vehicle, the fuselage and the wing are more integrated together than it is for the wing-body. This means that more geometry parameters are dependent on one another for the blended-body compared to the wing-body which means that less constraints are required.

For example, the length of the vehicle for the wing-body cross-section configuration was considered independent from the sizing of the wing, while for the blended-body cross-section this is not the case as the wing and fuselage are integrated together. Since there are less geometry components to constrain for the blended-body, data maps were able to be created using the MATLAB GUI as was used with the verification vehicles.

As mentioned, one constraint on the geometry is that the length of the blended-body vehicle is dependent on the wing size. Then the remaining geometry to be constrained is the overall wing geometry, which includes the span, leading-edge sweep, etc., and the max height of the vehicle. For the wing geometry, the scaling method to constrain these parameters is the same method as has been presented for Concorde, which uses the leading-edge flow parameter by keeping it constant and changing Mach number to define the leading-edge sweep. Then assuming the root chord is constant, the other wing geometry parameters can be defined. A visualization of the wing being scaled with increasing Mach number is shown in Fig. 4.20.

For the main tau scaling, the max height of the vehicle is varied as shown in Fig. 4.21. As with Concorde, even though the wing scaling with Mach number affects the overall tau value of

the vehicle, the wing scaling provides a base tau value, and then the height change varies tau from this base value which is the tau scaling.

As for scaling with PAX, Concorde's cross-sectional fuselage dimensions scaled with PAX, but this is not the same for Sänger. The effects of PAX for Sänger are more of a limit than a scaling method as it was for Concorde. Since the overall vehicle is scaled with the planform area and the height of the vehicle is scaled with tau, the size of the vehicle can be limited to ensure the required PAX volume, along with any other known/sized volumes, will fit inside the sized vehicle.

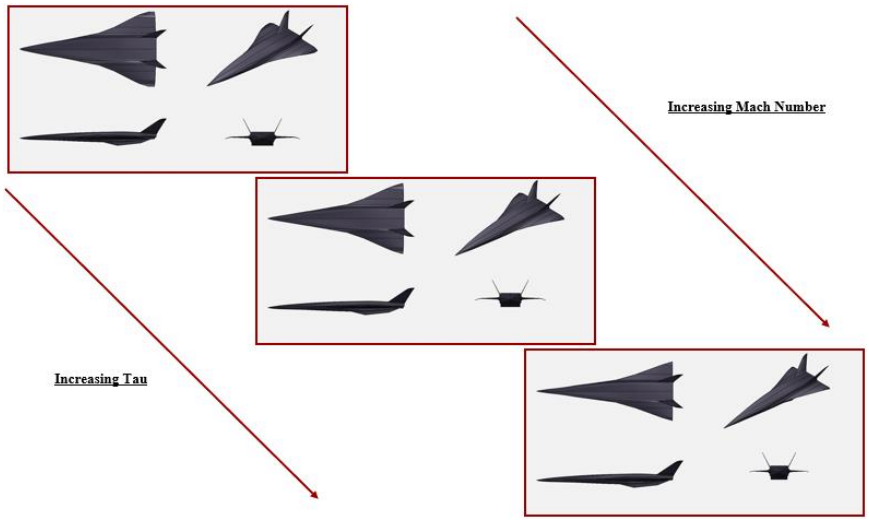

Fig. 4.20 Mach number variation for scaling of Sänger HST-230.

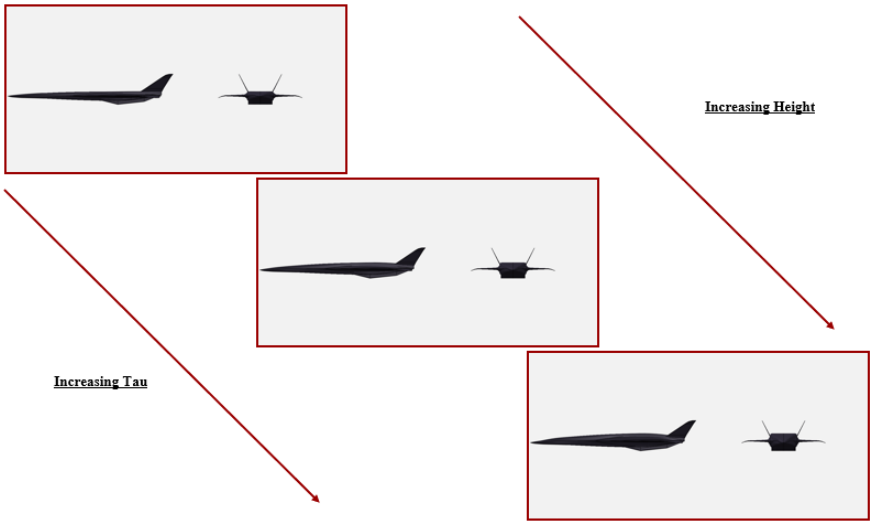

Fig. 4.21 Height variation for tau scaling of Sänger HST-230.

4.4.2.6.3 Orient Express

In terms of the method to constrain and scale the geometry of the all-body vehicle with respect to PAX, Mach number, and tau, the same method used for the blended-body vehicle is used for the all-body vehicle. This is because as with the blended-body, the fuselage and lifting-surface of the all-body are integrated together. Unlike the blended-body though, who does have separate components for the fuselage and wing, but are blended to be indistinguishable, the fuselage of the all-body is the lifting-surface. While it does not have a traditional wing, the geometry parameters to constrain are the same, or the free geometry parameters are the same for the considered trades, so the scaling method between the all-body and blended-body are the same. The scaling with respect to tau for the Orient Express is shown in Fig. 4.22 and Fig. 4.23.

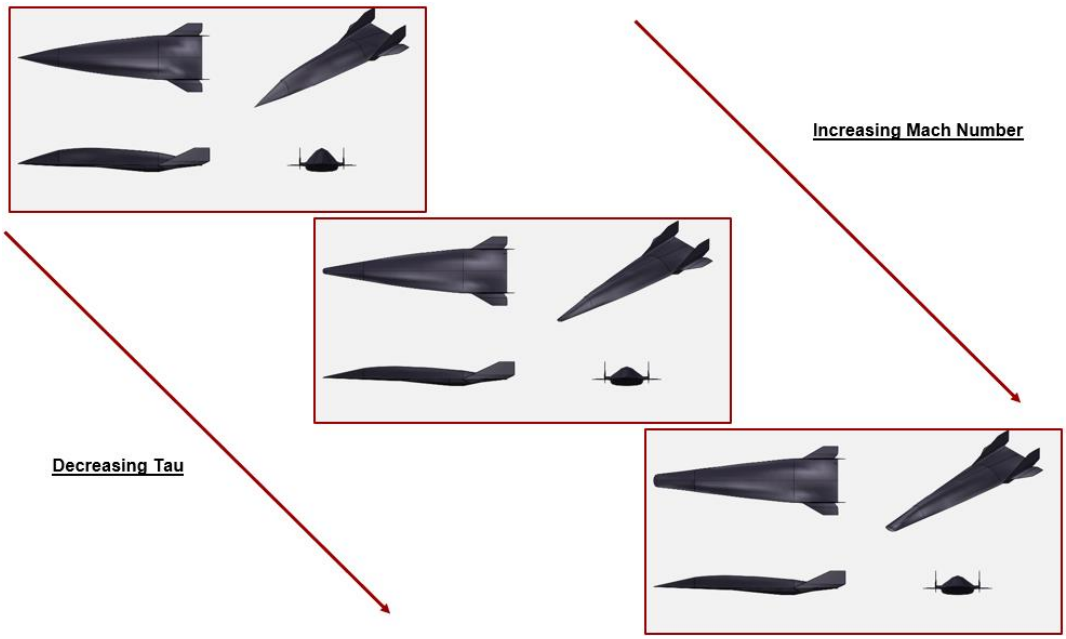

Fig. 4.22 Mach number variation for tau scaling of Orient Express.

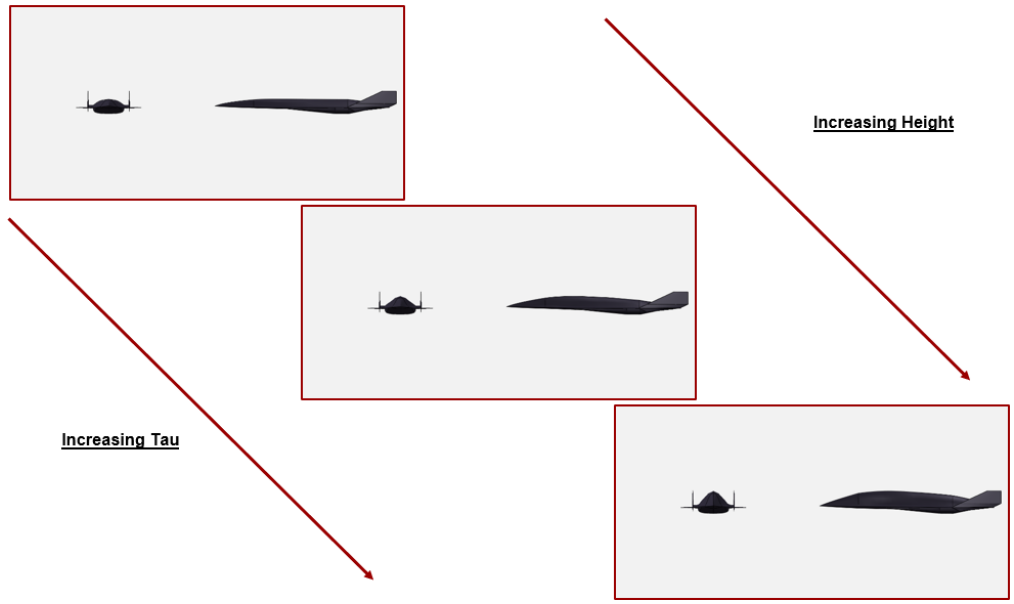

Fig. 4.23 Height variation for tau scaling of Orient Express.

4.4.3 Disciplinary Method and Synthesis System Verification

With the scaling process covered of how VSP can be used to scale vehicles for AVDS, the last main use for VSP within AVDS is for verification purposes which can be split between verification for disciplinary methods and synthesis systems. For the verification of disciplinary methods and synthesis systems, the VSP model is able to help with this through providing geometric information that was not available. As previously mentioned, each model is verified through comparing to known data. The more data available to verify against, the more reliable the model is. With the verified model, any geometric information required can be obtained with reasonable reliability that the value is an accurate representation of the actual value.

For the disciplinary methods, the geometric information extracted from the model is primarily used to run the method to compare to actual known data. An example is if the aerodynamic discipline's method to calculate C_L requires certain geometric data that is unavailable within the VCC, it can use the value from the verified VSP model instead and compare it to the C_L

values stored within VCC. This would then verify the method, but if the actual values were ever found, then the methods can be re-verified with the found data. This leads to the verification of the synthesis system.

For synthesis systems in general, the information extracted from the verified models can be used to compare to the outputs of the synthesis system to determine its verification. While the primary verification for the synthesis systems would come from data of the actual vehicles, the geometric information from the models could provide supplemental verification. This is the case for AVDS where when a vehicle is sized and provides a converged point, the data from the point is verified against actual data from the base vehicle and any other information that could be compared to the model. Complete examples of method verification for each discipline and of the synthesis system for the X-43A and XB-70 are shown in the next chapter, Chapter 5.

CHAPTER 5: VCC METHOD AND SYNTHESIS VERIFICATION

Verification within a vehicle synthesis system is important as the results of the verification determine how trustworthy the results of the synthesis system will be. For a synthesis system, there are methods which calculate the wanted vehicle parameters (e.g., empirical, analytic, numerical), and an overall logic, or solver, which takes these parameters and iterates them until a required convergence is met. While the methods for the synthesis system are carefully selected to match with what is wanted to be solved, such as sizing a commercial airliner, single-stage-to-orbit (SSTO) vehicle, hypersonic cruiser, etc., a method should be selected that calculates the least amount of error when comparing to an actual vehicle. For high-speed vehicles, verifying methods become a problem, especially for hypersonic vehicles, as available data is either scarce or restricted. The problem is increased in that with what data or information is available, the ability to obtain it is not an easy one. Even with the methods verified, the overall synthesis system results need to be verified against actual data as the accumulation of errors within the methods, or how the convergence logic is constructed, may cause excess error, producing invalid results. This is where the Vehicle Configuration Compendium (VCC) comes in with its database system which strives to obtain, contain, and make easily available high-speed vehicle data.

For this chapter, it will be shown how the VCC verifies the selected methods for the synthesis system and the synthesis system itself for two of the vehicles used within the NASA study, the X-43A and the XB-70. The reason these two vehicles were selected is to show how the VCC can be used for verification when a vehicle has very little publicly available data, the X-43A, and when one has an abundance of publicly available data, the XB-70.

5.1 X-43A Methods and Synthesis Verification

Starting with the X-43A, the disciplinary methods that were selected for the synthesis system are shown in Table 5.1 As discussed in Chapter 2, there are two iterations of the AVDS system developed during the NASA contract, the AVDS^{CE} and the AVDS^{PS}. The verification of the X-43A used the AVDS^{CE} version, so the methods were selected accordingly. This section will focus on what was available within the VCC, how that data/information was used to verify the selected disciplinary methods, and how they in turn verified the respective synthesis system.

Table 5.1 Disciplinary methods utilized in the AVDS^{CE} system for sizing the X-43A.

#	Method Title	Discipline	Page #	Last Name	Reference
1	Flight Condition	Environment			
2	Standard Earth Atmosphere Model	Environment	15-116	NASA	[57]
3	Supersonic/Hypersonic Lifting Body Aerodynamics	Aerodynamics	4-16	McDonnell Aircraft Company	[58]
4	X-43A Vehicle Geometry	Geometry	17	Morelli	[59]
			14	Vachan, Grindle, St. John, and Dowdell	[60]
5	Scramjet Lifting Body OWE Estimation	Weights	16	Sverdrup Technology, Inc. (for NASA)	[61]
			79	Czysz	[33]
			4-138	McDonnell Aircraft Company	[62]
6	Scramjet HAP Stream Thrust CEA (GH2 - Air) Look-Up Table	Propulsion	32	Billig	[63]
			151-168	Bradford	[64]
			-	NASA	[65]
			173-180	Heiser, Pratt	[66]
7	Constant Dynamic Pressure Climb	Trajectory	67	Miele	[67]
			374, 375, 421	Roskam	[68]
			266-267	Vinh	[69]
			111	Kundu	[70]
8	Constant Mach Endurance Cruise (used for trade study)	Trajectory	167	Miele	[67]
			266-267	Vinh	[69]

5.1.1 Geometry

The geometry data gathered within the VCC for the X-43A is minimal. The 3-view shown in Fig. 5.1 sums up most of the available geometric data, with the only other parameter found being the planform area which is 36.14 ft^2 or 3.36 m^2 [59]. For the geometry method, a model is created of the respective vehicle using NASA's open-source parametric aircraft geometry tool called *Open VSP* (Vehicle Sketch Pad), which will be referred to now as VSP. Using the available data as inputs

within VSP, and assuming the 3-view shown is proportionally accurate, a VSP model has been created as shown in a 4-view in Fig. 5.2. As the geometric parameters shown in the 3-view were used as inputs within VSP, they are not free to use as points of verification, this means that the only available data point for verification is the planform area. Comparing the VCC value to the model generated value as shown in Table 5.2, the error produced is less than 5%, which means that the model is deemed sufficient for use. This created model does not only serve for the geometry method but is also used when geometric information is required for other disciplines, but not available, so keeping the error as low as possible to what is available, will reduce the error introduced initially into the other disciplines.

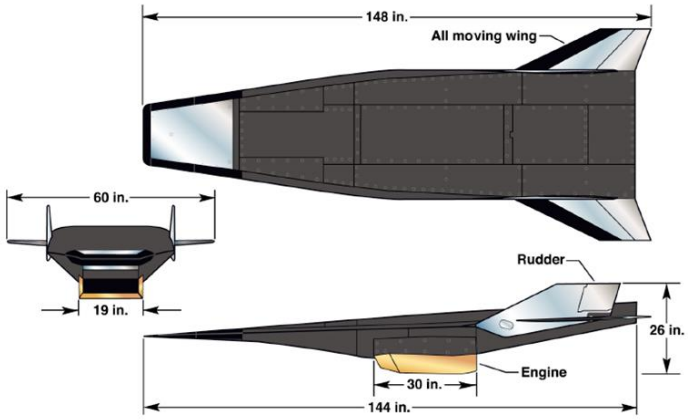

Fig. 5.1 Three-view of X-43A [60].

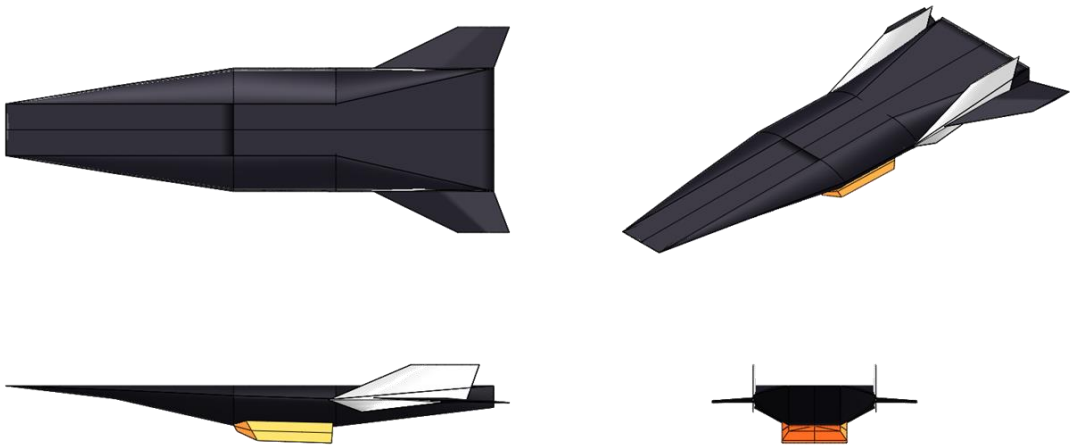

Fig. 5.2 Four-view of the VSP model representing the X-43A.

Table 5.2 Verification of X-43A VSP model [59].

	Actual (VCC)	VSP Model	% Error
S_{pln} (m^2)	3.36	3.27	2.68

5.1.2 Aerodynamics

For aerodynamics, there was almost no verification data available for the X-43A. The reason is because the majority of the aerodynamic data gathered within the VCC is in the form of figures as shown in Fig. 5.3. As shown, the values along the y-axis are removed, so this data becomes unusable for verification. Even though it is unfortunate that this data is unusable, a lift coefficient with respect to the angle of attack, or lift-curve slope, at Mach 7 is available to use for verification purposes. This is shown in Fig. 5.4 under three different conditions: inlet closed, inlet open power off, and inlet open power on.

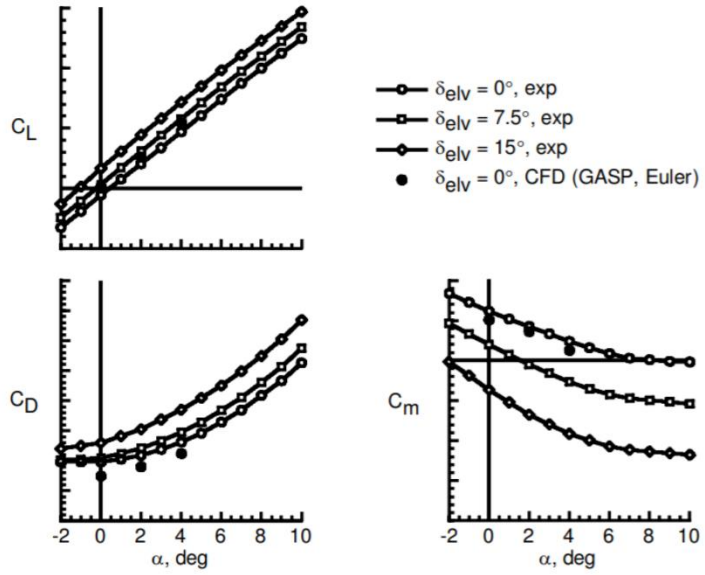

Fig. 5.3 Example of unusable data due to lack of axis values [71].

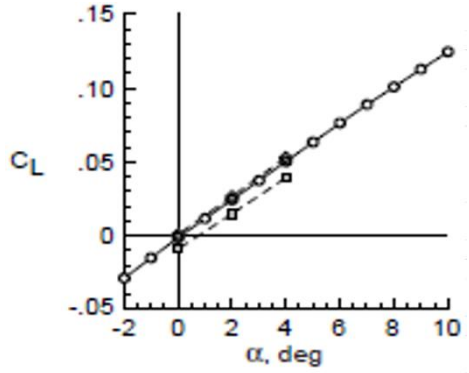

Fig. 5.4 Lift coefficient versus angle of attack at Mach 7 for X-43A [72].

With the lift-curve slope being the only aerodynamic data available, the process used for verifying the method is not only to produce a lift-curve slope at Mach 7 for comparison, but to produce a range of lift-curve slopes from Mach 2 to 10. The purpose of this is to not only verify at the particular known point, but to create a sanity check to determine that the results of the method, such as trends and overall behavior, are reasonable. As mentioned in the geometry section, some of the other disciplines require geometric values that are not available, so the verified VSP model is used in place of the actual data. This is the case for the aerodynamic method used. Even with this though, the error produced from lift-curve slope at Mach 7 of the actual vehicle and the

calculated one is under 5%. The results are shown in Table 5.3, along with Fig. 5.5 showing the range of lift-curve slopes from Mach 2 to 10. The lift-curve slopes pass the sanity check as it shows the expected trend of decreasing slope with increasing Mach number. While the method was determined sufficient with verification only available for one point and a sanity check of the produced trends, as there is an insufficient amount of available data, the verification of the synthesis system will also determine if the method is usable. If, despite this verification, the results of the total synthesis system create a huge percent error, each method will be reexamined, but if the results are within an acceptable error range, then the methods will be assumed to be acceptable for this vehicle.

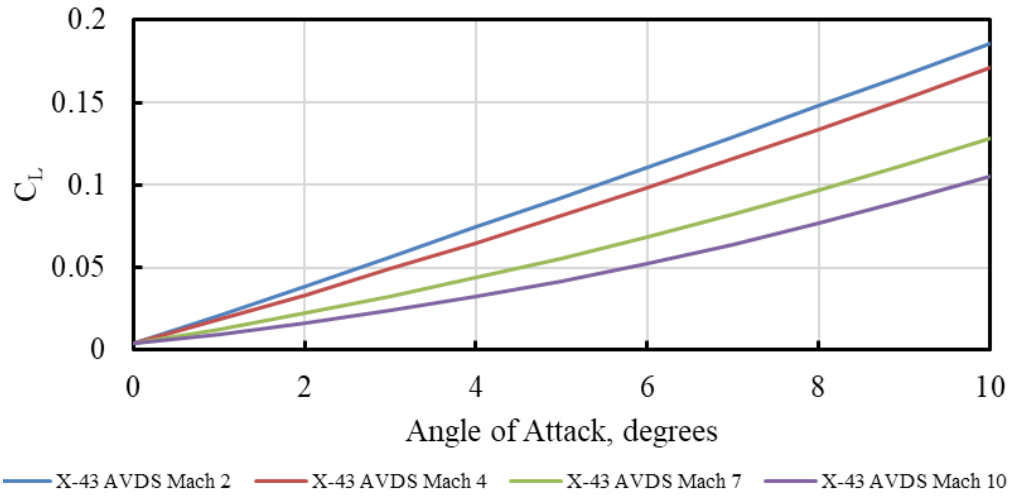

Fig. 5.5 Lift-curve slope for the X-43A at varying Mach.

Table 5.3 Verification results comparison for the X-43A lift-curve slope at Mach 7.

X-43A, Mach 7	
$C_{L\alpha}$ X-43A	0.0128
$C_{L\alpha}$ Results	0.0124
% Error	3.23

5.1.3 Propulsion

For propulsion, there was no easily identifiable verification data available. The data that was obtained within the VCC are similar to aerodynamics where an axis was missing to make the data unviable, or it was not usable for the conceptual design phase. Some examples are Fig. 5.6 and Fig. 5.7 which are not currently usable, but contained within the VCC so that it could possibly be used for verification during a later design phase, such as the detail design phase. As mentioned, there was no easily identifiable verification data for the propulsion system, but through manipulating two figures, a specific impulse value for the X-43A at Mach 6.83 was able to be obtained. These are shown in Fig. 5.8 and Fig. 5.9. Figure 5.8 is produced by Voland [73] and shows the I_{sp} values for X-43A at Mach 6.83 and 9.68, but as shown, the y-axis is missing. Using this with Fig. 5.9, which was produced by Moses [74], it shows the same plot with the y-axis but no X-43A values on it. The combination of these figures allows the determination of the specific impulse at Mach 6.83 which is 2,900 sec.

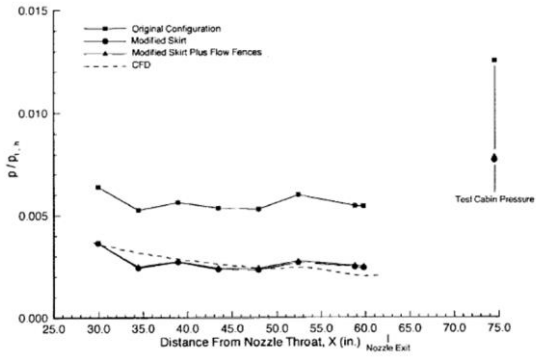

Fig. 5.6 Static pressure distribution along nozzle throat [75].

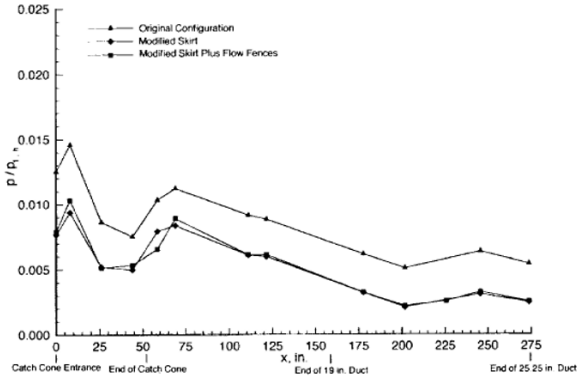

Fig. 5.7 Static pressure distribution along diffuser duct [75].

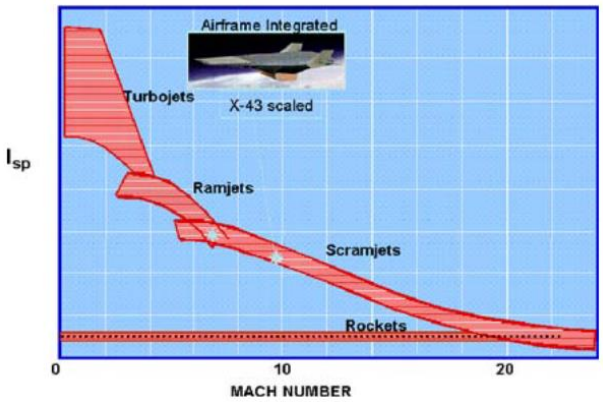

Fig. 5.8 Specific impulse vs mach number for X-43A, but with no y-axis values [73].

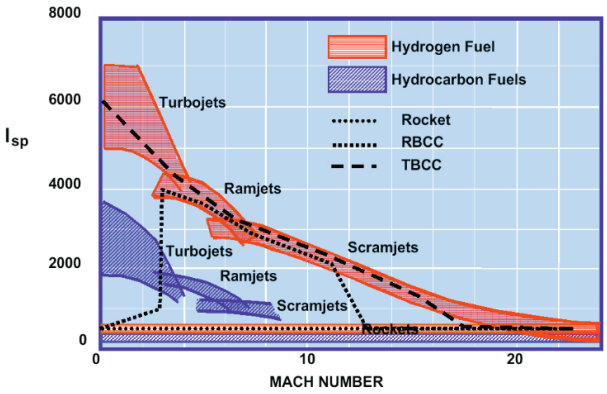

Fig. 5.9 Specifc impulse vs mach number with full axes [74].

The method created to calculate the propulsion performance uses Heiser and Pratt [66] and Bradford [64] (for nozzle analysis), as well as NASA's CEA [65] to calculate the gas properties of the fuel and air mixer through the engine. The X-43A was determined to be a two-fuel system, with gaseous silane as the igniter fuel and gaseous hydrogen as the main fuel. Using this method to calculate the engine performance at Mach 6.83 to compare for verification, it was found that the method produced an 8.17% error from the VCC value. This is shown in Table 5.4 below. As the produced error is below 10%, the method is assumed verified, and as with aerodynamics, since the number of verification points are low, the final verification determination is dependent on the synthesis sizing results.

Table 5.4 Verification results comparison for the X-43A Specific Impulse at Mach 6.83.

X-43A, Mach 6.83	
Actual *Isp*, s	2900.00
Calculated *Isp*, s	3137.08
% Error	8.17

5.1.4 Trajectory

For trajectory, the actual trajectory of the X-43A during its cruise portion is unknown, so a surrogate trajectory is developed to use for the synthesis system from what is known and contained within the VCC. From the few test flights that X-43A accomplished, the one that will be considered is test flight 2, which demonstrated accelerated climbing flight at Mach 6.83, as test flight 1 was not successful, and while test flight 3 was successful in demonstrating cruise at Mach 9.68 [73], the available information for the trajectory at that condition is less than what is available for test flight 2. After settling on which trajectory to consider, the primary trajectory information provided within the VCC is shown from Fig. 5.10 to Fig. 5.13.

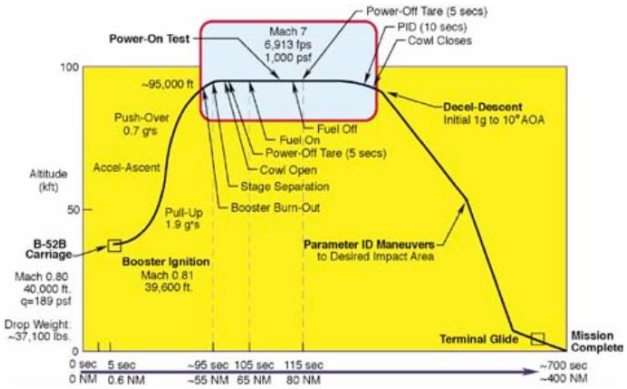

Fig. 5.10 X-43A flight mission profile [73].

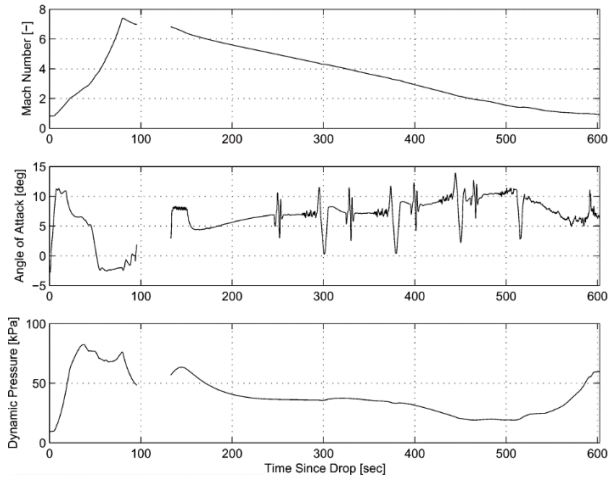

Fig. 5.11 X-43A flight 2 Mach number, angle of attack, and dynamic pressure [76].

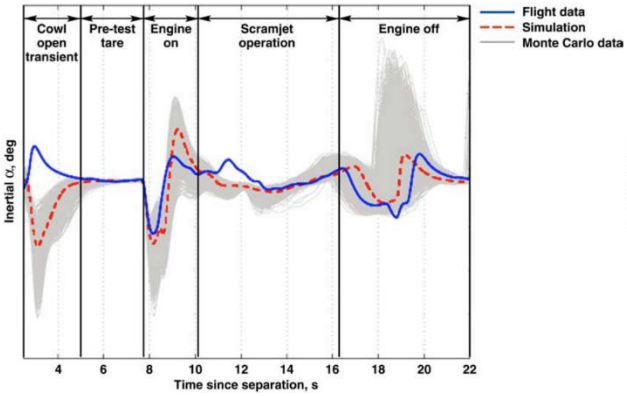

Fig. 5.12 X-43A flight 2 engine test phases [77].

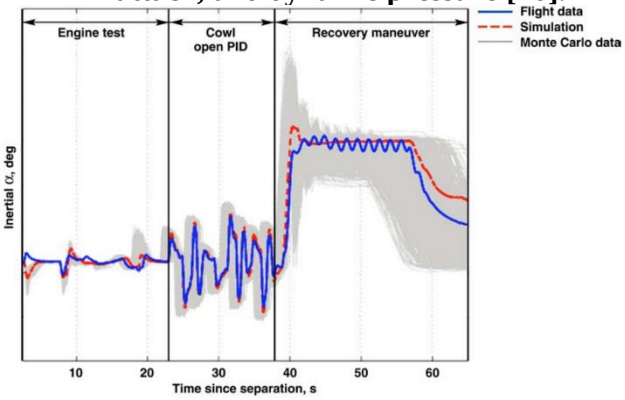

Fig. 5.13 X-43A flight 2 engine test, parameter identification, and recovery maneuver phases [77].

From the provided trajectory, only the flight segment where the X-43A flew with the engine on is of interest, so the flight segments with the Pegasus booster (including the booster separation) and the glide phase are not considered. As shown in Fig. 5.11 (also noted in Ref. [78]), there are about 39 seconds of trajectory that is not available from booster separation to the beginning of the recovery maneuver. This is noted by comparing the angle of attack over time trends from Fig. 5.12 and Fig. 5.13, and that the trend of the recovery maneuver in Fig. 5.13 is also shown in Fig. 5.11. Even though this missing section contains the wanted flight segment, a surrogate trajectory can still be determined with the provided figures as they contain information of the trajectory before and after the scramjet powered phase, as well as the timing details of when the engine is on and off.

Table 5.5 summarizes the known and unknown parameters that are required inputs for the surrogate trajectory. First, the accelerated climb is assumed to be a constant dynamic pressure climb. With this assumption, only the starting Mach number is required as this value would determine the climb's starting altitude and acceleration. This is accomplished as the starting altitude can be determined from the constant dynamic pressure and the starting Mach number, and the climb acceleration can be determined from the starting Mach number, the ending Mach number of 6.83, and the 11 sec scramjet operation duration time. After experimenting with several starting Mach numbers, the impact on the overall weight of the vehicle was determined to be small (as a 0.1 change in Mach number produced a 1.0 lb change in TOGW), the starting Mach number chosen was Mach 6.70. With this, the starting altitude is determined to be 28,520 m (93,570 ft).

Table 5.5 Summary of determined X-43A flight 2 trajectory attributes for the AVDS X-43A surrogate trajectory.

X-43A Flight 2 Attributes	Values	Reference
Trajectory method	Accelerated climbing flight	[73]
Scramjet climb starting Mach number	-	-
Scramjet climb starting altitude	-	-
Scramjet climb starting dynamic pressure	980 lb/ft^2 (taken to be a constant dynamic pressure climb)	-
Scramjet climb acceleration	-	-

Dynamic pressure at max Mach number	980 lb/ft^2	[73]
Maximum scramjet Mach number	6.83	[78]
Scramjet operation duration time	11 sec	[73]
Ignition phase duration time	1.5 sec	[73]
Booster separation details:		
Time to booster separation	93.44 sec	[77]
Engine ignition time (first possibility)	5 sec after booster separation	[73]
Engine ignition time (second possibility)	7.5 sec after booster separation	Fig. 5.12
Engine ignition time (third possibility)	10 sec after booster separation	Fig. 5.10
X-43A booster separation Mach number	6.95	[77]
X-43A booster separation dynamic pressure	1,024 lb/ft^2	[77]

As mentioned in the propulsion section, the X-43A is assumed to be a two-fuel system with gaseous silane as an ignition fuel and hydrogen as the main fuel. This means that the surrogate trajectory needs to be split between these two cases. Table 5.6 below summarizes these two cases with the starting Mach and altitude discussed previously with the silane phase, which is assumed to have an ignition duration of 1.5 sec, and the ending Mach and altitude with the hydrogen phase, which is assumed to have a duration of 9.5 sec to bring the total flight time to 11 sec.

Table 5.6 X-43A flight 2 surrogate trajectory flight segments and their parameters.

	Flight Segment	Parameters
1	Constant *q* Climb (scramjet, silane)	Duration: 1.5 sec Const *q* = 46.92 kPa (980 lb/ft^2) Start Altitude: 28,519 m (93,567 ft) Start Climb Mach = 6.70
2	Constant *q* Climb (scramjet, hydrogen)	Duration: 9.5 sec Const *q* = 46.92 kPa (980 lb/ft^2) End Climb Mach = 6.83 End Altitude: 28,781 m (94,425 ft)

Using Table 5.6 with Fig. 5.11, the created surrogate trajectory for the X-43A during its scramjet operation phase can be superimposed with the VCC available trajectory to show how they compare. This is shown in Fig. 5.14 and Fig. 5.15. The time placement of the surrogate trajectory was determined from the booster separation values shown in Table 5.5, with the separation occurring ~93.5 sec since the start, and using the ignition start time of 7.5 sec after booster separation to obtain the 101 sec placement. As shown, the overall placement of the surrogate trajectory falls within the redacted section. It should be noted that this method cannot be verified

separately from other disciplines as the past sections have been able to accomplish, so the verification of the surrogate trajectory is dependent on the results generated by the synthesis system.

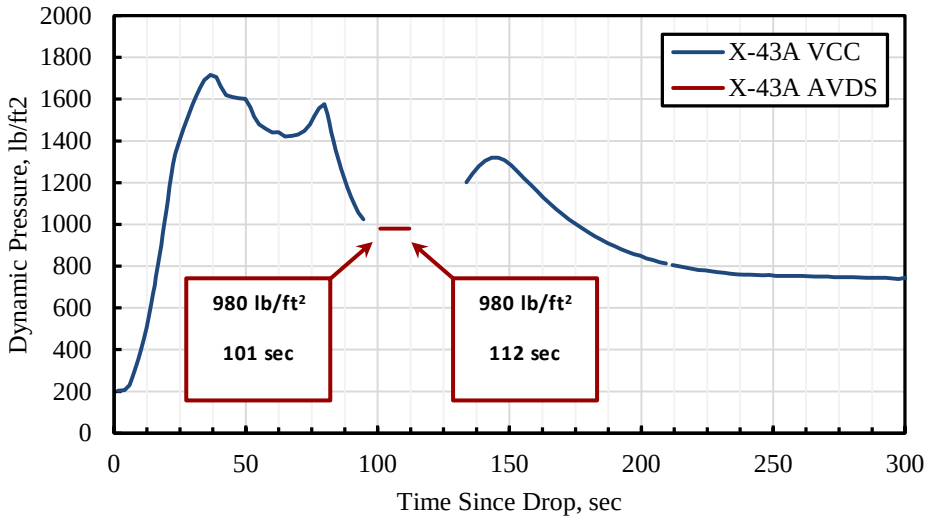

Fig. 5.14 Comparison of the AVDS^{CE} X-43A trajectory data and the X-43A flight #2 trajectory data from VCC for dynamic pressure and time.

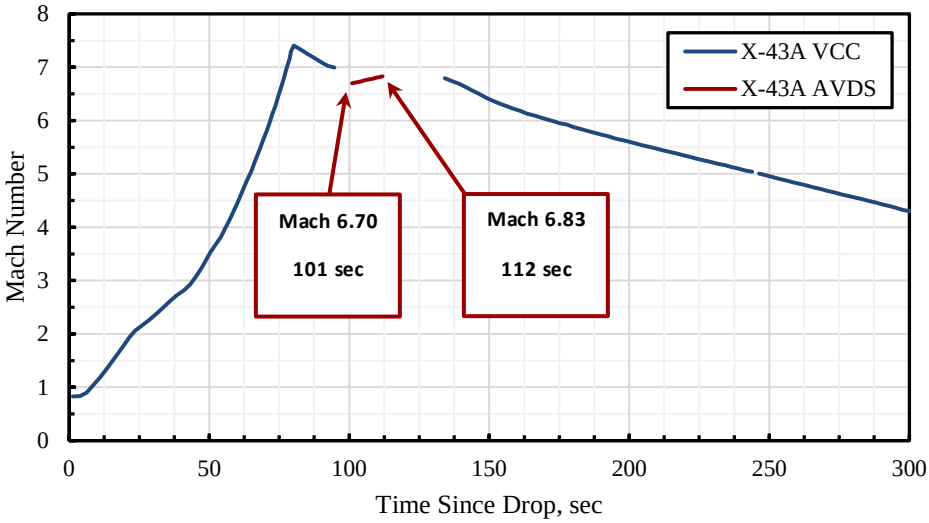

Fig. 5.15 Comparison of the AVDS^{CE} X-43A trajectory data and the X-43A flight #2 trajectory data from VCC for Mach number and time.

5.1.5 Weight and Volume

As has been for every other discipline, the verification data available within the VCC for the weight and volume discipline is scarce. The only weight values available are the takeoff gross weight (TOGW), the fuel weight, the weight of the tungsten ballast [79,80], and the weight of an electromechanical actuator [81]. The electromechanical actuator weight is not considered as verification point but added in list of known values for completion. With only a few points, the method to determine component weights is not possible, but the accumulation of the components can be verified with the TOGW value, as well as being used during the synthesis sizing verification. Table 5.7 provides a summary of available verification data.

Table 5.7 X-43A Synthesis weight verification data.

Component	Weight, lb	Weight, kg	Reference
Takeoff Gross Weight	2,824	1,281	[82,83]
Empty Weight	2,822	1,280	-
Propellant	2	1	[84]
Tungsten Ballast	865	392	[79,80]
Payload	0	0	

A unique challenge during the selection of the weight method for the X-43A is that since it is a demonstrator-scale vehicle, many of the conventional component weight estimations fell out as they are for full-scale vehicle due to the population of vehicles used to determine them. With this, the weight method used are the weight relations within HASA [61] which are for hypersonic vehicles and proved most reliable for this size of vehicle. With the HASA relations calculating the vehicle component weights, the ballast weight was determined by using the density of tungsten with the estimated volume of the nose in which the ballast encompassed. As will be shown, the tungsten ballast makes up a large part of the total weight of the vehicle. This is because the primary purpose of the ballast was to move the c.g. forward to make the vehicle nearly neutrally stable [82,

83]. The ability to act as a heat sink at the extreme temperatures it faced was an additional, but not primary, use as well.

Visuals of the breakdown of the calculated component weights are provided in Fig. 5.16 and Fig. 5.17. Figure 5.16 displays the relative magnitude in which each component weighs, with Fig. 5.17 showing the same, but compared to the total weight of the X-43A provided from the VCC. The verification results are also shown in Table 5.8. As shown, the largest known error is roughly ten percent, so despite not being able to verify every component, this weight method is considered verified.

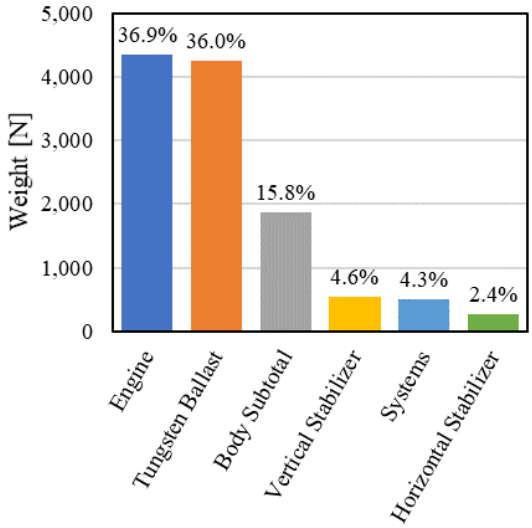

Fig. 5.16 Proportions of calculated weights for the X-43A.

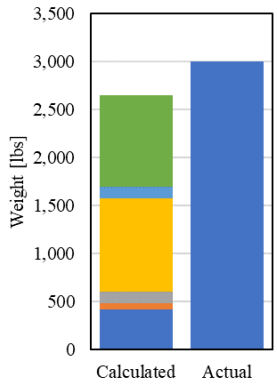

Fig. 5.17 Comparison of calculated weights to reference weight.

Table 5.8 X-43A weight verification results.

Component	Calculated Weight, N	lb
Basic Body	1,240	279
Thrust Structure	357	80
TPS	267	60
Body Subtotal	**1,864**	**419**
Horizontal Stabilizer	278	62
Vertical Stabilizer	538	121
Engine	4,351	978
Systems	506	114
Subsystems Subtotal	**5,673**	**1,275**
Tungsten Ballast	4,248	955
Total	**11,786**	**2,650**

5.1.6 Synthesis

With the disciplinary methods verified as discussed above, the selected methods can now be joined with the overall inputs and assumptions for the synthesis system to obtain sizing results for the X-43A. Table 5.9 provides a list of the inputs and assumptions used within AVDS^{CE} for the X-43A. Some of the inputs and assumptions shown are not available for the actual vehicle, so either the verified VSP model was used, or the range of values provided in Hypersonic Convergence for the respective parameter was reviewed [33].

Table 5.9 AVDS^{CE} X-43A inputs and assumptions.

Variable Discipline	Variable	Value
Geometry	Küchemann's tau	0.0945
	Nose spatula width percentage: Nose width measured as a percentage of the maximum fuselage width	42
Propulsion	Area ratio of viscous captured flow to inviscid captured flow	0.95
	Reference fuel equivalence ratio	1
	Design Mach	7
Trajectory	Constant *q* climb segment: Start altitude, m	28,519
	Constant *q* climb segment: Start velocity, m/s	2,014
	Constant *q* climb segment: Maximum longitudinal acceleration, m/s^2	0.35
	Constant *q* climb segment: Minimum longitudinal acceleration, m/s^2	0.01
	Constant *q* climb segment: End Mach number	6.83
	Constant *q* climb segment: Time to climb, sec	11
	Constant *q* climb segment: Ignition phase time, sec	1.5
Weights and Volume	Number of crew	0
	Number of passengers	0
	Weight of unmanned fixed systems, N	2,547
	Weight of each crew member, N/person	-
	Weight fixed manned systems per crew member, N/person	-
	Weight of each passenger, N/person	-
	Weight of passenger provisions per passenger, N/person	-

Weight of variable systems per vehicle dry weight	0.4542
Weight of cargo, N	0
Minimum dry weight (OEW) margin	0.1
Volume of provision for each crew member, m^3/person	-
Volume per crew member, m^3/person	-
Volume of manned fixed systems per crew member, m^3/person	-
Volume of each passenger space, m^3/person	-
Volume of variable systems per total vehicle volume, m^3	0.03
Volume of vehicle void space per total vehicle volume, m^3	0.1
Volume of unmanned fixed system, m^3	0.4244
Error band around the structural fraction, $m^{-0.138}$	0
Cargo density, kg/m^3	-
Fuel density, kg/m^3	47.7

For the X-43A sizing verification, the AVDS^{CE} system was run for two different cases. Case 1 is where the gaseous silane ignition phase was not considered, so the whole fuel phase was only hydrogen, and case 2 is where the silane ignition phase is included. There are also two reasons why these two cases are considered: 1) The provided 2 lb fuel weight was not determined from literature whether it included the silane fuel or not, and 2) it provided a chance to test the implementation of having multiple fuels during the trajectory analysis. It should be noted that the actual ignition process is not modeled, only the fuel type being burned is changed. The results for case 1 are provided in Table 5.10, and the results for case 2 are provided in Table 5.11.

As shown in Table 5.10 for case 1 where no silane ignition phase is considered, the majority of the sizing results are within 5.5% error. The notable exceptions are the fuel weight (80.3% error), the propulsion index (-45.9% error), and the total fuel fraction (84.6% error). The source of the high error for the last two parameters lies with the first parameter, the fuel weight. The calculated fuel weight was 3.61 lb compared to the actual fuel weight of 2 lb. With such a small amount of fuel, this parameter becomes very sensitive, and with the inclusion of the low fidelity propulsion method used for the sizing phase in conceptual design, it may not be sensitive enough for these small amounts. As the propulsion index and fuel fraction are functions of the fuel weight, the large fuel weight error propagates into these parameters. Despite the relatively large error in the fuel weight, it does not affect the overall weight much as the TOGW's error is low at -2.36%.

Table 5.10 Comparison of the AVDS^{CE} X-43A sizing results with (VCC) actual X-43A data. The results shown are the verification results where no silane ignition phase is considered (Case 1).

Sized Vehicle Attributes	X-43A [EN]	AVDS X-43A [EN]	X-43A [SI]	AVDS X-43A [SI]	% Error
Operating Weight Empty, lb or kg	2,821	2,753	1,279	1,248	-2.42
Operating Empty Weight, lb or kg	2,821	2,753	1,279	1,248	-2.42
Takeoff Gross Weight, lb or kg	2,823	2,756	1,280	1,250	-2.36
Structural Weight, lb or kg	-	635	-	288	-
Fuel Weight, lb or kg	2	3.61	1	1.63	80.3
Payload Weight, lb or kg	0	0	0	0	-
Tau, $V_{tot}/S_{pln}^{1.5}$	0.0945*	0.0945	0.0945*	0.0945	-
Total Planform Area, ft^2 or m^2	35.2*	36.3	3.27*	3.37	3.19
Wing Planform Area, ft^2 or m^2	35.2*	36.3	3.27*	3.37	3.19
Wetted Surface Area, ft^2 or m^2	89.6*	92.4	8.32*	8.59	3.17
Total Volume, ft^3 or m^3	19.7*	20.7	0.558*	0.585	4.85
Ratio of Wetted to Total Planform Area	2.55*	2.55	2.55*	2.55	-0.01
Structural Index, $I_{str} = W_{str}/S_{wet}$, lb/ft^2 or N/m^2	-	6.87	-	33.5	-
Propulsion Index, $I_p = \rho_{fuel}/(WR\text{-}1)$, lb/ft^3 or kg/m^3	4,200	2,274	67,262	36,411	-45.9
Industrial Capability Index, $10 \cdot I_p/I_{str}$	-	3,311	-	10,863	-
Total Fuel Fraction, W_{fuel}/TOGW	0.00071	0.00131	0.00071	0.00131	84.6
Total Weight Ratio, TOGW/OWE	1.00071	1.00131	1.00071	1.00131	0.06
Total Planform Wing Loading, TOGW/S_{pln}, lb/ft^2 or N/m^2	80.3*	75.9	3,843*	3,636	-5.38
Wing Planform Wing Loading, TOGW/S_w, lb/ft^2 or N/m^2	80.3*	75.9	3,843*	3,636	-5.38

*Values that have been obtained using the X-43A VSP geometry model

The sizing results for case 2, which includes the silane ignition phase, is shown below in Table 5.11. As with case 1, the majority of the sizing results are within 5.5% error, except for the same parameters of fuel weight, propulsion index, and fuel fraction. Comparing case 2 with case 1, the error increased for the fuel weight as the silane fuel has a lower specific impulse compared to the hydrogen fuel. This means that with the silane fuel, the AVDS^{CE} X-43A is less efficient for the first 1.5 sec, requiring more fuel overall compared to straight hydrogen fuel. Comparing the other parameters between the two cases, the takeoff gross weight, the empty weight, and the propulsion index are the only parameters whose error decreases, while all others increase. As mentioned, one of the reasons for the two cases was that it was not clear whether the 'actual' fuel weight includes the silane fuel or not, but as is shown between the two cases, the inclusion of silane for the ignition phase does not have a huge impact on the sizing results, as the greatest change is in the fuel fraction and fuel weight, with an increase of 1.7% and 1.6% respectively. After these,

every other parameter either increased or decreased in error up to 0.2%. From these observations between the two cases, the synthesis system is deemed verified for this vehicle.

Table 5.11 Comparison of the AVDS^{CE} X-43A sizing results with (VCC) actual X-43A data. The results shown are the verification results where a 1.5 second silane ignition phase has been considered (Case 2).

Sized Vehicle Attributes	X-43A [EN]	AVDS X-43A [EN]	X-43A [SI]	AVDS X-43A [SI]	% Error
Operating Weight Empty, lb or kg	2,821	2,753	1,279	1,248	-2.41
Operating Empty Weight, lb or kg	2,821	2,753	1,279	1,248	-2.41
Takeoff Gross Weight, lb or kg	2,823	2,757	1,280	1,250	-2.35
Structural Weight, lb or kg	-	635	-	288	-
Fuel Weight, lb or kg	2	3.64	1	1.65	81.9
Payload Weight, lb or kg	0	0	0	0	-
Tau, $V_{tot}/S_{pln}^{1.5}$	0.0945*	0.0945	0.0945*	0.0945	-
Total Planform Area, ft^2 or m^2	35.2*	36.3	3.27*	3.37	3.23
Wing Planform Area, ft^2 or m^2	35.2*	36.3	3.27*	3.37	3.23
Wetted Surface Area, ft^2 or m^2	89.6*	92.5	8.32*	8.59	3.22
Total Volume, ft^3 or m^3	19.7*	20.7	0.558*	0.59	4.92
Ratio of Wetted to Total Planform Area	2.55*	2.55	2.55*	2.55	-0.01
Structural Index, $I_{str} = W_{str}/S_{wet}$, lb/ft^2 or N/m^2	-	6.87	-	33.5	-
Propulsion Index, $I_p = \rho_{fuel}/(WR\text{-}1)$, lb/ft^3 or kg/m^3	4,200	2,281	67,262	36,527	-45.7
Industrial Capability Index, $10 \cdot I_p/I_{str}$	-	3,323	-	10,901	-
Total Fuel Fraction, W_{fuel}/TOGW	0.00071	0.00132	0.00071	0.00132	86.3
Total Weight Ratio, TOGW/OWE	1.00071	1.00131	1.00071	1.00131	0.06
Total Planform Wing Loading, TOGW/S_{pln}, lb/ft^2 or N/m^2	80.3*	75.9	3,843*	3,635	-5.41
Wing Planform Wing Loading, TOGW/S_w, lb/ft^2 or N/m^2	80.3*	75.9	3,843*	3,635	-5.41

*Values that have been obtained using the X-43A VSP geometry model

5.2 XB-70 Methods and Synthesis Verification

With the X-43A verification process complete, the XB-70 is now considered for comparison as a vehicle with an abundance of verification data available. For the XB-70, the disciplinary methods that were selected for the synthesis system are shown in Table 5.12. As can already be compared, there are more methods considered for the XB-70 than were considered for the X-43A. This is because the X-43A was a demonstrator within only the cruise portion considered, while the XB-70 was a full-scale vehicle and the entire takeoff to landing trajectory is considered. As was with the X-43A, this section for the XB-70 will focus on what was available within the VCC, how that data/information was used to verify the selected disciplinary methods, and how they in turn, verified the respective synthesis system.

Table 5.12 Disciplinary methods utilized in the AVDS^{CE} system for sizing the XB-70.

#	Method Title	Discipline	Page #	Last Name	Reference
1	Flight Condition	Environment			
2	Standard Earth Atmosphere Model	Environment	15-116	NASA	[57]
3	Subsonic Lift-Curve Slope at Low AoA	Aerodynamics	-	Spencer	[85]
4	Vortex Lift Contribution of Delta Wing	Aerodynamics	-	Polhamus	[86]
5	Wing Tip Droop Effects	Aerodynamics	-	Petersen	[87]
6	Shock-Mach Relations	Aerodynamics	-	Bartlett	[88]
7	Compression Lift	Aerodynamics	-	Eggers and Syvertson	[89]
8	Wave Drag	Aerodynamics	-	Mason	[90]
9	Irregular Planform Wing Aerodynamics	Aerodynamics	-	Benepe	[91]
10	Ground Effect	Aerodynamics	-	Baker, Schweikard, and Young	[92]
11	Pressure Ratios and Shock Angles	Aerodynamics	-	Becker	[93]
12	XB-70 Vehicle Geometry	Geometry	15-19	Andrews	[94]
			15	Dussart, Lone, O'Rourke, and Wilson	[95]
13	Turbojet Wing Body OWE Estimation	Weights	16-20	Sverdrup Technology, Inc. (for NASA)	[61]
			79	Czysz	[33]
			4-138	McDonnell Aircraft Company	[62]
			555	Nicolai	[96]
			8, 20	Glatt	[97]
			-	Raymer	[98]
			-	Torenbeek	[99]
14	Turbojet with Afterburner - YJ93-GE-3 Engine NPSS/pyCycle Model	Propulsion	-	NPSS	[100]
			-	pyCycle	[101]
			-	Mattingly	[102]
15	Takeoff and Climb Out	Trajectory	275	Miele	[67]
			435-477	Roskam	[68]
16	Constant Acceleration Climb	Trajectory	67	Miele	[67]
			375,420	Roskam	[68]
17	Constant Mach Climb	Trajectory	67	Miele	[67]
			375, 423	Roskam	[68]
			266-267	Vinh	[69]
18	Constant Altitude Acceleration	Trajectory	264	Miele	[67]
			-	Roskam	[68]
			266-267	Vinh	[69]
19	Constant Altitude Range Cruise	Trajectory	157	Miele	[67]
			-	Roskam	[68]
20	Constant Altitude Deceleration	Trajectory	264	Miele	[67]
			-	Roskam	[68]
21	Constant Dynamic Pressure Descent	Trajectory	67	Miele	[67]
			374, 375, 421	Roskam	[68]
			266-267	Vinh	[69]
			11	Kundu	[70]

5.2.1 Geometry

The geometric data gathered within the VCC for the XB-70 is extensive and provides more verification for the VSP model as compared to the X-43A. As the geometric information available would be too overwhelming to show here, most of it can be found in the 'Summary of Preliminary Data Derived from the XB-70 Airplanes' reference [94]. The majority of the data repeats itself

throughout the available sources, but this reference contains the most in a single location. With this data and a 3-view of the XB-70, shown in Fig. 5.18, a VSP model is able to be created as shown in Fig. 5.19. It is also noted that in the 3-view, the figure shows that the XB-70 had wing tips that could be deflected from the horizontal down. This is important as this changes the overall geometry, so geometric parameters such as planform area, side area, etc. become a function of these tip deflections.

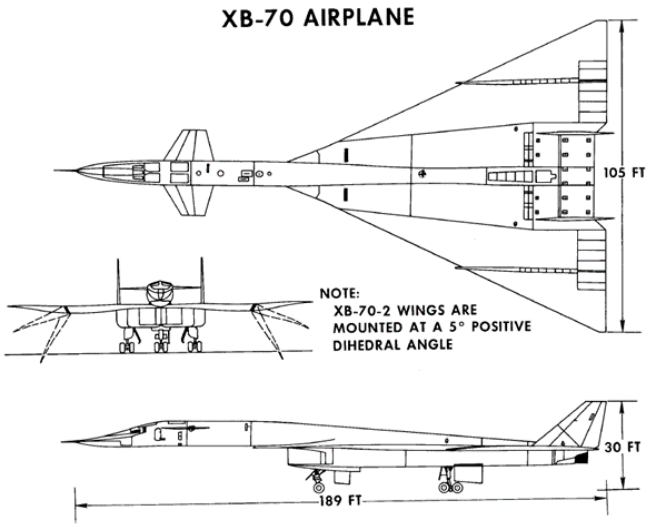

Fig. 5.18 Three-view of XB-70 [94].

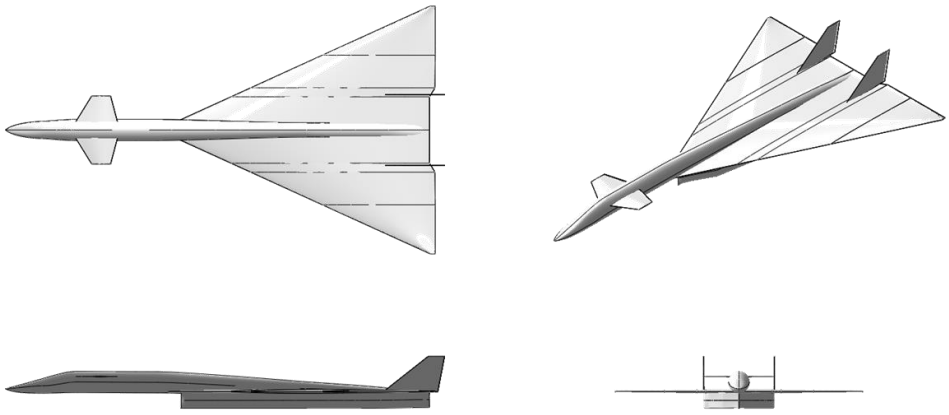

Fig. 5.19 Four-view of the VSP model representing the XB-70.

For the verification of the VSP model, Table 5.13 shows several of the values used to verify with. The model is assumed sufficiently verified as the largest error is 1.56% as shown. As there was more available geometric data for the XB-70, it is observed that the percentage error is smaller than that of the X-43A, who had significantly less available information. Another comparison between the XB-70 and X-43A VSP models is that the XB-70 uses wingspan as a verification parameter, while the X-43A does not, even though this value is available. The reason is because the span is an input into VSP for the X-43A to create the model, while it was not for the XB-70. For this model, the wing was created using analytical equations with aspect ratio (*AR*) as the input.

Table 5.13 Verification of XB-70 VSP model [93].

	Actual (VCC)	VSP Model	% Error
Wing Area (m^2)	585.08	584.862	0.04
Wingspan (m)	32	32.009	0.02
LE Sweep (degrees)	65.57	65.566	0.01
Wing Tip Area (one tip only) (m^2)	48.39	48.310	0.16
Wing Tip Span (m)	6.33	6.329	0.02
Wing Tip Root Chord (m)	14.61	14.599	0.08
Canard Area (m^2)	38.61	38.609	0.00
Engine Planform Area (m^2)	217.61	221.013	1.56
Engine Side Area (m^2)	66.58	65.784	1.20

5.2.2 Aerodynamics

For aerodynamics, as with geometry, there was an abundance of possible verification data available, but not all of it was needed. To filter out what should be used and what is not necessarily needed, two filters were used. First, the data was filtered to the data that could be used to verify critical Mach number points along the trajectory, along with data available for how the wing-tip droop affects the corresponding points. Second, as there is an abundance of information, the verification data selected were consistent across several sources, as some sources may have a different value for the same parameter due to certain conditions. Unlike the X-43A, whose considered trajectory only consisted of the cruise portion of the flight due to it being a demonstrator, the XB-70 was a fully operational vehicle, so the verification points span across the

entire speed regime from takeoff to subsonic flight, to supersonic flight, and finally to landing. This is shown in the list of verification points in Table 5.14. It is noted that currently the transonic region was neglected from verification due to the time constraints of the contract and to avoid unnecessary computing time to attempt to solve an often numerically challenging speed regime. As it is known that the vehicle was able to overcome the rise in drag due to the transonic region, it is not a significant limitation to neglect this at this time.

Table 5.14 Verification data for XB-70 compiled from VCC.

Data	Value	Reference	Flight Condition
C_L, takeoff	0.73-1.3	[103]	Subsonic, TO/Landing Configuration
C_L, landing	0.626	[103]	Subsonic, TO/Landing Configuration
C_{D0}	0.007	[103]	Subsonic, M = 0.76
$C_{L\alpha}$	0.046	[104]	Subsonic, M = 0.76
C_L at α=4.5°	0.167	[104]	Subsonic, M = 0.76
C_{Dbase}	0.001	[104]	Subsonic, M = 0.76
C_D	0.0106	[104]	Subsonic, M = 0.76
L/D	9.5	[104]	Subsonic, M = 0.76
C_D	0.0158	[96]	Supersonic, Mach 2.39, Wing Tips Deflected 65 deg
C_L	0.161	[96]	Supersonic, Mach 2.39, Wing Tips Deflected 65 deg
$C_{L\alpha}$	0.0214	[104]	Supersonic, Mach 2.5, Wing Tips Deflected 65 deg, cruise
L/D	6.45	[104]	Supersonic, Mach 2.5, Wing Tips Deflected 65 deg, cruise
C_L	0.1-0.13	[103]	Supersonic, Mach 3, Wing Tips Deflected 65 deg, cruise
C_D	0.059	[104]	Supersonic, Mach 3, Wing Tips Deflected 65 deg, cruise
L/D	5.5	[104]	Supersonic, Mach 3, Wing Tips Deflected 65 deg, cruise
$C_{Lcompression}/C_{Ltotal}$	0.3	[87]	Supersonic, Mach 3, Wing Tips Deflected 65 deg, cruise

The methods that are used within the verification process for the XB-70 are significantly different than those used in X-43A, not only because of the full range of flight considered, but because of the variable wing-tip droop feature. The reason is because the wing-tip droop creates an aerodynamic phenomenon where it 'captures' the generated shock wave at supersonic speeds to increase the pressure underneath the vehicle to create 'free' lift. This is called compression lift and is a key feature of waveriders. While the specification of whether the XB-70 is truly a waverider is up for debate, this compression lift is still a feature of the XB-70 and needs to be captured within the aerodynamic analysis. With this, a lift and drag buildup is used rather than the simplified total coefficient estimation method used for the X-43A.

Using this buildup, the verification results calculated are shown in Table 5.15 and Table 5.16. Along with the verification results, Fig. 5.20 and Fig. 5.21 show the calculated lift and drag coefficients throughout the speed regimes. The aerodynamic results from the used methods are relatively low, with most results being under 5%, with three notable exceptions. The first two exceptions are the lift coefficient at takeoff and at Mach 3 cruise. While these were noted as they were almost double the error as compared to other results, these are not considered significant as they are below 10% error and are provided from a range of values, with the largest difference used for the error value. Also, the calculated values are within the ranges provided by the VCC so, the larger error is considered not significant. The third exception is considered significant as the error is around 20% for the drag coefficient at Mach 2.39. The drag at this flight condition is over-estimated, so it leads to a conservative performance estimation. Even with this over-estimation, the error does not contribute significantly to the overall analysis and performance estimation as the vehicle accelerates through this point, so it does not remain long. The major flight points, such as cruise at Mach 2.25 and 3, are shown to have low error.

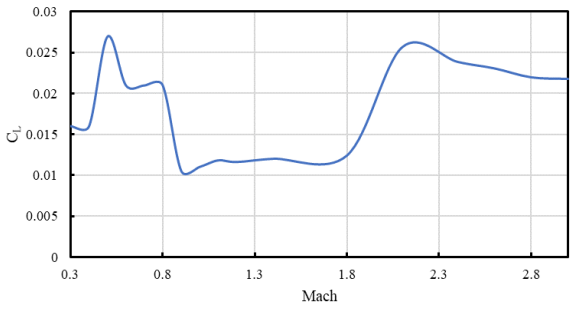

Fig. 5.20 Verification results of lift coefficient versus Mach for the XB-70.

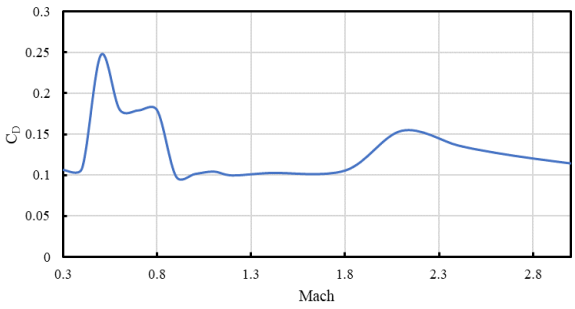

Fig. 5.21 Verification results of drag coefficient versus Mach for the XB-70.

Table 5.15 Subsonic verification error results for the XB-70.

Subsonic TO/Landing Configuration			
	Method	**VCC**	**% Error**
$C_{L,\ Takeoff}$	0.92	0.73-1.3	9.35%
$C_{L,\ Landing}$	0.649	0.626	3.67%
Subsonic M = 0.76			
$C_{L\alpha}$	0.0449	0.046	2.39%
C_L *at AoA 4.5 degrees*	0.178	0.167	6.58%
C_{D0}	0.0073	0.007	4.29%
C_{Dbase}	0.001	0.001	0%
C_D	0.0102	0.0106	3.77%
L/D	9.1	9.5	4.21%

Table 5.16 Supersonic verification error results for the XB-70.

Supersonic Mach 2.39, Wing Tips Deflected 65 deg			
	Method	**VCC**	**% Error**
C_D	0.0194	0.0158	22.78%
C_L	0.1578	0.161	1.98%
Supersonic Mach 2.5, Wing Tips Deflected 65 deg, cruise			
$C_{L\alpha}$	0.0207	0.0214	3.31%
L/D	6.22	6.45	3.57%
Supersonic, Mach 3, Wing Tips Deflected 65 deg, cruise			
$C_{Lcompression}/C_{Ltotal}$	0.3	0.3	0%
C_L	0.118	0.1-0.13	9.23%
C_D	0.062	0.059	5.08%
L/D	5.2	5.5	5.45%

5.2.3 Propulsion

For propulsion, unlike for the X-43A which had a single value, the XB-70 had usable data to verify with within the VCC. Some examples of the usable information are shown from Fig. 5.22 to Fig. 5.25. A similar challenge with the data obtained for the propulsion discipline as with the aerodynamic discipline, is with conflicting data between sources. It is assumed because the XB-70 became a test vehicle, that the conflicts are due to publications of different flights tests, but the actual specifications of the flights have not been clear. With this, as with aerodynamics, the values that are the most consistent, or relatively consistent, throughout the sources are the ones selected. An example is the thrust of the engines used by the XB-70. Most of the references determine the thrust to be 30,000 lbf per engine, with some being a little higher or lower. As the values tend to be around 30,000 lbf, this is the value selected for the thrust of the engines with after burner. The varying engine thrusts can be found in references [105-116].

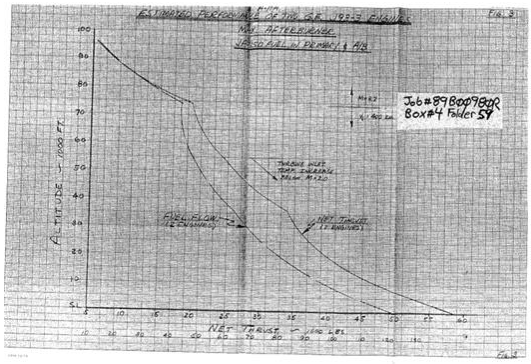

Fig. 5.22 Altitude vs net thrust [117].

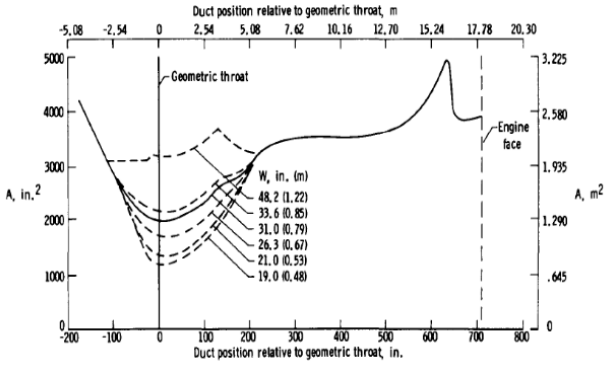

Fig. 5.23 Change in throat area [118, 119].

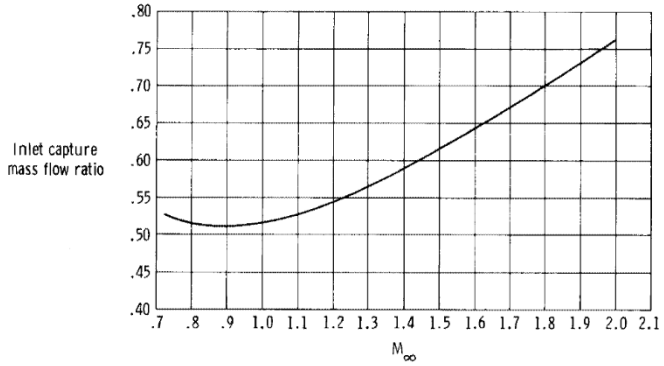

Fig. 5.24 Capture mass flow ratio for XB-70 [104, 106].

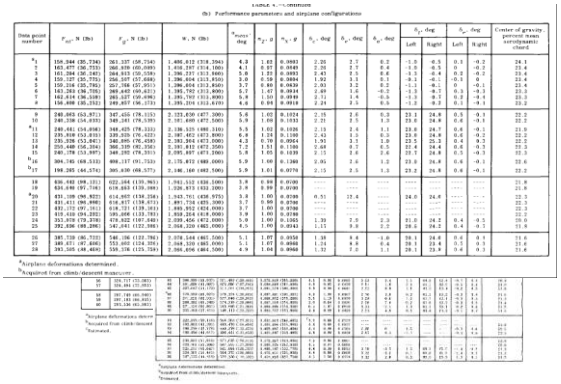

Fig. 5.25 Thrust data for various test flights [104, 120].

With the verification data available from the VCC, the method chosen for the XB-70 can be verified. The propulsion method that was selected is a component based 1D flow analysis software developed by NASA called *Numerical Propulsion System Simulation* (NPSS) [100]. For the sizing of the propulsion system for the XB-70, component efficiencies are used as defined by Mattingly [102]. The efficiencies selected are shown in Table 5.17.

Table 5.17 Component efficiency used for the YJ-93.

Efficiency	XB-70/YJ-93
Diffuser	0.9
Compressor	0.8
Fan	0.78
Burner	0.88
Turbine	0.8
Afterburner	0.85
Nozzle	0.9

While the thrust with afterburner and the component efficiencies was selected as discussed previously, the thrust without afterburner, the temperature after the afterburner (T_{ab}), and the turbine entry temperature (TET) values are missing for the propulsion method. To determine these values, the engine was first sized for a fixed dry thrust, which was varied between 18,000 lbf and 22,000 lbf. For each thrust value between the provided range, the TET was varied between 2,100 °R and 2,500 °R. From the results generated with these trades, a point was selected which matched the required mass flow rate of the XB-70 (265 lb/sec) and had a relatively low SFC value. From this selection, the TET was determined to be roughly 2,500 °R. This is shown in the left side of Fig. 5.26. After the selection of the TET, and with the known value of the mass flow rate, the maximum thrust produced by the engine can be determined (rubber engine concept). This is shown on the right side of Fig. 5.26. Again, using the TET selected and the known mass flow rate from the VCC, the dry thrust for the YJ-93 engine was determined to be about 20,800 lbf. It should be noted that the results shown in Fig. 5.26 are only a portion of the tests run for these calculations, with the most relevant ones shown.

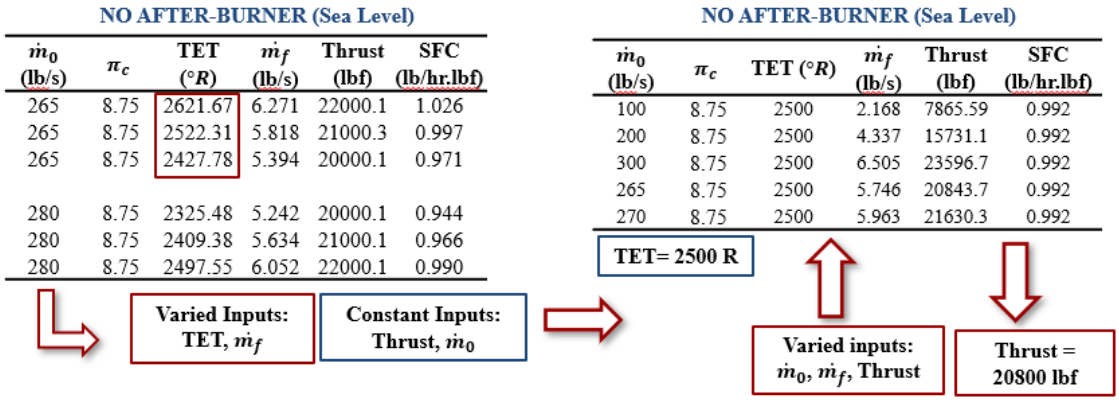

Fig. 5.26 Derivation of thrust, TET, and T_{ab} for the XB-70 engine (YJ-93) with no afterburner.

With the wet thrust (thrust with afterburner) provided from the VCC, and the TET and dry thrust determined as discussed, the temperature after the afterburner (T_{ab}) can be calculated. Table

5.18 shows some of the iterations to determine this value. As is shown from the results, two points were considered. While the last point was observed to be the best point as it was closest to the known mass flow rate, the calculated max T_{ab} is around 3,600 °R, which seemed too high to be achievable at the time when the XB-70 was developed, so the first point was investigated as it had a max T_{ab} of 3,000 °R. After investigating the first point, it was determined that the off-design results (not shown) were not acceptable, so the last point with max T_{ab} of 3,600 °R was selected.

Table 5.18 YJ-93 sizing results with afterburner (sea level).

$\dot{m}_0$ (lb/s)	Thrust (lbf)	π_c	TET (°R)	T_{ab} (°R)	SFC (lb/hr.lbf)	$\dot{m}_0/\dot{m}_f$	
258.065	29,000	8.75	2,500	3,569.763	1.776	0.03	
262.882	29,000	8.75	2,500	3,459.243	1.726	0.0275	
263.883	29,000	8.75	2,500	3,436.774	1.716	0.027	
268.024	29,000	8.75	2,500	3,345.782	1.674	0.025	
279.429	29,000	8.75	2,500	3,111.089	1.567	0.02	
269.793	30,000	8.75	2,500	3,111.089	1.567	0.02	
275.928	30,000	8.75	2,500	2,990.086	1.512	0.0175	⇦
289.064	30,000	8.75	2,500	3,111.089	1.567	0.020	
285.348	30,000	8.75	2,500	3,182.534	1.599	0.0215	
277.266	30,000	8.75	2,500	3,345.782	1.674	0.025	
266.963	30,000	8.75	2,500	3,569.763	1.776	0.03	⇦

With these values finally determined, a thrust vs. altitude plot can be created to compare to the one available within the VCC for final verification. As shown in Fig. 5.27, while the calculated thrust results are slightly lower than the actual, the results from the designed engine match closely with the data from the VCC. A summary of the designed XB-70 engine is shown in Table 5.19.

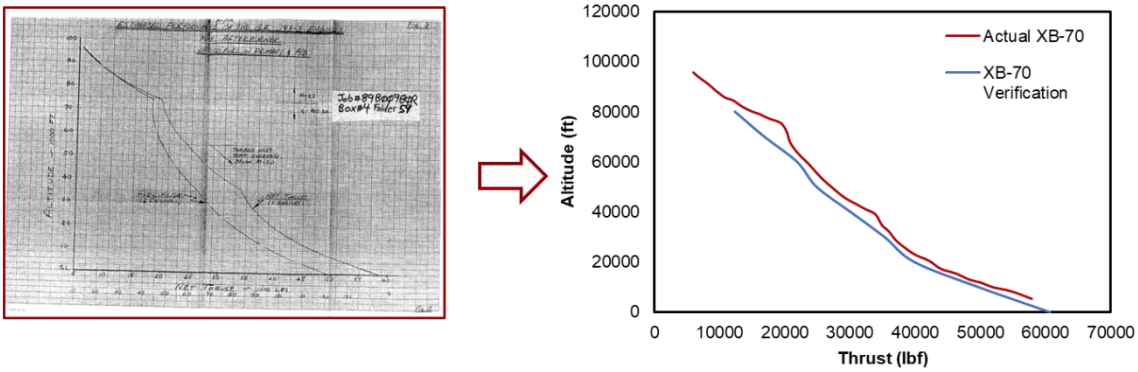

Fig. 5.27 Verification of thrust as function of altitude for the XB-70 engine J-93.

Table 5.19 Summary of J-93/YJ-93 engine specification.

Available Information	Value
Engine Type	Turbojet
Fuel Type	JP-6
Thrust (Wet)	30,000 lbf
Thrust (Dry)	20,800 lbf
Overall efficiency	40%
SFC	1.8 lb/hr.lb (SL wet)
Max Mach	3.07
Capture Area	5,600 in^2
Length	108.84 in
Inlet Ramp Angles	7°, 12°, 16°
Compressor Pressure Ratio	8.75
Mass Flow Rate	261 lb/sec
Shaft Speed	6,825 rpm
Compressor Type	11 stage axial compressors
Burner Type	Annular Combustor
Turbine Type	Two-stage Axial turbine

5.2.4 Trajectory

For trajectory, there is a significant amount of available verification data with the whole flight regime able to be verified. This contrasts with the X-43A whose prominent flight portion was redacted from the publicly available sources. As the trajectory of the XB-70 is from takeoff to landing, it contains many more flight segments to build the surrogate trajectory than it did for the X-43A. Along with the extended trajectory, the XB-70 also employs morphing wing geometry which must be accounted for in the trajectory on when the wing-tips droop and how much. The wing-tip folding schedule throughout the XB-70 trajectory is shown in Fig. 5.28 and Fig. 5.29.

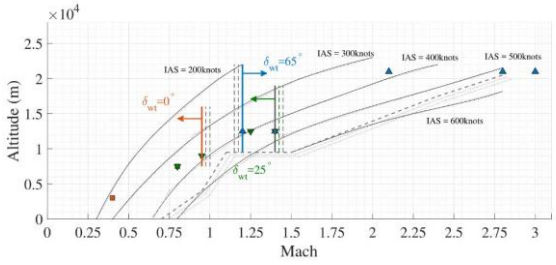

Fig. 5.28 XB-70 wing-tip folding schedule as a function of Mach number [95].

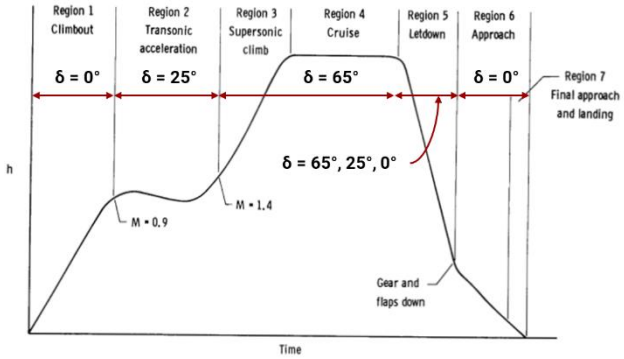

Fig. 5.29 XB-70 mission profile with annotated wing-tip folding schedule [121].

For the XB-70's trajectory, the VCC provides takeoff, climb, cruise, descent, and landing data, however, only the climb, cruise, and descent data will be discussed. The climb portion of the surrogate trajectory is determined from Fig. 5.30 and Fig. 5.31 below. The flight path of the 'typical climb profile' shown in Fig. 5.30 is used to determine the transition points between trajectory segments. Using these figures for the ascent trajectory a breakdown for the climb can be determined. As shown, there is a subsonic constant acceleration climb (maximum afterburner with full payload) until Mach 0.9, a constant Mach 0.9 climb until 10,050 m (33,000 ft), a constant altitude acceleration to Mach 1.44, and then a supersonic (maximum afterburner) constant acceleration climb to the Mach 3.0 cruising altitude of 21,830 m (71,600 ft). In addition, the XB-70 flight manual allows for a manual determination of the distance covered, time covered, and fuel used during the subsonic and supersonic climb. This is accomplished by using Fig. 5.32 and Fig. 5.33.

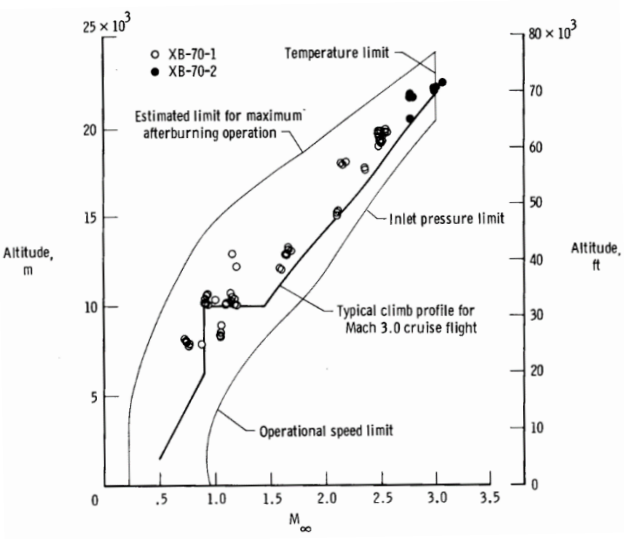

Fig. 5.30 Altitude and Mach number trajectory data used for the surrogate trajectory [104].

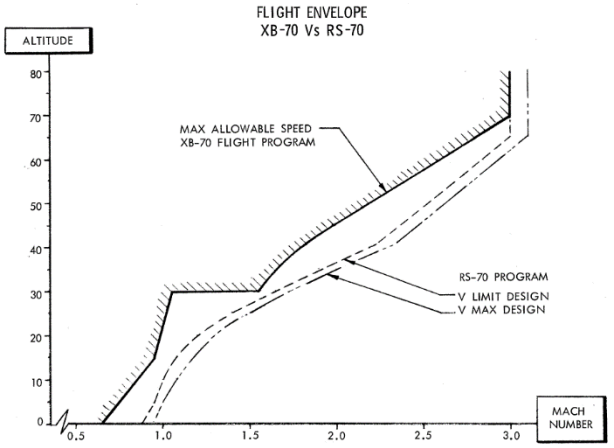

Fig. 5.31 Comparison of XB-70 flight speed limits to RS-70 flight speed limits [122].

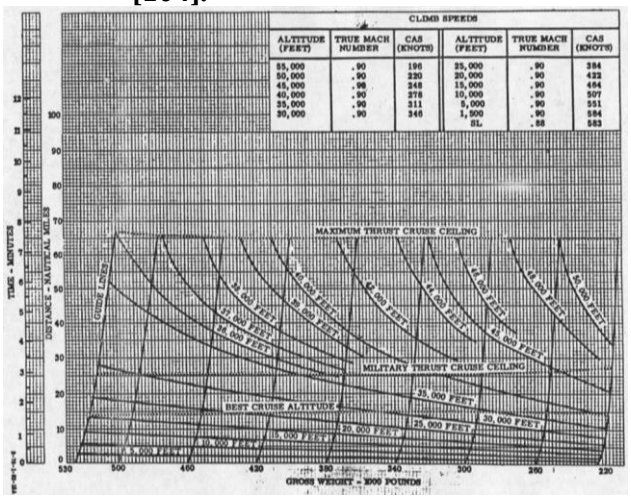

Fig. 5.32 XB-70A subsonic climb with max thrust (with afterburner) [123].

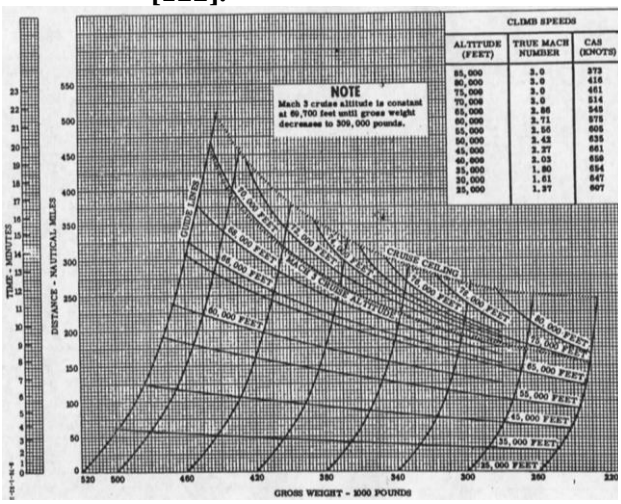

Fig. 5.33 XB-70A supersonic climb with max thrust (with afterburner) [123].

For cruise, the primary information required is the type of cruise, the cruising Mach number, the range of the cruise, and the cruise altitude(s). First to help with this determination, a collection of cruise data and overall mission range data was gathered for the XB-70, RS-70, and the B-70 as shown in Table 5.20. The range values for specific flight segments, such as the climb, cruise, and descent, have not been able to be identified, however. As for the type of cruise, it has been indicated that the XB-70 either had a cruise climb (Fig. 5.34), a constant altitude cruise, or

combination of both (Fig. 5.35 and Fig. 5.36 respectively). To simplify the cruise, the selected cruise type for the XB-70 trajectory will be a constant altitude cruise at Mach 3.0 and at an altitude of 69,700 ft. The range of the cruise has been selected to be 5,000 km (2,700 nmi) by going through a trial-and-error process using the AVDS^{CE} to see the vehicle converge.

Table 5.20 B-70, RS-70, XB-70, and YB-70 mission ranges and cruise attributes.

Vehicle	Cruising Mach	Payload [lb]	Cruising Altitude [m]	Cruising Altitude [ft]	Range [km]	Range [nmi]	Refueled?	Ref.
XB-70	3.0	-	21,946	72,000	6,901	3,726	-	[124]
XB-70	3.0	-	21,336	70,000	-	-	-	[125]
RS-70	-	-	-	-	11,940	6,447	No	[122]
RS-70	-	-	-	-	14,349	7,748	Yes	[122]
RS-70	-	-	-	-	9,838	5,312	Yes	[122]
RS-70	3.0	10,000	-	-	11,112	6,000	No	[126]
XB-70	3.0	-	21,336 to 24,384	70,000 to 80,000	-	-	-	[120]
XB-70A	3.0	-	21,336	70,000	12,038	6,500	-	[127]
B-70	-	50,000	-	-	11,112	6,000	-	[105]
B-70	3.0+	50,000	21,336	70,000	14,075	7,600*	No	[105]
B-70	3.0	50,000	-	-	12,964	7,000 plus†	Yes	[105]
XB-70	3.0	50,000	21,336	70,000	12,069	6,517	-	[128]
XB-70	3.0	-	-	-	5,499	2,969	-	[114]
YB-70	3.0	10,000	19,812 to 23,866	65,000 to 78,300	11,945	6,450	No	[129]
XB-70B-3	3.0	10,000	19,812 to 22,281	65,000 to 73,100	8,600	4,644	No	[130]
XB-70	3.0	None	19,812 to 23,348	65,000 to 76,600	10,399	5,615	No	[131]
XB-70	3.0	10,000	19,812 to 21,915	65,000 to 71,900	8,621	4,655	No	[132]
XB-70A-1	3.0	-	19,812 to 21,632	65,000 to 70,970	6,988	3,773	No	[133]
XB-70A-1	3.0	-	19,812 to 22,098	65,000 to 72,500	6,901	3,726	No	[134]
XB-70A-1	3.0	-	19,812 to 22,098	65,000 to 72,500	6,901	3,726	No	[135]
XB-70A-2	3.0	-	19,812 to 21,862	65,000 to 71,725	7,551	4,077	No	[136]
XB-70A-2	3.0	-	19,812 to 21,946	65,000 to 72,000	7,425	4,009	No	[137]
XB-70A-2	3.0	-	19,812 to 21,869	65,000 to 71,750	7,425	4,009	No	[138]
XB-70A-2	3.0	-	19,812 to 21,869	65,000 to 71,750	7,341	3,964	No	[139]

* Using six GE YJ93-GE-5 boron-burner engines
† Using six GE YJ93-GE-3 engines with JP-6 fuel. Without boron, the B-70 range was reduced by 10% [105]

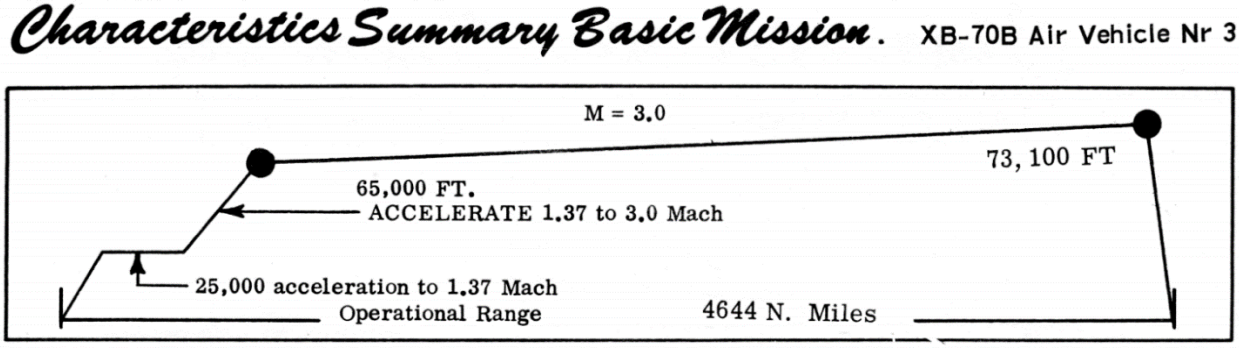

Fig. 5.34 XB-70B mission profile [130].

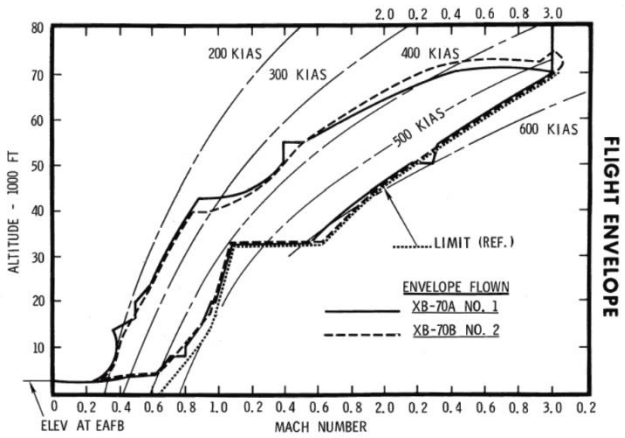

Fig. 5.35 XB-70A and XB-70B flight envelopes [122].

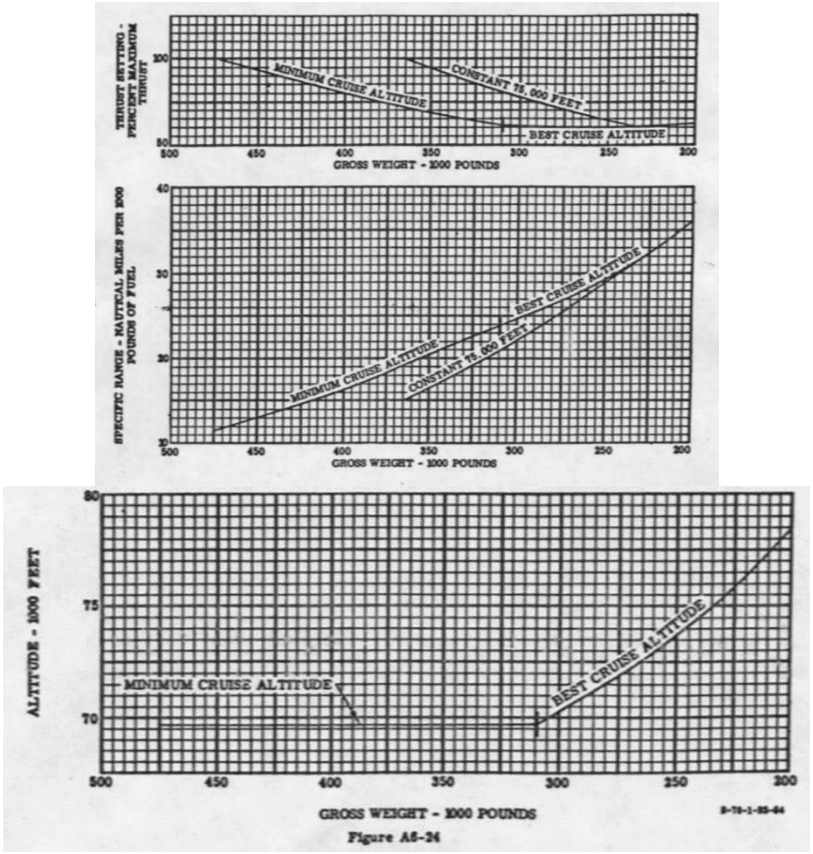

Fig. 5.36 XB-70A Mach 3.0 cruise altitude, range, and thrust settings [123].

Similar to the ascent portion of the trajectory, the descent portion uses Fig. 5.35 to determine the approximate transition altitudes and Mach numbers. The combination of the descent of Fig. 5.35 and the ascent of Fig. 5.30, Fig. 5.39 was able to be generated which will be used to

compare to the surrogate trajectory. Using this figure, it is determined that after cruise, the XB-70 decelerates at approximately constant altitude until it reaches Mach 2.4, but for the surrogate trajectory, the constant altitude deceleration ends at Mach 2.2 to better match the first descent trajectory as will be discussed. Figure 5.37 and Fig. 5.38 are used for descent as Fig. 5.35 and Fig. 5.36 were used for the ascent portion. Figure 5.37 provides more insight into the descent trajectory, while Fig. 5.38 provides the ability to determine the descent time, distance covered, and the fuel used, depending on the change in gross weight.

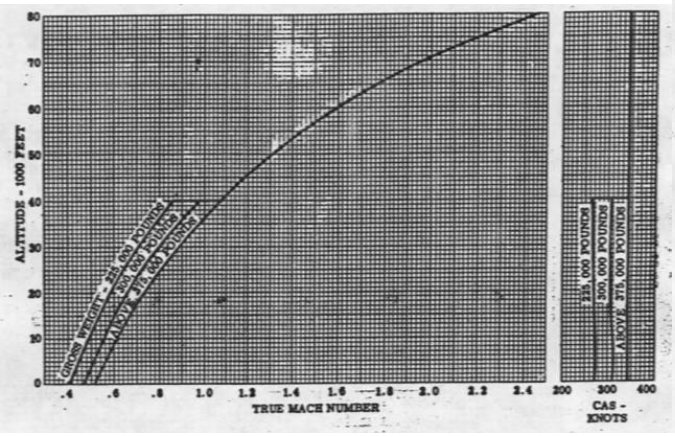

Fig. 5.37 XB-70A descent altitude, mach number, and speed for various weights [123].

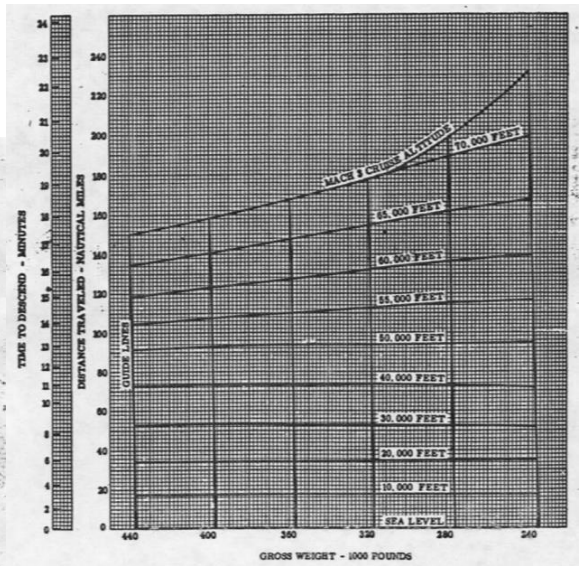

Fig. 5.38 XB-70A descent time, distance traveled, and fuel used (with change in gross weight) [123].

Continuing with the descent portion, depending on the ending weight of the constant altitude deceleration, the XB-70 begins to descend at a constant knots calibrated airspeed, or KEAS. For the surrogate trajectory, it has been decided to use a constant KEAS descent for both descent legs. For the first decent leg, a speed of 306 KEAS (317 lb/ft^2) is used. At the end of the first descent leg, which is roughly 40,000 ft, the XB-70 performs another constant altitude deceleration to obtain the speed for maximum glide range at lower altitude [123]. By selecting an

ending Mach number of 0.8 for the surrogate trajectory, the second descent leg has a constant KEAS of 228 KEAS (176 lb/ft^2). A summary of these trajectory parameters for the surrogate trajectory are shown in Table 5.21.

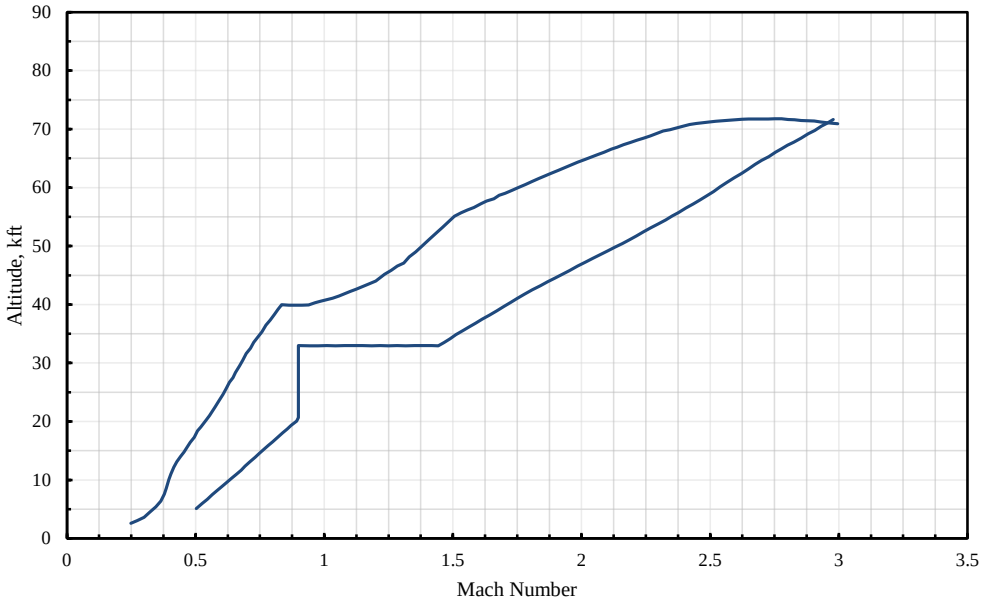

Fig. 5.39 Digitized XB-70 altitude and mach number mission profile [104,122].

Table 5.21 XB-70 surrogate trajectory input parameters.

	Flight Segment	Parameters	Method	Segment Termination
1	Takeoff and Climb Out	Start Altitude: 0 m Takeoff Distance = 2,256 m (7,400 ft) End Altitude = 50 m (164 ft)	Takeoff and Climb Out	Liftoff and specified end altitude
2	Subsonic Constant Acceleration Climb	Start Altitude = 50 m (164 ft) Start Climb Mach = 0.37 Acceleration dV/dh = 0.025 End Altitude = 6,493 m (21,300 ft) End Climb Mach = 0.9	Constant Acceleration Climb	Specified end altitude and Mach
3	Constant Mach Climb	Mach = 0.9 End Altitude = 10,060 m (33,000 ft)	Constant Mach Climb	Specified end altitude
4	Transonic Constant Altitude Acceleration	Start Mach = 0.9 End Mach = 1.44	Constant Altitude Acceleration	Specified end Mach
5	Supersonic Constant Acceleration Climb	Start Altitude = 10,060 m (33,000 ft) Start Climb Mach = 1.44 Acceleration dV/dh = 0.041 End Altitude = 21,245 m (69,700 ft) End Climb Mach = 3.0	Constant Acceleration Climb	Specified end altitude and Mach
6	Constant Altitude Cruise	Mach = 3.0 Range = 5000 km (2700 nmi)	Constant Altitude Cruise	Specified range
7	Constant Altitude Deceleration	Start Mach = 3.0 End Mach = 2.2	Powered Constant Altitude Deceleration	Specified end Mach
8	Supersonic Powered Descent with Constant EAS	KEAS = 306 kts Dynamic pressure = 317 lb/ft^2 End Altitude = 12,192 m (40,000 ft)	Powered Descent	Specified end altitude

9	Transonic Constant Altitude Deceleration	Start Mach = 1.08 End Mach = 0.8	Powered Constant Altitude Deceleration	Specified end Mach
10	Subsonic Powered Descent with Constant EAS	KEAS = 228 kts Dynamic pressure = 176 lb/ft^2 End Altitude = 30.5 m (100 ft)	Powered Descent	Specified end altitude
11	Approach and Landing	Landing Distance = 2,438 m (8,000 ft)	Approach and Landing	Touchdown and full stop

With the surrogate trajectory defined, the previous figures can be used as discussed to determine how much fuel is used, time spent, and distance covered during each trajectory segment. Table 5.22 and Table 5.23 provide these results, but it should be noted that these results were obtained by hand, with poor quality images, and corrections, such as corrections for inlet pressure recovery, have not been used in these results. Even with this, these results will be used for verification of this method when used within AVDS as no other results with the mission breakdown have been found or contained within VCC, especially for a full payload mission of 50,000 lb [105,128-130,132,140]. The reason this may have not been found and contained within the VCC is because the XB-70 never flew its intended mission after it was built, it became an experimental aircraft, carrying loads smaller than originally designed.

Table 5.22 Part one of the inputs and results from using the XB-70A flight manual to predict XB-70A performance for a mission that is similar to the surrogate XB-70 trajectory.

Mission Segment	Thrust Setting	Altitude [ft]	Weight [lb]	Time [min]	Range [nmi]	Mach Number
Subsonic Climb Start	Max AB Thrust	5,000	500,000	0.25	2.5	
Subsonic Climb End	Max AB Thrust	30,000	489,000	3	26	0.9
Transonic Acceleration Start	Max AB Thrust	30,000	489,000	1.125	8	0.9
Transonic Acceleration End	Max AB Thrust	30,000	469,800	5.9	67.5	1.61
Supersonic Climb Start	Max AB Thrust	30,000	469,800	1.80	30	1.61
Supersonic Climb End	Max AB Thrust	69,700	424,500	16.5	375	3.00
Supersonic Cruise Start	Max AB Thrust	69,700	424,500	0	0	3.00
Supersonic Cruise End	Max AB Thrust	71,000	286,500	95.98	2,760	3.00
Deceleration 1 Start	Idle Thrust	75,000	286,500	0	0	3.00
Deceleration 1 End	Idle Thrust	75,000	284,000	5.25	135	2.21
Descent 1 Start	Idle Thrust	75,000	284,000	0	0	2.21
Descent 1 End	Idle Thrust	40,000				
Deceleration 2 Start	Idle Thrust	40,000				1.08
Deceleration 2 End	Idle Thrust	40,000				0.948
Descent 2 Start	Idle Thrust	40,000				0.948
Descent 2 End	Idle Thrust	0	280,000	20.5	200	0.444

Table 5.23 Part two of the inputs and results from using the XB-70A flight manual to predict XB-70A performance for a mission that is similar to the surrogate XB-70 trajectory.

Mission Segment	Fuel Weight [lb]	Time of Segment [min]	Distance of Segment [nmi]	Rate of Climb [fpm]	Total Fuel [lb]	Total Time [min]	Total Range [nmi]
Subsonic Climb Start							
Subsonic Climb End	11,000	2.75	23.5	9,091	31,000	5.75	28.5
Transonic Acceleration Start							
Transonic Acceleration End	19,200	4.775	59.5	0	50,200	10.525	88
Supersonic Climb Start							
Supersonic Climb End	45,300	14.7	345	2,701	95,500	25.225	433
Supersonic Cruise Start							
Supersonic Cruise End	138,000	95.97981711	2,760	14	233,500	121.201	3,193
Deceleration 1 Start							
Deceleration 1 End	2,500	5.25	135	0	236,000	126.45	3328
Descent 1 Start							
Descent 1 End							
Deceleration 2 Start							
Deceleration 2 End							
Descent 2 Start							
Descent 2 End	4,000	20.5	200	-3,659	240,000	146.95	3,528
					Total Fuel [lb]	**Total Time[hr]**	**Total Range [km]**
					240,000	**2.45**	**6,534**

Finally, the determined surrogate trajectory for the XB-70 and the ascent and descent trajectory provided within the VCC are compared in Fig. 5.40. Overall, the trajectories match closely with one another, but there are a few discrepancies. Starting with the ascent portion of the trajectory, discrepancies begin right after the constant altitude acceleration until it reaches cruise, as the surrogate cruise point is at a lower altitude than what is shown from the VCC. The reason is because the cruise altitude selected was from the XB-70A flight manual as it specified at Mach 3, the starting cruise altitude should be 69,700 ft. The rest that was specified within the flight manual that was not considered though, was that once the vehicle weight reached 309,000 lb, the thrust was set to 61% of the maximum thrust and climbed to a higher altitude [123]. With the surrogate cruise altitude slightly lower than the ascent and descent plots in the VCC, the constant altitude deceleration after the cruise portion has a lower altitude as well. As previously mentioned, the surrogate trajectory for the constant altitude deceleration section ended at Mach 2.2 while it ends at Mach 2.4 from the VCC trajectory. The reason for this is so that the first leg of the descent

matches more closely to the VCC trajectory. If it ended at Mach 2.4, the first leg of the surrogate descent would be at a lower altitude overall creating a larger discrepancy than already presented. After this, the rest of the surrogate descent follows closely to the VCC trajectory.

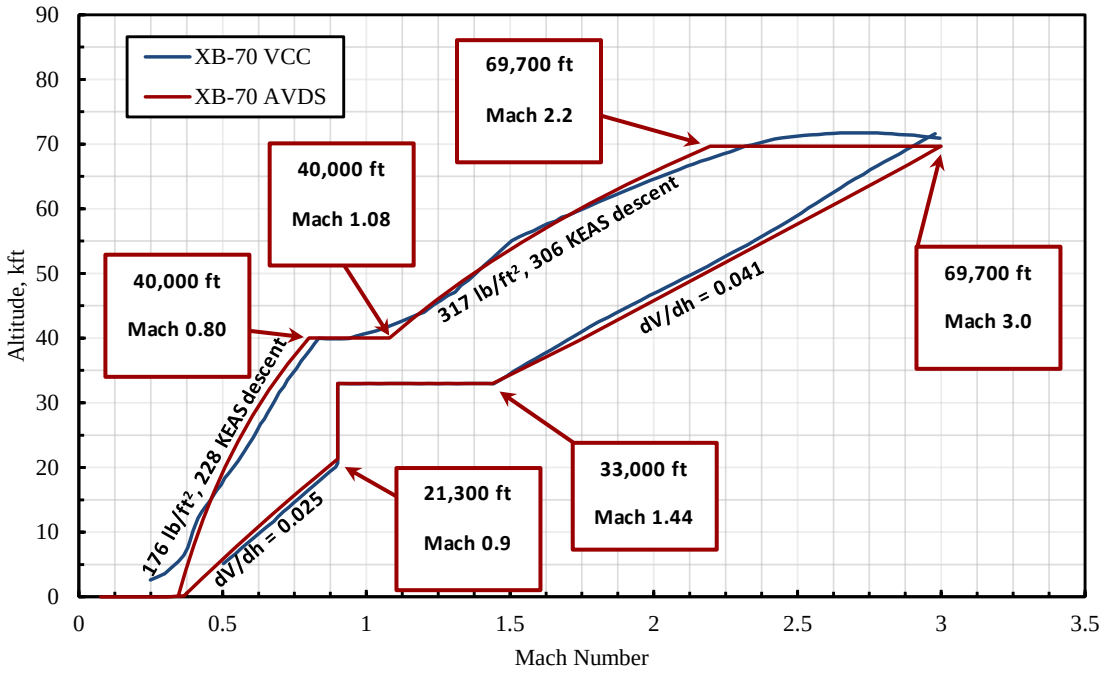

Fig. 5.40 Comparison of the AVDS^{CE} XB-70 trajectory data and the XB-70 trajectory data from VCC for altitude and Mach number.

With this surrogate trajectory, and the VCC available data from other disciplines, an initial sizing can be accomplished with AVDS^{CE} to further determine the verification of this method. From this, an altitude versus range profile was developed and is shown in Fig. 5.41. While there is not an altitude versus range profile provided in the VCC, the overall mission range can be compared to the overall mission ranges provided within the VCC, which are shown in Table 5.24. The mission range calculated as shown in Fig. 5.41 is 3,614 nmi, which compared to the range from entry 11 in Table 5.24, obtains an error of -4.2%. Out of the other entries shown, the reason entry 11, or the 1964 XB-70A-1, range value was selected for comparison is because the empty weight and the fuel weight (254,539 lb and 268,724 lb, respectively [133]) are the closest to the

ones used for verification of the synthesis system (256,148 lb and 285,881 lb, respectively [112]). The weights for the 1964 XB-70A-1 vehicle, or entry 11, are shown in Table 5.25.

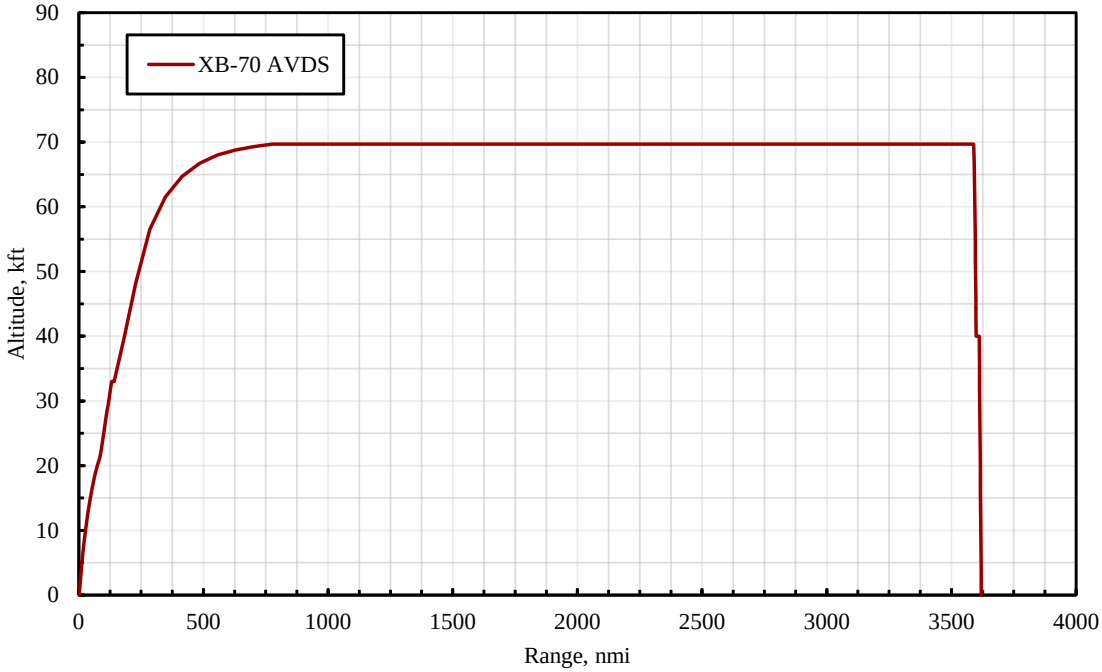

Fig. 5.41 AVDS^{CE} XB-70 altitude and range mission profile for a 50,000 lb payload.

Table 5.24 XB-70, XB-70A-1, and XB-70A-2 mission ranges and cruise attributes.

ID	Vehicle	Date	Cruising Mach	Payload [lb]	Cruising Altitude [m]	Cruising Altitude [ft]	Range [km]	Range [nmi]	Refueled?	Ref.
1	XB-70	2005	3.0	50,000	21,336	70,000	12,069	6,517	-	[128]
2	XB-70A	1964	3.0	-	21,336	70,000	12,038	6,500	-	[127]
3	XB-70	Dec. 1960	3.0	None	19,812 to 23,348	65,000 to 76,600	10,399	5,615	No	[131]
4	XB-70	April 1962	3.0	10,000	19,812 to 21,915	65,000 to 71,900	8,621	4,655	No	[132]
5	XB-70	2007	3.0	-	21,946	72,000	6,901	3,726	-	[124]
6	XB-70	1999	3.0	-	-	-	5,499	2,969	-	[114]
7	XB-70A-2	May 1964	3.0	-	19,812 to 21,862	65,000 to 71,725	7,551	4,077	No	[136]
8	XB-70A-2	Feb. 1965	3.0	-	19,812 to 21,946	65,000 to 72,000	7,425	4,009	No	[137]
9	XB-70A-2	Oct. 1965	3.0	-	19,812 to 21,869	65,000 to 71,750	7,425	4,009	No	[138]
10	XB-70A-2	April 1967	3.0	-	19,812 to 21,869	65,000 to 71,750	7,341	3,964	No	[139]
11	XB-70A-1	May 1964	3.0	-	19,812 to 21,632	65,000 to 70,970	6,988	3,773	No	[133]
12	XB-70A-1	Feb. 1965	3.0	-	19,812 to 22,098	65,000 to 72,500	6,901	3,726	No	[134]
13	XB-70A-1	April 1967	3.0	-	19,812 to 22,098	65,000 to 72,500	6,901	3,726	No	[135]
14	XB-70A FM*	Feb. 1967	3.0	-	21,245 to 21,641	69,700 to 71,000	6,534	3,528	No	[123]

*Calculated using XB-70A flight manual.

Table 5.25 XB-70A-1 and XB-70A-2 takeoff gross weights, empty weights, and fuel weights.

ID	Vehicle	Date	TOGW [lb]	Empty Weight [lb]	Mission Fuel Weight [lb]	Max Fuel Weight [lb]	Ref.
7	XB-70A-2	May 1964	542,029	248,600	283,584	283,584	[136]
8	XB-70A-2	Feb. 1965	542,029	228,965	293,407	310,929	[137]
9	XB-70A-2	Oct. 1965	542,029	230,876	291,075	310,929	[138]
10	XB-70A-2	April 1967	542,029	230,876	291,075	310,929	[139]
11	**XB-70A-1**	**May 1964**	**533,105**	**254,539**	**268,724**	**268,724**	**[133]**
12	XB-70A-1	Feb. 1965	521,056	231,215	273,056	285,881	[134]
13	XB-70A-1	April 1967	521,056	231,215	273,056	285,881	[135]

For a final comparison, the previously calculated fuel weights, and ranges for each trajectory segment from the VCC are compared to the values calculated with the initial sizing of the AVDS^{CE} using values from the VCC. The results from this comparison are shown in Table 5.26. From these results, first, the fuel calculated from AVDS is higher than the VCC, but this is because of the higher TOGW for the AVDS vehicle. The higher TOGW is most likely attributed to needing more fuel to overcome the higher drag produced with a higher angle of attack to maintain the same flight path angles during climb. For cruise weight, this difference could be attributed to not considering the exact path provided by the XB-70A flight manual, which is after reaching 309,000 lb, the vehicle than climbs with 61% of the maximum thrust setting. Out of these trajectory segments, the descent segment has the greatest error in fuel. This could be attributed to the selected flight path angles and throttle settings as these were not known. Lastly, the total fuel weights are not compared, as the fuel weight that the example in the flight manual starts with is 500,000 lb, which is less than the max fuel weight found to be for the XB-70. This fuel value is used for verification of the synthesis system results which is 285,881 lb. The error produced between the total fuel weight calculated for AVDS shown below to this value ~4%. Even though there were a few large discrepancies in the individual fuel weights for the trajectory segments with possible reasons as discussed, as the total fuel weight matches closely with the verification value, this method and surrogate trajectory is assumed verified.

Table 5.26 Comparison of the AVDS^{CE} XB-70 and the VCC XB-70 flight manual calculated ranges and fuel weights.

	VCC Fuel	AVDS Fuel	% Error	VCC Range	AVDS Range	% Error
Ascent, lb or nmi	95,500	116,657	22%	433	697	61%
Cruise, lb or nmi	138,000	156,031	13%	2,760	2,773	0.5%
Descent, lb or nmi	6,500	2,127	-67%	335	144	-57%
Totals, lb or nmi	240,000	274,815	-	3,528	3,614	-

This section was important to show the power of the VCC in terms of verification, as even though some verification values were not explicitly stated, such as the fuel weights for each trajectory segment, representative values could be determined from available figures that were not originally directly useful.

5.2.5 Weight and Volume

As for every other discipline for the XB-70, the verification values available within the VCC for weights are significant, especially compared to the X-43A who had only a few available points. With the amount of available weight values, the method of calculating component weights will be able to have a better verification for the XB-70. For the breakdown of the weights, the reference [140] was selected as it provides a very detailed account of these weights for the three versions of the vehicle. These are shown in Table 5.27 and Table 5.28. From observing these weight values, the XB-70-1 configuration was selected to use for verification as this is the version whose data was used for other disciplinary method verifications. Much of the data contained within these tables are too detailed to use within the conceptual design verification phase, so certain items will be grouped, and their summed values will be compared to the lower-fidelity weight estimation results. It is noted that none of the payloads shown for these configurations match the originally designed payload of 50,000 lb stated in other references [105]. This appears to be due to the XB-70 becoming an experimental aircraft for NASA, so it contained experimental payloads and ballast, but did not reach the max payload value. For the sake of reverse engineering and verifying the

originally designed XB-70 with the AVDS system, the original design payload of 50,000 lb is used instead. It is also noted that while this discipline is Weight and Volume, no meaningful volumes for either the XB-70 or the X-43A have been found.

Table 5.27 XB-70 weight data for verification part 1, units are lb [140].

Component	RS-70	XB-70-1	XB-70-2
Total Vehicle			
Dry Weight	207,571	250,817	253,601
Take Off Gross Weight	554,609	519,878	542,029
Max. Taxi Weight	562,609	542,029	542,029
Max. Landing Weight	282,661	296,292	296,292
Payload	10,000	0	0
Airframe Structure	**89,022**	**124,203**	**125,422**
H. Stab. & Flaps	2,240	3,244	3,285
V. Stab.	2,250	3,965	3,965
Wing	25,494	27,399	31,133
Fuselage Subtotal	**55,601**	**85,301**	**82,580**
Forward Fuselage	7,490	9,143	9,186
Interim Fuselage	40,699	64,992	62,626
Aft Fuselage	7,412	11,166	10,768
Misc. Items	2,109	1,927	2,078
Engine Mounts & Shroud	1,328	2,367	2,372
Environmental Control	**4,770**	**11,306**	**11,393**
Cabin Air Recirculation	2,069	2,336	2,441
Fluid	13	0	0
Gas	70	75	75
Water Supply System		5,682	5,696
Water (Normal)	1,515	4,076	4,076
Water (Emergency)	0	324	324
Ammonia Supply System		930	924
Remote Eqpmt. Cooling	611	1,190	1,178
Fluid (Glycol)	89	98	98
Anti-Icing	575	1,168	1,154
Propulsion	**37,630**	**39,116**	**39,189**
Engines	30,018	31,041	31,098
Engine Installation	270	301	312
Engine Cooling	179		
Drains & Vents		87	87
Fuel Pressure & Inerting	489	716	716
Nitrogen LN2	730	700	700
Fuel System	3,854	4,434	4,303
	51,797	43,646	45,971
Volume	gal	gal	gal
Weight	347,040	285,881	301,110
Engine Thrust Control	288	581	581
Engine Indicating	1,111	795	863
Starting Subsystem	397	309	324
Fire Protection	294	202	205
Detection	94	194	197
Extinguishing - Wet	185		
Extinguishing - Portable	15	8	8

Table 5.28 XB-70 weight data for verification part 2, units are lb [140].

Component	RS-70	XB-70-1	XB-70-2
Secondary Power Supply	**12,132**	**11,273**	**12,594**
Hydraulic Power Supply	8,618	6,455	7,145
Accessory Drive System	1,367	1,504	1,510
Electrical Power Supply	1,995	3,072	3,567
Air Induction System	**7,638**	**16,185**	**15,686**
Inlet Subsystem	5,486	3,372	3,462
By-pass Section	1,648	3,055	3,124
Air Induction Control		1,411	915
Controls and Displays		3,709	3,471
Boundary Layer Control	504	700	709
Cooling and Control		3,938	3,971
Cooling Nitrogen			1,050
Fod Screens			34
Flight Control	**7,751**	**7,610**	**7,705**
Primary Flight Controls	4,236	4,433	4,502
Secondary Flight Controls	3,145	2,818	2,842
Flight Augment. Controls	370	359	361
Accommodations & Escape	**3,267**	**1,830**	**1,827**
Personnel Equipment	2,281	1,256	1,256
Liquid Oxygen System	136	110	109
Crew Accommodations	850	464	492
Alighting & Arresting	**17,008**	**19,772**	**20,173**
Main Landing Gear	13,049	14,209	14,649
Nose Gear	1,794	1,978	1,988
Drag Chut Subsystem	450	516	512
Controls and Displays	1,715	2,769	3,024
Mission & Traffic Control	**1,310**	**1,096**	**1,144**
Comm. Equipment	632	304	352
Nav. Aids Equipment	146	308	309
IFF	308	100	100
Integrated Power Supply	65		
Racks & Supports	110	384	383
Flight Indication System	**10,615**	**665**	**661**
Aux. Gyro Platform	315	169	169
Flight Instruments	168	341	337
Control Air Data System	543	155	155
Offense Electronics	2,848		
Defense Electronics	6,216		
Weapon Platform	525		
Test Equipment		**16,263**	**18,369**
Misc. Items	100	**12,179**	**11,287**
Ballast (Design)		10,000	9,072
Ballast (Alternate)		2,078	2,078

With the verification data above, the compiled weights estimation library for this vehicle can now be used for verification. This weights estimation library can be viewed in reference [14]. As there are several methods to estimate the weight of a particular component, such as the fuselage, the result that produced the least error was selected. The final results for the verification are shown in Table 5.29. As observed, a few of the components have high error such as the wing weight with an error of 60.67%. While this is significant on its own, when compared to the whole vehicle, it contributes a small portion to the total weight as the dry weight error of the vehicle is 4.21%. With this, not only are the individual component errors shown on their own, but their component proportion is provided to show how much of the overall error that particular component is contributing. It should be noted that error in some of the component weights is possibly due to how the weights in the verification data table above were grouped. It is unknown which portions of the components were considered in the weight estimations. An example is for the weight estimation of the wing. While the weight method states wing, the weight-breakdown of the actual vehicle could be attributed to parts of the fuselage, thrust structure, or the air induction system. Despite the errors in some of the individual components, the important weights used within the AVDS system sizing process are the dry weight, fuel weight, and the takeoff gross weight, so with a percent error 4.21% for the dry weight, this method is deemed verified for this vehicle.

Table 5.29 XB-70 weights estimation verification results.

Group	Reference Weight [lb]	Calculated Weight [lb]	Difference*	Absolute Difference	Error†	Absolute Error	Component Proportion	Error Contribution†	Method Reference
Fuselage	85,301	88,597	3,296	3,296	3.86%	3.86%	39.34%	1.52%	[96]
Engine	31,041	30,086	-955	955	-3.08%	3.08%	14.31%	-0.44%	[61]
Wing	27,399	44,023	16,624	16,624	60.67%	60.67%	12.63%	7.67%	[97]
Landing Gear	19,772	25,671	5,899	5,899	29.83%	29.83%	9.12%	2.72%	[61]
Inlet	16,185	13,601	-2,584	2,584	-15.96%	15.96%	7.46%	-1.19%	[98]
Avionics	7,610	7,812	202	202	2.65%	2.65%	3.51%	0.09%	[61]
Tanks	4,434	3,025	-1,409	1,409	-31.77%	31.77%	2.04%	-0.65%	[99]
Vertical Stabilizer	3,965	3,660	-305	305	-7.70%	7.70%	1.83%	-0.14%	[61]
Horizontal Stabilizer	3,244	2,237	-1,007	1,007	-31.05%	31.05%	1.50%	-0.46%	[61]
Electrical Systems	3,072	3,166	94	94	3.07%	3.07%	1.42%	0.04%	[61]

Fuselage - Thrust Structure	2,367	1,232	-1,136	1,136	-47.97%	47.97%	1.09%	-0.52%	[61]
Fuselage - Secondary Structure	1,927	2,883	956	956	49.59%	49.59%	0.89%	0.44%	[97]
Total	216,854	225,992	9,138	9,138	4.21%	4.21%	100.00%	4.21%	

* Positive values highlighted in blue, negative values in yellow
† The product of Error and the Component Proportion

5.2.6 Synthesis

With the disciplinary methods verified as discussed above, the selected methods can now be joined with the overall inputs and assumptions for the synthesis system to obtain sizing results for the XB-70. Table 5.30 provides a list of the inputs and assumptions used within AVDS^{CE} for the XB-70. Some of the inputs and assumptions shown are not available for the actual vehicle, so either the verified VSP model was used, or the range of values provided in Hypersonic Convergence for the respective parameter was reviewed [33].

Table 5.30 AVDS^{CE} XB-70 inputs and assumptions [14].

Variable Discipline	Variable	Value
Geometry	Wing tip droop angles, deg	0, 25, 65
Aerodynamics	Ratio of square of Oswald efficiency factor to skin friction drag coefficient	200
Propulsion*	Number of engines	6
Trajectory	Takeoff segment: Starting altitude, m	0
	Takeoff segment: Starting velocity, m/s	0
	Takeoff segment: Obstacle altitude, m	15.24
	Takeoff segment: Climb flight path angle, degrees	1.5
	Takeoff segment: Angle of attack at liftoff, degrees	11.5
	Takeoff segment: Change in velocity before the liftoff velocity, m/s	10.29
	Takeoff segment: Rotation angular velocity, deg/s	2.1
	Takeoff segment: Rolling ground friction coefficient	0.025
	Constant acceleration climb segment (1): End Mach	0.9
	Constant acceleration climb segment (1): End altitude, m	6,300
	Constant acceleration climb segment (1): Change in velocity per change in altitude, sec^{-1}	0.025
	Constant Mach climb segment: Flight path angle, degrees	2
	Constant Mach climb segment: End altitude, m	10,058
	Constant altitude acceleration segment: Desired acceleration, m/s^2	0.3
	Constant altitude acceleration segment: End Mach	1.44
	Constant acceleration climb (2) segment: End Mach	3.0
	Constant acceleration climb (2) segment: End altitude, m	21,245
	Constant acceleration climb (2) segment: Change in velocity per change in altitude, sec^{-1}	0.041
	Constant altitude cruise segment: range, km	5,000
	Constant altitude powered deceleration segment (1): End Mach	2.2
	Constant q powered descent segment (1): End altitude, m	12,192
	Constant q powered descent segment (1): End Mach	1.08
	Constant q powered descent segment (1): Maximum longitudinal acceleration, m/s^2	-0.01
	Constant q powered descent segment (1): Minimum longitudinal acceleration, m/s^2	-1.5
	Constant altitude powered deceleration segment (2): End Mach	0.8
	Constant q powered descent segment (2): End altitude, m	30
	Constant q powered descent segment (2): End Mach	0.31
	Constant q powered descent segment (2): Maximum longitudinal acceleration, m/s^2	-0.1
	Constant q powered descent segment (2): Minimum longitudinal acceleration, m/s^2	-0.9

Weights and Volume	Number of crew	2
	Number of passengers	0
	Weight of cargo, N	222,411
	Weight of unmanned fixed systems, N	18,639
	Weight of each crew member, N/person	1,265
	Weight fixed manned systems per crew member, N/person	10,301
	Weight of each passenger, N/person	-
	Weight of passenger provisions per passenger, N/person	-
	Weight of variable systems per vehicle dry weight	0.16
	Minimum dry weight (OEW) margin	0.05
	Volume of unmanned fixed system, m^3	1.55
	Volume of provision for each crew member, m^3/person	1.5
	Volume per crew member, m^3/person	1.5
	Volume of manned fixed systems per crew member, m^3/person	1
	Volume of each passenger space, m^3/person	-
	Volume of variable systems per total vehicle volume, m^3	0.1
	Volume of vehicle void space per total vehicle volume, m^3	0.095
	Error band around the structural fraction, $m^{-0.138}$	0.049
	Cargo density, kg/m^3	2,000
	Fuel density, kg/m^3	810

*The inputs used in the NPSS method have been left out.

For the XB-70 sizing verification using the AVDS^{CE}, the XB-70 was a unique challenge as it was the first vehicle within the NASA study to attempt sizing using a full flight regime (from takeoff to landing), to consider aerodynamic phenomenon such as compression lift, and to attempt variable geometry changes through the trajectory with the folding wing tips. Using the verified method above and the provided inputs within the AVDS^{CE} system, the sized results for the XB-70 were able to be obtained as shown in Table 5.31. From the results, it is shown that the majority of the results are within 6.0% error except for the structural weight (-14.8% error), the structural index (-14.7% error) and the Industrial Capability Index (24.2% error). The error in the structural weight is not a significant problem as the operating empty weight (OEW) was within 5% error. The error in the structural index is directly related to the error in the structural weight. The large error within the Industrial Capability Index, ICI, is mostly due to the error from the structural index as it had the larger error between it and the propulsion index. Even with these relatively high errors due to the structural weight, the major weights of OEW and OWE are less than 5%, with even the TOGW having an error of 0.51%. With these, the AVDS^{CE} system is assumed verified for the XB-70.

Table 5.31 Comparison of the AVDS^{CE} XB-70 sizing results to the (VCC) actual XB-70 data. The results shown are the verification results with a 50,000 lb payload.

Sized Vehicle Attributes	XB-70 [EN]	AVDS XB-70 [EN]	XB-70 [SI]	AVDS XB-70 [SI]	% Error
Operating Weight Empty, lb or kg	256,148	265,258	116,147	120,277	3.56
Operating Empty Weight, lb or kg	206,148	214,668	93,475	97,338	4.13
Takeoff Gross Weight, lb or kg	542,029	544,814	245,776	247,038	0.51
Structural Weight, lb or kg	124,203	105,837	56,318	47,990	-14.8
Fuel Weight, lb or kg	285,881	279,557	129,629	126,761	-2.21
Payload Weight, lb or kg	50,000	50,000	22,672	22,672	-
Tau, $V_{total}/S_{pln}^{1.5}$	0.0549*	0.0549	0.0549*	0.0549	-
Total Planform Area, ft^2 or m^2	7,099*	7,093	660*	659	-0.09
Wing Planform Area, ft^2 or m^2	6,297	6,291	585	584	-0.09
Wetted Surface Area, ft^2 or m^2	18,981*	18,964	1,763*	1,762	-0.09
Total Volume, ft^3 or m^3	27,442*	27,406	777*	776	-0.13
Ratio of Wetted to Total Planform Area	2.67*	2.67	2.67*	2.67	0.00
Structural Index, $I_{str} = W_{str}/S_{wet}$, lb/ft^2 or N/m^2	6.54*	5.58	313*	27.2	-14.7
Propulsion Index, $I_p = \rho_{fuel}/(WR\text{-}1)$, lb/ft^3 or kg/m^3	45.3	48.0	726	769	5.90
Industrial Capability Index, $10 \cdot I_p/I_{str}$	69.26*	86.0	227*	282	24.2
Total Fuel Fraction, W_{fuel}/TOGW	0.527	0.513	0.527	0.513	-2.71
Total Weight Ratio, TOGW/OWE	2.12	2.05	2.12	2.05	-2.94
Total Planform Wing Loading, TOGW/S_{pln}, lb/ft^2 or N/m^2	76.3*	76.8	3,656*	3,678	0.60
Wing Planform Wing Loading, TOGW/S_{wing}, lb/ft^2 or N/m^2	86.1	86.6	4,122	4,146	0.60

*Values that have been obtained using the XB-70 VSP geometry model

With the methods and now the synthesis system deemed verified for the XB-70, it was again shown how indispensable the VCC was to the verification process. As discussed at the beginning of this chapter, the verification process for the XB-70 was chosen to be discussed as the verification data available is abundant. This was to provide a direct contrast with the X-43A whose verification data was scarce. From this process, it was shown how the VCC can be used for verification whether the data available is abundant or not. The importance of this is that the information was gathered, stored, and made available all from one location, and can be easily accessed for future projects. As the VCC is a dynamic system, which means it is constantly updated when more information is made available, for the vehicles that are currently scarce on verification data, these could eventually be updated, and the methods and synthesis system could be further verified.

CHAPTER 6: PARAMETER TREND INVESTIGATION

6.1 Purpose of Parameter Trend Investigation

For the parameter trend investigation, as this was initiated during the NASA contract, the main objectives were to develop possible correlations to help with input parameter values into the AVDS system, method development, and geometric scaling law development. Another purpose for this investigation was to provide insights into the behavior of the sizing results generated within AVDS.

For the input parameter values, the AVDS system requires an 'input deck' which houses all the required inputs to run the system such as cruise Mach number, mission range, tau value, etc. Some of these values, such as K_v, which is a propellant volume parameter, are determined from provided range values, but these values may only be applicable to certain vehicle missions or sizes, so new correlations would be required to obtain more reasonable values to use. For the scaling law development, an example is provided previously in Chapter 4, where the cabin size of the wing body vehicle is scaled with respect to number of passengers from created correlations. An example for the final main objective of method development, is the main discussion of this chapter to show how the parameter trend investigation was accomplished to create a method to use within AVDS. This method was created to determine the structural index value of each sized point as will be discussed.

6.2 Case Study: Structural Index (I_{str}) Investigation

6.2.1 Structural Index (I_{str}) Background

Before investigating the structural index, I_{str}, parameter and its relation to other parameters, the background of where this parameter came from and how it has been used must be discussed. This is because the structural index is not a geometric or mission parameter such as planform area and range, that does not necessarily require a buildup of its history but is a technology level parameter developed by Paul Czysz in the 1980's [33]. It was first shown within a hypersonic aerospace vehicle design and forecasting methodology called Hypersonic Convergence, along with two other technology parameters, the propulsion index, I_p, and the industrial capability index, *ICI*. As shown in Table 6.1, the structural index is a function of structural weight (W_{str}) and wetted area (S_{wet}), the propulsion index is a function of propellant density (ρ_{ppl}) and weight ratio (*WR*), and *ICI* being a function of these two technology parameters. These are known as technology parameters as they represent the technology level of a designed vehicle or provides a technology limit when current industry values are known, by being functions of technology as shown in Table 6.1 as well. While there are three technology parameters, one of the reasons that the structural index parameter was selected for this process is because it is an input within AVDS, while the other two are calculated within the synthesis system.

Table 6.1 Summary of how I_{str}, I_p, and *ICI* behave when decreasing and increasing the level of technical capability required to develop a design.

	Structural Index	Propulsion Index	Industrial Capability Index
	$I_{str} = \frac{W_{str}}{S_{wet}}$	$I_p = \frac{\rho_{ppl}}{WR - 1}$	$ICI = 10 \cdot \frac{I_p}{I_{str}}$
Decrease Technical Capability Required:	⇧	⇩	⇩

Increase Technical Capability Required:	⇩	⇧	⇧
Types of Technology:	• Structural concept • Materials • Manufacturing Capability	• Propulsion concept • Fuel choice • Aerodynamics • Combustion energy	• A combination of structural and propulsion technology
Example:	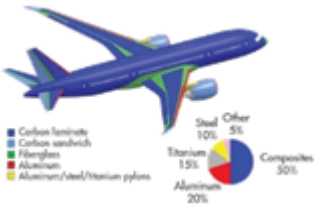	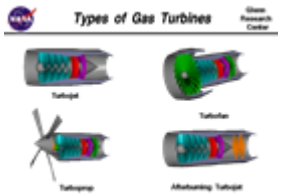	

Starting with Hypersonic Convergence where the structural index was first shown, a range of values were determined as shown in Table 6.2. These values cover the experience range of J. Vandenkerckhove (VDK) and the author of Hypersonic Convergence, Paul Czysz, for operationally sized hypersonic cruise vehicles with active TPS and hypersonic gliders with passive TPS. VDK's structural index values of 'reference' and 'advanced', were determined through discussions with British, French, German, and Russian sources in 1987 to 1990. The U.S. 1967-1970 structural index value was based on the values obtained from the Hypersonic Research Facilities Study (HyFAC), a NASA-sponsored research program in 1968-1970, while the 1983-1985 projection was determined though the Advanced Engineering Department of McDonnell Aircraft [33]. Even though the HyFAC study was roughly 20 years old when this range of values were considered, a NASA Langley AIAA report by Pegg et al [141] which documents a waverider design that produced the same I_{str} values. This means that the HyFAC study and results are still relevant today, and as will be shown from more modern studies, this range and/or these limits for the structural index are still used.

Table 6.2 Range of Structural Indices Encompassed by Investigation [33].

Minimum Value Considered	U.S. 1967-1970 SOA	VDK European 'Advanced'	VDK LACE Study	VDK European 'reference'	U.S. 1983-1985 Projection	Maximum Value Considered
17.0 kg/m^2	17.1	18.0	19.0	21.0	22.0	23.0
3.48 lb/ft^2	3.50	3.69	3.89	4.30	4.5	4.71

To help determine these structural index values, McDonnell Douglas used the structural concept shown below in Fig. 6.1. While the shingle and insulation materials were varied depending on the thermal input, the materials used for the main structure stayed the same with it being primarily aluminum with steel and titanium where strength was required. The values presented along with the structural concept are specific weights, or individual I_{str} values, for a passive insulated structure at Mach 12 for a demonstrator (Demo) with a flight time of 10 min or less, and a 1968 calculation and 1983 projection of a fully operational vehicle with a flight time of 90 min [33].

Figure 6.1 also shows values for three different structural configurations: integral tank, non-integral tank, and un-insulated tank. The integral tank configuration is where the tank is conformal to the body, so a separate tank to hold the fuel is not needed, this produces the lightest of the three configurations. The non-integral tank configuration is where the tank is separate from the structure of the body to hold the fuel, this produces the second lightest of the three configurations. These first two structural configurations are cold structures, meaning that the primary structure experiences relatively small temperature change as the shingle and insulation handle the thermal input. The third configuration, the un-insulated tank, means it is a hot structure with a non-integral tank, so the structure for this case does experience great temperature changes as the primary structure handles both the aerodynamic loads and the thermal input. With this and the separate tank, the un-insulated tank configuration is the heaviest of the three.

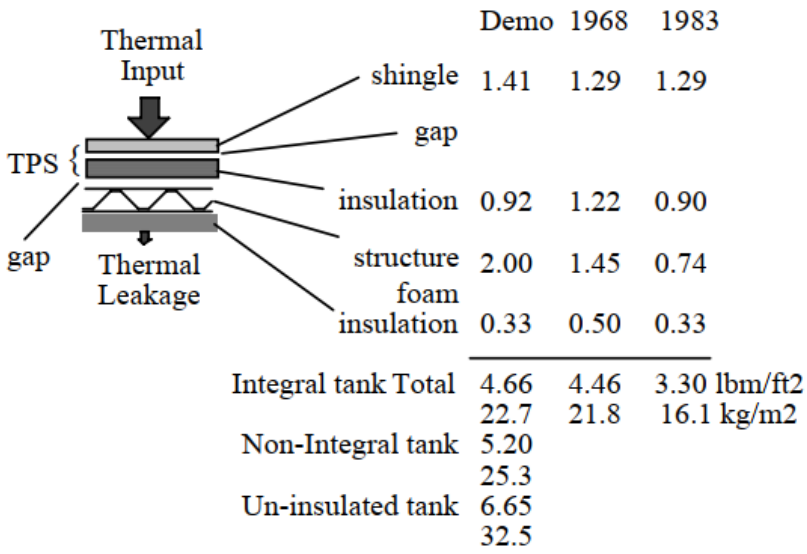

Fig. 6.1 Structural concept for hypersonic vehicles [33].

Using this structural concept, a structural index vs temperature plot shown in Fig. 6.2, was able to be developed. When this was originally developed in the 1970s, high-temperature refractory metals were used for the shingles such as columbium (niobium), tantalum, molybdenum, and Rene 41. These had densities greater than steel (9 to 17 kg/m^3 or 0.56 to 1.06 lb/ft^3) though, so the original figure would have had greater structural index values, shifting the trend in Fig. 6.2 up. The materials shown in Fig. 6.2, the rapid solidification rate (RSR) titanium, RSR metal matrix composites (MMC), carbon-carbon, etc., are relatively newer materials that achieved the same temperature performance as the high-temperature refractory metals at a much lower weight [33]. The newer materials were not directly calculated as the older materials were, but instead, the weights were scaled from the original 1970 data, so even though these I_{str} values are lower than the original, they are still conservative estimates. These structural index values were estimated to be possible at the beginning of the 21st century [33].

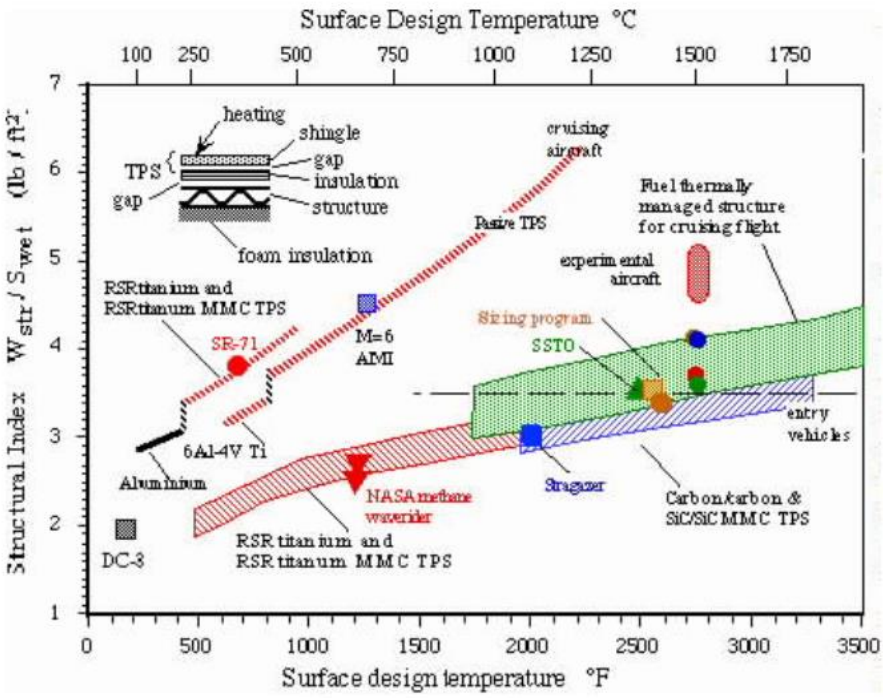

Fig. 6.2 Representative structural specific weights for a near-term demonstrator [33].

With the structural index values provided previously, these were then used as inputs or limits to compare to, for sizing vehicles and observing their behavior with respect to this parameter. Beginning again with Hypersonic Convergence, as this is where the parameter was developed, several sizing results and sensitivities were conducted using the geometries shown in Fig. 6.3. An example of one of the sizing results developed is shown in Fig. 6.4. This figure shows the feasible design space for each geometry configuration by using the 3.5 lb/ft^2 value from the HyFAC study, shown in Table 6.2, as a constant line for the lower limit, while the upper limit is the maximum possible I_{str} value for the tau (τ) and propulsion index (I_p) combination. The propulsion index (I_p) for this case, is determined by calculating the effect due to tau from the reference I_p value. From this, it is observed that the right-circular cone has the largest available design space and design margin, with the margin being the difference between the highest calculated I_{str} value, which is the maximum structural index that will allow convergence, and the lower limit, which is considered

the industrial capability. After the cone, from largest available design space to smallest is the blended-body, winged-body, and then the waverider. This figure shows one of the powers of the structural index by relating the material, structural, and manufacturing technology to sizing, and allowing the screening of several geometries. This shows that while three of the geometric configurations have possible feasible solutions for the provided mission, the waverider configuration would require an increase in some field of technology related to the structural index to lower the current industry value and provide a larger feasible design space.

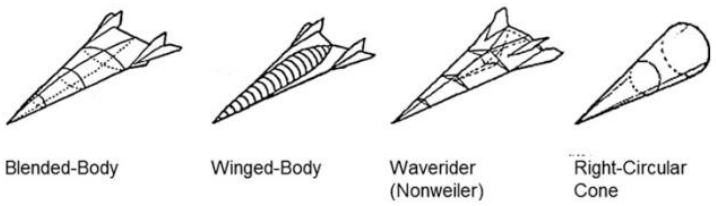

Fig. 6.3 Propulsion integrated configurations, 78° leading edge angle [33].

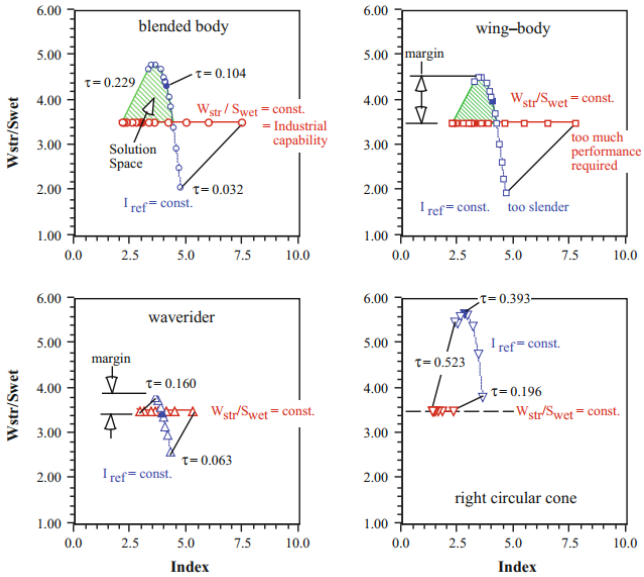

Fig. 6.4 Summary of the available design space for four different configuration concepts [33].

Outside of Hypersonic Convergence, the structural index has seen some use. While I_{str} was mostly solved originally, some cases used it as an input to observe the sensitivities of this

parameter on the design to determine which value should be used. Most of these cases also used the previous tables and figures for the inputs and ranges of the structural index. Some examples of more modern publications that use the structural index are provided and will be presented from the oldest to the most recent. The first publication considered is a dissertation by Gary Colemon from the University of Texas at Arlington (UTA), which was published in 2010 [13]. The structural index in this case was used as an input for two designs that were being sized, the Sänger EHTV and the LAPCAT II as shown in Fig. 6.5. The values selected for these vehicles were VDK's 'reference' and 'advanced' values as shown in Table 6.2. While only one I_{str} value was selected for the LAPCAT II as the structure was assumed to be thermally managed, for the Sänger EHTV, two I_{str} values were selected with the assumption of a passive TPS, so that both values could be sized to determine whether one of these limits could be used for this vehicle. Figure 6.6 below shows the results of this comparison and that the structural index value of 21.0 kg/m^2 (VDK's 'reference' value) produces a design point that matches closely with the actual Sänger vehicle. This shows that the structural index could be used as an input to estimate the technology level of a vehicle, as the LAPCAT II is assumed to require 'advanced' technology to be manufactured, the Sänger EHTV is shown that it could potentially be manufactured with today's material, structural, and manufacturing technology.

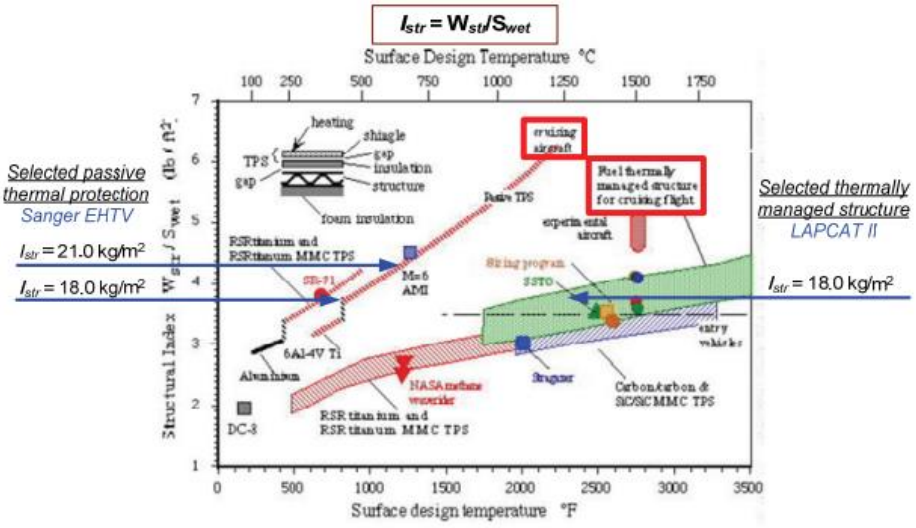

Fig. 6.5 Selected structural indices for the Sänger EHTV and LAPCAT II missions [13].

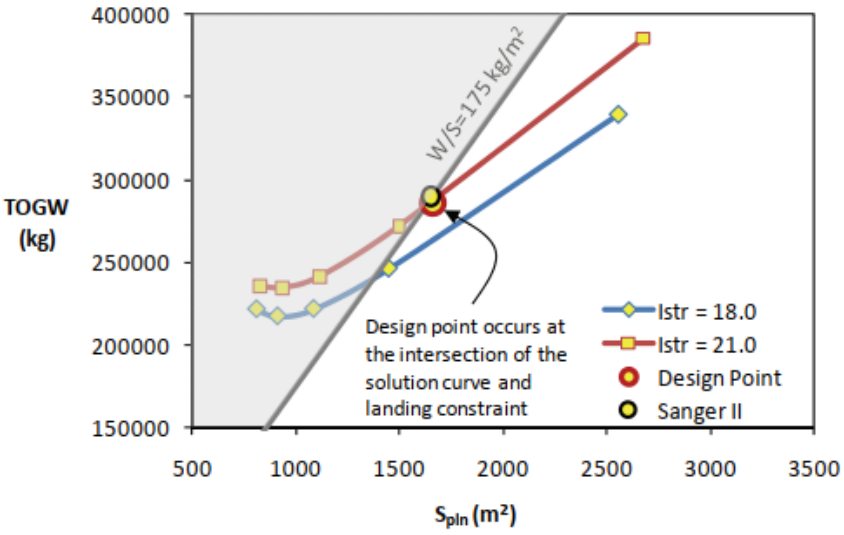

Fig. 6.6 Sänger II design space for two structural indices [13].

The next publication considered was published within the Journal of Aircraft in 2011 by Ingenito et al, where the structural index was used to size a fully integrated hypersonic commercial airliner [142]. For this case, the structural index was selected as an input again, but was used to determine the sensitivity of the parameter on the design instead of determining the closest I_{str} value to the original as the previous case for the Sänger EHTV. The selected values were again VDK's 'reference' and 'advanced' values, along with an even further advanced technology level of 15.1

kg/m^2 as shown in Fig. 6.7. It is shown that as the structural index is increased, the sized points along the emergency landing constraint line increase in planform area, but decrease in tau, or decrease in volume per planform area. Even though the structural index does affect the size, but as this vehicle is a fuel-dominated aircraft, the weight and size are primarily impacted by fuel weight and available volume, so the structural technology is considered a second-order design variable. With this, the I_{str} value selected was the mid-value of 18 kg/m^2 as it is a moderate structural technology level and produced relatively negligible weight savings when compared to the more technologically advanced 15.1 kg/m^2 structural index value. This shows that the technology level could be varied to determine how sensitive the design is to it, and then a technology level could be selected that is a compromise between what is industrially available, how much technology needs to advance, and performance, size, and weight of the vehicle.

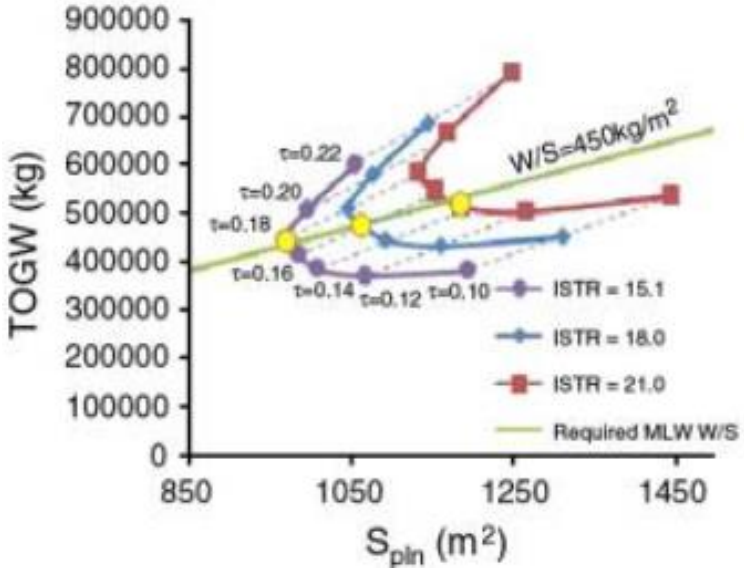

Fig. 6.7 Vehicle configuration sensitivity to I_{str}. (*W/S* denotes the wing loading, or weight over surface) [142].

The next publication is a NASA contractor report by the Aerospace Vehicle Design Laboratory (AVD Laboratory) at UTA published in 2012, where several hypersonic endurance

demonstrator configurations were screened [18]. For this case, the structural index was calculated and used as a primary constraint for the generated solution spaces. An example of one of the solution spaces that were generated is shown in Fig. 6.8. As shown for each sized point, the structural index is calculated, as the x-axis of the plot is for I_{str}, and the left bound of the solution space is limited by the structural index. These limits were considered the industrial capability of this parameter and is calculated in Fig. 6.9 for both a hydrogen vehicle and a kerosene vehicle. The reason that there are four limits for the structural index value, creating four solution spaces with the left bound depending on the selected limit, as shown in Fig. 6.8, is because for both the hydrogen and the kerosene vehicle, there are four structural concepts. These concepts are 1) a lithium-aluminum structure with refractory shingles, 2) a lithium-aluminum structure with advanced shingles (assumed SEP SiC/SiC MMC shingles), 3) a composite structure with refractory shingles, and 4) a composite structure with advanced shingles. The breakdown of the structural index value for the limit of each structural configuration for the hydrogen vehicle are from a combination of the values provided in Fig. 6.1 and Table 6.2. The kerosene fueled vehicle uses the same values for its structural limits, except the foam insulation, or the tank insulation, is removed as kerosene fuel is not cryogenic as hydrogen fuel is and could potentially be used as a heat sink. This case shows how the structural index could be used to constrain feasible design spaces, and that more than a single value could be used with these limits providing possible structural technology to obtain these values. It is noted that the structural configuration used for the fuel tank is assumed to be an integral tank for both hydrogen and kerosene fuel.

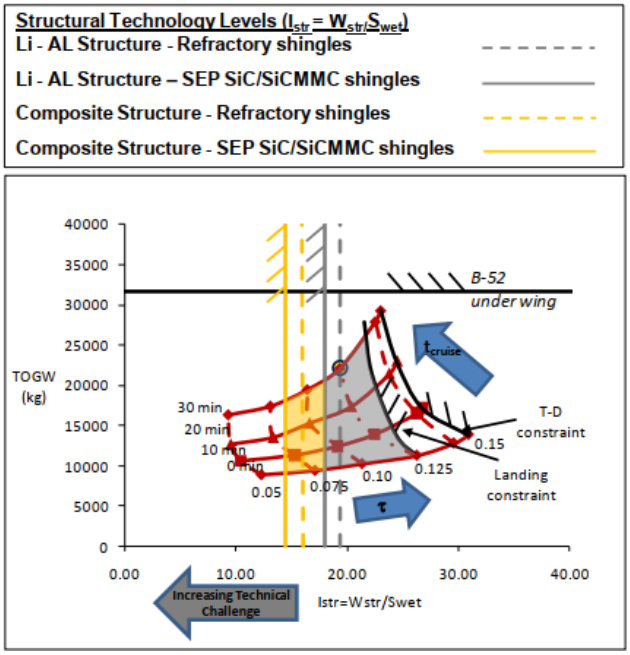

Fig. 6.8 Superposition of structural indices provides the final constraint to determine the technical solution space [18].

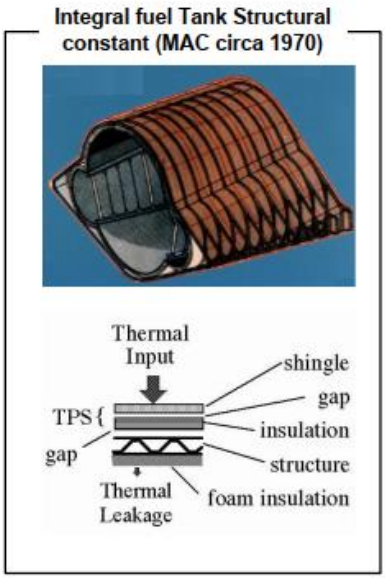

Break-down of industrial capability index

Integral Hydrogen Fuel tank

	Li-AL structure		Composite strucutre	
	Refractory shingles	Advanced schingles	Refractory shingles	Advanced schingles
	kg/m²	kg/m²	kg/m²	kg/m²
Shingle	6.30	4.88	6.30	4.88
Insulation	4.39	4.39	4.39	4.39
Structure	7.08	7.08	3.61	3.61
Foam insulation	1.61	1.61	1.61	1.61
total	***19.38***	***17.97***	***15.92***	***14.50***

Integral Kerosene fuel tank

	Li-AL structure		Composite strucutre	
	Refractory shingles	Advanced schingles	Refractory shingles	Advanced schingles
	kg/m²	kg/m²	kg/m²	kg/m²
Shingle	6.30	4.88	6.30	4.88
Insulation	4.39	4.39	4.39	4.39
Structure	7.08	7.08	3.61	3.61
Foam insulation	0.00	0.00	0.00	0.00
total	***17.77***	***16.36***	***14.31***	***12.89***

Fig. 6.9 Definition of structural capability indices used for this study [18].

The last publication that will be considered is an AIAA Space Forum conference paper from 2017 by Rana et al, which conducted a parametric sizing study to determine the effects of configuration geometry on a lifting-body reentry vehicle [143]. For this case, the structural index is calculated for each point and used primarily to compare the manufacturability of each sized

point and geometrical change. A couple of examples of results obtained from this study are shown in Fig. 6.10 and Fig. 6.11. Along with the structural index, a performance efficiency index defined by Eggers in 1956 [144] was used as well to compare the effects of the geometry changes as shown in these figures. The results are normalized to the max calculated value for each parameter. Figure 6.10 shows how the manufacturability and performance is affected for a single lifting-body cross-section with variation in spatula width and tau. Focusing on the structural index, this shows that for a single cross-section configuration, that increasing the spatula width increases the difficulty at which the vehicle is manufactured and increasing the tau value of the vehicle decreases the difficulty at which the vehicle is manufactured.

For Fig. 6.11, the lifting-body cross-sectional shape is changed to determine its effect on the manufacturability and performance. Again, for the structural index, at the lowest tau value, from most difficult to manufacture cross-section to least difficult is the half-ellipse, trapezoid, half-diamond, ellipse, and then diamond. For the highest tau value, the manufacturability of the cross-sections from most difficult to least is half-ellipse, half-diamond, trapezoid, diamond, and then ellipse. This shows how the combination of geometric changes, in this case the cross-sectional shape and the tau value, can affect the manufacturability of a vehicle design as at a certain tau value, the vehicles changed the order on which was more difficult to manufacture. It is also interesting to note that only for the half-ellipse cross-sectional shape that the vehicle designs increase in difficulty to manufacture with increase in tau value.

This study shows the importance of the structural index parameter during conceptual design as several vehicle cross-sectional shapes and geometrical variations, such as the spatula width change, were able to be compared using this parameter, and if current industry limit lines were added such as with the previous discussed study, then possible configurations that could be

manufactured could be selected. While I_{str} was used to compare manufacturability for this case, it could still be taken as the technology level required for each vehicle and which configurations would require more technical capability, with respect to materials, structures, and manufacturing, than others.

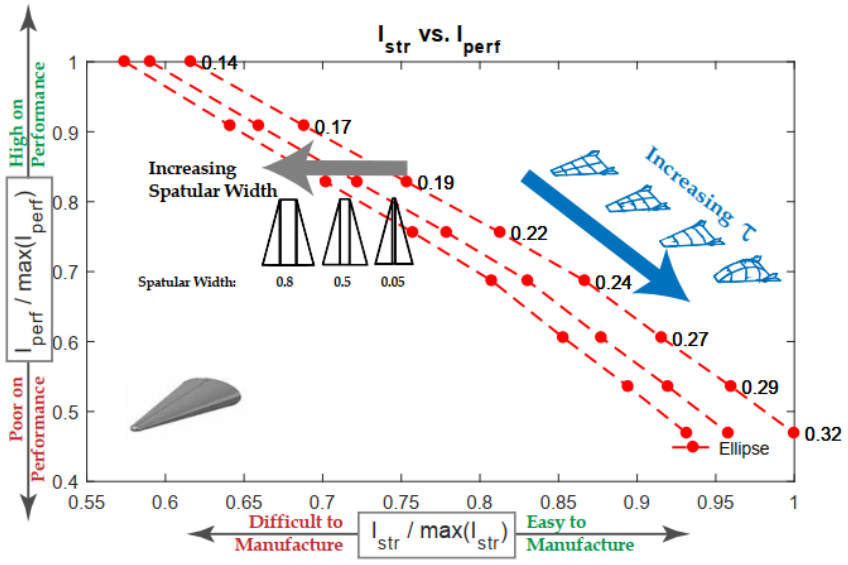

Fig. 6.10 I_{str} vs I_{perf} with varying spatula width and tau [143].

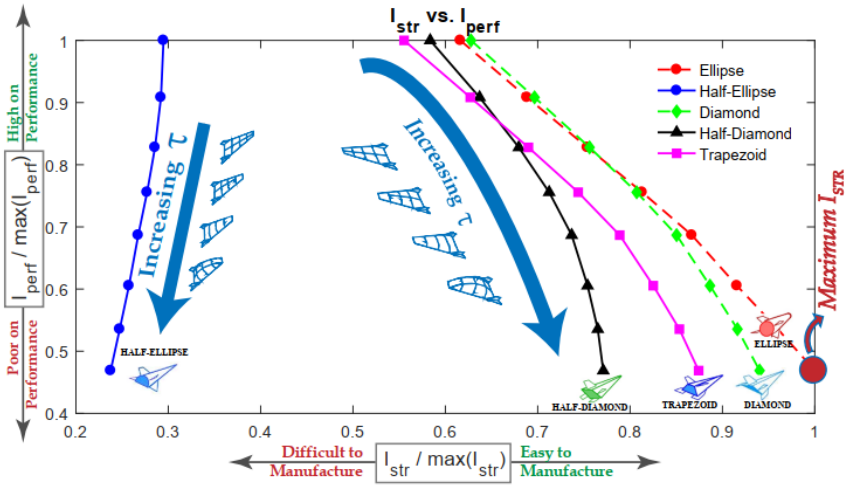

Fig. 6.11 I_{str} vs I_{perf} with varying vehicle cross-section and tau [143].

6.2.2 Structural Index (I_{str}) Trend Investigation

With the background of the structural index (I_{str}) parameter covered, the comparisons to selected parameters can be made and possible trends can be observed. As mentioned, the parameters that were selected to compare to I_{str} were primarily determined from the inputs used within AVDS, as the purpose of this case study is to improve AVDS and to show how parameter trend investigation can be used for a synthesis system. As this parameter comparison was investigated during the NASA contract [14], the main parameters investigated were number of passengers (PAX), payload weight (W_{pay}), and planform area (S_{pln}). While Mach number is another input into AVDS, it is not shown as the temperature experienced during flight is a function of cruise Mach number, and vice versa, so the original figure of I_{str} vs. temperature as shown in Fig. 6.2 in the background section was used for this case. A couple more parameters investigated for comparison to determine trends are the wetted area (S_{wet}) and the industrial capability index (ICI), as these are known functions.

Beginning with the input values, PAX and W_{pay} are shown in Fig. 6.12 and Fig. 6.13. Even though PAX is the main input value into AVDS, not W_{pay}, both are observed as a vehicle may have a payload but no passengers. The vehicles that are observed for the correlations are a collection of wing-body commercial aircraft vehicles, advanced commercial aircraft (e.g., Boeing 787) labeled N+1, vehicle configurations used within Hypersonic Convergence, and the verification vehicles selected during the NASA contract. The verification vehicles are the primary vehicles considered for the correlation, but the other ones are added to possibly determine if a trend spans across speed regimes. As observed, there is a clear correlation between the payload weight/number of passengers with respect to the structural index, but there are less outliers for the payload weight, due to vehicles having payload weight but no passengers. On these figures, estimations of the

structural index provided from Hypersonic Convergence are shown for comparison, but there is an additional line added for these two figures which divides the main commercial airlines from the verification vehicles to determine if there is a possible limit that could be observed. The X-43A is an outlier for the verification vehicles though as it has such a large structural index value in comparison. A reason for this could be that since the X-43A was to be the first operational scramjet demonstrator, the structure was overdesigned to ensure that it could survive the flight.

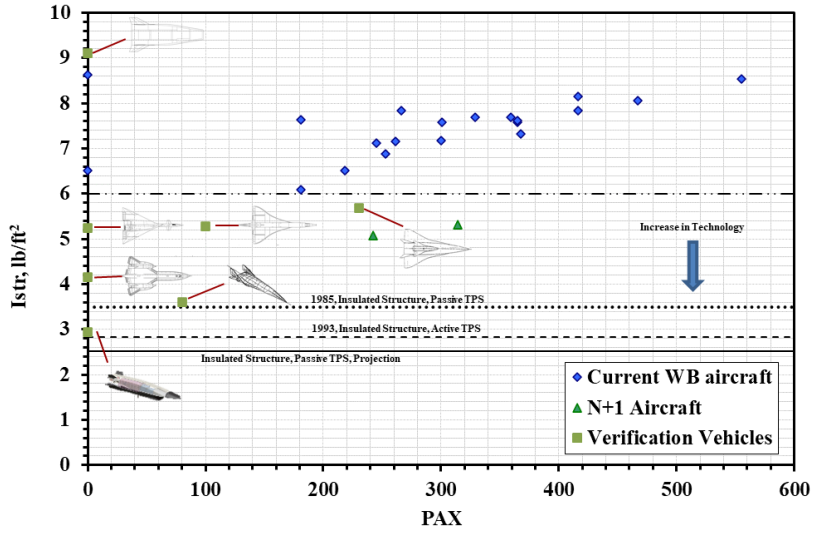

Fig. 6.12 Structural index vs. number of passengers.

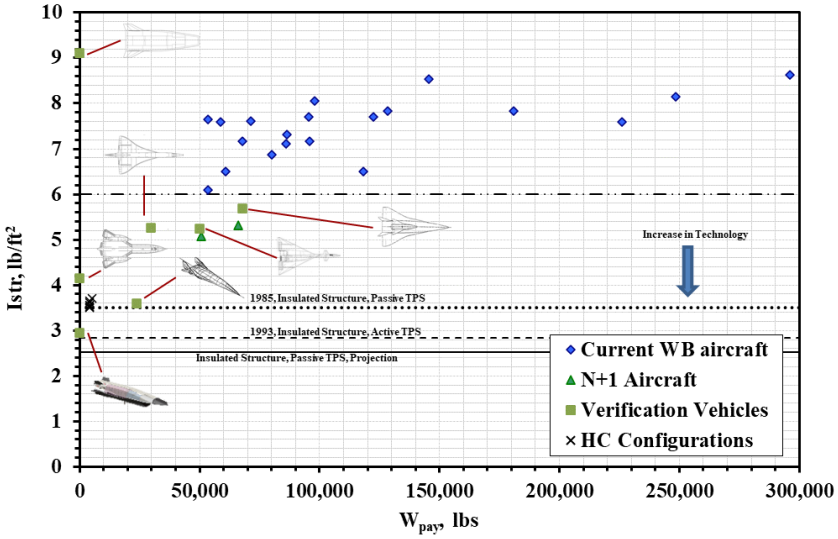

Fig. 6.13 Structural index vs. payload weight.

For the planform area comparison shown in Fig. 6.14, a correlation does appear to be made, but unlike the payload weight and PAX which appear to be able to have a single correlation with no regard to speed regime, the verification vehicles and the commercial vehicles appear to have separate discernable trends. While the overall trend is the same, that I_{str} increases with planform area, the commercial airline trend produces higher structural index values for the same planform area. This is most likely due to the greatly increased volume required to house passengers that the verification vehicles do not have.

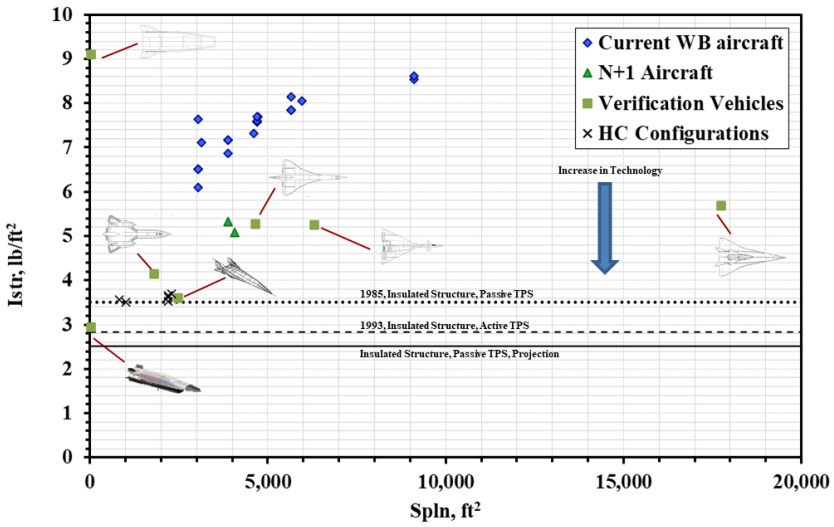

Fig. 6.14 Structural index vs. total planform area.

The last two figures, Fig. 6.15 and Fig. 6.16, show the comparison of the structural index to the industrial capability index and the wetted area respectively. For the industrial capability index, it was shown in Table 6.1 that if I_{str} decreases, then ICI should increase if I_p is kept constant. With this known relation and observing Fig. 6.15, it is shown that for the verification vehicles, in general, they do not appear to follow this trend while the commercial airliners do. This means that in general, the structural technology has increased for commercial airliners with relatively little improvement in propulsion technology in terms of reducing weight ratio, while it is varied for the

verification vehicles, which are all high-speed vehicles. One of these cases is the X-43A which has the highest structural index of the verification vehicles, but also has the second highest *ICI* value, meaning that it is the second most technologically advanced of these. As mentioned, this is most likely due to the X-43A being primarily a scramjet operation demonstrator, so while the structural technology is relatively low (well within industry capability), the propulsion technology was greatly increased for this vehicle to achieve the higher *ICI* value.

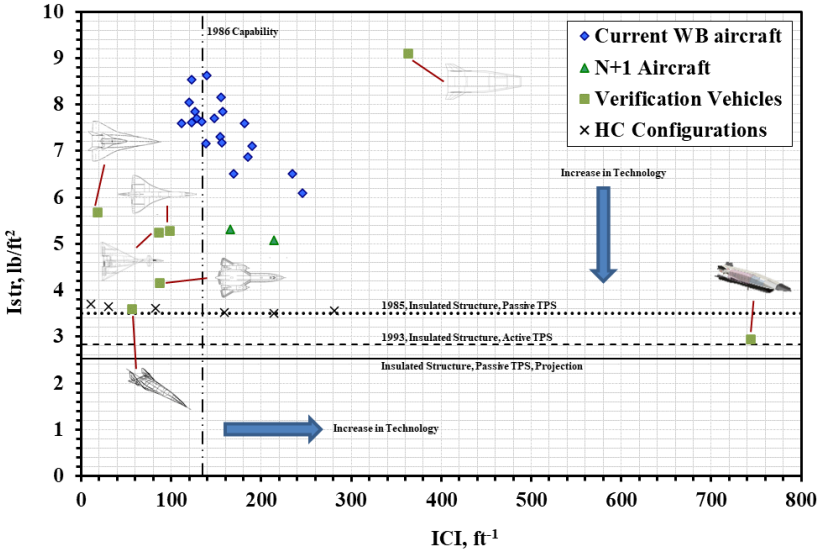

Fig. 6.15 Structural index vs. industrial capability index.

For the wetted area, this parameter is within the main definition of the structural index which is the structural weight over the wetted area as previously shown in Table 6.1. Assuming that the structural weight stays constant, if the wetted area is increased, the structural index should decrease by the relation. In actuality, when the wetted area is increased, the structural weight increases due to the increase area to support. So, this means that for I_{str} to decrease with increased S_{wet}, the wetted area must increase faster than the weight of the structure. Figure 6.16 primarily shows the former case for both vehicle types, the verification high-speed vehicles and the commercial airliners, where an increase in S_{wet} increases the structural index. At the smaller values

of wetted area for the commercial airliners though, I_{str} does appear to decrease slightly before increasing overall. From the trends shown, the X-43A is assumed an outlier, so is not considered within the correlation provided.

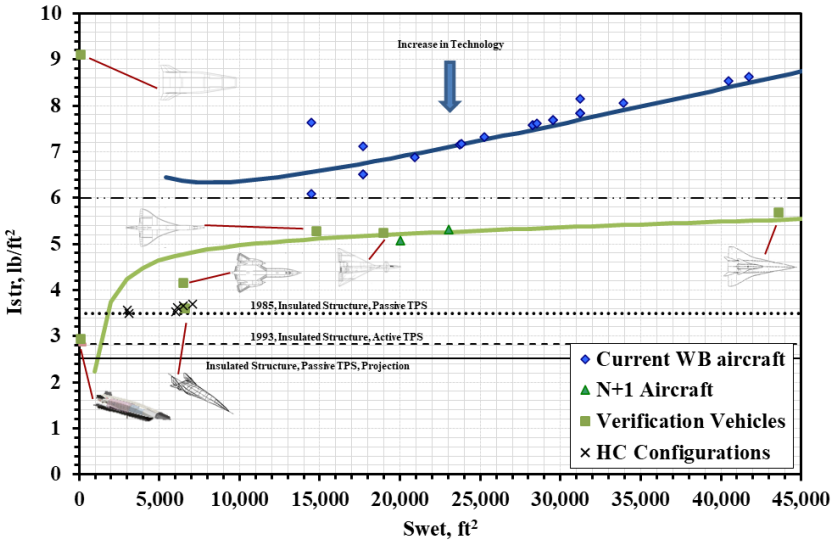

Fig. 6.16 Structural index vs. wetted area.

With these correlations investigated for these parameters, these can help determine the structural index to use during the convergence process of AVDS. From these observations, the parameter trends that were selected to determine the structural index for each trade study point were payload weight/PAX and Mach number. While the Mach number correlation is not shown above, as previously mentioned, it is a function of temperature, so the I_{str} vs. temperature plot shown in Fig. 6.2 is used for this correlation, which will be discussed below.

6.2.3 Developed I_{str} Parameter Trend Method

For this section, the trend investigation conducted previously will be used in conjunction with a figure developed within Hypersonic Convergence to be able to create a method to calculate I_{str} with mission inputs. The reason for this is that the way that I_{str} is calculated within Hypersonic

Convergence requires two correlation parameters to be used, which were correlated from unknown vehicles. While it is used for a range of Mach numbers and configurations, the fact that the limitations of these parameters are unknown causes concern for applicability, especially for the range of vehicles considered within AVDS. So, with this, the I_{str} parameter trend method is developed using the payload weight correlation for the verification vehicles discussed in the previous section, and the I_{str} vs. temperature figure provided within Hypersonic Convergence (Fig. 6.2). For the temperature figure, a way to determine temperature with an input Mach number without boundary layer equations, thermal model, etc., for this parameter trend method is required. Starting with observing Fig. 6.2, different trendlines are shown for how the structural index, I_{str}, varies with temperature along with the mission considered, such as cruising aircraft and entry vehicles. As cruising aircraft were the focus of the NASA study, the top trendline is the one used.

Through an investigation of correlations between temperature and Mach number that could be used during the conceptual design phase, a few relationships have been found, digitized, and superimposed into a single plot shown in Fig. 6.17. To determine which temperature lines to use, a temperature line from Concorde and a verification point from Concorde [33,145,146,147] has been added as shown in Fig. 6.17. From the temperature lines it can be observed that the Concorde temperature lines, the Concorde verification point, and the equilibrium radiation temperature line appear to follow the same trend with increasing Mach number. With this, the excess temperature lines have been removed, and the remaining ones are shown in Fig. 6.18. Using the average temperature of the trends in Fig. 6.18, the temperature at a given Mach number can be determined.

With the temperature at a given Mach number known, Fig. 6.2 is updated with an average I_{str} line showing the I_{str} limit used for a given temperature/Mach number combination, and the verification vehicle points added. Most of these vehicles lie above this line, with the X-51 and

Orient Express located below the line as an exception, see Fig. 6.19. The explanation for these exceptions is that the X-51 only flew a couple of minutes, so the structural technical capability required to survive the temperature exposure is much lower. On the other hand, the Orient Express's I_{str} matches that of the HyFAC value provide in Table 6.2 in the background section.

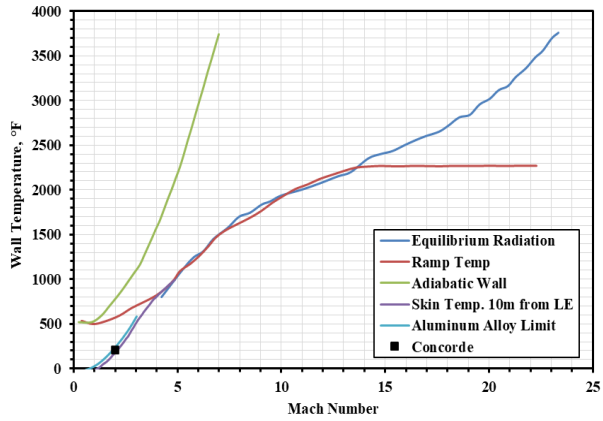

Fig. 6.17 Temperature versus Mach number [33,145,146,147].

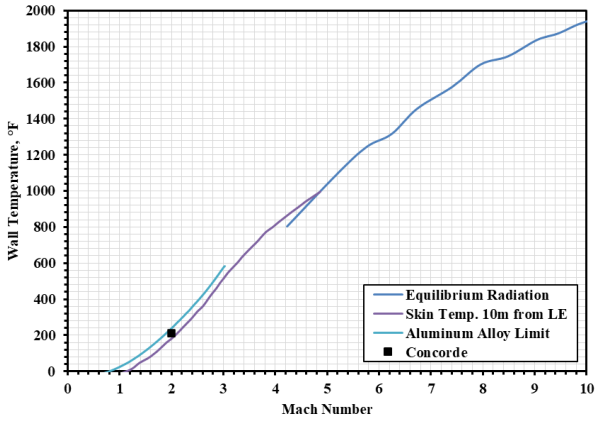

Fig. 6.18 Temperature versus Mach number reduction to usable correlation.

As mentioned, it is observed that most of the vehicles are above the I_{str} line, with some of the vehicles being farther away from the line than others. Therefore, payload weight or passenger weight has been considered with respect to its impact of the structural index.

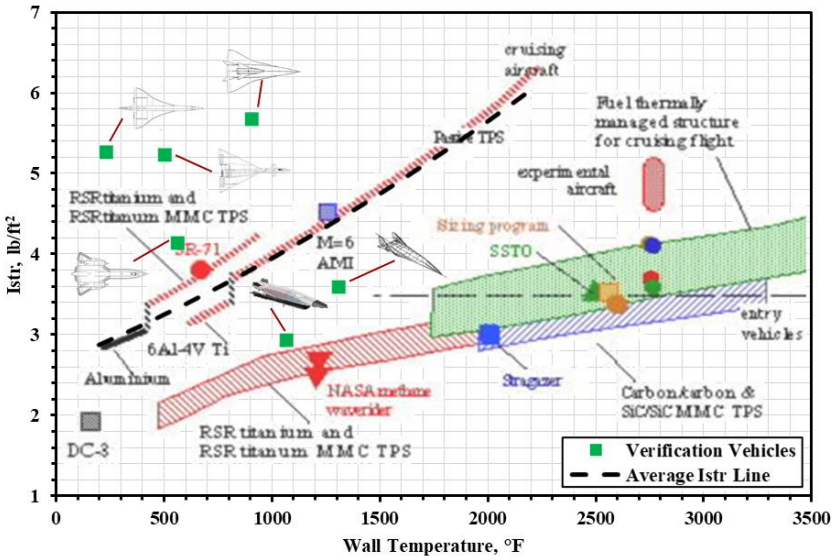

Fig. 6.19 Structural index vs temperature with verification vehicles and used correlation line [33].

With the Mach number relationship to the temperature and the payload correlation discussed, these can now be used to determine the structural index for a vehicle design point. This is accomplished by calculating I_{str} with both methods, comparing them, and selecting the larger of the two. The larger value is selected to create as much of a structural index margin as possible for the selected points. From observations of calculating several I_{str} points for varying payload weights, it is determined that at smaller payload weights, the structural index is more sensitive to the temperature, or cruise Mach number, while for larger payload weights, the structural index is more sensitive to the payload value.

With this, it has been shown how the parameter trend investigation can be used to observe the relationship between the wanted parameter and the parameters that were selected which were dependent on the purpose of the investigation. As shown, the purpose of the investigation in the structural index parameter was to determine the relationship between the inputs into AVDS and I_{str} to create an alternate method of selecting a reasonable value for the convergence point. While these parameters are compared using the verification vehicles to determine possible trends, it

should be noted that even though this does help AVDS with developing methods and/or interpreting results, that it is possible for the sizing results to obtain trends different to these. The reason for this is because, while the base geometry within AVDS is one of the verification vehicles, the alterations to the geometry for the conducted trades could produce non-explored configurations which could produce results different to these trends. It would then be up to the vehicle designer whether the difference in the trend is a reasonable one, or an issue with the design, methods, scaling, etc.

6.3 Summary of Other Parameter Trends Investigated

Even though the case study of the structural index parameter covered most of the parameter trends considered during the investigation, there were a few more parameter trends that wanted to be discussed. These are shown in the figures below which consist of explored trends for the other two technology index parameters, the propulsion index (I_p) and the industrial capability index (*ICI*). Since these parameters are outputs from the AVDS sizing results, these trends do not affect the overall results, but they can provide insights into the behavior of the results.

The first figure shown in Fig. 6.20, shows the comparison between the propulsion index (I_p) and the Mach number. This figure was a recreation of the I_p vs. Mach figure created within Hypersonic Convergence [33]. In general, the trend produced the same results as from Hypersonic Convergence, where with increase Mach number beyond supersonic speeds, the propulsion index would decrease. This can be observed with the comparison between the verification vehicles and the HC configurations. As can also be observed though, the X-43A and the X-51 are outliers to this general trend. This is most likely due to these vehicles being demonstrators, and with I_p being only a function of weight ratio (*WR*) with constant fuel density, meaning that for the demonstrator vehicles, the *WR* is smaller due to less fuel required for the small cruise times. It is also interesting

that the hydrocarbon fueled vehicles lie closely with the HC configurations for the same Mach number, meaning that 1) the figure in Hypersonic Convergence is most likely for hydrocarbon fueled vehicles, and 2) that as the HC configuration vehicles lie above the verification vehicles, that the trend from Hypersonic Convergence is potentially slightly optimistic. The reason that the propulsion index decreases with the Mach number though, is because with increased Mach number, more fuel is required in general to complete the same mission which increases the *WR*, thus decreasing I_p.

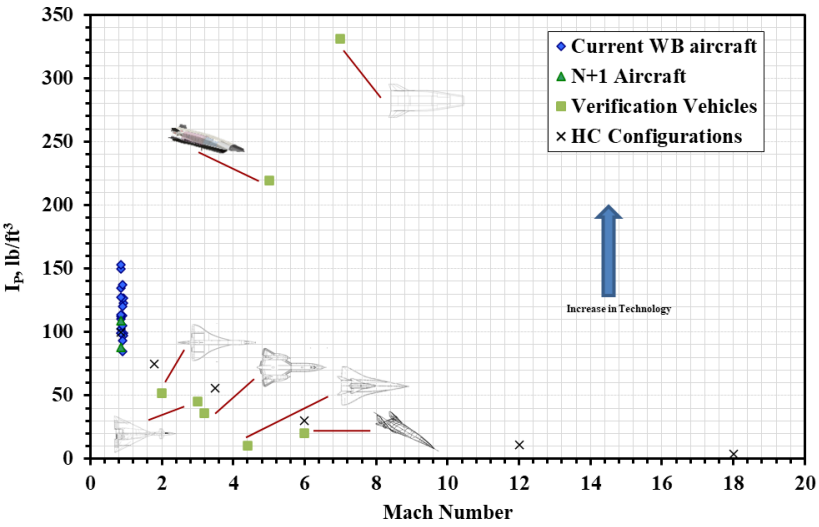

Fig. 6.20 Propulsion index vs. cruise mach number.

The next figure shown in Fig. 6.21, is for the propulsion index vs. the total range of the vehicle. As shown, there is a clear distinction between the commercial airliners and the high-speed verification vehicles, while both trends decrease in I_p with increase range, the correlation between the commercial airliners is higher than the trend for the verification vehicles. The reason that the propulsion index decreases with increase range follows the same reasoning as with the Mach number increase, where increase range requires more fuel, which increases the weight ratio (*WR*), thus decreasing I_p. An interesting note about this figure is that it shows that if the propulsion

efficiency/technology of the high-speed vehicles is wanted to be on the same level as the commercial airliners, either the density of the fuel needs to be increased, or if density is constant, the *WR* needs to significantly decrease. This means that if the same hydrocarbon fuel is used between the commercial airliners and the high-speed vehicles, the high-speed engines will need to be as fuel efficient as the transonic engines to reduce *WR*.

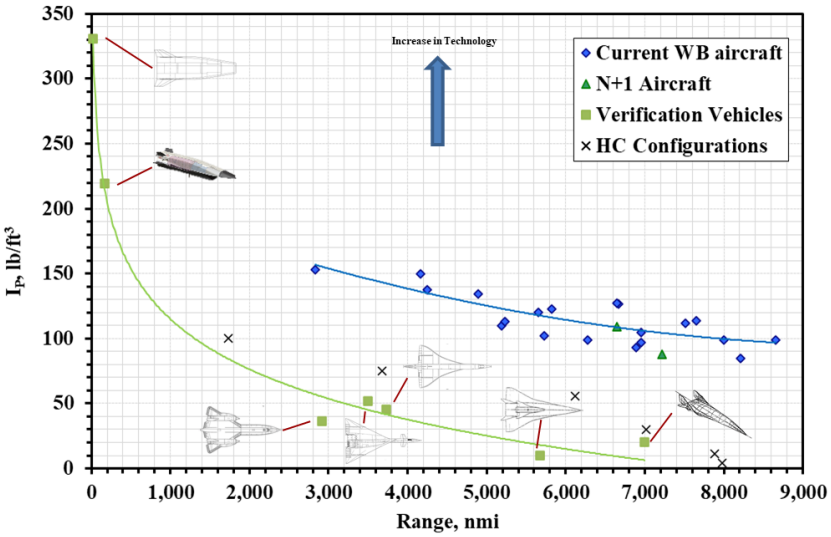

Fig. 6.21 Propulsion index vs. mission range.

The last figure, shown in Fig. 6.22, shows the industrial capability index (*ICI*) vs. the total planform area (S_{pln}) of the vehicles. As observed, overall, as the planform area increases *ICI* decreases, meaning that as size increases, the industry technology level required actually decreases. While it may seem counterintuitive, this shows that a demonstrator requires a higher technology level than a full-scale vehicle. A couple of examples of possible reasons why demonstrators would require a higher industry technology level is 1) aerothermodynamics, the smaller vehicle will experience higher heating than the larger vehicle, and 2) propulsion, smaller vehicles require smaller engines, which may need to be more fuel efficient to keep the propellant

volume lower to fit within the vehicle size, or cruise time and range must be lower to keep propellant volume lower for less fuel efficient engines.

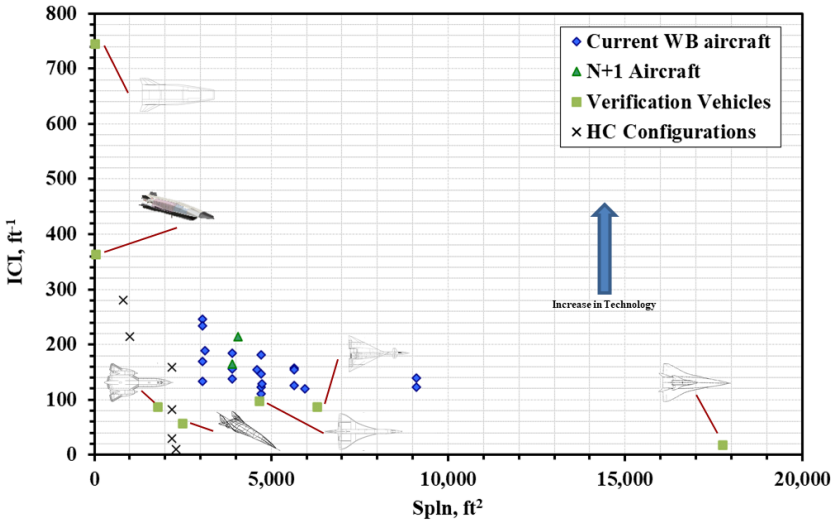

Fig. 6.22 Industry capability index vs. total planform area.

As with the structural index parameter investigation, these trends also improve AVDS as these trends can be used to provide insights into the sizing results by comparing the trends from the results to these. As previously mentioned, it is possible for the sizing results to produce different trends than these, but primarily, these are the expected trends to see. A note that has not been mentioned yet, is that while these parameter trend investigations were conducted independently and then implemented within AVDS, the task of this investigation will be taken over by the knowledgebase function of the VCC, which was discussed in Chapter 3.

CHAPTER 7: AEROTHERMODYNAMICS DISCIPLINE DEVELOPMENT FOR AVDS

7.1 Aerothermodynamics Discipline Overview

The aerothermodynamics discipline is the consideration of the effects of the aerodynamics discipline and thermodynamics discipline together on a system, which means that temperature becomes an important factor. Aerothermodynamics is mostly considered for hypersonic vehicles where the high temperatures not only affect the vehicle body, but the chemistry of the air, or type of flow, as well. These temperature effects introduce problems during vehicle design as certain assumptions must be made. With the air chemistry (type of flow) involved, the air may no longer be considered a calorically perfect gas, where the specific heat values are constant, but may be assumed to be a thermally perfect gas, where the specific heat values vary with temperature, or even a chemically reacting gas (equilibrium, non-equilibrium, or frozen flow), where the specific heat values vary with temperature, pressure, and air composition. Further definition of these types of flows can be found in the following references [148,149]. Figure 7.1 shows an example of these air chemistry locations with respect to altitude and Mach number. As a note, the calorically perfect and thermally perfect assumptions both fall within the 'no gas chemistry effects' section of the figure.

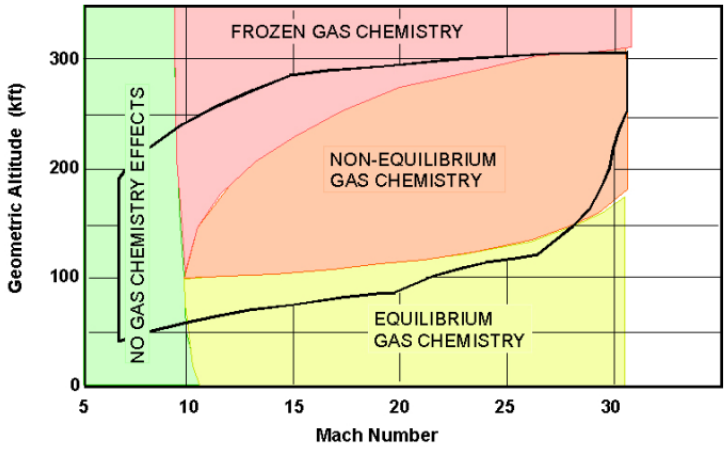

Fig. 7.1 Air flow chemistry boundaries [33].

Even though the temperature experienced in flight determines the air chemistry that will be experienced, when designing a high-speed vehicle, the surface temperature is usually one of the unknowns of the design [148]. This is where the assumptions for the type of air flow take place and figures similar to Fig. 7.1 can help in determining the correct assumption. The reason that this assumption is so important is because it will determine the surface temperatures expected to experience, and the wrong assumption can overpredict the temperatures, thus making valid vehicle designs invalid, or underpredict the temperatures, thus making invalid vehicle designs valid. An example of this importance is shown in Fig. 7.2 where the comparison of the temperature behind a normal shockwave against velocity is shown with the calorically perfect gas and equilibrium chemically reacting gas assumption. As shown, if the calorically perfect gas assumption was used during the design of the vehicles shown, then the temperature expected would have been so great that none of these vehicles would have been possible, but with the equilibrium chemically reacting gas assumption, it was possible.

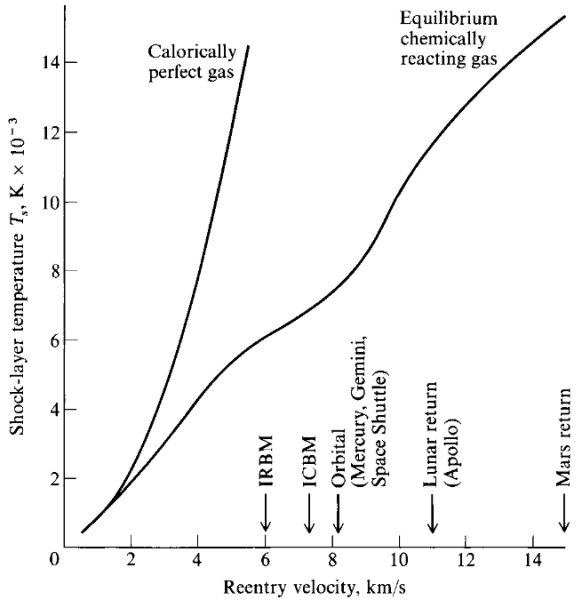

Fig. 7.2 Temperature behind a normal shock wave as a function of freestream velocity at a standard altitude of 52 km [150].

As mentioned, the temperature is usually unknown and requires the air chemistry, or type of flow, assumption to be able to determine these values. This is possible through the determination of the convective heat rate into the surface which is calculated through boundary layer analysis, and the heat rate that is radiated away from the surface. While the heat rate being radiated away is relatively simple with being a function of the emissivity of the surface material, and the surface temperature which is calculated in conjunction with the convective heat rate, the convective heat rate is more difficult to determine due to the boundary layer analysis. The convective heat rate calculated from the boundary layer analysis can be determined from either empirical data, or methods such as the reference temperature method. When selecting the method to determine this though, the type of boundary layer (laminar or turbulent), and the type of flow is required, as in the case for analytical equations, as they were derived for a specific type of flow.

While difficult in general to accurately model the surface temperature experienced by the hypersonic vehicle, this difficulty is enhanced during the conceptual design phase where access to

finite element models, or complex calculations are either limited or not used at all due to the processing time, number of unknown elements, number of considered configurations, etc. To enhance the aerothermodynamics discipline within AVDS with these complications in mind, the structural index (I_{str}) parameter was considered again, moving past the parameter trend investigation discussed in Chapter 6, to determine an I_{str} value from an aerothermodynamic analysis that will provide a better representation of each sized vehicle point.

7.2 Development of Aerothermodynamic Methods for AVDS

To determine the structural index (I_{str}) parameter from the perspective of aerothermodynamic analysis for the AVDS system, two overall methods will be introduced, 1) the constant temperature 'solution spaces' method that was discovered within the HyFAC reports [151], and 2) a method to determine the temperature distribution through the TPS. While the parameter trend method to determine I_{str} previously discussed proved useful during the NASA study, there were some limitations within the temperature portion of the method. An example of one of the limitations is that cruise time was not considered for I_{str}, and that the assumption is that the margin created between the temperature and payload values would cover the increased cruise time. Also, while materials were used to create the temperature I_{str} figure used (Fig. 6.19), if updated materials, or other materials, wanted to be considered, it would not be possible with that figure. These two methods were investigated to correct these limitations and to expand the aerothermodynamics discipline within AVDS.

7.2.1 HyFAC Constant Temperature ‘Solution Spaces’

7.2.1.1 Purpose of Method for AVDS

The first method to introduce is the constant temperature ‘solution space’ method provided within the HyFAC reports. As will be further discussed, this method produced ‘solution spaces’ as a function of altitude, Mach number, angle of attack, and wing loading, where each combination of these within a specific ‘solution space’ experiences the same equilibrium temperature. The purpose of this method to improve AVDS and the aerothermodynamics discipline is that with a nominal trajectory for the vehicle design, it provides an estimated equilibrium temperature that will be experienced during the flight. This helps with material selection as well, as knowing the expected max temperature beforehand helps narrow down which materials are viable. The material selection process is primarily the use of this method, but also improves AVDS by allowing temperature to be a factor before sizing during the mission selection.

7.2.1.2 HyFAC Method Overview and Verification

In aerospace vehicle design, material choice is an important aspect as the selected materials must be able to withstand the loads experienced by the vehicle during its designed trajectory. All aerospace vehicles experience aerodynamic loads, such as lift, dynamic pressure, in-flight maneuvers, etc., but for high-speed vehicles, temperature starts becoming a factor as heat loads. With the addition of heat loads, the material selection becomes even more complex as not only do they have to withstand the aerodynamic loads, but they must be able to withstand them at an increased temperature. Compromises must be made, as typically, material strength decreases with increase in temperature [33], so if a specific material is supposed to carry the structural loads experienced during flight and carry them at the elevated temperature, then more material is required to ensure the structural integrity of the vehicle, which means the structure of the vehicle

will be heavier. This specific type of structure is known as a hot structure. The aerodynamic loads and the heat loads can be assumed to be decoupled when a passive thermal protection system (TPS) is considered. This system has a thermal protection system consisting of a radiation shingle (high emissivity material to radiate heat away), and insulation to protect the inner structure. Thus, the radiation shingle and the insulation handle the heat loads, while the protected inner structure handles the aerodynamics loads. An active TPS can be used when the heat loads experienced are extreme, which protects the inner structure with insulation, but also some other method, whether a water wall, fuel, coolant, etc., that takes the heat away from the structure. These thermal protection systems are known as reusable systems, as they are designed to be used multiple times without being replaced. There are non-reusable systems which use ablative material, but these are mostly used for expandable reentry vehicles, or reentry vehicles who experience temperatures that reusable materials are not currently able to withstand. This discussion on the different types of TPS systems shows the importance and range of consideration when determining which materials to use.

As the selection process of materials is complex, this is normally considered beyond the conceptual design phase, where finite analysis is used, and the properties of the materials are thoroughly examined. While the final material used is not determined during the conceptual design phase, considering a range or family of materials would be beneficial during the conceptual design phase as materials determine the weight of the vehicle. An example is an aircraft that uses composite materials would be lighter than an aircraft that uses metallic materials. During the conceptual design phase, empirical relations are used to estimate weights of the vehicle, but there are several assumptions behind these relations, such as structural material and mission (e.g.,

bomber, fighter, commercial airline), so to decide between which relations to use, a material family (composite, metallic, etc.) that works with the provided mission, must be decided.

The material selection for structural weight during conceptual design example leads to the added high-speed consideration of temperature. This adds the categories of TPS systems and materials that resist the elevated temperatures (i.e., ceramics, metallics, C/C), that need to be considered when selecting a material, or family of materials. While the temperature that is estimated to be experienced during flight can be determined after a trajectory is established, during conceptual design, especially the sizing phase, the trajectory is normally not established yet, or in the middle of being established. This is where the method discussed here is used.

Figure 7.3 shows an altitude vs. Mach plot with several 'solution spaces' on it. Each of these 'solution spaces' represent an area of constant equilibrium temperature, ranging from 310 °F to 2600 °F as shown. Each of these areas are functions of angle of attack, lift loading, Mach number, and temperature, providing corresponding altitude for each point. The colored outlines are the full areas, but the shaded regions are smaller as the airbreathing dynamic pressure limits are used to constrain the areas further. From this figure, a notional trajectory can be determined with the ability to estimate the temperatures that will be experienced during the flight. Also, it can help modify the trajectory, to determine if there are any points during the flight, that could potentially 'overtemperature' the vehicle, or reach a temperature that was not designed for, such as with any in-flight maneuvers at supersonic and hypersonic speeds [33]. In terms of material selection, there are two uses for this figure, 1) knowing estimated temperatures at the beginning of vehicle design allows earlier selection of materials, or investigation into materials, and 2) if the materials are known beforehand, or materials wanted to be used, the figure shows what combination of speed, altitude, angle of attack, etc., this material can withstand, or function in.

Continuing the second use, vehicle forecasting can be completed if an in-development material is expected to function at a known temperature, or if material development in general is expected to function at a more elevated temperature in the next 10, 20, and so on, years.

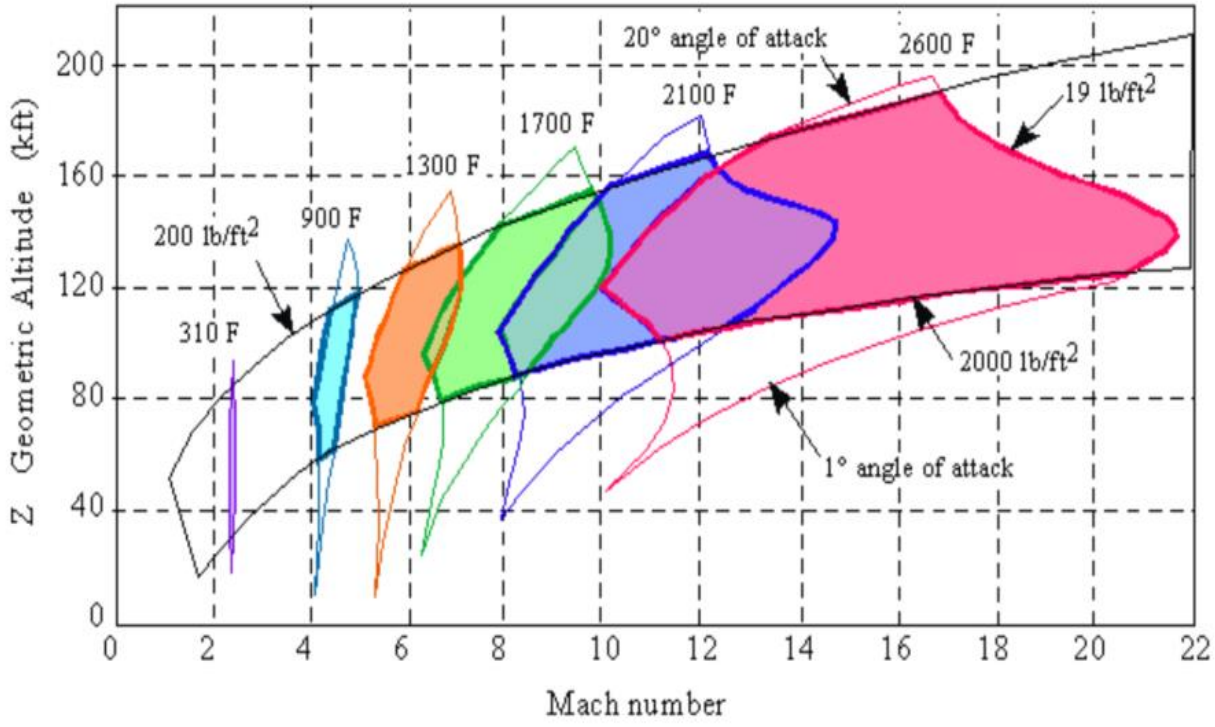

Fig. 7.3 Altitude vs. mach with constant equilibrium temperature solution space [33].

This method was originally used during the Hypersonic Research Facilities (HyFAC) Study. The 'solution spaces' were made by finding the intersection points of calculated lift loading lines and temperature lines. Starting with the lift loading lines, Eqn. (9) shown below is used. For the 'solution spaces,' the lift loading lines determine the right and left boundary, with the lowest lift loading value on the right, and decreasing in value to the left. Looking at Eqn. (9), the lift loading term is the numerator on the right side of the equation, which is the product of the load factor and wing loading of the vehicle. With this term, the change in wing loading across the trajectory can be estimated, and it can show how flight maneuvers effect the temperature value,

with a turn possibly requiring a reduction in speed and altitude to keep the vehicle within the required temperature range. As a quick note, the constant value of 1481 currently in the denominator is for when English units are used for the lift loading (lb/ft^2), while the constant value of 70,900 is for when metric units are used for the lift loading (N/m^2).

$$\frac{P_\infty}{P_{S.L.}} = \frac{n_z\ (W/S_W)}{1481\ C_L\ M_\infty^2} \tag{9}$$

In Fig. 7.3, the top and bottom boundaries of the 'solution space' are angle of attack limits with the range shown being from 1° to 20°. Looking at Eqn. (9), angle of attack is not directly used, but used through the Coefficient of Lift, C_L. During the Hypersonic Research Facilities Study, C_L was estimated for a 70° to 80° leading edge sweep vehicle at selected Mach numbers and range of angle of attacks. This is shown in Fig. 7.4, which was also used to calculate C_L for each wanted angle of attack and Mach number. Lastly, the freestream Mach number is used within Eqn. (9). With these parameters, the pressure ratio, and therefore the altitude can be determined, and lift loading lines can be created.

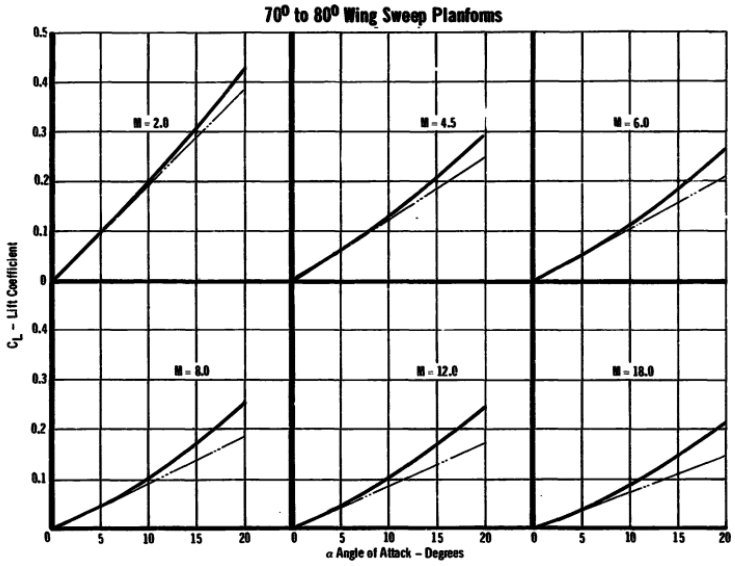

Fig. 7.4 Coefficient of lift vs. angle of attack at various mach numbers [151].

For the temperature lines, these were calculated during the HyFAC Study by using a 'MCAIR Boundary Layer Heating Analysis'. This analysis outputs the Mach number and altitude combination which produces a given temperature and angle of attack [151]. Figure 7.5 is one of the figures created using this method at several angles of attack and at a given temperature of 1700 °F. A few of the assumptions used within this analysis are also shown which is assuming a turbulent boundary layer that is located 5 to 10 ft downstream of the leading edge, and a surface emissivity of 0.8. Besides this, not much else is known about this portion of the method that was used.

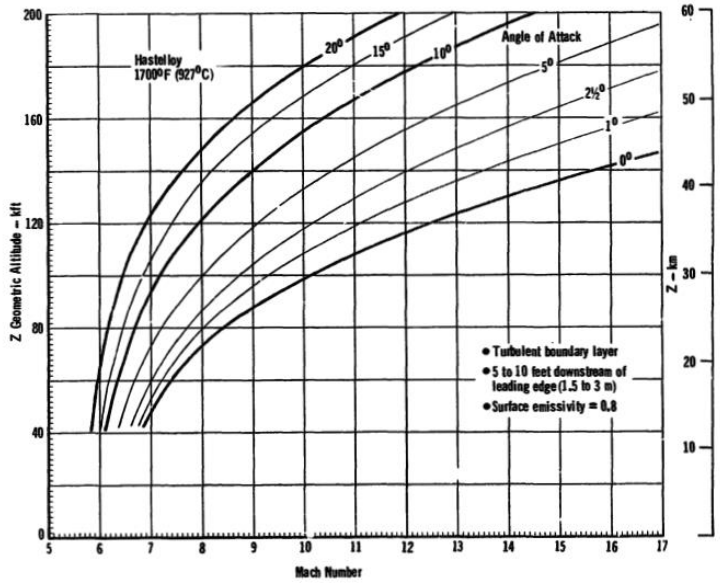

Fig. 7.5 Constant equilibrium temperature lines for temperature of 1700 °F [151].

With both the lift loading and the temperature lines, the intersection of these lines produces Fig. 7.6. Unlike Fig. 7.3, this one shows the various angles of attack and lift loading lines within the 'solution space'. As mentioned, these 'solution spaces' help in determining a trajectory with temperature as a restriction, and in selecting the materials that will withstand the temperatures experienced during the trajectory. This is useful especially during conceptual design to provide an

initial estimate of expected temperatures and provides an earlier start in material selection and thermal analysis.

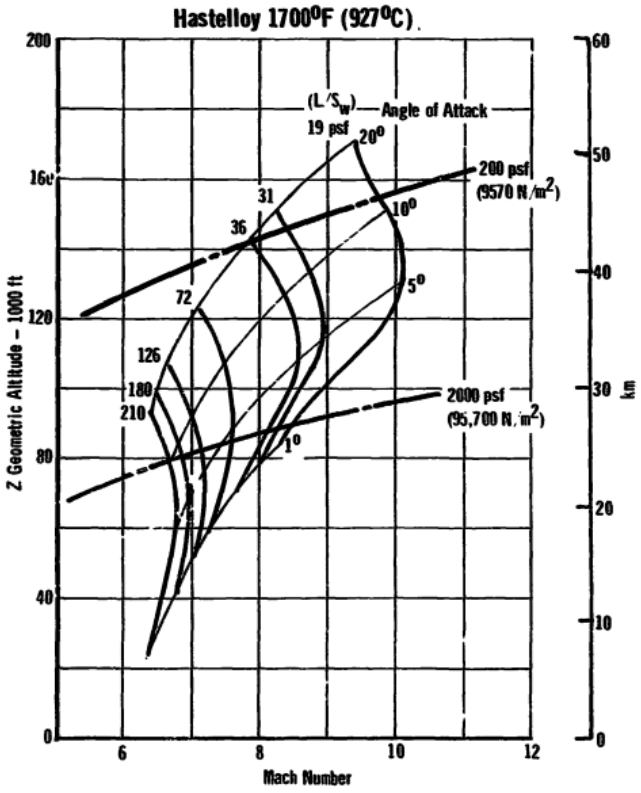

Fig. 7.6 Constant equilibrium temperature solution space for 1700 °F [151].

For the verification of this method, the lift loading lines, and the temperature lines are recreated where able, as will be discussed, to create a constant temperature 'solution space'. Starting with recreating the lift loading lines, Eqn. (9) as previously discussed is used. Looking at Fig. 7.6, the Mach range considered is 6 to 11, angles of attack of 1°, 5°, 10°, and 20°, and the temperature of 1700 °F. For the lift loading values, 19 psf and 210 psf were used for the outer boundaries. To determine C_L from Fig. 7.4 using the considered angles of attack and Mach range, it was assumed that the Mach 8 plot in Fig. 7.4 was constant throughout the considered Mach range. With this assumption, for this Mach range, C_L does not vary with Mach number and is only a function of angle of attack, so C_L is assumed constant along each angle of attack line. Figure 7.7

below shows the angle of attack lines for a lift loading of 19 psf, which will provide the right border of the 'solution space' as will be shown.

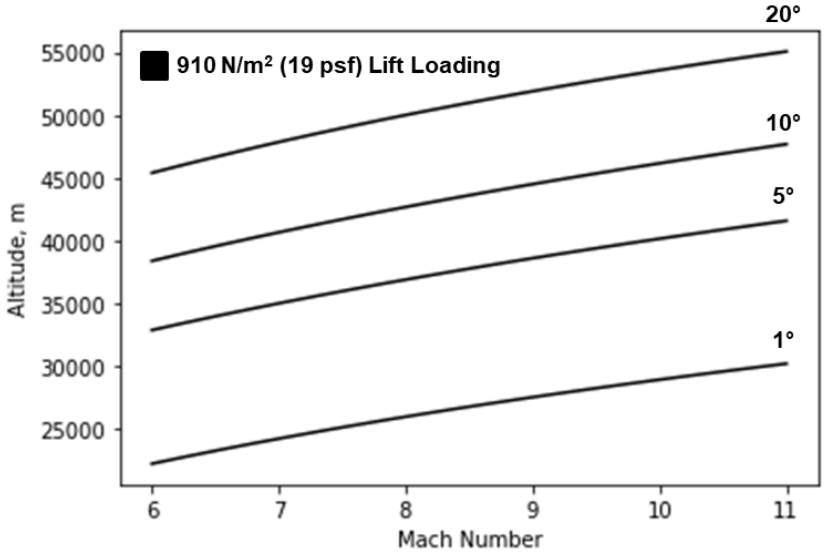

Fig. 7.7 Calculated lift loading lines at a value of 19 psf at various angles of attack.

For recreating the temperature lines from HyFAC shown in Fig. 7.5, as the method in which these were created was not explicitly stated, Fig. 7.5 was imported into *WebPlotDigitizer* and the considered angle of attack lines mentioned previously were digitized. Figure 7.8 shows these plotted lines. The explicit investigation to recreate these lines using boundary layer theory, etc., is further discussed in the next section, but as this verification section is primarily to create an understanding of how these figures were created within HyFAC, digitizing the temperature lines and using them with the calculated lift loading lines is sufficient for this, as if the combination of these lines creates the solution space shown in Fig. 7.6, then only the temperature lines need to be further investigated. Again, this approach was taken as the temperature line method was only referred to being created with the 'MCAIR Boundary Layer Heating Analysis' with no discussion on the internal calculations of the method, only the inputs and outputs.

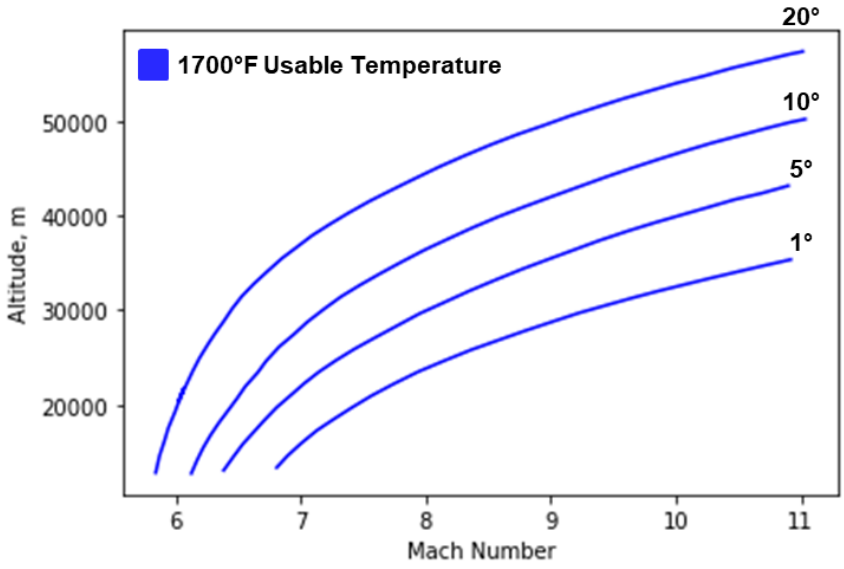

Fig. 7.8 Digitized constant equilibrium temperature lines.

With the digitized temperature lines and the ability to create the lift loading lines, these are then overlayed together in the same plot. Figure 7.9 shows the temperature lines with the previously shown lift loading lines. To obtain the full 'solution space', the left boundary is required, so Fig. 7.10 shows the temperature lines with two sets of lift loading lines, one with a lift loading value of 19 psf and the other with a lift loading value of 210 psf. With these lines, the 'solution space' can be created. First, intersection points of the corresponding angle of attack line between the temperature defined one and each of the lift loading defined ones are marked. Next, as this will create an area of constant temperature, the constant temperature lines are followed when possible. So, starting with the bottom left intersection point, in this case being at 1° for temperature and the 210 psf lift loading line, the bottom temperature line is traced until the next intersection point is reached. As this is the intersection point between both 1° angle of attack lines for temperature and the 19 psf lift loading line, the tracing stops here, and lines are drawn to each intersection point for the corresponding lift loading. This creates the right boundary of the 'solution space' depicting the lower lift loading limit. From the last intersection point, in this case being at

20° for temperature and the 19 psf lift loading line, the top temperature line is then traced to the next intersection point, in this case being at 20° for temperature and the 210 psf lift loading line. The lower and upper temperature lines create the bottom and top boundaries which depict the angle of attack limits to keep the wanted vehicle within the temperature range. From this intersection point, lines are drawn to each intersection point for the corresponding lift loading as was done for the right boundary, this creates the left boundary for the 210 psf lift loading and closes the 'solution space'. This is shown in Fig. 7.11 with Fig. 7.12 showing the shaded region that constitutes the constant temperature region. Comparing Fig. 7.12 below with Fig. 7.6 above, not only does the general shape of the recreated 'solution space' match closely to the original, but the values of Mach number and altitude does as well.

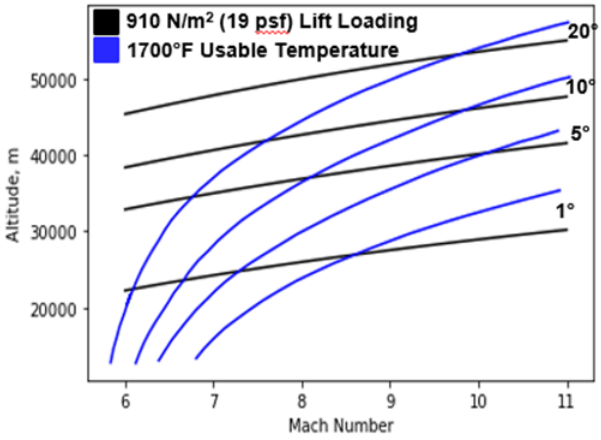

Fig. 7.9 Overlay of constant equilibrium temperature lines and 19 psf lift loading lines.

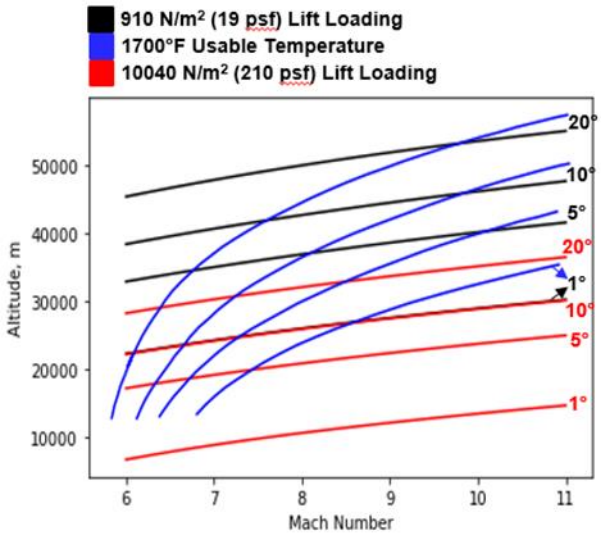

Fig. 7.10 Overlay of constant equilibrium temperature lines and 19 psf and 210 psf loading lines.

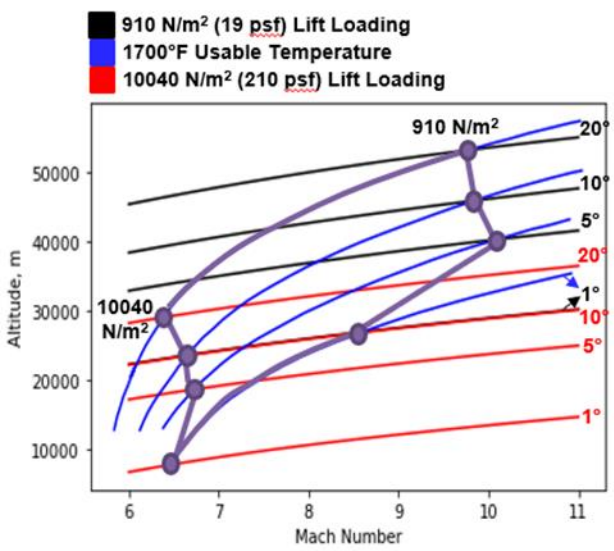

Fig. 7.11 Outlining the boundary of the solution space with the overlayed temperature and lift loading lines.

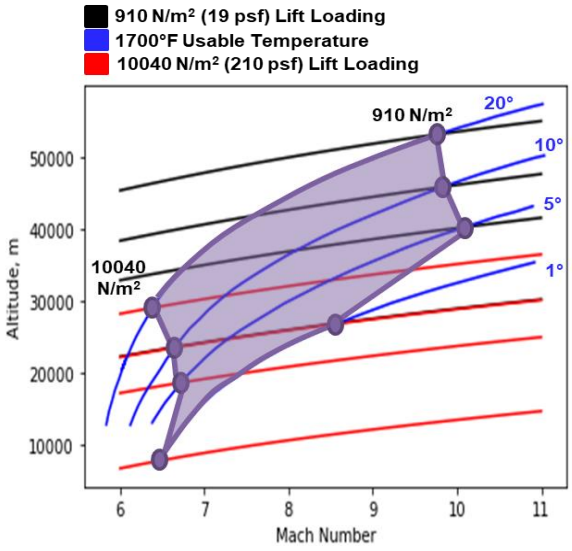

Fig. 7.12 Final created constant equilibrium temperature solution space.

7.2.1.3 Constant Temperature Line Method Investigation

Now that the constant temperature 'solution space' from HyFAC has been recreated to determine how they were made, the temperature lines can be further explored to determine how these were calculated. To determine the surface temperature, the convective heat flux and the heat flux radiated away from the surface was required. While determining the heat flux radiated away from the surface is relatively straightforward, the convective heat flux provided a more difficult problem to calculate. After investigating several analytical methods [148,152-157], which used boundary layer analysis, and empirical methods [148,156-160], to determine the convective heat flux, the method selected to use was the reference temperature method [148,156]. Most of the assumptions for this method are the same as was used from HyFAC, which is turbulent boundary layer, 5 to 10 ft downstream of the leading edge, and an emissivity of 0.8. As these were the only known assumptions, several other assumptions had to be made to use the reference temperature method. One of the other assumptions is using Oblique Shock Theory over a flat plate to calculate

the properties of air behind the shock wave generated at supersonic/hypersonic speeds. A flat plate is assumed initially so that the method is not a function of geometry. Another assumption made is assuming that the air is calorically perfect. This simplifies the method as the air properties are not a function of temperature (for thermally perfect) and pressure (for equilibrium flow). As a side note, equilibrium flow assumption was attempted, and while properties behind a shock wave using this assumption were calculated and verified, a method to calculate equilibrium flow properties within a turbulent boundary layer, especially to be used within the sizing phase, was not found [148,153,154,157,161]. The last assumption which is not explicitly stated in the HyFAC temperature method, is the assumption of equilibrium radiation temperature, which means that the heat flux going into the system (convective heat flux) is the same as the heat flux being radiated away from the system, or the surface. With these assumptions and using the equations shown in Appendix E, an input temperature and range of Mach numbers and angles of attack, allow an altitude to be solved that matches these conditions, similar to HyFAC's temperature method. The results of this method as compared to HyFAC's method are shown below.

7.2.1.4 Results and Observations

Observing Fig. 7.13, it is shown that the calculated constant temperature lines and the ones from HyFAC do not match well at all. The first reason considered is due to the assumption of calorically perfect air, as the temperature of 1700 °F is considered outside its suitable range. Even with that though, lower value temperature lines were digitized that were within the calorically perfect assumption range, but the relationship to the calculated lines at that lower temperature still matched that shown in Fig. 7.13. This means that even though the calorically perfect assumption could be an issue, there are more issues between the two methods than just this one assumption.

Reviewing the other assumptions that were considered, another issue that could be producing this difference is how the properties of the turbulent boundary layer are calculated. The method currently being used is an analytical method, but it is possible that an empirical method was used within the 'MCAIR Boundary Layer Analysis' method used by HyFAC. As mentioned, an empirical method was attempted along with the analytical method, but through several iterations of the empirical method, all the results produced more error than the current analytical method. Even though this was not able to be currently corrected, future efforts in modifying boundary layer analysis from calorically perfect air assumption to thermally perfect air assumption and researching into possible empirical equations for turbulent boundary layer, is recommended.

Figure 7.14 shows how the current calculated temperature lines shift the 'solution space' from HyFAC's to AVD's. While this method has not been fully verified to be able to create more constant temperature 'solution spaces' or to change the angle of attack range to possibly be used for reentry missions, the current HyFAC created 'solution spaces', shown previously in Fig. 7.3, can be used in the meantime as they do cover a wide range of temperatures and Mach numbers. As for the material selection, even though HyFAC specifies a certain material for each 'solution space', as each 'space' is a constant temperature, any material whose usable temperature is above the temperature indicated for that 'solution space' would be acceptable, if it also has at least an emissivity of 0.8, which was used for the temperature lines.

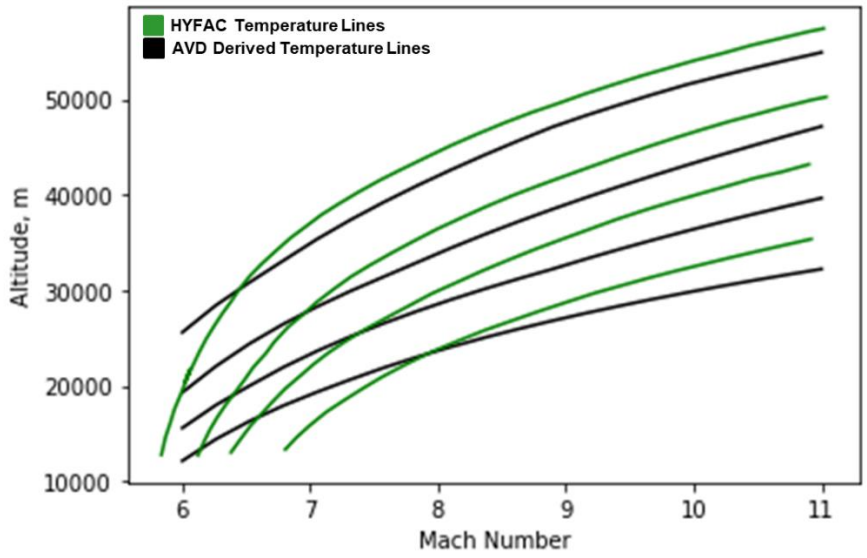

Fig. 7.13 Comparison of digitized to calculated constant equilibrium temperature lines.

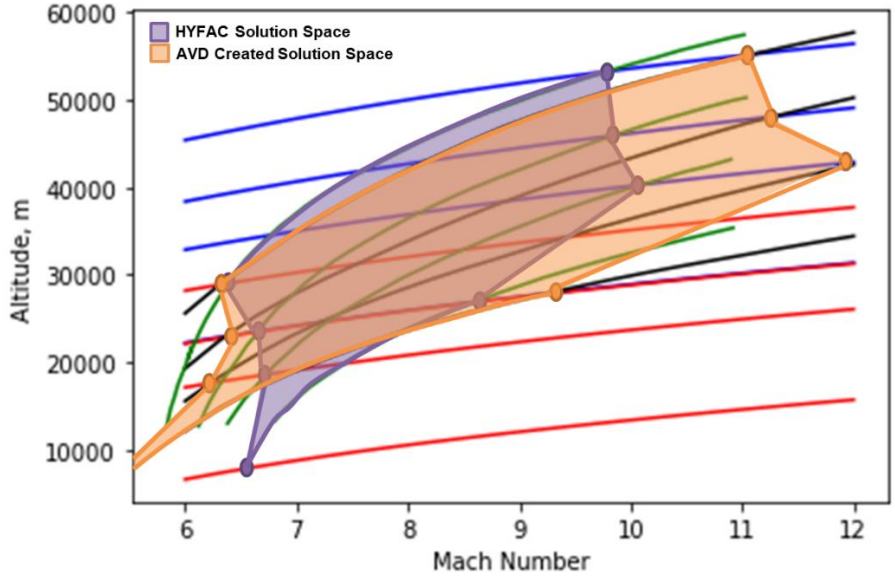

Fig. 7.14 Comparison of the generated constant equilibrium temperature solution spaces.

7.2.2 Temperature Distribution through TPS Method

7.2.2.1 Purpose of Method (change in cruise time, materials, etc.)

The second method to introduce is the method to determine the temperature distribution through the TPS. The purpose of this method for the improvement of AVDS and the aerothermodynamics discipline is to update the structural index (I_{str}) method from the parameter

trend method introduced in Chapter 6, to a more analytical one. This method will allow the use of the aerothermodynamic analysis of determining either the heat flux, or equilibrium temperature, along the trajectory of a sized vehicle to determine the required TPS thickness to maintain the structure within its temperature limits. While the parameter trend method provides a simpler method to determine the I_{str} value and would provide a shorter run time during the convergence process, the analytical method would allow multiple considerations that the parameter trend method would not, such as change in cruise time and alternate material selections. Even though the analytical method would provide a unique I_{str} value for the converged vehicle, the temperature I_{str} figure used from the parameter trend method can be recreated to show the sensitivities of cruise times, material selection, etc. These will all be shown and discussed below.

7.2.2.2 Analytical I_{str} Method Development

For this more analytical method to determine the structural index (I_{str}), there were two methods investigated to determine which one to use. The first method that will be shown was also the first one found, but during development of this method, the second one was found, so a comparison was made to determine how their results compare. From the results, several considerations will be made, such as time to calculate results, accuracy of results, method complexity, etc.

The focus of these new methods has been to determine the temperature distribution throughout the TPS system for a given mission, so that the material thicknesses can be determined, and finally the structural index value. During the beginning of the investigation to determine the temperature distribution through the TPS system, it was found that this can be calculated by solving the unsteady 1D conduction partial derivative shown in Fig. 7.15 with corresponding boundary conditions. A method was found to solve the partial derivative with the corresponding boundary

conditions through finite difference [162], which is the first method found to determine the temperature distribution through the TPS system.

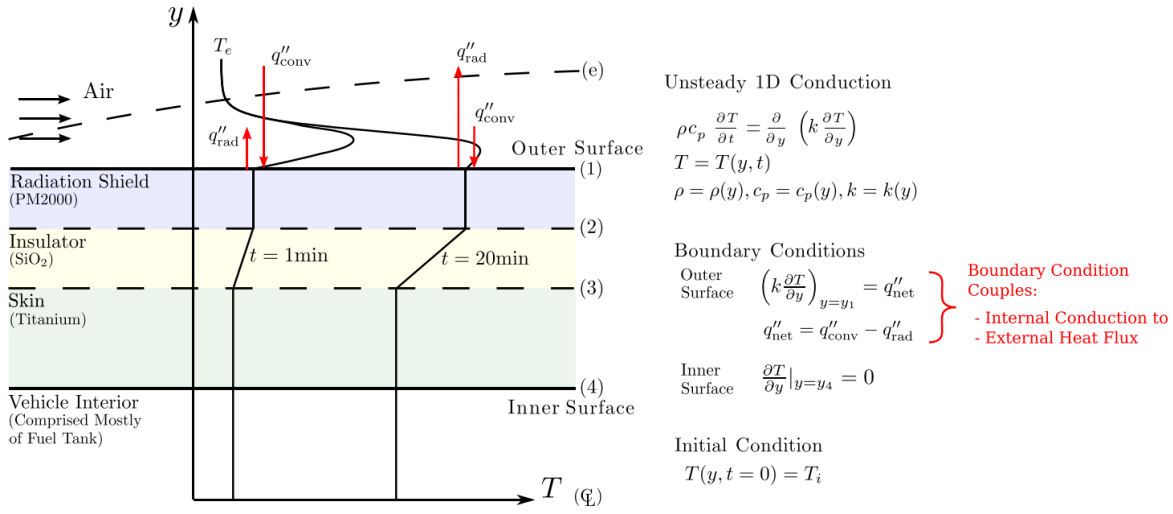

Fig. 7.15 Schematic of a thermal protection system with temperature distribution [152].

7.2.2.2.1 Finite Difference Method

For the finite difference method, Fig. 7.16 shows a representative model of a three-material TPS system, with the first material representing the radiation shield, the second material representing the insulation, and the third material representing the material of the skin or structure of the vehicle. This three-material system is also shown in Fig. 7.15. Looking at the representative model there are four distinct node types: 1) the surface node denoted at i = 1, 2) interior nodes, the nodes within each specified material, 3) material interface nodes, or nodes at where each new material meets, and 4) the n^{th} node, or the last node that denotes the interior of the vehicle.

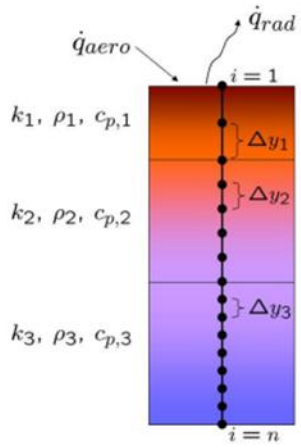

Fig. 7.16 Representative finite element model of a thermal protection system [162].

For each distinct node type, equations were available to determine the temperature at that point with respect to material properties, net heat rate (for surface node), previous node temperature, and time step. These equations are available in Appendix E. Examples of results of using these equations are shown in Fig. 7.17 and Fig. 7.18. The material used is PM2000 for the radiation shield, SiO2 for the insulation, and titanium for the structure, and calculated at a cruise time of 2 hrs. Figure 7.17 shows the temperature over time for each node, with the top clustered nodes being for the radiation shield, the more separated nodes in the middle being for the insulation, and the bottom clustered nodes being for the structure of the vehicle. With this, it can be determined whether the materials are within their usable temperature range, and if so, when it occurs. It also shows when the vehicle reaches equilibrium radiation temperature, which is when the surface nodes, or the radiation shield, reaches constant temperature, shown to be about 2000 sec in this case. Figure 7.18 shows the temperature through the depth or thickness of the TPS at three separate times. With this, the temperature distribution through the TPS system can be observed, and how it is distributed at distinct times. While Fig. 7.17 is useful in determining

whether the material stays within its specified limits, Fig. 7.18 allows the determination of how material thickness effects the temperature within the TPS system.

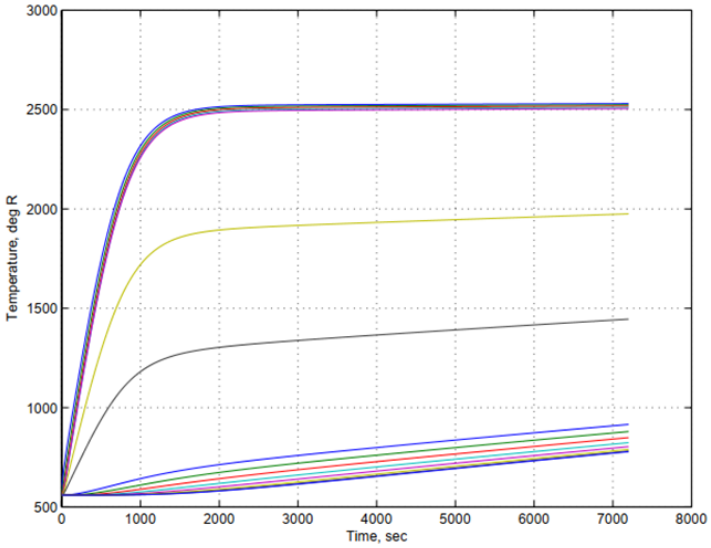

Fig. 7.17 Temperature of each node of the thermal protection system over time [162].

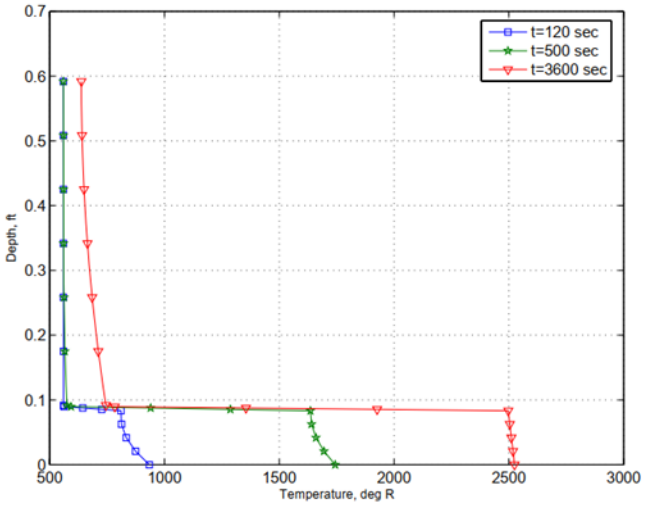

Fig. 7.18 Temperature through the thickness of the thermal protection system at various times [162].

For this first method investigated, the verification results for this method are shown below. The results that the method is being verified against is the results provided in Fig. 7.17 and Fig. 7.18 above. This is to make sure that the equations provided are correct and that any additional assumptions required to obtain the results that are not explicitly stated, are reasonable enough.

Most of the assumptions to use the equations, such as Mach number, cruise altitude, material properties and thicknesses, were provided, but a couple more assumptions were required, which were the node length (Δy) for the material interface node, and the time step for each calculation. Assuming that the node length for the material interface node is equal to the smallest of the interior node lengths of the two materials, and that the time step is 0.1s, initial results were obtained, but the temperature distribution showed to increase from the middle of the TPS system instead of from the surface. While investigating this phenomenon, it was found that the equation provided for the surface temperature had a typo within the original document [162]. Each provided equation was rederived to determine whether there were any more typos, but only the surface node equation was determined to have one. After fixing this equation and rerunning the results, Fig. 7.19 was obtained. Comparing Fig. 7.19 shown below to Fig. 7.17 above, it is observed that while the separation of the nodes between the radiation shield, insulation, and the structure, match with each other, the slope of the overall trends do not match.

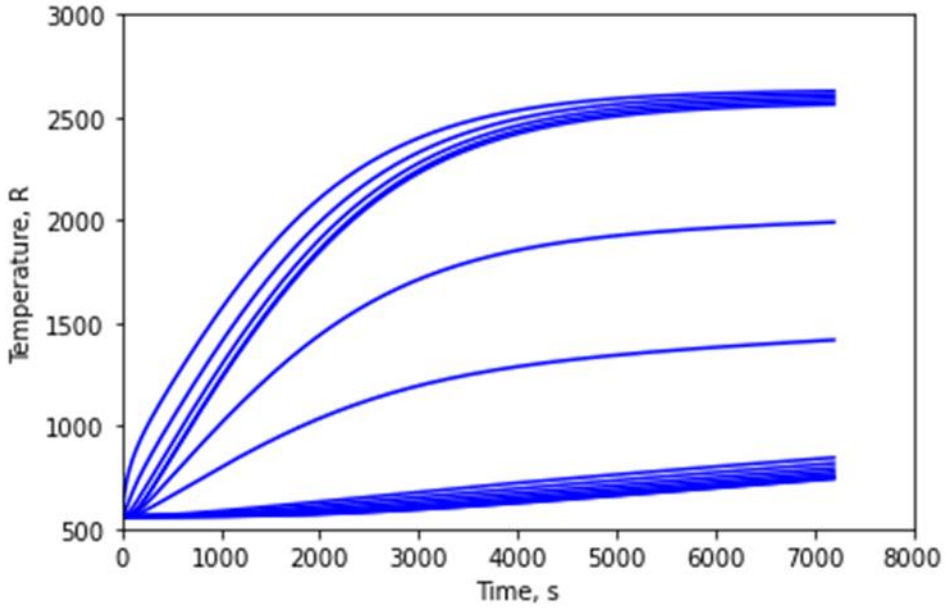

Fig. 7.19 Calculated temperature of each node of the thermal protection system over time.

From this, it was observed that the total combined thickness of the provided material thicknesses from the method reference was 0.15 m larger than that shown in Fig. 7.18. After noticing this, Fig. 7.18 was digitized within *WebPlotDigitizer* and each material thickness was estimated, and found that the structural thickness was the same, but the radiation shingle and the insulation thickness were smaller in the figure than what was provided in the text. By reducing the material thicknesses, the time step also had to be reduced from 0.1s to 0.01s to be able to run the method. After these changes, Fig. 7.20 and Fig. 7.21 were obtained. Comparing Fig. 7.20 shown below with Fig. 7.17 above, it is observed that the trends now match between the original results and the calculated results. Figure 7.21 below is also shown to compare to Fig. 7.18 above. It is observed that the overall trends and the max temperature for the 120s and 500s match closely with each other, but the max temperature for the 3600s trend is almost 100 °R over. This means there is a less than 4% error from the calculated results to the original results with this method slightly overpredicting the temperature experienced. This is taken to be sufficient, with errors attributed to the assumptions made that were not provided. With this method verified against their own results, it can now be used to compare generated results with the new method found.

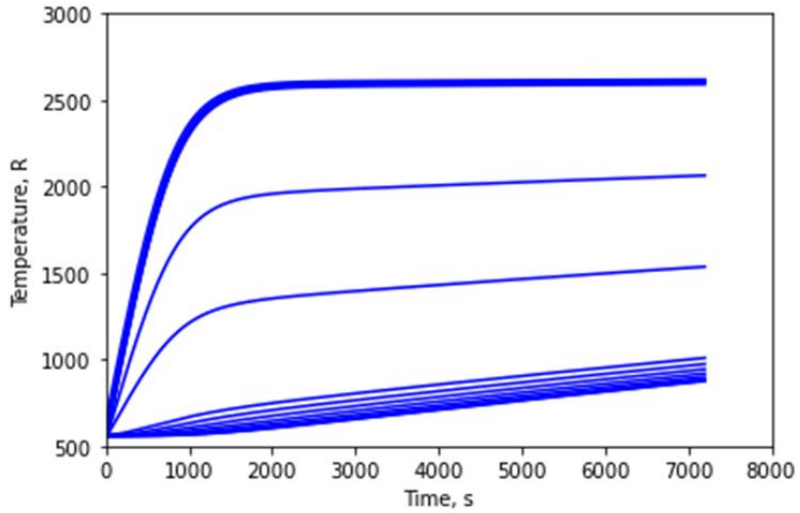

Fig. 7.20 Updated calculated temperature of each node of the thermal protection system over time.

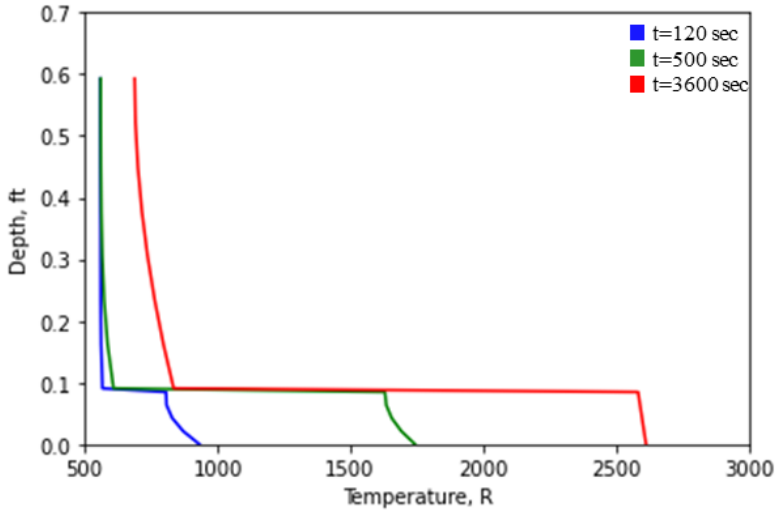

Fig. 7.21 Calculated temperature through the thickness of the thermal protection system at various times.

7.2.2.2.2 Heat Pulse Method

Before comparing results between these two methods, the second method (Heat Pulse Method) should be discussed [163]. As with the Finite Difference method, the assumed thermal model is shown in Fig. 7.22. As shown, the model considered is only the insulator material and the inner face sheet, with the top insulation surface exposed to the thermal environment. Also, the thermal input for this method is a heat pulse, with temperature as the input, and analytical equations were able to be developed with these boundary conditions. This varies from the Finite Difference method which includes the radiation shield in the calculations, the input is the heat flux, which can vary during the mission, and required a finite difference method to solve for the boundary conditions.

The difference between the Heat Pulse and Finite Difference method are due to the boundary conditions, which the Finite Difference method can have varying heat flux, while this method uses the heat pulse. The reason that the radiation shield is not considered for the Heat Pulse method in terms of the model, is that it is assumed that the radiation shield is thin and does not

contribute to reducing the heat that reaches the inner face sheet [163], as would be the case if the radiation shield was relatively thick to act as a heat sink. The heat sink case could be considered for the Finite Difference method, but not this one due to this assumption. Also, with the thermal input being temperature instead of heat flux, emissivity of the material is required if converting from a heat flux input, so the radiation shield material could be considered here as the emissivity would affect the surface temperature even if given the same heat flux profile. An example of emissivity changing with outer material is that the Finite Difference method uses PM2000 as the radiation shield for their example, which has an emissivity of 0.6 [162], and the Heat Pulse method uses LI-900 tiles from the Space Shuttle which had a reaction cured glass (RCG) coating with an emissivity of about 0.85 [164]. As this method would need to calculate the total structural index though, the radiation shield material would be selected and either a constant thickness across materials would be selected, or a minimum manufacturing thickness would be determined to calculate the I_{str} value for this portion.

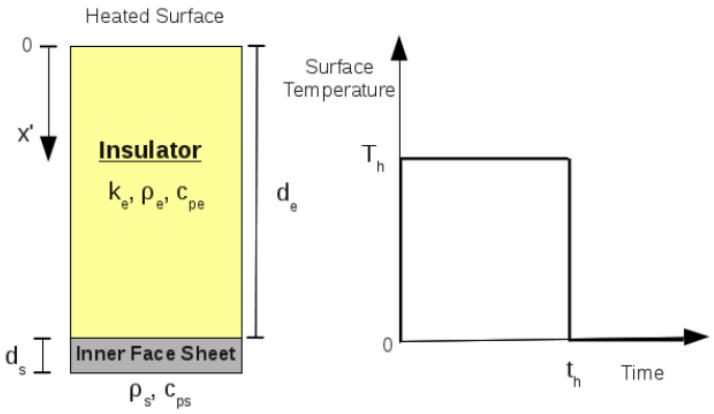

Fig. 7.22 Illustration of simplified problem [163].

As mentioned, the Finite Difference method uses heat flux as the thermal input while this method uses temperature. Also, the Finite Difference method allows transient heat flux, while the Heat Pulse method uses a heat pulse for its calculations. Despite this Heat Pulse method having a

simpler thermal input, the analytical equations developed with this assumption were compared to a finite element model using several heat profiles and temperature dependent material properties. For the simplified analytical equations, each heat profile was converted to a representative heat pulse as shown in Fig. 7.23. This representative heat pulse is used to compare to the finite element model to determine the accuracy of the developed analytical equations. One of the results for this comparison, the structural temperature vs. the insulation thickness, is shown in Fig. 7.24. As shown, the analytical equations (Series, Eqn 20, and Eqn 21) match closely with the finite element models with the largest error produced at the smaller insulation thickness, and the smallest error produced at the larger insulation thickness. It also shows that the analytical equation that uses a series produces the least error compared to the FE model than the other analytical equations.

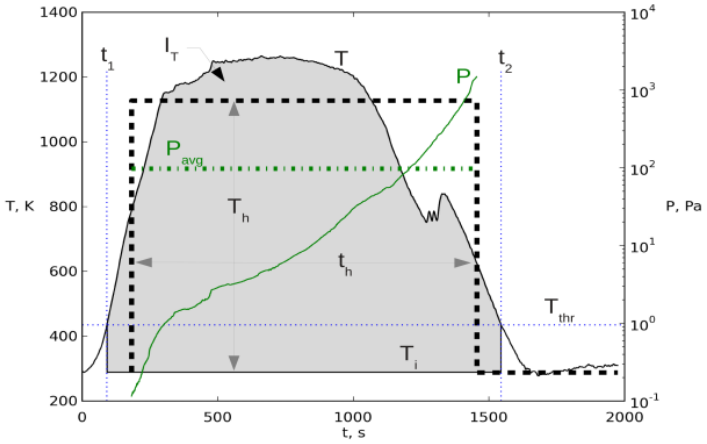

Fig. 7.23 Simplified heating and pressure histories for BP9740 [163].

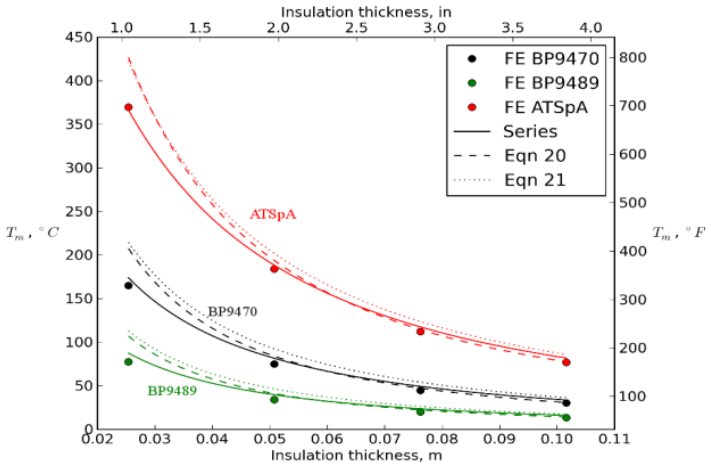

Fig. 7.24 Maximum structural temperature rise vs insulation thickness [163].

For this Heat Pulse method investigated, the verification results are presented in Fig. 7.25 with the equations used provided in Appendix E. These results are compared to the series solution of Fig. 7.24 as they produced the smallest error compared to the FE results. As observed, the verification series results match closely with all three heat profiles, with the largest error of 6% occurring for the heat profile of ATSpA (Access to Space point A) when compared to Blosser's series results. This error is due to the method of interpolation when calculating the material properties, specifically the thermal conductivity, *k*, as it is a function of both temperature and pressure. For Fig. 7.25, the material properties were calculated using 'linear' interpolation. After using other interpolation methods to observe their effect on the results, it was found that 'spline' interpolation produced the smallest error for ATSpA, but with increase in error for the other two heat profiles, especially for BP9470 (Body Point 9470), as shown in Fig. 7.26. From this, the 'linear' interpolation method was selected as the default method to calculate the material properties as it produced the least overall error across the three heat profiles.

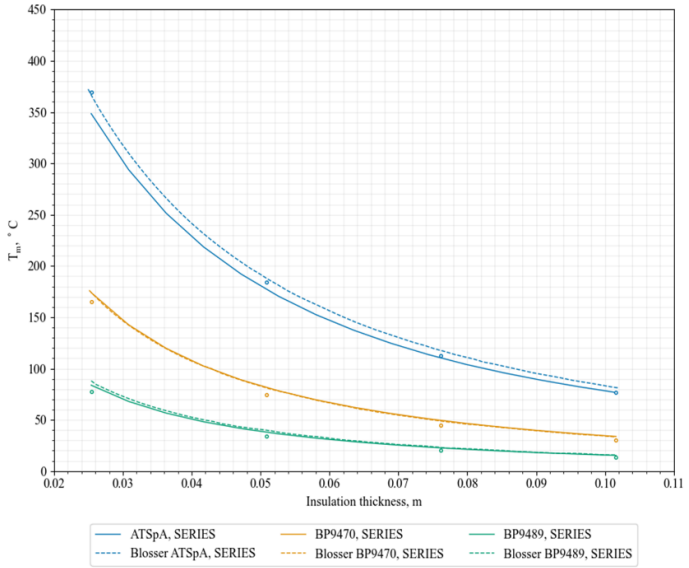

Fig. 7.25 Comparison of Blosser series results with AVD results (linear interpolation).

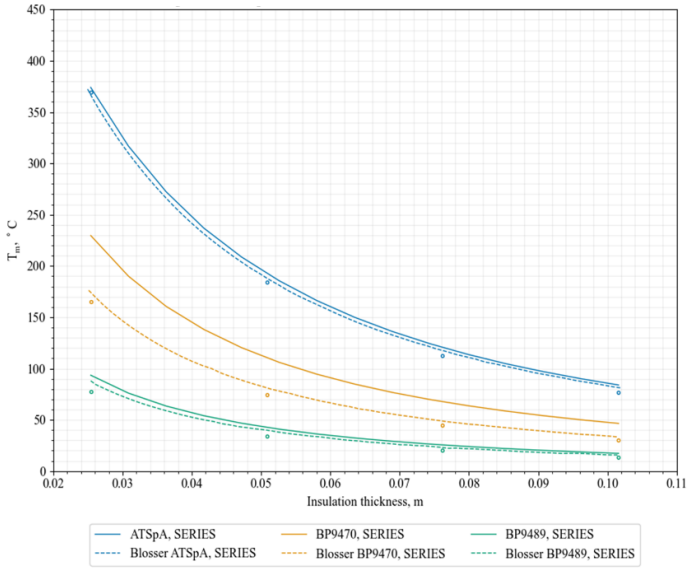

Fig. 7.26 Comparison of Blosser series results with AVD results (spline interpolation).

7.2.2.2.3 Comparison of Temperature Methods

Using Fig. 7.24 above, the results for ATSpA were used to compare the two investigated methods to determine which method to continue with. As the Finite Difference method requires heat flux as the thermal input instead of temperature, the original heat flux profile for ATSpA was found and provided in reference [165]. Using this heat profile and modeling the first method as

close as possible to match the Heat Pulse method, which required using only the insulation and the structure for the thermal calculations, the results between the two methods for the same thermal input are shown in Fig. 7.27. It is observed that the first method appears to vary greatly from the second method at large thicknesses but is comparable at smaller thicknesses. From this, it was originally unknown whether the Finite Difference method was underpredicting results, or the Heat Pulse method was overpredicting. With this in mind, a separate value, the verification value, was determined using data within the ATSpA heat profile reference [165], where the thickness of LI-900 insulation was determined for this heat profile. This now shows that the Finite Difference method was underpredicting results, while the Heat Pulse method matched very well.

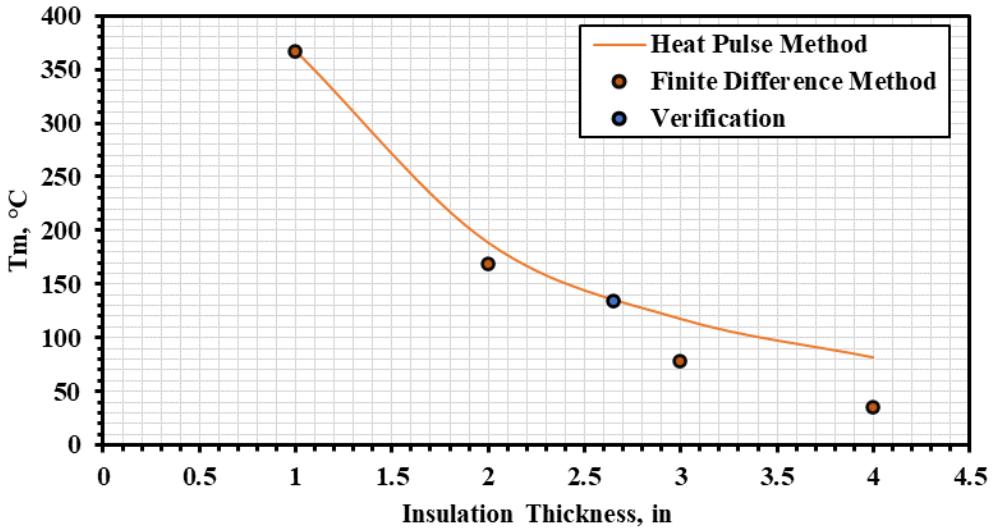

Fig. 7.27 Results for temperature method comparison.

From these results and other considerations, it was determined that the second method was the method to continue with. Observing the results, the second method matches very well with the verification point lying just below its line, meaning that the Heat Pulse method may overpredict the structural temperature slightly. When it comes to overpredicting or underpredicting results, overprediction is preferred in terms of vehicle design as if a vehicle's values are overpredicted, it

can still be designed if lower values are obtained, if a vehicle's values are underpredicted though, it would not be able to be designed if higher values are obtained without changes. As for the other considerations, they are 'time to execute' and 'complexity of the method', which typically go hand in hand. In comparison, the Finite Difference method is more complex and time consuming to run due to it being a finite difference method, requiring the materials to be broken down into multiple elements, or nodes, to run, and requiring the time step to be on the order of 0.01 s – 0.001 s, due to the thickness values. With the Heat Pulse method using analytical equations, even the one with a series, these execute quicker in comparison. For example, one of the points for the Finite Difference Method shown in Fig. 7.27 can take around 3hrs to run, while the Heat Pulse method is on the order of a few seconds for one point.

Both methods considered only really help with the TPS portion of the total I_{str} by being able to determine the thickness of the insulation required to keep the structure within the defined max temperature limit. Also, the radiation shield thickness can be determined from manufacturing limits, or assuming a previous TPS shingle thickness. These combined determine the TPS I_{str}, but the primary structure I_{str} has not been determined. For both cases, only a thickness or an I_{str} value was provided for the primary structure to calculate the other values, these were never calculated themselves. This is because the primary structure in both these cases are cold structures, so the structure thickness/I_{str} is independent of temperature, meaning that they are functions of other parameters such as the aerodynamic forces experienced during flight. These methods do not deal with the forces on the primary structure, so another method or assumption is required for the I_{str} for the primary structure. One assumption that could be made is to use either the structural index value for the primary structure assumed by either the 1983 structure assumption of Hypersonic Convergence shown in Chapter 6 in Fig. 6.1, or the structure assumption used for calculations

within the Heat Pulse method reference [163] which is 8.89 kg/m^2 (1.82 lb/ft^2). There is a difference for these though, in that for Hypersonic Convergence, the value is for a Mach 12 cruiser, while the value for the Heat Pulse method reference is for a space access vehicle as these are the vehicles considered within each study.

Instead of the assumptions, regressions could be made to determine the primary structural weight versus some parameter. An example is shown in Fig. 7.28 where the structural weight is a function of the wetted area. For this though, a weight breakdown for each vehicle is required to remove the TPS from the structural weight and any other elements that are not wanted to be considered within this, such as possibly the landing gear weight. The reason that structural design is not considered is due to it being considered within the preliminary design phase and not the conceptual design phase, especially for vehicle sizing. With either the regression method or assuming a primary structure I_{str} value, this combined with the TPS calculations with the selected heat pulse method, the total structural index value can be calculated. These will be used to create updated maps of the original temperature I_{str} figure made within Hypersonic Convergence, to primarily show time effects with updated materials.

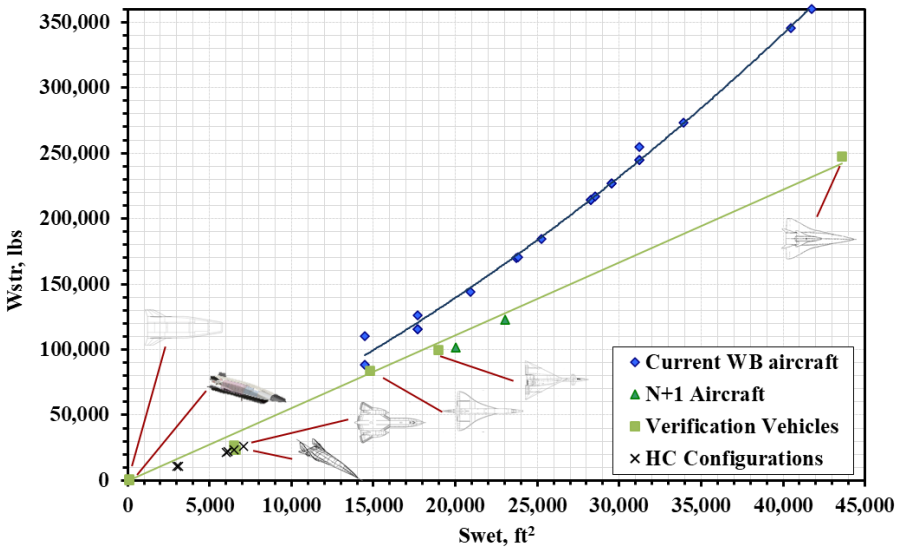

Fig. 7.28 Total structural weight vs wetted area.

7.2.2.3 Results and Observations

Using the temperature through the thickness method selected from the previous section, structural index maps and sensitivities can be generated and observed. While the generated maps that will be discussed are important for sensitivities and can show the rough magnitude of the structural index for certain TPS concepts, when a vehicle design trade point is being converged upon within AVDS, these maps will not be consulted, but a unique value pertaining to the design will be calculated. As mentioned, these maps are to show how the structural index is impacted with certain variables, such as insulation material, structural material, cruise time, etc. These will provide insight into which variables provide the greatest change in structural index, and which ones should be considered when investigating which technology should be improved upon.

For the maps generated, the variables that will be considered are the effects of change in insulation material, structural material, radiation shield material, cruise time, and average atmospheric pressure during the flight. Along with these sensitivities, each map generated will

show how each of these changes with temperature as well. The materials considered for this study are shown in Table 7.1.

The density of each material is used to determine the I_{str} for each specific section of the TPS with the combination of all three being the total structural index of the vehicle. The max usable temperature for each material is used to cut off where a material is usable. This shows which materials/TPS concepts are viable at a certain temperature.

For the structural material, there is a range of max usable temperatures as the limits were dependent on the application, so an upper and lower limit were selected [163]. It is noted that the temperature used within the figure may not be the max temperature experienced when compared to an actual flight envelope as the method selected uses a representative heat pulse as shown in Fig. 7.22 and Fig. 7.23 above. This will change which materials are usable, but for the sake of these sensitivity maps this is not considered.

The average atmospheric pressure, P_{avg}, is required for the selected method as well as shown in Fig. 7.23 above, so as mentioned for one of the sensitivity maps, the effects of this parameter will be investigated. The specific heat capacity (c_p) and thermal conductivity (k) of each material are provided as well, but as these values change with temperature and possibly pressure, the tables with the full range of values used are provided in Appendix F. The specific heat capacity and thermal conductivity of the radiation shield are not provided as they are not used in the selected method. This is because the assumption for the radiation shield is that it does not act as a heat sink, so the temperature at the surface of the radiation shield is the same as at the interface to the insulation. As the name suggests, the purpose of the radiation shield is the radiate away the incoming heat flux, so the only considerations for the radiation shield are the density of the material, the max temperature that it can resist, and the emissivity of the material as the higher the

emissivity, the lower the surface temperature. As a heat flux profile is not considered for this study, the emissivity is not considered at this time, but in practical use it would be.

Table 7.1 List of material properties used for I_{str} sensitivity study.

Material	Density, lb/ft^3	Max Usable Temperature, °F	c_p	k	Reference
		Radiation Shield			
Carbon/Carbon	117	2550	N/A	N/A	[166]
2D CVI SiC/SiC	140	2550	N/A	N/A	[167,168]
PM2000	444	2200	N/A	N/A	[162]
ZrB2-30Vol%SiC	339	3630	N/A	N/A	[169]
Ti-SF61	285	1830	N/A	N/A	[170]
		Insulation			
Saffil	3.0	2191	Table F.1 Table F.2	Table F.1 Table F.2	[171]
Q-Felt	3.5	1800	Table F.3 Table F.4	Table F.3 Table F.4	[172]
Cerrachrome	6.0	2400	Table F.5	Table F.5	[173]
AETB-8	8.0	2750	Table F.6	Table F.6	[174]
AFRSI	6.0	1750	Table F.7	Table F.7	[174]
LI-900	9.0	2300	Table F.8	Table F.8	[164]
		Structure			
Aluminum 2024-T4	173	300 – 350	Table F.9	Table F.9	[163,175]
Titanium 6Al-4V	276	500 – 800	Table F.10	Table F.10	[163,175]
Aluminum-Beryllium Alloy AM162	131	450 – 550	Table F.11	Table F.11	[163,176]
Graphite/Epoxy	99	200 – 300	Table F.12	Table F.12	[163,177]

Before generating the sensitivity maps for I_{str}, the selected method to calculate I_{str} with the different variables was used to verify against the structural index trends generated by Paul Czysz in Hypersonic Convergence. This verification is shown in Fig. 7.29 along with the constants used in Table 7.2. The trends shown are for passive TPS as the assumption for these sensitivity maps are for passive TPS. As will be discussed, observations can be made on when an active TPS should be used depending on the TPS concept, and the assumption would be that the structural index would decrease given an active TPS as shown in Czsyz's original I_{str} figure, Fig. 6.2 shown previously in Chapter 6.

The range of I_{str} values for each material is due to the structural max usable temperature range that the insulation thickness is iterated to maintain. Using Fig. 6.1 which provides a structural

index breakdown of a Mach 12 vehicle at a cruise time of 1.5 hrs, it was assumed that the radiation shield and structural I_{str} of 1.29 lb/ft^3 and 1.45 lb/ft^3 respectively were constant, so the only value that needed to be calculated was the insulation I_{str}. The reason that the radiation shield and structural I_{str} were held constant is because these values are determined separate from the temperature method, with structural analysis for the structure and radiation shield concept (e.g., honeycomb, standoff), and/or manufacturing capabilities for the radiation shield (minimum thickness), so only the insulation I_{str} can be directly calculated. It is noted that while the I_{str} value of the structure is kept constant, the material properties of the selected structural material still play a part in the insulation I_{str} calculations.

Observing Fig. 7.29, it is shown that Czysz's I_{str} line appears to match with a couple of insulation materials. Removing the extraneous insulation materials, it is shown in Fig. 7.30 that Czysz's I_{str} line matches with the lower structural temperature bound for LI-900 and Cerrachrome. This not only verifies the selected method to calculate I_{str}, but this also means that a trend that was generated in the 80's was able to be recreated with a modern method. It is noted that the insulation material that matches with Czysz's I_{str} line may not be the same insulation material that was considered at that time but could have had similar properties in those temperature ranges. This is observed because the Cerrachrome insulation material produces a lower I_{str} than the LI-900 until just over 1500 °F when LI-900 produces a lower I_{str}. If Cerrachrome was the actual insulation used, then Czysz's line would have followed along Cerrachrome's bound for longer until switching to the LI-900 material. As this is not the case, similar materials to these were most likely used. With the selected method to calculate I_{str} verified with historic data, the sensitivity maps can now be created.

Table 7.2 Variables for I_{str} verification study.

Radiation Shield Material	Insulation Material	Structural Material	Cruise Time, hrs	P_{avg}, Pa
PM2000	Varying	Titanium 6Al-4V	1.5	98

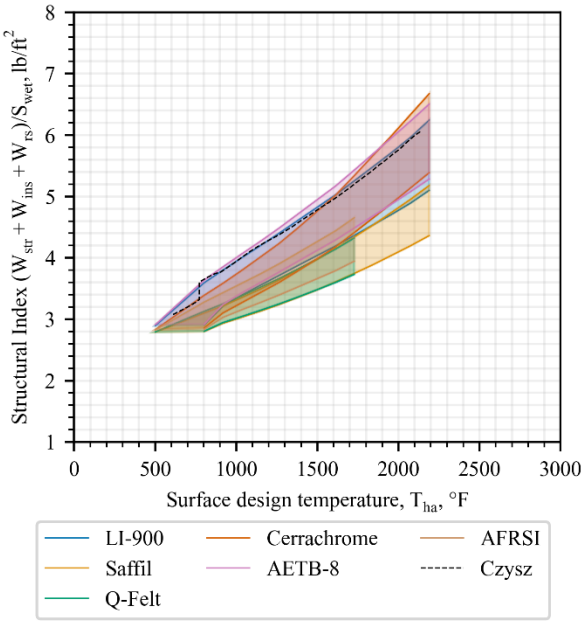

Fig. 7.29 Verification between selected method and results by Czysz.

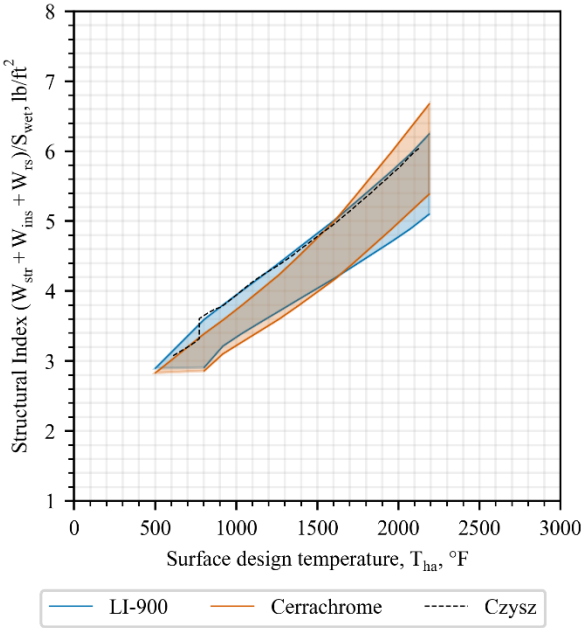

Fig. 7.30 Verification between selected method and results by Czysz (reduced).

7.2.2.3.1 Effects of Insulation Material Variation

The first structural index sensitivity map generated is how varying insulation material affects I_{str} as shown in Fig. 7.31. The constants for this figure are provided in Table 7.3. While this is similar to the verification figure above, the structural material and cruise time are different, and the radiation shield weight is not considered. Except for the sensitivity map concerning the radiation shield, this set of materials are not considered for the other maps to maintain one changing variable between each one.

For the variation in insulation, the main observation is that primarily I_{str} decreases with a decrease in insulation density. The reason this is primarily the case is because overall this is observed as the higher density insulation materials are the top trendlines and the lower density materials are the bottom trend lines. There are exceptions though, with LI-900 producing slightly lower I_{str} values than AETB-8 at lower temperatures, but then produces noticeably lower values than both AETB-8 and Cerrachrome at higher temperatures despite having a higher density. This means that while the material thermal properties are important, allowing higher density insulation materials to produce lower I_{str} values than lower density materials in certain cases, the main driver for the structural index in terms of insulation material is the density.

Table 7.3 Variables for I_{str} sensitivity study 1.

Radiation Shield Material	Insulation Material	Structural Material	Cruise Time, hrs	P_{avg}, Pa
None	Varying	Aluminum 2024-T4	2	98

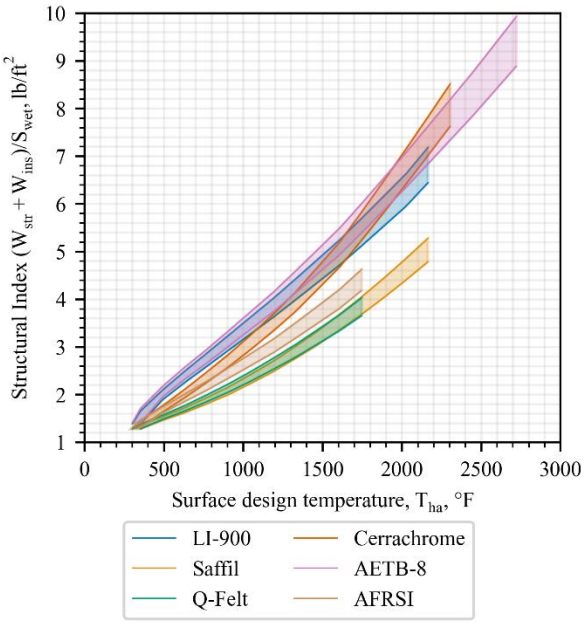

Fig. 7.31 Structural index sensitivity map for varying insulation material.

Along with its effect on the structural index, I_{str}, shown above, the required thickness for each insulation to maintain the max usable temperature limits of aluminum 2024 with increasing temperature is shown in Fig. 7.32. It is interesting to note that the insulation materials that produce the lowest I_{str} require the largest thicknesses and vice versa. Unlike its effects on the structural index (I_{str}), the insulation material density has a lesser effect on the thickness required to maintain the max temperature of the structure, meaning that in the case of thickness, the material thermal properties are the main drivers. This is shown primarily through the comparison of the materials Q-felt and Cerrachrome, and AETB-8 and AFRSI. In the case of Q-felt and Cerrachrome, these two materials' trend lines lie almost completely on one another even though Cerrachrome's density is roughly twice that of Q-felt. For AETB-8 and AFRSI, AETB-8 requires a smaller thickness overall compared to AFRSI despite having a higher density.

Another interesting note is that at lower temperatures (roughly lower than 750 °F) the material thermal properties nor density affect the required thickness, with all six insulations requiring the

same thickness. Beyond this point though, the insulations begin to fan out with the material thermal properties taking over.

Observing the thickness required for each insulation to maintain the max structural temperature, it is shown that the thickness required greatly increases with temperature, with some of the thicknesses even reaching and exceeding a foot thick. This, of course, is an unreasonable thickness to use, but some insights can be obtained. First, these thickness values provide a possible limit in which active TPS would be required. For example, if it was required that the insulation thickness had to be 4 inches or lower for various reasons, then using the insulation outer limits, Saffil would require active TPS above 950 °F and LI-900 would require active TPS above 1400 °F. While LI-900 produces a higher structural index (I_{str}) than Saffil, as LI-900 can maintain as a passive TPS at a higher temperature, the weight penalty of LI-900 as a passive TPS may provide a lower weight than Saffil as an active TPS.

Another insight of the insulation thickness values is that, in conjunction with Fig. 7.31 above, a compromise can be made between weight and volume of the TPS. While in reality not the case, if the thickness selected was assumed throughout the whole of the vehicle, then a notional volume for the TPS can be determined. This notional TPS volume can be iterated within a synthesis system, like AVDS, to determine the total volume of the vehicle required to house this TPS volume and all the other volumes such as the fuel and cargo. As the weight of the vehicle impacts the fuel weight and volume required, the thinner but heavier insulations may produce a smaller, lighter vehicle than the thicker but lighter insulation, keeping all other volumes and weights constant.

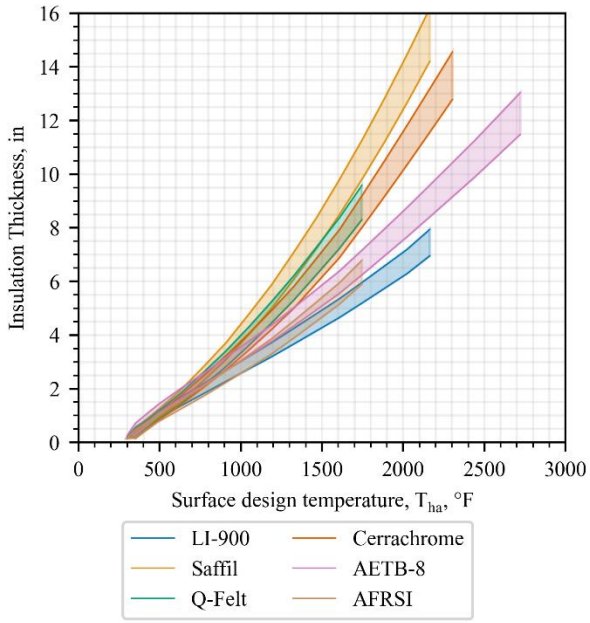

Fig. 7.32 Insulation thickness sensitivity map for varying insulation material.

7.2.2.3.2 Effects of Structural Material Variation

The second structural index sensitivity map generated is how varying structural material affects I_{str} as shown in Fig. 7.33. The constants for this figure are provided in Table 7.4. For the variation in structural material, it is shown that the structural material producing the largest structural index (I_{str}) to the lowest is graphite/epoxy, aluminum 2024, and titanium 6Al-4V and beryllium aluminum sharing the bottom boundary line.

Comparing the material density first, it is observed that density is not the primary driver that effects the structural index as the densities do not correlate, with the lowest density producing the highest I_{str}, the second highest density producing the second highest I_{str}, and the highest and second lowest densities producing the lowest I_{str}. Next, the max temperature of the structural material was compared. From this, it is observed that the max temperature is the primary driver that affects the structural index in varying structural material as an increase in max temperature reduces I_{str}.

Graphite/epoxy, while having the lowest density, also has the lowest max temperature range, so a thicker insulation is required to maintain these temperatures, increasing the structural index. As the max temperature range increases, the required insulation thickness decreases, decreasing the structural index. This is observed for each structural material except for beryllium aluminum's relationship with titanium 6Al-4V. Beryllium Aluminum's total max temperature range is around the lower temperature limit of titanium, but it produces I_{str} values along the higher temperature limit of titanium. This could be attributed to the density of the materials. While structural density is not the primary driver, it does have some effect as beryllium aluminum's density is over half that of titanium's. This means that if two structural materials have the same max temperature value, then the one with the lowest density will produce the lowest structural index value.

While this seems straightforward, it is noted that this is only in terms of temperature, and other factors, such as strength of the material, could make the lowest density material require a heavier structure than the higher density one. The material strength required to withstand the aerodynamic loads is not currently considered as previously mentioned, so the observations obtained for varying structural material are only from their thermal capabilities.

Table 7.4 Variables for I_{str} sensitivity study 2.

Radiation Shield Material	Insulation Material	Structural Material	Cruise Time, hrs	P_{avg}, Pa
None	AETB-8	Varying	2	98

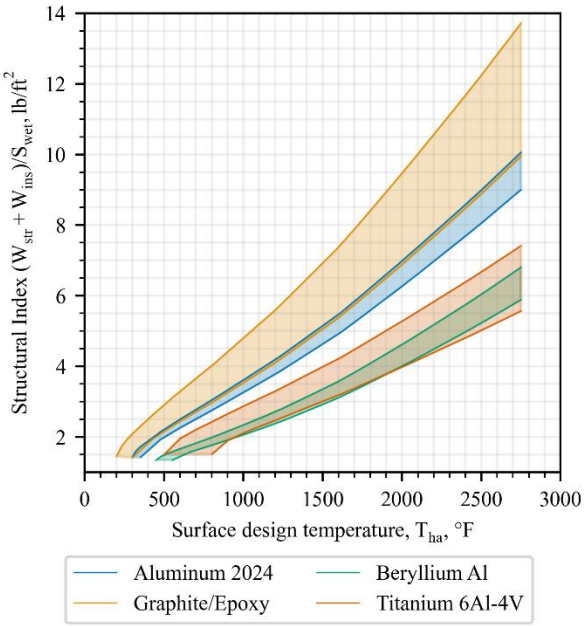

Fig. 7.33 Structural index sensitivity map for varying structural material.

Along with its effect on the structural index, I_{str}, shown above, the required thickness for the insulation to maintain the max usable temperature limits of each structural material with increasing temperature is shown in Fig. 7.34. As observed, the trends of varying structural material for the insulation thickness match that of the structural index.

As mentioned previously, the structural materials with the lowest max temperature limits require thicker insulation, while the ones with a higher max temperature limit have thinner insulation. This is proved with graphite/epoxy requiring the thickest insulation and titanium and beryllium aluminum requiring the thinnest.

In terms of active TPS, the selected structural material also affects when active TPS would be required. Using the previous example of a limit of a 4 inch insulation thickness, graphite/epoxy would require active TPS above 900 °F to 1300 °F, aluminum above 1300 °F to 1400 °F, titanium above 1700 °F to 2200 °F, and beryllium aluminum above 2000 °F to 2200 °F. Observing the total

temperature range of this example from 900 °F to 2200 °F, the max temperature limit of the selected structural material greatly effects when active TPS would be required.

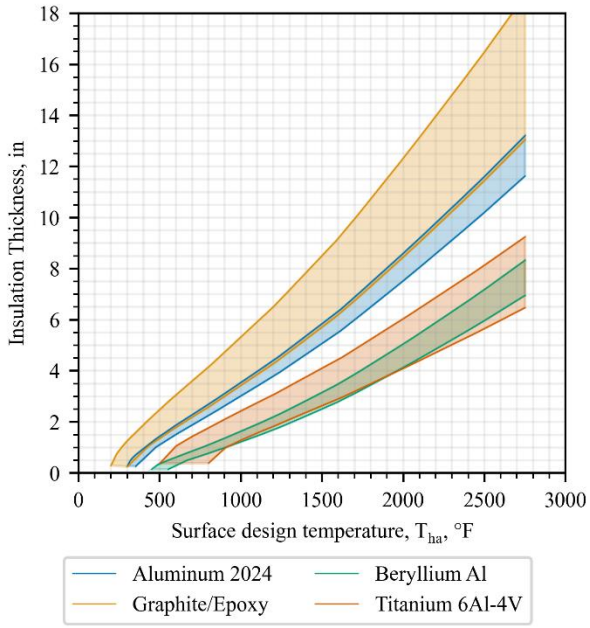

Fig. 7.34 Insulation thickness sensitivity map for varying structural material.

7.2.2.3.3 Effects of Radiation Shield Material Variation

The third structural index sensitivity map generated is how varying the radiation shield material affects I_{str} as shown in Fig. 7.35. The constants for this figure are provided in Table 7.5. For the variation in radiation shield material, the primary driver of the structural index for these trend lines is the density of the radiation shield. This is shown as the material with the highest density (PM2000) produces the highest I_{str}, while the material with the lowest density (Carbon/Carbon) produces the lowest I_{str}.

This relationship is expected as for the current consideration of radiation shield material only adds weight to the TPS, so density would be its only effect on I_{str}. This may seem a simple case to consider, but there is an assumption that has been made that may greatly change the results. The assumption was to maintain the same radiation shield thickness of 0.001 m across each material,

which also would limit the comparison to the density only. The thickness was determined by taking PM2000 and calculating the thickness that would produce the same I_{str} value of 1.29 lb/ft^2 for the shingle used within Hypersonic Convergence shown back in Fig. 6.1. The PM2000 material was used for this calculation as this was accomplished during the use of the Finite Difference method discussed in the previous section before finding and using the Heat Pulse method. The reason this is an assumption that could greatly change the results is because this thickness may be larger or smaller depending on the material and radiation shield concept.

For the material, the thickness is dependent on the manufacturing capability, so a material that can be made thinner but has a high density can potentially have a smaller I_{str} than a material with a low density but is harder to work with so has a greater minimum thickness. This concept is the same discussed with the insulation thickness but applies here as well.

For the radiation shield concept, this includes concepts such as honeycomb core sandwiches, standoffs, etc., which while does affect the thickness, is not used directly in calculating the structural index. The weight of this concept over the area would need to be determined by other means than direct calculation between thickness and density as has been currently used.

With these considerations, only the effects of density with a constant thickness were observed for this sensitivity map as the others require further investigation. A property of the radiation shield that would not affect the trend lines but affect the output value given the same input is the emissivity value. The emissivity value determines the amount of heat flux that is radiated away, which in turn determines the temperature that the surface reaches. The higher the emissivity, the more heat flux is radiated way, the lower the surface temperature, and vice versa. This means that given a heat profile from a mission, depending on the radiation shield material and its corresponding emissivity, the temperature that is experienced for each one could be different,

which may make certain materials have a lower I_{str} despite a higher density. As high emissivity values are wanted, and coatings can be applied to raise this value, this consideration may have a small effect on the structural index.

Lastly, it is noted that comparing the trends of the varying radiation shield material to the other material variations, that the radiation shield has the smallest effect on the structural index. This means that the primary materials for consideration in terms of significantly changing the structural index would be the insulation and structural material. While it does influence the total structural index value, the primary purpose of the radiation shield is to obtain the lowest surface temperature possible from the given heat profile, to survive at these elevated temperatures, and to protect the insulation and structure.

Table 7.5 Variables for I_{str} sensitivity study 3.

Radiation Shield Material	Insulation Material	Structural Material	Cruise Time, hrs	P_{avg}, Pa
Varying	AETB-8	Aluminum 2024-T4	2	98

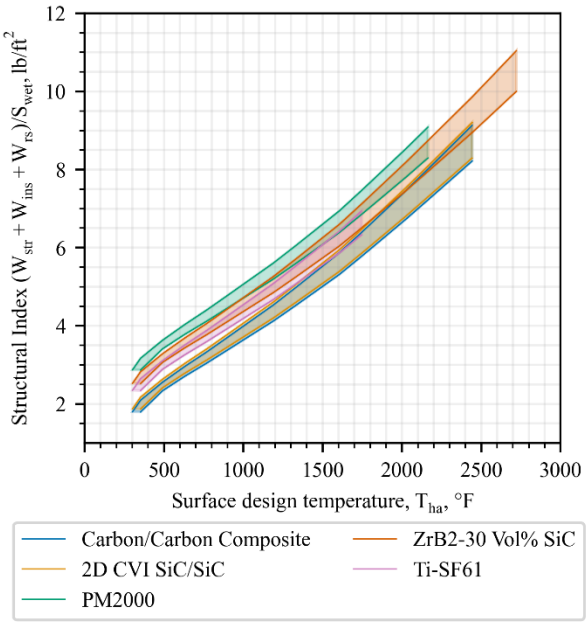

Fig. 7.35 Structural index sensitivity map for varying radiation shield material.

7.2.2.3.4 Effects of Cruise Time Variation

The fourth structural index sensitivity map generated is how varying the cruise time affects I_{str} as shown in Fig. 7.36. The constants for this figure are provided in Table 7.6. For the variation in cruise time, it is shown that as the cruise time increases the structural index increases and the rate at which it increases with temperature also increases. Interestingly though, the rate at which I_{str} increases decreases as cruise time increases, meaning that the difference between each cruise time trendline is decreasing, with the trendlines for a cruise time of 4 and 5 hrs overlapping. This means that a vehicle with an aluminum structure that is designed to withstand its upper temperature limit at a cruise time of 5 hrs can have the same, or slight lower, I_{str} value as a vehicle at a cruise time of 4 hrs but designed with the more conservative lower temperature limit.

Except for the boundary cases at the higher cruise times, the results shown are to be expected. Even though the insulation thickness is not provided, the insulation thickness increases with cruise time as more material is needed to maintain the structural max temperature limit, which increases I_{str}. As previously mentioned, these sensitivity maps are for passive TPS, so the rate these trend lines increase may be at a shallower slope for an active TPS.

Table 7.6 Variables for I_{str} sensitivity study 4.

Radiation Shield Material	Insulation Material	Structural Material	Cruise Time, hrs	P_{avg}, Pa
None	AETB-8	Aluminum 2024-T4	Varying	98

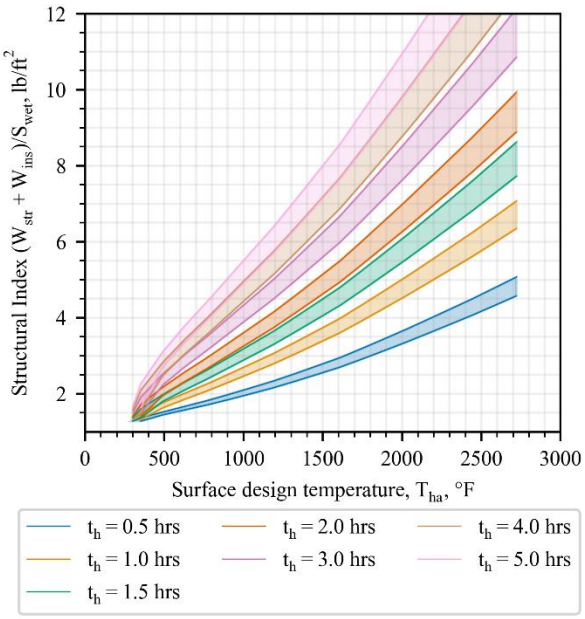

Fig. 7.36 Structural index sensitivity map for varying cruise time.

7.2.2.3.5 Effects of Average Atmospheric Pressure Variation

The last structural index sensitivity map generated is how varying P_{avg} effects I_{str} as shown in Fig. 7.37. The constants for this figure are provided in Table 7.7. For the variation in P_{avg}, it is shown that as the average atmospheric pressure along the given trajectory increases, the structural index (I_{str}) increases as well. As was also shown with an increase in cruise time, the trend lines for increasing P_{avg} begin to coalesce at higher pressures with the last two highest pressures (10,747 and 12,000 Pa) overlapping each other. This means that further increase in P_{avg} beyond 10,747 Pa (roughly 0.1 atm) will not further increase the structural index.

Since P_{avg} is used within the material property calculations, it is material specific, so this pressure in which the trend lines are collapsing upon may not be the same for a different insulation material. Despite this though, it can be assumed that other insulation materials will behave similarly, so at higher atmospheric pressure averages, the insulation thermal properties could be

considered only dependent on temperature, while at lower P_{avg}, the thermal properties are dependent on temperature and pressure.

For the atmospheric pressure averages, an example of missions that would have lower P_{avg} values would be boost glide, reentry, and SSTO. These missions generally have vehicles in the less dense atmosphere for most of the mission which reduces P_{avg}. For the higher P_{avg} values, this would consist of cruisers where most of their mission is within the denser portion of the atmosphere. Taking the reentry and cruise vehicle mission examples, the results obtained for the sensitivity map of P_{avg} matches the expected outcome that a vehicle with a cruising mission would require more insulation to withstand the aerothermal environment than a reentry vehicle. While a reentry vehicle technically does experience higher temperatures than a cruise vehicle, the time experienced at these temperatures is significantly less. Also, when converting the heat profile into an equivalent heat pulse, the heat pulse for the reentry vehicle would have the potential to be lower than the cruiser, while the cruiser's heat pulse would be close to the equilibrium temperature at cruise.

As a side note, the reason this sensitivity map does not have the full structural temperature range for each trend line, as in the previous sensitivity studies, is because the close proximity of the lines produced issues in distinguishing these lines, so only the lower structural max temperature value was used.

Table 7.7 Variables for I_{str} sensitivity study 5.

Radiation Shield Material	Insulation Material	Structural Material	Cruise Time, hrs	P_{avg}, Pa
None	AETB-8	Aluminum 2024-T4	2	Varying

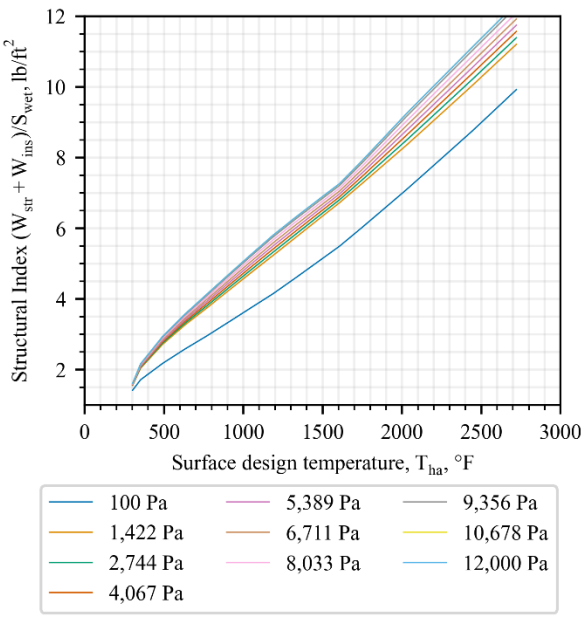

Fig. 7.37 Structural index sensitivity map for varying average atmospheric pressure (P_{avg})

With these sensitivity maps generated, it is shown how the material properties and a few parameters affect the structural index. While only one parameter was changing for each sensitivity to clearly show its relationship to I_{str}, full maps of each structural material with each insulation material and cruise time are provided in Appendix G. These full maps provide insight into how each combination affects I_{str}, but also allows the use of them as how Fig. 6.2 from Hypersonic Convergence was originally used with using the figure directly to select an estimated structural index value for a vehicle. It is again noted that these maps do not consider the radiation shield, but this value can be directly added to the selected I_{str} value once determined separately.

CHAPTER 8: FUTURE WORK

8.1 Improvement to the Vehicle Configuration Compendium (VCC)

With the alpha version of the VCC developed and while the software mostly provides a preview of how it could look and run, it provides a starting point in which the VCC can now be improved by implementing more high-speed vehicles, integrating it with AVDS, and developing the GUI further. The implementation of more vehicles will further increase the usefulness of the VCC, especially the knowledgebase side as it deals with trends and forecasting through past vehicles. Even with just 7 vehicles as a test case, the VCC has proved its power through its use of the database, as was shown in Chapter 5, where the data stored is used for the verification of methods used within AVDS and the synthesis system, AVDS itself, and the knowledgebase, as was shown in Chapter 6, where parameter trends are investigated to use within AVDS.

As the VCC is currently a standalone system, the process of using the data within AVDS is a manual process where all the data wanted for verification must be manually entered. When the VCC is eventually integrated with AVDS it will allow most of these processes to be automatic, such as pulling the data wanted for verification, selecting trends from the predefined knowledge plots for methods, or to superimpose the synthesis data from AVDS of new designs on to the knowledge plots to compare them to legacy vehicles. This will improve the functionality of AVDS by reducing the time required to run and improve the quality of the results of verification and trade studies.

For the further development of the GUI, this is more for the user of the VCC as when used in conjunction with AVDS, the GUI is not needed. While it is not needed directly with AVDS, the GUI provides a visual for future researchers and design engineers to view the digitized data of the

stored vehicles and to make the configuration/cross-section comparisons without having to do them on their own. This allows a single location where the user can be acquainted with these high-speed legacy vehicles without having to investigate themselves, 'catch-up' with previous researchers and engineers by observing the knowledge that they found/developed through the knowledgebase, and to possibly obtain new knowledge from investigating the parameter combinations for each configuration comparison. Lastly, it will allow them to pass on knowledge themselves to the next set of researchers by updating the knowledgebase with what they have learned. So, while the current GUI is a first look or 'preview' into how the VCC software could look like and function, improving it further is also a major step for the future of the VCC.

8.2 VCC Synthetic Development

Alongside the improvements of the VCC as previously discussed, another form of the VCC could be developed where synthetic data created during verification studies could be used in place of the unknown wanted data of the database. This form, called the VCC Synthetic as mentioned in Chapter 4, would be able to fill up the database of the wanted parameters, even for vehicles that have a low data richness value. As reasonable methods have to be selected and used to determine a value that is required within AVDS for the verification of the vehicle, when the vehicle is verified, these values could be place holders within the database to provide 'ballpark' values that users could view. While these values are not the actual values, since the vehicle has been verified within AVDS, the synthetic values could be used as the actual values, such as within the knowledge plots and method creation, until actual values are found or released.

This would improve the VCC experience in being able to flesh out the data that the user is able to view for each vehicle as there would be no holes, or missing data, within the database.

There would be a note, or some sort of marker, that would distinguish between the actual and synthetic data. The data richness within the database 'snapshot' would remain the same, showing how the actual data extraction process fared, but in cases where no wanted data could be found such as with the propulsion discipline for the X-51, the VCC would not have a blank page, and would provide users with a view of how the vehicle potentially behaves.

8.3 Geometry Module of AVDS

As with the VCC, the geometry method, which uses *OpenVSP* to create 3D models of the selected vehicles to obtain values for AVDS, is a standalone method, working independently from AVDS. As discussed in Chapter 4, when trades are selected to run within AVDS that affect the geometry, it must be programmed within *OpenVSP* for that vehicle, and then maps generated within MATLAB to be entered into AVDS. This is a time extensive process and having to make maps of the trades limits the number of geometric trades possible, as the maps become large and convoluted. This can be resolved through the creation of a geometry module within python for AVDS.

Instead of having the geometry method coded directly into AVDS, the geometry module would be a separate code that AVDS could call that would contain the ability to run *OpenVSP* through the desired trades without the need for the creation of maps. While the wanted geometric trades will still have to be coded within *OpenVSP*, the geometry module could then solve for the specific geometric values with the provided tau and planform area without interpolating through maps. This would remove the limit of geometric trades due to map size and obtain more accurate values from the verified VSP model.

This geometry module, with the integration of *OpenVSP*, would also improve the scaling process of the vehicles in which trade studies are being conducted. For more integrated vehicles, such as Sänger II and Orient Express, the scaling process has less parameters that need to be constrained, no major improvements other than removing the maps would be gained from the integration. For less integrated vehicles though, such as Concorde with the fuselage and wing considered separate from one another, the scaling process has more parameters that need to be constrained, so being able to integrate *OpenVSP*, conduct multiple geometric variations for the scaling, and obtain the geometric values from the verified VSP model would greatly improve the time and performance for these types of vehicles.

8.4 Improvements to Aerothermodynamics Method

8.4.1 Constant Temperature 'Solution Spaces'

One of the aerothermodynamics methods that was considered for AVDS was recreating and using the constant temperature 'solution spaces' developed by HyFAC. As mentioned in Chapter 7 where this method was discussed, several issues arose while attempting to recreate these 'solution spaces' as the created ones were not able to match the originals. As the exact methods/process in which HyFAC used to create the 'solution spaces' is not known, a possible solution is to improve the boundary layer analysis that is used. While boundary layer analysis may fall outside what is considered conceptual design, if it helps with the creation of these 'solution spaces', these can be used during conceptual design to provide an expected temperature and allow the selection of materials for the TPS to be determined.

8.4.2 Temperature Distribution through the TPS Method

Another one of the aerothermodynamic methods that was considered for AVDS was an analytical method to calculate the temperature distribution through the TPS to determine the minimum required insulation thickness to keep the temperature that reaches the structure under the max usable temperature of the material, and to the determine the corresponding structural index. For this method, while the method to determine the insulation thickness/structural index was determined successful and sensitivity maps were developed from it, a couple of assumptions that were used should be researched further. These assumptions were for the structural index of the structure and the radiation shield.

For the structural index of the structure, currently this value is assumed constant and to be the same as that used for Hypersonic Convergence. This is because this value was for a Mach 12 cruiser, and as the max Mach number considered for the sensitivity maps was Mach 5, it was deemed reasonable as an initial assumption. For the future though, this particular structural index value should be investigated to improve the ability to determine the structural weight of the vehicle. This could be accomplished through developing regressions, but as only the structural weight is wanted, excluding the TPS, a weight breakdown for each vehicle would be required which may not always be available. While there are some methods that exist to estimate the structural weight, further research to determine their viability is required.

For the structural index of the radiation shield, this value is also currently assumed constant. As the method does not use the radiation shield within its calculations, it is assumed that the radiation shield quickly reaches the equilibrium temperature to match the model used. This is in line with the purpose of the radiation shield as a high emissivity is wanted to reach this temperature as soon as possible. While this is the case, there are considerations for the design of

the radiation shield which are not considered. Assuming that the structural index value is constant, the thickness of the radiation shield can be determined from the material density. It is possible that this thickness is not realistic due to manufacturing capabilities, or structural capabilities such as buckling with temperature, etc. This may prove to be considered more for detailed design, but for the conceptual design phase and to improve the determination of the total structural index for a vehicle, this still needs to be researched further.

CHAPTER 9: SUMMARY OF CONTRIBUTIONS

To conclude the research presented here, a summary of the contributions completed by the author will be discussed. The reason for this is that the research presented, especially what has been used during the NASA study, is multi-collaboration, meaning that multiple people contributed to it. The purpose of this chapter is to make clear the specific contributions that the author completed.

Starting with the Vehicle Configuration Compendium (VCC), the primary contributions completed by the author was 1) contributed to defining the process on how to build up the VCC, 2) contributed to mapping out the GUI and database 'snapshot' layout, 3) the collection and storage of all the references for each of the 7 vehicles considered within the NASA study, 4) the generation of each vehicle bibliography, and 5) wrote the 'Statement of Authenticity' used within the VCC. The author did contribute to the extraction, digitization, and storage of vehicle data, but to a lesser extent compared to the other contributors, Stenila Simon and Ramlingam Pillai. For the collection of the references for each considered vehicle, this was not from scratch. The AVD Laboratory has been systematically collecting vehicle references/data since its inception, and even before that during Dr. Chudoba's personal research. Gathering these references, documenting them, and completing a new updated search was what the author contributed to this portion. Even with this 'head start', the accumulation and documentation took several months for all 7 vehicles.

For the 'VSP Model Creation and Use', the model creation and method processes presented were not original to the author, but the specific vehicle models created and the uses of VSP within the VCC and AVDS is. While tau scaling has been used within the AVD Laboratory previously,

the specific scaling laws presented for the WB, BB, and AB, were investigated, and created by the author.

For the use of the VCC Database for method and synthesis verification, the primary contribution completed by the author is the creation and verification of the VSP models of the selected vehicles that are used for 1) method verification of other disciplines, if needed, by providing geometry data, and 2) the verification of the synthesis system as it serves as the base for sizing within AVDS. While the other disciplines equally serve to verify the synthesis system, in the case of the method verification, many of the methods used required geometric information that was not known, so the generated models contributed heavily to these verifications, especially for the vehicles that had very low verification data, or low data richness.

For the use of the VCC Knowledgebase for parameter trend investigation, the full work presented here was contributed solely by the author, in the case of the parameter trends investigated, the explanations of the results, and the creation of the I_{str} trend method. It is noted that the data points used for the verification vehicles were contributed also by AVD Researchers Ian Maynard and Harin Patel. The commercial airliner data points were contributed by an accumulation of past AVD Researchers.

Lastly for the 'Aerothermodynamics Discipline', besides the huge contribution by Ian Maynard of coding the Heat Pulse method for verification and the creation of the I_{str} maps, the rest of the presented work was contributed by the author. This includes 1) the investigation of the HyFAC constant temperature 'solution spaces', 2) the investigation, coding, and verification of the Finite Difference method, 3) the gathering of the material properties used within the Heat Pulse method, 4) the comparison of the two methods, and 5) the conduction of the I_{str} sensitivity study and creation of the updated I_{str} vs. temperature maps.

REFERENCES

[1] McCullough, D., *The Wright Brothers*, Simon & Schuster, New York, NY, 2015.

[2] Rich, B. R. and Janos, L., *Skunk Works – A Personal Memoir of My Years at Lockheed*, 1st ed., Little Brown and Company, 1994.

[3] "HOTOL," Astronautix Available: http://www.astronautix.com/h/hotol.html.

[4] Sarson, P., "HOTOL," *Eagle Comic*, issue 424, May 1990, pp. 16-17. Available: https://www.flickr.com/photos/ausdew/49149768886/in/album-72157662557631854/

[5] Bowcutt, K. G., "Hypersonic Technology Status and Development Roadmap." AIAA HyTasp, 2003.

[6] Fuchs, R. P., Chaput, A. J., Frost, D. E., McMahan, T., and Vesely, D. L., "Why and Whither Hypersonics Research in the US Air Force." SCIENTIFIC ADVISORY BOARD (AIR FORCE), Washington DC, 2000.

[7] Pape, G. R. and Campbell, J. M., *Northrop Flying Wings – A History of Jack Northrop's Visionary Aircraft*, 1st ed., Schiffer Publishing Ltd., 1995.

[8] Scott, B., *Inside the Stealth Bomber – The B-2 Story*, TAB/AERO Books, 1991.

[9] Santayana, G., "Flux and Constancy in Human Nature," *Life of Reason*, Vol. 1, Ch. XII, 1905-1906.

[10] Heinze, W., "Ein Beitrag Zur Quantitativen Analyse Der Technischen Und Wirtschaftlichen Auslegungsgrenzen Verschiedener Flugzeugkonzepte Fur Den Transport Grosser Nutzlasten," Ph.D. Dissertation, TU Braunschweig, ZLR Forschungsbericht, 1994.

[11] McCall, T. P. D., "Automating Aerospace Synthesis Code Generation," Ph.D. Dissertation, Department of Mechanical and Aerospace Engineering, The University of Texas at Arlington, Arlington, TX, 2020.

[12] Chudoba, B. and Heinze, W., "Evolution of Generic Flight Vehicle Design Synthesis," The Aeronautical Journal, vol. 114, September 2010, pp. 549-567.

[13] Coleman, G., "Aircraft Conceptual Design: An Adaptable Parametric Sizing Methodology," Ph.D. Dissertation, Department of Mechanical and Aerospace Engineering, The University of Texas at Arlington, Arlington, TX, 2010.

[14] Chudoba, B., Maynard, I. W., Patel, H. R., Connerly, C. N., Atchison, S. C., and Van Ausdoll, A. S., "Hypersonic Commercial Transportation Feasibility Study – Paving the Way to Revolutionary Aircraft Shapes and Propulsion," NASA-CR-2021-017755, Hypersonic Technology Project (HTP), NASA Langley Research Center, NASA, 06 July 2021 [Available only with approval of the following issuing office: NASA Langley Research Center, System and Analysis Concepts Directorate, Hypersonic Technology Project, Hampton, Virginia].

[15] Chudoba, B., *Stability and Control of Conventional and Unconventional Aerospace Configurations – A Generic Approach from Subsonic to Hypersonic Speeds*, 1st ed., Springer International Publishing, July 2019. https://doi.org/10.1007/978-3-030-16856-8

[16] Moore, W. F., "A Model for the Configuration Integration Process," AIAA Paper 95-3905, *Aircraft Engineering, Technology, and Operations Congress*, Los Angeles, CA, 19-21 September 1995.

[17] Dirks, G. A., and Schneegans, A., "Scenario Based Aerospace Vehicle Design Using Knowledge Based Software Methods," ICAS Paper 5103, *22nd International Congress of*

Aeronautical Sciences, Harrogate International Conference Centre, UK, 27 August - 01 September 2000.

[18] Chudoba, B., Coleman, G., Oza, A., Gonzalez, L., and Czysz, P., "Solution-Space Screening of a Hypersonic Endurance Demonstrator," NASA-CR-2012-217774, Vehicle Analysis Branch (VAB), NASA LaRC, October 2012.

[19] Chudoba, B., Coleman, G., Gonzalez, L., Haney, E., Oza, A., and Ricketts, V., "Orbital Transfer Vehicle (OTV) System Sizing Study for Manned GEO Satellite Servicing," The Aeronautical Journal, vol. 120, April 2016, pp. 573-599.

[20] Chudoba, B. and Gonzalez, L., "Air-Launched Hypersonic Demonstrator Solution Space Screening – Mathematical Optimization in Multidisciplinary Design," Contractor Report AFRL-RQ-WP-TR-2015-0000, Air Force Summer Faculty Fellowship Program (SFFP) by AVD Laboratory, MAE-UTA for Aerospace Systems Directorate, WPAFB, OH, August 2015.

[21] Kreth, P., Schmisseur, J., Pap, R., Sanders, R., and Chudoba, B., "Design, Analysis, and Technology Base Maturation in Support of the AFRL REACH Program," Final Report for Phase I: 18 Dec. 2015 – 30 Sept. 2016, Submitted to the Air Force Research Laboratory, AFRL/RQHX (J. Staines), 30 September 2016.

[22] Haley, J., Gonzalez, L., and Chudoba, B., "Generic Hypersonic Vehicle Design Configuration Verification," AIAA 2018-5258, *2018 AIAA SPACE and Astronautics Forum and Exposition*, Orlando, FL, 17-19 September 2018.

[23] Rana, L., McCall, T., Haley, J., Gonzalez, L., Omoragbon, A., Oza, A., and Chudoba, B., "A Paradigm-Shift in Aerospace Vehicle Design Synthesis and Technology Forecasting," AIAA 2018-5210, *2018 AIAA SPACE and Astronautics Forum and Exposition*, Orlando, FL, 17-19 September 2018.

[24] Haley, J., McCall, T., Maynard, I., and Chudoba, B., "A Sizing-Based Approach to Evaluate Near Term Hypersonic Hypersonic Demonstrators: Demonstrator-Carrier Constraints and Sensitivities," *JANNAF 37th Air-Breathing Propulsion Meeting, Hypersonic Airbreathing Vehicle Designs and Methods – I*, JANNAF, Dayton, OH, 2019.

[25] Patel, H. and Chudoba, B., "A Sizing Study Comparison of Hypersonic Demonstrator Vehicles with a Pre-Cooled Turbojet Cycle" AIAA 2020-2442, *23rd AIAA International Space Planes and Hypersonic Systems and Technologies Conference*, Montreal, Quebec, Canada, 10-12 March 2020.

[26] Simon, S., Atchison, S., and Chudoba, B., "Conceptual Design Decision-Making Assisted by a Comprehensive High-Speed Vehicle Knowledgebase Library," AIAA 2021-4231, *ASCEND 2021*, Las Vegas, NV, 15-17 November 2021.

[27] Davenport, T. H. and Prusak, L., *Working Knowledge – How Organisations Manage What They Know*, Harvard Business School Press, 1998.

[28] Haney, E., "Data Engineering in Aerospace Systems Design & Forecasting," Ph.D. Dissertation, Department of Mechanical and Aerospace Engineering, The University of Texas at Arlington, Arlington, TX, April 2016.

[29] Vincenti, W. G., *What Engineers Know and How They Know It: Analytical Studies from Aeronautical History*, Johns Hopkins University Press, 1990.

[30] Simon, S., "Development of the Vehicle Configuration Compendium: A Comprehensive Data-Information-Knowledge System to Aid in High-Speed Vehicle Design," Department of Mechanical and Aerospace Engineering, The University of Texas at Arlington, M.S. Thesis, Arlington, TX, 2021.

[31] Simon, S., Atchison, S., and Chudoba, B., "Development of a High-Speed Vehicle Configuration Compendium," AIAA 2021-2791, *AIAA AVIATION 2021 FORUM*, VIRTUAL EVENT, 02-06 August 2021.

[32] Peng, X., "Formalization of the Engineering Science Discipline – Knowledge Engineering," Ph.D. Dissertation, Department of Mechanical and Aerospace Engineering, The University of Texas at Arlington, Arlington, TX, 2015.

[33] Czysz, P. A., "Hypersonic Convergence – High-Speed Aircraft Aero-Propulsion-Structure Systems Integration – Integrated Systems Approach to Identifying Solution Space," Volumes I-III, Course AE-P-452-50, 1992-93, Aerospace and Mechanical Engineering Department, Parks College, Saint Louis University, 1st ed., 1986.

[34] Gonzalez, L., "Complex Multidisciplinary System Composition for Aerospace Vehicle Conceptual Design," Ph.D. Dissertation, Department of Mechanical and Aerospace Engineering, The University of Texas at Arlington, Arlington, TX, 2016.

[35] Omoragbon, A., "Complex Multidisciplinary Systems Decomposition for Aerospace Vehicle Conceptual Design and Technology Acquisition," Ph.D. Dissertation, Department of Mechanical and Aerospace Engineering, The University of Texas at Arlington, Arlington, TX, 2016.

[36] Oza, A. R., "A Generic Methodology for Flight Test and Safety Evaluation at Conceptual Design," M.S. Thesis, Department of Mechanical and Aerospace Engineering, The University of Texas at Arlington, Arlington, TX, 2009.

[37] Rana, L., "Designing Space Access Systems," Ph.D. Dissertation, Department of Mechanical and Aerospace Engineering, The University of Texas at Arlington, Arlington, TX, 2017.

[38] "Why is Python Best Adapted to AI and Machine Learning?," *Turing*, URL: https://www.turing.com/kb/python-best-adapted-to-ai-and-machine-learning [cited 15 April 2023].

[39] Czysz. P. A., Bruno, C., and Chudoba, B., "Commercial Near-Earth Space Launcher: Understanding System Integration," *Future Spacecraft Propulsion Systems and Integration: Enabling Technologies for Space Exploration*, 3rd ed., Springer, Praxis Publishing, Chichester, UK, 2018, pp. 52-53.

[40] "About OpenVSP," *OpenVSP*, URL: https://openvsp.org/learn.shtml [cited 15 April 2023].

[41] Haimes, R. and Dannenhoffer III, J. F., "The Engineering Sketch Pad: A Solid-Modeling, Feature-Based, Web-Enabled System for Building Parametric Geometry," [PowerPoint], *21st AIAA Computational Fluid Dynamics Conference CFD-38 Grid Generation and Effects of Grid Quality II*, San Diego, CA, 24-27 June 2013.

[42] Weiland, C., *Aerodynamic Data of Space Vehicles*, Springer-Verlag, Berlin, Germany, 2014.

[43] Zahringer, C. "Untersuchung Der Separationsdynamik Eines Zweistufigen Hyperschall-Flugsystems Unter Besonderer Berücksichtigung Der Seitenbewegung," Doktor-Ingenieur Dissertation, Lehrstuhl fur Flugmechanik und Flugregelung, Technische Universitat Munchen, Munich, Germany, 19 April 2005.

[44] Drexler, E., *Nanosystems: Molecular Machinery, Manufacturing and Computation*, A. Wiley Interscience Publication, 1992.

[45] Phoenix, C., "Scaling Laws: Back to Basics," URL: http://crnano.typepad.com/crnblog/2004/08/scaling_lawsbac.html, 03 August 2004.

[46] Voland, R. and Rock, K., "NASP Concept Demonstration Engine and Subscale Parametric Engine Tests," AIAA-95-6055, *AIAA 6th International Aerospace Planes and Hypersonics Technologies Conference*, American Institute of Aeronautics and Astronautics, Chattanooga, TN, 03-07 April 1995. https://doi.org/10.2514/6.1995-6055

[47] Tegler, J., "Scaling UP," *Aerospace America*, American Institute of Aeronautics and Astronautics, January 2021. URL: https://aerospaceamerica.aiaa.org/features/scaling-up/?utm_source=Informz&utm_medium=email&utm_campaign=AerospaceAmerica.

[48] Corke, T., "Horizontal and Vertical Tail Design," *Design of Aircraft*, Pearson Education, Inc., Upper Saddle River, NJ, 2003.

[49] Balaba, D. and Mavris, D., "An Empirical Approach Towards the Rapid Derivation of Vehicle Scaling Laws in Conceptual Design," AIAA-2011-643, *49th AIAA Aerospace Sciences Meeting including the New Horizons Forum and Aerospace Exposition*, Orlando, FL, 04-07 January 2011.

[50] Werner, R. and Wislicenus, G. F., "Analysis of Airplane Design by Similarity Considerations," AIAA-68-1017, *AIAA 5th Annual Meeting and Technical Display*, Philadelphia, PA, 21-24 October 1968.

[51] Raymer, D., *Aircraft Design: A Conceptual Approach*, 3rd ed., *AIAA Education Series*, American Institute of Aeronautics and Astronautics, Reston, VA, 1999.

[52] Raymer, D., "Enhancing Aircraft Conceptual Design Using Multidisciplinary Optimization," Ph.D. Dissertation, Department of Aeronautics, Royal Institute of Technology, Stockholm, Sweden, 2002.

[53] Segel, L., "Simplification and Scaling," *SIAM review*, vol. 14, no. 4, October 1972, pp. 547-571.

[54] Mendez, P. and Ordonez, F., "Scaling Laws from Statistical Data and Dimensional Analysis," *Transactions of the ASME*, vol. 72, 2005.

[55] Küchemann, D., *The Aerodynamic Design of Aircraft*, *AIAA Education Series*, American Institute of Aeronautics and Astronautics, Reston, VA, 2012.

[56] Torenbeek, E., *Essentials of Supersonic Commercial Aircraft Conceptual Design*, *Aerospace Series*, John Wiley & Sons, Inc., Hoboken, NJ, 2020.

[57] Anon, "U.S. Standard Atmosphere, 1976," NASA TM-X-74335, NOAA, NASA, USAF, Washington, D.C., October 1976.

[58] McDonnell Aircraft Company, "Hypersonic Research Facilities Study: Phase 2 Parametric Studies, Research Requirements and Ground Facility Synthesis," Vol. III Part 1, NASA CR-114325, NASA, Moffet Field, California, 1970.

[59] Morelli, E. A., "Flight-Test Experiment Design for Characterizing Stability and Control of Hypersonic Vehicles," *U.S. Air Force T&E Days*, American Institute of Aeronautics and Astronautics, Los Angeles, CA, 05-07 February 2008.

[60] Vachon, M., Grindle, T., St. John C., and Dowdell, D., "X-43A Fluid and Environmental Systems: Ground and Flight Operation and Lessons Learned," *AIAA/CIRA 13th International Space Planes and Hypersonic Systems and Technologies Conference*, American Institute of Aeronautics and Astronautics, Capua, Italy, 16 May 2005. https://doi.org/10.2514/6.2005-3337

[61] Berkowitz, M., "HASA – Hypersonic Aerospace Sizing Analysis for the Preliminary Design of Aerospace Vehicles," 1988.

[62] McDonnell Douglas Aerospace, "Hypersonic Research Facilities Study," *HyFAC*, Vol. 2.2, NASA, 1970.

[63] Billig, F. S., "Hypersonic Vehicles II," *Proceedings of the Short Course of Engine Airframe Integration*, School of Mechanical Engineering, Purdue University, July 1989.
[64] Bradford, J. E., "A Technique for Rapid Prediction of Aftbody Nozzle Performance for Hypersonic Launch Vehicle Design," Ph.D. Dissertation, Georgia Institute of Technology, Atlanta, GA, June 2001.
[65] Sanford, G., and Mcbride, B. J., "Computer Program for Calculation of Complex Chemical Equilibrium Compositions and Applications. Part 1: Analysis," NASA RP-1311, NASA, Washington, D.C., 01 October 1994.
[66] Heiser, W. H., Pratt, D. T., Daley, D. H., and Mehta, U. B., *Hypersonic Airbreathing Propulsion, AIAA Education Series*, American Institute of Aeronautics and Astronautics, Inc., Washington, D.C., 1994.
[67] Miele, A., *Flight Mechanics: Theory of Flight Paths*, Dover Publications, Inc., NY, 1990.
[68] Edward Lan, C.-T., and Roskam, J., *Airplane Aerodynamics and Performance*, Design, Analysis and Research Corporation, Lawrence, KS, 2016.
[69] Vinh, N. X., *Optimal Trajectories in Atmospheric Flight*, Elsevier Scientific Publishing Company, NY, 01 January 1981.
[70] Kundu, A. K., Price, M. A., and Riordan, D., *Theory and Practice of Aircraft Performance*, John Wiley & Sons, Ltd., U.K., 2016.
[71] Engelund, W. C., Holland, S. D., Jr, C. E. C., and Bittner, R., "Aerodynamic Database Development for the Hyper-X Airframe-Integrated Scramjet Propulsion Experiments," *Journal of Spacecraft and Rockets*, Vol. 38, No. 6, p. 8, 2001.
[72] Engelund, W. C., Holland, S. D., Cockrell, C. E., and Bittner, R., "Propulsion System Airframe Integration Issues and Aerodynamic Database Development for the Hyper-X Flight Research Vehicle," ISOABE-99-7215, *XIV ISOABE*, Florence, Italy, 05-10 September 1999.
[73] Voland, R. T., Huebner, L. D., and McClinton, C. R., "X-43A Hypersonic Vehicle Technology Development," IAC-05-D2.6.01, *56th International Astronautical Congress*, Fukuoka, Japan, 17-21 October 2005.
[74] Moses, P., "X-43C Flight Demonstrator Project Overview," *Joint JANNAF Subcommitee Meeting 39th Combustion*, Colorado Springs, CO, 01-05 December 2003.
[75] Albertson, C., and Emami, S., "Alleviation of Facility/Engine Interactions in an Open-Jet Scramjet Test Facility," AIAA-2001-3677, *37th AIAA/ASME/SAE/ASEE Joint Propulsion Conference and Exhibit*, American Institute of Aeronautics and Astronautics, Salt Lake City, UT, 08-11 July 2001.
[76] Karlgaard, C., Tartabini, P., Blanchard, R., Kirsch, M., and Toniolo, M., "Hyper-X Post-Flight-Trajectory Reconstruction," *Journal of Spacecraft and Rockets*, Vol. 43, No. 1, pp. 105-115, January-February 2006.
[77] Bahm, C., Baumann, E., Martin, J., Bose, D., Beck, R., and Strovers, B., "The X-43A Hyper-X Mach 7 Flight 2 Guidance, Navigation, and Control Overview and Flight Test Results," AIAA-2005-3275, *AIAA/CIRA 13th International Space Planes and Hypersonics Systems and Technologies Conference*, American Institute of Aeronautics and Astronautics, Capua, Italy, 2005.
[78] Marshall, L., Corpening, G., and Sherrill, R., "A Chief Engineer's View of the NASA X-43A Scramjet Flight Test," *AIAA/CIRA 13th International Space Planes and Hypersonics Systems and Technologies Conference*, American Institute of Aeronautics and Astronautics, Capua, Italy, 16 May 2005.

[79] Harsha, P., Keel, L., Castrogiovanni, A., and Sherrill, R., "X-43A Vehicle Design and Manufacture," AIAA-2005-3334, *AIAA/CIRA 13th International Space Planes and Hypersonics Systems and Technologies Conference*, American Institute of Aeronautics and Astronautics, Capua, Italy, 16 May 2005.

[80] Orton, G., "Air-Breathing Hypersonics Research at Boeing Phantom Works," AIAA-2002-5251, *AIAA/AAAF 11th International Space Planes and Hypersonics Systems and Technology*, American Institute of Aeronautics and Astronautics, Orleans, France, 29 September 2002.

[81] Lin, Y., Baumann, E., Bose, D., Beck, R., and Jenney, G., "Test and Techniques for Characterizing and Modeling X-43A Electromechanical Actuators," NASA/TM-2008-214637, Dryden Flight Research Center, NASA, Edwards, CA, December 2008.

[82] Tartabini, P., Bose, D., Thornblom, M., Lien, J., and Martin, J., "Mach 10 Stage Separation Analysis for the X-43A," *44th AIAA Aerospace Sciences Meeting and Exhibit*, American Institute of Aeronautics and Astronautics, Reno, NV, 09 January 2006.

[83] Redifer, M., Lin, Y., Bessent, C. A., and Barklow, C., "The Hyper-X Flight Systems Validation Program," NASA/TM-2007-214620, Dryden Flight Research Center, NASA, Edwards, CA, May 2007.

[84] Anon, "NASA X-43A" [Website], Wikipedia, URL: https://en.wikipedia.org/wiki/NASA_X-43 [retrieved 01 May 2020].

[85] Bernard Spencer, J., "A Simplified Method for Estimating Subsonic Lift-Curve Slope at Low Angles of Attack for Irregular Planform Wings," TM X-525, Langley Research Center, Langley Field, VA, 1961.

[86] Polhamus, E. C., "A Concept of the Vortex Lift of Sharp-Edge Delta Wings Based on a Leading-Edge-Suction Analogy," NASA-TN-D-3767, National Aeronautics and Space Administration, Washington, D. C., December 1966.

[87] Petersen, R. H., "The Effects of Wing-Tip Droop on the Aerodynamic Characteristics of a Delta-Wing Aircraft at Supersonic Speeds," NASA-TM-X-363, National Aeronautics and Space Administration, Washington, D.C., May 1960.

[88] Barlett, R. S., "Tables of Supersonic Symmetrical Flow Around Right Circular Cones, with and without the Addition of Heat at the Wave," R & M 3521, Aeronautical Research Council, London, 1968.

[89] Eggers, A. J., and Syvertson, C. A., "Aircraft Configurations Developing High Lift-Drag Ratios at High Supersonic Speeds," NACA-RM-A55L05, National Advisory Committee for Aeronautics, Washington, D.C., 05 March 1956.

[90] Mason, W. H., "Supersonic Aerodynamics," Department of Aerospace and Ocean Engineering, Virginia Polytechnic Institute and State University, Blacksburg, VA, 31 July 2016.

[91] Benepe, D. B., "Development of Aerodynamic Prediction Methods for Irregular Planform Wings," CR 3664, General Dynamics, Fort Worth, TX, 1983.

[92] Baker, P. A., Schweikhard, W. G., and Young, W. R., "Flight Evaluation of Ground Effect on Several Low-Aspect-Ratio Airplanes," NASA-TN-D-6053, National Aeronautics and Space Administration, Washington, D. C., October 1970.

[93] Becker, J. V., "Studies of High Lift/Drag Ratio Hypersonic Configurations," *Studies of Hypersonic Configurations*, Fourth Congress – Aeronautical Sciences, Hampton, VA.

[94] Andrews, W., "Summary of Preliminary Data Derived from the XB-70 Airplanes," NASA-TM-X-1240, National Aeronautics and Space Administration, Washington, D. C., June 1966.
[95] Dussart, G., Lone, M., O'Rourke, C., and Wilson, T., "In-Flight Wingtip Folding: Inspiration from the XB-70 Valkyrie," *International Journal of Aviation, Aeronautics, and Aerospace*, Vol. 6, No. 3, 2019.
[96] Nicolai, L. M., and Carichner, G. E., *Fundamentals of Aircraft and Airship Design Volume I – Aircraft Design*, *AIAA Education Series*, American Institute of Aeronautics and Astronautics, Reston, VA, 2010, p. 881.
[97] Glatt, C. R., "WAATS – a Computer Program for Weight Analysis of Advanced Transportation Systems," NASA-CR-2420, NASA, Washington, D. C., September 1974.
[98] Raymer, D., *Aircraft Design: A Conceptual Approach*, 6th ed., *AIAA Education Series*, American Institute of Aeronautics and Astronautics, Inc., Reston, VA, 2018.
[99] Torenbeek, E., *Synthesis of Subsonic Airplane Design*, Delft University Press, Delft, The Netherlands, 1982.
[100] Anon, "NPSS™ User Guide," Document Revision 4, Numerical Propulsion System Simulation Consortium, 20 December 2003.
[101] Hendricks, E. S., and Gray, J. S., "pyCycle: A Tool for Efficient Optimization of Gas Turbine Engine Cycles," *Aerospace*, Vol. 6, No. 8, p. 87, 2019.
[102] Mattingly, J. D., and Boyer, K. M., *Elements of Propulsion: Gas Turbines and Rockets*, *AIAA Education Series*, 2nd ed., American Institute of Aeronautics and Astronautics, Inc., Reston, VA, 2016.
[103] Campbell, J. M., *North American XB-70 Valkyrie: The Legacy*, *Schiffer Military History*, Schiffer Publishing, Atglen, PA, 1998, p. 96.
[104] Arnaiz, H. H., "Flight-Measured Lift and Drag Characteristics of a Large, Flexible, High Supersonic Cruise Airplane," NASA-TM-X-3532, National Aeronautics and Space Administration, Washington, D. C., May 1977.
[105] Pace, S., *North American Valkyrie XB-70A*, *Aero Series*, Vol. 30, Aero Publishers, Fallbrook, CA, 1984, p. 104.
[106] Arnaiz, H. H., Peterson, J. B., and Daugherty, J. C. "Wind-Tunnel/Flight Correlation Study of Aerodynamic Characteristics of a Large Flexible Supersonic Cruise Airplane (XB-70-1): III - a Comparison between Characteristics Predicted from Wind-Tunnel Measurements and Those Measured in Flight," NASA-TP-1516, Dryden Flight Research Center, NASA, Edwards, CA, March 1980.
[107] Wolowicz, C. H., and Yancey, R. B. "Summary of Stability and Control Characteristics of the XB-70 Airplane," NASA-TM-X-2933, National Aeronautics and Space Administration, Washington, D. C., October 1973.
[108] Wilson, R. J., and McKay, J. M. "Landing Loads and Accelerations of the XB-70-1 Airplane," NASA-TN-D-4836, National Aeronautics and Space Administration, Washington, D. C., October 1968.
[109] Tinetti, A. F., Maglieri, D. J., Driver, C., and Bobbitt, P. J. "Equivalent Longitudinal Area Distributions of the B-58 and XB-70-1 Airplanes for Use in Wave Drag and Sonic Boom Calculations," NASA/CR-2011-217078, Langley Research Center, NASA, Hampton, VA, March 2011.

[110] Maglieri, D. J., Henderson, H. R., and Tinetti, A. F. "Measured Sonic Boom Signatures above and Below the XB-70 Airplane Flying at Mach 1.5 and 37,000 Feet," NASA/CR-2011-217077, Langley Research Center, NASA, Hampton, VA, April 2011.
[111] Wilson, R. J., and Larson, R. R. "Statistical Analysis of Landing-Contact Conditions for the XB-70 Airplane," NASA-TN-D-4007, National Aeronautics and Space Administration, Washington, D. C., June 1967.
[112] Wolowicz, C. H., Strutz, L. W., Gilyard, G. B., and Matheny, N. W. "Preliminary Flight Evaluation of the Stability and Control Derivatives and Dynamic Characteristics of the Unaugmented XB-70-1 Airplane Including Comparisons with Predictions," NASA-TN-D-4578, National Aeronautics and Space Administration, Washington, D. C., May 1968.
[113] Taube, L. J. "B-70 Aircraft Study Final Report: Volume III," SD-72-SH-0003, Space Division, North American Rockwell, April 1972.
[114] Sotham, J. "The Legend of the Valkyrie," *Air & Space*, pp. 46-57, September 1999.
[115] Beatovich, G. "A Case Study of Manned Strategic Bomber Acquisition: The B-70 Valkyrie," Master's Defense, School of Systems and Logistics, Air Force Institute of Technology, Air University, Wright-Patterson Air Force Base, OH, September 1990.
[116] Lewis, T. J., Dods, J. B., and Hanly, R. D. "Measurements of Surface-Pressure Fluctuations on the XB-70 Airplane at Local Mach Numbers up to 2.45," National Aerospace and Space Administration, Washington, D. C., March 1973.
[117] Anon, "Estimated Performance of G.E. J93-3 Engines Max. Afterburner JP-150," *A-12 OXCART Reconnaissance Aircraft Documentation Collection*, Document Number: 0001465820, 01 January 1967. URL: https://www.cia.gov/readingroom/document/0001465820
[118] Putnam, T. W., and Smith, R. H., "XB-70 Compressor-Noise Reduction and Propulsion-System Performance for Chocked Inlet Flow," NASA-TN-D-5692, National Aeronautics and Space Administration, Washington, D. C., March 1970.
[119] Gallagher, R. J., "Investigation of a Digital Simulation of the XB-70 Inlet and Its Application to Flight-Experienced Free-Stream Disturbances at Mach Numbers of 2.4 to 2.6," NASA-TN-D-5827, National Aeronautics and Space Administration, Washington, D. C., June 1970.
[120] Arnaiz, H. H., and Schweikhard, W. G., "Validation of the Gas Generator Method of Calculating Jet-Engine Thrust and Evaluation of XB-70-1 Airplane Engine Performance at Ground Static Conditions," NASA-TN-D-7028, National Aeronautics and Space Administration, Washington, D. C., December 1970.
[121] Powers, B. G., "Statistical Survey of XB-70 Airplane Responses and Control Usage with an Illustration of the Application to Handling Qualities Criteria," NASA-TN-D-6872, National Aeronautics and Space Administration, Washington, D. C., July 1972.
[122] Taube, L. J., "B-70 Aircraft Study Final Report: Volume II," SD-72-SH-0003, Space Division, North American Rockwell, April 1972.
[123] Anon, "Flight Handbook Supplement: XB-70A," *USAF Series Aircraft*, United States Air Force, 30 September 1964 (Changed 15 February 1967).
[124] Crede, E., Simpson, A., and Shannon, J., "XB-70 Valkyrie," [Presentation], Department of Aerospace and Ocean Engineering, Virginia Polytechnic Institute and State University, Blacksburg, VA, 2007.
[125] Anon, "XB-70," *NASAFacts*, Dryden Flight Research Center, NASA, Edwards, CA, 2003.

[126] Carichner, G., and Nicolai, L. M., *Fundamentals of Aircraft and Airship Design: Volume 2 – Airship Design and Case Studies*, American Institute of Aeronautics and Astronautics, March 2013.
[127] Anon, "Faster Than a Bullet: Premier of the North American XB-70A," *Interavia*, pp. 982-984, 1964.
[128] Roedts, R., Somero, R., and Waskiewicz, C., "XB-70 Valkyrie," [Presentation], Department of Aerospace and Ocean Engineering, Virginia Polytechnic Institute and State University, Blacksburg, VA, 2005.
[129] Anon, "Characteristics Summary," YB-70, System 110A, Historical Section of the US Air Force Museum, Dayton, OH, March 1961. URL: http://www.alternatewars.com/SAC/SAC.htm
[130] Anon, "Characteristics Summary," XB-70B Air Vehicle Number 3, System 110A, Historical Section of the US Air Force Museum, Dayton, OH, 09 May 1963. URL: http://www.alternatewars.com/SAC/SAC.htm
[131] Anon, "Characteristics Summary," XB-70, System 110A, Historical Section of the US Air Force Museum, Dayton, OH, 20 December 1960. URL: http://www.alternatewars.com/SAC/SAC.htm
[132] Anon, "Characteristics Summary," XB-70 Air Vehicle Number 3, System 110A, Historical Section of the US Air Force Museum, Dayton, OH, 18 April 1962. URL: http://www.alternatewars.com/SAC/SAC.htm
[133] Anon. "Characteristics Summary," XB-70A Air Vehicle Number 1, System 110A, Historical Section of the US Air Force Museum, Dayton, Ohio, 11 May 1964. URL: http://www.alternatewars.com/SAC/SAC.htm
[134] Anon. "Characteristics Summary," XB-70A Air Vehicle Number 1, System 110A, Historical Section of the US Air Force Museum, Dayton, Ohio, February 1965. URL: http://www.alternatewars.com/SAC/SAC.htm
[135] Anon. "Characteristics Summary," XB-70A Air Vehicle Number 1, System 110A, Historical Section of the US Air Force Museum, Dayton, Ohio, April 1967. URL: http://www.alternatewars.com/SAC/SAC.htm
[136] Anon. "Characteristics Summary," XB-70A Air Vehicle Number 2, System 110A, Historical Section of the US Air Force Museum, Dayton, Ohio, 11 May 1964. URL: http://www.alternatewars.com/SAC/SAC.htm
[137] Anon. "Characteristics Summary," XB-70A Air Vehicle Number 2, System 110A, Historical Section of the US Air Force Museum, Dayton, Ohio, February 1965. URL: http://www.alternatewars.com/SAC/SAC.htm
[138] Anon. "Characteristics Summary," XB-70A Air Vehicle Number 2, System 110A, Historical Section of the US Air Force Museum, Dayton, Ohio, October 1965. URL: http://www.alternatewars.com/SAC/SAC.htm
[139] Anon. "Characteristics Summary," XB-70A Air Vehicle Number 2, System 110A, Historical Section of the US Air Force Museum, Dayton, Ohio, April 1967. URL: http://www.alternatewars.com/SAC/SAC.htm
[140] Taube, L. J., "B-70 Aircraft Study Final Report: Volume I," SD-72-SH-0003, Space Division, North American Rockwell, April 1972.
[141] Pegg, R. J., Hunt, J. L., Petley, D. H., Burkardt, L., Stevens, D. R., Moses, P. L., Pinckney, S. Z., Kabis, H. Z., Spoth, K. A., Dziedzic, W. M., Kreis, R. I., Martin, J. G., and Barnhart,

P. J., "Design of a Hypersonic Waverider-Derived Airplane," AIAA-93-0401, *31st Aerospace Sciences Meeting*, Reno, NV, 11-14 January 1993.
[142] Ingenito, A., Gulli, S., Bruno, C., Coleman, G., Chudoba, B., and Czysz, P. A., "Sizing of a Fully Integrated Hypersonic Commercial Airliner," *Journal of Aircraft*, Vol. 48, No. 6, pp. 2161-2164, November-December 2011.
[143] Rana, L., McCall, T., Haley, J., and Chudoba, B., "A Parametric Sizing Study on the Effects of Configuration Geometry on a Lifting-Body Reentry Vehicle," AIAA-2017-5356, *AIAA SPACE and Astronautics Forum and Exposition*, Orlando, FL, 12-14 September 2017.
[144] Eggers Alfred, J., Julian, A. H., and Neice Stanford, E., "A Comparative Analysis of the Performance of Long-Range Hypervelocity Vehicles," *NACA Research Memorandum, Washington: National advisory committee for Aeronautical*, 1955.
[145] McKim, F R., *Vol Supersonique: De Bernoulli a Concorde*, 1974.
[146] Carlier, P., Debelmas, C., Pilon, J. C., and Velot-Lerou, A., "Avant-Projet D'un Avion De Transport Commercial Supersonique," Aerospatiale, 1992.
[147] Skinner, S., *Concorde*, Midland Publishing, Surrey, England, 2009.
[148] Anderson, Jr., J. D., *Hypersonic and High-Temperature Gas Dynamics*, *AIAA Education Series*, 2nd ed., American Institute of Aeronautics and Astronautics, Inc., Reston, VA, 2006.
[149] Bertin, J. J., *Hypersonic Aerothermodynamics*, *AIAA Education Series*, American Institute of Aeronautics and Astronautics, Inc., Washington, D.C., 1994.
[150] Anderson, Jr., J. D., *Modern Compressible Flow: with Historical Perspective*, 3rd ed., McGraw-Hill, NY, 2003.
[151] Pirrelo, C. J., and Czysz, P. A., "Hypersonic Research Facilities Study," Volumes I-IV, National Aeronautics and Space Administration Contact NAS2-5458 by McDonnell Aircraft Company, NASA CR 114322-114331, October 1970.
[152] Marley, C. D., and Driscoll, J. F., "Heat Transfer Operability Limits for an Actively and Passively Cooled Hypersonic Vehicle," *Journal of Aircraft*, Vol. 55, No. 44, pp. 1655-1674, July-August 2018.
[153] Srinivasan, S., Tannehill, J. C., and Weilmuenster, K. J., "Simplified Curve Fits for the Thermodynamic Properties of Equilibrium Air," NASA Reference Publication 1181, National Aeronautics and Space Administration, August 1987.
[154] Hansen, C. F., "Approximations for the Thermodynamic and Transport Properties of High-Temperature Air," NACA-TC-4150, National Advisory Committee for Aeronautics, Washington, March 1958.
[155] Hirschel, E. H., and Weiland, C., *Selected Aerothermodynamic Design Problems of Hypersonic Flight Vehicles*, Springer-Verlag, Berlin, Germany, 2009.
[156] Arthur, P. D., Schultz, H. D., and Guard, F. L., "Flat Plate Turbulent Heat Transfer at Hypervelocities," *Journal of Spacecraft and Rockets*, Vol. 3, No. 10, pp. 1549-1551, October 1966.
[157] Eckert, E. R. G., "Survey of Boundary Layer Heat Transfer at High Velocities and High Temperature," Contract No. AF 33(616)-5676, Wright Air Development Center, Air Research and Development Command, Wright Patterson Air Force Base, OH, April 1960.
[158] Spruijt, M. R. F., and Zandbergen, B. T. C., "Spaceplane Aeroheating: Some Simple Estimation Methods," AE-DUT-TN-9405, Delft University of Technology, Delft, The Netherlands, 10 April 1996.

[159] Tauber, M. E., Menees, G. P., and Adelman, H. G., "Aerothermodynamics of Transatmospheric Vehicles," *Journal of Aircraft,* Vol. 24, No. 9, pp. 594-602, 1987.

[160] Quinn, R. D., and Gong, L., "A Method for Calculating Transient Surface Temperatures and Surface Heating Rates for High-Speed Aircraft," NASA/TP-2000-209034, Dryden Flight Research Center, NASA, Edwards, CA, December 2000.

[161] Moura, A. F., and Rosa, M. A. P., "A Computer Program for Calculating Normal and Oblique Shock Waves for Airflows in Chemical and Thermodynamic Equilibrium," *22nd International Congress of Mechanical Engineering*, Ribeirao Preto, SP, Brazil, 03-07 November 2013.

[162] Bolender, M. A., and Doman, D. B., "Modeling Unsteady Heating Effects on the Structural Dynamics of a Hypersonic Vehicle," AIAA-2006-6646, *AIAA Atmospheric Flight Mechanics Conference and Exhibit,* Keystone, CO, 21-24 August 2006.

[163] Blosser, M. L., "Analysis and Sizing for Transient Thermal Heating of Insulated Aerospace Vehicle Structures," NASA/TP-2012-217595, Langley Research Center, NASA, Hampton, VA, August 2012.

[164] Williams, S. D., and Curry, D. M., "Thermal Protection Materials: Thermophysical Property Data," NASA Reference Publication 1289, National Aeronautics and Space Administration, December 1992.

[165] Myers, D. E., Martin, C. J., and Blosser, M. L., "Parametric Weight Comparison of Current and Proposed Thermal Protection System (TPS) Concepts," AIAA-99-3459, *33rd Thermophysics Conference*, Norfolk, VA, 28 June – 01 July 1999.

[166] Macias, J. D., Bante-Guerra, J., Cervantes-Alvarez, F., Rodrìguez-Gattorno, G., Arés-Muzio, Romero-Paredes, H., Arancibia-Bulnes, C. A., Ramos-Sánchez, V., Villafán-Vidales, H. I., Ordonez-Miranda, J., Voti, R., and Alvarado-Gil, J. J., "Thermal Characterization of Carbon Fiber-Reinforced Carbon Composites," *Applied Composite Materials*, Vol. 26, No. 1, pp. 321-337, February 2019.

[167] Morscher, G. N., and Pujar, V. V., "Design Guidelines for In-Plane Mechanical Properties of SiC Fiber-Reinforced Melt-Infiltrated SiC Composites," *International Journal of Applied Ceramic Technology*, Vol. 6, No. 2, pp. 151-163, March 2009.

[168] Lamon, J., "Chemical Vapor Infiltrated SiC/SiC Composites (CVI SiC/SiC)," *Handbook of Ceramic Composites*, Kluwer Academic Publishers, 2005.

[169] Stadelmann, R., "ZrB2-SiC Based Ultra High Temperature Ceramic Composites: Mechanical Performance and Measurement and Design of Thermal Residual Stresses for Hypersonic Vehicle Applications," Ph.D. Dissertation, Department of Mechanical and Aerospace Engineering, University of Central Florida, Orlando, FL, 2015.

[170] Purwar, A., and Basu, B., "Thermo-Structural Design of ZrB2-SiC-Based Thermal Protection System for Hypersonic Space Vehicles," *Journal of the American Ceramic Society*, Vol. 100, No. 4, pp. 1618-1633, February 2017.

[171] Daryabeigi, K., "Analysis and Testing of High Temperature Fibrous Insulation for Reusable Launch Vehicles," AIAA-99-1044, *37th AIAA Aerospace Sciences Meeting and Exhibit,* Reno, NV, January 1999.

[172] Daryabeigi, K., "Effective Thermal Conductivity of High Temperature Insulations for Reusable Launch Vehicles," NASA-TM-1999-208972, February 1999.

[173] Gorton, M. P., Shideler, J. L., and Webb, G. L., "Static and Aerothermal Tests of a Superalloy Honeycomb Prepackaged Thermal Protection System," NASA-TP-3257, March 1993.

[174] Myers, D. E., Martin, C. J., and Blosser, M. L., "Parametric Weight Comparison of Advanced Metallic, Ceramic Tile, and Ceramic Blanket Thermal Protection Systems," NASA/TM-2000-210289, Langley Research Center, NASA, Hampton, VA, June 2000.

[175] Brown, W. F., Mindlin, Jr., H., and Ho, C. Y., *Aerospace Structural Metals Handbook*, CINDAS/USAF CRDA Handbooks Operation, Purdue University, 1994.

[176] Grensing, F. C., and Hashiguchi, D., "Mechanical and Thermal Properties of Aluminum-Beryllium Alloy AM162," *Advances in Powder Metallurgy & Particulate Materials – 1995*, Proceedings of the 1995 International Conference & Exhibition on Powder Metallurgy & Particulate Materials, 1995.

[177] Ehrlich, Jr., C. F., Potts, J., Brown, J., Schell, K., Manley, M., Chen, I., Earhart, R., Urrutia, C., Randolph, R., and Morris, J., "Advanced Manned Launch System (AMLS) Study – Final Report," NASA-CR-189673, Langley Research Center, NASA, Hampton, VA, 30 September 1992.

APPENDIX A
VERIFICATION VEHICLE INPUTS AND ASSUMPTIONS FOR AVDS^{CE}

Table A.1 AVDS^{CE} X-51 inputs and assumptions [14].

Variable Discipline	Variable	Value
Geometry	Küchemann's tau	0.214
Propulsion	Area ratio of viscous captured flow to inviscid captured flow	0.95
	Reference fuel equivalence ratio	1
	Design Mach	6
Trajectory	Constant *q* climb segment: Start altitude, m	18,517
	Constant *q* climb segment: Start velocity, m/s	1,416
	Constant *q* climb segment: End altitude, m	19,290
	Constant *q* climb segment: Maximum longitudinal acceleration, m/s^2	0.1
	Constant *q* climb segment: Minimum longitudinal acceleration, m/s^2	0.01
	Constant Mach endurance cruise segment: Cruise endurance time, sec	109
Weights and Volume	Number of crew	0
	Number of passengers	0
	Weight of unmanned fixed systems, N	2,053
	Weight of each crew member, N/person	-
	Weight fixed manned systems per crew member, N/person	-
	Weight of each passenger, N/person	-
	Weight of passenger provisions per passenger, N/person	-
	Weight of variable systems per vehicle dry weight	0.0161
	Weight of cargo, N	0
	Minimum dry weight (OEW) margin	0.1
	Volume of provision for each crew member, m^3/person	-
	Volume per crew member, m^3/person	-
	Volume of manned fixed systems per crew member, m^3/person	-
	Volume of each passenger space, m^3/person	-
	Volume of variable systems per total vehicle volume, m^3	0.1
	Volume of vehicle void space per total vehicle volume, m^3	0.1
	Volume of unmanned fixed system, m^3	0.3724
	Error band around the structural fraction, $m^{-0.138}$	-0.02
	Cargo density, kg/m^3	-
	Fuel density, kg/m^3	800

Table A.2 AVDS^{CE} X-43A inputs and assumptions [14].

Variable Discipline	Variable	Value
Geometry	Küchemann's tau	0.0945
	Nose spatula width percentage: Nose width measured as a percentage of the maximum fuselage width	42
Propulsion	Area ratio of viscous captured flow to inviscid captured flow	0.95
	Reference fuel equivalence ratio	1
	Design Mach	7
Trajectory	Constant q climb segment: Start altitude, m	28,519
	Constant q climb segment: Start velocity, m/s	2,014
	Constant q climb segment: Maximum longitudinal acceleration, m/s^2	0.35
	Constant q climb segment: Minimum longitudinal acceleration, m/s^2	0.01
	Constant q climb segment: End Mach number	6.83
	Constant q climb segment: Time to climb, sec	11
	Constant q climb segment: Ignition phase time, sec	1.5
Weights and Volume	Number of crew	0
	Number of passengers	0
	Weight of unmanned fixed systems, N	2,547
	Weight of each crew member, N/person	-
	Weight fixed manned systems per crew member, N/person	-
	Weight of each passenger, N/person	-
	Weight of passenger provisions per passenger, N/person	-
	Weight of variable systems per vehicle dry weight	0.4542
	Weight of cargo, N	0
	Minimum dry weight (OEW) margin	0.1
	Volume of provision for each crew member, m^3/person	-
	Volume per crew member, m^3/person	-
	Volume of manned fixed systems per crew member, m^3/person	-
	Volume of each passenger space, m^3/person	-
	Volume of variable systems per total vehicle volume, m^3	0.03
	Volume of vehicle void space per total vehicle volume, m^3	0.1
	Volume of unmanned fixed system, m^3	0.4244
	Error band around the structural fraction, m$^{-0.138}$	0
	Cargo density, kg/m^3	-
	Fuel density, kg/m^3	47.7

Table A.3 AVDS^{CE} XB-70 inputs and assumptions [14].

Variable Discipline	Variable	Value
Geometry	Wing tip droop angles, deg	0, 25, 65
Aerodynamics	Ratio of square of Oswald efficiency factor to skin friction drag coefficient	200
Propulsion*	Number of engines	6
Trajectory	Takeoff segment: Starting altitude, m	0
	Takeoff segment: Starting velocity, m/s	0
	Takeoff segment: Obstacle altitude, m	15.24
	Takeoff segment: Climb flight path angle, degrees	1.5
	Takeoff segment: Angle of attack at liftoff, degrees	11.5
	Takeoff segment: Change in velocity before the liftoff velocity, m/s	10.29
	Takeoff segment: Rotation angular velocity, deg/s	2.1
	Takeoff segment: Rolling ground friction coefficient	0.025
	Constant acceleration climb segment (1): End Mach	0.9
	Constant acceleration climb segment (1): End altitude, m	6,300
	Constant acceleration climb segment (1): Change in velocity per change in altitude, sec^{-1}	0.025
	Constant Mach climb segment: Flight path angle, degrees	2
	Constant Mach climb segment: End altitude, m	10,058
	Constant altitude acceleration segment: Desired acceleration, m/s^2	0.3
	Constant altitude acceleration segment: End Mach	1.44
	Constant acceleration climb (2) segment: End Mach	3.0
	Constant acceleration climb (2) segment: End altitude, m	21,245
	Constant acceleration climb (2) segment: Change in velocity per change in altitude, sec^{-1}	0.041
	Constant altitude cruise segment: range, km	5,000
	Constant altitude powered deceleration segment (1): End Mach	2.2
	Constant *q* powered descent segment (1): End altitude, m	12,192
	Constant *q* powered descent segment (1): End Mach	1.08
	Constant *q* powered descent segment (1): Maximum longitudinal acceleration, m/s^2	-0.01
	Constant *q* powered descent segment (1): Minimum longitudinal acceleration, m/s^2	-1.5
	Constant altitude powered deceleration segment (2): End Mach	0.8
	Constant *q* powered descent segment (2): End altitude, m	30
	Constant *q* powered descent segment (2): End Mach	0.31
	Constant *q* powered descent segment (2): Maximum longitudinal acceleration, m/s^2	-0.1
	Constant *q* powered descent segment (2): Minimum longitudinal acceleration, m/s^2	-0.9
Weights and Volume	Number of crew	2
	Number of passengers	0
	Weight of cargo, N	222,411
	Weight of unmanned fixed systems, N	18,639
	Weight of each crew member, N/person	1,265
	Weight fixed manned systems per crew member, N/person	10,301
	Weight of each passenger, N/person	-
	Weight of passenger provisions per passenger, N/person	-
	Weight of variable systems per vehicle dry weight	0.16
	Minimum dry weight (OEW) margin	0.05
	Volume of unmanned fixed system, m^3	1.55
	Volume of provision for each crew member, m^3/person	1.5
	Volume per crew member, m^3/person	1.5
	Volume of manned fixed systems per crew member, m^3/person	1
	Volume of each passenger space, m^3/person	-
	Volume of variable systems per total vehicle volume, m^3	0.1
	Volume of vehicle void space per total vehicle volume, m^3	0.095
	Error band around the structural fraction, $m^{-0.138}$	0.049
	Cargo density, kg/m^3	2,000
	Fuel density, kg/m^3	810

*The inputs used in the NPSS method have been left out.

Table A.4 AVDS^{CE} SR-71 inputs and assumptions [14].

Variable Discipline	Variable	Value
Aerodynamics	Ratio of square of Oswald efficiency factor to skin friction drag coefficient	200
Propulsion*	Number of engines	2
Trajectory	Takeoff segment: Starting altitude, m	0
	Takeoff segment: Starting velocity, m/s	0
	Takeoff segment: Obstacle altitude, m	15.24
	Takeoff segment: Climb flight path angle, degrees	1.5
	Takeoff segment: Angle of attack at liftoff, degrees	11
	Takeoff segment: Change in velocity before the liftoff velocity, m/s	15.43
	Takeoff segment: Rotation angular velocity, deg/s	2.1
	Takeoff segment: Rolling ground friction coefficient	0.025
	Constant *q* climb segment (1): Flight path angle, deg	4
	Constant *q* climb segment (1): End Mach	0.9
	Constant *q* climb segment (1): End altitude, m	6,233
	Constant *q* climb segment (1): Maximum longitudinal acceleration, m/s^2	5
	Constant *q* climb segment (1): Minimum longitudinal acceleration, m/s^2	0.01
	Constant Mach climb segment: Flight path angle, degrees	4
	Constant Mach climb segment: End altitude, m	7,620
	Constant altitude acceleration segment: Desired acceleration, m/s^2	0.9
	Constant altitude acceleration segment: End Mach	1.10
	Constant *q* climb segment (2): Flight path angle, deg	4
	Constant *q* climb segment (2): End Mach	3.0
	Constant *q* climb segment (2): End altitude, m	21,336
	Constant *q* climb segment (2): Transition altitude, m	18,288
	Constant *q* climb segment (2): Maximum longitudinal acceleration, m/s^2	5
	Constant *q* climb segment (2): Minimum longitudinal acceleration, m/s^2	0.01
	Constant altitude cruise segment: Range, km	5,000
	Constant altitude powered deceleration segment (1): End Mach	2.53
	Constant *q* powered descent segment (1): End altitude, m	12,802
	Constant *q* powered descent segment (1): End Mach	1.30
	Constant *q* powered descent segment (1): Minimum longitudinal acceleration, m/s^2	-1.2
	Constant altitude powered deceleration segment (2): End Mach	0.80
	Constant *q* powered descent segment (2): End altitude, m	30
	Constant *q* powered descent segment (2): End Mach	0.31
	Constant *q* powered descent segment (2): Minimum longitudinal acceleration, m/s^2	-0.3
Weights and Volume	Number of crew	2
	Number of passengers	0
	Weight of cargo, N	17,793
	Weight of unmanned fixed systems, N	1,000
	Weight of each crew member, N/person	1,265
	Weight fixed manned systems per crew member, N/person	0
	Weight of each passenger, N/person	-
	Weight of passenger provisions per passenger, N/person	-
	Weight of variable systems per vehicle dry weight	0.12
	Minimum dry weight (OEW) margin	0.1
	Volume of provision for each crew member, m^3/person	1.5
	Volume per crew member, m^3/person	1.5
	Volume of manned fixed systems per crew member, m^3/person	0.1
	Volume of each passenger space, m^3/person	-
	Volume of variable systems per total vehicle volume, m^3	0.1
	Volume of vehicle void space per total vehicle volume, m^3	0.1
	Volume of unmanned fixed system, m^3	7.75
	Error band around the structural fraction, m$^{-0.138}$	0.049
	Cargo density, kg/m^3	240
	Fuel density, kg/m^3	787

*The inputs used in the NPSS method have been left out.

APPENDIX B
VEHICLE BIBLIOGRAPHIES

B.1. X-51 Bibliography

[1] Anon. “Roadmap for the Hypersonics Programs of the Department of Defense,” No. 109-364, Report to Congress, Joint Technology Office on Hypersonics Director, Defense Research & Engineering, 01 February 2008.

[2] Anon. “US Military to Test Hypersonic Vehicle over Pacific: X-51A to Reach Mach 6,” *The Associated Press*. http://phys.org/news/2012-08-military-hypersonic-vehicle-pacific-X-51a.html, 14 August 2012.

[3] Anon. “Unmanned US Military Hypersonic Craft Failed,” *The Associated Press*. http://phys.org/news/2012-08-unmanned-military-hypersonic-craft.html, 15 August 2012.

[4] Anon. “USAF Vehicle Breaks Record for Hypersonic Flight,” *The Associated Press*. https://phys.org/news/2010-5-usaf-vehicle-hypersonic-flight.html, 27 May 2010.

[5] Anon. “High-Speed Air-Breathing Propulsion,” *Aerospace America,* AIAA High-Speed Air-Breathing Propulsion Technical Committee, December 2008.

[6] *AVD Internal*----------

[7] Anon. “Assessment of Aerothermodynamic Flight Prediction Tools through Ground and Flight Experimentation,” RTO-TR-AVT-136, Research & Technology Organisation, November 2011.

[8] Borg, M. P. “Laminar Instability and Transition on the X-51A,” Ph.D. Dissertation, Purdue University, West Lafayette, IN, August 2009.

[9] Borger, W. U. “Disruptive Technology: Hypersonic Propulsion,” AFRL HQ 07-0083, [Presentation], Air Force Research Laboratory, Wright-Patterson Air Force Base, OH, September 2007.

[10] Bowcutt, K. G. “Tackling the Extreme Challenges of Air-Breathing Hypersonic Vehicle Design, Technology, and Flight.” *Mathematics, Computing & Design Symposium*, [Presentation], Boeing, Stanford University, CA, 21 November 2014.

[11] Brink, C. “X-51 Flight Four Results and What's Next for High Speed Weapons,” Presentation for the WPAFB Chapter of the Daedalians, Air Force Research Laboratory, Wright-Patterson Air Force Base, OH, 20 August 2013.

[12] Candler, G., Johnson, H., Alba, C., and MacLean, M. “Analysis of Modal Growth on the Leeward Centerplane of the X-51 Vehicle,” AFRL-RB-WP-TM-2010-3001, Air Force Research Laboratory, Wright-Patterson Air Force Base, OH, September 2009.

[13] Chen, P. C., Starkey, R., Chang, K. T., and Sengupta, A. “Integrated Aero-Servo-Thermo-Propulso-Elasticity (ASTPE) for Hypersonic Scramjet Vehicle Design/Analysis:,” United States Air Force Office of Scientific Research, Arlington, VA, 04 December 2009.

[14] Eichhorn, D. J. “Test Like You Train…Train Like You Fight: How Today’s Complexity Drives Future Range Requirements,” [Presentation], Air Force Flight Test Center, Edwards Air Force Base, CA, October 2008.

[15] *AVD Internal*----------

[16] Hank, J., Murphy, J., and Mutzman, R. “The X-51A Scramjet Engine Flight Demonstration Program,” AIAA-2008-2540. *15th AIAA International Space Planes and Hypersonic Systems and Technologies Conference*, American Institute of Aeronautics and Astronautics, Dayton, OH, 28 April 2008. https://doi.org/10.2514/6.2008-2540

[17] Kazmar, R. “Hypersonic Propulsion at Pratt & Whitney — Overview.” *AIAA/CIRA 13th International Space Planes and Hypersonics Systems and Technologies Conference*, American Institute of Aeronautics and Astronautics, Capua, Italy, 16-20 May 2012.

[18] Kelly, C. “Speeding into the Future: In a History-Making Flight, the X-51A Showed the Possibilities of Hypersonic Travel,” *Boeing Frontiers*, July 2010.

[19] Lane, J. “Design Processes and Criteria for the X-51A Flight Vehicle Airframe,” RTO-MP-AVT-145. *UAV Design Processes / Design Criteria for Structures*, Research and Technology Organisation, Neuilly-sur-Seine, France, 2007.

[20] Leugers, J. “Airbreathing Hypersonic Technologies in the Air Force S&T Portfolio.” *13th Annual Science & Engineering Technology Conference*, [Presentation], NDIA, North Charleston, SC, 18 April 2012.

[21] Lewis, M. “X-51 Scrams into the Future,” *Aerospace America,* pp. 26-31, October 2010.

[22] Moerel, J.-L., and Halswijk, W. “Ramjets: Airframe Integration,” RTO-EN-AVT-185, TNO Defence, Rijswijk, The Netherlands, September 2010.

[23] *AVD Internal*----------

[24] Murphy, J. S., Hank, J. M., and Mutzman, R. C. “The X-51A Scramjet Engine Demonstration Program: Technology Maturation Thru Flight Tests 1 & 2,” RTO-MP-AVT-208-P-16, Air Force Research Laboratory, Wright-Pattterson Air Force Base, OH.

[25] Mutzman, R., and Murphy, S. “X-51 Development: A Chief Engineer’s Perspective.” *17th AIAA International Space Planes and Hypersonic Systems and Technologies Conference*, [Presentation], American Institute of Aeronautics and Astronautics, San Francisco, CA, 11-14 April 2011.

[26] Norris, G. “High-Speed Strike Weapon to Build on X-51 Flight,” *Aviation Week & Space Technology*. http://aviationweek.com/awin/high-speed-strike-weapon-build-x-51-flight, 20 May 2013.

[27] Ormsby, C. “Air Force FY15 S&T Program,” [Presentation], U.S. Air Force, Arlington, VA, 12 March 2014.

[28] Osborn, K. “AF Chief Scientist: Air Force Working on New Hypersonic Air Vehicle,” *Defense Tech*. https://www.military.com/defensetech/2015/06/01/af-chief-scientist-air-force-working-on-new-hypersonic-air-vehicle, 01 June 2015.

[29] Reed, J. “X-51A Scramjet Engine Demonstrator - Waverider,” [Presentation], Air Force Research Laboratory, Wright-Patterson Air Force Base, OH, 26 April 2010.

[30] Rondeau, C. M., and Jorris, T. R. “X-51A Scramjet Demonstrator Program: Waverider Ground and Flight Test.” *SFTE 44th International / SETP Southwest Flight Test Symposium*, Ft Worth, TX, 28 October 2013.

[31] Shaffer, A. “Technology Surprise - Need for Rebalance of R&E Investments,” Department of Defense, Arlington, VA, 18 March 2014.

[32] Stephenson, D. “'Pretty Cool' Vehicles,” *Boeing Frontiers*, pp. 30-33, February 2008.

[33] Vogel, J. “X-51A Scramjet Engine Demonstrator - Waverider,” 2010 Aviation Week Program Excellence Initiative, 2010.

[34] *AVD Internal*----------

B.2. X-43A Bibliography

[1] Albertson, C., and Emami, S. "Alleviation of Facility/Engine Interactions in an Open-Jet Scramjet Test Facility," AIAA-2001-3677. *37th AIAA/ASME/SAE/ASEE Joint Propulsion Conference and Exhibit*, American Institute of Aeronautics and Astronautics, Salt Lake City, UT, 08-11 July 2001. https://doi.org/10.2514/6.2001-3677

[2] Anon. "Nasa's X-43A Scramjet Achieves Record-Breaking Mach 10 Speed Using Model-Based Design," MathWorks.

[3] Anon. "Real-Time Simulation of Aeroheating of the Hyper-X Airplane," Dryden Flight Research Center, NASA, Edwards, California.

[4] Anon. "X43 Program." Accurate Automation Corporation, Chattanooga, TN.

[5] Anon. "X-43A Hyper-X Launch Vehicle Fact Sheet," Orbital, Dulles, VA.

[6] Anon. "X-43 Emergency Summary," 04 November 2004.

[7] Anon. "Report of Findings: X-43A Mishap," Vol. 1, X-43A Mishap Investigation Board, 08 May 2003.

[8] Anon. "Advances on Propulsion Technology for High-Speed Aircraft. Volume 2." von Karman Institute for Fluid Dynamics, Belgium, 12-15 March 2007.

[9] Anon. "Advances on Propulsion Technology for High-Speed Aircraft. Volume 1." von Karman Institute for Fluid Dynamics, Belgium, 12-15 March 2007.

[10] Anon. "Fiscal Year 2001 Accountability Report," NASA, 2001.

[11] Anon. "X-43A Project Overview: Adventures in Hypersonics," [Presentation], NASA, 2005.

[12] Anon. "NASA Hyper-X Program Demonstrates Scramjet Technologies: X-43A Flight Makes Aviation History," *NASAFacts*, NASA, 2006.

[13] Anon. "Pegasus User's Guide," Release 7.0, Orbital Sciences Corporation, April 2010.

[14] Anon. "NASA "Hyper-X" Program Demonstrates Scramjet Technologies: X-43a Being Readied for Reflight," *FactSheet*, Langley Research Center, NASA, Hampton, VA, July 2003.

[15] Anon. "Technical Training on High-Order Spectral Analysis and Thermal Anemometry Applications," Langley Research Center, NASA, Hampton, VA, September 2003.

[16] Bahm, C., Baumann, E., Martin, J., Bose, D., Beck, R., and Strovers, B. "The X-43A Hyper-X Mach 7 Flight 2 Guidance, Navigation, and Control Overview and Flight Test Results," AIAA-2005-3275. *AIAA/CIRA 13th International Space Planes and Hypersonics Systems and Technologies Conference*, American Institute of Aeronautics and Astronautics, Capua, Italy, 2005. https://doi.org/10.2514/6.2005-3275

[17] Bakos, D. R. "Current Hypersonic Research in the USA," RTO-EN-AVT-150. *Advances on Propulsion Technology for High-Speed Aircraft*, Research and Technology Organisation, Neuilly-sur-Seine, France, 2008.

[18] Bakos, R., Tsai, C.-Y., Rogers, R., and Shih, A. "Hyper-X Mach 10 Engine Flowpath Development - Fifth Entry Test Conditions and Methodology," AIAA-2001-1814. *10th AIAA/NAL-NASDA-ISAS International Space Planes and Hypersonic Systems and Technologies Conference*, American Institute of Aeronautics and Astronautics, Kyoto, Japan, 24 April 2001. https://doi.org/10.2514/6.2001-1814

[19] Bakos, R. J., Tsai, C.-Y., Rogers, R., and Shih, A. "The Mach 10 Component of Nasa's Hyper-X Ground Test Program," Langley Research Center, NASA, Hampton, VA, 01 January 1999.

[20] Bathel, B., Danehy, P., Inman, J., Alderfer, D., and Berry, S. "PLIF Visualization of Active Control of Hypersonic Boundary Layers Using Blowing," *26th AIAA Aerodynamic Measurement Technology and Ground Testing Conference*, American Institute of Aeronautics and Astronautics, Seattle, WA, 23 June 2008, https://doi.org/10.2514/6.2008-4266

[21] Baumann, E. "X-43A Flight Controls," [Presentation], Dryden Flight Research Center, NASA, Edwards, CA, 06 March 2006.

[22] Baumann, E. "Tailored Excitation for Frequency Response Measurement Applied to the X-43A Flight Vehicle," NASA/TM-2007-214609, Dryden Flight Research Center, NASA, Edwards, CA, January 2007.

[23] Baumann, E., Bahm, C., Strovers, B., Beck, R., and Richard, M. "The X-43A Six Degree of Freedom Monte Carlo Analysis," NASA/TM-2007-214630, Dryden Flight Research Center, NASA, Edwards, CA, December 2007.

[24] Baumann, E., Pahle, J. W., Davis, M. C., and White, J. T. "The X-43A Flush Airdata Sensing System Flight Test Results." *AIAA Atmospheric Flight Mechanics Conference and Exhibit*, American Institute of Aeronautics and Astronautics, Honolulu, Hawaii, 18-21 August 2008.

[25] Bermudez, L., Gladden, R., Jeffries, M., McMillan, D., Porter, J., Allen, V., and Engelund, W. C. "Aerodynamic Characterization of the Hyper-X Launch Vehicle." *12th AIAA International Space Planes and Hypersonic Systems and Technologies*, American Institute of Aeronautics and Astronautics, Norfolk, VA, 15-19 December 2003. https://doi.org/10.2514/6.2003-7074

[26] Berry, S., and Berger, K. "NASA Langley Experimental Aerothermodynamic Contributions to Slender and Winged Hypersonic Vehicles," Langley Research Center, NASA, Hampton, VA.

[27] Berry, S., Daryabeigi, K., Wurster, K., and Bittner, R. "Boundary Layer Transition on X-43A," AIAA-2008-3736. *38th AIAA Fluid Dynamics Conference*, American Institute of Aeronautics and Astronautics, Seattle, WA, 23-26 June 2008.

[28] Berry, S., DiFulvio, M., and Kowalkowski, K. "Forced Boundary-Layer Transition on X-43 (Hyper-X) in NASA Larc 31-Inch Mach 10 Air Tunnel," NASA/TM-2000-210315, Langley Research Center, NASA, Hampton, VA, August 2000.

[29] Berry, S., DiFulvio, M., and Kowalkowski, K. "Forced Boundary-Layer Transition on X-43 (Hyper-X) in NASA Larc 20-Inch Mach 6 Air Tunnel," NASA/TM-2000-210316, Langley Research Center, NASA, Hampton, VA, August 2000.

[30] Berry, S., and Nowak, R. "A Comparison of Active and Passive Methods for Control of Hypersonic Boundary Layers on Airbreathing Configurations." *JANNAF 27th Airbreathing Propulsion Subcommittee Meeting*, Langley Research Center, NASA, Colorado Springs, CO, 01-05 December 2003.

[31] Berry, S., Nowak, R., and Horvath, T. "Boundary Layer Control for Hypersonic Airbreathing Vehicles," AIAA-2004-2246. *34th AIAA Fluid Dynamics Conference and Exhibit*, American Institute of Aeronautics and Astronautics, Portland, OR, 28 June 2004. https://doi.org/10.2514/6.2004-2246

[32] Berry, S. A., Auslender, A. H., Dilley, A. D., and Calleja, J. F. "Hypersonic Boundary-Layer Trip Development for Hyper-X," AIAA-2000-4012. *18th AIAA Applied Aerodynamics Conference*, American Institute of Aeronautics and Astronautics, Denver, CO, 14-17 August 2000.

[33] Berry, S. A., and Horvath, T. J. "Discrete Roughness Transition for Hypersonic Flight Vehicles." *45th AIAA Aerospace Sciences Meeting and Exhibit*, American Institute of Aeronautics and Astronautics, Reno, NV, 08-11 January 2007.

[34] Blocker, W., and Ruebush, D. "X-43A Stage Separation System - a Flight Data Evaluation," AIAA-2005-3335. *AIAA/CIRA 13th International Space Planes and Hypersonics Systems and Technologies Conference*, American Institute of Aeronautics and Astronautics, Capua, Italy, 16 May 2005. https://doi.org/10.2514/6.2005-3335

[35] Bowcutt, K. G. "Tackling the Extreme Challenges of Air-Breathing Hypersonic Vehicle Design, Technology, and Flight." *Mathematics, Computing & Design Symposium*, [Presentation], Boeing, Stanford University, CA, 21 November 2014.

[36] Brock, M. A. "Performance Study of Two-Stage-to-Orbit Reusable Launch Vehicle Propulsion Alternatives," Master's Defense, Department of Aeronautics and Astronautics, Graduate School of Engineering and Management, Air Force Institute of Technology, Air University, Wright-Patterson Air Force Base, OH, March 2004.

[37] Buning, P., Wong, T.-C., Dilley, A., and Pao, J. "Prediction of Hyper-X Stage Separation Aerodynamics Using CFD." *18th Applied Aerodynamics Conference*, American Institute of Aeronautics and Astronautics, Denver, CO, 14-17 August 2000. https://doi.org/10.2514/6.2000-4009

[38] Choudhari, M., Li, F., and Edwards, J. "Stability Analysis of Roughness Array Wake in a High-Speed Boundary Layer." *47th AIAA Aerospace Sciences Meeting including The New Horizons Forum and Aerospace Exposition*, American Institute of Aeronautics and Astronautics, Orlando, FL, January 2009. https://doi.org/10.2514/6.2009-170

[39] Cockrell, C. "Aerosciences, Aero-Propulsion and Flight Mechanics Technology Development for NASA's Next Generation Launch Technology Program." *12th AIAA International Space Planes and Hypersonic Systems and Technologies*, American Institute of Aeronautics and Astronautics, Norfolk, VA, 15-19 December 2003. https://doi.org/10.2514/6.2003-6948

[40] Cockrell, C., Auslender, A. H., White, J., and Dilley, A. "Aeroheating Predictions for the X-43 Cowl-Closed Configuration at Mach 7 and 10," AIAA 2002-0218. *40th AIAA Aerospace Sciences Conference & Exhibit*, American Institute of Aeronautics and Astronautics, Reno, Nevada, 14-17 January 2002.

[41] Cockrell, C., Davis, S., Robinson, K., Tuma, M., and Sullivan, G. "NASA Crew Launch Vehicle Flight Test Options." *57th International Astronautical Congress*, Valencia, Spain, 02-06 October 2006.

[42] Cockrell, J., Charles, Engelund, W., Dilley, A., Bittner, R., Jentink, T., and Frendi, A. "Integrated Aero-Propulsive CFD Methodology for the Hyper-X Flight Experiment." *18th Applied Aerodynamics Conference*, American Institute of Aeronautics and Astronautics, Denver, CO, 14-17 August 2000. https://doi.org/10.2514/6.2000-4010

[43] Cook, M., Murphy, K. L., and Schneider, T. "Advanced Materials for Exploration Task Research Results," NASA/TM-2008-215465, Marshall Space Flight Center, NASA, MSFC, AL, July 2008.

[44] Corpening, G. "X-43A: The First Flight of a Scramjet Powered Airplane." *AIAA Space 2004 Conference*, [Presentation], American Institute of Aeronautics and Astronautics, San Diego, CA, 28 September 2004.

[45] Crawford, J. L., and Cruciani, E. "2000 - 2001 Research Engineering Annual Report," NASA/TM-2004-212025, Dryden Flight Research Center, NASA, Edwards, California, January 2004.

[46] Crawford, J. L., and Cruciani, E. "2002 Research Engineering Annual Report," NASA/TM-2004-212851, Dryden Flight Research Center, NASA, Edwards, CA, September 2004.

[47] Danehy, P. M., Bathel, B., Inman, J. A., Alderfer, D. W., and Jones, S. B. "Stereoscopic Imaging in Hypersonics Boundary Layers Using Planar Laser-Induced Fluorescence." *38th AIAA Fluid Dynamics Conference and Exhibit*, American Institute of Aeronautics and Astronautics, Seattle, WA, 23-26 June 2008.

[48] Daryabeigi, K., Berry, S. A., Horvath, T. J., and Nowak, R. J. "Finite Volume Numerical Methods for Aeroheating Rate Calculations from Infrared Thermographic Data," AIAA-2003-3634. *36th AIAA Thermophysics Conference*, American Institute of Aeronautics and Astronautics, Orlando, FL, 23-26 June 2003.

[49] Davidson, J., Lallman, F., McMinn, J., Martin, J., Pahle, J., Stephenson, M., Selmon, J., and Bose, D. "Flight Control Laws for NASA's Hyper-X Research Vehicle," AIAA-99-4124. *Guidance, Navigation, and Control Conference and Exhibit*, American Institute of Aeronautics and Astronautics, Portland, OR, 09 August 1999. https://doi.org/10.2514/6.1999-4124

[50] Davis, M., and White, J. "Flight-Test-Determined Aerodynamic Force and Moment Characteristics of the X-43A at Mach 7.0." *14th AIAA/AHI Space Planes and Hypersonic Systems and Technologies Conference*, American Institute of Aeronautics and Astronautics, Canberra, Australia, 06-09 November 2006. https://doi.org/10.2514/6.2006-8028

[51] Davis, M. C., Sim, A. G., Rhode, M., and Johnson, K. D. "Wind-Tunnel Results of the B-52B with the X-43A Stack," *Journal of Spacecraft and Rockets*, Vol. 44, No. 4, pp. 871-877, 2007. https://doi.org/10.2514/1.27191.

[52] Dennehy, N., Lebsock, K., and West, J. "Guidance, Navigation & Control (Gn&C) Best Practices for Human-Rated Spacecraft Systems," Presentation for Program Management Challenge 2008, Daytona Beach, FL, 26-27 February 2008.

[53] Dickeson, J., Rodriguez, A., Sridharan, S., and Korad, A. "Elevator Sizing, Placement, and Control-Relevant Tradeoffs for Hypersonic Vehicles." *AIAA Guidance, Navigation, and Control Conference*, American Institute of Aeronautics and Astronautics, Toronto, Ontario, Canada, 2010. https://doi.org/10.2514/6.2010-8339

[54] Dickeson, J., Rodriguez, A., Sridharan, S., Soloway, D., Korad, A., Khatri, J., Benavides, J., Kelkar, A., and Vogel, J. "Control-Relevant Modeling, Analysis, and Design for Scramjet-Powered Hypersonic Vehicles." *16th AIAA/DLR/DGLR International Space Planes and Hypersonic Systems and Technologies Conference*, American Institute of Aeronautics and Astronautics, Bremen, Germany, 2009. https://doi.org/10.2514/6.2009-7287

[55] Douglas, M., and Lindgren, J. "Hypersonic Weapons Technology for the Time Critical Mobile Ground Threat: A State-of-the-Art Review," DMSTTIAC SOAR 99-01, DMSTTIAC IIT Research Institute, Huntsville, AL, January 1999. [retrieved 2020-01-21 18:36:41].

[56] Drummond, J. P. "Methods for Prediction of High-Speed Reacting Flows in Aerospace Propulsion," *AIAA Journal*, Vol. 52, No. 3, pp. 465-485, 2014. https://doi.org/10.2514/1.J052283.

[57] Drummond, J. P., Cockrell, C., Pellett, G., Diskin, G., Auslender, A. H., Exton, R., Guy, R. W., Hoppe, J., Puster, R., Rogers, R., Trexler, C. A., and Voland, R. T. "Hypersonic Airbreathing Propulsion - an Aerodynamics, Aerothermodynamics, and Acoustics Competency White Paper," NASA/TM-2002-211951, Langley Research Center, NASA, Hampton, VA, November 2002.

[58] Ellsworth, J. "An Analytical Explanation for the X-43A Flush Air Data Sensing System Pressure Mismatch between Flight and Theory." *28th AIAA Applied Aerodynamics Conference*, American Institute of Aeronautics and Astronautics, Chicago, Illinois, 2010. https://doi.org/10.2514/6.2010-4964

[59] Engelund, W., and Neal, B. "X-43A Lessons Learned," [Presentation], Hypersonic Lessons Learned Workshop, Arlington, VA, 10 December 2013.

[60] Engelund, W. C. "Hyper-X Program Overview," Aerospace and Ocean Engineering Dept. Seminar, Virginia Tech, 02 May 2001.

[61] Engelund, W. C., Holland, S. D., Cockrell, C. E., and Bittner, R. “Propulsion System Airframe Integration Issues and Aerodynamic Database Development for the Hyper-X Flight Research Vehicle,” ISOABE-99-7215. *XIV ISOABE*, Florence, Italy, 05-10 September 1999.

[62] Engelund, W. C., Holland, S. D., Jr, C. E. C., and Bittner, R. “Aerodynamic Database Development for the Hyper-X Airframe-Integrated Scramjet Propulsion Experiments,” *Journal of Spacecraft and Rockets*, Vol. 38, No. 6, p. 8, 2001.

[63] Erdos, J., Bakos, R., Castrogiovanni, A., and Rogers, R. “Dual Mode Shock-Expansion/Reflected-Shock Tunnel.” *35th Aerospace Sciences Meeting and Exhibit*, American Institute of Aeronautics and Astronautics, Reno, NV, 1997. https://doi.org/10.2514/6.1997-560

[64] Erickson, G. E. “Overview of Supersonic Aerodynamics Measurement Techniques in the NASA Langley Unitary Plan Wind Tunnel,” NASA/TM-2007-214894, Langley Research Center, NASA, Hampton, VA, August 2007.

[65] Ferleman, P. “Comparison of Hyper-X Mach 10 Scramjet Preflight Predictions and Flight Data,” AIAA-2005-3352. *AIAA/CIRA 13th International Space Planes and Hypersonics Systems and Technologies Conference*, American Institute of Aeronautics and Astronautics, Capua, Italy, 16-20 May 2005.

[66] Ferleman, S., McClinton, C., Rock, K., and Voland, R. T. “Hyper-X Mach 7 Scramjet Design, Ground Test and Flight Results.” *AIAA/CIRA 13th International Space Planes and Hypersonics Systems and Technologies Conference*, American Institute of Aeronautics and Astronautics, Capua, Italy, 16-20 May 2005.

[67] Fidan, B., Mirmirani, M., and Ioannou, P. “Flight Dynamics and Control of Air-Breathing Hypersonic Vehicles: Review and New Directions.” *12th AIAA International Space Planes and Hypersonic Systems and Technologies*, American Institute of Aeronautics and Astronautics, Norfolk, VA, 15-19 December 2003. https://doi.org/10.2514/6.2003-7081

[68] Freeman, D., Reubush, D., McClinton, C., Rausch, V., and Crawford, L. “The NASA Hyper-X Program,” IAF-97-V.4.07. *48th International Astronautical Congress*, Turin, Italy, 06-10 October 1997.

[69] Freeman, M. “The Space Plane: Hypersonic Flight Is Ready for Take-Off,” *Executive Intelligence Review*, Vol. 31, No. 45, p. 8, 19 November 2004.

[70] Gibson, C., Neidhoefer, J., Cooper, S., Carlton, L., Cox, C., and Jorgensen, C. “Development and Flight Test of the X-43A-Ls Hypersonic Configuration UAV.” *AIAA's 1st Technical Conference and Workshop on Unmanned Aerospace Vehicles*, American Institute of Aeronautics and Astronautics, Portsmouth, VA, 20-23 May 2002. https://doi.org/10.2514/6.2002-3462

[71] Gibson, C., Vess, R., and Pegg, R. “Low Speed Flight Testing of a X-43A Hypersonic Lifting Body Configuration,” AIAA-2003-7086. *12th AIAA International Space Planes and Hypersonic Systems and Technologies*, American Institute of Aeronautics and Astronautics, Norfolk, VA, 15-19 December 2003. https://doi.org/10.2514/6.2003-7086

[72] Glaessgen, E. H., Dawicke, D. S., Johnston, W. M., James, M. A., Simonsen, M., and Mason, B. H. “X-43A Rudder Spindle Fatigue Life Estimate and Testing,” NASA/TM-2005-213525, Langley Research Center, NASA, Hampton, VA, March 2005.

[73] Grindle, L. “Hyper-X/ X-43A: Dryden’s Role,” Presentation for Lockheed Martin Interchange, Dryden Flight Research Center, NASA, Edwards, CA, 14 August 2012.

[74] Grindle, L., and Bahm, C. “The X-43A (Hyper-X) Flies into the Record Books,” Dryden Flight Research Center, NASA.

[75] Gupta, K. K., Choi, S. B., and Ibrahim, A. “Aeroelastic-Acoustics Simulation of Flight Systems.” *47th AIAA Aerospace Sciences Meeting*, [Presentation], American Institute of Aeronautics and Astronautics, Orlando, FL, 05-08 January 2009.

[76] Harrington, B. H. “Magnetogasdynamic Flow Acceleration in a Scramjet Nozzle,” Master's Defense, Department of Aeronautics and Astronautics, Graduate School of Engineering and Management, Air Force Institute of Technology, Air University, Wright-Patterson Air Force Base, OH, June 2004.

[77] Harsha, P., Keel, L., Castrogiovanni, A., and Sherrill, R. “X-43A Vehicle Design and Manufacture,” AIAA-2005-3334. *AIAA/CIRA 13th International Space Planes and Hypersonics Systems and Technologies Conference*, American Institute of Aeronautics and Astronautics, Capua, Italy, 16 May 2005. https://doi.org/10.2514/6.2005-3334

[78] Holland, S. D., Woods, C., and Engelund, W. C. “Hyper-X Research Vehicle (HXRV) Experimental Aerodynamics Test,” AIAA-2000-4011. *AIAA 18th Applied Aeronautics Conference*, American Institute of Aerounautics and Astronautics, Denver, CO.

[79] Horvath, T. J., Berry, S. A., and Merski, N. R. “Hypersonic Boundary/Shear Layer Transition for Blunt to Slender Configurations - a NASA Langley Experimental Perspective,” RTO-MP-AVT-111, RTO AVT Specialists' Meeting on “Enhancement of NATO Military Flight Vehicle Performance by Management of Interacting Boundary Layer Transition and Separation”, Prague, Czech Republic, 04-07 October 2004.

[80] Huebner, L., Rock, K., Ruf, E., Witte, D., and Andrews, E. “Hyper-X Flight Engine Ground Testing for X-43 Flight Risk Reduction,” AIAA-2001-1809. *10th AIAA/NAL-NASDA-ISAS International Space Planes and Hypersonic Systems and Technologies Conference*, American Institute of Aeronautics and Astronautics, Kyoto, Japan, 24-27 April 2001. https://doi.org/10.2514/6.2001-1809

[81] Huebner, L., Rock, K., Witte, D., Ruf, E., and Andrews, E. “Hyper-X Engine Testing in the NASA Langley 8-Foot High Temperature Tunnel,” AIAA-2000-3605. *36th AIAA/ASME/SAE/ASEE Joint Propulsion Conference and Exhibit*, American Institute of Aeronautics and Astronautics, Huntsville, AL, 17-19 July 2000. https://doi.org/10.2514/6.2000-3605

[82] Hunt, J., and Rausch, V. “Airbreathing Hypersonic Systems Focus at NASA Langley Research Center.” *8th AIAA International Space Planes and Hypersonic Systems and Technologies Conference*, American Institute of Aeronautics and Astronautics, Norfolk, VA, 27-30 April 1998. https://doi.org/10.2514/6.1998-1641

[83] Hunt, J. L. “Airbreathing/Rocket Single-Stage-to-Orbit Design Matrix,” AIAA-95-6011. *Sixth International Aerospace Planes and Hypersonics Technologies Conference*, American Institute of Aeronautics and Astronautics, Chattanooga, TN, 03-07 April 1995.

[84] Hunt, J. L., Pegg, R. J., and Petley, D. H. “Airbreathing Hypersonic Vision-Operational-Vehicles Design Matrix.” *World Aviation Congress & Exposition*, 1999. https://doi.org/10.4271/1999-01-5515

[85] Jenkins, D., Landis, T., and Miller, J. *American X-Vehicles: An Inventory X-1 to X-50*, Centennial of Flight Edition ed., National Aeronautics and Space Administration, Washington, DC, June 2003.

[86] Johnson, W., and Weeks, C. “Evaluation of a Gamma Titanium Aluminide for Hypersonic Structural Applications,” NAG-1-02018, Georgia Institute of Technology, Atlanta, GA, April 2005.

[87] Joyce, P., Pomroy, J., and Grindle, L. “The Hyper-X Launch Vehicle: Challenges and Design Considerations for Hypersonic Flight Testing,” AIAA-2005-3333. *AIAA/CIRA 13th International Space Planes and Hypersonics Systems and Technologies Conference*, American Institute of Aeronautics and Astronautics, Capua, Italy, 16 May 2005. https://doi.org/10.2514/6.2005-3333

[88] Karlgaard, C., Martin, J., Tartabini, P., and Thornblom, M. "Hyper-X Mach 10 Trajectory Reconstruction." *AIAA Atmospheric Flight Mechanics Conference and Exhibit*, American Institute of Aeronautics and Astronautics, San Francisco, CA, 15 August 2005. https://doi.org/10.2514/6.2005-5920
[89] Karlgaard, C., Tartabini, P., Blanchard, R., Kirsch, M., and Toniolo, M. "Hyper-X Post-Flight Trajectory Reconstruction," AIAA-2004-4829. *AIAA Atmospheric Flight Mechanics Conference and Exhibit*, American Institute of Aeronautics and Astronautics, Providence, RI, 16-19 August 2004. https://doi.org/10.2514/6.2004-4829
[90] Karlgaard, C., Tartabini, P., Blanchard, R., Kirsch, M., and Toniolo, M. "Hyper-X Post-Flight-Trajectory Reconstruction," Journal of Spacecraft and Rockets, Vol. 43, No. 1, pp. 105-115, January-February 2006.
[91] *AVD Internal*----------
[92] Ko, W. L. "Stress Analysis of B-52B and B-52H Air-Launching Systems Failure-Critical Structural Components," NASA/TP-2005-212862, Dryden Flight Research Center, NASA, Edwards, CA, April 2005.
[93] Ko, W. L. "Thermal Buckling Analysis of Rectangular Panels Subjected to Humped Temperature Profile Heating," NASA/TP-2004-212041, Dryden Flight Research Center, NASA, Edwards, CA, January 2004.
[94] Ko, W. L., and Chen, T. "Extended Aging Theories for Predictions of Safe Operational Life of Critical Airborne Structural Components," NASA/TP-2006-213676, Dryden Flight Research Center, NASA, Edwards, CA, May 2006.
[95] Ko, W. L., and Gong, L. "Thermostructural Analysis of Unconventional Wing Structures of a Hyper-X Hypersonic Flight Research Vehicle for the Mach 7 Mission," NASA/TP-2001-210398, Dryden Flight Research Center, NASA, Edwards, CA, October 2001.
[96] Ko, W. L., and Gong, L. "Thermoelastic Analysis of Hyper-X Camera Windows Suddenly Exposed to Mach 7 Stagnation Aerothermal Shock," NASA/TP-2000-209030, Dryden Flight Research Center, NASA, Edwards, CA, September 2000.
[97] Ko, W. L., Tran, V. T., and Chen, T. "Incorporation of Half-Cycle Theory into Ko Aging Theory for Aerostructural Flight-Life Predictions," NASA/TP-2007-214608, Dryden Flight Research Center, NASA, Edwards, CA, January 2007.
[98] Labbe, S. G., Gilbert, M. G., and Kehoe, M. W. "Possible Deficiencies in Predicting Transonic Aerodynamics on the X-43A," NASA/TM-2009-215711, Langley Research Center, NASA, Hampton, VA.
[99] LaRouche, L. H. "We Must Save the X-43A: How I Defined the Scramjet," *Executive Intelligence Review*, Vol. 31, No. 45, p. 2, 19 November 2004.
[100] Leonard, C., Amundsen, R., and Bruce, W. "Hyper-X Hot Structures Design and Comparison with Flight Data." *AIAA/CIRA 13th International Space Planes and Hypersonics Systems and Technologies Conference*, American Institute of Aeronautics and Astronautics, Capua, Italy, 16 May 2005. https://doi.org/10.2514/6.2005-3438
[101] Lin, Y., Baumann, E., Bose, D., Beck, R., and Jenney, G. "Tests and Techniques for Characterizing and Modeling X-43A Electromechanical Actuators," NASA/TM-2008-214637, Dryden Flight Research Center, NASA, Edwards, CA, December 2008.
[102] Liu, Y.-b., and Lu, Y.-p. "Conceptual Research on Modelling and Control Integrative Design Methods for Hypersonic Waverider," *Proceedings of the Institution of Mechanical Engineers, Part G: Journal of Aerospace Engineering*, Vol. 225, No. 12, pp. 1291-1301, December 2011. https://doi.org/10.1177/0954410011406629.
[103] Lockwood, M. K., Hunt, J., Kabis, H., Moses, P., Pao, J.-L., Yarrington, P., and Collier, C. "Design and Analysis of a Two-Stage-to-Orbit Airbreathing Hypersonic Vehicle Concept," AIAA-96-2890. *32nd AIAA/ASME/SAE/ASEE Joint Propulsion Conference*, American Institute of Aeronautics and Astronautics, Lake Buena Vista, FL, 01-03 July 1996.
[104] Lux, J., and Burkes, D. A. "Hyper-X (X-43A) Flight Test Range Operations Overview," NASA/TM-2008-214626, Dryden Flight Research Center, NASA, Edwards, CA, January 2008.
[105] Lux-Baumann, J., Dees, R., and Fratello, D. "Control Room Training for the Hyper-X Program Utilizing Aircraft Simulation." *AIAA Modeling and Simulation Technologies Conference and Exhibit*, American Institute of Aeronautics and Astronautics, Keystone, CO, 21 August 2006. https://doi.org/10.2514/6.2006-6264
[106] Lux-Baumann, J., Dees, R., and Fratello, D. "Control Room Training for the Hyper-X Project Utilizing Aircraft Simulation," NASA/TM-2006-213685, Dryden Flight Research Center, NASA, Edwards, CA, November 2006.
[107] Malmuth, N. D., Shalaev, V., and Fedorov, A. "Mathematical Fluid Dynamics of Store and Stage Separation," SC71193.RFRFTV, Rockwell Scientific Company, Thousand Oaks, CA, May 2005.
[108] Mangus, D., Mendelsohn, C., Starin, S., Stengle, T., and Truong, S. "Flight Dynamics Analysis Branch End of Fiscal Year 2002 Report," Flight Dynamics Analysis Branch, Goddard Space Flight Center, NASA, Greenbelt, Maryland, December 2002.
[109] Marshall, L., Bahm, C., Corpening, G., and Sherrill, R. "Overview with Results and Lessons Learned of the X-43A Mach 10 Flight," AIAA-2005-3336. *AIAA/CIRA 13th International Space Planes and Hypersonics Systems and Technologies Conference*, American Institute of Aeronautics and Astronautics, Capua, Italy, 16 May 2005. https://doi.org/10.2514/6.2005-3336
[110] Marshall, L., Corpening, G., and Sherrill, R. "A Chief Engineer's View of the NASA X-43A Scramjet Flight Test." *AIAA/CIRA 13th International Space Planes and Hypersonics Systems and Technologies Conference*, American Institute of Aeronautics and Astronautics, Capua, Italy, 16 May 2005. https://doi.org/10.2514/6.2005-3332
[111] McClinton, C. R., Holland, S. D., Rock, K. E., Engelund, W. C., Voland, R. T., Huebner, L. D., and Rogers, R. C. "Hyper-X Wind Tunnel Program," AIAA-98-0553. *36th AIAA Aerospace Sciences Meeting and Exhibit*, American Institute of Aeronautics and Astronautics, Reno, NV, 12-15 January 1998.
[112] McClinton, C. R., Rausch, V., Sitz, J., and Reukauf, P. "Hyper-X Program Status," AIAA-2001-0828. *39th AIAA Aerospace Sciences Meeting and Exhibit*, American Institute of Aeronautics and Astronautics, Reno, NV, 08-12 January 2001.
[113] McClinton, C. "X-43: Mach 7 and Beyond," Langley Research Center, NASA, Hampton, VA.
[114] McClinton, C. "X-43: Scramjet Power Breaks the Hypersonic Barrier." *44th AIAA Aerospace Sciences Meeting and Exhibit*, [Presentation], American Institute of Aeronautics and Astronautics, Reno, NV, 09 January 2006.
[115] McClinton, C. "X-43 - Scramjet Power Breaks the Hypersonic Barrier: Dryden Lectureship in Research for 2006," AIAA-2006-1. *44th AIAA Aerospace Sciences Meeting and Exhibit*, American Institute of Aeronautics and Astronautics, Reno, NV, 09-12 January 2006. https://doi.org/10.2514/6.2006-1
[116] McClinton, C., Hunt, J., Ricketts, R., Reukauf, P., and Peddie, C. "Airbreathing Hypersonic Technology Vision Vehicles and Development Dreams," AIAA-99-4978. *9th International Space Planes and Hypersonic Systems and Technologies Conference and 3rd Weakly Ionized Gases Workshop*, American Institute of Aeronautics and Astronautics, Norfolk, VA, 01-05 November 1999. https://doi.org/10.2514/6.1999-4978
[117] McClinton, C. R. "High Speed/Hypersonic Aircraft Propulsion Technology Development," RTO-EN-AVT-150. *Advances on Propulsion Technology for High-Speed Aircraft*, Research and Technology Organisation, Neuilly-sur-Seine, France, 2008.

[118] McClinton, C. R., Rausch, V. L., Nguyen, L. T., and Sitz, J. R. "Preliminary X-43 Flight Test Results," *Acta Astronautica*, Vol. 57, No. 2-8, pp. 266-276, 2005. https://doi.org/10.1016/j.actaastro.2005.03.060.

[119] McNamara, J., Friedmann, P., Powell, K., Thuruthimattam, B., and Bartels, R. "Three-Dimensional Aeroelastic and Aerothermoelastic Behavior in Hypersonic Flow." *46th AIAA/ASME/ASCE/AHS/ASC Structures, Structural Dynamics and Materials Conference*, American Institute of Aeronautics and Astronautics, Austin, TX, 18 April 2005. https://doi.org/10.2514/6.2005-2175

[120] Meyer, B. "A Comparison of Computational Results to Transonic Test Data from a Hypersonic Airbreathing Model with Exhaust Simulation," AIAA-2003-4411. *39th AIAA/ASME/SAE/ASEE Joint Propulsion Conference and Exhibit*, American Institute of Aeronautics and Astronautics, Huntsville, AL, 20-23 July 2003. https://doi.org/10.2514/6.2003-4411

[121] Miller, C. "Aerothermodynamic Flight Simulation Capabilities for Aerospace Vehicles," AIAA-98-2600. *20th AIAA Advanced Measurement and Ground Testing Technology Conference*, American Institute of Aeronautics and Astronautics, Albuquerque, NM, 15-18 June 1998. https://doi.org/10.2514/6.1998-2600

[122] Miller, J., Leggett, J., and Kramer-White, J. "Design Development Test and Evaluation (DDT&E) Considerations for Safe and Reliable Human Rated Spacecraft Systems," NASA/TM-2008-215126/Vol II, Langley Research Center, NASA, Hampton, VA, April 2008.

[123] Morelli, E., Derry, S., and Smith, M. "Aerodynamic Parameter Estimation for the X-43A (Hyper-X) from Flight Data," AIAA-2005-5921. *AIAA Atmospheric Flight Mechanics Conference and Exhibit*, American Institute of Aeronautics and Astronautics, San Francisco, CA, 15-18 August 2005. https://doi.org/10.2514/6.2005-5921

[124] Morelli, E. A. "Flight-Test Experiment Design for Characterizing Stability and Control of Hypersonic Vehicles." *U.S. Air Force T&E Days*, American Institute of Aeronautics and Astronautics, Los Angeles, CA, 05-07 February 2008.

[125] Moses, P., Bouchard, K., Vause, R., Pinckney, S., Taylor, L., Ferlemann, S., Leonard, C., Robinson, J., Martin, J., Petley, D., and Hunt, J. "An Airbreathing Launch Vehicle Design with Turbine-Based Low-Speed Propulsion and Dual Mode Scramjet High-Speed Propulsion," AIAA-99-4948. *9th International Space Planes and Hypersonic Systems and Technologies Conference and 3rd Weakly Ionized Gases Workshop*, American Institute of Aeronautics and Astronautics, Norfolk, VA, 01-05 November 1999. https://doi.org/10.2514/6.1999-4948

[126] Nilsen, J. K. "Performance Study of Staging Variables on Two-Stage-to-Orbit Reusable Launch Vehicles," Master's Defense, Department of Aeronautics and Astronautics, Graduate School of Engineering and Management, Air Force Institute of Technology, Air University, Wright-Patterson Air Force Base, OH, March 2005.

[127] Ohlhorst, C. W., Glass, D. E., Bruce, W. E., Lindell, M. C., Vaughn, W. L., Smith, R. W., Dirling, R. B., Hogenson, P. A., Nichols, J. M., Risner, N. W., Thompson, D. R., Kowbel, W., Sullivan, B. J., Koenig, J. R., and Cuneo, J. C. "Development of X-43A Mach 10 Leading Edges." *56th International Astronautical Congress*, Fukuoka, Japan, 17-21 October 2005.

[128] Pak, C. "Aeroservoelastic Stability Analysis of the X-43A Stack," NASA/TM-2008-214635, Dryden Flight Research Center, NASA, Edwards, CA, April 2008.

[129] Parikh, P., Engelund, W., Armand, S., and Bittner, R. "Evaluation of a CFD Method for Aerodynamic Database Development Using the Hyper-X Stack Configuration." *22nd AIAA Applied Aerodynamics Conference and Exhibit*, American Institute of Aeronautics and Astronautics, Providence, RI, 16-19 August 2004.

[130] Peebles, C. *The X-43A Flight Research Program: Lessons Learned on the Road to Mach 10*, edited by Allen, N., *Library of Flight*, American Institute of Aeronautics and Astronautics, Reston, VA, 01 March 2008, p. 311.

[131] Peebles, C. "Learning from Experience: Case Studies of the Hyper-X Project," AIAA-2009-1523. *47th AIAA Aerospace Sciences Meeting including The New Horizons Forum and Aerospace Exposition*, American Institute of Aeronautics and Astronautics, Orlando, FL, 05-08 January 2009. https://doi.org/10.2514/6.2009-1523

[132] Peebles, C. "The X-43 Fin Actuation System Problem – Reliability in Shades of Gray." *Space Conference*, American Institute of Aeronautics and Astronautics, San Jose, CA, 19-21 September 2006.

[133] Peebles, C. *Eleven Seconds into the Unknown: A History of the Hyper-X Program*, edited by Allen, N., *Library of Flight*, American Institute of Aeronautics and Astronautics, Reston, VA, 31 March 2011, p. 342.

[134] Petersen, K. "X-43A Mach 7 Flight: A Defining Moment in Hypersonics," [Presentation], Dryden Flight Research Center, NASA, Edwards, CA.

[135] Quinlan, J., McDaniel, J. C., Drozda, T. G., Lacaze, G., and Oefelein, J. C. "A Priori Analysis of Flamelet-Based Modeling for a Dual-Mode Scramjet Combustor." *50th AIAA/ASME/SAE/ASEE Joint Propulsion Conference*, American Institute of Aeronautics and Astronautics, Cleveland, OH, 28 July 2014. https://doi.org/10.2514/6.2014-3743

[136] Rausch, V., McClinton, C. R., and Crawford, J. L. "Hyper-X: Flight Validation of Hypersonic Airbreathing Technology," Langley Research Center, NASA, Hampton, VA, 01 January 1997.

[137] Rausch, V., McClinton, C., and Sitz, J. "NASA's Hyper-X Program," IAF-00-V.4.01. *51st International Astronautical Congress*, Rio de Janeiro, Brazil, 02-06 October 2000.

[138] Reddy, D. R. "70 Years of Aeropropulsion Research at NASA Glenn Research Center," NASA/TP-2013-216524, Glenn Research Center, NASA, Cleveland, OH, September 2013.

[139] Redifer, M., Lin, Y., Bessent, C. A., and Barklow, C. "The Hyper-X Flight Systems Validation Program," NASA/TM-2007-214620, Dryden Flight Research Center, NASA, Edwards, CA, May 2007.

[140] Reubush, D. "Hyper-X Stage Separation - Background and Status," AIAA-99-4818. *9th International Space Planes and Hypersonic Systems and Technologies Conference and 3rd Weakly Ionized Gases Workshop*, American Institute of Aeronautics and Astronautics, Norfolk, VA, 01-05 November 1999. https://doi.org/10.2514/6.1999-4818

[141] Reubush, D., Martin, J., Robinson, J., Bose, D., and Strovers, B. "Hyper-X Stage Separation--Simulation Development and Results," AIAA-2001-1802. *10th AIAA/NAL-NASDA-ISAS International Space Planes and Hypersonic Systems and Technologies Conference*, American Institute of Aeronautics and Astronautics, Kyoto, Japan, 24-27 April 2001. https://doi.org/10.2514/6.2001-1802

[142] Reubush, D., Nguyen, L., and Rausch, V. "Review of X-43A Return to Flight Activities and Current Status." *12th AIAA International Space Planes and Hypersonic Systems and Technologies*, American Institute of Aeronautics and Astronautics, Norfolk, VA, 15 December 2003. https://doi.org/10.2514/6.2003-7085

[143] Rivers, H. K., and Glass, D. "Advances in Hot-Structure Development." *5th European Workshop on Thermal Protection Systems and Hot Structures*, Noordwiji, Netherlands, 17 May 2006.

[144] Robinson, J., and Martin, J. "SACD's Support of the Hyper-X Program," AIAA-2006-7031. *11th AIAA/ISSMO Multidisciplinary Analysis and Optimization Conference*, American Institute of Aeronautics and Astronautics, Portsmouth, VA, 06-08 September 2006. https://doi.org/10.2514/6.2006-7031

[145] Rogers, R., Capriotti, D., and Guy, R. "Experimental Supersonic Combustion Research at NASA Langley," AIAA-98-2506. *20th AIAA Advanced Measurement and Ground Testing Technology Conference*, American Institute of Aeronautics and Astronautics, Albuquerque, NM, 15-18 June 1998. https://doi.org/10.2514/6.1998-2506
[146] Rogers, R., Shih, A., and Hass, N. "Scramjet Development Tests Supporting the Mach 10 Flight of the X-43," AIAA-2005-3351. *AIAA/CIRA 13th International Space Planes and Hypersonics Systems and Technologies Conference*, American Institute of Aeronautics and Astronautics, Capua, Italy, 16 May 2005. https://doi.org/10.2514/6.2005-3351
[147] Rogers, R., Shih, A., Tsai, C.-Y., and Foelsche, R. "Scramjet Tests in a Shock Tunnel at Flight Mach 7, 10, and 15 Conditions," AIAA-2001-3241. *37th AIAA/ASME/SAE/ASEE Joint Propulsion Conference and Exhibit*, American Institute of Aeronautics and Astronautics, Salt Lake City, UT, 09-11 July 2001. https://doi.org/10.2514/6.2001-3241
[148] Schultz, J. *Crafting Flight: Aircraft Pioneers and the Contributions of the Men and Women of NASA Langley Research Center, NASA History Series*, 2003.
[149] Smith, R., Sikora, J., and Lindell, M. C. "Test and Analysis of a Hyper-X Carbon-Carbon Leading Edge Chine," NASA/TM-2005-213765, Langley Research Center, NASA, Hampton, VA, May 2005.
[150] Sparkman, B. "Scramjet Fuel Injection Array Optimization Utilizing Mixed Variable Pattern Search with Kriging Surrogates," Master's Defense, Department of Operational Sciences, Graduate School of Engineering and Management, Air Force Institute of Technology, Air University, Wright-Patterson Air Force Base, OH, March 2008.
[151] Spivey, N. "NASA Armstrong's Structural Dynamics Airworthiness Processes for Aircraft." *NESC Loads & Dynamics TDT Annual Face-to-Face Meeting*, [Presentation], San Diego, CA, 27-29 October 2015.
[152] Stoliker, P., Flick, B., and Cruciani, E. "2004 Research Engineering Annual Report," NASA/TM-2006-213677, Dryden Flight Research Center, NASA, Edwards, CA, June 2006.
[153] Stoliker, P. C., Flick, B., and Cruciani, E. "2003 Research Engineering Annual Report," NASA/TM-2005-212874, Dryden Flight Research Center, NASA, Edwards, CA, July 2005.
[154] Tartabini, P., Bose, D., McMinn, J., Martin, J., and Strovers, B. "Hyper-X Stage Separation Trajectory Validation Studies," AIAA-2003-5819. *AIAA Modeling and Simulation Technologies Conference and Exhibit*, American Institute of Aeronautics and Astronautics, Austin, TX, 11-14 August 2003. https://doi.org/10.2514/6.2003-5819
[155] Tartabini, P., Bose, D., Thornblom, M., Lien, J., and Martin, J. "Mach 10 Stage Separation Analysis for the X43-A." *44th AIAA Aerospace Sciences Meeting and Exhibit*, American Institute of Aeronautics and Astronautics, Reno, NV, 09 January 2006. https://doi.org/10.2514/6.2006-1038
[156] Tartabini, P. V., Roithmayr, C., Toniolo, M. D., Karlgaard, C., and Pamadi, B. N. "Verification of the Constraint Force Equation Methodology for Modeling Multibody Stage Separation," AIAA-2008-7039. *AIAA Modeling and Simulation Technologies Conference and Exhibit*, American Institute of Aeronautics and Astronautics, Honolulu, Hawaii, 18-21 August 2008.
[157] Thomas, D. J. "Design and Analysis of UHTC Leading Edge Attachment," NASA/CR-2002-211505, Glenn Research Center, NASA, Cleveland, OH, July 2002.
[158] Thomas, J. "Flight Test of the Engine Fuel Schedules of the X-43A Hyper-X Research Vehicles," Dryden Flight Research Center, NASA, Edwards, CA, 01 June 2006.
[159] Vachon, M., Grindle, T., St. John, C., and Dowdell, D. "X-43A Fluid and Environmental Systems: Ground and Flight Operation and Lessons Learned." *AIAA/CIRA 13th International Space Planes and Hypersonics Systems and Technologies Conference*, American Institute of Aeronautics and Astronautics, Capua, Italy, 16 May 2005. https://doi.org/10.2514/6.2005-3337
[160] Voland, R., Rock, K., Huebner, L., Witte, D., Fischer, K., and McClinton, C. "Hyper-X Engine Design and Ground Test Program," AIAA-98-1532. *8th AIAA International Space Planes and Hypersonic Systems and Technologies Conference*, American Institute of Aeronautics and Astronautics, Norfolk, VA, 27-30 April 1998. https://doi.org/10.2514/6.1998-1532
[161] Voland, R. T., Huebner, L. D., and McClinton, C. R. "X-43A Hypersonic Vehicle Technology Development," IAC-05-D2.6.01. *56th International Astronautical Congress*, Fukuoka, Japan, 17-21 October 2005.
[162] Woods, W. C., Holland, S. D., and DiFulvio, M. "Hyper-X Stage Separation Wind-Tunnel Test Program," *Journal of Spacecraft and Rockets*, Vol. 38, No. 6, pp. 811-819, 2001. https://doi.org/10.2514/2.3770.

B.3. XB-70 Bibliography

[1] Andrews, W. “Summary of Preliminary Data Derived from the XB-70 Airplanes,” NASA-TM-X-1240, National Aeronautics and Space Administration, Washington, D. C., June 1966.

[2] Anon. "Standard Aircraft Characteristics: B-70 Valkyrie," 57WC-4984, 08 June 1960.

[3] Anon. “Interim Flight Manual: XB-70A,” *USAF Series Aircraft*, United States Air Force, 25 June 1965.

[4] Anon. "Flight Handbook Supplement: XB-70A," USAF Series Aircraft, United States Air Force, 30 September 1964 (Changed 15 February 1967).

[5] Anon. "B-70 Technology Applicable to the Supersonic Transport," NA-62-601, Los Angeles Division, North American Aviation, Los Angeles, CA, 1962.

[6] Anon. “Faster Than a Bullet: Premiere of the North American XB-70A,” *Interavia*, pp. 982-984, 1964.

[7] Anon. “XB-70,” *NASAFacts*, Dryden Flight Research Center, NASA, Edwards, CA, 2003.

[8] Anon. "Estimated Performance of Two G.E. J93-3 Engines," 89B00980R, August 2007.

[9] Anon. “Flight Control Systems: XB-70 Air Vehicle,” NA-60-2, Control Systems Group, North American Aviation, January 1960.

[10] Anon. “Analysis of External Aerodynamic Effect of Inlet Operation on the XB-70 at Mach Numbers of 1.2 to 3.5 in the North American Aviation Trisonic Wind Tunnel and the Ames 8x7 Supersonic Wind Tunnel,” NA-62-575, Aero-Thermo Design, B-70 Division, North American Aviation, June 1962.

[11] Anon. “Estimated Rigit and Flexible Aerodynamic Derivatives for XB-70 Air Vehicle No. 1,” TFD-65-396, Aerodynamics Group, North American Aviation, June 1965 (rev. October 1966).

[12] Arnaiz, H. H. “Flight-Measured Lift and Drag Characteristics of a Large, Flexible, High Supersonic Cruise Airplane,” NASA-TM-X-3532, National Aeronautics and Space Administration, Washington, D. C., May 1977.

[13] Arnaiz, H. H., Peterson, J. B., and Daugherty, J. C. “Wind-Tunnel/Flight Correlation Study of Aerodynamic Characteristics of a Large Flexible Supersonic Cruise Airplane (XB-70-1): III - a Comparison between Characteristics Predicted from Wind-Tunnel Measurements and Those Measured in Flight,” NASA-TP-1516, Dryden Flight Research Center, NASA, Edwards, CA, March 1980.

[14] Arnaiz, H. H., and Schweikhard, W. G. “Validation of the Gas Generator Method of Calculating Jet-Engine Thrust and Evaluation of XB-70-1 Airplane Engine Performance at Ground Static Conditions,” NASA-TN-D-7028, National Aeronautics and Space Administration, Washington, D. C., December 1970.

[15] Baker, P. A., Schweikhard, W. G., and Young, W. R. “Flight Evaluation of Ground Effect on Several Low-Aspect-Ratio Airplanes,” NASA-TN-D-6053, National Aeronautics and Space Administration, Washington, D. C., October 1970.

[16] Bartley, S., Urquidi, N., and Lurie, D. “XB-70, SR-71, & TU-144: Large Supersonic Transports,” [Presentation], Department of Aerospace and Ocean Engineering, Virginia Polytechnic Institute and State University, Blacksburg, VA, 22 March 2006.

[17] Beatovich, G. “A Case Study of Manned Strategic Bomber Acquisition: The B-70 Valkyrie,” Master's Defense, School of Systems and Logistics, Air Force Institute of Technology, Air University, Wright-Patterson Air Force Base, OH, September 1990.

[18] Beaulieu, W., Campbell, R., and Burcham, W. “Measurement of XB-70 Propulsion Performance Incorporating the Gas Generator Method.,” *Journal of Aircraft*, Vol. 6, No. 4, pp. 312-317, 1969. https://doi.org/10.2514/3.44057.

[19] Berry, D. T., and Powers, B. G. “Handling Qualities of the XB-70 Airplane in the Landing Approach,” NASA-TN-D-5676, National Aeronautics and Space Administration, Washington, D. C., February 1970.

[20] Blume, J. A., Sharpe, R. L., Kost, G., and Proulx, J. “Response of Structures to Sonic Booms Produced by XB-70, B-58 and F-104 Aircraft,” AF-49(368)-1739, John A. Blume & Associates Research Division, San Francisco, CA, October 1967.

[21] Boyne, W. J. “The Ride of the Valkyrie,” *AIR FORCE Magazine*, Vol. 89, No. 6, pp. 76-79, Air Force Association, Arlington, VA, June 2006.

[22] Campbell, J. M. *North American XB-70 Valkyrie: The Legacy*, *Schiffer Military History*, Schiffer Publishing, Atglen, PA, 1998, p. 96.

[23] Campbell, J. M., and Pape, G. R. *North American XB-70 Valkyrie: A Photo Chronicle*, *Schiffer Military/Aviation History*, Schiffer Publishing, Atglen, PA, 1996, p. 48.

[24] Child, R. D., and Schlosser, D. C. “Substantiation of the XB-70 Air Vehicle Drag,” NA-61-703-1, North American Aviation, Los Angeles, CA, 28 March 1963.

[25] Conrady, T. “The Experimental Aircraft XB-70 Valkyrie,” *Euroavia News*, pp. 12-14, April 1996.

[26] Cox, T. H., and Jackson, D. W. “Evaluation of High-Speed Civil Transport Handling Qualities Criteria with Supersonic Flight Data,” NASA-TM-4791, Dryden Flight Research Center, NASA, Edwards, CA, 1997.

[27] Cox, T. H., and Marshall, A. “Longitudinal Handling Qualities of the Tu-144LL Airplane and Comparisons with Other Large, Supersonic Aircraft,” NASA/TM-2000-209020, Dryden Flight Research Center, NASA, Edwards, CA, May 2000.

[28] Crede, E., Simpson, A., and Shannon, J. “XB-70 Valkyrie,” [Presentation], Department of Aerospace and Ocean Engineering, Virginia Polytechnic Institute and State University, Blacksburg, VA, 2007.

[29] Daugherty, J. C. “Wind-Tunnel/Flight Correlation Study of Aerodynamic Characteristics of a Large Flexible Supersonic Cruise Airplane (XB-70-1): I - Wind-Tunnel Tests of a 0.03-Scale Model at Mach Numbers from 0.6 to 2.53,” NASA-TP-1514, Ames Research Center, NASA, Moffett Field, CA, November 1979.

[30] Davidson, D. L., and Domal, A. F. "Emission Measurements of a J93 Turbojet Engine," AEDC-TR-73-132, Engine Test Facility, Arnold Engineering Development Center, Air Force Systems Command, Arnold Air Force Station, Tennessee, September 1973.

[31] Davies, P. E. *North American XB-70 Valkyrie*, *X-Planes*, Vol. 7, Osprey Publishing, Oxford, England, United Kingdom, 2018, p. 80.

[32] Domack, C. S. “Results of a Preliminary Investigation of Inlet Unstart on a High-Speed Civil Transport Airplane Concept.” *First Annual NASA High-Speed Research Workshop*, National Aeronautics and Space Administration, Williamsburg, VA, 16 May 1991.

[33] Dussart, G., Lone, M., O'Rourke, C., and Wilson, T. “In-Flight Wingtip Folding: Inspiration from the XB-70 Valkyrie,” *International Journal of Aviation, Aeronautics, and Aerospace*, Vol. 6, No. 3, 2019. https://doi.org/https://doi.org/10.15394/ijaaa.2019.1343.

[34] Eggers, A. J., and Syvertson, C. A. “Aircraft Configurations Developing High Lift-Drag Ratios at High Supersonic Speeds,” NACA-RM-A55L05, National Advisory Committee for Aeronautics, Washington, 5 March 1956.

[35] Ehernberger, L. J. “Meteorological Aspects of High-Altitude Turbulence Encountered by the XB-70 Airplane.” *AIAA 3rd National Conference on Aerospace Meteorology*, American Institute of Aeronautics and Astronautics, New Orleans, LA, 6-9 May 1968.
[36] Ehernberger, L. J. “Atmospheric Conditions Associated with Turbulence Encountered by the XB-70 Airplane above 40,000 Feet Altitude,” NASA-TN-D-4768, National Aeronautics and Space Administration, Washington, D. C., September 1968.
[37] Elmer, K. R., and Joshi, M. C. “Variability of Measured Sonic Boom Signatures.” *NASA HSR Sonic Boom Workshop*, National Aeronautics and Space Administration, Ames Research Center, NASA, 12-14 May 1993.
[38] Elmer, K. R., and Joshi, M. C. “Variability of Measured Sonic Boom Signatures: Volume 2 - Data Report,” NASA-CR-191483, Langley Research Center, NASA, Hampton, VA, January 1994.
[39] Elmer, K. R., and Joshi, M. C. “Variability of Measured Sonic Boom Signatures: Volume 1 - Technical Report,” NASA-CR-191483, Langley Research Center, NASA, Hampton, VA, January 1994
[40] Filippone, A. “Data and Performances of Selected Aircraft and Rotorcraft,” *Progress in Aerospace Sciences*, Vol. 36, No. 8, pp. 629-654, 2000. https://doi.org/10.1016/S0376-0421(00)00011-7.
[41] Findley, D. S., Huckel, V., and Henderson, H. R. “Vibration Responses of Test Structure No. 1 During the Edwards Air Force Base Phase of the National Sonic Boom Program,” NASA-TM-X-72706, Langley Research Center, NASA, Hampton, VA, June 1975.
[42] Fisher, D. F., and Saltzman, E. J. “Local Skin Friction Coefficients and Boundary-Layer Profiles Obtained in Flight from the XB-70-1 Airplane at Mach Numbers up to 2.5,” NASA-TN-D-7220, National Aeronautics and Space Administration, Washington, D. C., June 1973.
[43] Foxworth, T. G. “North American XB-70: Half Airplane - Half Spacecraft Part I,” *Historical Aviation Album: All American Series*, Vol. VII, pp. 76-87, Historical Aviation Album, Temple City, CA, 1969.
[44] Freschl, E., and Steel, E. S. “Development of the XB-70A Propulsion System.,” *Journal of Aircraft*, Vol. 3, No. 2, pp. 147-153, 1966. https://doi.org/10.2514/3.43719.
[45] Fulton, F. L. “Lessons from the XB-70 as Applied to the Supersonic Transport.” *21st Annual International Air Safety Seminar*, Anaheim, CA, 7-11 October 1968.
[46] Gainer, T. G. “Low-Speed Investigation of Effects of Vertical Tails on the Static Stability Characteristics of a Canard-Bomber Configuration Having a Very Thin Wing and a Slender Elliptical Fuselage,” NASA-TM-X-436, Langley Research Center, NASA, Langley Field, VA, January 1961.
[47] Gallagher, R. J. “Investigation of a Digital Simulation of the XB-70 Inlet and Its Application to Flight-Experienced Free-Stream Disturbances at Mach Numbers of 2.4 to 2.6,” NASA-TN-D-5827, National Aeronautics and Space Administration, Washington, D. C., June 1970.
[48] Goecke, S. A. “Flight-Measured Base Pressure Coefficients for Thick Boundary-Layer Flow over an Aft-Facing Step for Mach Numbers from 0.4 to 2.5,” NASA-TN-D-7202, National Aeronautics and Space Administration, Washington, D. C., May 1973.
[49] Greene, L. P. “Airframe Systems Design Evaluation,” *AGARD Preliminary Design Aspects of Military Aircraft*, March 1970.
[50] Griffin, J. A., and Gable, F. A. “XB-70A Electrical System - a Unique Environment for Equipment,” ASME Publication.
[51] Hallion, R. P. *NASA's Contributions to Aeronautics*, Vol. 2, National Aeronautics and Space Administration, Washington, D.C., 2010.
[52] Hatton, W. H., and Modiest, L. J. “The XB-70 Reliability Program.” *Symposium on Deep Submergence Propulsion and Marine Systems*, American Institute of Aeronautics and Astronautics, Forest Park, IL, 28 February 1966.
[53] Incrocci, T. P., and Scoggins, J. R. “An Investigation of the Relationships between Mountain-Wave Conditions and Clear Air Turbulence Encountered by the XB-70 Airplane in the Stratosphere,” NASA-CR-1878, National Aeronautics and Space Administration, Washington D.C., July 1971.
[54] Irwin, K. S., and Andrews, W. H. “Summary of XB-70 Airplane Cockpit Environmental Data,” NASA-TN-D-5449, National Aeronautics and Space Administration, Washington, D.C., October 1969.
[55] Jenkins, D., and Landis, T. *Valkyrie: North American's Mach 3 Superbomber*, Specialty Press, North Branch, MN, 2004, p. 264.
[56] Jenkins, J. M., DeAngelis, V. M., Friend, E. L., and Monaghan, R. C. “Flight Measurements of Canard Loads, Canard Buffeting, and Elevon and Wing-Tip Hinge Moments on the XB-70 Aircraft Including Comparisons with Predictions,” NASA-TN-D-5359, National Aeronautics and Space Administration, Washigton, D.C., August 1969.
[57] Jones, L. S. *U.S. Bombers: B1-B70*, Aero Publishers, Fallbrook, CA, 1966, p. 237.
[58] Jung, T. P., Starkey, R. P., and Argrow, B. “Modified Linear Theory Sonic Booms Compared to Experimental and Numerical Results,” *Journal of Aircraft*, Vol. 52, No. 6, pp. 1821-1837, 2015. https://doi.org/10.2514/1.C033088.
[59] Kordes, E. E., and Love, B. J. “Preliminary Evaluation of XB-70 Airplane Encounters with High-Altitude Turbulence,” NASA-TN-D-4209, National Aeronautics and Space Administration, Washington, D. C., October 1967.
[60] Larson, T. J., and Schweikhard, W. G. “Verification of Takeoff Performance Predictions for the XB-70 Airplane,” NASA-TM-X-2215, National Aeronautics and Space Administration, Washington, D. C., March 1971.
[61] Lasagna, P. L., and McLeod, N. J. “Preliminary Measured and Predicted XB-70 Engine Noise,” NASA-TM-X-1565, National Aeronautics and Space Administration, Washington, D. C., April 1968.
[62] Lasagna, P. L., and Putnam, T. W. “Engine Exhaust Noise During Ground Operation of the XB-70 Airplane,” NASA-TN-D-7043, National Aeronautics and Space Administration, Washington, D. C., January 1971.
[63] Lewis, T. J., Dods, J. B., and Hanly, R. D. “Measurements of Surface-Pressure Fluctuations on the XB-70 Airplane at Local Mach Numbers up to 2.45,” National Aerospace and Space Administration, Washington, D. C., March 1973.
[64] Lock, W. P., Kordes, E. E., McKay, J. M., and Wykes, J. H. “Flight Investigation of a Structural Mode Control System for the XB-70 Aircraft,” NASA-TN-D-7420, National Aeronautics and Space Administration, Washington, D. C., October 1973.
[65] Lorell, M. A., Saunders, A., and Levaux, H. P. *Bomber R & D since 1945: The Role of Experience*, RAND, Santa Monica, CA, 1995, p. 77.
[66] Maglieri, D., Sothcott, V., and Hicks, J. “Influence of Vehicle Configuration and Flight Profile on X-30 Sonic Booms.” *AIAA 2nd International Aerospace Planes Conference*, American Institute of Aeronautics and Astronautics, Orlando, FL, 29-31 October 1990. https://doi.org/10.2514/6.1990-5224
[67] Maglieri, D. J., Henderson, H. R., and Tinetti, A. F. “Measured Sonic Boom Signatures Above and Below the XB-70 Airplane Flying at Mach 1.5 and 37,000 Feet,” NASA/CR-2011-217077, Langley Research Center, NASA, Hampton, VA, April 2011.

[68] Maglieri, D. J., Sothcott, V. E., and Keefer, T. N. “A Summary of XB-70 Sonic Boom Signature Data,” NASA-CR-189630, Eagle Engineering, Inc., Hampton, VA, April 1992.
[69] Martin, A. W., and Beaulieu, W. D. “XB-70 Flight Test Data Comparisons with Simulation Predictions of Inlet Unstart and Buzz,” NASA-CR-1631, National Aeronautics and Space Administration, Washington, D. C., June 1970.
[70] Martin, R. A. “Dynamic Analysis of XB-70-1 Inlet Pressure Fluctuations During Takeoff and Prior to a Compressor Stall at Mach 2.5,” NASA-TN-D-5826, National Aeronautics and Space Administration, Washington, D. C., June 1970.
[71] Mason, W. H. "Some Supersonic Aerodynamics," [Presentation], Department of Aerospace and Ocean Engineering, Virginia Polytechnic Institute and State University, Blacksburg, VA.
[72] Mason, W. H. "Supersonic Aerodynamics," Department of Aerospace and Ocean Engineering, Virginia Polytechnic Institute and State University, Blacksburg, VA, 31 July 2016.
[73] Matranga, G., and Schweikhard, W. G. “Early Supersonic Flight and Technology Contributions at Edwards AFB in Retrospect.” *AIAA Guidance, Navigation, and Control Conference and Exhibit*, American Institute of Aeronautics and Astronautics, Austin, TX, 11-14 August 2003. https://doi.org/10.2514/6.2003-5766
[74] McKay, J. M., Kordes, E. E., and Wykes, J. H. “Flight Investigation of XB-70 Structural Response to Oscillatory Aerodynamic Shaker Excitation and Correlation with Analytical Results,” NASA-TN-D-7227, National Aeronautics and Space Administration, Washington, D. C., April 1973.
[75] McLeod, N. J. “Acoustic Attenuation Determined Experimentally During Engine Ground Tests of the XB-70 Airplane and Comparison with Predictions,” NASA-TM-X-2223, National Aeronautics and Space Administration, Washington, D. C., March 1971.
[76] Nangia, R. K. “Assessment of Air Vehicle Design Evolution over Mach Number and Altitude Operating Envelope with and without S&C Considerations as Part of the Design Synthesis,” Defense Technical Information Center, Fort Belvoir, VA, August 2011.
[77] Nicolai, L. M., and Carichner, G. E. *Fundamentals of Aircraft and Airship Design Volume I - Aircraft Design*, *AIAA Education Series*, American Institute of Aeronautics and Astronautics, Reston, VA, 2010, p. 881.
[78] Oliveira, P. D., and Libeau, M. “The Blackbird, Revisited in Blacksburg,” [Presentation], Department of Aerospace and Ocean Engineering, Virginia Polytechnic Institute and State University, Blacksburg, VA, 21 April 2000.
[79] Pace, S. *North American Valkyrie XB-70A*, *Aero Series*, Vol. 30, Aero Publishers, Fallbrook, CA, 1984, p. 104.
[80] Petersen, R. H. “The Effects of Wing-Tip Droop on the Aerodynamic Characteristics of a Delta-Wing Aircraft at Supersonic Speeds,” NASA-TM-X-363, National Aeronautics and Space Administration, Washington, May 1960.
[81] Peterson, J. B., Mann, M. J., Sorrells, R. B., Sawyer, W. C., and Fuller, D. E. “Wind-Tunnel/Flight Correlation Study of Aerodynamic Characteristics of a Large Flexible Supersonic Cruise Airplane (XB-70-1): II - Extrapolation of Wind-Tunnel Data to Full-Scale Conditions,” NASA-TP-1515, Langley Research Center, NASA, Hampton, VA, February 1980.
[82] Pike, I. “B-70: The State-of-the-Art Improver Part 2,” *Flight International*, pp. 18-24, 2 July 1964.
[83] Pike, I. “B-70: The State-of-the-Art Improver Part 1,” *Flight International*, pp. 1055-1062, 25 June 1964.
[84] Polhamus, E. C. “A Concept of the Vortex Lift of Sharp-Edge Delta Wings Based on a Leading-Edge-Suction Analogy,” NASA-TN-D-3767, National Aeronautics and Space Administration, Washington, D. C., December 1966.
[85] Powers, B. G. “Statistical Survey of XB-70 Airplane Responses and Control Usage with an Illustration of the Application to Handling Qualities Criteria,” NASA-TN-D-6872, National Aeronautics and Space Administration, Washington, D. C., July 1972.
[86] Powers, B. G. “A Review of Transport Handling-Qualities Criteria in Terms of Preliminary XB-70 Flight Experience,” NASA-TM-X-1584, National Aeronautics and Space Administration, Washington, D. C., May 1968.
[87] Putnam, T. W., and Smith, R. H. “XB-70 Compressor-Noise Reduction and Propulsion-System Performance for Choked Inlet Flow,” NASA-TN-D-5692, National Aeronautics and Space Administration, Washington, D. C., March 1970.
[88] Razgonyaev, V., and Mason, W. H. “An Evaluation of Aerodynamic Prediction Methods Applied to the XB-70 for Use in High Speed Aircraft Stability and Control System Design.” *33rd Aerospace Sciences Meeting and Exhibit*, American Institute of Aeronautics and Astronautics, Reno, NV, 9-12 January 1995. https://doi.org/10.2514/6.1995-759
[89] Remak, J., and Ventolo, J. *XB-70 Valkyrie: The Ride to Valhalla*, MBI Publishing Company, Osceola, WI, 1998, p. 128.
[90] Roedts, R., Somero, R., and Waskiewicz, C. “XB-70 Valkyrie,” [Presentation], Department of Aerospace and Ocean Engineering, Virginia Polytechnic Institute and State University, Blacksburg, VA, 2005.
[91] Rogerson, D. B. “Technological Advancements Resulting from XB-70 Performance Requirements,” SAE Technical Paper 650798. *Aeronautic and Space Engineering and Manufacturing Meeting*, February 1965. https://doi.org/10.4271/650798
[92] Ross, J., and Rogerson, D. “XB-70 Technology Advancements.” *Aircraft Prototype and Technology Demonstrator Symposium*, American Institute of Aeronautics and Astronautics, Dayton, OH, 23-24 March 1983.
[93] Saltzman, E. J., and Ayers, T. G. “Selected Examples of NACA/NASA Supersonic Flight Research,” NASA-SP-513, Dryden Flight Research Center, NASA, Edwards, CA, May 1995.
[94] Saltzman, E. J., Goecke, S. A., and Pembo, C. “Base Pressure Measurements on the XB-70 Airplane at Mach Numbers from 0.4 to 3.0,” NASA-TM-X-1612, National Aeronautics and Space Administration, Washington, D. C., September 1968.
[95] Simons, G. M. *Valkyrie the North American XB-70: The USA's Ill-Fated Supersonic Heavy Bomber*, Pen & Sword Aviation, Barnsley, South Yorkshire, England, United Kingdom, 2015, p. 256.
[96] Sisk, T. R., and Andrews, W. “Utilization of Existing Aircraft in Support of Supersonic-Transport Research Programs.” *Testing of Manned Flight Systems Conference*, American Institute of Aeronautics and Astronautics, Edwards Air Force Base, CA, 04-06 December 1963.
[97] Sisk, T. R., Irwin, K. S., and McKay, J. M. “Review of the XB-70 Flight Program.” *NASA Conference on Aircraft Operating Problems*, National Aeronautics and Space Administration, Langley Research Center, NASA, Hampton, VA, 10-12 May 1965.
[98] Smith, R. E., and Lum, E. L. “Linear Optimal Control Theory and Angular Acceleration Sensing Applied to Structural Bending Control on the XB-70,” AFFDL-TR-66-88, February 1967.
[99] Smith, R. H., and Schweikhard, W. G. “Initial Flight Experience with the XB-70 Air-Induction System.” *Conference on Aircraft Aerodynamics*, National Aeronautics and Space Administration, Flight Research Center, NASA, Edwards, CA, May 1966.
[100] Soban, D. S. “Subsonic Wing Optimization for Handling Qualities Using ACSYNT,” Master's Defense, Aeronautical Engineering, California Polytechnic State University, October 1996.

[101] Sotham, J. “The Legend of the Valkyrie,” *Air & Space*, pp. 46-57, September 1999.
[102] Spivak, W. A. "XB-70A Mach 3 Design and Operating Experiences," SAE Transactions, Vol. 75, No. 2, pp. 114-126, 1967.
[103] Stenton, T. E. “Theoretical Frequency Response Functions and Power Spectra of the XB-70 Response to Atmospheric Turbulence,” NASA-CR-1621, National Aeronautics and Space Administration, Washington, D. C., August 1970.
[104] Stricker, J. M. “The Gas Turbine Engine Conceptual Design Process- an Integrated Approach.” *Design Principles and Methods for Aircraft Gas Turbine Engines*, Research and Technology Organisation, Toulouse, France, 11-15 May 1998.
[105] Tanner, C. S., and McLeod, N. J. “Preliminary Measurements of Take-Off and Landing Noise from a New Instrumented Range.” *NASA Conference on Aircraft Operating Problems*, National Aeronautics and Space Administration, Langley Research Center, NASA, Hampton, VA, 10-12 May 1965.
[106] Taube, L. J. “B-70 Aircraft Study Final Report: Volume I,” SD-72-SH-0003, Space Division, North American Rockwell, April 1972.
[107] Taube, L. J. “B-70 Aircraft Study Final Report: Volume II,” SD-72-SH-0003, Space Division, North American Rockwell, April 1972.
[108] Taube, L. J. “B-70 Aircraft Study Final Report: Volume III,” SD-72-SH-0003, Space Division, North American Rockwell, April 1972.
[109] Taube, L. J. “B-70 Aircraft Study Final Report: Volume IV,” SD-72-SH-0003, Space Division, North American Rockwell, April 1972.
[110] Taylor, J. W. *North American Valkyrie: XB-70*, *Jane's All the World's Aircraft 1965-66*, Jane's All the World's Aircraft Publishing, England, United Kingdom, 1965, p. 533.
[111] Thorpe, D. G., Escher, D., and Rhodes, R. E. “Sub-Orbital Passenger Aircraft for Space Launch Operations.” *51st AIAA/SAE/ASEE Joint Propulsion Conference*, American Institute of Aeronautics and Astronautics, Orlando, FL, 27-29 July 2015. https://doi.org/10.2514/6.2015-3894
[112] Tinetti, A. F., Maglieri, D. J., Driver, C., and Bobbitt, P. J. “Equivalent Longitudinal Area Distributions of the B-58 and XB-70-1 Airplanes for Use in Wave Drag and Sonic Boom Calculations,” NASA/CR-2011-217078, Langley Research Center, NASA, Hampton, VA, March 2011.
[113] Walker, H. J. “Performance Evaluation Method for Dissimilar Aircraft Designs,” NASA-RP-1042, Dryden Flight Research Center, NASA, Edwards, CA, September 1979.
[114] Wilson, R. J., and Larson, R. R. “Statistical Analysis of Landing-Contact Conditions for the XB-70 Airplane,” NASA-TN-D-4007, National Aeronautics and Space Administration, Washington, D. C., June 1967.
[115] Wilson, R. J., Love, B. J., and Larson, R. R. “Evaluation of Effects of High-Altitude Turbulence Encounters on the XB-70 Airplane,” NASA-TN-D-6457, National Aeronautics and Space Administration, Washington, D. C., July 1971.
[116] Wilson, R. J., and McKay, J. M. “Landing Loads and Accelerations of the XB-70-1 Airplane,” NASA-TN-D-4836, National Aeronautics and Space Administration, Washington, D. C., October 1968.
[117] Wolowicz, C. H. “Analysis of an Emergency Deceleration and Descent of the XB-70-1 Airplane Due to Engine Damage Resulting from Structural Failure,” NASA-TM-X-1195, National Aeronautics and Space Administration, Washington, D. C., March 1966.
[118] Wolowicz, C. H., Strutz, L. W., Gilyard, G. B., and Matheny, N. W. “Preliminary Flight Evaluation of the Stability and Control Derivatives and Dynamic Characteristics of the Unaugmented XB-70-1 Airplane Including Comparisons with Predictions,” NASA-TN-D-4578, National Aeronautics and Space Administration, Washington, D. C., May 1968.
[119] Wolowicz, C. H., and Yancey, R. B. “Comparison of Predictions of the XB-70-1 Longitudinal Stability and Control Derivatives with Flight Results for Six Flight Conditions,” NASA-TM-X-2881, National Aeronautics and Space Administration, Washington, D. C., August 1973.
[120] Wolowicz, C. H., and Yancey, R. B. “Summary of Stability and Control Characteristics of the XB-70 Airplane,” NASA-TM-X-2933, National Aeronautics and Space Administration, Washington, D. C., October 1973.
[121] Wykes, J. H., and Lawrence, R. E. “Estimated Performance and Stability and Control Data for Correlation with XB-70-1 Flight Test Data,” Los Angeles Division, North American Rockwell, Los Angeles, CA, July 1971.
[122] Wykes, J. H., and Mori, A. S. “XB-70 Aerodynamic, Geometric, Mass, and Symmetric Structural Mode Data,” Los Angeles Division, North American Rockwell, Los Angeles, CA, March 1970.
[123] Wykes, J. H., Nardi, L. U., and Mori, A. S. “XB-70 Structural Mode Control System Design and Performance Analyses,” NASA-CR-1557, National Aeronautics and Space Administration, Washington, D. C., July 1970.

B.4. SR-71 Bibliography

[1] Anderson, E., and Lopata, J. "Using a Modified SR-71 Aircraft and Air-Launched Expendable Rockets to Place Small Payloads into Orbit." *32nd AIAA, ASME, SAE, and ASEE Joint Propulsion Conference and Exhibit*, American Institute of Aeronautics and Astronautics, Lake Buena Vista, FL, 1-3 July 1996. https://doi.org/10.2514/6.1996-2774

[2] Anderson, E., Lopata, J., Hoar, P., and Nelson, D. "Performance Analysis and Optimized Design of an SR-71 Based Air Launch System for Small Payloads." *33rd AIAA/ASME/SAE/ASEE Joint Propulsion Conference and Exhibit*, American Institute of Aeronautics and Astronautics, Seattle, WA, 06-09 July 1997. https://doi.org/10.2514/6.1997-3123

[3] *AVD Internal*----------

[4] *AVD Internal*----------

[5] Anon. "Functional Check Flight Procedures: SR-71A and SR-71B Aircraft," SR-71-6CF-1, Technical Manual, 1 March 1986.

[6] Anon. "Black Shield Mission BX6723," NPIC/R-194/67, National Photographic Interpretation Center, 17 September 1967.

[7] Anon. "Inventing the SR-71 Engine Inlets," *Air & Space Magazine*, Smithsonian Institute, Washington, D. C., 22 March 2006.

[8] Anon. "SR-71 Current Status," 24 January 1996.

[9] Anon. "SR-71A Flight Manual," 25 May 1987.

[10] Anon. "Black Shield," *Air Force Magazine*, Air Force Association, Arlington, VA, 30 August 2008.

[11] Anon. "The Oxcart Story," *Air Force Magazine*, Air Force Association, Arlington, VA, 30 August 2008.

[12] Anon. *Lockheed SR-71 Supersonic/Hypersonic Research Facility Researcher's Handbook*, Vol. II: Technical Description, Lockheed Advanced Development Company, Palmdale, CA, 1995.

[13] Anon. "Deactivation of the SR-71 Program at Beal Air Force Base, California," Department of the Air Force Headquarters, Strategic Air Command, Offutt Air Force Base, NE, July 1989.

[14] Anon. "SR-71 Group Weight Estimate," May 1966.

[15] Bartley, S., Urquidi, N., and Lurie, D. "XB-70, SR-71, & TU-144: Large Supersonic Transports," [Presentation], Department of Aerospace and Ocean Engineering, Virginia Polytechnic Institute and State University, Blacksburg, VA, 22 March 2006.

[16] Bouchard, G. "Lockheed Advanced Development Company (LADC), Aka Skunkworks, May 12, 1993," 25 July 1995.

[17] Boyne, W. J. "The Early Overflights," *Air Force Magazine*, Air Force Association, Arlington, VA, 2 July 2008.

[18] Boyne, W. J. "Reconnaissance on the Wing," *Air Force Magazine*, Air Force Association, Arlington, VA, 10 July 2008.

[19] Byrnes, D. A., Byrnes, S. L., Hurley, K. D., and Hurley, J. *Blackbird Rising: Birth of an Aviation Legend*, Sage Mesa Publications, Los Lunas, NM, 1999.

[20] Colville, J., and Lewis, M. "An Aerodynamic Redesign of the SR-71 Inlet with Applications to Turbine Based Combined Cycle Engines." *40th AIAA/ASME/SAE/ASEE Joint Propulsion Conference and Exhibit*, American Institute of Aeronautics and Astronautics, Fort Lauderdale, FL, 11-14 July 2004. https://doi.org/10.2514/6.2004-3481

[21] Colville, J., Starkey, R., and Lewis, M. "Extending the Flight Mach Number of the SR-71 Inlet." *AIAA/CIRA 13th International Space Planes and Hypersonics Systems and Technologies Conference*, American Institute of Aeronautics and Astronautics, Capua, Italy, 16-20 May 2005. https://doi.org/10.2514/6.2005-3284

[22] Conners, T. R. "Predicted Performance of a Thrust-Enhanced SR-71 Aircraft with an External Payload," NASA-TM-104330, Dryden Flight Research Center, NASA, Edwards, CA, 1997.

[23] Corda, S., Moes, T. R., Mizukami, M., Hass, N., Jones, D., Monaghan, R. C., Ray, R. J., Jarvis, M. L., and Palumbo, N. "The SR-71 Test Bed Aircraft: A Facility for High-Speed Flight Research," NASA/TP-2000-209023, Dryden Flight Research Center, NASA, Edwards, CA, June 2000.

[24] Corda, S., Neal, B. A., Moes, T. R., Cox, T. H., Monaghan, R. C., Voelker, L. S., Corpening, G. P., Larson, R. R., and Powers, B. G. "Flight Testing the Linear Aerospike SR-71 Experiment (LASRE)," NASA/TM-1998-206567, Dryden Flight Research Center, Edwards, CA, September 1998.

[25] Cox, T. H., and Jackson, D. "Supersonic Flying Qualities Experience Using the SR-71." *Atmospheric Flight Mechanics*, American Institute of Aeronautics and Astronautics, New Orleans, LA, 11-13 August 1997.

[26] Cox, T. H., and Jackson, D. W. "Evaluation of High-Speed Civil Transport Handling Qualities Criteria with Supersonic Flight Data," NASA-TM-4791, Dryden Flight Research Center, Edwards, CA, 1997.

[27] Cox, T. H., and Marshall, A. "Longitudinal Handling Qualities of the Tu-144LL Airplane and Comparisons with Other Large, Supersonic Aircraft," NASA/TM-2000-209020, Dryden Flight Research Center, NASA, Edwards, CA, May 2000.

[28] Crickmore, P. *SR-71 Blackbird: Lockheed's Mach 3 Hot Shot, Osprey Colour Series*, Osprey Publishing, London, England, United Kingdom, 1987, p. 128.

[29] Crickmore, P. *Lockheed SR-71: The Secret Missions Exposed*, Osprey Publishing, London, England, United Kingdom, 1993, p. 222.

[30] Crickmore, P. *Lockheed's Black World Skunk Works: The U-2, SR-71, and F-117*, Osprey Publishing, Oxford, England, United Kingdom, 2000, p. 112.

[31] Crickmore, P. *Lockheed A-12: The CIA's Blackbird and Other Variants, Air Vanguard*, Vol. 12, Osprey Publishing, Oxford, England, United Kingdom, 2014, p. 64.

[32] Davies, S., and Crickmore, P. *Lockheed SR-71, Haynes Owners' Workshop Manual*, Haynes Publishing, Somerset, England, United Kingdom, 2012, p. 156.

[33] DeHart, R. M. "High Altitude Radiation Exposure in the SR-71: A Preliminary Report," Air War College, Air University, Maxwell Air Force Base, AL, April 1974.

[34] Drendel, L. *SR-71 Blackbird in Action*, Squadron/Signal Publications, Carrollton, TX, 1982, p. 50.

[35] Elam, S. K. "Test Report for NASA MSFC Support of the Linear Aerospike SR-71 Experiment (LASRE)," NASA/TM-2000-210076, Marshall Space Flight Center, NASA, Marshall Space Flight Center, AL, February 2000.

[36] Ennix, K. A., and Corpening, G. P. "Evaluation of the Linear Aerospike SR-71 Experiment (LASRE) Oxygen Sensor," NASA/TM-1999-206589, Dryden Flight Research Center, NASA, Edwards, CA, November 1999.

[37] Fouladi, K. "CFD Predictions of Sonic-Boom Characteristics for Unmodified and Modified SR-71 Configurations." *High-Speed Research: 1994 Sonic Boom Workshop*, National Aeronautics and Space Administration, Hampton, VA, 1-3 June 1999.

[38] Goodall, J. *SR-71 Blackbird*, Squadron/Signal Publications, Carrollton, TX, 1995, p. 80.

[39] Goodall, J., and Miller, J. *Lockheed's SR-71 'Blackbird' Family: A-12, F-12, M-21, D-21, SR-71*, Midland Publishing, Hinckley, England, United Kingdom, 2002, p. 128.

[40] Graham, R. H. *The Complete Book of the SR-71 Blackbird*, Zenith Press, Minneapolis, MN, 2015, p. 288.

[41] Green, K. S., and Putnam, T. W. "Measurements of Sonic Booms Generated by an Airplane Flying at Mach 3.5 and 4.8," NASA-TM-X-3126, National Aeronautics and Space Administration, Washington, D. C., October 1974.

[42] Haering, E. A., Ehernberger, L. J., and Whitemore, S. A. "Preliminary Airborne Measurements for the SR-71 Sonic Boom Propagation Experiment." *NASA High Speed Research Program Sonic Boom Workshop*, National Aeronautics and Space Administration, Hampton, VA, 11-13 September 1995.

[43] Haering, E. A., Whitmore, S. A., and Ehernberger, L. J. "Measurement of the Basic SR-71 Airplane Near-Field Signature." *High-Speed Research: 1994 Sonic Boom Workshop*, National Aeronautics and Space Administration, Hampton, VA, 1-3 June 1994.

[44] Hallion, R. P. *NASA's Contributions to Aeronautics*, Vol. 2, National Aeronautics and Space Administration, Washington, D.C., 2010.

[45] Hass, N., Mizukami, M., Neal, B. A., St. John, C., Beil, R. J., and Griffin, T. P. "Propellant Feed System Leak Detection: Lessons Learned from the Linear Aerospike SR-71 Experiment (LASRE)," NASA/TM-1999-206590, Dryden Flight Research Center, NASA, Edwards, CA, November 1999.

[46] Hildebrant, D. "Time Line of the SR-71," 2002.

[47] Iorio, C., and Lind, R. "Parameter Estimation of the SR-71 Fuselage Dynamics Using an Additive Beam Model." *39th AIAA/ASME/ASCE/AHS/ASC Structures, Structural Dynamics, and Materials Conference and Exhibit*, American Institute of Aeronautics and Astronautics, Long Beach, CA, 20-23 April 1998. https://doi.org/10.2514/6.1998-1730

[48] Iorio, C., Napolitano, M., Seanor, B., An, Y., and Bowers, A. "Parameter Estimation for the NASA SR-71 Longitudinal and Lateral/Directional Dynamics." *24th Atmospheric Flight Mechanics Conference*, American Institute of Aeronautics and Astronautics, Portland, OR, 09-11 August 1999. https://doi.org/10.2514/6.1999-4172

[49] Ivanteyeva, L. G., Kovalenko, V. V., Pavlyukov, E. V., Teperin, L. L., and Rackl, R. G. "Validation of Sonic Boom Propagation Codes Using SR-71 Flight Test Data," *The Journal of the Acoustical Society of America*, Vol. 111, No. 1, pp. 554-561, January 2002.

[50] Jenkins, D. *Lockheed SR-71/YF-12 Blackbirds, Warbird Tech Series*, Vol. 10, Specialty Press Publishers and Wholesalers, North Branch, MN, 1997, p. 100.

[51] Johnson, C. L., and Smith, M. *Kelly: More Than My Share of It All*, Smithsonian Books, Washington, D. C., 1985, p. 209.

[52] Kloesel, K. J., Ratnayake, N. A., and Clark, C. M. "A Technology Pathway for Airbreathing, Combined-Cycle, Horizontal Space Launch through SR-71 Based Trajectory Modeling." *17th AIAA International Space Planes and Hypersonic Systems and Technologies Conference*, American Institute of Aeronautics and Astronautics, San Francisco, CA, 11-14 April 2011.

[53] Klyde, D. H., and Mitchell, D. G. "Development of Supersonic Demonstration Maneuvers with the NASA SR-71 Aircraft and Simulator." *36th AIAA Aerospace Sciences Meeting and Exhibit*, American Institute of Aeronautics and Astronautics, Reno, NV, 12-15 January 1998. https://doi.org/10.2514/6.1998-493

[54] Larson, R. R. "Automated Testing Experience of the Linear Aerospike SR-71 Experiment (LASRE) Controller," NASA/TM-1999-206588, Dryden Flight Research Center, Edwards, CA, September 1999.

[55] Law, P. "SR-71 Propulsion System P&W J-58 Engine (JT11D-20)," [Presentation].

[56] Lux, D., Ehernberger, L. J., Moes, T. R., and Haering, E. A. "Low-Boom SR-71 Modified Signature Demonstration Program." *High-Speed Research: 1994 Sonic Boom Workshop*, National Aeronautics and Space Administration, Hampton, VA, 1-3 June 1999.

[57] Maglieri, D., Sothcott, V., and Hicks, J. "Influence of Vehicle Configuration and Flight Profile on X-30 Sonic Booms." *2nd AIAA International Aerospace Planes Conference*, American Institute of Aeronautics and Astronautics, Orlando, FL, 29-31 October 1990. https://doi.org/10.2514/6.1990-5224

[58] Maglieri, D. J., Huckel, V., and Henderson, H. R. "Sonic-Boom Measurements for SR-71 Aircraft Operating at Mach Numbers to 3.0 and Altitudes to 24384 Meters," NASA-TN-D-6823, National Aeronautics and Space Administration, Washington, D. C., September 1972.

[59] Mason, W. H. "Some Supersonic Aerodynamics," [Presentation], Department of Aerospace and Ocean Engineering, Virginia Polytechnic Institute and State University, Blacksburg, VA.

[60] Mason, W. H. "Supersonic Aerodynamics," Department of Aerospace and Ocean Engineering, Virginia Polytechnic Institute and State University, Blacksburg, VA, 31 July 2016.

[61] Matranga, G., and Schweikhard, B. "Early Supersonic Flight and Technology Contributions at Edwards AFB in Retrospect." *AIAA Guidance, Navigation, and Control Conference and Exhibit*, American Institute of Aeronautics and Astronautics, Austin, TX, 11-14 August 2003. https://doi.org/10.2514/6.2003-5766

[62] Merlin, P. W. "SR-71 Blackbird," *Advanced Materials & Processes*, Vol. 161, No. 5, pp. 27-29, ASM International, Materials Park, OH, 01 May 2003.

[63] Merlin, P. W. "Design and Development of the Blackbird: Challenges and Lessons Learned." *47th AIAA Aerospace Sciences Meeting including The New Horizons Forum and Aerospace Exposition*, American Institute of Aeronautics and Astronautics, Orlando, FL, 05-08 January 2009. https://doi.org/10.2514/6.2009-1522

[64] Merlin, P. W. "Mach 3 Legend: Design and Development of the Lockheed Blackbird." *2012 National Space and Missile Materials Symposium (NSMMS)*, [Presentation], Tampa, FL, 25-28 June 2012.

[65] Merlin, P. W. *From Archangel to Senior Crown: Design and Development of the Blackbird, Library of Flight*, American Institute of Aeronautics and Astronautics, Reston, VA, 2008, p. 202.

[66] Miller, J. *Lockheed SR-71 (A-12/YF-12/D-21), Aerofax Minigraph*, Vol. 1, Aerofax, inc, Arlington, TX, 1985, p. 40.

[67] Miller, J. *Lockheed Martin's Skunk Works*, Rev. ed., Midland Publishing, Leicester, England, United Kingdom, 1995, p. 216.
[68] Mixon, B., and Chudoba, B. "The Lockheed SR-71 Blackbird - a Senior Capstone Re-Engineering Experience." *45th AIAA Aerospace Sciences Meeting and Exhibit*, American Institute of Aeronautics and Astronautics, Reno, NV, 08-11 January 2007. https://doi.org/10.2514/6.2007-698
[69] Mizukami, M., Corpening, G. P., Ray, R. J., Hass, N., Ennix, K. A., and Lazaroff, S. M. "Linear Aerospike SR-71 Experiment (LASRE): Aerospace Propulsion Hazard Mitigation Systems." *34th Joint Propulsion*, American Institute of Aeronautics and Astronautics, Cleveland, OH, 13-15 July 1998.
[70] Mizukami, M., Jones, D., and Weinstock, V. D. "Flow-Field Survey in the Test Region of the SR-71 Aircraft Test Bed Configuration," NASA/TM-2000-209025, Dryden Flight Research Center, NASA, Edwards, CA, August 2000.
[71] Moes, T. R., Cobleigh, B. R., Conners, T. R., Cox, T. H., Smith, S. C., and Shirakata, N. "Wind-Tunnel Development of an SR-71 Aerospike Rocket Flight Test Configuration," NASA-TM-4749, Dryden Flight Research Center, NASA, Edwards, CA, June 1996.
[72] Moes, T. R., Cobleigh, B. R., Cox, T. H., Conners, T. R., Iliff, K. W., and Powers, B. G. "Flight Stability and Control and Performance Results from the Linear Aerospike SR-71 Experiment (LASRE)." *Atmosphere Flight Mechanics*, American Institute of Aeronautics and Astronautics, Boston, MA, 10-12 August 1998.
[73] Moes, T. R., and Iliff, K. W. "Stability and Control Estimation Flight Test Results for the SR-71 Aircraft with Externally Mounted Experiments," NASA/TP-2002-210718, Dryden Flight Research Center, NASA, Edwards, CA, June 2002.
[74] *AVD Internal*----------
[75] Morgenstern, J. M., Bruns, D. B., and Camacho, P. P. "SR-71A Reduced Sonic Boom Modification Design." *High-Speed Research: 1994 Sonic Boom Workshop*, National Aeronautics and Space Administration, Hampton, VA, 01-03 June 1994.
[76] Nicolai, L. M., and Carichner, G. E. *Fundamentals of Aircraft and Airship Design Volume I - Aircraft Design*, *AIAA Education Series*, American Institute of Aeronautics and Astronautics, Reston, VA, 2010, p. 881.
[77] Norris, S. R., Haering, E. A., and Murray, J. E. "Ground-Based Sensors for the SR-71 Sonic Boom Propagation Experiment." *1995 NASA High-Speed Research Program Sonic Boom Workshop Volume I*, National Aeronautics and Space Administration, Hampton, VA, 12-13 September 1996.
[78] Oliveira, P. D., and Libeau, M. "The Blackbird, Revisited in Blacksburg," [Presentation], Department of Aerospace and Ocean Engineering, Virginia Polytechnic Institute and State University, Blacksburg, VA, 21 April 2000.
[79] Pedlow, G. W., and Welzenbach, D. E. "Chapter 6 - the U-2's Intended Successor: Project Oxcart, 1956-1968," *The Central Intelligence Agency and Overhead Reconnaissance: The U-2 and Oxcart Programs 1954-1974*, Skyhorse Publishing, New York City, NY, 15 March 2016, pp. 259-313.
[80] Peebles, C. *Dark Eagles: A History of Top Secret U.S. Aircraft*, Revised ed., Presidio Press, Novato, CA, 1999, p. 353.
[81] Poling, H. W. "Sonic Boom Propagation Codes Validated by Flight Test," NASA-CR-201634, Langley Research Center, NASA, Hampton, VA, October 1996.
[82] Powers, B. G. "Structural Dynamic Model Obtained from Flight Use with Piloted Simulation and Handling Qualities Analysis," NASA-TM-4747, National Aeronautics and Space Administration, Washington, D. C., 1996.
[83] Reithmaier, L. "Appendix B: Development of the Lockheed SR-71 Blackbird," *Mach 1 and Beyond: The Illustrated Guide to High-Speed Flight*, TAB Books, Blue Ridge Summit, PA, 1995, pp. 219-237.
[84] Ricco, P. "The Heart of the SR-71 "Blackbird" : The Mighty J-58 Engine," 2002. URL: www.aerostories.org
[85] Rich, B. R. "F-12 Series Aircraft Aerodynamic and Thermodynamic Design in Retrospect," *Journal of Aircraft*, Vol. 11, No. 7, pp. 401-406, July 1974. https://doi.org/10.2514/3.60356.
[86] Robarge, D. S. *Archangel: CIA's Supersonic A-12 Reconnaissance Aircraft*, 2nd ed., Center for the Study of Intelligence, Washington, D.C., January 2012.
[87] Suhler, P. A. *From RAINBOW to GUSTO: Stealth and the Design of the Lockheed Blackbirds*, *Library of Flight*, American Institute of Aeronautics and Astronautics, Reston, VA, 2009, p. 284.
[88] Thornborough, A. M., and Davies, P. E. *Lockheed Blackbirds*, Ian Allan Ltd, Shepperton, Surrey, England, United Kingdom, 1988, p. 144.
[89] Thorpe, D. G., Escher, D., and Rhodes, R. E. "Sub-Orbital Passenger Aircraft for Space Launch Operations." *51st AIAA/SAE/ASEE Joint Propulsion Conference*, American Institute of Aeronautics and Astronautics, Orlando, FL, 27-29 July 2015. https://doi.org/10.2514/6.2015-3894
[90] Tomaro, R. F., and Wurtzler, K. E. "High Speed Configuration Aerodynamics: SR-71 to SMV." *17th Applied Aerodynamics Conference*, American Institute of Aeronautics and Astronautics, Norfolk, VA, 28 June 1999. https://doi.org/10.2514/6.1999-3204
[91] Urie, D. "Case Studies in Engineering: The SR-71 Blackbird," Course AE107, California Institute of Technology, Pasadena, CA, 1991.
[92] Whittenbury, J. R. "Lockheed Blackbirds (A-12, YF-12, M-21, and SR-71)," *Fundamentals of Aircraft and Airship Design Volume 2 - Airship Design and Case Studies*, *AIAA Education Series*, American Institute of Aeronautics and Astronautics, Reston, VA, 2011, pp. 431-512.
[93] Xue, H., Khawaja, H., and Moatamedi, M. "Conceptual Design of High Speed Supersonic Aircraft: A Brief Review on SR-71 (Blackbird) Aircraft." *10th International Conference on Mathematical Problems in Engineering, Aerospace and Sciences*, AIP Publishing, Narvik, Norway, 15-18 July 2014. https://doi.org/10.1063/1.4904694
[94] Yenne, B. *Area 51 Black Jets: A History of the Aircraft Developed at Groom Lake, America's Secret Aviation Base*, New ed., Zenith Press, Minneapolis, MN, 06 March 2018, p. 192.

B.5. Concorde Bibliography

[1] *AVD Internal*----------
[2] *AVD Internal*----------
[3] *AVD Internal*----------
[4] Anon. "History of Concorde G-BBDG (202)," *Concorde at Brooklands.* http://www.brooklandsconcorde.com/history.html,
[5] Anon. "Concorde: The Supersonic Passenger Aircraft," Aerospatiale-British Aerospace.
[6] Anon. "BAC-SUD Concorde." http://www.aemann.pwp.blueyonder.co.uk/aircraft/british/concorde.html,
[7] *AVD Internal*----------
[8] Anon. "25 Years Ago...Concorde," p. 62.
[9] Anon. "Additional Considerations for Supersonic Aircraft," *Supersonic Aircraft Fuselage Design.* http://adg.stanford.edu/aa241/fuselayout/sstfuse.html,
[10] Anon. "Accident on 25 July 2000 at La Patte d'Oie in Gonesse (95) to the Concorde Registered F-BTSC Operated by Air France," Report Translation f-sc000725a, BEA, France.
[11] Anon. "The Supersonic Transport: A Factual Basis for Decision," American Institute of Aeronautics and Astronautics, Reston, VA, 01 March 1971.
[12] *AVD Internal*----------
[13] *AVD Internal*----------
[14] *AVD Internal*----------
[15] *AVD Internal*----------
[16] Anon. "Fuel Leak Seals Concorde's Fate," *Flight International*, p. 4, 06-12 May 2003.
[17] *AVD Internal*----------
[18] *AVD Internal*----------
[19] *AVD Internal*----------
[20] *AVD Internal*----------
[21] *AVD Internal*----------
[22] Anon. "Concorde Crash Negotiations Break Down." SPACE.com, http://www.space.com/businesstechnology/business/concorde_breakdown_010108_wg.html, 08 January 2001.
[23] Anon. "Type Certificate Data Sheet No. A45EU," Federal Aviation Administration, Department of Transportation, 09 January 1979.
[24] *AVD Internal*----------
[25] *AVD Internal*----------
[26] *AVD Internal*----------
[27] *AVD Internal*----------
[28] Anon. *Concorde Flying Manual*, Vol. 2(b), British Airways, 11 November 1994.
[29] *AVD Internal*----------
[30] Anon. *Concorde Flying Manual*, Vol. 2(a), British Airways, 11 October 1994.
[31] *AVD Internal*----------
[32] *AVD Internal*----------
[33] *AVD Internal*----------
[34] *AVD Internal*----------
[35] *AVD Internal*----------
[36] *AVD Internal*----------
[37] *AVD Internal*----------
[38] *AVD Internal*----------
[39] *AVD Internal*----------
[40] *AVD Internal*----------
[41] *AVD Internal*----------
[42] *AVD Internal*----------
[43] *AVD Internal*----------
[44] *AVD Internal*----------
[45] *AVD Internal*----------
[46] *AVD Internal*----------
[47] *AVD Internal*----------
[48] *AVD Internal*----------
[49] *AVD Internal*----------
[50] *AVD Internal*----------
[51] *AVD Internal*----------
[52] *AVD Internal*----------
[53] *AVD Internal*----------
[54] Anon. "Concorde Crashes in France." SPACE.com, http://www.space.com/news/concorde_crash_000725.html, 25 July 2000.
[55] *AVD Internal*----------
[56] *AVD Internal*----------
[57] *AVD Internal*----------
[58] Anon. "AFCS: Automatic Flight Control System for SST Concorde," Elliot-Sfena, London, England, 27 May 1971.
[59] *AVD Internal*----------
[60] *AVD Internal*----------
[61] *AVD Internal*----------
[62] *AVD Internal*----------

[63] Anon. “Concorde for the Airlines,” *Flight International*, London, England, 1971.
[64] *AVD Internal*----------
[65] *AVD Internal*----------
[66] *AVD Internal*----------
[67] Anon. “Concorde Engineering Notes Sections 1, 2 & 3,” Commercial Aircraft Division, British Aircraft Corporation, Bristol, England, 1975.
[68] Anon. *Concorde TSS Standards: Supersonic Transport Aircraft*, 1976.
[69] Anon. “Noise-Induced Building Vibrations Caused by Concorde and Conventional Aircraft Operations at Dulles and Kennedy International Airports - Final Report,” NASA-TM-78769, Langley Research Center, NASA, Hampton, VA, 1978.
[70] Anon. “Concorde.” Aircraft Group, British Aerospace, Weybridge, England, 1980, p. 39.
[71] Anon. “Study of High-Speed Civil Transports,” NASA-CR-4235, National Aeronautics and Space Administration, Washington, D. C., 1989.
[72] Anon. *Concorde Flying Manual*, Vol. 1, British Airways, 1990.
[73] *AVD Internal*----------
[74] Anon. *U.S. Supersonic Commercial Aircraft: Assessing NASA’s High Speed Research Program*, National Academy Press, Washington, D.C., 1997.
[75] Anon. “Concorde,” [Lecture Slides], Cranfield University, Cranfield, England, 1997.
[76] Anon. “A Study of Concorde Performance,” *AAE 190*, 2000.
[77] Anon. “Concorde: The Supersonic Passenger Aircraft,” British Aerospace, 2005.
[78] Anon. “De Concorde Aux Nouveaux Projets D’avions Supersoniques,” AAE Dossier #46, Academie de L’Air et de L’Espace, 2019.
[79] Anon. “Design of a New Generation Supersonic Transport Aircraft,” 2019-3332-AJTE-MEC, 2019.
[80] Anon. “Concorde Noise-Induced Building Vibrations: John F. Kennedy International Airport - Report No. 3,” NASA-TM-78727, Langley Research Center, NASA, Hampton, VA, April 1978.
[81] Anon. *Part 1: Advanced High-Speed Aircraft, Impact of Advanced Air Transport Technology*, Office of Technology Assessment, Washington, D. C., April 1980, p. 93.
[82] Anon. “Concorde Noise-Induced Building Vibrations, Montgomery County, Maryland - Report No. 3,” NASA-TM-X-73947, Langley Research Center, NASA, Hampton, VA, August 1976.
[83] *AVD Internal*----------
[84] *AVD Internal*----------
[85] Anon. “Concorde Noise-Induced Building Vibrations, Sully Plantation - Report No. 2, Chantilly, Virginia,” NASA-TM-X-73926, Langley Research Center, NASA, Hampton, VA, June 1976.
[86] Anon. “Concorde Noise-Induced Building Vibrations for Sully Plantation, Chantilly, Virginia,” NASA-TM-X-73919, Langley Research Center, NASA, Hampton, VA, June 1976.
[87] Anon. “21 Years of Supersonic Majesty,” *Aerospace Magazine*, pp. 8-12, March 1997.
[88] *AVD Internal*----------
[89] *AVD Internal*----------
[90] Anon. “Concorde Noise-Induced Building Vibrations: International Airport Dulles - Final Report,” NASA-TM-74083, Langley Research Center, NASA, Hampton, VA, September 1977.
[91] Becker, H. J. *Concorde, Flugzeuge Die Geschichte Machten*, Motorbuch Verlag, Stuttgart, Germany, 1991, p. 149.
[92] Beniada, F., and Fraile, M. *Concorde*, Zenith Press, Minneapolis, MN, 2006.
[93] Berger, J. “A Comparison of Predictions Obtained from Wind Tunnel Tests and the Results from Cruising Flight (Airbus and Concorde),” NASA-TM-75238, National Aeronautics and Space Administration, Washington, D. C., August 1979.
[94] Bohme, F., Cadete, S., and Dannet, G. "Concorde 2.0: On-Going Supersonic Projects." *TMAL02 Expert Conference 2019*, Linkoping University, Linkoping, Sweden, 2019.
[95] *AVD Internal*----------
[96] Burdun, I. Y. “Virtual Test and Evaluation of Air France Concorde Flight No. AF4590: Preliminary Case Study,” 26 July 2000.
[97] Burgess, E. “Concorde Inaugurates the Supersonic Era.” *9th Annual Meeting and Technical Display*, American Institute of Aeronautics and Astronautics, Washington, D. C., 08-10 January 1973. https://doi.org/10.2514/6.1973-16
[98] Cado, and Broihanne. “The Flight Control System for the Concorde Supersonic Civil Transport Aircraft,” Library Translation No. 1615, Royal Aircraft Establishment, July 1973.
[99] Calder, P. H., and Gupta, P. C. “Engine Options for Supersonic Cruise Aircraft.” *AIAA/SAE 14th Joint Propulsion Conference*, American Institute of Aeronautics and Astronautics, Las Vegas, NV, 25-27 July 1978. https://doi.org/10.2514/6.1978-1054
[100] Calvert, B. *Flying Concorde*, Airlife Publishing, Shrewsbury, England, 1989.
[101] Candel, S. “Concorde and the Future of Supersonic Transport,” *Journal of Propulsion and Power*, Vol. 20, No. 1, pp. 59-68, 2004.
[102] Carioscia, S. A., Locke, J. A., Boyd, I. D., Lewis, M. J., and Hallion, R. P. "Commercial Development of Civilian Supersonic Aircraft," IDA Science & Technology Policy Institute, Washington, D. C., August 2019.
[103] Carlier, P., Debelmas, C., Pilon, J. C., and Velot-Lerou, A. “Avant-Projet D’un Avion De Transport Commercial Supersonique,” Aerospatiale, 1992.
[104] Castel, F. “Concorde: A Space Age Relic.” SPACE.com, http://www.space.com/news/concorde_techno_000725.html, 15 June 2005.
[105] Chudoba, B. “Investigation of Inherent Slender-Body Characteristics Using the CONCORDE Simulator,” Cranfield University, Cranfield, England, 27 February 1997.
[106] Chudoba, B. “Primary Control Surfaces on Supersonic Transport Aircraft,” Final Thesis, Fachbereich Flugzeugbau, Fachhochschule Aachen, Aachen, Germany, 1994.
[107] Chudoba, B., Coleman, G., Oza, A., and Czysz, P. A. “What Price Supersonic Speed? A Design Anatomy of Supersonic Transportation Part 1,” *The Aeronautical Journal*, March 2008.
[108] Clark, F. G., and Gibson, A. *Concorde: The Story of the World’s Most Advanced Passenger Aircraft*, Paradise Press.
[109] Coen, P. G. “The Effect of Advanced Technology on the Second-Generation SST.” *AIAA/AHS/ASEE Aircraft Systems, Design and Technology Meeting*, American Institute of Aeronautics and Astronautics, Dayton, OH, 20-22 October 1986. https://doi.org/10.2514/6.1986-2672

[110] Collard, D. “Concorde Airframe Design and Development,” SAE-TP-912162. *Aerospace Technology Conference and Exposition*, SAE International, Long Beach, CA, 23-26 September 1991.
[111] Cormery, G. "Supersonic Transport Vis-a-Vis Energy Savings," NASA-TM-75464, National Aeronautics and Space Administration, Washington, D.C., September 1979.
[112] Cowell, A. “British and French to Halt Concorde Flights.” The New York Times, http://www.nytimes.com/2003/04/10/business/worldbusiness/10CND-CONC.html, 10 April 2003.
[113] Curwen, K. R. “Turbine Blade Pyrometer System in the Control of the Concorde Engine,” *Instrumentation for Airbreathing Propulsion*, Massachusetts Institute of Technology, Cambridge, Massachusetts, 1971, pp. 399-407.
[114] Davies, R. E. G. *Fallacies and Fantasies of Air Transport History*, Paladwr Press, McLean, VA, 1994.
[115] Davies, R. E. G. *Supersonic (Airliner) Non-Sense: A Case Study in Applied Market Research*, Paladwr Press, McLean, VA, 1998.
[116] Domini, A., and Chicot, J. "Case Study Report from Concorde to Airbus," Mission-Oriented R&I Policies: In-Depth Case Studies, European Commission, February 2018.
[117] Donin, R. B. “Safety Regulation of the Concorde Supersonic Transport: Realistic Confinement of the National Environmental Policy Act,” *Transportation Law Journal*, Vol. 8, pp. 47-69, 1976.
[118] Dornheim, M. A. “Concorde Report Uncovers Inflight Fire in 1979 Incident,” *Aviation Week & Space Technology*, pp. 52-54, 04 February 2002.
[119] Dornheim, M. A. “Engine, Fuel Tank Show Damage in 1979 Concorde Incident,” *Aviation Week & Space Technology*, p. 75, 04 September 2000.
[120] Dornheim, M. A. “Concorde Had a Chance until 2nd Engine Failed,” *Aviation Week & Space Technology*, pp. 54-55, 11 September 2000.
[121] Dornheim, M. A. “Details Emerge of Earlier Fuel Tank Penetrations,” *Aviation Week & Space Technology*, pp. 33-34, 28 August 2000.
[122] Dornheim, M. A., and Morrocco, J. D. “BA Plans Concorde Ops into Next Decade,” *Aviation Week & Space Technology*, pp. 39-40, 14 August 2000.
[123] Dornheim, M. A., and Sparaco, P. “Concorde Probe Finds Accident Oddities,” *Aviation Week & Space Technology*, pp. 440-441, 15 January 2001.
[124] Doyle, A. “Twenty Years Young,” *Flight International*, pp. 41-43, 07-13 February 1996.
[125] Doyle, A., Moxon, J., and Kingsley-Jones, M. “Broken Water Deflector Probed in French Concorde Crash Inquiry,” *Flight International*, pp. 4-5, 08-14 August 2000.
[126] Driver, C. “What Gross Weight and Range for an Advanced HSCT?”. *High-Speed Research: Sonic Boom Volume II*, National Aeronautics and Space Administration, Hampton, VA, 25-27 February 1992.
[127] Dubin, A. P. “Supersonic Transport Market Penetration Model.” *AIAA Conference on Air Transportation: Technical Perspectives and Forecasts*, American Institute of Aeronautics and Astronautics, Los Angeles, CA, 21-24 August 1978. https://doi.org/10.2514/6.1978-1557
[128] Edwards, G. “Review Lecture: The Technical Aspects of Supersonic Civil Transport Aircraft,” Philosophical Transactions of the Royal Society of London. Series A, Mathematical and Physical Sciences, Vol. 275, No. 1254, pp. 529-565, 21 March 1974.
[129] Emling, S. “Concorde Is Grounded after a Life of High-Tech and Low Returns.” SMH, http://www.smh.com.au/articles/2003/05/30/1054177726628.html?oneclick=true, 31 May 2003.
[130] Field, E. J. “Appendix K: British Aircraft Corporation/Aerospatiale Concorde,” *Flying Qualities of Transport Aircraft: Precognitive or Compensatory?* College of Aeronautics, Cranfield University, Cranfield, England, June 1995, pp. 283-288.
[131] Fiorino, F. “Concorde Tire Blowout Concerns Date Back to Late ‘70s,” *Aviation Week & Space Technology*, pp. 36-37, 31 July 2000.
[132] Flottau, J. “Concorde Victim Cases Could End up in U.S.,” *Aviation Week & Space Technology*, pp. 75-76, 04 September 2000.
[133] Forsgren, R. “The Concorde Accident: A Case Study,” APPEL, Knowledge Services, NASA.
[134] Funtanilla, J. G. “Supersonic Commercial Aircraft,” American Institute of Aeronautics and Astronautics, 13 December 2016.
[135] Gardner, J. H., and Rogers, P. H. “Thermospheric Propagation of Sonic Booms from the Concorde Supersonic Transport,” NRL-MR-3904, Naval Research Laboratory, Washington, D. C., 14 February 1979.
[136] George, A. R., and Kim, Y. N. “High-Altitude Long-Range Sonic Boom Propagation,” *Journal of Aircraft*, Vol. 16, No. 9, pp. 637-639, September 1979.
[137] Gillman, P. "Supersonic Bust - the Story of the Concorde," *The Atlantic Monthly*; Vol. 239, No. 1, pp. 72-81. https://www.theatlantic.com/past/docs/issues/77jan/gillman.htm, January 1977.
[138] H. O. F. “Concorde Then, Now and in the Future,” *Guild News*, No. 106, pp. 12-14, The Guild of Air Pilots and Air Navigators, London, England, January 1998.
[139] Hamilton, J. “Concorde - An Exercise in Collaboration.” *AIAA 5th Annual Meeting and Technical Display*, American Institute of Aeronautics and Astronautics, Philadelphia, PA, 21-24 October 1968. https://doi.org/10.2514/6.1968-990
[140] Harpur, N. “Structural Testing of Concorde Aircraft: Further Report on United Kingdom Tests.” *Advanced Approaches to Fatigue Evaluation, Sixth ICAF Symposium*, National Aeronautics and Space Administration, Miami Beach, FL, 13-14 May 1971.
[141] Harpur, N. F. “Concorde Structural Development.” *AIAA Commercial Aircraft Design and Operation Meeting*, American Institute of Aeronautics and Astronautics, Los Angeles, CA, 12-14 June 1967. https://doi.org/10.2514/6.1967-402
[142] Harpur, N. F. “Structural Development of the Concorde: An Account of the Design Philosophy Adopted to Meet the New Considerations Involved in the Construction of a Supersonic Transport,” *Aircraft Engineering and Aerospace Technology*, Vol. 40, No. 3, pp. 18-25, March 1968. https://doi.org/10.1108/eb034351.
[143] Harriss, J. A. “The Concorde Redemption: Can the Superplane Make a Comeback?”. *Air & Space Magazine*, Smithsonian Institute, Washington, D. C., August/September 2001.
[144] Henne, P. A. “Case for Small Supersonic Civil Aircraft,” *Journal of Aircraft*, Vol. 42, No. 3, pp. 765-774, May-June 2005. https://doi.org/10.2514/1.5119.
[145] Hitch, H. P. Y. “Concorde Dynamics - A Review.”*AIAA/ASME/SAE 13th Structures, Structural Dynamics, and Materials Conference*, American Institute of Aeronautics and Astronautics, San Antonio, TX, 10-12 April 1972. https://doi.org/10.2514/6.1972-381
[146] Horinouchi, S. “Conceptual Design of a Low Boom SSBJ.” *43rd AIAA Aerospace Sciences Meeting and Exhibit*, American Institute of Aeronautics and Astronautics, Reno, NV, 10-13 January 2005. https://doi.org/10.2514/6.2005-1018
[147] Horwitch, M. *Clipped Wings: The American SST Conflict*, The MIT Press, Cambridge, MA, 1982.

[148] Humi, P. “Supersonic Concorde Wings Its Way to 30,” *Travel Guide News*. CNN, http://www.cnn.com/TRAVEL/NEWS/9903/02/aging.concorde/, 02 March 1999.
[149] Johnston, J., Trivellini, G., Rodriguez, R., Kirkby, N., and Parraguirre, C. “Revisiting the Concorde: A New Approach to Delta-Winged Flight,” 22 July 2010.
[150] Kingsley-Jones, M. “Retrospective: Concorde as Viewed from the Flightdeck,” *Flight International*. https://www.flightglobal.com/programmes/retrospective-concorde-as-viewed-from-the-flightdeck/131502.article, 01 March 2019.
[151] Kingsley-Jones, M. “The Fast Show,” *Flight International*, pp. 36-37, 06-12 November 2001.
[152] Kingsley-Jones, M. “BA Cautious on Concorde Plans,” *Flight International*, p. 27, 12-18 February 2002.
[153] Kingsley-Jones, M. “Flawed Icon,” *Flight International*, pp. 34-45, 21-27 October 2003.
[154] Kloster, M. "Die Bewertung Kunftiger Uberschall-Verkehrs-Flugzeuge Mittels Des Schallknallkriteriums," D-85747. *DLGR - Workshop "Bewertung von Flugzeugen"*, Technische Universitat Munchen Luftfahrttechnik, Garching, Germany, 26-27 October 1998.
[155] Koff, B. L., and Koff, S. G. “Engine Design and Challenges for the High Mach Transport,” AIAA-2007-5344. *43rd AIAA/ASME/SAE/ASEE Joint Propulsion Conference & Exhibit*, American Institute of Aeronautics and Astronautics, Cincinnati, OH, 08-11 July 2007. https://doi.org/10.2514/6.2007-5344
[156] Lassere, J. "ICARE - No 34 Summer 1965 Why Did the "CONCORDE" Project Have to Be Saved?," *Cap Avenir CONCORDE - The Shared Passion*. http://cap-avenir-concorde.fr/les-dossiers-de-presse/icare/icare-n-34-ete-1965-pourquoi-le-projet-concorde-devait-etre-sauve,
[157] Learmount, D. “Damage Leads to Checks for Concorde Elevons,” *Flight International*, p. 17, 03-09 June 1998.
[158] Learmount, D. “‘Poor Repair’ to DC-10 Was Cause of Concorde Crash,” *Flight International*, p. 4, 24-30 October 2000.
[159] Learmount, D., Doyle, A., and Moxon, J. “Concorde Grounded: Investigations Shed New Light on Tyre and Engines,” *Flight International*, p. 6, 22-28 August 2000.
[160] Learmount, D., and Moxon, J. “The Concorde Dilemma,” *Flight International*, p. 39, 12-18 September 2000.
[161] Learmount, D., and Moxon, J. “Trials of Strength,” *Flight International*, pp. 34-35, 23-29 January 2001.
[162] Leney, D., and Macdonald, D. *Aerospatial/Bac Concorde, Haynes Owners’ Workshop Manual*, Haynes Publishing, Somerset, England, July 2010.
[163] Lewis, R. *Supersonic Secrets: The Unofficial Biography of Concorde*, Expose, London, England, 2003.
[164] Leyman, C. S. “A Review of the Technical Development of Concorde,” *Progress in Aerospace Sciences*, Vol. 23, No. 3, pp. 185-238, 1986. https://doi.org/10.1016/0376-0421(86)90007-2.
[165] Leyman, C. S., and Scotland, R. L. “The Effect of Engine Failure at Supersonic Speeds on a Slender Aircraft - Predicted and Actual,” AGARD-CP-119, April 1972.
[166] Maglieri, D., Sothcott, V., and Hicks, J. “Influence of Vehicle Configuration and Flight Profile on X-30 Sonic Booms.” *AIAA 2nd International Aerospace Planes Conference*, American Institute of Aeronautics and Astronautics, Orlando, FL, 29-31 October 1990. https://doi.org/10.2514/6.1990-5224
[167] Mann, P. “Concorde Sparks Debate on Criminalizing Crashes,” *Aviation Week & Space Technology*, pp. 41-42, 14 August 2000.
[168] Marlow, P. *Concorde: Last Summer*, Thames & Hudson, London, England, 2006.
[169] Mason, W. H. "Some Supersonic Aerodynamics," [Presentation], Department of Aerospace and Ocean Engineering, Virginia Polytechnic Institute and State University, Blacksburg, VA.
[170] Mason, W. H. "Supersonic Aerodynamics," Department of Aerospace and Ocean Engineering, Virginia Polytechnic Institute and State University, Blacksburg, VA, 31 July 2016.
[171] McKim, F. R. *Vol Supersonique: De Bernoulli a Concorde*, 1974.
[172] McKinlay, R. M. “Concorde Systems in Airline Operation,” AIAA-76-925. *AIAA Aircraft Systems and Technology Meeting*, American Institute of Aeronautics and Astronautics, Dallas, TX, 27-29 September 1976. https://doi.org/10.2514/6.1976-925
[173] McKinlay, R. M., Heaton, G. R. I., and Franchi, J. “Operational Experience on Concorde,” *10th Congress of the International Council of the Aeronautical Sciences (ICAS), ICAS Proceedings*, International Council of the Aeronautical Sciences (ICAS), Ottawa, Ontario, Canada, 04-08 October 1976.
[174] McLean, F. E. “Supersonic Cruise Technology,” NASA-SP-472, National Aeronautics and Space Administration, Washington, D. C., 1985.
[175] Ménéxiadis, G., and Varnier, J. “Long-Range Propagation of Sonic Boom from the Concorde Airliner: Analyses and Simulations,” *Journal of Aircraft*, Vol. 45, No. 5, pp. 1612-1618, September-October 2008. https://doi.org/10.2514/1.33899.
[176] Merritt, L. R. “Concorde Landing Requirement Evaluation Tests,” AD/A-000 014, Federal Aviation Administration, Washington, D. C., August 1974.
[177] Morgan, M. “A New Shape in the Sky,” *Aeronautical Journal*, January 1972.
[178] Morrocco, J. D. “BA Keeps Its Fleet of Concordes Flying,” *Aviation Week & Space Technology*, p. 31, 07 August 2000.
[179] Morrocco, J. D. “Technical Team Forges Concorde Work Plan,” *Aviation Week & Space Technology*, pp. 44-45, 13 November 2000.
[180] Morrocco, J. D. “BA Tests Concorde Safety Modification,” *Aviation Week & Space Technology*, pp. 46-47, 23 July 2001.
[181] Morrocco, J. D., and Sparaco, P. “Concorde Team Activates Return-to-Flight Plan,” *Aviation Week & Space Technology*, pp. 38-40, 22 January 2001.
[182] Nangia, R. K. “Assessment of Air Vehicle Design Evolution over Mach Number and Altitude Operating Envelope with and without S&C Considerations as Part of the Design Synthesis,” AFRL-AFOSR-UK-TR-2011-0035, Air Force Research Laboratory, August 2011.
[183] Nangia, R. K., Palmer, M. E., and Doe, R. H. “Towards Design of Mach 1.6+ Cruise Aircraft,” AIAA-2004-5070. *22nd AIAA Applied Aerodynamics Conference and Exhibit*, American Institute of Aeronautics and Astronautics, Providence, RI, 16-19 August 2004. https://doi.org/10.2514/6.2004-5070
[184] Nguyen, V. P., and Perrais, J. P. “Fatigue Tests on Big Structure Assemblies of Concorde Aircraft.” *Advanced Approaches to Fatigue Evaluation, Sixth ICAF Symposium*, National Aeronautics and Space Administration, Miami Beach, FL, 13-14 May 1971.
[185] Orlebar, C. *The Concorde Story*, Fully Revised ed., The Hamlyn Publishing Group, London, England, 1994.
[186] Orlebar, C. *The Concorde Story: 21 Years in Service*, New ed., Osprey Publishing, Oxford, England, 1997.
[187] Orlebar, C. *The Concorde Story*, Sixth ed., Osprey Publishing, Botley, Oxford, England, 2004.
[188] Owen, K. *Concorde: New Shape in the Sky*, Jane’s Publishing Company, London, England, 1982.
[189] Owen, K. *Concorde and the Americans, Smithsonian History of Aviation Series*, Smithsonian Institution Press, 1997.

[190] Owen, K. *Concorde: Story of a Supersonic Pioneer*, Science Museum, London, England, 2001.
[191] *AVD Internal*----------
[192] Pinet, J. "Aircraft Simulation Application to the Development of the Concorde Project," AIAA-70-923. *AIAA 2nd Aircraft Design and Operations Meeting*, American Institute of Aeronautics and Astronautics, Los Angeles, CA, 20-22 July 1970. https://doi.org/10.2514/6.1970-923
[193] Plotkin, K. J., and Maglieri, D. J. "Sonic Boom Research: History and Future," AIAA-2003-3575. *33rd AIAA Fluid Dynamics Conference and Exhibit*, American Institute of Aeronautics and Astronautics, Orlando, FL, 23-26 June 2003. https://doi.org/10.2514/6.2003-3575
[194] Powell, C. A., and McCurdy, D. A. "Comparison of Low-Frequency Noise Levels of the Concorde Supersonic Transport with Other Commercial Service Airplanes," NASA-TM-78736, National Aeronautics and Space Administration, Washington, D. C., October 1978.
[195] *AVD Internal*----------
[196] Rech, J., and Leyman, C. *A Case Study by Aerospatiale and British Aerospace on the Concorde*, American Institute of Aeronautics and Astronautics, New York, 1980.
[197] Reithmaier, L. *Mach 1 and Beyond: The Illustrated Guide to High-Speed Flight*, TAB Books, Blue Ridge Summit, PA, 1995.
[198] Renaudie, J. "Concorde and C.E.V. - Cooperation between Firms and Government Offices or Establishment in the Flight Test Program - Certification Flights," AIAA-71-784. *AIAA 3rd Aircraft Design and Operations Meeting*, American Institute of Aeronautics and Astronautics, Seattle, WA, 12-14 July 1971. https://doi.org/10.2514/6.1971-784
[199] Reuters. "Concorde - An Uneconomic Triumph." SPACE.com, http://www.space.com/news/concorde_sidebar_000725_wg.html, 25 July 2000.
[200] Richter, G., and Hoch, R. "Concept and Characteristics of the Concorde Flight Silencer." *AIAA Commercial Aircraft Design and Operation Meeting*, American Institute of Aeronautics and Astronautics, Los Angeles, CA, 12-14 June 1967. https://doi.org/10.2514/6.1967-391
[201] Richter, G., and Hoch, R. "Concept and Characteristics of the Concorde Exhaust Noise Suppressor," *Journal of Aircraft*, Vol. 6, No. 2, pp. 98-101, March 1969.
[202] Ripley, E. L. "The Philosophy Which Underlies the Structural Tests of a Supersonic Transport Aircraft with Particular Attention to the Thermal Cycle." *Advanced Approaches to Fatigue Evaluation, Sixth ICAF Symposium*, Miami Beach, FL, 13-14 May 1971.
[203] Robinson, W. "Coming of Age," *Flight International*, pp. 46-47, 16-22 December 2003.
[204] Salmon, M. "Concorde and the Aeronautical Research," NASA-TM-76973, National Aeronautics and Space Administration, Washington, D. C., August 1982.
[205] Satre, P. "Supersonic Air Transport - True Problems and Misconceptions," *Journal of Aircraft*, Vol. 7, No. 1, pp. 3-12, Jan.-Feb. 1970. https://doi.org/10.2514/3.44113.
[206] Seebass, A. "The Prospects for Commercial Supersonic Transport," AIAA-94-0017. *32nd Aerospace Sciences Meeting and Exhibit*, American Institute of Aeronautics and Astronautics, Reno, NV, 10-13 January 1994. https://doi.org/10.2514/6.1994-17
[207] Seebass, R. "History and Economics of, and Prospects for, Commercial Supersonic Transport." *Fluid Dynamics Research on Supersonic Aircraft*, RTO AVT, Rhode-Saint-Genese, Belgium, 25-29 May 1998.
[208] *AVD Internal*----------
[209] *AVD Internal*----------
[210] *AVD Internal*----------
[211] Shackleton, E. *Bristol Aero Collection Celebrates 25 Years of Concorde*, Bristol Aero Collection, 1994.
[212] *AVD Internal*----------
[213] Sieker, B. "Why-Because-Analysis Tools and the Concorde Accident." *First Bieleschweig Workshop on Systems Engineering*, RVS Group, Bielefeld, Germany, 2002.
[214] Siuru, B., and Busick, J. D. *Future Flight: The Next Generation of Aircraft Technology*, 2nd ed., TAB AERO, Blue Ridge Summit, PA, 1994.
[215] Skinner, S. *Concorde*, Midland Publishing, Surrey, England, 2009.
[216] Smith, D. G., Yamartino, R. J., Benkley, C., Isaacs, R., Lee, J., and Chang, D. "Concorde Air Quality Monitoring and Analysis Program at Dulles International Airport," Vol. 1, FAA-AEQ-77-14, Office of Environmental Quality, Federal Aviation Administration, U.S. Department of Transportation, Washington, D. C., December 1977.
[217] Smith, M. J. T., Lowrie, B. W., Brooks, J. R., and Bushell, K. W. "Future Supersonic Transport Noise - Lessons from the Past," AIAA-88-2989. *AIAA/SAE/ASME/ASEE 24th Joint Propulsion Conference*, American Institute of Aeronautics and Astronautics, Boston, MA, 11-13 July 1988. https://doi.org/10.2514/6.1988-2989
[218] Sparaco, P. "Concorde Tire Blowout Expected to Stir Controversy," *Aviation Week & Space Technology*, p. 74, 04 September 2000.
[219] Sparaco, P. "Concorde Accident to Affect Paris Airports," *Aviation Week & Space Technology*, p. 32, 07 August 2000.
[220] Sparaco, P. "France's Concordes Still Grounded," *Aviation Week & Space Technology*, pp. 28-30, 07 August 2000.
[221] Sparaco, P. "A Concorde Comeback Is Becoming More Elusive," *Aviation Week & Space Technology*, pp. 56-57, 11 September 2000.
[222] Sparaco, P. "Concorde Fuel Line Testing Progresses," *Aviation Week & Space Technology*, pp. 34-35, 12 February 2001.
[223] Sparaco, P. "Pace of Concorde Probe Angers British," *Aviation Week & Space Technology*, pp. 43-44, 13 November 2000.
[224] Sparaco, P. "Concorde Investigation Focuses on Burst Tire," *Aviation Week & Space Technology*, pp. 38-39, 14 August 2000.
[225] Sparaco, P. "Judging the Judiciary," *Aviation Week & Space Technology*, p. 49, 17 October 2005.
[226] Sparaco, P. "Upgraded Concorde Awaits New Flight Tests," *Aviation Week & Space Technology*, pp. 96-98, 18 June 2001.
[227] Sparaco, P. "Concorde Crash Upsets French Airport Strategy," *Aviation Week & Space Technology*, pp. 43-44, 18 September 2000.
[228] Sparaco, P. "Official Optimism Grows for Concorde's Return," *Aviation Week & Space Technology*, p. 41, 19 February 2001.
[229] Sparaco, P. "French, British Prepare Fresh Concorde Start," *Aviation Week & Space Technology*, p. 42, 27 August 2001.
[230] Sparaco, P. "Franco-British Team Plans Concorde Modifications," *Aviation Week & Space Technology*, pp. 32-33, 28 August 2000.
[231] Sparaco, P., and Dornheim, M. A. "Final Concorde Report Supports Past Findings," *Aviation Week & Space Technology*, pp. 46-48, 28 January 2002.
[232] Sparaco, P., Fiorino, F., and Dornheim, M. A. "Concorde Troubles Began on Takeoff Roll," *Aviation Week & Space Technology*, pp. 32-34, 31 July 2000.
[233] Sparaco, P., and Flottau, J. "End of an Era," *Aviation Week & Space Technology*, p. 34, 14 April 2003.
[234] Stratford, A. H. *Air Transport Economics in the Supersonic Era*, 2nd ed., The MacMillan Press, London, England, 1973.

[235] Strohmeyer, D., and Seubert, R. "Improvement of a Preliminary Design and Optimization Program for the Evaluation of Future Aircraft Projects," AIAA-98-4828. *7th AIAA/USAF/NASA/ISSMO Symposium on Multidisciplinary Analysis and Optimization*, American Institute of Aeronautics and Astronautics, St. Louis, MO, 15-18 September 1998.
[236] *AVD Internal*----------
[237] *AVD Internal*----------
[238] Sun, Y., and Smith, H. "Sonic Boom and Drag Evaluation of Supersonic Jet Concepts," AIAA-2018-3278. *2018 AIAA/CEAS Aeroacoustics Conference*, American Institute of Aeronautics and Astronautics, Atlanta, GA, 25-29 June 2018. https://doi.org/10.2514/6.2018-3278
[239] Swadling, S. J. "Commercial Supersonic Operations - Thirteen Years of Experience with Concorde,"
[240] Swadling, S. J. "Prospects for a Second Generation Supersonic Transport." *ICAS 1992*, International Council of the Aeronautical Sciences, Beijing, China, 1992.
[241] Syon, G. "Consuming Concorde," Technology and Culture, Vol. 44, No. 3, pp. 650-654, July 2003.
[242] Tanner, C. S., and McLeod, N. J. "Preliminary Measurements of Take-Off and Landing Noise from a New Instrumented Range." *NASA Conference on Aircraft Operating Problems*, National Aeronautics and Space Administration, Hampton, VA, 10-12 May 1965.
[243] Taverna, M. A., and Morrocco, J. D. "Concorde Moves Closer to Resuming Service," *Aviation Week & Space Technology*, pp. 43-44, 30 July 2001.
[244] Taylor, J. W. "Concorde," *Jane's All the World's Aircraft 19??-??*, Jane's All the World's Aircraft Publishing, England, United Kingdom, pp. 104-106.
[245] Thorpe, D. G., Escher, D., and Rhodes, R. E. "Sub-Orbital Passenger Aircraft for Space Launch Operations," AIAA-2015-3894. *51st AIAA/SAE/ASEE Joint Propulsion Conference*, American Institute of Aeronautics and Astronautics, Orlando, FL, 27-29 July 2015. https://doi.org/10.2514/6.2015-3894
[246] Trubshaw, B. *Concorde: The inside Story*, Sutton Publishing, Gloucestershire, England, 2000.
[247] *AVD Internal*----------
[248] *AVD Internal*----------
[249] Truscott, P. R., Dyer, C. S., and Flatman, J. C. "Surface Activation of Concorde by Be-7." *First Post-Retrieval Symposium*, National Aeronautics and Space Administration, Langley Research Center, NASA, 1992.
[250] Turnill, R. *Celebrating Concorde*, Ian Allen Publishing, Surrey, England, 1994.
[251] Walsh, D. "Concorde: Its History and Tragedy," *World Socialist Web Site*. The International Committee of the Fourth International, http://www.wsws.org/articles/2000/jul2000/con1-j28_prn.shtml, 28 July 2000.
[252] Webber, D. "Point-to-Point People with Purpose—Exploring the Possibility of a Commercial Traveler Market for Point-to-Point Suborbital Space Transportation," AA-2-2011-22. *2nd International IAA Conference on Private Human Access to Space*, Arcachon, France, 2011. https://doi.org/10.1016/j.actaastro.2012.04.046
[253] Wilde, M. G., and Cormery, G. "The Aerodynamic Derivation of the Concorde Wing." *11th Anglo-American Aeronautical Conference*, London, England, 08-12 September 1969.
[254] *AVD Internal*----------
[255] *AVD Internal*----------
[256] Wolz, R. "A Summary of Recent Supersonic Vehicle Studies at Gulfstream Aerospace," AIAA-2003-0558. *41st Aerospace Sciences Meeting and Exhibit*, American Institute of Aeronautics and Astronautics, Reno, NV, 06-09 January 2003. https://doi.org/10.2514/6.2003-558
[257] Woolley, P. K. "A Cost-Benefit Analysis of the Concorde Project," *Journal of Transport Economics and Policy*, Vol. 6, No. 3, pp. 225-239, September 1972.
[258] Zaitsev, M. ""Consent" ("Concorde") Does Not Exist Any More " *"Tupolev" PSC in Mass Media*. Public-Stock Company Tupolev, http://www.tupolev.ru/English/Show.asp?SectionID=60,

B.6. Sänger-II Bibliography

[1] Anon. “Revell Sänger 3-View Drawing.”

[2] Anon. *Round Trip to Orbit: Human Spaceflight Alternatives*, 1st ed., Books for Business, 24 May 2002.

[3] Anon. “Reusable Launch Vehicle Programs and Concepts,” Associate Administrator for Commercial Space Transportation (AST), January 1998.

[4] Anon. “Aerospace Plane Technology: Research and Development Efforts in Europe,” Report to the Chairman, Committee on Science, Space, and Technology, House of Representatives, GAO/NSIAD-91-194, National Security and International Affairs Division, United States General Accounting Office, Washington, D.C., July 1991.

[5] Bardenhagan, A. “Massenabschatzung Und Gesamtauslegung Der Unterstufe Von Hyperschall-Raumtransportern,” Dr.-Ing. Dissertation, ZLR-Forschungsbericht 98-04, Institut fur Flugzeugbau und Leichtbau, Technische, Universitat Braunschweig, Zentrum fur Luft- und Raumfahrttechnik, Braunschweig, Germany, 05 November 1997.

[6] Bardenhagen, A., Kossira, H., and Heinze, W. “Weight Estimation of Hypersonic Waveriders within the Integrated Design Program PrADO-Hy,” AIAA-96-4546. *Space Plane and Hypersonic Systems and Technology Conference*, American Institute of Aeronautics and Astronautics, Norfolk, VA, 18-22 November 1996.

[7] Bardenhagen, A., Kossira, H., and Heinze, W. “Interdisciplinary Design of Modern Hypersonic Waveriders Using the Integrated Program PrADO-Hy,” ICAS-94-1.4.1, ICAS 1994. *19th Congress of the International Council of the Aeronautical Sciences*, Anaheim, CA, 18-23 September 1994.

[8] Bayer, M. “Comparative Assessment of Rocket Propelled SSTO Concepts,” AIAA-98-1555. *AIAA 8th International Space Planes and Hypersonic Systems and Technologies Conference*, American Institute of Aeronautics and Astronautics, Norfolk, VA, 27-30 April 1998.

[9] Berens, T. M., and Bissinger, N. C. “Study on Forebody Precompression Effects and Inlet Entry Conditions for Hypersonic Vehicles,” AIAA-96-4531. *AIAA 7th International Space Planes and Hypersonic Systems and Technologies Conference*, American Institute of Aeronautics and Astronautics, Norfolk, VA, 18-22 November 1996.

[10] Berens, T. M., and Bissinger, N. C. “Forebody Precompression Performance of Hypersonic Flight Test Vehicles.” *AIAA 8th International Space Planes and Hypersonic Systems and Technologies Conference*, American Institute of Aeronautics and Astronautics, Norfolk, VA, 27-30 April 1998.

[11] Bertin, J. J. *Hypersonic Aerothermodynamics, AIAA Education Series*, American Institute of Aeronautics and Astronautics, Washington, D.C, 1994.

[12] Beyes, G. “Eugen Sänger: Astronautical Pioneer and Trailblazer,” *EIR Science & Technology*, Vol. 14, No. 9, pp. 22-28, 27 February 1987.

[13] Breitsamter, C., Laschka, B., Zahringer, C., and Sachs, G. “Wind Tunnel Tests for Separation Dynamics Modeling of a Two-Stage Hypersonic Vehicle,” AIAA-2001-1811. *AIAA/NAL-NASDA-ISAS 10th International Space Planes and Hypersonic Systems and Technologies Conference*, American Institute of Aeronautics and Astronautics, Kyoto, Japan, 24-27 April 2001.

[14] Bruhl, C., Crutzen, P., Grabl, H., and Kley, D. “The Impact of the Spacecraft System SÄNGER in the Composition of the Middle Atmosphere,” AIAA-92-5071. *AIAA 4th International Aerospace Planes Conference*, American Institute of Aeronautics and Astronautics, Orlando, FL, 01-04 December 1992.

[15] Buhl, W., Ebert, K., and Herbst, H. “Optimal Ascent Trajectories for Advanced Launch Vehicles,” AIAA-92-5008. *AIAA 4th International Aerospace Planes Conference*, American Institute of Aeronautics and Astronautics, Orlando, FL, 01-04 December 1992.

[16] Chiesa, S., Russo, G., Fioriti, M., and Corpino, S. “Status and Perspectives of Hypersonic Systems and Technologies with Emphasis on the Role of Sub-Orbital Flight,” *Aerotecnica Missili & Spazio*, Vol. 94, No. 2, pp. 81-90, April-July 2015.

[17] Chiesa, S. G., and Maggiore, P. “Hypersonic Aircraft Conceptual Design Methodology,” ICAS-94-1.4.2. *19th Congress of the International Council of the Aeronautical Sciences*, Anaheim, CA, 18-23 September 1994.

[18] Decker, K., and Laschka, B. “Unsteady Aerodynamics of a Hypersonic Vehicle During a Separation Phase,” AIAA-2001-1852. *AIAA/NAL-NASDA-ISAS 10th International Space Planes and Hypersonic Systems and Technologies Conference*, American Institute of Aeronautics and Astronautics, Kyoto, Japan, 24-27 April 2001.

[19] Dujarric, C. “Proposed Orientations for Future European Launchers Concepts and Associated Aerothermodynamics Technology Development Requirements.” *3rd European Symposium on Aerothermodynamics for Space Vehicles, ESTEC*, Noordwiik, The Netherlands, 24-26 November 1998.

[20] Dujarric, C. “Possible Future European Launchers - A Process of Convergence,” *ESA Bulletin 97*, February 1999.

[21] Dujarric, C., Caporicci, M., Kuczera, H., and Sacher, P. “Conceptual Studies and Technology Requirements for a New Generation of European Launchers - A FESTIP Status Report,” *Acta Astronautica*, Vol. 41, No. 4-10, pp. 219-228, August-November 1997.

[22] Eggers, T. “Aerodynamischer Entwurf Von Wellenreiter-Konfigurationen Fur Hyperschallflugzeuge,” Dr.-Ing. Disseration, Forschungsbericht 1999-10, Institut fur Entwurfsaerodynamik des DLR, Deutsches Zentrum fur Luft- und Raumfahrt, e. V., Braunschweig, Germany, 08 December 1998.

[23] Eggers, T., and Novelli, P. “Design Studies for a Mach 8 Dual Mode Ramjet Flight Test Vehicle,” AIAA-99-4877. *9th International Space Planes and Hypersonic Systems and Technologies Conference*, American Institute of Aeronautics and Astronautics, Norfolk, VA, 01-05 November 1999.

[24] Eggers, T., Radespiel, R., Waibel, M., and Hummel, D. “Flow Phenomena of Hypersonic Waveriders and Validation of Design Methods,” AIAA-93-5045. *AIAA/DGLR 5th International Aerospace Planes and Hypersonics Technologies Conference*, American Institute of Aeronautics and Astronautics, Munich, Germany, 30 November - 03 December 1993.

[25] Engler, V., Coors, D., and Jacob, D. “Optimization of a Space Transportation System Including Design Sensitivities,” AIAA-98-1553. *AIAA 8th International Space Planes and Hypersonic Systems and Technologies Conference*, American Institute of Aeronautics and Astronautics, Norfolk, VA, 27-30 April 1998.

[26] Fossati, F. A., and Denaro, A. “A RLV Concept Selection from the Thermo-Mechanical Outlook the Lessons Learned in FESTIP,” AIAA-99-4976. *9th International Space Planes and Hypersonic Systems and Technologies Conference*, American Institute of Aeronautics and Astronautics, Norfolk, VA, 01-05 November 1999.

[27] Furniss, T. “Sänger Aerospaceplane Gains Momentum,” *Flight International*, pp. 39-41, 12 August 1989.

[28] Gonzalez, P. “Influence of the Abort Capability in Reusable Systems Reliability. FESTIP Results Overview,” AIAA-99-4928. *9th International Space Planes and Hypersonic Systems and Technologies Conference,* American Institute of Aeronautics and Astronautics, Norfolk, VA, 01-05 November 1999.
[29] Grallert, H. “Synthesis of a FESTIP Air-Breathing TSTO Space Transportation System,” AIAA-99-4884. *9th International Space Planes and Hypersonic Systems and Technologies Conference*, American Institute of Aeronautics and Astronautics, Norfolk, VA, 01-05 November 1999.
[30] *AVD Internal*----------
[31] Grallert, H., and Herrmann, O. “Generic Derivation of a Promising Air-Breathing TSTO Space Transportation System - from Sänger to FESTIP,” AIAA-98-1552. *8th AIAA International Space Planes and Hypersonic Systems and Technologies Conference,* American Institute of Aeronautics and Astronautics, Norfolk, VA, 27-30 April 1998.
[32] Grallert, H., and Keller, K. “Metallic Thermal Protection Concept for Aerodynamic Controlled Hypersonic Vehicles,” ICAS-88-2.3.2. *16th Congress of the International Council of the Aeronautical Sciences*, Jerusalem, Israel, 28 August - 02 September 1988.
[33] Grallert, H., and Kuczera, H. “Kick-Stages - A Mandatory Element of Future Reusable Space Transportation Systems,” AIAA-99-4885. *9th International Space Planes and Hypersonic Systems and Technologies Conference*, American Institute of Aeronautics and Astronautics, Norfolk, VA, 01-05 November 1999.
[34] Grallert, H., and Vollmer, K. “Conceptual Design of the Thermal Protection System for the Reference Concept SÄNGER by Means of Advanced Methods,” AIAA-93-5085. *AIAA/DGLR 5th International Aerospace Planes and Hypersonics Technologies Conference,* American Institute of Aeronautics and Astronautics, Munich, Germany, 30 November - 03 December 1993.
[35] Gruhn, P. “Einfluss Einer Heckklappe Auf Die Dusenstromung Im Hyperschall,” PhD Dissertation, Rheinisch-Westfalischen Technischen Hochschule Aachen (RWTH Aachen), Aachen, Germany, 30 July 2004.
[36] Hald, H., Petersen, D., Reimer, T., Ruhle, F., Winkelmann, P., and Weihs, H. “Development of a CMC-Based TPS for Two Representative Specimens of Cryogenic Tank RLVs,” AIAA-98-1609. *AIAA 8th International Space Planes and Hypersonic Systems and Technologies Conference,* American Institute of Aeronautics and Astronautics, Norfolk, VA, 27-30 April 1998.
[37] Hall, R. C. “Essays on the History of Rocketry and Astronautics: Proceedings of the Third through the Sixth History Symposia of the International Academy of Astronautics,” Vol. 1, NASA-CP-2014, 1977.
[38] Hanel, D., Krause, E., and Henze, A. "Supersonic and Hypersonic Flow Computations for the Research Configuration ELAC I and Comparison to Experimental Data," *Zeitschrift fur Flugwissenschaften und Weltraumforschung*, Vol. 17, No. 2, pp. 90-98, 1993.
[39] Hannigan, R. J. *Spaceflight in the Era of Aero-Space Planes*, Krieger Publishing Company, Malabar, FL, 1994.
[40] *AVD Internal*----------
[41] Haug, T., Ehrmann, U., and Knabe, H. “Air Intake Ramp Made from C/Sic Via the Polymer Route for Hypersonic Propulsion Systems.” *AIAA/DGLR 5th International Aerospace Planes and Hypersonics Technologies Conference*, American Institute of Aeronautics and Astronautics, Munich, Germany, 30 November - 03 December 1993.
[42] Heitmeir, F., Lederer, R., and Herrmann, O. “German Hypersonic Technology Programme - Airbreathing Propulsion Activities,” AIAA-92-5057. *AIAA 4th International Aerospace Planes Conference,* American Institute of Aeronautics and Astronautics, Orlando, FL, 01-04 December 1992.
[43] Hendrick, P. “SSTO & TSTO LOX Collection System Performances: Influence of LOX Plant Architecture,” ICAS-96-5.7.5. *20th Congress of the International Council of the Aeronautical Sciences*, Sorrento, Italy, September 1996.
[44] Hendrick, P., and Saint-Mard, M. “Sänger-Type T.S.T.O. Using in-Flight LOX Collection,” AIAA-97-2858. *33rd Joint Propulsion Conference and Exhibit,* American Institute of Aeronautics and Astronautics, Seattle, WA, 06-09 July 1997.
[45] Herholz, J. “European Space Transportation System Projects Since 1998.” *9th International Mars Society Conference*, [Presentation], Washington, D.C., 03-06 August 2006.
[46] Hirschel, E. “Aerothermodynamics and Propulsion Integration in the SÄNGER Technology Programme,” AIAA-91-5041. *AIAA 3rd International Aerospace Planes Conference*, American Institute of Aeronautics and Astronautics, Orlando, FL, 03-05 December 1991.
[47] Hirschel, E. “The Hypersonics Technology Development and Verification Strategy of the German Hypersonics Technology Programme,” AIAA-93-5072. *AIAA/DGLR 5th International Aerospace Planes and Hypersonics Technologies Conference*, American Institute of Aeronautics and Astronautics, Munich, Germany, 30 November - 03 December 1993.
[48] Hirschel, E., Arlinger, B., Lind, I., and Norstrund, H. “German-Scandinavian Cooperation in the Field of Aerothermodynamics of the German Hypersonics Technology Programme,” AIAA-95-6073. *AIAA 6th International Aerospace Planes and Hypersonics Technologies Conference,* American Institute of Aeronautics and Astronautics, Chattanooga, TN, 03-07 April 1995.
[49] Hirschel, E. H., and Kuczera, H. “The FESTIP Technology Development and Verification Plan,” AIAA-98-1567. *8th AIAA International Space Planes and Hypersonic Systems and Technologies Conference,* American Institute of Aeronautics and Astronautics, Norfolk, VA, 27-30 April 1998.
[50] Hirschel, E. H., and Kuczera, H. “Technologische Herausforderungen Des Hyperschallfluges: Das Technologieentwicklungs- Und Verifikationskonzept Des Deutschen Hyperschalltechnologie - Programms 1988-1995,” EHHuHk/RAeS/25.4.2013, [Presentation], DGLR Vortrag, Hamburg, Germany, 28 November 2013.
[51] Hirschel, E. H., Prem, H., and Madelung, G. *Luftfahrtforschung in Deutschland*, Band 30, Die deutsche Luftfahrt, Buchreihe uber die Entwicklungsgeschichte der deutschen Luftfahrttechnik, Bernard & Graefe, Bonn, Germany, 2001.
[52] Hirschel, E. H., Prem, H., and Madelung, G. *Aeronautical Research in Germany - from Lilienthal until Today*, Springer Publisher, 2004.
[53] Hirschel, E. H., and Weiland, C. *Selected Aerothermodynamic Design Problems of Hypersonic Flight Vehicles, Progress in Astronautics and Aeronautics*, Vol. 229, American Institute of Aeronautics and Astronautics, Springer, Reston, VA, 2009.
[54] Hirschel, E. H., and Weiland, C. “Design of Hypersonic Flight Vehicles: Some Lessons from the Past and Future Challenges,” *CEAS Space Journal*, Vol. 1, No. 3-22, September 2011.
[55] Hogenauer, E. “Entwicklungstendenzen Bei Raumtransportern,” in Jahrbuch 1986 II. *DGLR-Jahrestagung 1986*, DGLR, Munich, Germany, 08-10 October 1986.
[56] Hogenauer, E. “A Space Transporter for the Year 2000,” *EIR Science & Technology*, Vol. 14, No. 8, pp. 28-37, 20 February 1987.
[57] Hogenauer, E., and Koelle, D. “SÄNGER - the German Aerospace Vehicle Program,” AIAA-89-5007. *AIAA 1st National Aero Space Plane Conference*, American Institute of Aeronautics and Astronautics, Dayton, OH, 20-21 July 1989.
[58] Hornung, M. “Entwurf Eines Luftatmenden Oberstufe Und Gesamtoptimierung Eines Transatmospharischen Raumtransportsystems,” PhD Thesis, Fakultat fur Luft- und Raumfahrttechnik, Universitat der Bundeswehr Munchen, Neubiberg, Germany, 15 January 2003.

[59] Husken, D., and Funk, D. “Der Neue Weg Ins All. Raumtransporter Der Nachsten Generation: Eine Ausstellung Der Deutschen Forschungsgemeinschaft (DFG).” Broschure, Kollen Druck, December 2002.
[60] Jabs, A. “Turboramjet Engine,” Patent No.: 5,094,071, MTU Motoren und Turbinen Union Muenchen GmbH, Fed. Rep. of Germany, United States, 10 March 1992.
[61] Jackson, A. A. “Eugen Sänger, from the Silverbird to Interstellar Voyages,” [Presentation], History Lunch & Learn, Visiting Scientist Lunar and Planetary Institute, American Institute of Aeronautics and Astronautics (AIAA) Houston Section, Organized by the Section's History Technical Committee (Chair: Douglas Yazell members Ted Kenny and Chester Vaughan), 22 April 2016.
[62] Jacob, D., Sachs, G., and Wagner, S. *Basic Research and Technologies for Two-Stage-to-Orbit Vehicles: Final Report of the Collaborative Research Centres 253, 255 and 259*, Deutsche Forschungsgemeinschaft, Wiley-VCH Verlag GmbH & Co. KGaA, Weinheim, Germany, 2005.
[63] Jadhav, V. B., and Warke, A. “Investigation of ELAC 1 Aerodynamics Using CFD in Supersonic Flow,” *Applied Mechanics and Materials*, Vol. 592-594, pp. 1955-1961, 2014.
[64] *AVD Internal*----------
[65] Kania, P. “The German Hypersonics Technology Program,” AIAA-95-6005. *6th International Aerospace Planes and Hypersonics Technologies Conference*, American Institute of Aeronautics and Astronautics, Chattanooga, TN, 03-07 April 1995.
[66] Kerstein, A., and Matko, D. “Eugen Sänger: Eminent Space Pioneer,” *Acta Astronautica*, Vol. 61, No. 11-12, pp. 1085-1092, December 2007.
[67] Keuk, J., J, B., Schneider, A., and Koschel, W. “Numerical Simulation of Hypersonic Inlet Flows,” AIAA-98-1526. *AIAA 8th International Space Planes and Hypersonic Systems and Technologies Conference*, American Institute of Aeronautics and Astronautics, Norfolk, VA, 27-30 April 1998.
[68] Knoblock, E. *The Shoulders on Which We Stand - Wegbereiter Der Wissenschaft*, 1st ed., Springer, 25 October 2012.
[69] Koelle, D. E. Figures, Diagrams, Photos, Personal Conversation with B. Chudoba.
[70] Koelle, D. E. “Launch Cost Assessment of Operational Winged Launch Vehicles,” AIAA-92-5021. *AIAA 4th International Aerospace Planes Conference*, American Institute of Aeronautics and Astronautics, Orlando, FL, 01-04 December 1992.
[71] Koelle, D. E. “Advanced Two-Stage Vehicle Concepts (SÄNGER),” AIAA-90-1933. *AIAA/SAE/ASME/ASEE 26th Joint Propulsion Conference*, American Institute of Aeronautics and Astronautics, Orlando, FL, 16-18 July 1990.
[72] Koelle, D. E. “SÄNGER II, A Hypersonic Flight and Space Transportation System,” ICAS-88-1.5.1. *16th Congress of the International Council of the Aeronautical Sciences*, Jerusalem, Israel, 28 August - 02 September 1988.
[73] Koelle, D. E. “Launch Cost Analyses for Reusable Space Transportation Systems (Sänger II),” *Acta Astronautica*, Vol. 19, No. 2, pp. 191-197, February 1989.
[74] Koelle, D. E. “Handbook of Cost Engineering and Design of Space Transportation Systems,” Report No. TCS-TR-200, Registered Copy No. 568, Revision 4c, TransCost 8.2 Model Description, Statistical-Analytical Model for Cost Estimation and Economic Optimization of Launch Vehicles, TCS-TransCostSystems, Ottobrunn, Germany, February 2020.
[75] Koelle, D. E. “On the Optimum Cruise Speed of a Hypersonic Aircraft,” *IEEE Aerospace and Electronic Systems Magazine*, Vol. 4, No. 5, May 1989.
[76] Koelle, D. E., and Kuczera, H. “Sänger II, An Advanced Launcher System for Europe,” *Acta Astronautica*, Vol. 19, No. 1, pp. 63-72, 1989.
[77] Koelle, D. E., Sacher, P., and Grallert, H. *Deutsche Raketenflugzeuge Und Raumtransporter-Projekte*, Band 34, Die deutsche Luftfahrt, Buchreihe uber die Entwicklungsgeschichte der deutschen Luftfahrttechnik, Berndard & Graefe, Bonn, Germany, 2007.
[78] Kopp, S., Hollmeier, S., Rick, H., and Herrmann, O. “Airbreathing Hypersonic Propulsion System Integration within FESTIP FSSC-12,” AIAA-99-4813. *9th International Space Planes and Hypersonic Systems and Technologies Conference*, American Institute of Aeronautics and Astronautics, Norfolk, VA, 01-05 November 1999.
[79] Kordulla, W., Radespiel, R., Krogmann, P., and Maurer, F. “Aerothermodynamics Activities in Hypersonics at DLR,” AIAA-92-5032. *AIAA 4th International Aerospace Planes Conference*, American Institute of Aeronautics and Astronautics, Orlando, FL, 01-04 December 1992.
[80] Koschel, W., Rick, W., and Ruggeberg, T. “Study of Flow Phenomena in High Speed Intakes,” AIAA-92-5029. *AIAA 4th International Aerospace Planes Conference*, American Institute of Aeronautics and Astronautics, Orlando, FL, 01-04 December 1992.
[81] Koschel, W. W. “Basic Research in German Universitites and DLR on High Speed Airbreathing Propulsion,” AIAA-96-4579. *AIAA 7th International Space Planes and Hypersonics Systems and Technologies Conference*, American Institute of Aeronautics and Astronautics, Norfolk, VA, 18-22 November 1996.
[82] Kossira, H., Bardenhagan, A., and Heinze, W. “Investigations on the Potential of Hypersonic Waveriders with the Integrated Aircraft Design Program PrADO-Hy,” AIAA-93-5098. *5th International Aerospace Planes and Hypersonics Technologies Conference*, American Institute of Aeronautics and Astronautics, Munich, Germany, 30 November - 03 December 1993.
[83] Kossira, H., Bardenhagen, A., and Heinze, W. “An Integrated Computer-Program-System for the Preliminary Design of Advanced Hypersonic Aircraft (PrADO-Hy),” A95-87373. *3rd Aerospace Symposium, Braunschweig, Germany*, in: “Orbital Transport: Technical, Meteorological and Chemical Aspects”, 26-28 August 1991.
[84] Krammer, P., Heitmeir, F., Bissinger, N. C., and Voss, N. “German Hypersonics Technology Programme Propulsion Technology - Status 1993,” AIAA-93-5094. *AIAA/DGLR 5th International Aerospace Planes and Hypersonics Technologies Conference*, American Institute of Aeronautics and Astronautics, Munich, Germany, 30 November - 03 December 1993.
[85] Krause, E. “German University Research in Hypersonics,” AIAA-92-5033. *AIAA 4th International Aerospace Planes Conference*, American Institute of Aeronautics and Astronautics, Orlando, FL, 01-04 December 1992.
[86] Krause, E. “Numerical Simulation of Supersonic and Hypersonic Flow Around Delta Wings in Comparison to Experimental Results,” RWTH-CONV-177871. *European Congress on Computational Methods in Applied Sciences and Engineering (ECCOMAS 2000)*, Barcelona, Spain, 11-14 September 2000.
[87] Krause, E., Limberg, W., Kharitonov, A. M., Brodetsky, M. D., and Henze, A. "An Experimental Investigation of the ELAC 1 Configuration at Supersonic Speeds," *Experiments in Fluids*, Vol. 26, pp. 423-436, 1999.
[88] Kuczera, H. Figures, Diagrams, Photos, Personal Conversation with B. Chudoba.
[89] *AVD Internal*----------
[90] *AVD Internal*----------
[91] *AVD Internal*----------

[92] Kuczera, H. “FESTIP (Future European Space Transportation Investigations Programme).” *Proceedings of the International Workshop on Spaceplane/RLV Technology Demonstrator*, Tokyo, Japan, 10-12 March 1997.
[93] Kuczera, H. “FESTIP System Study - An Overview.” *AIAA 8th International Space Planes and Hypersonic Systems and Technologies Conference*, [Presentation], American Institute of Aeronautics and Astronautics, Norfolk, VA, 27-30 April 1998.
[94] Kuczera, H., and Hauck, H. “The German Hypersonics Technology Programme - Status Report 1992.” *AIAA 4th International Aerospace Planes Conference*, American Institute of Aeronautics and Astronautics, Orlando, FL, 01-04 December 1992.
[95] Kuczera, H., Hauck, H., Sacher, P., and Krammer, P. “The German Hypersonics Technology Programme Status 1993 and Perspectives,” AIAA-93-5159. *AIAA/DGLR 5th International Aerospace Planes and Hypersonics Technologies Conference*, American Institute of Aeronautics and Astronautics, Munich, Germany, 30 November - 03 December 1993.
[96] Kuczera, H., and Johnson, C. “The Major Results of the FESTIP System Study.” *9th International Space Planes and Hypersonic Systems and Technologies Conference*, [Presentation], American Institute of Aeronautics and Astronautics, Norfolk, VA, 01-05 November 1999.
[97] Kuczera, H., and Sacher, P. *Reusable Space Transportation Systems*, Springer-Praxis Books in Astronautical Engineering, 2011.
[98] Kuczera, H., Sacher, P., and Dujarric, C. “FESTIP System Study - An Overview.” *AIAA 7th International Space Planes and Hypersonic Systems and Technologies Conference*, American Institute of Aeronautics and Astronautics, Norfolk, VA, 18-22 November 1996.
[99] Kuczera, H., Sacher, P., and Krammer, P. “The German Hypersonics Programme - Status Report 1991,” AIAA-91-5001. *AIAA 3rd International Aerospace Planes Conference*, American Institute of Aeronautics and Astronautics, Orlando, FL, 03-05 December 1991.
[100] Kunkler, H. “Airbreathing Propulsion for Space Transport - New Concepts, Special Problems and Attempts at Solutions,” AD-P007 943, AGARD Conference Proceedings No. 479 (AGARD-CP-479). *Hypersonic Combined Cycle Propulsion*.
[101] Lang, N. “Investigation of the Supersonic Flow-Field Around a Delta Wing Using Particle-Image-Velocimetry,” 2000.
[102] Lederer, R. “Testing the Actively Cooled, Fully Variable Hypersonic Demonstrator Nozzle - Results from the Test Campaign 1995/96,” AIAA-96-4500-CP. *AIAA 7th International Space Planes and Hypersonic Systems and Technologies Conference*, American Institute of Aeronautics and Astronautics, Norfolk, VA, 18-22 November 1996.
[103] Lederer, R., Schwab, R., and Voss, N. “Hypersonic Airbreathing Propulsion Activities for SÄNGER,” AIAA-TP-91-5040. *3rd AIAA International Aerospace Planes Conference*, American Institute of Aeronautics and Astronautics, Orlando, FL, 03-05 December 1991.
[104] Lentz, S. “Gesamtentwurf Eines Zweistufigen Raumtransportsystems Mit Einer Anlage Zur Extraktion Von Sauerstoff an Bord Der Unterstufe,” PhD Dissertation, Fakultat fur Luft- und Raumfahrttechnik, Universitat der Bundeswehr Munchen, Neubiberg, Germany, 2006.
[105] Lentz, S., Hornung, M., and Staudacher, W. “Conceptual Design of a Reusable Aces TSTO Space Transportation System,” AIAA-2005-3246. *AIAA/CIRA 13th International Space Planes and Hypersonics Systems and Technologies*, American Institute of Aeronautics and Astronautics, Capua, Italy, 16-20 May 2005.
[106] Leyland, P., Perez, A., Perusset, X., Olivier, H., Henze, H., and Bleilebens, M. “ELAC: A Case Study for High Speed Transportation,” ESA-SP-487. *4th European Symposium on Aerothermodynamics for Space Vehicles*, European Space Agency, Capua, Italy, 15-18 October 2001.
[107] Limberg, W., and Stromberg, A. "Pressure Measurements at Supersonic Speeds on the Research Configuration ELAC I," *Zeitschrift fur Flugwissenschaften und Weltraumforschung*, Vol. 17, No. 2, pp. 82-89, April 1993.
[108] Longo, J. M. A., Barth, T., and Eggers, T. “Aerothermodynamics Issues of the DLR Hypersonic Flight Experiment SHEFEX-I,” AIAA-2008-4038. *38th Fluid Dynamics Conference & Exhibit*, American Institute of Aeronautics and Astronautics, Seattle, Washington, 23-26 June 2008.
[109] Lopez-Reig, J., Rebolo, R., Matesanz, A., Velazquez, A., and Rodriguez, M. “Integration of Hypersonic Aerothermodynamics Design Methods,” AIAA-96-4502-CP. *AIAA 7th International Space Planes and Hypersonic Systems and Technologies Conference*, American Institute of Aeronautics and Astronautics, Norfolk, VA, 18-22 November 1996.
[110] Mayrhofer, M., and Sachs, G. “A Contribution to Mission Safety for a Two-Stage Hypersonic Vehicle,” AIAA-99-4886. *9th International Space Planes and Hypersonic Systems and Technologies Conference*, American Institute of Aeronautics and Astronautics, Norfolk, VA, 01-05 November 1999.
[111] Mayrhofer, M., and Sachs, G. “Mission Safety Concept for a Two-Stage Space Transportation Vehicle,” AIAA-2001-1789. *AIAA/NAL-NASDA-ISAS 10th International Space Planes and Hypersonic Systems and Technologies Conference*, American Institute of Aeronautics and Astronautics, Kyoto, Japan, 24-27 April 2001.
[112] Mayrhofer, M., and Sachs, G. “Mission Safety Improvement: A Key Factor for the Success of Next Generation Launchers,” AIAA-2005-5255. *AIAA/AAAF 11th International Space Planes and Hypersonic Systems and Technologies Conference*, American Institute of Aeronautics and Astronautics, Orleans, France, 29 September - 04 October 2002.
[113] Mayrhofer, M., Sachs, G., and da Costa, O. “Mission Abort Trajectories of Orbital Stage with Maximum Longitudinal and Lateral Ranges,” AIAA-2003-7078. *12th AIAA International Space Planes and Hypersonic Systems and Technologies*, American Institute of Aeronautics and Astronautics, Norfolk, VA, 15-19 December 2003.
[114] Messe, C. “Thermostructural Problem of Hypersonic Airbreathing Flight Systems - Modeling and Simulation,” PhD Thesis, Department of Aerospace Engineering and Geodesy, University of Stuttgart, Stuttgart, Germany, 04 August 2017.
[115] Moelyadi, M. A., Jiang, L., and Breitsamter, C. “Investigation of Steady and Unsteady Flow Characteristics of Space Transport System During Separation,” AIAA-2005-3248. *AIAA/CIRA 13th International Space Planes and Hypersonics Systems and Technologies Conference*, American Institute of Aeronautics and Astronautics, Capua, Italy, 16-20 May 2005.
[116] Mooij, E. “Direct Model Reference Adaptive Control of a Winged Re-Entry Vehicle,” AIAA-99-4834. *9th International Space Planes and Hypersonic Systems and Technologies Conference*, American Institute of Aeronautics and Astronautics, Norfolk, VA, 01-05 November 1999.
[117] Mooij, E. “Linear Quadratic Regulator Re-Entry Control: Performance Assessment Using a Taguchi Approach,” AIAA-98-1629. *AIAA 8th International Space Planes and Hypersonic Systems and Technologies Conference*, American Institute of Aeronautics and Astronautics, Norfolk, VA, 27-30 April 1998.
[118] Moore, G. “European Spaceplanes Hermes, Sänger, or Hotol?,” *Electronics & Power*, pp. 252-254, April 1987.
[119] Muller, H. “The High-Flying Legacy of Eugen Sänger,” *Air & Space*, pp. 92-99, Smithsonian Institution, Washington, D.C., August/September 1987.
[120] Myhra, D. *Sänger: Germany's Orbital Rocket Bomber in World War II, Schiffer Military History*, Schiffer Publishing, Atglen, PA, 2002.

[121] Neuwerth, G., Peiter, U., Decker, F., and Jacob, D. “Reynolds Number Effects on the Low-Speed Aerodynamics of the Hypersonic Configuration ELAC-1,” AIAA-98-1578. *AIAA 8th International Space Planes and Hypersonic Systems and Technologies Conference*, American Institute of Aeronautics and Astronautics, Norfolk, VA, 27-30 April 1998.
[122] Oertel, H. “Gaskinetical and Navier-Stokes Simulation of Reentry Flows.” *Proceedings of INRIA and GAMNI-SMAI Workshop on Hypersonic Flows for Reentry Problems*, Antibes, France, 22-25 January 1990.
[123] Olivier, H., and Gronig, H. “Hypersonic Model Testing in a Shock Tunnel,” AIAA-93-5004. *AIAA/DGLR 5th International Aerospace Planes and Hypersonics Technologies Conference*, American Institute of Aeronautics and Astronautics, Munich, Germany, 30 November - 03 December 1993.
[124] Olivier, H., Gronig, H., and Le Bozec, A. “Hypersonic Model Testing in a Shock Tunnel,” *AIAA Journal*, Vol. 33, No. 2, pp. 262-265, February 1995.
[125] Paschen, H., Coenen, R., Gloede, F., Sardemann, G., and Tangen, H. “Technikfolgenabschatzung Zum Raumtransportsystem SÄNGER,” Drucksache 12/4277, Deutscher Bundestag 12. Wahlperiode, Bonner Universitats-Buchdruckerei, Bonn, Germany, June 1992.
[126] Pfeffer, H. “The Actions of the European Space Agency to Prepare for Future Space Transportation Systems - the FESTIP Programme,” AIAA-92-5003. *AIAA 4th International Aerospace Planes Conference*, American Institute of Aeronautics and Astronautics, Orlando, FL, 01-04 December 1992.
[127] Rahn, M., and Schoettle, U. “Safety and Flight Abort Aspects of the SÄNGER Space Transportation System,” AIAA-93-5092. *AIAA/DGLR Fifth International Aerospace Planes and Hypersonics Technologies Conference*, American Institute of Aeronautics and Astronautics, Munich, Germany, 30 November - 03 December 1993.
[128] Rahn, M., Schottle, U. M., and Messerschmid, E. “Impact of Mission Requirements and Constraints on Conceptual Launch Vehicle Design,” AIAA-98-1554. *AIAA 8th International Space Planes and Hypersonic Systems and Technologies Conference*, American Institute of Aeronautics and Astronautics, Norfolk, VA, 27-30 April 1998.
[129] Raible, T., and Jacob, D. “Sensitivity-Based Optimization of Two-Stage-to-Orbit Space Planes with Lifting Body and Waverider Lower Stages,” AIAA-2003-7048. *12th AIAA International Space Planes and Hypersonic Systems and Technologies*, American Institute of Aeronautics and Astronautics, Norfolk, VA, 15-19 December 2003.
[130] Rocci Denis, S., Kau, H. P., and Brandstetter, A. “Experimental Study on Transition between Ramjet and Scramjet Modes in a Dual-Mode Combustor,” AIAA-2003-7048. *12th AIAA International Space Planes and Hypersonic Systems and Technologies*, American Institute of Aeronautics and Astronautics, Norfolk, VA, 15-19 December 2003.
[131] Rocci Denis, S., Maier, D., Erhard, W., and Kau, H. P. “Free Stream Investigations on Methane Combustion in a Supersonic Air Flow,” AIAA-2005-3314. *AIAA/CIRA 13th International Space Planes and Hypersonics Systems and Technologies*, American Institute of Aeronautics and Astronautics, Capua, Italy, 16-20 May 2005.
[132] *AVD Internal*----------
[133] *AVD Internal*----------
[134] Sacher, P. “European Experimental Test Vehicle Options (EXTV) Proposed within FESTIP,” AIAA-99-4876. *9th International Space Planes and Hypersonic Systems and Technologies Conference and 3rd Weakly Ionized Gases Workshop*, American Institute of Aeronautics and Astronautics, Norfolk, VA, 01-05 November 1999.
[135] Sacher, P. “The Engineering Design of Engine/Airframe Integration for the SÄNGER Fully Reusable Space Transportation System,” Chapter 16, RTO-EN-AVT-185, NATO Science and Technology Organization, 16 September 2010.
[136] Sacher, P. “Engineering Engine/Airframe Integration for Fully Reusable Space Transportation Systems,” Chapter 1, RTO-EN-AVT-185, NATO Science and Technology Organization, 16 September 2010.
[137] *AVD Internal*----------
[138] Sacher, P. “Hypersonic Flight Testing Issues,” AIAA-93-5078. *AIAA/DGLR 5th International Aerospace Planes and Hypersonics Technologies Conference*, American Institute of Aeronautics and Astronautics, Munich, Germany, 30 November - 03 December 1993.
[139] Sacher, P. “European Experimental Test Vehicle Options: Proposed within FESTIP,” *Air & Space Europe*, Vol. 3, No. 1-2, pp. 85-91, January-April 2001.
[140] Sachs, G., and Schoder, W. “Robust Control of the Separation of Hypersonic Lifting Vehicles,” AIAA-92-5013. *AIAA 4th International Aerospace Planes Conference*, American Institute of Aeronautics and Astronautics, Orlando, FL, 01-04 December 1992.
[141] Samuelsson, L., and Satmark, T. “Design and Testing of an Actively Cooled Nozzle Component for a Hypersonic Ram Engine,” AIAA-96-4551. *AIAA 7th International Space Planes and Hypersonic Systems and Technologies Conference*, American Institute of Aeronautics and Astronautics, Norfolk, VA, 18-22 November 1996.
[142] Sänger, E. “Recent Results in Rocket Flight Technique,” NACA-TM-1012, National Advisory Committee for Aeronautics, Washington, D.C., 01 April 1942.
[143] Sänger, E. “Accurate Calculation of Multispar Cantilever and Semicantilever Wings with Parallel Webs under Direct and Indirect Loading,” NACA-TM-662, National Advisory Committee for Aeronautics, Washington, D.C., 01 March 1932.
[144] Sänger, E. “Dinner Speech on the Occasion.” *16th AIAA/DLR/DGLR International Space Planes and Hypersonic Systems and Technologies Conference*, Bremen, Germany, 19-22 October 2009.
[145] Sänger, E. *Raketen-Flugtechnik*, Verlag von R. Oldenbourg, Munchen und Berlin, 1933.
[146] Sänger, E. “Zur Theorie Der Photoraketen,” Band 21, Ingenieur-Archiv, 1953.
[147] Sänger, E. *Raumfahrt-Technische Uberwindung Des Krieges - Aktuelle Aspekte Der Uberschall-Luftfahrt Und Raumfahrt*, Rowohlt, Hamburg, Germany, 1958.
[148] Sänger, E. “Photon Propulsion,” *Handbook of Astronautical Engineering*, edited by Koelle, H. H., McGraw-Hill, New York, 1961.
[149] Sänger, E. *Space Flight - Countdown for the Future*, McGraw-Hill Book Company, 1965.
[150] Sänger, E. “Rocket Flight Engineering,” NASA-TT-F-223, National Aeronautics and Space Administration, Washington, D.C., September 1965.
[151] Sänger, E., and Bredt, I. *A Rocket Drive for Long Range Bombers*, Technical Information Branch Buaer, Navy Department, Santa Barbera, CA, August 1944.
[152] Sänger, E., and Bredt, I. “A Ram-Jet Engine for Fighters,” NACA-TM-1106, National Advisory Committee for Aeronautics, Washington, D.C., October 1947.

[153] Sänger, H. E., and Szames, A. D. "From the Silverbird to Interstellar Voyages," IAC-03-IAA.2.4.a.07. *54th International Astronautical Congress of the International Astronautical Federation, International Academy of Astronautics, International Institute of Space Law*, Bremen, Germany, 03 October 2003.
[154] Sänger-Bredt, I. "The Silver Bird Story: A Memoir," *Essays on the History of Rocketry & Astronautics: Proceedings of the Third to the Sixth History Symposium of the International Academy of Astronautics (IAA)*, Vol. 1, National Aeronautics and Space Administration, Washington, D.C., 1977.
[155] Sänger-Bredt, I., and Engel, R. "The Development of Regeneratively Cooled Liquid Rocket Engines in Austria and Germany, 1926-42," No. 10, Smithsonian Annals of Flight. *First Steps Towards Space: Proceedings of the First and Second History Symposia of the International Academy of Astronautics*, Belgrad, Yugoslavia, 26 September 1967, and New York, USA, 17 October 1968.
[156] Schoettle, U., and Rahn, M. "Effects of Extended Airbreathing Operation by Scramjet Propulsion on Vehicle Design of a Two-Stage Launch System," AIAA-93-5009. *AIAA/DGLR 5th International Aerospace Planes and Hypersonics Technologies Conference*, American Institute of Aeronautics and Astronautics, Munich, Germany, 30 November - 03 December 1993.
[157] Schoettle, U. M., Grallert, H., and Hewitt, F. A. "Advanced Air-Breathing Propulsion Concepts for Winged Launch Vehicles," *Acta Astronautica*, Vol. 20, pp. 117-129, 1989.
[158] Sobieczky, H., and Stroeve, J. C. "Generic Supersonic and Hypersonic Configurations," AIAA-91-3301CP. *9th AIAA Applied Aerodynamics Conference*, American Institute of Aeronautics and Astronautics, Baltimore, MD, 23-26 September 1991.
[159] *AVD Internal*----------
[160] Staudacher, W., and Wimbauer, J. "Design Sensitivities of Airbreathing Hypersonic Vehicles," AIAA-93-5099. *AIAA/DGLR 5th International Aerospace Planes and Hypersonics Technologies Conference*, American Institute of Aeronautics and Astronautics, Munich, Germany, 30 November - 03 December 1993.
[161] Staufenbiel, R. "Horizontal Aerospace Transport Systems," Paper No. 21. *Space Course on Low Earth Transportation and Orbital Systems*, Aachen, Germany, 1991.
[162] Steinebach, D., Kuhl, W., and Gallus, H. "Design Aspects of the Propulsion System for Aerospace Planes," AIAA-93-5127. *AIAA/DGLR 5th International Aerospace Planes and Hypersonics Technologies Conference*, American Institute of Aeronautics and Astronautics, Munich, Germany, 30 November - 03 December 1993.
[163] Steinhoff, J., and Mersch, T. "Computation of Vortex Formation over ELAC-1 Configuration Using Vorticity Confinement," AIAA-95-6157. *AIAA Sixth International Aerospace Planes and Hypersonics Technologies Conference*, American Institute of Aeronautics and Astronautics, Chattanooga, TN, 03-07 April 1995.
[164] Strobel, C., Knott, U., and Kruger, W. "Lightweight Structures for Hypersonic Propulsion Systems," AIAA-93-5037. *AIAA/DGLR 5th International Aerospace Planes and Hypersonics Technologies Conference*, American Institute of Aeronautics and Astronautics, Munich, Germany, 30 November - 03 December.
[165] Strohmeyer, D., Eggers, T., Heinze, W., and Bardenhagen, A. "Planform Effects on the Aerodynamics of Waveriders for TSTO Missions," AIAA-96-4544-CP. *AIAA 7th International Space Planes and Hypersonic Systems and Technologies Conference*, American Institute of Aeronautics and Astronautics, Norfolk, VA, 18-22 November 1996.
[166] Stromberg, A., and Decker, F. "Aachener Hyperschallkonfiguration ELAC I Im Hochdruckwindkanal Der DLR," *Luft- und Raumfahrt*, pp. 14-17, DGLR, June 1993.
[167] Treinies, N., and et al. "Das Raumtransportsystem SÄNGER - Billiger in den Orbit?," DLR-IB 30106-91/4, Vorstudie für eine Technikfolgenabschätzung, Im Auftrag des Büros für Technikfolgen-Abschätzung des Deutschen Bundestags, DLR Hauptabteilung Systemanalyse Raumfahrt (HA-SR), Leitung: H. Sax, Koln-Porz, Germany, 21 December 1990.
[168] Trollheden, S., and Streifinger, H. "Secondary Power System Study for the SÄNGER First Stage Vehicle," AIAA-93-5033. *AIAA/DGLR 5th International Aerospace Planes and Hypersonics Technologies Conference*, American Institute of Aeronautics and Astronautics, Munich, Germany, 30 November - 03 December 1993.
[169] Van den Abeelen, L. "Competition and the Others: Spacecraft from Around the World," *Spaceplane Hermes - Europe's Dream of Independent Manned Spaceflight*, Spring-Praxis Books, Cham, Switzerland, 2017, pp. 173-177.
[170] Weiland, C. *Aerodynamic Data of Space Vehicles*, Springer-Verlag, Berlin, Germany, 2014.
[171] Weingartner, S. "SÄNGER - the Reference Concept of the German Hypersonics Technology Program," AIAA-93-5161. *AIAA/DGLR 5th International Aerospace Planes and Hypersonics Technologies Conference*, American Institute of Aeronautics and Astronautics, Munich, Germany, 30 November - 03 December 1993.
[172] Weingartner, S., and Kuczera, H. "Selection and Design Guidelines for Future Space Transportation Systems," AIAA-93-5013. *AIAA/DGLR 5th International Aerospace Planes and Hypersonics Technologies Conference*, American Institute of Aeronautics and Astronautics, Munich, Germany, 30 November - 03 December 1993.
[173] Williamson, M. "Hypersonic Transport ... 30 Years and Holding?," *Aerospace America*, pp. 40-45, May 2012.
[174] Winter, F. H. "History of Rocketry and Astronautics," *AAS History Series Proceedings of the 33rd History Symposium of the International Academy of Astronautics*, Vol. 28, Amsterdam, The Netherlands, 1999.
[175] Wolf, D., and Daum, A. "DSL - A Near Term Aerospace Plane Concept," AIAA-93-5100. *AIAA/DGLR 5th International Aerospace Planes and Hypersonics Technologies Conference*, American Institute of Aeronautics and Astronautics, Munich, Germany, 30 November - 03 December 1993.
[176] Zaganescu, N.-F. "Dr. Irene Sänger-Bredt: A Life for Astronautics," *Acta Astronautica*, Vol. 55, No. 11, pp. 889-894, December 2004.
[177] Zahringer, C. "Untersuchung Der Separationsdynamik Eines Zweistufigen Hyperschall-Flugsystems Unter Besonderer Berücksichtigung Der Seitenbewegung," Doktor-Ingenieur Dissertation, Lehrstuhl fur Flugmechanik und Flugregelung, Technische Universitat Munchen, Munich, Germany, 19 April 2005.
[178] Zahringer, C., Heller, M., and Sachs, G. "Lateral Separation Dynamics and Stability of a Two-Stage Hypersonic Vehicle," AIAA-2003-7080. *12th AIAA International Space Planes and Hypersonic Systems and Technologies*, American Institute of Aeronautics and Astronautics, Norfolk, VA, 15-19 December 2003.
[179] *AVD Internal*----------
[180] Zellner, B., Sterr, W., and Herrmann, O. "Integration of Turbo-Expander- and Turbo-Ramjet-Engines in Hypersonic Vehicles," 92-GT-204. *ASME 1992 International Gas Turbine and Aeroengine Congress and Exposition*, The American Society of Mechanical Engineers, Cologne, Germany, 01-04 June 1992.

B.7. NASP/X-30/Orient Express Bibliography

[1] Acosta, M. G. “The Retro-Rotary (REM) - NASP Aerospace Plane - Concept Design Evaluation,” CIFRA doc. 09-021, Bogota, Colombia, 14 July 2012.

[2] Alberico, J. “The Development of an Interactive Computer Tool for Synthesis and Optimization of Hypersonic Airbreathing Vehicles,” AIAA-92-5076. *AIAA 4th International Aerospace Planes Conference*, American Institute of Aeronautics and Astronautics, Orlando, FL, 1992. https://doi.org/10.2514/6.1992-5076

[3] Anderson, R. H. “Zero Margin Requirements Allocation for WBS 1133 and 1200,” BN09879, NASP General Dynamics, Fort Worth Division, 27 February 1991.

[4] Anon. X-30 Timeline.

[5] Anon. “Accessibility - Margin Issues,” NPO-SE-9101, National Program Office, NASP.

[6] Anon. “Compatibility of SCS-6/Beta 21S with the NASP Environment to 1500 °F,” New Aircraft and Missile Products, McDonnell Douglas Aerospace, St. Louis, MO.

[7] Anon. “Engine Weight Reduction Plan Near-Term Goals,” [Presentation], NASP.

[8] Anon. “HYFLITE Hypersonic Flight Test Experiment Technical Status,” [Presentation], NASP.

[9] Anon. “Impact of Engine Performance and Empty Weight Reductions on the NASP Vehicle Closure.”

[10] Anon. “Multidisciplinary Methods Used in CSO,” Press Flyer, Double-Side, Final NASP Configuration.

[11] Anon. “NASP Low-Speed System Summary.”

[12] Anon. “X-30 National Aero-Space Plane (NASP) - Made in America, Our Nation Cannot Afford the Alternative.”

[13] Anon. “NDV Airbreather/Rocket HT/HL SSTO Technology Level Evaluation.”

[14] Anon. “Vehicle 200 Hot vs. Cold Structure Trade Study - Qualitative Summary,” NASP Special Program Data, Structures/Materials Team, NASP.

[15] *AVD Internal*----------

[16] *AVD Internal*----------

[17] *AVD Internal*----------

[18] Anon. Cabin Layout, Top View, Economy/First Class. McDonnell Douglas.

[19] Anon. “Beta-21S Titanium Alloy.”

[20] Anon. “Aerospaceplane to NASP: The Lure of Air-Breathing Hypersonics,” *AERONAUTICS*. http://ourairports.biz/?p=2411, 02 November 2015.

[21] Anon. “Williams Names 6 Topics for Academic Research,” *Military Space*, Pash Publications, Arlington, VA, 03 August 1987.

[22] Anon. “National Aero-Space Plane: Restructuring Future Research and Development Efforts,” GAO/NSIAD-93-71, Report to Congressional Requesters, National Security and International Affairs Division, United States General Accounting Office, Washington, D.C., 03 December 1992.

[23] Anon. “Aerospace Plane Technology: Research and Development Efforts in Japan and Australia,” GAO/NSIAD-92-5, National Security and International Affairs Division, United States General Accounting Office, Washington, D.C., 04 October 1991.

[24] Anon. “DSB Review of NASP - 1987,” DSB CH14, Charter and Results, 10 March 1992.

[25] Anon. “NASP Status Report - Response to Defense Science Board,” 12 May 1992.

[26] Anon. “Ten-Year Space Launch Technology Plan,” NASA-TM-108701, National Aeronautics and Space Administration, 12 November 1992.

[27] Anon. “Comparison of Current NASP Configuration to DARPA Government Baseline Vehicle (GBV) Concept (U),” Memo, 15 August 1991.

[28] Anon. “Weekly Design Review Agenda,” CFG-9001-CF13, National Program Office, NASP, 16 August 1990.

[29] Anon. “National Aero-Space Plane: A Need for Program Direction and Funding Decisions,” GAO/NSIAD-93-207, Report to Congressional Requesters, National Security and International Affairs Division, United States General Accounting Office, Washington, D.C., 18 June 1993.

[30] Anon. “Engine System Weight Status,” [Presentation], NASP, 21 July 1992.

[31] Anon. “Aerospace Plane Technology: Research and Development Efforts in Europe,” GAO/NSIAD-91-194, Report to the Chairman, Committee on Science, Space, and Technology, House of Representatives, National Security and international Affairs Division, United States General Accounting Office, Washington, D.C., 25 July 1991.

[32] Anon. “Alternate Low Speed Accelerator Study - Trade Study #130,” LSA 100, NPO Engineering Council Review, National Program Office, NASP, 26 February 1991.

[33] Anon. “National Aero-Space Plane: A Technology Development and Demonstration Program to Build the X-30,” GAO/NSIAD-88-122, Report to Congressional Committees, National Security and International Affairs Division, United States General Accounting Office, Washington, D.C., 27 April 1988.

[34] Anon. “Propulsion System Margin Summary,” RD-835-MDC-01, NASP, 27 February 1991.

[35] Anon. “Base Pressure Control and Mixing at High Speeds,” RD-RE-4/91-CC001, Informal Discussions at NASA-LaRC, NASP, 29 February 1991.

[36] Anon. “Propulsion System Status Volume - E22A Preliminary,” NASP, 29 June 1992.

[37] Anon. “Integrated Technology Plan for the Civil Space Program,” NASA-TM-107988, Office of Aeronautics and Space Technology, NASA, Washington, D.C., 1991.

[38] Anon. “Low Speed Nozzle Performance - Factors Considered in Estimates,” misc., around 1989.

[39] Anon. “Round Trip to Orbit: Human Spaceflight Alternatives - Special Report,” OTA-ISC-419, Office of Technology Assessment, U.S. Congress, U.S. Government Printing Office, Washington, D.C., August 1989.

[40] Anon. NASP and Md-2001 Flight Vehicle Renderings. McDonnell Douglas Corporation, St. Louis, MO, January 1989.

[41] Anon. “Into Orbit with Reusable Spacecraft,” *Spaceflight: The International Magazine of Space and Astronautics*, Vol. 35, No. 3, The British Interplanetary Society, March 1993.

[42] *AVD Internal*----------

[43] Anon. “Five Firms Will Study Advanced Avionics Design,” *Defense Week*, Monday, 14 February 1983.

[44] Atamanchuk, T., Sislian, J., and Dudebout, R. “An Aerospace Plane as a Detonation Wave Ramjet/Airframe Integrated Waverider,” AIAA-92-5022. *AIAA 4th International Aerospace Planes Conference*, American Institute of Aeronautics and Astronautics, Orlando, FL, 01-04 December 1992. https://doi.org/10.2514/6.1992-5022
[45] Augenstein, B. W., and Harris, E. D. “The National Aerospace Plane (NASP): Development Issues for the Follow-on Vehicle - Executive Summary,” R-3878/1-AF, A Project Air Force Report, RAND, 1993.
[46] Augustine, N. R., Letter to Harold D. Altis, Executive Vice President. McDonnell Douglas Corporation, 06 October 1983.
[47] Ault, D., and Van Wie, D. “Comparison of Experimental Results and Computational Analysis for the External Flowfield of a Scramjet Inlet at Mach 10 and 13,” AIAA-92-5100. *AIAA 4th International Aerospace Planes Conference*, American Institute of Aeronautics and Astronautics, Orlando, FL, 01-04 December 1992. https://doi.org/10.2514/6.1992-5100
[48] Balepin, V., Czysz, P. A., Maita, M., and Vandenkerckhove, J. “Assessment of S.S.T.O. Performance with In-Flight LOX Collection,” AIAA-95-6047. *6th International Aerospace Planes and Hypersonics Technologies*, American Institute of Aeronautics and Astronautics, Chattanooga, TN, April 1995.
[49] Balepin, V., Czysz, P. A., and Moszee, R. H. “Combined Engine for a Reusable Launch Vehicle (KLIN Cycle),” AIAA-2001-1911. *10th International Space Planes and Hypersonic Systems and Technologies Conference*, American Institute of Aeronautics and Astronautics, Kyoto, Japan, 24-27 April 2001.
[50] Bardina, J., Coakley, T., and Marvin, J. “Two-Equation Turbulence Modeling for 3-D Hypersonic Flows,” AIAA-92-5064. *AIAA 4th International Aerospace Planes Conference*, American Institute of Aeronautics and Astronautics, Orlando, FL, 01-04 December 1992. https://doi.org/10.2514/6.1992-5064
[51] Barthelemy, R. R. “The National Aerospace Plane Program: A Revolutionary Concept,” *John Hopkins APL Technical Digest*, Vol. 11, No. 3 and 4, pp. 312-318, 1990.
[52] Bennett, G. “X-30 National Aero-Space Plane Mockup Set to Roll Out,” Release: 92-XX, 10 June 1992.
[53] Benson, J. “Requirements and Integration - External Rocket System (ERS),” WBS 1311.7, Engineering Council Review, External Rocket System Team, National Program Office, NASP, 02 May 1991.
[54] Benson, J. “External Rocket System (ERS) Concept Trade Study (#217) Final Results,” No. 91-195, System Engineering Use, Coordination Memorandum, National Program Office, NASP, 26 April 1991.
[55] Benton, M. G. “Design Synthesis of Shuttle-Class Hypersonic SSTO Vehicle,” AIAA-90-0297. *28th Aerospace Sciences Meeting*, American Institute of Aeronautics and Astronautics, Reno, NV, 08-11 January 1990. https://doi.org/10.2514/6.1990-297
[56] Billig, F. S., and Schetz, J. A. “Analysis of Penetration and Mixing of Gas Jets in Supersonic Cross Flow,” AIAA-92-5061. *AIAA 4th International Aerospace Planes Conference*, American Institute of Aeronautics and Astronautics, Orlando, FL, 01-04 December 1992. https://doi.org/10.2514/6.1992-5061
[57] *AVD Internal*----------
[58] Bogue, R., and Erbland, P. “Perspective on the National Aero-Space Plane Program Instrumentation Development,” AIAA-92-5086. *AIAA 4th International Aerospace Planes Conference*, American Institute of Aeronautics and Astronautics, Orlando, FL, 01-04 December 1992. https://doi.org/10.2514/6.1992-5086
[59] Borling, J. E. “High-Speed Propulsion Overview,” [Presentation], Pratt & Whitney, June 1991.
[60] Bowcutt, K. “Hypersonic Aircraft Optimization Including Aerodynamic, Propulsion, and Trim Effects,” AIAA-92-5055. *AIAA 4th International Aerospace Planes Conference*, American Institute of Aeronautics and Astronautics, Orlando, FL, 01-04 December 1992. https://doi.org/10.2514/6.1992-5055
[61] Boyden, R. P., Dress, D. A., Fox, C. H., Huffman, J. K., and Cruz, C. I. “Subsonic Static and Dynamic Stability Characteristics of a NASP Configuration,” *Journal of Aircraft*, Vol. 31, No. 4, pp. 879-885, July-August 1994.
[62] Brewer, G. D. “Hypersonic Aircraft,” *Hydrogen Aircraft Technology*, 1st ed., CRC Press, 1991, pp. 247-300.
[63] Brinson, M. “Phase 2D Technical Objectives Document and National Aero-Space Plane Phase 2 Exit Criteria,” NASP Facsimile Record, 06 February 1991.
[64] Brinson, M. “201 Sensitivities,” message to Larry Hunt, 24 March 1992.
[65] Brown, S. F. “Reusable Rocket Ships: New Low-Cost Rides to Space,” *Popular Science*, pp. 49-55, February 1994.
[66] Brown, S. F. “X-30 - Out of This World in a Scramjet,” *Popular Science*, pp. 70-112, November 1991.
[67] Brumfield, G. “On Wings and a Prayer,” *Nature*, Vol. 421, News Feature, pp. 684-685, Nature Publishing Group, 13 February 2003.
[68] Bruner III, W. W. “National Security Implications of Inexpensive Space Access,” *Beyond the Paths of Heaven: The Emergence of Space Power Thought*, Air University Press, Maxwell AFB, AL, September 1999, pp. 365-436.
[69] Burkardt, L. A. “NASA Lewis Two Stage to Orbit System Studies,” TSTO1a.DRW LAB/KMH, [Presentation], Propulsion Analysis Branch, 15 November 1990.
[70] Butler, D., and Moore, R. “Liquid and Slush Hydrogen Ground Support Facilities for Aerospace Planes,” AIAA-92-5068. *AIAA 4th International Aerospace Planes Conference*, American Institute of Aeronautics and Astronautics, Orlando, FL, 01-04 December 1992. https://doi.org/10.2514/6.1992-5068
[71] Butrica, A. J. “Reusable Launch Vehicles or Expendable Launch Vehicles? A Perennial Debate,” *Critical Issues in the History of Spaceflight, The NASA History Series*, CreateSpace Independent Publishing Platform, 09 November 2013, pp. 301-341.
[72] Calise, A. J., Corban, J. E., and Flandro, G. A. “Trajectory Optimization and Guidance Law Development for National Aerospace Plane Applications,” Final Report, Langley Research Center, NASA Supported, December 1988. https://doi.org/10.23919/ACC.1988.4789941
[73] Canan, J. W. “Mastering the Transatmosphere,” *AIR FORCE Magazine*, pp. 48-54, June 1986.
[74] Carter, P. “Ground System Requirements for Aerospace Planes,” AIAA-92-5069. *AIAA 4th International Aerospace Planes Conference*, American Institute of Aeronautics and Astronautics, Orlando, FL, 01-04 December 1992. https://doi.org/10.2514/6.1992-5069
[75] Castleberry, G. “External Rocket Concept Trade Study Status,” No. 90-181, System Engineering Use, Coordination Memorandum, National Program Office, NASP, 15 November 1990.
[76] Chang, K. T. “25 Years Ago, NASA Envisioned Its Own 'Orient Express',” *The New York Times*, 20 October 2014.
[77] Chaput, A. J. “International Competition - the NASP Challenge,” AIAA-89-5018. *AIAA National Aerospace Plane Conference*, American Institute of Aeronautics and Astronautics, Dayton, OH, 20-21 July 1989. https://doi.org/10.2514/6.1989-5018
[78] Chaput, A. J., and Imfeld, W. F. “CTM/GTM Technical Exchanges,” ED-NPO-91-001, Engineering Directive.

[79] Chase, R. L. “Performance Assessment of Single-Stage-to-Orbit Vehicle Propulsion Concepts, or Is Atmospheric Oxygen Really Free?,” AIAA-89-2293. *AIAA/ASME/SAE/ASEE 25th Joint Propulsion Conference*, American Institute of Aeronautics and Astronautics, Monterey, CA, 10-12 July 1989.
[80] Chase, R. L. “A Comparison of Horizontal and Vertical Launch Modes for Earth-to-Orbit NASP-Technology Enabled Vehicles,” AIAA-91-2388. *AIAA/SAE/ASME 27th Joint Propulsion Conference*, American Institute of Aeronautics and Astronautics, Sacramento, CA, 24-26 June 1991.
[81] Chase, R. L., and Tang, M. H. “A History of the NASP Program from the Formation of the Joint Program Office to the Termination of the HySTP Scramjet Performance Demonstration Program,” AIAA-95-6031. *AIAA 6th International Aerospace Planes and Hypersonics Technologies Conference*, American Institute of Aeronautics and Astronautics, Chattanooga, TN, 03-07 April 1995. https://doi.org/10.2514/6.1995-6031
[82] Chavez, F. R., and Schmidt, D. K. “Analytical Aeropropulsive/Aeroelastic Hypersonic-Vehicle Model with Dynamic Analysis,” *Journal of Guidance, Control, and Dynamics*, Vol. 17, No. 6, pp. 1308-1319, November - December 1994.
[83] Cheng, P., Chan, S., Myers, T., Klyde, D., and McRuer, D. “Aeroservoelastic Stabilization Technique Refinement for Hypersonic Flight Vehicles,” AIAA-92-5014. *AIAA 4th International Aerospace Planes Conference*, Orlando, FL, 01-04 December 1992.
[84] Clifton, J. V. “Margin Issues WBS 1133 - Engine-Airframe Integration,” NPO-AERO-9101, NASP, National Program Office, 27 February 1991.
[85] Cole, S. R., Florance, J. R., Thomason, L. B., Spain, C. V., and Bullock, E. P. “Supersonic Aeroelastic Instability Results for A NASP-Like Wing Model,” NASA-TM-107739, Langley Research Center, NASA, Hampton, VA, April 1993. https://doi.org/10.2514/6.1993-1369
[86] Collier, C. “Structural Analysis and Sizing of Stiffened, Metal Matrix Composite Panels for Hypersonic Vehicles,” AIAA-92-5015. *AIAA 4th International Aerospace Planes Conference*, American Institute of Aeronautics and Astronautics, Orland, FL, 01-04 December 1992. https://doi.org/10.2514/6.1992-5015
[87] Conesa, E. “Organizational Dynamics and the Evolutionary Dilemma between Diversity and Standardization in Mission-Oriented Research Programmes: An Illustration,” IR-97-023, International Institute for Applied Systems Analysis (IIASA), Laxenburg, Austria, May 1997.
[88] Cook, R. “External Rocket Trade Study Plans,” No. 90-139, System Engineering Use, Coordination Memorandum, National Program Office, NASP, 23 October 1990.
[89] Cooper, H. F. “On Spaceplane and X Vehicles,” Testimony to the House Subcommittee on Space and Aeronautics Committee on Science, 11 October 2001.
[90] Corsmeyer, C. “NASP News Reference,” Viewgraphs, Aerospace Technology Innovation Workshop, NASA Ames, Sponsored by NSF, McDonnell Douglas.
[91] Cox, T. H., Sachs, G., Knoll, A., and Stich, R. “A Flying Qualities Study of Longitudinal Long-Term Dynamics of Hypersonic Planes,” NASA-TM-104308, Dryden Flight Research Center, NASA, Edwards AFB, CA, April 1995. https://doi.org/10.2514/6.1995-6150
[92] Cribbs, D. “Performance Uncertainty Briefing,” NASP Special Program Data, General Dynamics Fort Worth Division, NASP, 10 January 1991.
[93] Cribbs, D. “Performance Uncertainty,” NPO-SE-AJC, National Program Office, NASP, 15 January 1991.
[94] Cribbs, D. “Performance Uncertainty Analysis for NASP.” *2nd International Aerospace Planes Conference*, American Institute of Aeronautics and Astronautics, Orlando, FL, 29-31 October 1990. https://doi.org/10.2514/6.1990-5209
[95] Czysz, P., and Warnecke, M. “Earth to Orbit Aerospace Planes - Dream or Reality?,” AIAA-92-5083. *AIAA 4th International Aerospace Planes Conference*, American Institute of Aeronautics and Astronautics, Orlando, FL, 01-04 December 1992. https://doi.org/10.2514/6.1992-5083
[96] Czysz, P. A., Geometric Descriptors.
[97] Czysz, P. A., Paired Comparison.
[98] Czysz, P. A. “McDonnell Aircraft Company Hypersonic Configuration and Control Development,”
[99] Czysz, P. A., K_w, S_p, K_{geo}, S_{wet}, K_{total}, K_p, Etc. Correlations.
[100] Czysz, P. A., Flight Boundaries Based on Wing Loading, Load Factor, and Material Temperature Limits.
[101] Czysz, P. A., Cross-Section Study for Fighters.
[102] Czysz, P. A., Spatula Sänger, Modified Sänger.
[103] Czysz, P. A. “Combined Cycle Propulsion - Is It the Key to Achieving Low Payload to Orbit Costs?.” *14th International Symposium on Air Breathing Engines (ISABE)*, Florence, Italy, 05-12 September 1999.
[104] Czysz, P. A. “System Concepts and Technology Challenges for the XXI Century.” *Short Course on Integration of Space Transportation Vehicles*, Marshall Space Flight Center (MSFC), NASA, 07-11 February 2000.
[105] Czysz, P. A. “Testing Hypersonic Airbreathing Engines: A Perspective,” ISABE-97-7036. *13th International Symposium on Air Breathing Engines*, Chattanooga, TN, 07-12 September 1997.
[106] Czysz, P. A. “A SSTO Launcher/Demonstrator Concept for International Development of a Flight Test Vehicle,” St. Louis University. *Proceeding of the International Workshop on Spaceplane/RLV Technology Demonstrators*, Tokyo, Japan, 10-12 March 1997.
[107] Czysz, P. A. “Interaction of Propulsion Performance with Available Design Space.” *12th International Symposium on Air Breathing Engines (ISABE)*, Melbourne, Australia, 10-15 September 1995.
[108] Czysz, P. A. “Energy Analysis of High Speed Flight Systems - Size and Thrust Potential.” *JANNAF Workshop on Scramjet Performance*, Albuquerque, NM, 11-12 December 1996. 2
[109] Czysz, P. A. “'Supersonic Hydrogen Combustion Studies' - Retrospective 1993.” *1st JANNAF Workshop Scramjet Combustor Performance, AIAA 31st Aerospace Sciences Meeting and Exhibit*, Reno, NV, 14 January 1993.
[110] Czysz, P. A. “System Concepts and Technology Challenges for the XXI Century Integration of Rocket and Air-Breathing Propulsion Systems.” *The AIAA Space Transportation Technical Committee 'Great Debate'*, 14 March 2000.
[111] Czysz, P. A. “SSTO Launcher/Demonstrator with Combined Cycle Propulsion Options,” *Hypersonic Aircraft: Lifting Re-Entry and Launch, Philosophical Transactions: Mathematical, Physical and Engineering Sciences*, Vol. 357, No. 1759, pp. 2285-2316, 15 August 1999.
[112] Czysz, P. A. “SSTO Launcher Design Space Convergence and Rocket Based Combined Cycle (RBCC) Propulsion Systems,” by invitation. *2nd National Conference on Air Breathing and Aerospace Propulsion*, Thriuvananthapuram, India, 15-17 December 1994.

[113] Czysz, P. A. "Rocket Based Combined Cycle (RBCC) Offers Developmental and Operational Advantages," IAF-93-S.4.477. *44th Congress of the International Astronautical Federation*, Graz, Austria, 16-22 October 1993.
[114] *AVD Internal*----------
[115] Czysz, P. A. "Advanced Propulsion Concepts for the XXIst Century." *IAA Workshop on Advanced Space Propulsion Concepts, A World View of Space Propulsion for the Next 40 Years*, 20-21 January 1998.
[116] Czysz, P. A. "Air Breather vs. Rocket, Is the Rocket the Only Reliable, Demonstrable Space Propulsion System?," Presented at Hypersonic Propulsion Session, 3HP2. *1993 SAE Aerospace Atlantic Conference*, Dayton, OH, 20-23 April 1993.
[117] Czysz, P. A. "Hypersonic Aircraft as a Vehicle to Teach Practical Aircraft Design," Presented at Hypersonic Systems Concepts Session 3HP3. *1993 SAE Aerospace Atlantic Conference*, Dayton, OH, 20-23 April 1993.
[118] Czysz, P. A. "Rocket Based Combined Cycle (RBCC) Propulsion Systems Offer Additional Options." *11th International Symposium on Air Breathing Engines (ISABE)*, American Institute of Aeronautics and Astronautics, Tokyo, Japan, 20-24 September 1993.
[119] *AVD Internal*----------
[120] Czysz, P. A. "Propulsion Concepts and Technology Challenges for the XXIst Century," Propulsion in Space Transportation. *5th Symposium International*, Carre des Sciences, Paris, France, 22-24 May 1996.
[121] Czysz, P. A. "Oral Introduction to Paper: Propulsion Concepts and Technology Challenges for the XXIst Century." *5th International Symposium*, Carre des Sciences, Paris, France, 22-24 May 1996.
[122] Czysz, P. A. "Combined Cycle Propulsion for the XXIst Century." *RBCC Workshop*, The University of Alabame in Huntsville, Huntsville, AL, 25-26 February 1998.
[123] Czysz, P. A. "Foreign SpacePlane Concepts," AIAA-90-3836. *AIAA Space Programs and Technologies Conference*, American Institute of Aeronautics and Astronautics, Huntsville, AL, 25-28 September 1990.
[124] Czysz, P. A. "Can Combined Cycle Propulsion Lower Launch 21st Century Launch Costs." *NSJSASS Meeting*, Sendai, Japan, 27 February 1998.
[125] Czysz, P. A. "Space Transportation Systems Requirements Derived from the Propulsion Performance," IAF-92-0858, Hypersonic and Combined Cycle Propulsion Session, 1991 IAF Congress. *43rd Congress of the International Astronautical Federation (IAF)*, Washington, D.C., 28 August - 05 September 1992.
[126] Czysz, P. A. "Earth to Orbit Aerospace Planes: What Prevents the Realization of This Long Held Dream," by invitation. *International Workshop on Aerospace Planes/Hypersonic Technology*, Tokyo, Japan, 28 February - 02 March 1994.
[127] *AVD Internal*----------
[128] Czysz, P. A. "Conservation of Available Energy - An Excellent Return on Investment," invited keynote address. *NASA Langley Workshop on 'Performance Enhancement for Hypervelocity Airbreathing Propulsion'*, [Presentation], by invitation only, 29-31 July 1991.
[129] Czysz, P. A. "Addendum to Presentation Conservation of Available Energy." *NASA Langley Workshop on 'Performance Enhancement for Hypervelocity Airbreathing Propulsion'*, [Presentation], by invitation only, 29-31 July 1991.
[130] *AVD Internal*----------
[131] Czysz, P. A. "Hypersonic Vehicles," *Aeronautical Technology 2000: A Projection of Advanced Vehicle Concepts*, Report of the Panel on Vehicle Applications, National Research Council, National Academy Press, Washington, D.C., 1985, pp. 45-58.
[132] Czysz, P. A. "Transatmospheric Vehicle," *Aeronautical Technology 2000: A Projection of Advanced Vehicle Concepts*, Report of the Panel on Vehicle Applications, National Research Council, National Academy Press, Washington, D.C., 1985, pp. 45-58.
[133] Czysz, P. A. "Definition of the Design Space in Which Convergence Can Occur with a Combined Cycle Propulsion System," *Acta Astronautica*, Vol. 37, pp. 179-192, 1995.
[134] Czysz, P. A. "A Demonstrator for the SSTO Launcher with Combined Cycle Propulsion," *Phil Trans, Royal Society London*, Vol. 357, pp. 2285-2316, 1999.
[135] Czysz, P. A. "Propulsion Sharpens the Focus for Hypersonic Design," AIAA-93-4012. *Aircraft Design Systems, and Operations Conference*, American Institute of Aeronautics and Astronautics, Monterey, CA, August 1993.
[136] Czysz, P. A. "Hypersonic Convergence Interdependence: Airframe - Propellant - Propulsion," McDonnell Douglas Corporation, February 1987.
[137] Czysz, P. A. "Maximize the Energy Conserved, Minimized the Energy Expended, Yields Excellent ROI," invited keynote address. *European Space Agency FESTIP Workshop*, Frascati, Italy, February 1992.
[138] Czysz, P. A. "Definition of the Design Space in Which Convergence Can Occur with a Combined Cycle Propulsion System," IAF-94-S.4.427. *45th Congress of the International Astronautical Federation*, Jerusalem, Israel, October 1994.
[139] Czysz, P. A., and Bruno, C. "Interaction of the Propulsion System and System Parameters Determine the Design Space Available for Solutions," IAF Paper 00-S.5.07. *51st International Astronautical Congress*, Rio de Janeiro, Brazil, 02-06 October 2000.
[140] Czysz, P. A., Bruno, C., and Kato, K. "Interactions between Propulsion Systems and the Configuration Concepts Defines the Design Space," AIAA-2001-1924. *10th International Space Planes and Hypersonic Systems and Technologies Conference*, American Institute of Aeronautics and Astronautics, Kyoto, Japan, 24-27 April 2001.
[141] Czysz, P. A., Bruno, C., and Lee, Y. M. "Is the Most Versatile Earth-to-Orbit Launcher a TSTO and Not a SSTO," Paper IAC-04-V.P.10. *55th International Astronautical Congress*, Vancouver, Canada, 04-08 October 2004.
[142] Czysz, P. A., and Froning, H. D. "A Propulsion Technology Challenge - An Abortable, Continuous Use Vehicles," IAF-95-S.2.03. *46th International Astronautical Congress*, Oslo, Norway, 02-06 October 1995.
[143] Czysz, P. A., and Froning, H. D. "A Propulsion Technology Challenge - An Abortable, Continuous Use Vehicles," *Acta Astronautica*, Vol. 38, No. 4-8, pp. 235-249, 1996.
[144] Czysz, P. A., Froning, H. D., and Longstaff, R. "A Concept for an International Project to Develop a Hypersonic Flight Test Vehicle," AIAA-97-2808. *33rd IAAA/ASME/SAE/ASEE Joint Propulsion Conference and Exhibit*, American Institute of Aeronautics and Astronautics, Seattle, WA, 06-09 July 1997.
[145] Czysz, P. A., Froning, H. D., and Longstaff, R. "A Concept for an International Project to Develop a Hypersonic Flight Test Vehicle." *Proceedings of the International Workshop on Spaceplanes/RLV Technology Demonstrators*, Tokyo, Japan, March 1998.
[146] Czysz, P. A., Froning, H. D., and Murthy, S. N. B. "Payload Mass and RBCC Engine Performance Determine the Industrial Capability Required," IAF-95-S.5.05. *IAF 46th International Astronautical Congress*, Oslo, Norway, 02-06 October 1995.

[147] Czysz, P. A., and Little, M. J. "The Rocket Based Combined Cycle Engine (RBCC) - A Propulsion System for the 21st Century," AIAA-93-5096. *AIAA/DGLR 5th International Aerospace Planes and Hypersonics Technologies Conference*, American Institute of Aeronautics and Astronautics, Munich, Germany, 30 November - 03 December 1993.
[148] *AVD Internal*----------
[149] *AVD Internal*----------
[150] Czysz, P. A., and Murthy, S. N. B. "Energy Management and Vehicle Synthesis," AIAA-95-6101. *6th International Aerospace Planes and Hypersonics Technologies Conference*, American Institute of Aeronautics and Astronautics, Chattanooga, TN, 03-07 April 1995.
[151] *AVD Internal*----------
[152] Czysz, P. A., and Murthy, S. N. B. "SSTO Launcher Demonstrator for Flight Test," AIAA-96-4574. *7th International Spaceplanes and Hypersonics Systems and Technology Conference*, American Institute of Aeronautics and Astronautics, Norfolk, VA, 18-22 November 1996.
[153] Czysz, P. A., and Murthy, S. N. B. "Energy Management and Vehicle Synthesis," *Developments in High-Speed-Vehicle Propulsion Systems*, *Progress in Astronautics and Aeronautics*, Vol. 165, American Institute of Aeronautics and Astronautics, Reston, VA, 1996, pp. 581-686.
[154] Czysz, P. A., and Murthy, S. N. B. "Energy Analysis of High-Speed Flight Systems," *High-Speed Flight Propulsion Systems*, *Progress in Astronautics and Aeronautics*, Vol. 137, American Institute of Aeronautics and Astronautics, Reston, VA, September 1991, pp. 143-235.
[155] Czysz, P. A., Murthy, S. N. B., Froning, H. D., and McKinney, L. "Space Launchers," ISABE-97-7202. *13th International Symposium on Air Breathing Engines*, Chattanooga, TN, 07-12 September 1997.
[156] Czysz, P. A., and Rahaim, C. P. "Perspective of Launch Vehicle Size and Weight Based on Propulsion System Concept," IAC-02-V.4.08. *53rd International Astronautical Congress - The World Space Congress - 2002*, Houston, TX, 10-19 October 2002.
[157] Czysz, P. A., and Rahaim, C. P. "Comparison of SSTO Launchers Powered by an RBCC Propulsion System and a Pulse Detonation Wave Propulsion System," Paper S19-2. *6th International Symposium on Propulsion for Space Transportation XXIst Century*, Versailles, France, 14-16 May 2002.
[158] Czysz, P. A., and Rahaim, C. P. "Conceptual Design of a Hypersonic Deep Interdiction Aircraft," ISABE-2003-1199. *AIAA Proceedings of the XVIIIth ISABE*, 31 August - 02 September 2003.
[159] Czysz, P. A., and Rahaim, C. P. "Perspective of Launch Vehicle Size and Weight Based on Propulsion System Concept," *Space Technology*, Vol. 23, No. 1, pp. 37-62, 2003.
[160] Czysz, P. A., and Richards, M. J. "Benefits from Incorporation of Combined Cycle Propulsion," IAF-98-S.5.10. *49th International Astronautical Congress*, Melbourne, Australia, 28 September - 02 October 1998.
[161] Czysz, P. A., and Richards, M. J. "Benefits from Incorporation of Combined Cycle Propulsion," *Acta Astronautica*, Vol. 44, No. 7-12, pp. 445-460, 1999.
[162] Czysz, P. A., and Vandenkerckhove, J. "Transatmospheric Launcher Sizing," *Scramjet Propulsion, Progress in Astronautics and Aeronautics*, Vol. 189, American Institute of Aeronautics and Astronautics, Reston, VA, 2000, pp. 979-1103.
[163] *AVD Internal*----------
[164] Davies, R. E. G. *Supersonic (Airliner) Non-Sense: A Case Study in Applied Market Research*, Paladwr Press, McLean, VA, 1998.
[165] Davis, J., Campbell, R., Medley, J., and Hornung, H. "Hypervelocity Scramjet Capabilities of the T5 Free-Piston Tunnel at Caltech," AIAA-92-5037. *AIAA 4th International Aerospace Planes Conference*, American Institute of Aeronautics and Astronautics, Orlando, FL, 01-04 December 1992. https://doi.org/10.2514/6.1992-5037
[166] Davis, J., and Murrow, H. "Enabling Technologies Research and Development Structures," AIAA-89-5011. *AIAA First National Aero-Space Plane Conference*, American Institute of Aeronautics and Astronautics, Dayton, OH, 20-21 July 1989.
[167] DeAngelis, M. V., and Anderson, K. F. "Thermal-Structural Test Facilities at NASA Dryden," NASA-TM-104249, Dryden Flight Research Facility, NASA, Edwards, CA, 1992.
[168] DeWitt, R. L., Hardy, T. L., Whalen, M. V., and Richter, G. P. "Slush Hydrogen (Slh2) Technology Development for Application to the National Aerospace Plane (NASP)," NASA-TM-102315. *Prepared for the Cryogenic Engineering Conference Sponsored by the University of California at Los Angeles*, Los Angeles, CA, 24-28 July 1989.
[169] DeWitt, R. L., Hardy, T. L., Whalen, M. V., Richter, G. P., and Tomsik, T. M. "Background, Current Status, and Prognosis of the Ongoing Slush Hydrogen Technology Development Program for the NASP," NAAS-TM-103220, Lewis Research Center, NASA, Cleveland, OH.
[170] Dress, D., Boyden, R., and Cruz, C. "Supersonic Dynamic Stability Characteristics of the Test Technique Demonstrator NASP Configuration," AIAA-92-5009. *AIAA 4th International Aerospace Planes Conference*, American Institute of Aeronautics and Astronautics, Orlando, FL, 01-04 December 1992.
[171] DuPont, T. "Effect of On Board Oxygen on NASP Gross Weight," Report, 28 March 1991.
[172] Edwards, J. B. "The Great Technology Race - Why We're Losing and What We Need to Compete," Hampton Roads Publishing Co., Inc., 1993.
[173] Edwards, T. A. "CFD Applications in Hypersonic Flight," AIAA-92-5025. *AIAA 4th International Aerospace Planes Conference*, American Institute of Aeronautics and Astronautics, Orland, FL, 01-04 December 1992. https://doi.org/10.2514/6.1992-5025
[174] Ehernberger, I. J. "Stratospheric Turbulence Measurement and Models for Aerospace Plane Design," NASA-TM-104262, Dryden Flight Research Center, NASA, Edwards, CA, December 1992.
[175] Ehernberger, L. J. "Stratospheric Turbulence Measurements and Models for Aerospace Plane Design," AIAA-92-5072. *AIAA 4th International Aerospace Planes Conference*, American Institute of Aeronautics and Astronautics, Orlando, FL, 01-04 December 1992. https://doi.org/10.2514/6.1992-5072
[176] Elias, T. "Consensus X-30 Boundary Layer Transition Prediction Method "BLT-1A"," No. 90-111, Coordination Memorandum, National Program Office, NASP, 02 October 1990.
[177] Ellis, D. A. "Overview - Design of an Efficient Lightweight Airframe Structure for the National Aerospace Plane," AIAA-89-1406-CP. *30th Structures, Structural Dynamics and Materials Conference*, American Institute of Aeronautics and Astronautics, Mobile, AL, 03-05 April 1989. https://doi.org/10.2514/6.1989-1406
[178] Ellison, J. C., Whitehead, P. R., and Tyson, R. W. "NASP Government Work Package Implementation," AIAA-95-6053. *6th International Aerospace Planes and Hypersonics Technologies Conference*, American Institute of Aeronautics and Astronautics, Chattanooga, TN, 03-07 April 1995. https://doi.org/10.2514/6.1995-6053

[179] Emanuel, G., and Rasmussen, M. L. "An Integrated Aerodynamic/Propulsion Study for Generic Aero-Space Planes Based on Waverider Concepts," NASA-CR-188691, Final Report, University of Oklahoma, National Aeronautics and Space Administration, August 1991.
[180] Escher, W. J. D. "A U.S. History of Airbreathing/Rocket Combined-Cycle (RBCC) Propulsion for Powering Future Aerospace Transports, with A Look Ahead to the Year 2020," Report/Patent Number IS-30, Document ID 19990062726, Approved Final Draft, American Institute of Aeronautics and Astronautics, Los Angeles, CA, 20-25 June 1999.
[181] Escher, W. J. D. "Technical Background for Vehicle Mass/Flight Speed Trends (SSTO Cases)," SAIC, NASA, 21 March 2003.
[182] Escher, W. J. D. "Extended Synopsis - Draft," about the Schweikart Report, 31 May 2001.
[183] Ferrante, R. "NASP Difference Interferometry Tests - Comments," Informal Memo to T. Bogar, 20 December 1988.
[184] Fields, R. A., Richards, W. L., and DeAngelis, M. V. "Combined Loads Test Fixture for Thermal-Structural Testing Aerospace Vehicle Panel Concepts," NASA-TM-2004-212039, Dryden Flight Research Center, NASA, Edwards AFB, CA, February 2004.
[185] Finley, D., Bender, E., and Hopping, B. "Assessment of the Effect of Inlet Fairings on a Powered Nozzle Plume Using 2-D PNS Codes," AIAA-92-5046. *AlAA 4th International Aerospace Planes Conference*, American Institute of Aeronautics and Astronautics, Orlando, FL, 01-04 December 1992. https://doi.org/10.2514/6.1992-5046
[186] Froning, D., Gaubatz, W., and Mathews, G. "NASP: Enabling New Space Launch Options," AIAA-90-5263. *2nd International Aerospace Planes Conference*, American Institute of Aeronautics and Astronautics, Orlando, FL, 29-31 October 1990. https://doi.org/10.2514/6.1990-5263
[187] Froning, H. D., and Czysz, P. A. "Exploitation of an Advanced Propulsion Development for Demonstration of Aerospace Plane Art," Abstract and Research Material, Unpublished.
[188] Froning, H. D., and Czysz, P. A. "Test Bed Vehicle for Demonstrating Both Rocket and Airbreathing Launch Vehicle Art," IAF-95-V.4.03. *46th International Astronautical Congress*, Oslo, Norway, 02-06 October 1995.
[189] Froning, H. D., and Czysz, P. A. "Impact of Emerging Technologies on Manned Transportation between Earth and Space," MDC 91H1076. *42nd Congress of the International Astronautical Federation*, Montreal, Canada, 07-11 October 1991.
[190] Gabrynowicz, J., Graham, J., Bille, M., and Bille, D. "The Case for International Cooperation on Hypersonic Technology Development," AIAA-92-5000. *AlAA 4th International Aerospace Planes Conference*, American Institute of Aeronautics and Astronautics, Orlando, FL, 01-04 December 1992. https://doi.org/10.2514/6.1992-5000
[191] Gallicao, P. "Planes Leaving for Shanghai - Paris - " *The Reader's Digest*, August, 1935.
[192] Gatlin, G. M. "Wind-Tunnel Investigation of the Low-Speed Aerodynamics of Slender Accelerator-Type Configurations," SAE-881356. *Advanced Aerospace Aerodynamics*, Society of Automotive Engineers, Warrendale, PA, October 1988.
[193] Goad, J., and Benson, J. "External Rocket System (ERS) Concept Trade Study (#54) Results," No. 90-207, System Engineering Use, Coordination Memorandum, National Program Office, NASP, December 1990.
[194] Gonzales, D., Eisman, M., Shipbaugh, C., Bonds, T., and Tuan Le, A. "Proceedings of the Rand Project Air Force Workshop on Transatmospheric Vehicles," MR-890-AF, Project AIR FORCE, 1995.
[195] Gottemoeller, R., and Brooks, N. "Soviet Reactions to the National Aerospace Plane," N-3127-AF, A Rand Note, Prepared for the United States Air Force, The RAND Corporation, November 1990.
[196] Gregory, I. M., McMinn, J. D., Shaughnessy, J. D., and Chowdhry, R. S. "Hypersonic Vehicle Control Law Development Using H Infinity and Mu-Synthesis," AIAA-92-5010. *AlAA 4th International Aerospace Planes Conference*, American Institute of Aeronautics and Astronautics, Orlando, FL, 01-04 December 1992. https://doi.org/10.2514/6.1992-5010
[197] Griffin, G. M. "Transmittal of Zero-Margin Requirements Allocation," No. NAA 91-024, System Engineering Use, Coordination Memorandum, North American Aircraft, NASP, 25 February 1991.
[198] Gulcher, R. "The Past as Prologue," AIAA-89-5004. *AIAA First National Aerospace Plane Conference*, American Institute of Aeronautics and Astronautics, Dayton, OH, 20-21 July 1989. https://doi.org/10.2514/6.1989-5004
[199] Gupta, K., Petersen, K., and Lawson, C. "On Some Recent Advances in Multidisciplinary Analysis of Hypersonic Vehicles," AIAA-92-5026. *AlAA 4th International Aerospace Planes Conference*, American Institute of Aeronautics and Astronautics, Orlando, FL, 01-04 December 1992. https://doi.org/10.2514/6.1992-5026
[200] Gwynne, P. "Space Plane," *Air & Space*, pp. 26-33, August/September 1986.
[201] Hall, K. R., Brown, S. W., Bennett, A. G., and Rais-Rohani, M. "Construction of a One-Third Scale Model of the National Aerospace Plane-NASP," *Int. J. Engng Ed.*, Vol. 13, No. 2, pp. 153-159, 1997.
[202] Hames, J. "Single-Stage-to-Orbit Vehicle Performance Evaluation Methods," AIAA-92-5056. *AlAA 4th International Aerospace Planes Conference*, American Institute of Aeronautics and Astronautics, Orlando, FL, 01-04 December 1992. https://doi.org/10.2514/6.1992-5056
[203] Hamm, D., and Best, D. "Hypersonic Design," AIAA-92-5077. *AlAA 4th International Aerospace Planes Conference*, American Institute of Aeronautics and Astronautics, Orlando, FL, 01-04 December 1992. https://doi.org/10.2514/6.1992-5077
[204] Hamm, D., and Best, D. "Hypersonic Design," ICAS-92-1.8.1. *18th Congress of the International Council of the Aeronautical Sciences*, Beijing, China, 20-25 September 1992.
[205] Hammond, W. E. *Space Transportation: A Systems Approach to Analysis and Design, AIAA Education Series*, American Institute of Aeronautics and Astronautics, Reston, VA, 1999.
[206] Hammond, W. E. *Design Methodologies for Space Transportation Systems, AIAA Education Series*, American Institute of Aeronautics and Astronautics, Reston, VA, 2001, pp. 85, 108, 112, 211-212, 315-316.
[207] Hank, J. M. "Comparative Analysis of Two-Stage-to-Orbit Rocket and Airbreathing Reusable Launch Vehicles for Military Applications," Master's Thesis, Department of Aeronautics and Astronautics, Graduate Schoool of Engineering and Management, Air Force Institute of Technology, Air University, March 2006.
[208] Hannigan, R., and Sved, J. "True Space Transportation: The Key to a New Era in Space Operations," AIAA-92-5082. *AlAA 4th International Aerospace Planes Conference*, American Institute of Aeronautics and Astronautics, Orlando, FL, 01-04 December 1992. https://doi.org/10.2514/6.1992-5082
[209] Hannigan, R., and Webb, D. "Spaceflight in the Aero-Space Plane Era," AIAA-91-5089. *AIAA 3rd International Aerospace Planes Conference*, American Institute of Aeronautics and Astronautics, Orlando, FL, 03-05 December 1991. https://doi.org/10.2514/6.1991-5089
[210] Hannum, N., and Berkopec, F. "Fueling the National Aero-Space Plane with Slush Hydrogen," AIAA-89-5014. *AIAA First National Aero-Space Plane Conference*, American Institute of Aeronautics and Astronautics, Dayton, OH, 20-21 July 1989.

[211] Harris, E. D. "The National Aerospace Plane: Cost Considerations for the Follow-On Vehicle." *5th International Aerospace Planes and Hypersonics Technologies Conference*, American Institute of Aeronautics and Astronautics, Munich, Germany, 30 November - 03 December 1993.
[212] Harris, W. "Aerospace Planes and Hypersonics Technologies - An Overview for the United States," AIAA-93-5157. *AIAA/DGLR 5th International Aerospace Planes and Hypersonics Technologies Conference*, American Institute of Aeronautics and Astronautics, Munich, Germany, 30 November - 03 December 1993. https://doi.org/10.2514/6.1993-5157
[213] Harsha, P., and Waldman, B. "The NASP Challenge: Testing for Validation," AIAA-89-5005. *AIAA First National Aerospace Plane Conference*, American Institute of Aeronautics and Astronautics, Dayton, OH, 20-21 July 1989. https://doi.org/10.2514/6.1989-5005
[214] Hattis, P., and Malchow, H. "Evaluation of Some Significant Issues Affecting Trajectory and Control Management for Air-Breathing Hypersonic Vehicles," AIAA-92-5011. *AIAA 4th International Aerospace Planes Conference*, American Institute of Aeronautics and Astronautics, Orlando, FL, 01-04 December 1992. https://doi.org/10.2514/6.1992-5011
[215] Hawkins, R., and Dilley, A. "CFD Comparisons with Wind Tunnel and Flight Data for the X-15," AIAA-92-5047. *AIAA 4th International Aerospace Planes Conference*, American Institute of Aeronautics and Astronautics, Orlando, FL, 01-04 December 1992. https://doi.org/10.2514/6.1992-5047
[216] Heeg, J., Zeiler, T. A., Pototzky, A. S., Spain, C. V., and Engelund, W. C. "Aerothermoelastic Analysis of a NASP Demonstrator Model," NASA-TM-109007, Langley Research Center, NASA, Hampton, VA, October 1993.
[217] *AVD Internal*----------
[218] *AVD Internal*----------
[219] Heppenheimer, T. A. *Hypersonic Technologies and the National AeroSpace Plane*, 1st ed., Pasha Publications Inc, 1990.
[220] Heppenheimer, T. A. "Toward Transatmospheric Flight: From V-2 to the X-51," *NASA's Contributions to Aeronautics*, edited by Hallion, R. P., Vol. 1, National Aeronautics and Space Administration, 2010, pp. 277-358.
[221] Heppenheimer, T. A. "The Hypersonic World of Robert Williams," *Air & Space*, pp. 52-55, February/March 1988.
[222] Heppenheimer, T. A. *Facing the Heat Barrier: A History of Hypersonics, The NASA History Series*, National Aeronautics and Space Administration, Washington, D.C., September 2007.
[223] Hermann, J. A., and Schmidt, D. K. "Fuel-Optimal SSTO Mission Analysis of a Generic Hypersonic Vehicle," AIAA-95-3372-CP. *Guidance, Navigation, and Control Conference*, American Institute of Aeronautics and Astronautics, Baltimore, MD, 07-10 August 1995.
[224] Hickman, R., and Adams, J. "Operational Design Factors for NASP Derived Vehicles," AIAA-91-5081. *AIAA 3rd International Aerospace Planes Conference*, American Institute of Aeronautics and Astronautics, Orlando, FL, 03-05 December 1991. https://doi.org/10.2514/6.1991-5081
[225] Hicks, J. W. "Propulsion Modeling Techniques and Applications for the NASA Dryden X-30 Real-Time Simulator," AIAA-91-2937. *AIAA Flight Simulation Technologies Conference*, American Institute of Aeronautics and Astronautics, New Orleans, LA, 12-14 August 1991.
[226] Hielm, L. N. "NASP Materials Lessons Learned Workshop," Air Force Research Laboratory Materials Directorate, Wright-Patterson AFB, OH, 28-29 October 1997.
[227] Hoekie, S. J., Outlaw, R. A., and Sankaran, S. N. "Surface Compositional Variations of Mo-47Re Alloy as a Function of Temperature," NASA-TP-3402, Office of Management, NASA, December 1993.
[228] Hoey, R. G. "X-15 Contributions to the X-30," NASA-CP-3105. *Proceedings of the X-15 First Flight 30th Anniversary Celebration*, National Aeronautics and Space Administration, Edwards, CA, 01 January 1991.
[229] Hoffman, E., Bird, R., and Dicus, D. "Effect of Braze Processing on the Microstructure and Mechanical Properties of SCS-6/Beta21s Titanium Matrix Composites," AIAA-92-5017. *AIAA 4th International Aerospace Planes Conference*, American Institute of Aeronautics and Astronautics, Orlando, FL, 01-04 December 1992. https://doi.org/10.2514/6.1992-5017
[230] Holland, S. D., and Murphy, K. J. "An Experimental Parametric Study of Geometric, Reynolds Number, and Ratio of Specific Heats Effects in Three-Dimensional Sidewall Compression Scramjet Inlets at Mach 6," AIAA-93-0740. *31st Aerospace Sciences Meeting*, American Institute of Aeronautics and Astronautics, Reno, NV, 11-14 January 1993. https://doi.org/10.2514/6.1993-740
[231] Horozak. "National Aerospace Plane (NASP) McDonnell Douglas Md-2001," [Artwork], Image Record: AC87-0754, NASA Ames Research Center Photo Library, 15 October 1987, URL: https://ails.arc.nasa.gov/index.html [retrieved 20 January 2021].
[232] Horton, D. "National Aero-Space Plane Project Overview," AIAA-89-5002. *AIAA First National Aero-Space Plane Conference*, American Institute of Aeronautics and Astronautics, Dayton, OH, 20-21 July 1989. https://doi.org/10.2514/6.1989-5002
[233] Hunt, J. L. "CSO Structures Support for NASP NPO Alternative Engine Study."
[234] Hunt, J. L. "Design Bias in Configuration 201," W/DSGN BS 201/Hunt.
[235] Hunt, J. L. "Exit Criteria Milestones," [Presentation].
[236] Hunt, J. L. "Material Benefits," [Presentation].
[237] Hunt, J. L. "NASP from a National Perspective," [Presentation].
[238] Hunt, J. L. "The National Aero-Space Plane Program."
[239] Hunt, J. L. "The Spinoff Potential for Technology Development in the National Aero-Space Plane (NASP) Program."
[240] Hunt, J. L. "Generic NASP SSTO Vehicle Sensitivities," G/GNRC NASP.
[241] Hunt, J. L., Handnotes. pp. 01-03.
[242] Hunt, J. L. "Propulsion Concepts Validated by 4 Years of Research and Hardware Development."
[243] Hunt, J. L. "Hypersonic Airbreathing Vehicle Conceptual Design (Focus on Aero-Space Plane)," N89-25210. *Recent Advances in Multidisciplinary Analysis and Optimization, Part 3*, National Aeronautics and Space Administration, Hampton, VA, 01 April 1989.
[244] Hunt, J. L. "Subscale Scramjet Free Flyer Design," SAO/NASPO/LaRC, Langley Research Center, NASA, Hampton, VA, 02 September 1991.
[245] Hunt, J. L. "Airbreathing/Rocket Single-Stage-to-Orbit Design Matrix," AIAA-95-6011. *Sixth International Aerospace Planes and Hypersonics Technologies Conference*, American Institute of Aeronautics and Astronautics, Chattanooga, TN, 03-07 April 1995.
[246] Hunt, J. L. "Possibility of Point-of-Departure Design Region Becoming a Premature Solution for the X-30 ... And How to Avoid It," Reply to Attention of 350, NASP JPO, NASA LaRC, 05 February 1991.
[247] Hunt, J. L. "NASP Design Activities in Hypersonic Technology Office (HTO)," Presented to OAST Management Council, CSO/HTO/LaRC, Langley Research Center, NASA, Hampton, VA, 07 April 1992.

[248] Hunt, J. L. “National Aero-Space Plane - Figures of Merit,” SAE Technical Paper SAE-92-XXXX. *Aerospace Atlantic Conference*, Society of Automotive Engineers, Dayton, OH, 07-10 April 1992.
[249] Hunt, J. L. “NASP Design Activities in Hypersonic Technology Office (HTO),” Presented to OAST Management Council, CSO/HTO/LaRC, Langley Research Center, NASA, Hampton, VA, 08 April 1992.
[250] Hunt, J. L. “NASP Vehicle Design Briefing,” [Presentation], CSO/HTO, Langley Research Center, NASA, Hampton, VA, 08 November 1991.
[251] Hunt, J. L. “NASP Interim Technical Review 2 - Debrief,” ITR-2, SAO/HVO/LaRC, Langley Research Center, NASA, Hampton, VA, 09 November 1994.
[252] Hunt, J. L. “NASP Overview,” Presentation to Aerospace Safety Advisory Panel, CSO/HTO/LaRC, Langley Research Center, NASA, Hampton, VA, 10 March 1992.
[253] Hunt, J. L. “Unclassified Figures - Airbreather to SSF (SSTO, HT/HL),” SAO/NASPO/LaRC, Langley Research Center, NASA, Hampton, VA, 10 March 1993.
[254] Hunt, J. L. “Air Core Enhanced Turboramjet (AceTR),” HVO/LaRC, Langley Research Center, NASA, Hampton, VA, 12 July 1994.
[255] Hunt, J. L. “A/R SSTO Vehicle Designs for Three Low-Speed Propulsion Systems,” HVO/LaRC, Langley Research Center, NASA, Hampton, VA, 12 July 1994.
[256] Hunt, J. L. “Trade Studies Conducted by HTO in Support of NASP,” [Presentation], Conceptual Studies Office, Langley Research Center, NASA, Hampton, VA, 17 June 1991.
[257] Hunt, J. L. “Airbreathing Orbital Concepts/Technology,” SAO/HVO/LaRC, Briefing to USAF Scientific Advisory Board, Space Launch Study Committee, 20 July 1994.
[258] Hunt, J. L. “GBL 3.2.1 Vehicle Sizing Trends,” [Presentation], Lessons Learned, Langley Research Center, NASA, Hampton, VA, 20 March 1991.
[259] Hunt, J. L. “Hypersonic Airbreathing Vehicle Design Issues,” [Presentation], Briefing to AFSAB, CSO/HTO, Langley Research Center, NASA, Hampton, VA, 21 June 1991.
[260] Hunt, J. L. “NASP Vehicle Status Briefing,” CSO/HTO/LaRC, Langley Research Center, NASA, Hampton, VA, 21 March 1991.
[261] Hunt, J. L. “Critique of NASP Vehicle Design at Preliminary Vehicle Baseline Review (PVBR),” Configuration/Flow Path Optimization Technical Team, NASP Status Report Response to Defense Science Board, 21 May 1991.
[262] Hunt, J. L. “Conceptual Studies Office (CSO) - Strategic Planning Review,” Conceptual Studies Office (CSO), Langley Research Center, NASA, Hampton, VA, 22 February 1991.
[263] Hunt, J. L. “NASP Vehicle Status,” [Presentation], SAO/NASPO/LaRC, Langley Research Center, NASA, Hampton, VA, 23 October 1992.
[264] Hunt, J. L. “Performance Appraisal for James L. Hunt,” W/SAO Accomplishment, Systems Analysis Office (SAO), 24 August 1994.
[265] Hunt, J. L. “Conceptual Study of Symmetric Scramjet Flight Experiment - Status,” [Presentation], 24 September 1992.
[266] Hunt, J. L. “NASP Interim Technical Review 2 - Debrief,” ITR-2, SAO/HVO/LaRC, Langley Research Center, NASA, Hampton, VA, 25-27 October 1994.
[267] *AVD Internal*----------
[268] Hunt, J. L. “Hypersonic Propulsion Research Peer Review - Systems Analysis Studies,” SAO/HVO/LaRC, Langley Research Center, NASA, Hampton, VA, 27 April 1994.
[269] Hunt, J. L. “Scramjet Accelerator Flight Test Vehicle - HYFLIGHT III,” Preliminary, SAO/NASP/LaRC, 27 January 1993.
[270] Hunt, J. L. “The Hypersonic Airbreathing Vehicles/Technologies,” SAO/HVO/LaRC, Langley Research Center, NASA, Hampton, VA, 27 September 1995.
[271] Hunt, J. L. “Propulsion Integration Characteristics/Sensitivities for LOX Augmented Aerospace Planes,” CSO/HTO/LaRC. *NASA Langley Workshop on 'Performance Enhancement for Hypervelocity Airbreathing Propulsion'*, [Presentation], 29 July 1991.
[272] *AVD Internal*----------
[273] Hunt, J. L. “Aero-Space Plane Matrix,” 1991.
[274] Hunt, J. L. “Configuration Trade Study Matrix - Relative to 201,” for J.R. Thompson, July 1991.
[275] Hunt, J. L., Dyer, D., Brinson, M., Burkardt, L., Bullock, R., Collier, C., Hicks, J., Martin, J., Moses, P., and Pinckney, Z. “Configuration/Flowpath Technical Team Report,” The National Aero-Space Plane Interim Technical Review, 19-21 November 1991, 11 December 1991.
[276] *AVD Internal*----------
[277] Hunt, J. L., and Martin, J. G. “Aero-Space Plane Figures of Merit,” AIAA-92-5058. *AIAA 4th International Aerospace Planes Conference*, American Institute of Aeronautics and Astronautics, Orlando, FL, 01-04 December 1992. https://doi.org/10.2514/6.1992-5058
[278] Imfeld, W. F. “Engineering,” ASD/NAE, [Presentation], 12 February 1991.
[279] Imfeld, W. F. “Technical Support Team Structure and Operating Procedures,” AFSC, Department of the Air Force, 19 February 1991.
[280] Imfeld, W. F. “NASP Interim Technical Review (ITR),” NASP JPO, WPAFB, AFSC, Department of the Air Force, 25 February 1991.
[281] Ishmael, S. D. “What Is the X-30?,” NASA-CP-3105. *Proceedings of the X-15 First Flight 30th Anniversary Celebration*, National Aeronautics and Space Administration, Edwards, CA, 01 January 1991.
[282] Jackman, C., Douglas, A., and Brueske, K. “A Simulation of the Effects of the National Aerospace Plane Testing on the Stratosphere Using a Two-Dimensional Model,” AIAA-92-5073. *AIAA 4th International Aerospace Planes Conference*, American Institute of Aeronautics and Astronautics, Orlando, FL, 01-04 December 1992. https://doi.org/10.2514/6.1992-5073
[283] Jenkins, D., Landis, T., and Miller, J. *American X-Vehicles: An Inventory X-1 to X-50*, Centennial of Flight Edition ed., National Aeronautics and Space Administration, Washington, DC, June 2003.
[284] Johnson, D. “Beyond the X-30: Incorporating Mission Capability,” AIAA-91-5078. *AIAA 3rd International Aerospace Planes Conference*, American Institute of Aeronautics and Astronautics, Orlando, FL, 03-05 December 1991. https://doi.org/10.2514/6.1991-5078
[285] Johnson, D., Espinosa, A., and Althuis, J. “NASP Derived Vehicles: Not Just to Space,” AIAA-92-5020. *AIAA 4th International Aerospace Planes Conference*, American Institute of Aeronautics and Astronautics, Orlando, FL, 01-04 December 1992. https://doi.org/10.2514/6.1992-5020

[286] Johnson, D., Hill, C., Brown, S., and Batts, G. "Natural Environment Application for NASP/X-30 Design and Mission Planning," AIAA-93-0851. *31st Aerospace Sciences Meeting and Exhibit*, American Institute of Aeronautics and Astronautics, Reno, NV, 11-14 January 1993. https://doi.org/10.2514/6.1993-851
[287] Johnson, D., Hill, C., Vaughan, W., Brown, S., and Batts, G. "Natural Environment Requirements Definition and Significance for Aerospace Plane Development," AIAA-93-5074. *AIAA/DGLR 5th International Aerospace Planes and Hypersonics Technologies Conference*, American Institute of Aeronautics and Astronautics, Munich, Germany, 30 November - 03 December 1993. https://doi.org/10.2514/6.1993-5074
[288] Johnson, K. "Around the World in 60 Minutes (or Less!)," Commentary, CSIS Aerospace Security Project, Center for Strategic and International Studies, 17 January 2018.
[289] Johnson, K. F. "The Need for Speed: Hypersonic Aircraft and the Transformation of Long Range Airpower," Master's Thesis, The School of Advanced Air and Space Studies, Air University, Maxwell AFB, AL, June 2005.
[290] Jones, G. "Q vs T Diagram," Pratt & Whitney, National Aero-Space Plane, 10 March 1992.
[291] Kamath, P., and Mao, M. "Computation of Transverse Injection into a Supersonic Flow with Ship3d PNS Code," AIAA-92-5062. *AIAA 4th International Aerospace Planes Conference*, American Institute of Aeronautics and Astronautics, Orlando, FL, 01-04 December 1992. https://doi.org/10.2514/6.1992-5062
[292] Kang, B. H. "Air Data and Surface Pressure Measurement for Hypersonic Vehicles," Master's Thesis, Aeronautics and Astronautics, Massachusetts Institute of Technology, Cambridge, Massachusetts, May 1989.
[293] Kasten, T. "Value of NASP to This Country - the Return on Investment from a National Perspective."
[294] Kazmar, R. "Hypersonic Propulsion at Pratt & Whitney — Overview," AIAA-2005-3256. *AIAA/CIRA 13th International Space Planes and Hypersonics Systems and Technologies Conference*, American Institute of Aeronautics and Astronautics, Capua, Italy, 16-20 May 2012.
[295] Kazmar, R. R. "Hypersonic Propulsion at Pratt & Whitney — Overview." *11th AIAA/AAAF International Conference on Space Planes and Hypersonic Systems and Technologies*, American Institute of Aeronautics and Astronautics, Orleans, France, 29 September - 04 October 2002.
[296] Kelly, H. N., and Blosser, M. L. "Active Cooling from the Sixties to NASP," NASA-TM-109079, Langley Research Center, NASA, Hampton, VA, 01 July 1994.
[297] Kock, B. "HYFLITE III Progress Report," Detachment 5, National Aero-Space Plane Joint Program Office, 15 January 1993.
[298] *AVD Internal*----------
[299] Konsewicz, R. "Configuration 200A Controllability Assessment," [Presentation], NASP, 28 February 1991.
[300] Kumar, A., Drummond, J. P., McClinton, C. R., and Hunt, J. L. "Research in Hypersonic Airbreathing Propulsion at the NASA Langley Research Center." *Fifteenth International Symposium on Airbreathing Engines (ISABE)*, Bangalore, India, 02-07 September 2001.
[301] Kuperman, G., and Sobel, A. "Information Requirements Analysis for NASP-Derived Vehicles," AIAA-92-5078. *AIAA 4th International Aerospace Planes Conference*, American Institute of Aeronautics and Astronautics, Orlando, FL, 01-04 December 1992. https://doi.org/10.2514/6.1992-5078
[302] Kussoy, M., and Huang, G. P. G. "Hypersonic Flows as Related to the National Aerospace Plane," NASA-CR-199365, Ames Research Center, NASA, Mountain View, CA, 09 May 1995.
[303] Lau, K. Y. "Effect of Turbulence Transition Prediction on Heating Rate," Informal Memo, 18 February 1991.
[304] Launius, R. D. "Chapter 10: History of Civil Space Activity and Spacepower," *Toward a Theory of Spacepower: Selected Essays*, Government Printing Office, 07 March 2011.
[305] Lawrence, S. "Application of Space-Marching Methods to Hypersonic Forebody Flow Fields," AIAA-92-5030. *AIAA 4th International Aerospace Planes Conference*, American Institute of Aeronautics and Astronautics, Orlando, FL, 01-04 December 1992. https://doi.org/10.2514/6.1992-5030
[306] Lindley, C. A. "International Aerospaceplane Efforts." *NASA Lewis Research Center Rocket-Based Combined-Cycle (RBCC) Propulsion Technology Workshop, Tutorial Session*, 1992.
[307] Little, M. J., and Czysz, P. A. "Rocket Based Combined Cycle Integrated with Liquid Air Collection, A Propulsion Concept for the 21st Century." *9th Annual Midwest Space Development Conference*, Indianapolis, IN, 22-24 October 1993.
[308] Liu, S. K. "Aerospace-Plane Flight and Stratospheric Ozone: Review and Preliminary Assessment of the National Aerospace Plane (NASP) Operations," N-3464-AF, A Rand Note, Prepared for the United States Air Force, The RAND Corporations, 1992.
[309] Liu, S. K. "Numerical Simulation of Hypersonic Aerodynamics and the Computational Needs for the Design of an Aerospace Plane," N-3253-AF, A Rand Note, Prepared for the United States Air Force, The RAND Corporation, 1992.
[310] *AVD Internal*----------
[311] Logsdon, J. M. ""A Failure of National Leadership": Why No Replacement for the Space Shuttle?," *Critical Issues in the History of Spaceflight*, CreateSpace Independent Publishing Platform, 09 November 2013, pp. 269-300.
[312] London III, J. R. "LEO on the Cheap: Methods for Achieving Drastic Reduction in Space Launch Costs," Report No. AU-AIR-93-8, Air University Press, Maxwell AFB, AL, October 1994.
[313] Lovell, T. A., and Schmidt, D. K. "A Parametric Sensitivity Study for Single-Stage-to-Orbit Hypersonic Vehicles Using Trajectory Optimization," NASA-CR-194618, Langley Research Center, NASA, Hampton, VA, 21 March 1994.
[314] Lu, P. "Trajectory Optimization for the National Aerospace Plane," NASA-CR-194618, Langley Research Center, NASA, Hampton, VA, November 1993.
[315] Lu, P., and Samsundar, J. "Closed Form Solutions of Constrained Trajectories: Application in Optimal Ascent of Aerospace Plane," AIAA-92-5012. *AIAA 4th International Aerospace Planes Conference*, American Institute of Aeronautics and Astronautics, Orlando, FL, 01-04 December 1992. https://doi.org/10.2514/6.1992-5012
[316] Maglieri, D., Sothcott, V., and Hicks, J. "Influence of Vehicle Configuration and Flight Profile on X-30 Sonic Booms," AIAA-90-5224. *AIAA 2nd International Aerospace Planes Conference*, American Institute of Aeronautics and Astronautics, Orlando, FL, 29-31 October 1990. https://doi.org/10.2514/6.1990-5224
[317] Magnuson, G. G. "Manufacturing Producibility," [Presentation], NASP, 25 February 1991.
[318] Martin, J., Kabis, H., and Hunt, J. L. "The Necessity of On Board Oxygen for Airbreathing Single-Stage-to-Orbit Vehicles," AIAA-91-5016. *AIAA 3rd International Aerospace Planes Conference*, Presentation, American Institute of Aeronautics and Astronautics, Orlando, FL, 03-05 December 1991.

[319] Martin, J. G., Kabis, H. Z., and Hunt, J. L. "The Necessity of On Board Oxygen for Airbreathing Single-Stage-to-Orbit Vehicles," AIAA-91-5016. *AIAA 3rd International Aerospace Planes Conference*, American Institute of Aeronautics and Astronautics, Orlando, FL, 03-05 December 1991.
[320] Martindale, D. "Frequent Flyers' Date with the Final Frontier - the U.S. Moves Closer to Launch of a Hypersonic Plane," March 1987.
[321] Mattern, S. "System Safety Activities Supporting an Aero-Space Plane Ground Support Technology," AIAA-92-5070. *AIAA 4th International Aerospace Planes Conference*, American Institute of Aeronautics and Astronautics, Orlando, FL, 01-04 December 1992. https://doi.org/10.2514/6.1992-5070
[322] Maurice, L., Leingang, J., and Carreiro, L. "The Benefits of In-Flight LOX Collection for Airbreathing Space Boosters," AIAA-92-5059. *AIAA 4th International Aerospace Planes Conference*, American Institute of Aeronautics and Astronautics, Orlando, FL, 01-04 December 1992. https://doi.org/10.2514/6.1992-5059
[323] McClinton, C. R., Mao, M., Bittner, R., and Riggins, D. "Experimental and Numerical Base Pressure at Mach 13.5 to 17," GWP 54, Numerical Applications Office, Langley Research Center, NASA, Hampton, VA, February 1992.
[324] McClinton, C., Bittner, R., and Kamath, P. "CFD Support of NASP Design," AIAA-90-5249. *AIAA 2nd International Aerospace Planes Conference*, American Institute of Aeronautics and Astronautics, Orlando, FL, 29-31 October 1990. https://doi.org/10.2514/6.1990-5249
[325] *AVD Internal*----------
[326] McClinton, C. R. "SSTO Studies - Tasks," National Program Office, NASP, 20 January 1993.
[327] McCormick, J. B. "NASP - Phase 3 Program Development Plan Reference Program Description Draft," X30NP91021, CDRL. ITEM A016 (DI-S-30559/T), First Draft Release, NASP, FSCM:ONPDO, 15 November 1991.
[328] McGrory, W., Huebner, L., Slack, D., and Walters, R. "Development and Application of Gasp 2.0," AIAA-92-5067. *AIAA 4th International Aerospace Planes Conference*, American Institute of Aeronautics and Astronautics, Orlando, FL, 01-04 December 1992. https://doi.org/10.2514/6.1992-5067
[329] McIver, D. E., and Morrell, F. R. "National Aero-Space Plane: Flight Mechanics." *AGARD 75th Symposium of the Flight Mechanics Panel on Space Vehicle Flight Mechanics*, Luxembourg, France, 13-16 November 1989.
[330] McLucas, J. L., and Marin, J. J. *Hypersonic Technology for Military Application*, 2nd Printing, National Academy Press, Washington, D.C., November 1990.
[331] McNelis, N., Hardy, T., Whalen, M., Kudlac, M., Moran, M., Tomsik, T., and Haberbusch, M. "A Summary of the Slush Hydrogen Technology Program for the National Aero-Space Plane," AIAA-95-6056. *AIAA 6th International Aerospace Planes and Hypersonics Technologies Conference*, American Institute of Aeronautics and Astronautics, Chattanooga, TN, 03-07 April 1995.
[332] Mcquilkin, F., and Logan, T. "Optimization and Validation of a Fuselage Fuel Tank Structural Concept for the NASP," AIAA-90-5262. *AIAA 2nd International Aerospace Planes Conference*, American Institute of Aeronautics and Astronautics, Orlando, FL, 29-31 October 1990. https://doi.org/10.2514/6.1990-5262
[333] Mehta, U. B. "The Aerospace Plane Design Challenge: Credible Computational Fluid Dynamics Results," NASA-TM-102887, Ames Research Center, NASA, Mountain View, CA, December 1990. https://doi.org/10.2514/6.1990-5248
[334] Mehta, U. B. "Air-Breathing Aerospace Plane Development Essential: Hypersonic Propulsion Flight Tests," NASA-TM-108857, Ames Research Center, NASA, Mountain View, CA, November 1994.
[335] Mendez, B. "The National Aero-Space Plane," 19890009016, NASA Ames Summer High School Apprenticeship Research Program: 1986 Research Papers pp. 49-53, Ames Research Center, NASA, Moffett Field, CA, 01 September 1988.
[336] Menees, G. P., Adelman, H. G., Cambier, J. L., and Bowles, J. V. "Wave Combustors for Trans-Atmospheric Vehicles," *Journal of Propulsion and Power*, Vol. 8, No. 3, May-June 1992.
[337] Miller, J. *The X-Planes - X-1 to X-45*, Chapter 34: X-30A, First Published by Midland Publishing, 2001, pp. 308-315.
[338] Morgan, M. G. "Access to Space: The Future of U.S. Space Transportation Systems," OTA-ISC-415, Office of Technology Assessment, U.S. Congress, U.S. Government Printing Office, Washington, D.C., April 1990.
[339] Morris, C. "NASP Technology Transfer," Presentation to ITP Workshop, Office of Aeronautics and Space Technology, 18 March 1992.
[340] Morris, C. E. K. "National Aero-Space Plane Achievements and U.S. Space-Launch Goals," AIAA-95-6052. *6th International Aerospace Planes and Hypersonics Technologies Conference*, American Institute of Aeronautics and Astronautics, Chattanooga, TN, 03-07 April 1995. https://doi.org/10.2514/6.1995-6052
[341] Moses, R. A. "Design Data Book - X-30 Configuration 202," X30NP92001, Book 6, Vol. 2, 10 August 1992.
[342] Moszee, R. H., and Snyder, C. D. "A Propulsion Development Strategy for the National Aero-Space Plane," AIAA-89-2751. *25th Joint Propulsion Conference*, American Institute of Aeronautics and Astronautics, Monterey, CA, 10-12 July 1989.
[343] Murthy, S. N. B., and Czysz, P. A. "An Approach to Air-Breathing High Speed Vehicle Synthesis," AIAA-91-0225. *29th AIAA Aerospace Sciences Meeting*, American Institute of Aeronautics and Astronautics, invited paper, Reno, NV, 07-10 January 1991.
[344] Odabas, O., and Sarigul-Klijn, N. "On the Coupled Thermomechanical Analysis of Hypersonic Flight Vehicle Structures," AIAA-92-5018. *AIAA 4th International Aerospace Planes Conference*, American Institute of Aeronautics and Astronautics, Orlando, FL, 01-04 December 1992. https://doi.org/10.2514/6.1992-5018
[345] Ohlhorst, C. W., Vaughn, W. L., and Bresina, J. J. "NASA Langley Research Center National Aero-Space Plane Mission Simulation Profile Sets," NASA-TM-102670, Langley Research Center, NASA, Hampton, VA, October 1990.
[346] Orloff, B. S. "A Comparative Analysis of Singe-State-to-Orbit Rocket and Air-Breathing Vehicles," Master's Thesis, Department of Aeronautics and Astronautics, Graduate School of Engineering and Management, Air Force Institute of Technology, Air University, June 2006.
[347] Orton, G. "External Rocket System Concept Trade Study - Interim Review/Concept Screening Agenda," [Presentation], NASP Subsystem Team, NASP, 28 November 1990.
[348] *AVD Internal*----------
[349] Pace, S. N. "The Aerospace Plane: Goals and Realities," *Issues in Science and Technology*, pp. 20-24, Spring 1987.
[350] *AVD Internal*----------
[351] *AVD Internal*----------
[352] Pamadi, B. N. "A Simple Analytical Aerodynamic Model of Langley Winged-Cone Aerospace Plane Concept," NASA-CR-194987, Langley Research Center, NASA, Hampton, VA, October 1994.

[353] Parks, S., and Waldman, B. “Flight Testing Hypersonic Vehicles - the X-30 and Beyond,” AIAA-90-5229. *AIAA 2nd International Aerospace Planes Conference*, American Institute of Aeronautics and Astronautics, Orlando, FL, 29-31 October 1990. https://doi.org/10.2514/6.1990-5229
[354] Pegg, R. J., and Hunt, J. L. “HYFLITE Design Review,” [Presentation], SAO, NASPO, Langley Research Center, NASA, Hampton, VA, 07 October 1993.
[355] Pegg, R. J., Hunt, J. L., Petley, D. H., Burkardt, L., Stevens, D. R., Moses, P. L., Pinckney, S. Z., Kabis, H. Z., Spoth, K. A., Dziedzic, W. M., Kreis, R. I., Martin, J. G., and Barnhart, P. J. “Design of a Hypersonic Waverider-Derived Airplane,” AIAA-93-0401. *31st Aerospace Sciences Meeting & Exhibit*, American Institute of Aeronautics and Astronautics, Reno, NV, 11-14 January 1993.
[356] Pinckney, S. Z. “Flight Test Inlet Design - NASP,” [Presentation], 11 September 1992.
[357] *AVD Internal----------*
[358] Pototzky, A. S., Spain, C. V., Soistmann, D. L., and Noll, T. E. “Application of Unsteady Aeroelastic Analysis Techniques on the National Aerospace Plane,” NASA-TM-100648, Langley Research Center, NASA, Hampton, VA, September 1988.
[359] Powell, W. E. “NASP X-30 Propulsion Technology Status,” NASA-CP-10090. *Rocket-Based Combined-Cycle (RBCC) Propulsion Technology, Tutorial Session*, National Aeronautics and Space Administration, Huntsville, AL, 01 January 1992.
[360] Ranger, R. “Red Horizons: The U.S. Response to Soviet Military Gains in Space,” *REPORT Europe*. 14 September 1988.
[361] Reda, H. “NASP and the Environment,” AIAA-91-5051. *AIAA 3rd International Aerospace Planes Conference*, American Institute of Aeronautics and Astronautics, Orlando, FL, 03-05 December 1991. https://doi.org/10.2514/6.1991-5051
[362] Reubush, D. E. “A Historical Perspective on Hypersonic Research at the NACA/NASA Langley Research Center (1944-1984),” AIAA-92-5034. *AIAA 4th International Aerospace Planes Conference*, American Institute of Aeronautics and Astronautics, Orlando, FL, 01-04 December 1992. https://doi.org/10.2514/6.1992-5034
[363] Richardson, P. F., McClinton, C. R., Bittner, R. D., Dilley, A. D., Edwards, K. W., Eppard, W. M., Morrison, J. H., Riggins, D. R., Switzer, G. F., and Parlette, E. B. “Hypersonic CFD Applications for the National Aero-Space Plane,” SAE-TP-892310. *Aerospace Technology Conference and Exposition*, Anaheim, CA, 25-28 September 1989.
[364] Riggins, D., McClinton, C., and Rogers, R. “Flow Enthalpy Effects on Scramjet Mixing and Combustion,” AIAA-92-5097. *AIAA 4th International Aerospace Planes Conference*, American Institute of Aeronautics and Astronautics, Orlando, FL, 01-04 December 1992. https://doi.org/10.2514/6.1992-5097
[365] Rizzi, S., Robinson, J., and Chiang, C. “Dynamic Response and Sonic Fatigue Analysis at NASA Langley for Hypersonic Vehicle Structures,” AIAA-92-5019. *AIAA 4th International Aerospace Planes Conference*, American Institute of Aeronautics and Astronautics, Orlando, FL, 01-04 December 1992. https://doi.org/10.2514/6.1992-5019
[366] Ronald, T. “Structural Materials for NASP,” AIAA-91-5101. *AIAA 3rd International Aerospace Planes Conference*, American Institute of Aeronautics and Astronautics, Orlando, FL, 03-05 December 1991. https://doi.org/10.2514/6.1991-5101
[367] Ronald, T. “Status and Applications of Materials Developed for NASP,” AIAA-95-6131. *AIAA Sixth International Aerospace Planes and Hypersonics Technologies Conference*, American Institute of Aeronautics and Astronautics, Chattanooga, TN, 03-07 April 1995. https://doi.org/10.2514/6.1995-6131
[368] Ronald, T. M. F. “Materials Challenges for NASP,” AIAA-89-5010. *AIAA First National Aerospace Plane Conference*, American Institute of Aeronautics and Astronautics, Dayton, OH, 20-21 July 1989. https://doi.org/10.2514/6.1989-5010
[369] Ronald, T. M. F. “Materials for Hypersonic Engines,” in AGARD-CP-479, Hypersonic Combined Cycle Propulsion. *75th Hypersonic Combined Cycle Propulsion Panel Symposium*, Madrid, Spain, 28 May - 01 June 1990.
[370] Rowland, F. “Future Roles for Hyper-Velocity Vehicles,” Fort Worth Division, General Dynamics Corporation, January 1990.
[371] Rumerman, J. A. “Hypersonics: The National Aerospace Plane Program,” NASA-SP-2000-4012, NASA Historical Data Book, Vol. VI, The NASA History Series, NASA History Office, Office of Policy and Plans, Washington, D.C., 2000.
[372] Salsbury, S. C. “Validation of License to Export Unclassified Technical Data Pertaining to the X-30 National Aerospace Plane (NASP) to the United Kingdom,” Memo, SCS-786-1125-EL0641-88, 27 June 1988.
[373] Sams, H. “The NASP Challenge - Management Innovation,” AIAA-89-5006. *AIAA First National Aerospace Plane Conference*, American Institute of Aeronautics and Astronautics, Dayton, OH, 20-21 July 1989. https://doi.org/10.2514/6.1989-5006
[374] Sanford, T. H. “2-4 April Preliminary Vehicle Baseline Review (PVBR),” Directorate of Engineering (ASD/NAE), NASP JPO, WPAFB, Dayton, OH, 20 May 1991.
[375] Schmidt, D. K. “Problems in Control System Design for Hypersonic Vehicles,” *IFAC Proceedings Volumes*, Vol. 25, No. 22, pp. 89-96, September 1992. https://doi.org/10.1016/S1474-6670(17)49638-8.
[376] Schmidt, D. K., and Lovell, T. A. “Mission Performance and Design Sensitivities of Air-Breathing Hypersonic Launch Vehicles,” *AIAA Journal of Spacecraft and Rockets*, Vol. 34, No. 2, pp. 158-164, March - April 1997. https://doi.org/10.2514/2.3204.
[377] Schwartz, I. “Revolutionary Hybrid,” AP Newsfeatures Photo, Bob Williams holds a model, 24 November 1986.
[378] Schweikart, L. *The Hypersonic Revolution - Case Studies in the History of Hypersonic Technology - the Quest for the Orbital Jet - the National Aero-Space Plane Program (1983-1995), Air Force History and Museums Program*, Vol. III, Bolling AFB, Washington, D.C., 1998.
[379] Schweikart, L. “Command Innovation - Lessons from the National Aerospace Plane Program,” *Innovation and the Development of Flight*, Texas A&M University Press, College Station, TX, 1999, pp. 299-323.
[380] Schweikart, L. “Hypersonic Hope: Planning for NASP, 1986-1991,” *Air Power History*, Vol. 41, No. 1, pp. 36-48, Spring 1994.
[381] Shea, J. F. “Report of the Defense Science Board Task Force on National Aero-Space Plane (NASP) Program,” AD-A274 530, Defense Science Board, Director of Defense Research and Engineering, Washington, D.C, November 1992.
[382] Shih, P., and Neumann, R. “The Value of Sub-Scale Flight Tests in the Development of NASP Vehicles,” AIAA-91-5048. *AIAA 3rd International Aerospace Planes Conference*, American Institute of Aeronautics and Astronautics, Orlando, FL, 03-05 December 1991. https://doi.org/10.2514/6.1991-5048
[383] Shore, C. P. “Review of Convectively Cooled Structures for Hypersonic Flight,” NASA-TM-87740, Langley Research Center, NASA, Hampton, VA, May 1986.
[384] Siebenhaar, A., Leonard, J. R., and Orton, G. F. “Thrust Cell Technology for Modular Engines,” AIAA-93-2561. *AIAA/SAE/ASME/ASEE 29th Joint Propulsion Conference and Exhibit*, American Institute of Aeronautics and Astronautics, Monterey, CA, 28-30 June 1993.
[385] Smith, B. C., Suarez, C. J., Porado, W. A., and Malcolm, G. N. “Aerodynamic Control of NASP-Type Vehicles Through Vortex Manipulation,” Vol. IV, NASA-CR-177626, Ames Research Center, NASA, Moffett Field, CA, September 1993.

[386] Smith, F. W. “Practical Applications of Hypersonic Flight ... Possibilities for Air Express.” *Proceedings of the 1st High Speed Commercial Flight Symposium*, in J.P. Loomis (Ed.), High Speed Commercial Flight, The Coming Era, Columbus, OH, 22-23 October 1986.
[387] Snyder, C. D., and Pinckney, S. Z. “A Configuration Development Strategy for the NASP,” AIAA-91-5044. *AIAA 3rd International Aerospace Planes Conference*, American Institute of Aeronautics and Astronautics, Orlando, FL, 03-05 December 1991. https://doi.org/10.2514/6.1991-5044
[388] Spain, C., Soistmann, D., Parker, E., Gibbons, M., and Gilbert, M. “An Overview of Selected NASP Aeroelastic Studies at the NASA Langley Research Center,” AIAA-90-5218. *AIAA 2nd International Aerospace Planes Conference*, American Institute of Aeronautics and Astronautics, Orlando, FL, 29-31 October 1990. https://doi.org/10.2514/6.1990-5218
[389] Spoth, K. A., and Moses, P. L. “Structural Design and Analysis of a Mach Zero-to-Five Turbo-Ramjet System,” AIAA-93-1983. *AIAA/SAE/ASME/ASEE 29th Joint Propulsion Conference and Exhibit*, American Institute of Aeronautics and Astronautics, Monterey, CA, 28-30 June 1993.
[390] Stafford, J. R. “SSTO RLVs: More Global Reach? A Study of the Use of Single Stage to Orbit Reusable Launch Vehicles as Airlift Platforms,” Master's Thesis, Graduate School of Logistics and Acquisition Management, Air Force Institute of Technology, Air University, November 1996.
[391] Stangeland, M. I. J. “Turbopumps for Liquid Rocket Engines,” SP-924. *9th Cliff Garrett Turbomachinery Award Lecture*, SAE International, 07 April 1992.
[392] Stull, F. D. “Scramjet Propulsion,” AIAA-89-5012. *AIAA First National Aero-Space Plane Conference*, American Institute of Aeronautics and Astronautics, Dayton, OH, 20-21 July 1989. https://doi.org/10.2514/6.1989-5012
[393] Suarez, C. J., Kramer, B. R., Smith, B. C., and Malcolm, G. N. “Aerodynamic Control of NASP-Type Vehicles Through Vortex Manipulation - Static Wind Tunnel Tests,” Vol. II, NASA-CR-177626, Ames Research Center, NASA, Moffett Field, CA, September 1993.
[394] Suarez, C. J., Ng, T. T., Ong, L. Y., and Malcolm, G. N. “Aerodynamic Control of NASP-Type Vehicles Through Vortex Manipulation - Static Water Tunnel Tests,” Vol. 1, NASA-CR-177626, Ames Research Center, NASA, Moffett Field, CA, September 1993.
[395] Sullivan, W. “Conducting the NASP Ground Test Program,” AIAA-91-5029. *AIAA 3rd International Aerospace Planes Conference*, American Institute of Aeronautics and Astronautics, Orlando, FL, 03-05 December 1991. https://doi.org/10.2514/6.1991-5029
[396] Swartwout, W., Erdos, J., Engers, R., and Prescott, C. “An Oxidation and Erosion Test Facility for Cooled Panels,” AIAA-92-5095. *AIAA 4th International Aerospace Planes Conference*, American Institute of Aeronautics and Astronautics, Orlando, FL, 01-04 December 1992. https://doi.org/10.2514/6.1992-5095
[397] Sweetman, B. *AURORA - the Pentagon's Secret Hypersonic Spyplane, Mil-Tech Series*, MBI Publishing Company, Osceola, WI, 1993.
[398] Swihart, J. “Keynote Address: Advanced Technology Demonstrators, Prototypes and Hypersonic Flight,” AIAA-92-4999. *AIAA 4th International Aerospace Planes Conference*, American Institute of Aeronautics and Astronautics, Orlando, FL, 01-04 December 1992. https://doi.org/10.2514/6.1992-4999
[399] Sypniewski, C. “The NASP Challenge: Technical Breakthrough,” AIAA-89-5017. *AIAA First National Aero-Space Plane Conference*, American Institute of Aeronautics and Astronautics, Dayton, OH, 20-21 July 1989. https://doi.org/10.2514/6.1989-5017
[400] Tang, M. H. “National Aero-Space Plane Organization and Management (Lessons Learned).” *NGLT Workshop*, Presentation, Williamsburg, VA, 11 December 2003.
[401] Tang, M. H. “National Aero-Space Plane (NASP) Program,” N91-28214, [Presentation], Pennsylvania State University, University Park, PA, 26-29 June 1990.
[402] Tarifa, C. S. “Hypersonic Propulsion: Past and Present.”
[403] Terry, C. E., and Kent, T. J. “Risk Analysis of Hot/Cold Structure Concepts,” BN09861, General Dynamics, NASP Program, NASP GD, 26 February 1991.
[404] Throckmorton, D. “Enabling Technologies Research and Development for the National Aero-Space Plane,” AIAA-89-5009. *AIAA First National Aero-Space Plane Conference*, American Institute of Aeronautics and Astronautics, Dayton, OH, 20-21 July 1989. https://doi.org/10.2514/6.1989-5009
[405] Toten, A., Fong, J., Murphy, R., and Powell, W. “NASP Derived Vehicle (NDV) Space Launch Operating Costs and Program Cost Recovery Options,” AIAA-91-5080. *AIAA 3rd International Aerospace Planes Conference*, American Institute of Aeronautics and Astronautics, Orlando, FL, 03-05 December 1991. https://doi.org/10.2514/6.1991-5080
[406] Townend, L., Broadbent, E., Nonweiler, T., Pagan, G., Parker, E., and Pike, J. “Aero-Propulsive Effects on Configuration Shaping,” AIAA-91-5064. *AIAA 3rd International Aerospace Planes Conference*, American Institute of Aeronautics and Astronautics, Orlando, FL, 03-05 December 1991. https://doi.org/10.2514/6.1991-5064
[407] *AVD Internal*----------
[408] Vandenkerckhove, J., and Czysz, P. A. “S.S.T.O. Performance Assessment with In-Flight LOX Collection,” IAF-94-S.4.426. *45th Congress of the International Astronautical Federation*, Jerusalem, Israel, 09-14 October 1994.
[409] Vandenkerckhove, J., and Czysz, P. A. “S.S.T.O. Performance Assessment with In-Flight LOX Collection,” *Acta Astronautica*, Vol. 37, pp. 167-178, 1995.
[410] Vaughan, W., and Anderson, B. “Environmental Effects Consideration: A Case Study - Lessons Learned,” AIAA-92-5075. *AIAA 4th International Aerospace Planes Conference*, American Institute of Aeronautics and Astronautics, Orlando, FL, 01-04 December 1992. https://doi.org/10.2514/6.1992-5075
[411] Ventura, T., and Czysz, P. “Aurora & Beyond: Paul Czysz on Hypersonic Aircraft.” American Antigravity.com, 26 July 2006.
[412] Voelcker, J. “The Iffy 'Orient Express',” *IEEE Spectrum*, pp. 31-33, August 1988.
[413] Voland, R., and Rock, K. “NASP Concept Demonstration Engine and Subscale Parametric Engine Tests,” AIAA-95-6055. *AIAA 6th International Aerospace Planes and Hypersonics Technologies Conference*, American Institute of Aeronautics and Astronautics, Chattanooga, TN, 03-07 April 1995. https://doi.org/10.2514/6.1995-6055
[414] Wagner, E., Li, I., Nguyen, D., and Nguyen, P. “NASP Guidance Design for Vehicle Autonomy,” AIAA-90-5245. *AIAA 2nd International Aerospace Planes Conference*, American Institute of Aeronautics and Astronautics, Orlando, FL, 29-31 October 1990. https://doi.org/10.2514/6.1990-5245
[415] Waldman, B., and Harsha, P. “NASP: Focus on Technology,” AIAA-92-5001. *AIAA 4th International Aerospace Planes Conference*, American Institute of Aeronautics and Astronautics, Orlando, FL, 01-04 December 1992. https://doi.org/10.2514/6.1992-5001

[416] Waldman, B., and Harsha, P. “The First Year of Teaming: A Progress Report,” AIAA-91-5008. *AIAA 3rd International Aerospace Planes Conference*, American Institute of Aeronautics and Astronautics, Orlando, FL, 03-05 December 1991.
[417] *AVD Internal*----------
[418] White, M. E. “The National Aerospace Plane Program and the APL Role,” *John Hopkins APL Technical Digest*, Vol. 13, No. 1, pp. 218-229, 1992.
[419] Whitehead, A. “NASP Aerodynamics,” AIAA-89-5013. *AIAA First National Aero-Space Plane Conference*, American Institute of Aeronautics and Astronautics, Dayton, OH, 01-04 December 1989. https://doi.org/10.2514/6.1989-5013
[420] Wierzbanowski, T., and Kasten, T. “Manned Versus Unmanned: The Implications to NASP,” AIAA-90-5265. *AIAA 2nd International Aerospace Planes Conference*, American Institute of Aeronautics and Astronautics, Orlando, FL, 29-31 October 1990. https://doi.org/10.2514/6.1990-5265
[421] Wierzbanowski, T., Reda, H., Duecker, G., and Brown, C. “An Environmental Study of the National Aero-Space Plane,” AIAA-92-5074. *AIAA 4th International Aerospace Planes Conference*, American Institute of Aeronautics and Astronautics, Orlando, FL, 01-04 December 1992. https://doi.org/10.2514/6.1992-5074
[422] Wilhite, A. W., Powell, R. W., Scotti, S. J., McClinton, C. R., Pinckney, S. Z., Cruz, C. I., Jackson, L. R., Hunt, J. L., Cerro, J. A., and Moses, P. L. “Concepts Leading to the National Aero-Space Plane Program,” AIAA-90-0294. *28th Aerospace Sciences Meeting*, American Institute of Aeronautics and Astronautics, Reno, NV, 08-11 January 1990.
[423] Wilson, G. “Time-Dependent Quasi-One-Dimensional Simulations of High Enthalpy Pulse Facilities,” AIAA-92-5096. *AIAA 4th International Aerospace Planes Conference*, American Institute of Aeronautics and Astronautics, Orlando, FL, 01-04 December 1992. https://doi.org/10.2514/6.1992-5096
[424] Wright, H. “National Aero-Space Plane Technology Development Overview,” AIAA-89-5003. *AIAA First National Aero-Space Plane Conference*, American Institute of Aeronautics and Astronautics, Dayton, OH, 20-21 July 1989. https://doi.org/10.2514/6.1989-5003
[425] Yeager, C. “America's Orient Express,” *Popular Mechanics*, pp. 72-75, August 1986.

APPENDIX C
DATABASE VEHICLE ‘SNAPSHOTS’

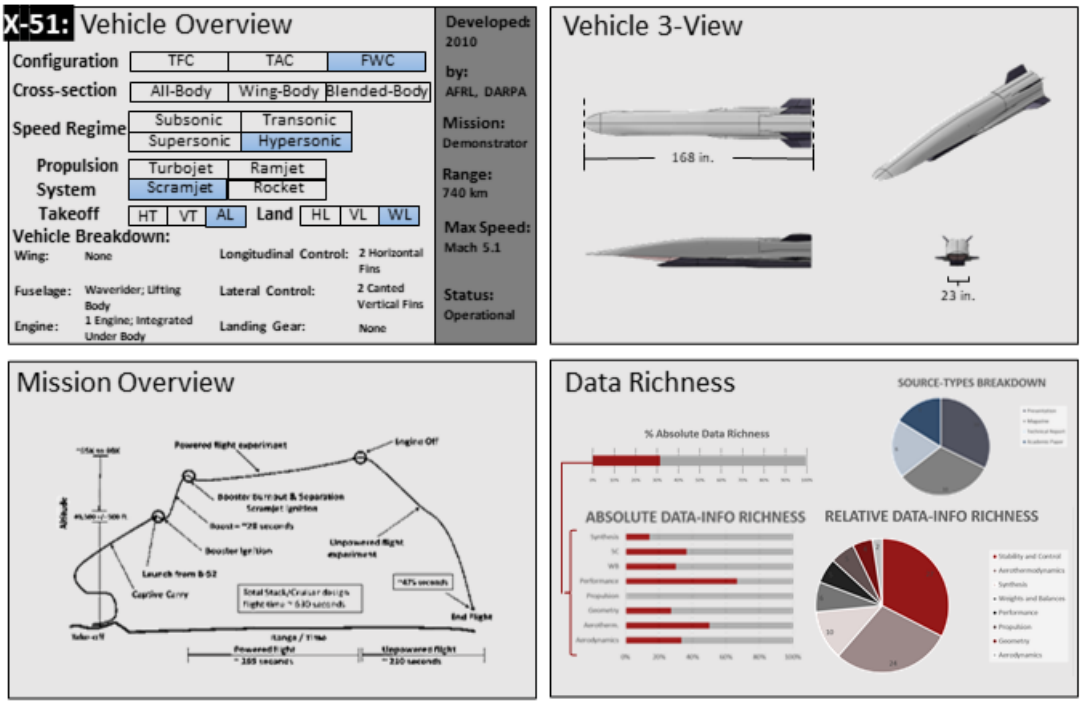

Fig. C.1 X-51 database 'snapshot'.

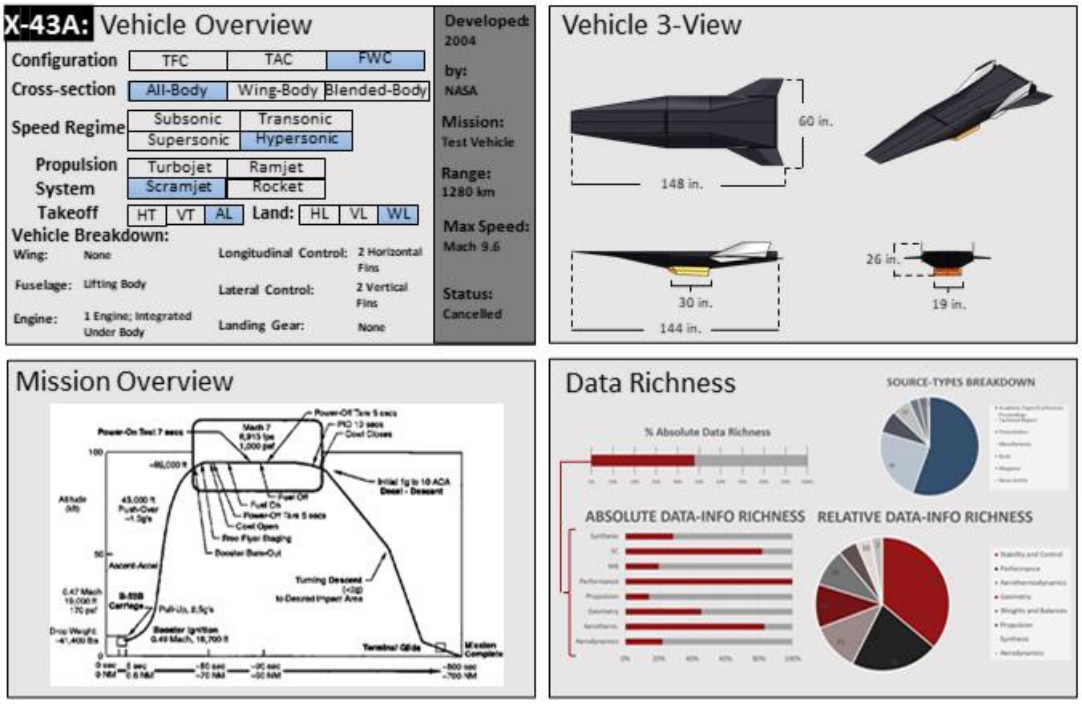

Fig. C.2 X-43A database 'snapshot'.

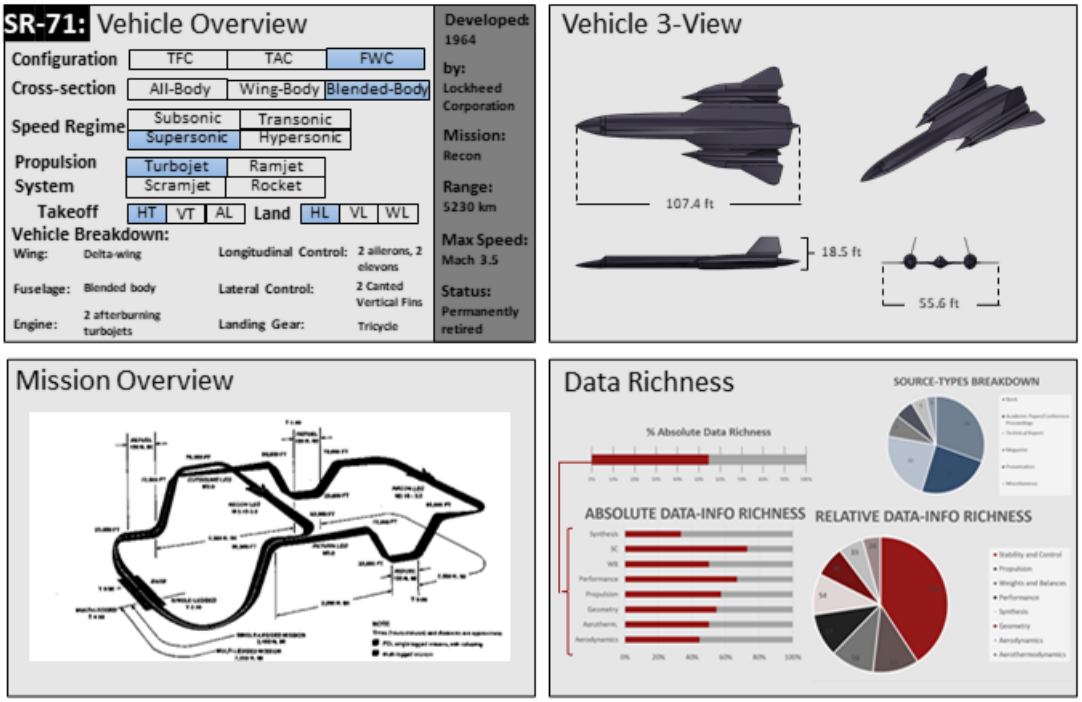

Fig. C.3 SR-71 database 'snapshot'.

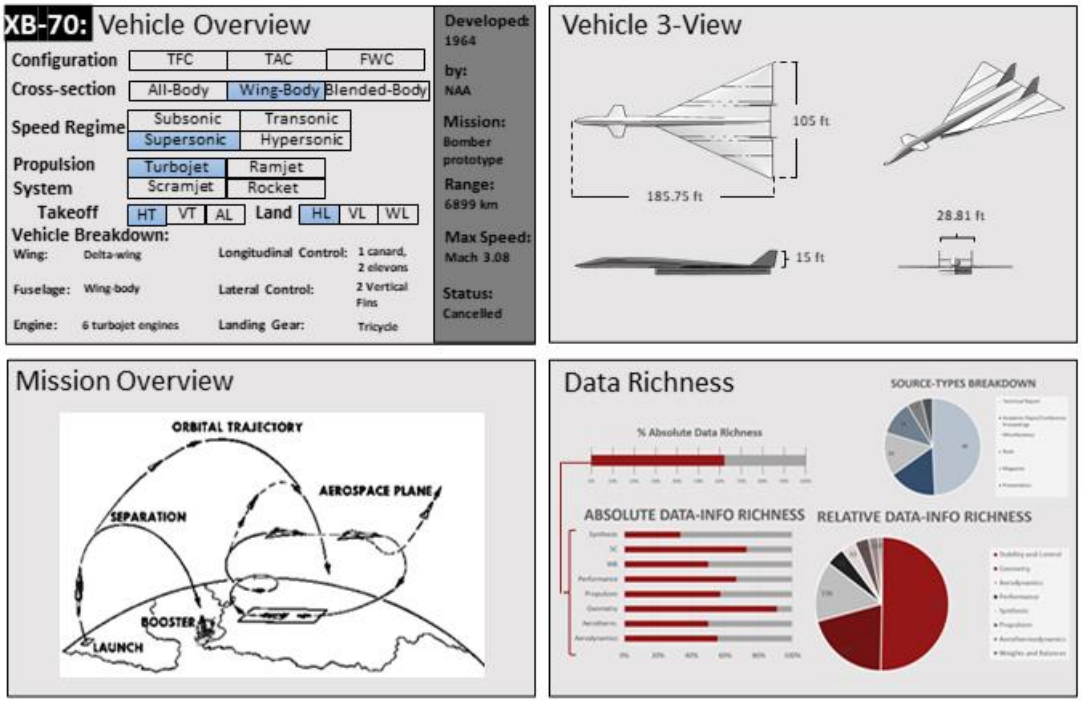

Fig. C.4 XB-70 database 'snapshot'.

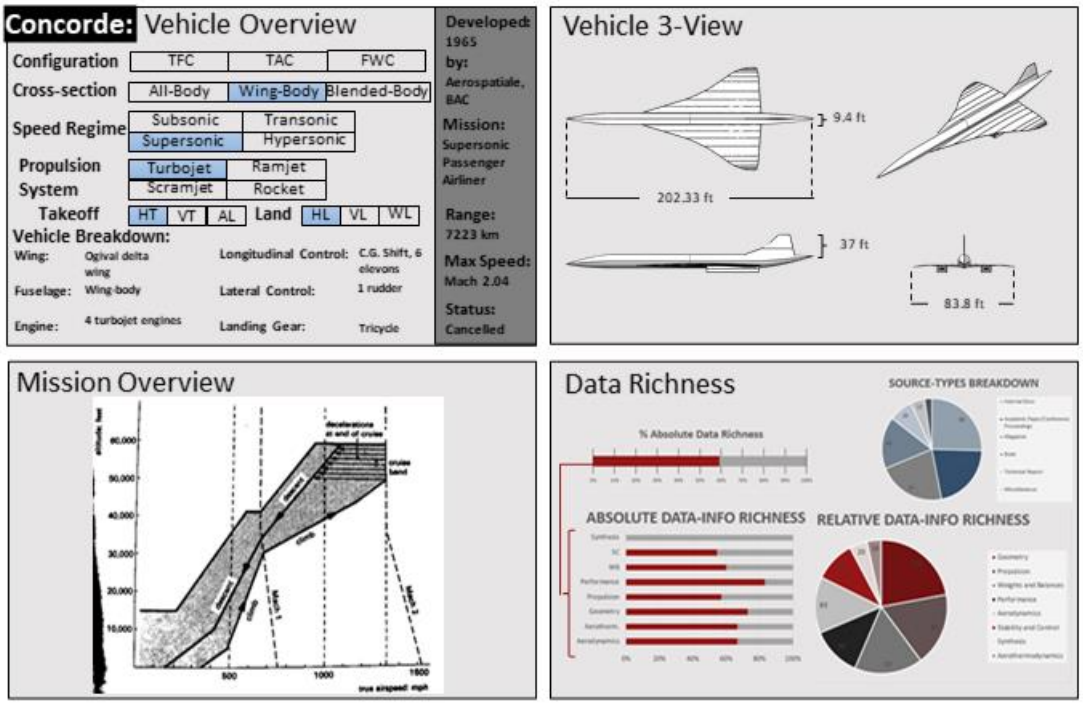

Fig. C.5 Concorde database 'snapshot'.

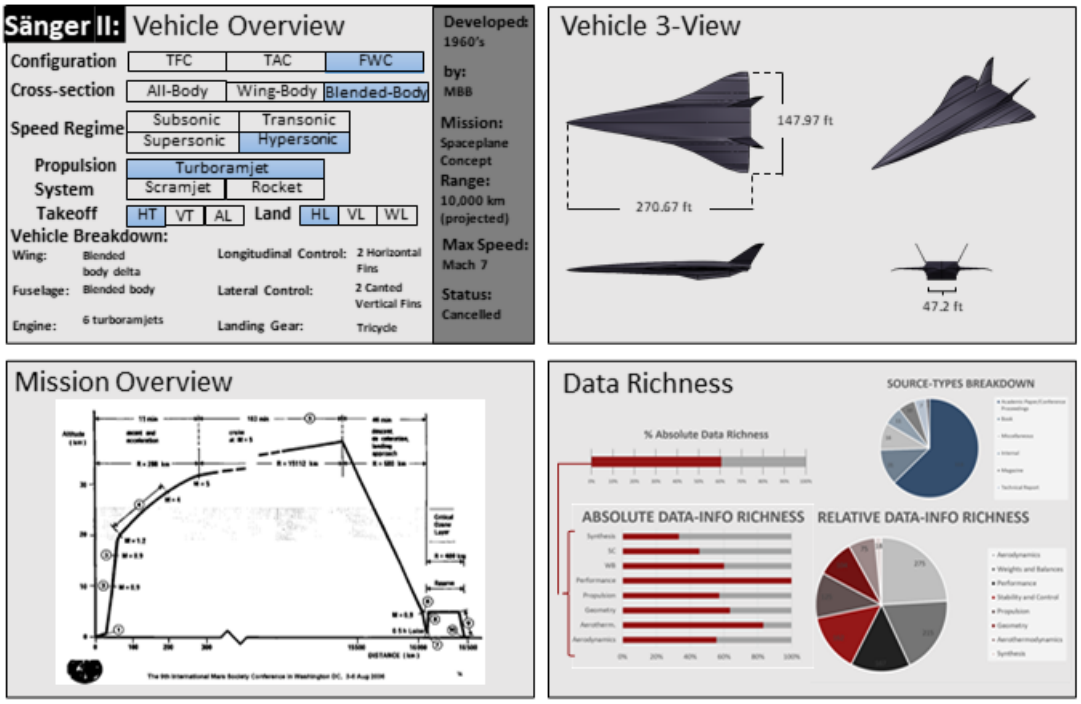

Fig. C.6 Sänger II database 'snapshot'.

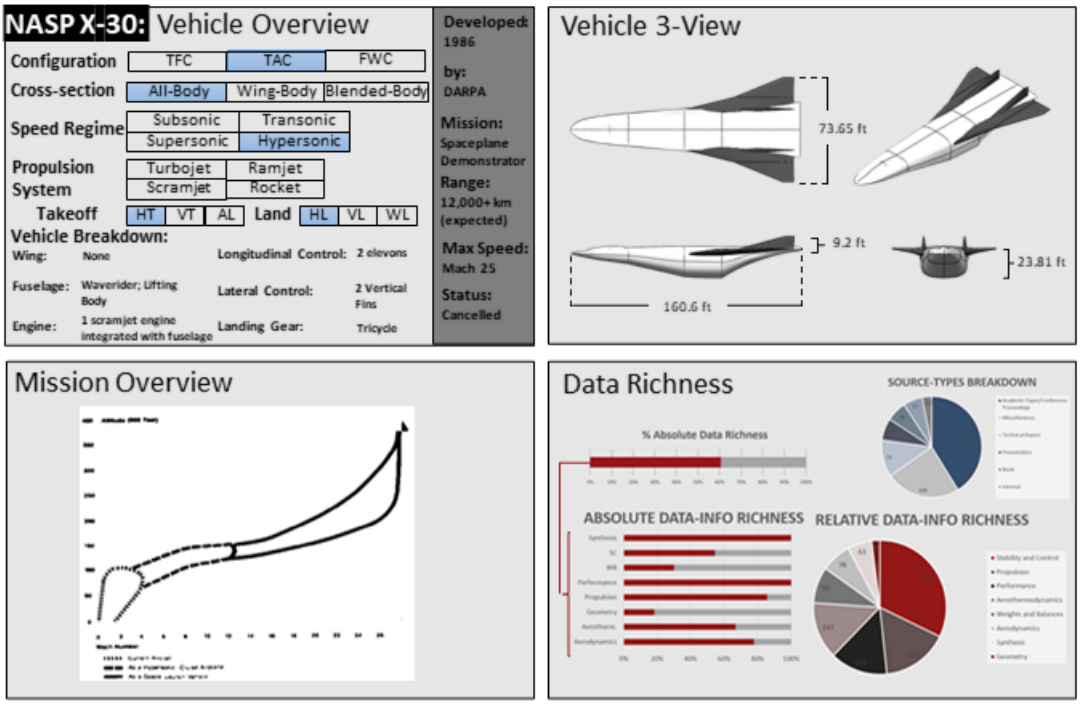

Fig. C.7 NASP X-30 database 'snapshot'.

APPENDIX D
VEHICLE GEOMETRIC METHODS USED WITHIN AVDS

D.1 AVDS Configuration Evaluation (AVDS^{CE}) Geometric Method

Discipline	Method Title	Method Type	Applicability
Geometry	XB-70 Wingtip Droop Geometry Changes	Analytical	Only for XB-70 Valkyrie

Summary of Analysis
This method provides the equations used to calculate the geometrical properties that are affected by the wingtip droop change.

Inputs	Outputs	Legacy Use
C_{in}, b_{tip}, δ_{droop}, S_{pln}, S_{wing}, b, V_{TOT}, C_{tip}, S_{side}, H_{engine}, θ_{tip}	$S_{pln,droop}$, $S_{wing,droop}$, b_{droop}, AR_{droop}, τ_{droop}, $S_{side,droop}$	XB-70

Design Fidelity	Assumptions	Comments
PS	Can be defined using simple geometrical shapes such as rectangles and triangles	

Source Material
Derived by Samuel Atchison

Planform Area Change:

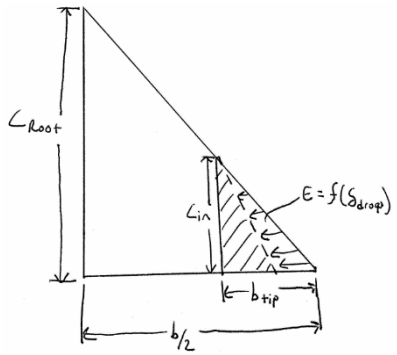

$$E = \frac{1}{2} C_{in} b_{tip} - (b_{tip} \cos \delta_{droop})$$

$$\tau_{droop} = \frac{V_{TOTAL}}{S_{pln_{droop}}^{1.5}}$$

$$S_{pln_{droop}} = S_{pln} - 2E$$

$$S_{wing_{droop}} = S_{wing} - 2E$$

$$b_{droop} = b - 2b_{tip} + 2b_{tip} \cos \delta_{droop}$$

$$AR_{droop} = \frac{b_{droop}^2}{S_{wing_{droop}}}$$

Side Area Change:

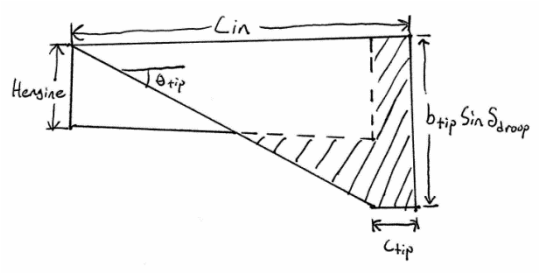

if $b_{tip} \sin \delta_{droop} \leq H_{engine}$ *and* $\delta_{droop} \neq 0$*:*

$$S_{side_{droop}} = S_{side} + C_{tip} b_{tip} \sin \delta_{droop}$$

if $b_{tip} \sin \delta_{droop} > H_{engine}$ *and* $\delta_{droop} \neq 0$*:*

$$S_{side_{droop}} = S_{side} + \frac{1}{2}\left(\frac{b_{tip} \sin \delta_{droop} - H_{engine}}{\tan \theta_{tip}}\right) + C_{tip} b_{tip} \sin \delta_{droop}$$

D.2 AVDS Parametric Sizing (AVDS^{PS}) Geometric Method

Discipline	Method Title	Method Type	Applicability
Geometry	Passenger Cabin Scaling	Empirical	WB, BB, and AB at supersonic/ hypersonic speeds

Summary of Analysis

This method is based on regression data gathered from past AVD members on passenger aircraft ranging from transonic to supersonic speeds. Trendlines were created separating the speed regimes.

Inputs	Outputs	Legacy Use
PAX	H_{cabin}, W_{cabin}, L_{cabin}, Vol_{cabin}	Concorde, Sänger II, Orient Express

Design Fidelity	Assumptions	Comments
PS		Vehicles used for regression are WB vehicles so outer dimensions of passenger cabin are more cylindrical. BB and AB used cabin volume parameter.

Source Material

Previous AVD study

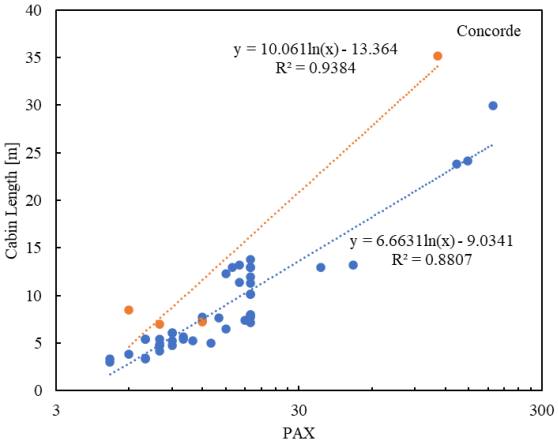

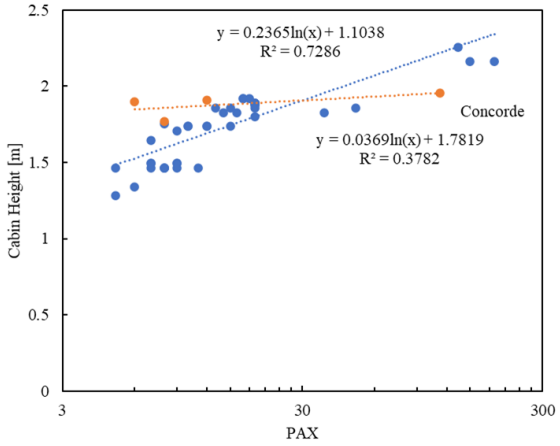

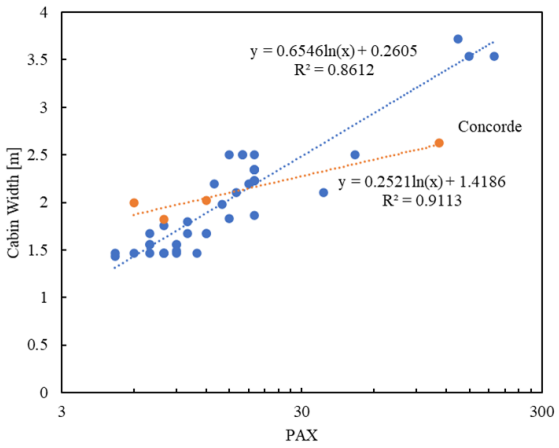

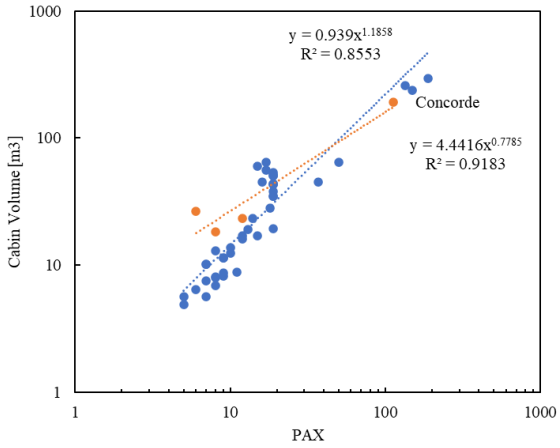

Transonic Equations:

$L_{cabin} = 6.6631\, ln\,(PAX) - 9.0341$

$H_{cabin} = 0.2365\, ln\,(PAX) + 1.1038$

$W_{cabin} = 0.6546\, ln(PAX) + 0.2605$

$Vol_{cabin} = 0.939 PAX^{1.1858}$

Supersonic Equations:

$L_{cabin} = 10.061\, ln\,(PAX) - 13.364$

$H_{cabin} = 0.0369\, ln\,(PAX) + 1.7819$

$W_{cabin} = 0.2521\, ln(PAX) + 1.4186$

$Vol_{cabin} = 4.4416 PAX^{0.7785}$

Discipline	Method Title	Method Type	Applicability
Geometry	Leading-Edge Flow Parameter Scaling	Analytical	AB, BB, and WB and all speeds

Summary of Analysis

This scaling method uses the leading-edge flow parameter defined by Torenbeek to calculate the parameter value with the original Mach number and leading-edge angle, and then while keeping the parameter constant, solve for a new leading-edge angle with the new Mach number wanted.

Inputs	Outputs	Legacy Use
$M_{original}$, $\Lambda_{original}$,, M_{new}	Λ_{new}	Concorde, Sänger II, Orient Express

Design Fidelity	Assumptions	Comments
PS	The flow perpendicular to the wing is constant with the Mach change	

Source Material

Torenbeek, E. *Essentials of Supersonic Commercial Aircraft Conceptual Design*, *Aerospace Series*, John Wiley & Sons, Inc., Hoboken, NJ, 2020. [56]

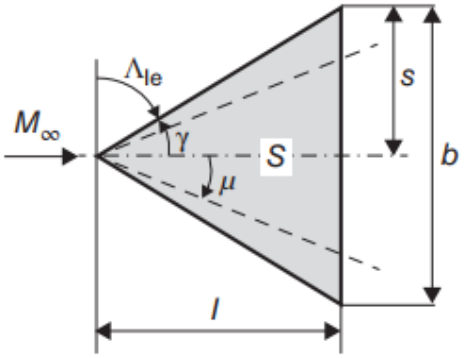

$$m = \frac{\tan\gamma}{\tan\mu} = \frac{\tan(90 - \Lambda_{original})}{\tan\left(\sin^{-1}\left(\frac{1}{M_{original}}\right)\right)}$$

$$\Lambda_{new} = 90 - \tan^{-1}\left(m \cdot \tan\left(\sin^{-1}\left(\frac{1}{M_{new}}\right)\right)\right)$$

APPENDIX E
AEROTHERMODYNAMIC DISCIPLINARY METHODS FOR AVDS

Discipline	Method Title	Method Type	Applicability
Aerothermodynamics	Reference Temperature Method	Analytical	M > 1

Summary of Analysis

This aerothermodynamic method is used to determine the heat flux that goes into the vehicle through convection and the heat flux that is radiated away from the vehicle. It was developed to provide a first order assumption of the expected heat flux/temperatures that the vehicle will experience.

Inputs	Outputs	Legacy Use
Pr, T_0, R, x_t, C_p, ε, v_{sb}, T_w Air properties behind shock: T_2, P_2, V_2	$\dot{q}_{conv}$, $\dot{q}_{rad}$	Concorde, XB-70, SR-71

Design Fidelity	Assumptions	Comments
PS	Calorically Perfect Air, Flat Plate Assumption, Radiation Equilibrium Temperature: $\dot{q}_{conv} = \dot{q}_{rad}$, Pr = 0.715, ε = 0.8, ν_{sb} = 5.67e-8	When using the Radiation Equilibrium Temperature assumption, T_w is a guess value that is iterated until true for each point along the trajectory

Source Material

Anderson, J. D., *Hypersonic and High Temperature Gas Dynamics*, *AIAA Education Series*, 2nd Ed., American Institute of Aeronautics and Astronautics, Reston, VA, 2006. [147]

Arthur, P. D., Schultz, H. D., and Guard, F. L., "Flat Plate Turbulent Heat Transfer at Hypervelocities," *Journal of Spacecraft and Rockets,* Vol. 3, No. 10, pp. 1549-1551, October 1966. [155]

$$r = Pr^{1/3}$$

$$T_{aw} = T_2 + r(T_0 - T_2)$$

$$T^* = T_2 + 0.5(T_w - T_2) + 0.22(T_{aw} - T_2)$$

$$\rho^* = \frac{P_2}{RT^*}$$

$$\mu^* = 1.789x10^{-5}\left(\frac{T^*}{288}\right)^{3/2}\left(\frac{288+110}{T^*+110}\right)$$

$$Re_x^* = \frac{\rho^* V_2 x_t}{\mu^*}$$

If Re_x^*<= 1e7:

$$\frac{c_f}{2} = \frac{0.0296}{Re_x^{*0.2}}$$

If Re_x^* > 1e7:

$$\frac{c_f}{2} = \frac{0.185}{\log_{10}(Re_x^*)^{2.584}}$$

$$C_H = \frac{c_f}{2} Pr^{-2/3}$$

$$\dot{q}_{conv} = \rho^* V_2 C_H C_p (T_{aw} - T_w)$$

$$\dot{q}_{rad} = \varepsilon v_{sb} T_w^4$$

Discipline	Method Title	Method Type	Applicability
Aerothermodynamics	Temperature through the Thickness Finite Difference Method	Analytical	Speeds/temperatures where TPS is required

Summary of Analysis

This aerothermodynamics method can determine the temperature through a TPS material system over time with a finite difference method by separating each material into nodes.

Inputs	Outputs	Legacy Use
Properties for each material: k, ρ, c_p $\dot{q}_{aero}$, $\dot{q}_{rad}$, Δt, Δy	T	

Design Fidelity	Assumptions	Comments
CE	TPS system starts at an initial temperature	Long run time Appears to have increased error for thicker TPS systems

Source Material

Bolender, M. A., Doman, D. B, "Modeling Unsteady Heating Effects on the Structural Dynamics of a Hypersonic Vehicle," AIAA-2006-6646, *AIAA Atmospheric Flight Mechanics Conference and Exhibit*, Keystone, CO, 21-24 August 2006. [161]

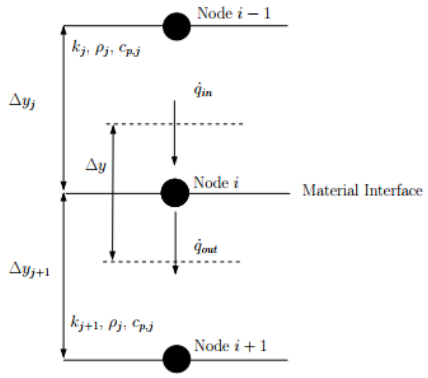

Heat Transfer at the Exterior Surface (corrected equation):

$$T_1^{(p+1)} = (\dot{q}_{aero} - \dot{q}_{rad})\frac{2\Delta t}{\rho_1 c_{p,1}\Delta y_1} + T_1^{(p)}\left(1 - \frac{2k_1\Delta t}{\rho_1 c_{p,1}(\Delta y_1)^2}\right) + T_2^{(p)}\left(\frac{2k_1\Delta t}{\rho_1 c_{p,1}(\Delta y_1)^2}\right)$$

Heat Transfer at Interior Nodes:

$$T_i^{(p+1)} = \frac{k_j\Delta t}{\rho_j c_{p,j}(\Delta y_j)^2}\left(T_{i+1}^{(p)} + T_{i-1}^{(p)}\right) + \left(1 - \frac{2k_j\Delta t}{\rho_j c_{p,j}(\Delta y_j)^2}\right)T_i^{(p)}$$

Heat Transfer at Material Interfaces:

$$T_i^{(p+1)} = \frac{2\Delta t}{(\rho_j c_{p,j} + \rho_{j+1} c_{p,j+1})\Delta y}\left\{\frac{k_j}{\Delta y_j} T_{i-1}^{(p)} + \frac{k_{j+1}}{\Delta y_{j+1}} T_{i+1}^{(p)}\right\} + \left\{1 - \left[\frac{k_j}{\Delta y_j} + \frac{k_{j+1}}{\Delta y_{j+1}}\right]\frac{2\Delta t}{(\rho_j c_{p,j} + \rho_{j+1} c_{p,j+1})\Delta y}\right\} T_i^{(p)}$$

Heat Transfer in Node n:

$$T_n^{(p+1)} = \left(1 - \frac{2k_3\Delta t}{\rho_3 c_{p,3}(\Delta y_3)^2}\right) T_n^{(p)} + \frac{2k_3\Delta t}{\rho_3 c_{p,3}(\Delta y_3)^2} T_{n-1}^{(p)}$$

Discipline	Method Title	Method Type	Applicability
Aerothermodynamics	Temperature through the Thickness Heat Pulse Method	Analytical	Speeds/temperatures where TPS is required

Summary of Analysis

This aerodynamics method can determine the temperature through the TPS over time through a representative heat pulse.

Inputs	Outputs	Legacy Use
Material Properties: ρ, c_p, k, d Temperature Profile from Trajectory Pressure Profile from Trajectory t, x, T_i, f_{thr}, T_{mx}, f_{ke}	$T(x,\tau)$	

Design Fidelity	Assumptions	Comments
PS, CE	Radiation shield is thin and contributes little to thermal response. Can be neglected. Varying transient temperature can be represented as a heat pulse. f_{ke} = 0.6, f_{thr} = 0.15	Shorter run time compared to Finite Difference Method. Higher error at thin insulation thickness, within acceptable range (5%).

Source Material

Blosser, M. L., "Analysis and Sizing for Transient Thermal Heating of Insulated Aerospace Vehicle Structures," AIAA-2006-6646, *AIAA Atmospheric Flight Mechanics Conference and Exhibit*, Keystone, CO, 21-24 August 2006. [162]

Temperature Equations:

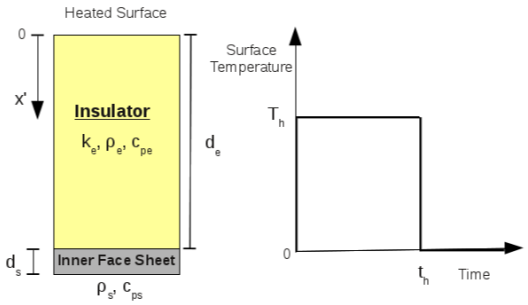

$$\beta = \frac{k_e}{\rho_e c_{pe} d_e^2}$$

$$\gamma = \frac{\rho_e c_{pe} d_e}{\rho_s c_{ps} d_s}$$

$$\tau_h = \frac{k_e}{\rho_e c_{pe} d_e^2} t_h$$

$$\lambda_m \tan \lambda_m = \gamma$$

$$c_m = \frac{2(\lambda_m^2 + \gamma^2)}{\lambda_m(\lambda_m^2 + \gamma^2 + \gamma)}$$

For $0 < \tau \leq \tau_h$:

$$\theta(x,\tau) = \frac{T(x,\tau)}{T_h} = 1 - \sum_{m=1}^{\infty} c_m \sin(\lambda_m x) e^{-\lambda_m^2 \tau}$$

For $\tau > \tau_h$:

$$\theta(x,\tau) = \frac{T(x,\tau)}{T_h} = \sum_{n=1}^{\infty} b_n \sin(\lambda_n x) e^{-\lambda_n^2(\tau - \tau_h)}$$

$$b_n = c_n\left(1 - e^{-\lambda_n^2 \tau_h}\right) - \sum_{\substack{m=1 \\ m \neq n}}^{\infty} \left(\frac{\frac{\sin(\lambda_m - \lambda_n)}{(\lambda_m - \lambda_n)} - \frac{\sin(\lambda_m + \lambda_n)}{(\lambda_m + \lambda_n)} + \frac{2 \sin \lambda_m \sin \lambda_n}{\gamma}}{1 - \frac{\sin(2\lambda_n)}{2\lambda_n} + \frac{2 \sin^2 \lambda_n}{\gamma}} \right) c_m e^{(-\lambda_m^2 \tau_h)}$$

Converting Temperature and Pressure Trajectory Information:

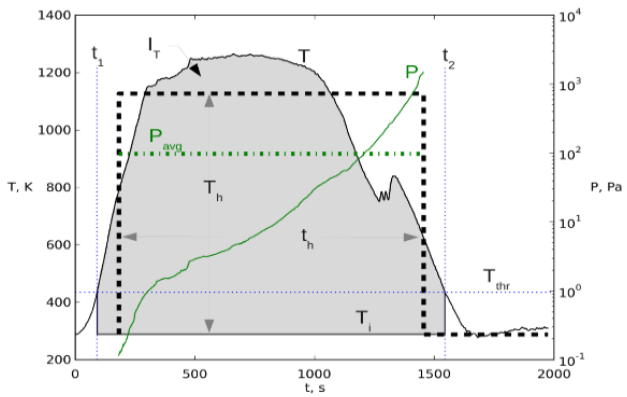

$$T_{thr} = T_i + f_{thr}(T_{mx} - T_i)$$

$$I_T = \int_{t_1}^{t_2} (T - T_i) dt$$

$$t_h = \frac{(t_2 - t_1) + \frac{I_T}{T_{mx} - T_i}}{2}$$

$$T_h = \frac{I_T}{t_h}$$

Approximate Temperatures for Variable Material Properties:

$$c_{ps} = c_{ps}(T_{cs}), \text{ where } T_{cs} = T_i + \frac{T_m}{2}$$

$$c_{pe} = c_{pe}(T_{ce}), \text{ where } T_{ce} = T_i + T_m$$

$$k_e = k_e(T_{ke}, P_{avg}), \text{ where } T_{ke} = T_i + f_{ke}T_h$$

APPENDIX F
MATERIAL PROPERTIES

E.1 Insulation Material Properties

Table F.1 Material properties of saffil [171].

		Thermal Conductivity, (Btu-in)/(s-in^2-°R)							
		Pressure, psi							
Temperature, °R	Specific Heat, Btu/lb$_m$/°R	1.93x10-6	9.67x10-6	1.93x10-5	9.67x10-5	1.93x10-5	9.67x10-4	1.93x10-3	9.67x10-3
455	0.164	3.11E-08	3.12E-08	3.14E-08	3.27E-08	3.43E-08	4.66E-08	6.07E-08	1.37E-07
491	0.173	3.81E-08	3.82E-08	3.84E-08	3.97E-08	4.13E-08	5.35E-08	6.74E-08	1.45E-07
671	0.227	9.00E-08	9.01E-08	9.02E-08	9.14E-08	9.29E-08	1.05E-07	1.18E-07	2.00E-07
851	0.244	1.74E-07	1.74E-07	1.75E-07	1.76E-07	1.77E-07	1.88E-07	2.02E-07	2.86E-07
1031	0.261	2.96E-07	2.97E-07	2.97E-07	2.98E-07	2.99E-07	3.10E-07	3.23E-07	4.08E-07
1211	0.272	4.61E-07	4.61E-07	4.61E-07	4.62E-07	4.64E-07	4.74E-07	4.87E-07	5.73E-07
1391	0.28	6.72E-07	6.72E-07	6.72E-07	6.73E-07	6.75E-07	6.85E-07	6.97E-07	7.83E-07
1571	0.286	9.33E-07	9.33E-07	9.33E-07	9.34E-07	9.35E-07	9.45E-07	9.58E-07	1.04E-06
1751	0.292	1.25E-06	1.25E-06	1.25E-06	1.25E-06	1.25E-06	1.26E-06	1.27E-06	1.35E-06
1931	0.296	1.62E-06	1.62E-06	1.62E-06	1.62E-06	1.62E-06	1.63E-06	1.64E-06	1.72E-06
2111	0.299	2.04E-O6	2.04E-06	2.04E-06	2.04E-06	2.04E-06	2.05E-06	2.06E-06	2.15E-06
2291	0.301	2.53E-06	2.53E-06	2.53E-06	2.53E-06	2.53E-06	2.54E-06	2.55E-06	2.63E-06
2471	0.303	3.07E-06	3.07E-06	3.07E-06	3.07E-06	3.08E-06	3.08E-06	3.10E-06	3.18E-06
2651	0.304	3.68E-06	3.68E-06	3.68E-06	3.68E-06	3.68E-06	3.69E-06	3.70E-06	3.78E-06

Table F.2 Material properties for saffil cont. [171].

		Thermal Conductivity, (Btu-in)/(s-in^2-°R)						
		Pressure, psi						
Temperature, °R	Specific Heat, Btu/lb$_m$/°R	0.0193	0.0967	0.193	0.967	1.93	9.67	14.7
455	0.164	1.87E-07	2.82E-07	3.03E-07	3.22E-07	3.25E-07	3.27E-07	3.27E-07
491	0.173	1.98E-07	3.01E-07	3.25E-07	3.47E-07	3.50E-07	3.52E-07	3.52E-07
671	0.227	2.63E-07	4.08E-07	4.45E-07	4.82E-07	4.87E-07	4.92E-07	4.92E-07
851	0.244	3.56E-07	5.39E-07	5.91E-07	6.45E-07	6.53E-07	6.59E-07	6.60E-07
1031	0.261	4.84E-07	6.99E-07	7.67E-07	8.41E-07	8.51E-07	8.60E-07	8.61E-07
1211	0.272	6.51E-07	8.96E-07	9.80E-07	1.07E-06	1.09E-06	1.10E-06	1.10E-06
1391	0.28	8.64E-07	1.13E-06	1.23E-06	1.35E-06	1.37E-06	1.38E-06	1.38E-06
1571	0.286	1.13E-06	1.42E-06	1.53E-06	1.67E-06	1.69E-06	1.71E-06	1.71E-06
1751	0.292	1.44E-06	1.75E-06	1.88E-06	2.04E-06	2.06E-06	2.08E-06	2.09E-06
1931	0.296	1.81E-06	2.13E-06	2.27E-06	2.45E-06	2.48E-06	2.51E-06	2.51E-06
2111	0.299	2.23E-06	2.57E-06	2.72E-06	2.93E-06	2.96E-06	2.99E-06	2.99E-06
2291	0.301	2.71E-06	3.06E-06	3.23E-06	3.45E-06	3.49E-06	3.52E-06	3.53E-06
2471	0.303	3.26E-06	3.62E-06	3.79E-06	4.03E-06	4.08E-06	4.11E-06	4.12E-06
2651	0.304	3.87E-06	4.23E-06	4.41E-06	4.68E-06	4.72E-06	4.76E-06	4.77E-06

Table F.3 Material properties for q-felt [172].

		Thermal Conductivity, (Btu-in)/(s-in^2-°R)							
		Pressure, psi							
Temperature, °R	Specific Heat, Btu/lb$_m$/°R	1.93x10-6	1.93x10-5	1.93x10-4	1.93x10-3	0.0193	0.193	0.967	1.93
530	0.169	4.63E-08	4.86E-08	5.09E-08	7.18E-08	1.44E-07	1.97E-07	3.13E-07	3.43E-07
660	0.204	8.80E-08	8.80E-08	9.03E-08	1.13E-07	1.88E-07	2.45E-07	3.94E-07	4.33E-07
860	0.227	1.76E-07	1.76E-07	1.78E-07	1.99E-07	2.75E-07	3.40E-07	5.28E-07	5.86E-07
1060	0.239	2.92E-07	2.92E-07	2.94E-07	3.13E-07	3.89E-07	4.58E-07	6.78E-07	7.55E-07
1260	0.248	4.38E-07	4.38E-07	4.40E-07	4.61E-07	5.35E-07	6.09E-07	8.56E-07	9.49E-07
1460	0.254	6.18E-07	6.18E-07	6.20E-07	6.39E-07	7.13E-07	7.87E-07	1.06E-06	1.17E-06
1660	0.259	8.45E-07	8.45E-07	8.47E-07	8.66E-07	9.38E-07	1.01E-06	1.30E-06	1.42E-06
1860	0.263	1.19E-06	1.19E-06	1.19E-06	1.21E-06	1.28E-06	1.35E-06	1.66E-06	1.80E-06
2060	0.267	1.61E-06	1.61E-06	1.62E-06	1.63E-06	1.70E-06	1.78E-06	2.10E-06	2.25E-06
2260	0.271	2.13E-06	2.13E-06	2.13E-06	2.15E-06	2.22E-06	2.30E-06	2.63E-06	2.79E-06

Table F.4 Material properties for q-felt cont. [172].

		Thermal Conductivity, (Btu-in)/(s-in^2-°R)	
		Pressure, psi	
Temperature, °R	Specific Heat, Btu/lb$_m$/°R	1.93	14.7
530	0.169	4.63E-08	4.86E-08
660	0.204	8.80E-08	8.80E-08
860	0.227	1.76E-07	1.76E-07
1060	0.239	2.92E-07	2.92E-07
1260	0.248	4.38E-07	4.38E-07
1460	0.254	6.18E-07	6.18E-07
1660	0.259	8.45E-07	8.45E-07
1860	0.263	1.19E-06	1.19E-06
2060	0.267	1.61E-06	1.61E-06
2260	0.271	2.13E-06	2.13E-06

Table F.5 Material properties for cerrachrome [173].

		Thermal Conductivity, (Btu-in)/(s-in^2-°R)							
		Pressure, psi							
Temperature, °R	Specific Heat, Btu/lb$_m$/°R	7.54x10-5	1.93x10-4	1.93x10-3	0.0193	0.193	0.967	1.93	14.7
460	0.1648	9.95E-08	9.95E-08	1.11E-07	2.04E-07	4.12E-07	4.77E-07	4.88E-07	4.98E-07
660	0.1958	9.95E-08	9.95E-08	1.11E-07	2.04E-07	4.12E-07	4.77E-07	4.88E-07	4.98E-07
860	0.2268	2.45E-07	2.45E-07	2.57E-07	3.47E-07	6.04E-07	7.08E-07	7.25E-07	7.41E-07
1060	0.2482	4.00E-07	4.00E-07	4.10E-07	4.95E-07	7.92E-07	9.33E-07	9.58E-07	9.84E-07
1260	0.264	5.90E-07	5.90E-07	6.00E-07	6.81E-07	1.00E-06	1.19E-06	1.22E-06	1.25E-06
1460	0.2726	8.54E-07	8.54E-07	8.63E-07	9.40E-07	1.28E-06	1.50E-06	1.55E-06	1.59E-06
1660	0.2789	1.23E-06	1.23E-06	1.24E-06	1.31E-06	1.66E-06	1.92E-06	1.98E-06	2.03E-06
1860	0.2808	1.63E-06	1.63E-06	1.64E-06	1.71E-06	2.07E-06	2.37E-06	2.44E-06	2.51E-06
2060	0.2839	2.15E-06	2.15E-06	2.16E-06	2.23E-06	2.59E-06	2.92E-06	3.00E-06	3.09E-06
2260	0.2871	2.68E-06	2.68E-06	2.68E-06	2.75E-06	3.11E-06	3.47E-06	3.56E-06	3.66E-06
2460	0.2902	3.39E-06	3.39E-06	3.40E-06	3.46E-06	3.83E-06	4.22E-06	4.32E-06	4.44E-06
2660	0.2934	4.23E-06	4.23E-06	4.23E-06	4.29E-06	4.66E-06	5.08E-06	5.19E-06	5.32E-06
2860	0.2965	5.03E-06	5.03E-06	1.11E-07	5.09E-06	5.46E-06	5.90E-06	6.03E-06	6.18E-06

Table F.6 Material properties of AETB-8 [174].

		Thermal Conductivity, Btu/(s-ft-°R)					
		Pressure, lb/ft^2					
Temperature, °R	Specific Heat, Btu/lb$_m$/°R	0.001	0.2116	2.116	21.16	211.6	2116
460	0.150	2.78E-06	2.78E-06	4.17E-06	7.22E-06	8.33E-06	8.33E-06
710	0.210	3.06E-06	3.06E-06	4.44E-06	8.06E-06	9.72E-06	1.00E-05
960	0.252	4.17E-06	4.17E-06	5.56E-06	9.44E-06	1.19E-05	1.22E-05
1210	0.275	6.11E-06	6.11E-06	7.22E-06	1.17E-05	1.47E-05	1.53E-05
1460	0.288	8.61E-06	8.61E-06	9.44E-06	1.42E-05	1.67E-05	1.86E-05
1710	0.296	1.14E-05	1.14E-05	1.25E-05	1.72E-05	2.14E-05	2.22E-05
1960	0.300	1.50E-05	1.50E-05	1.58E-05	2.06E-05	2.56E-05	2.64E-05
2210	0.303	2.11E-05	2.11E-05	1.94E-05	2.42E-05	2.97E-05	3.08E-05
2460	0.303	2.25E-05	2.25E-05	2.33E-05	2.83E-05	3.42E-05	3.56E-05
2710	0.303	2.67E-05	2.67E-05	2.75E-05	3.22E-05	3.86E-05	4.03E-05
2960	0.303	3.06E-05	3.06E-05	3.14E-05	3.67E-05	4.31E-05	4.47E-05
3210	0.303	3.17E-05	3.17E-05	3.25E-05	3.69E-05	4.36E-05	4.56E-05

Table F.7 Material properties of AFRSI [174].

		Thermal Conductivity, Btu/(s-ft-°R)				
		Pressure, lb/ft^2				
Temperature, °R	Specific Heat, Btu/lb$_m$/°R	0.2126	2.126	21.16	211.6	2116
460	0.177	1.11E-06	1.67E-06	4.17E-06	4.72E-05	5.28E-06
710	0.212	1.94E-06	2.78E-06	5.83E-06	7.22E-06	8.33E-06
960	0.244	2.78E-06	3.89E-06	7.22E-06	1.00E-05	1.14E-06
1210	0.270	4.17E-06	5.28E-06	8.89E-06	1.28E-05	1.47E-06
1460	0.277	5.83E-06	7.22E-06	1.11E-05	1.58E-05	1.83E-05
1710	0.269	8.33E-06	1.00E-05	1.44E-05	1.94E-05	2.22E-05
1960	0.282	1.11E-05	1.33E-05	1.83E-05	2.33E-05	2.64E-05
2210	0.295	1.50E-05	1.72E-05	2.22E-05	2.92E-05	3.33E-05

Table F.8 Material properties of LI-900 [164].

		Thermal Conductivity, Btu/(ft-hr-°R)				
		Pressure, atm				
Temperature, °R	Specific Heat, Btu/lb$_m$/°R	0.0001	0.001	0.01	0.1	1.0
460	0.150	0.0075	0.0100	0.0183	0.0250	0.0275
710	0.210	0.0092	0.0125	0.0225	0.0316	0.0341
960	0.252	0.0125	0.0167	0.0276	0.0400	0.0433
1210	0.275	0.0175	0.0216	0.0325	0.0492	0.0534
1460	0.288	0.0233	0.0275	0.0392	0.0600	0.0658
1710	0.296	0.0308	0.0350	0.0492	0.0725	0.0782
1960	0.300	0.0416	0.0459	0.0617	0.0875	0.0942
2210	0.303	0.0567	0.0610	0.0767	0.1060	0.1130
2460	0.303	0.0734	0.0782	0.0942	0.1270	0.1360
2760	0.303	0.0966	0.1020	0.1160	0.1550	0.1670
2960	0.303	0.1160	0.1230	0.1390	0.1790	0.1940
3260	0.303	0.1540	0.1620	0.1800	0.2220	0.2420
3460	0.303	0.1900	0.1960	0.2190	0.2620	0.2900

Table F.9 Material properties of aluminum 2024-T4 [175].

Temperature, °R	Density, lb_m/in^3	Specific Heat, $Btu/lb_m/°R$	Thermal Conductivity, $(Btu\text{-}in)/(s\text{-}in^2\text{-}°R)$
260	0.1	0.149	1.18E-03
360	0.1	0.174	1.36E-01
460	0.1	0.193	1.49E-03
560	0.1	0.207	1.64E-03
660	0.1	0.217	1.80E-03
760	0.1	0.225	2.00E-03
860	0.1	0.231	2.30E-03
960	0.1	0.237	2.46E-03
1060	0.1	0.245	2.50E-03
1160	0.1	0.256	2.43E-03
1260	0.1	0.270	2.31E-03

Table F.10 Material properties of titanium 6Al-4V [175].

Temperature, °R	Density, lb_m/in^3	Specific Heat, $Btu/lb_m/°R$	Thermal Conductivity, $(Btu\text{-}in)/(s\text{-}in^2\text{-}°R)$
60	0.16	0.014	3.01E-05
160	0.16	0.066	4.85E-05
260	0.16	0.101	6.51E-05
360	0.16	0.116	8.04E-05
460	0.16	0.125	9.43E-05
560	0.16	0.130	1.08E-04
660	0.16	0.134	1.18E-04
760	0.16	0.138	1.32E-04
860	0.16	0.141	1.43E-04
960	0.16	0.144	1.57E-04
1060	0.16	0.147	1.72E-04
1160	0.16	0.150	1.86E-04
1260	0.16	0.153	2.01E-04
1360	0.16	0.155	2.15E-04
1460	0.16	0.158	2.30E-04
1560	0.16	0.160	2.43E-04
1660	0.16	0.162	2.59E-04
1760	0.16	0.165	2.72E-04

Table F.11 Material properties of aluminum-beryllium alloy AM162 [176].

Temperature, °R	Density, lb_m/in^3	Specific Heat, $Btu/lb_m/°R$	Thermal Conductivity, $(Btu\text{-}in)/(s\text{-}in^2\text{-}°R)$
260	0.0758	0.131	4.60E-03
360	0.0758	0.240	3.70E-03
460	0.0758	0.321	3.00E-03
660	0.0758	0.392	2.50E-03
860	0.0758	0.435	2.20E-03
1060	0.0758	0.471	1.95E-03
1260	0.0758	0.506	1.80E-03

Table F.12 Material properties of graphite/epoxy [177].

Temperature, °R	Density, lb_m/in^3	Specific Heat, $Btu/lb_m/°R$	In-plane thermal conductivity, $(Btu\text{-}in)/(s\text{-}in^2\text{-}°R)$	Through-thickness thermal conductivity, $(Btu\text{-}in)/(s\text{-}in^2\text{-}°R)$
170	0.057	0.052	1.11E-05	4.86E-06
310	0.057	0.110	2.38E-05	7.64E-06
410	0.057	0.150	3.17E-05	9.26E-06
560	0.057	0.208	4.07E-05	1.13E-05
660	0.057	0.242	4.54E-05	1.23E-05
760	0.057	0.277	4.81E-05	1.32E-05

APPENDIX G
STRUCTURAL INDEX (I_{STR}) SENSITIVITY MAPS

G.1 Variation of Structural Index with an Aluminum 2024 Structure

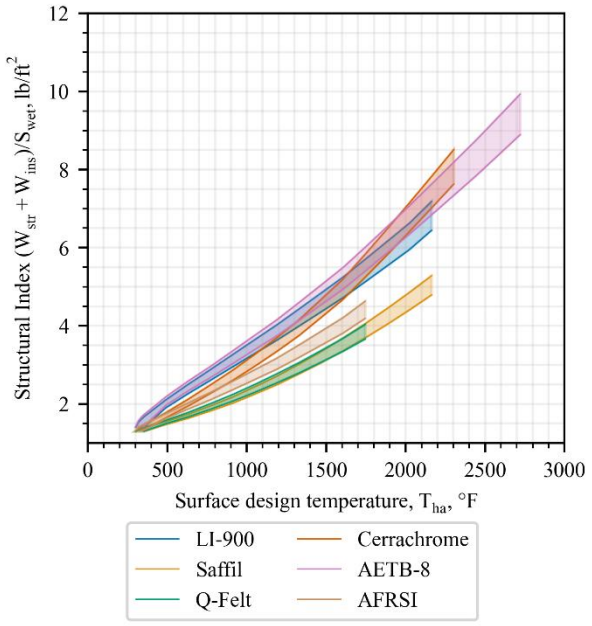

Fig. G.1 Structural index vs surface design temperature at a cruise time of 2 hrs.

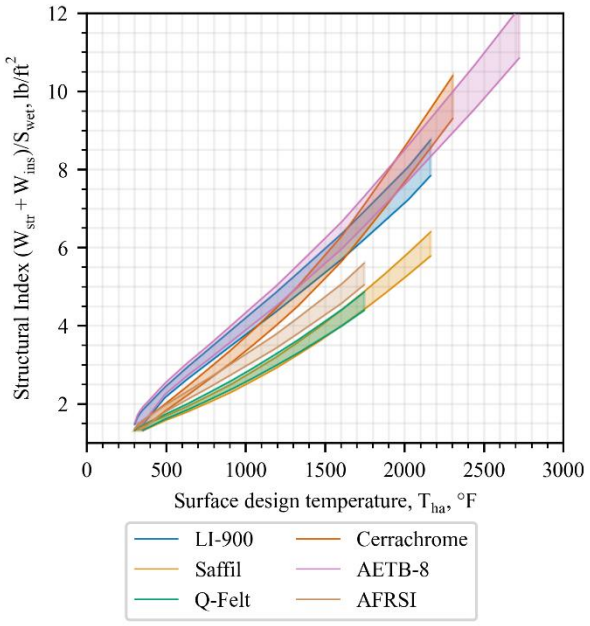

Fig. G.2 Structural index vs surface design temperature at a cruise time of 3 hrs.

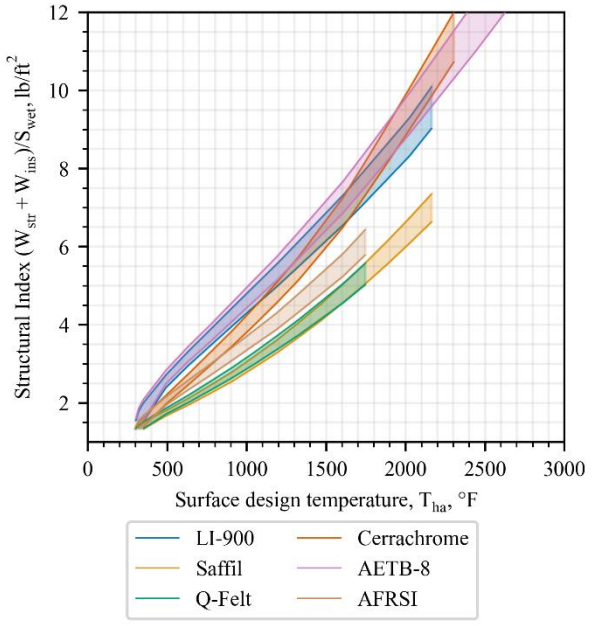

Fig. G.3 Structural index vs surface design temperature at a cruise time of 4 hrs.

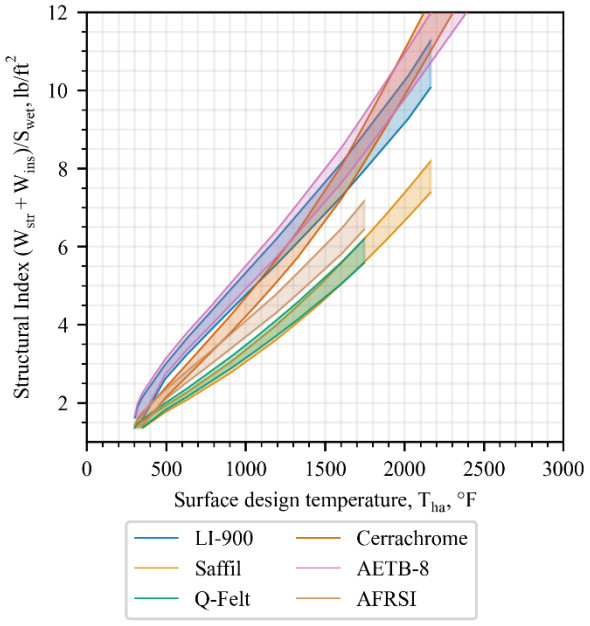

Fig. G.4 Structural index vs surface design temperature at a cruise time of 5 hrs.

G.2 Variation of Insulation Thickness with an Aluminum 2024 Structure

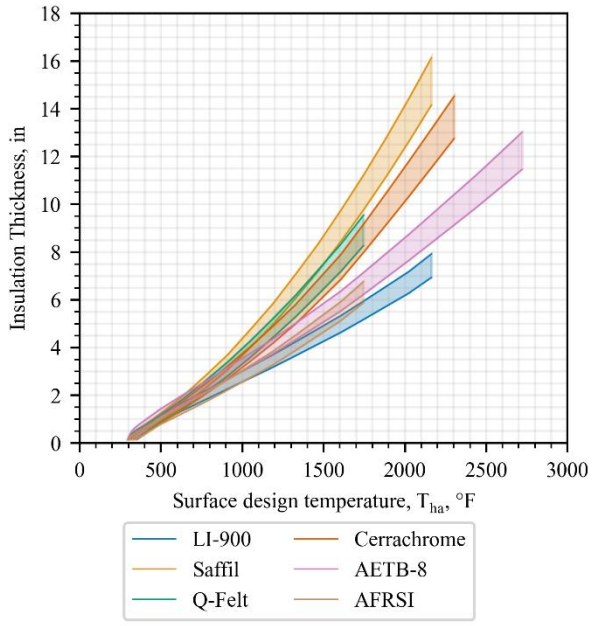

Fig. G.5 Insulation thickness vs surface design temperature at a cruise time of 2 hrs.

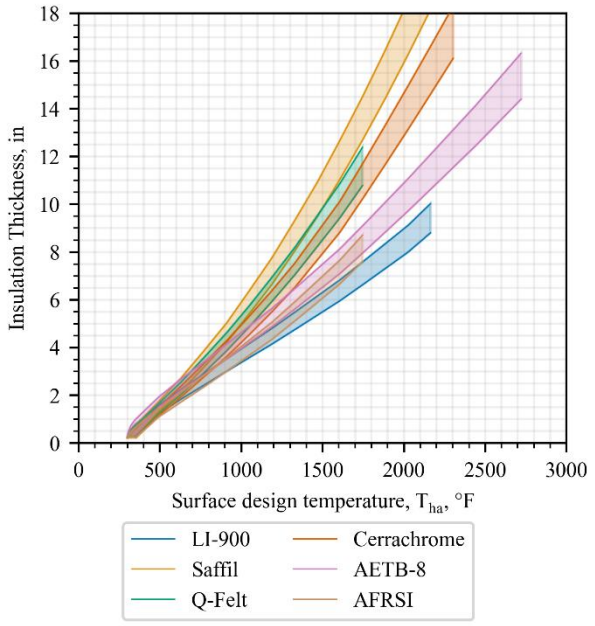

Fig. G.6 Insulation thickness vs surface design temperature at a cruise time of 3 hrs.

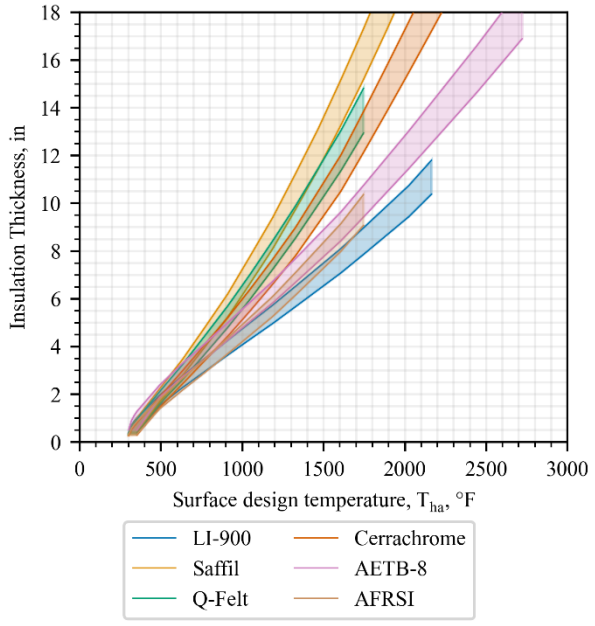

Fig. G.7 Insulation thickness vs surface design temperature at a cruise time of 4 hrs.

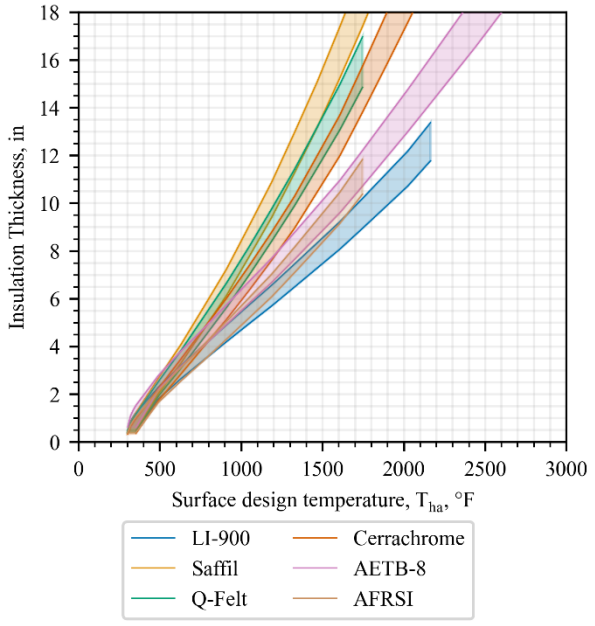

Fig. G.8 Insulation thickness vs surface design temperature at a cruise time of 5 hrs.

G.3 Variation of Structural Index with a Beryllium Aluminum Structure

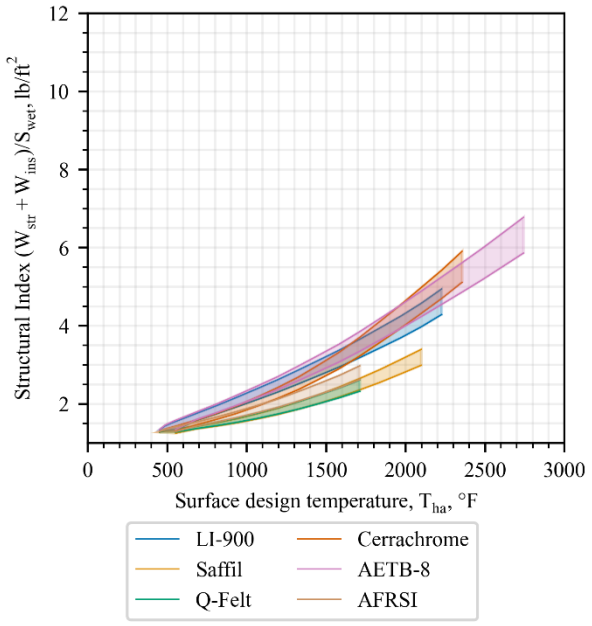

Fig. G.9 Structural index vs surface design temperature at a cruise time of 2 hrs.

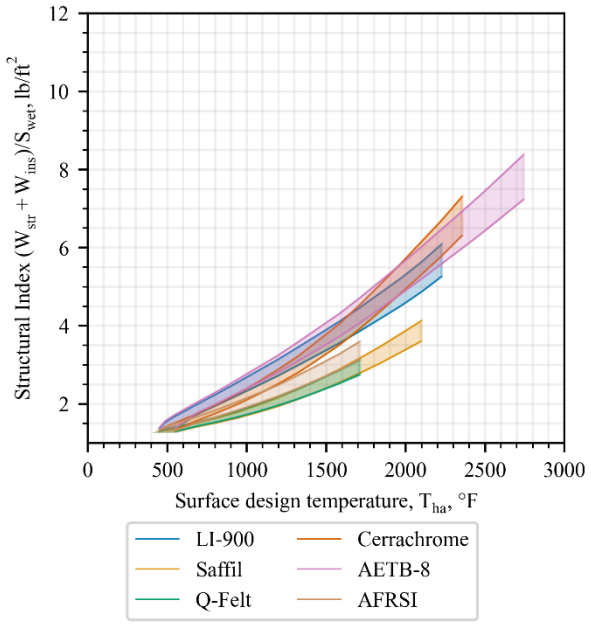

Fig. G.10 Structural index vs surface design temperature at a cruise time of 3 hrs.

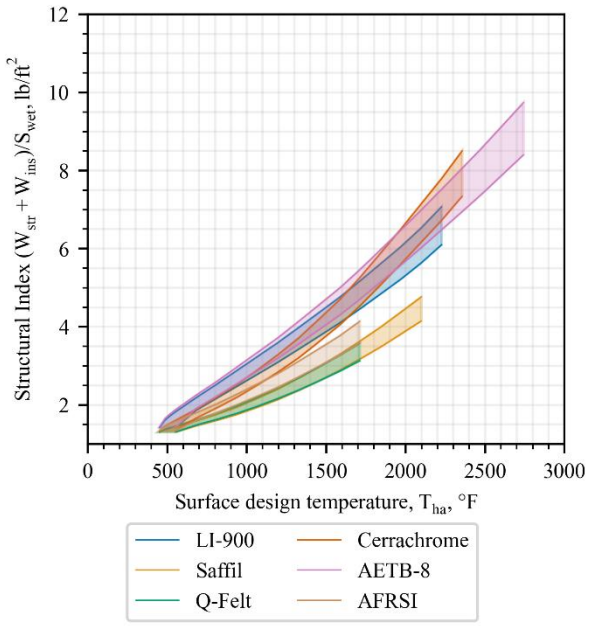

Fig. G.11 Structural index vs surface design temperature at a cruise time of 4 hrs.

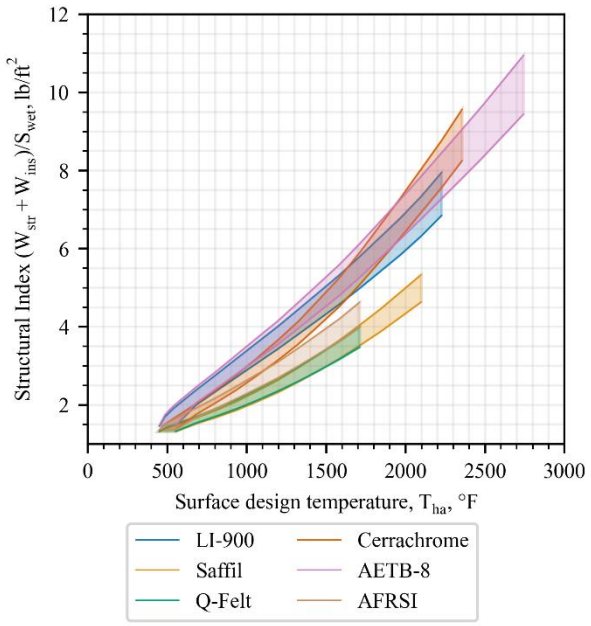

Fig. G.12 Structural index vs surface design temperature at a cruise time of 5 hrs.

G.4 Variation of Insulation Thickness with a Beryllium Aluminum Structure

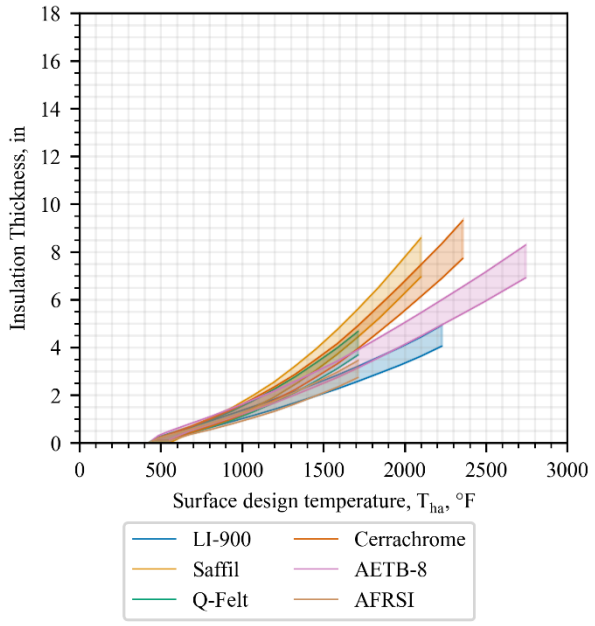

Fig. G.13 Insulation thickness vs surface design temperature at a cruise time of 2 hrs.

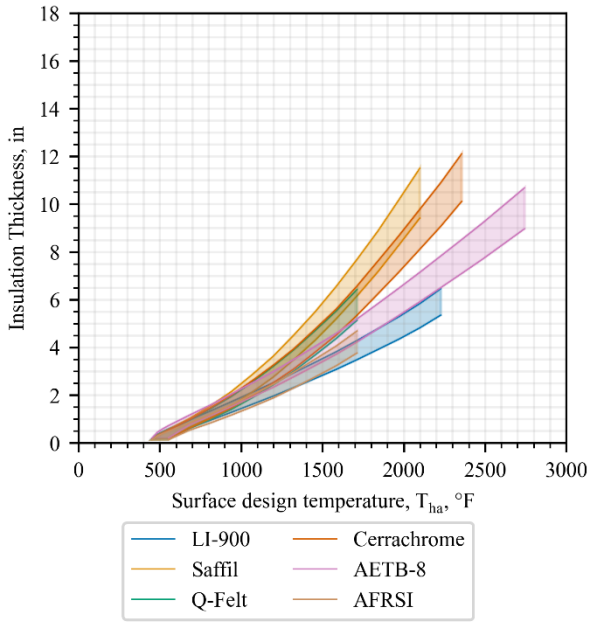

Fig. G.14 Insulation thickness vs surface design temperature at a cruise time of 3 hrs.

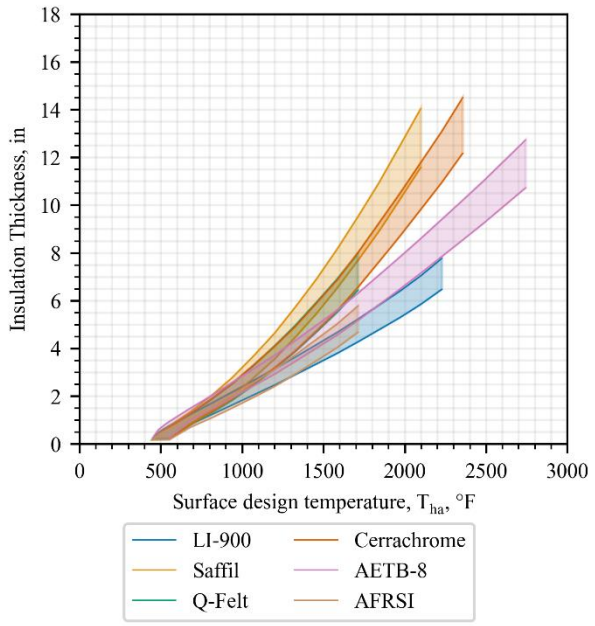

Fig. G.15 Insulation thickness vs surface design temperature at a cruise time of 4 hrs.

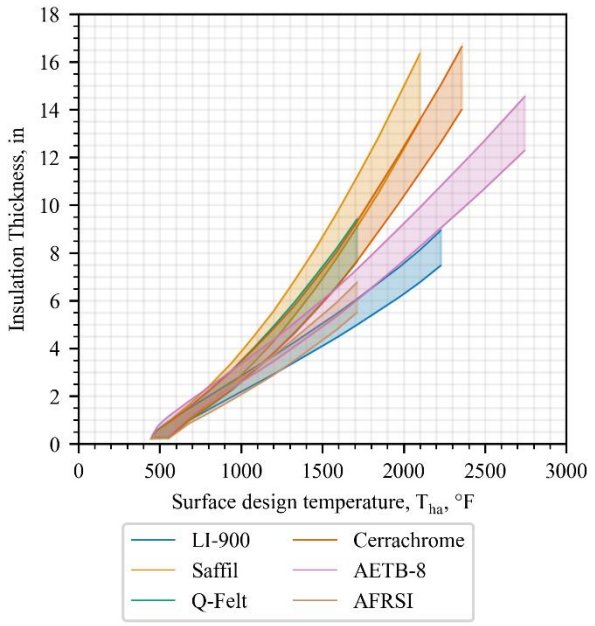

Fig. G.16 Insulation thickness vs surface design temperature at a cruise time of 5 hrs.

G.5 Variation of Structural Index with a Graphite/Epoxy Structure

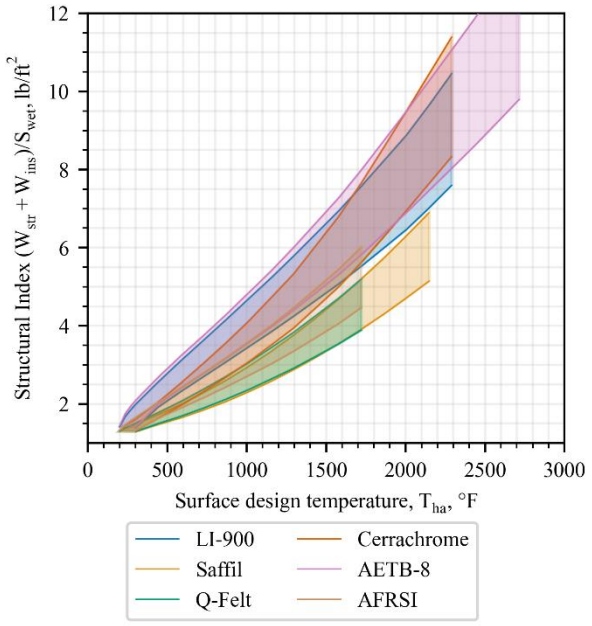

Fig. G.17 Structural index vs surface design temperature at a cruise time of 2 hrs.

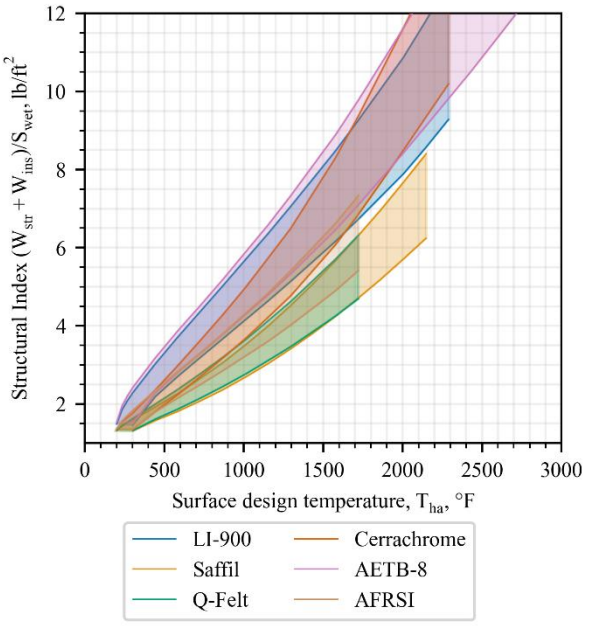

Fig. G.18 Structural index vs surface design temperature at a cruise time of 3 hrs.

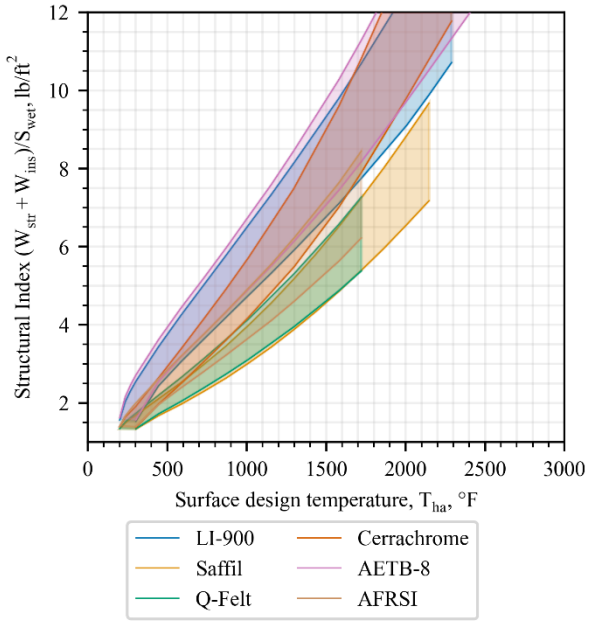

Fig. G.19 Structural index vs surface design temperature at a cruise time of 4 hrs.

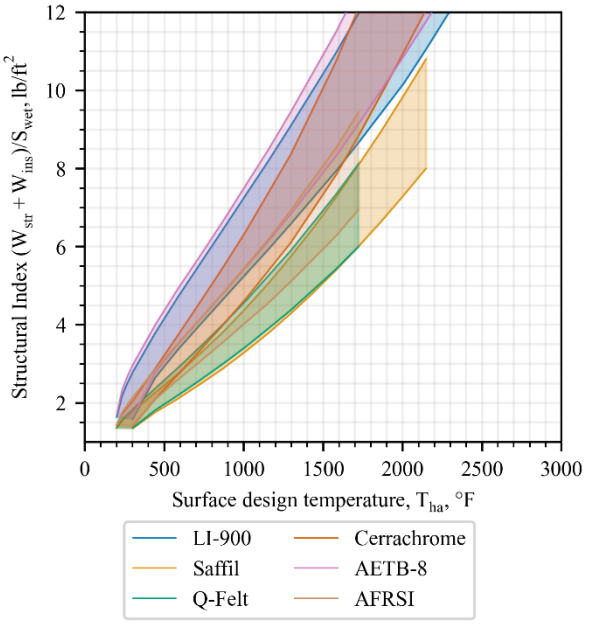

Fig. G.20 Structural index vs surface design temperature at a cruise time of 5 hrs.

G.6 Variation of Insulation Thickness with a Graphite/Epoxy Structure

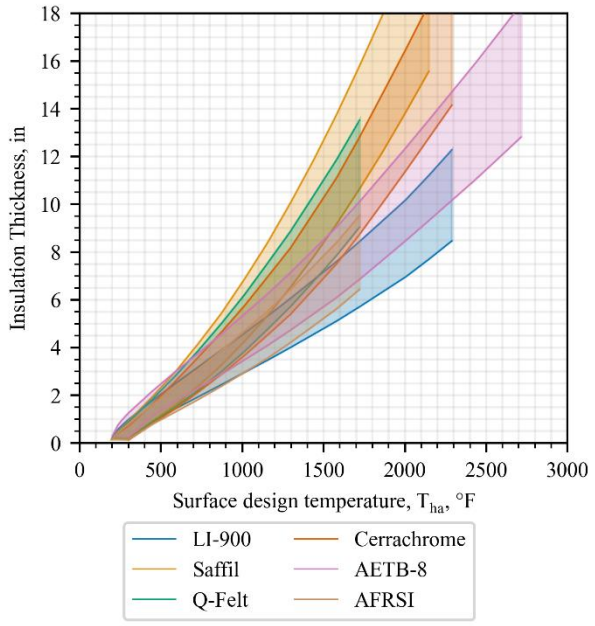

Fig. G.21 Insulation thickness vs surface design temperature at a cruise time of 2 hrs.

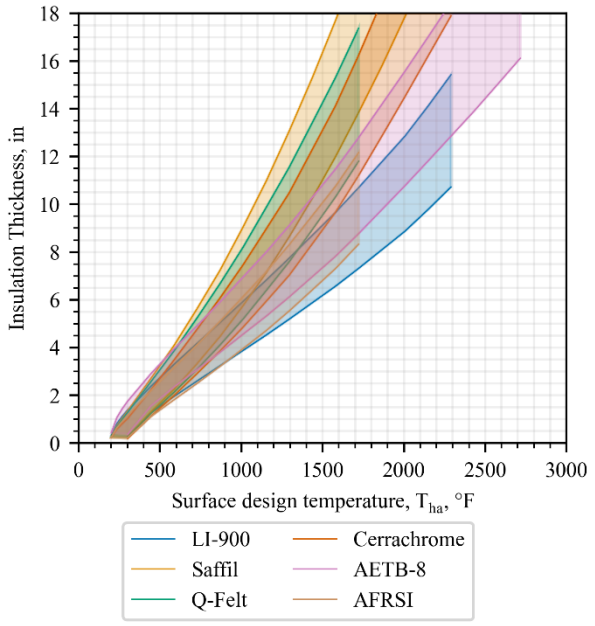

Fig. G.22 Insulation thickness vs surface design temperature at a cruise time of 3 hrs.

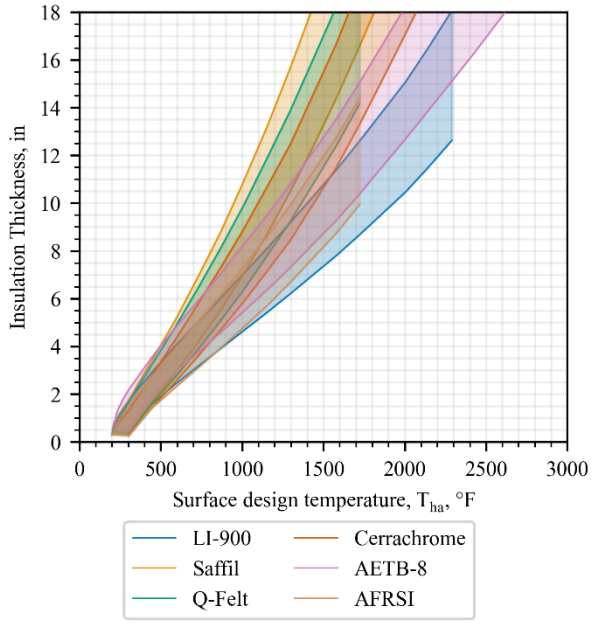

Fig. G.23 Insulation thickness vs surface design temperature at a cruise time of 4 hrs.

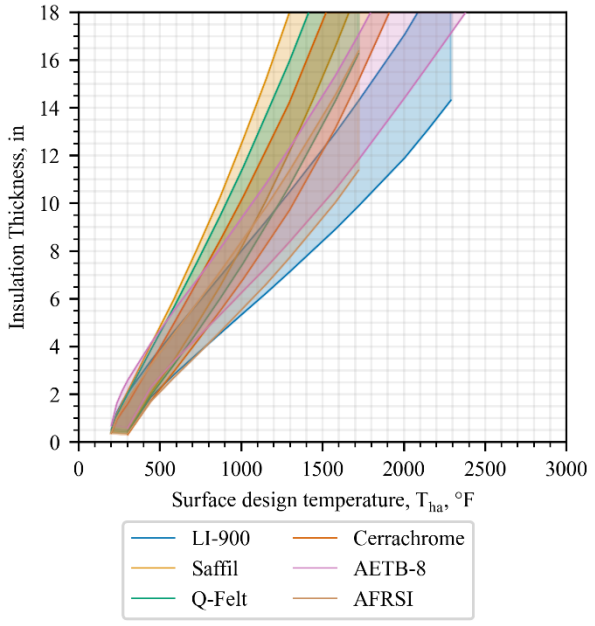

Fig. G.24 Insulation thickness vs surface design temperature at a cruise time of 5 hrs.

G.7 Variation of Structural Index with a Titanium 6Al-4V Structure

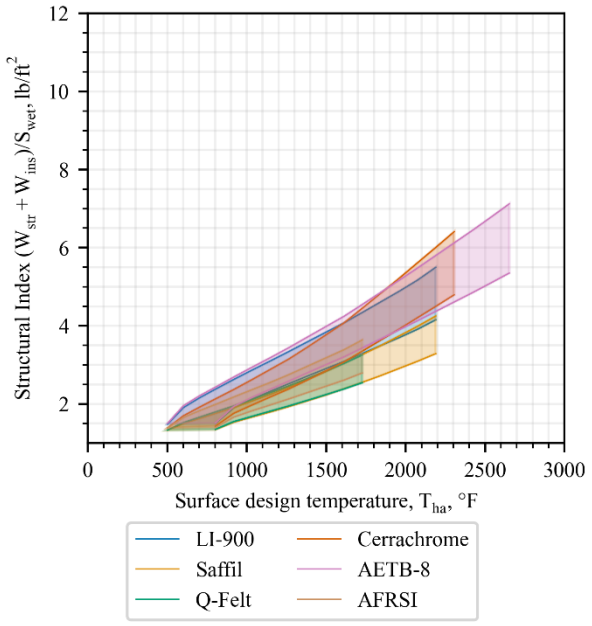

Fig. G.25 Structural index vs surface design temperature at a cruise time of 2 hrs.

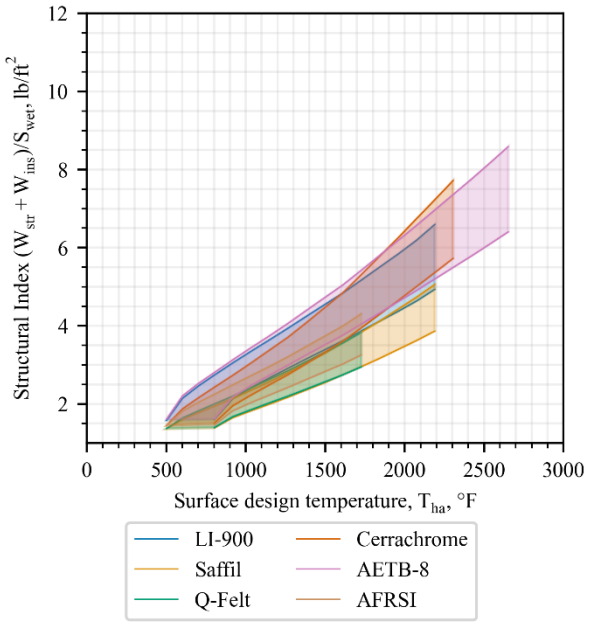

Fig. G.26 Structural index vs surface design temperature at a cruise time of 3 hrs.

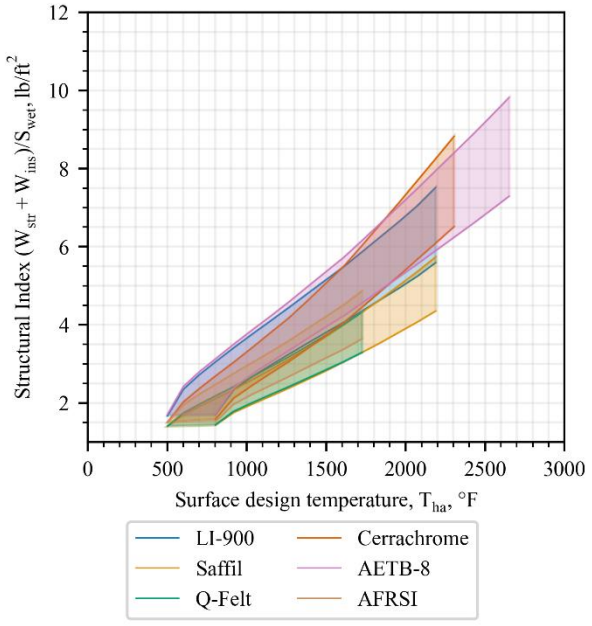

Fig. G.27 Structural index vs surface design temperature at a cruise time of 4 hrs.

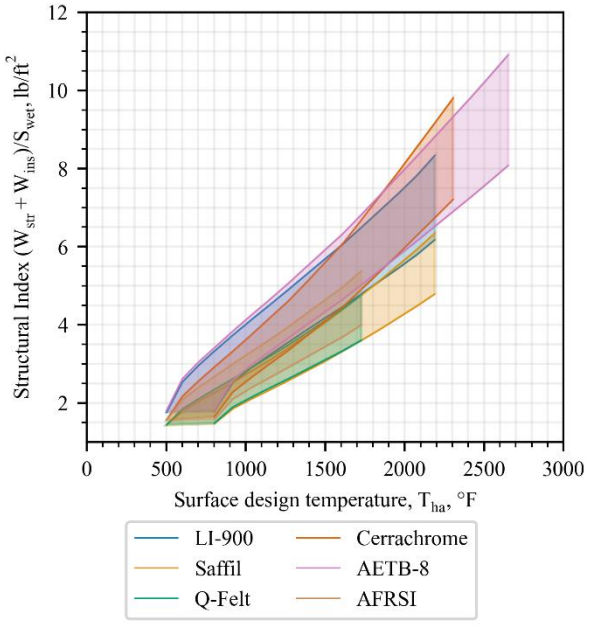

Fig. G.28 Structural index vs surface design temperature at a cruise time of 5 hrs.

G.8 Variation of Insulation Thickness with a Titanium 6Al-4V Structure

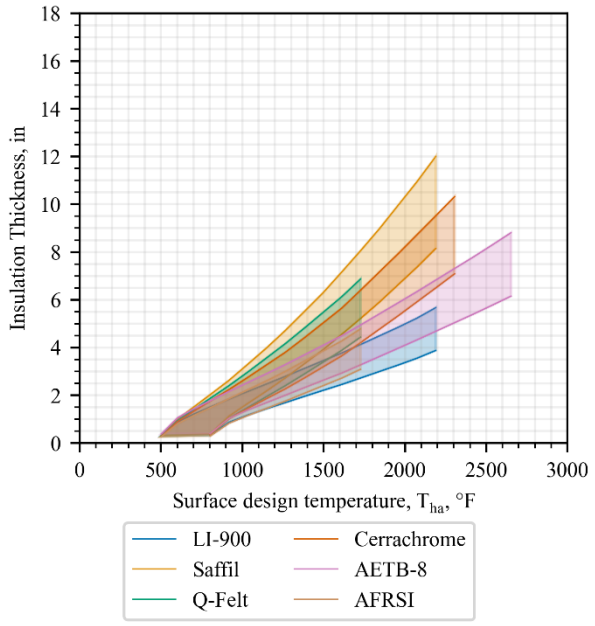

Fig. G.29 Insulation thickness vs surface design temperature at a cruise time of 2 hrs.

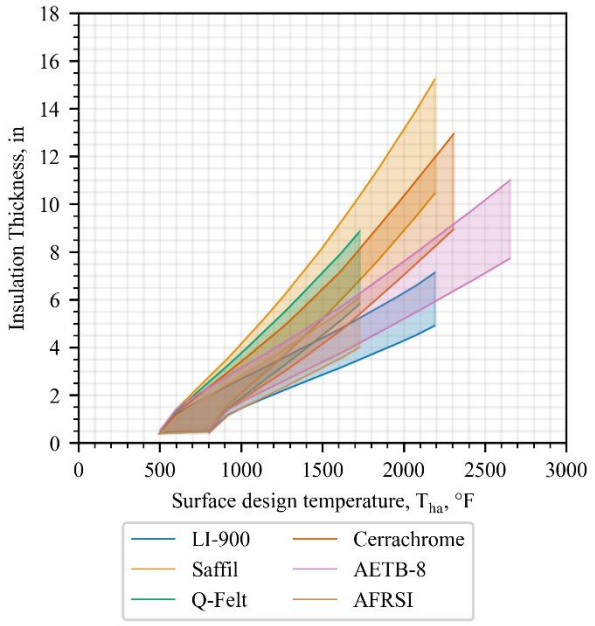

Fig. G.30 Insulation thickness vs surface design temperature at a cruise time of 3 hrs.

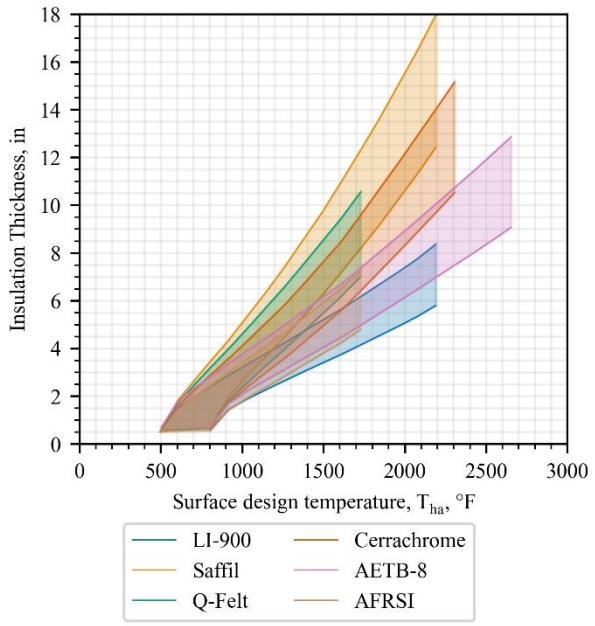

Fig. G.31 Insulation thickness vs surface design temperature at a cruise time of 4 hrs.

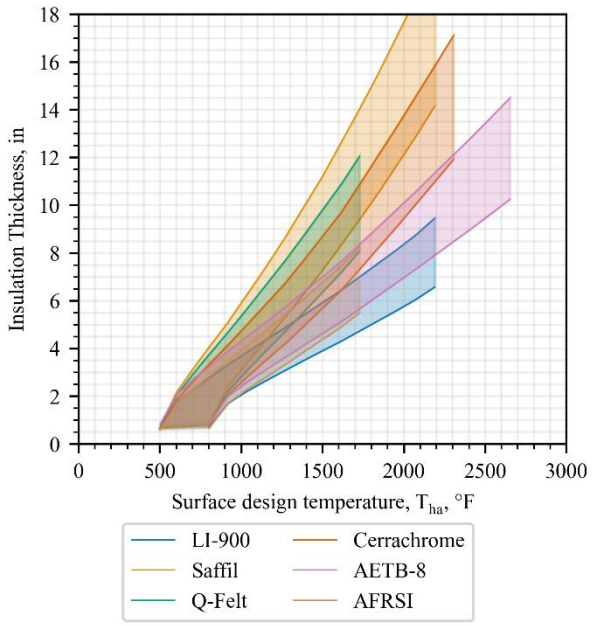

Fig. G.32 Insulation thickness vs surface design temperature at a cruise time of 5 hrs.